3D Modelling and Tissue-level Morphology of Trapeziometacarpal Joint

Yasser AL Harbi

Thesis submitted in fulfilment of the requirement for the degree of Doctor of Philosophy

Articulation Research Laboratory
College of Medical, Veterinary and Life Science
University of Glasgow
Glasgow, G12 8QQ
UK

September 2015

Acknowledgement

“In the name of Allah Almighty, the most merciful, the most beneficent”

I owe my deepest gratitude to my supervisors Dr Quentin Fogg and Prof. Willam Cushely for all their continuous guidance, advice and constructive criticism.

I am very thankful to David Russell, Gorden for all their technical assistance and fruitful collaboration.

I have been fortunate to know and work with fantastic people over the past few years. Special thanks go to Dr Stuart Macdonald for his kind help and support during the last three years.

A special thanks to all the donors and their families from the West of Scotland Body Donation Programme.

My deepest respect, great love and gratitude to my father **Ayish** my mother **Suad**, the most loving, kind, patient and intelligent parent I will ever know. This thesis is dedicated to both of them.

Finally, special thanks and great love goes to my lovely kids **Sama** and **Abdulrahman**, prayers and support this whole journey of PhD would have not been possible.

Publication

- 3D analysis of the Trapeziometacarpal (TMC) Ligaments during neutral and full abduction positions. British Association of Clinical Anatomy (Swansea 2012).

- Static and Dynamic Modeling of the Trapeziometacarpal Joint Ligaments. European Association of Clinical Anatomy (Lisbon2013).

- Microscopic Analysis of the Trapeziometacarpal Ligaments. European Association of Clinical Anatomy (Lisbon2013).

- Comparative study between the outcomes of the reconstruction and modelling of the volar, dorsal intermetacarpal ligaments of the trapeziometacarpal joint. American Association of Clinical Anatomist (Orlando 2014).

- Develop techniques of histological staining at the trapeziometacarpal ligament attachments. American Association of Clinical Anatomist (Orlando 2014).

- Morphological and statistical descriptions of the trapezium and first metacarpal bones. American Association of Clinical Anatomist (Las vagus 2015).

Abstract

The ligaments of the trapeziometacarpal joint (TMC) are complex and highly varied. Several studies have reported different patterns of ligament arrangement. Which ligaments are responsible for governing the stability of the TMC is still a source of controversy; the very naming of some of the ligaments is also in dispute.

The overall aim of the experiments in this thesis is to explore the stablization of the TMC ligaments during a specific positions (the neutral and full abduction positions), the mechanics of the attachment, the relaxing and stretching of the TMC ligaments, and the responsibilities of the TMC ligaments to prevent the TMC joint subluxations such as dorsal subluxation, palmar subluxation, and lateral subluxation. An additional aim is to describe the orientation of the TMC ligaments (origin, insertion) and the ligament fibres' directions.

The study used development devices to render the TMC ligaments into 2D reconstruction and 3D modelling in the 3D virtual environment such as Rhinoceros V5, 3D Landmark software, and 3D Amira software. Length, width, area, volume, thickness, and cross-sectional measurements were assessed in the neutral and full abduction positions. The ligament stretcher was designed to stretch the TMC ligaments after the ligaments were cut away from the joint. Also used in the thesis is a new technique to develop staining procedures by combining two different stains with accurate timing and re-timing the procedures of the Miller's Elastin Staining protocol. Also, the entheses investigations have been applied on the attachments of the TMC ligaments with trapezuim and first metacarpal bones (proximal and distal).

Moreover, the technique of the high resolution episcopic microscopy (HREM) was used to identify the relation of the TMC ligaments fibres to the flexor retinaculum, especially at dorso-ulnar trapeziometacarpal ligament (DUTML). The layers of the palmar trapeziometacarpal ligament (PTML) were also investigated to identify the nature of this ligament. The osteological descriptions were noted for the first metacarpal and trapezium bones, the geometrical measurement experiments on the articular surface of both bones allowed for a description of the effects of the degenerative disease, especially osteioarthritis disease (OA), and

comparisons between both genders, the right and left specimens, embalmed and fresh cadavers were investigated to achieve the most accurate and precise results. The index procedures against the third metacarpal assisted in describing the relation between the actual reading and index reading.

Seven ligaments were shown in the 3D virtual environment: radial trapeziometacarpal ligament (RTML), superficial palmar trapeziometacarpal ligament (sPTML), deep palmar trapeziometacarpal ligament (dPTML), palmo-ulnar trapeziometacarpal ligament (PUTML), dorso-ulnar trapeziometacarpal ligament (DUTML), palmar intermetacarpal ligament (PIML), and dorsal intermetacarpal ligament (DIML). Also, the results revealed that the PIML and DIML were the main stabilizers through the experiments, and the DUTML and PUTML served as associated ligaments to prevent TMC joint dislocation. The RTML prevented radial subluxation, while the superficial and deep layers of the PTML acted as a pivot for the movement of the TMC joint and assisted in preventing a palmar subluxation. In addition, there were no significant differences ($p>0.05$) between embalmed and fresh cadavers, but there were significant differences ($p<0.05$) between male and female cadavers as well as between the right and left hands, especially in the measurement investigations.

Moreover, the TMC ligament attachments were found to be of the fibrocartilagenous type; this was found at both attachments, proximal and distal. The combination beginning with Miller Elastin stain (ME) was better than that starting with Modified Masson Trichrome stain (MME) and the colours were nearer to those of the MMT results; however, the MMT alone was clearest. Also, a re-timing of the ME stain revealed that the experiment involving 2.5 hours of Miller's Elastin and 15 seconds of Van Gieson Solution was the best of all experiments. The HREM technique revealed no connection between the collagen fibres of both the DUTML and the flexor retinaculum. The single coordination points of each of the first metacarpal (1st MC) and trapezium (TM) bones revealed varieties of prominences and declines in the bones' surfaces, especially the articular surface.

New names of the TMC ligaments as following:

Old Name	New Name
Ulnar collateral ligament (UCL).	Radial trapeziometacarpal ligament (RTML).
Superficial anterior oblique ligament (sAOL).	Superficial palmar trapeziometacarpal ligament (sPTML).
Deep anterior oblique ligament (dAOL).	Deep palmar trapeziometacarpal ligament (dPTML).
Posterior oblique ligament (POL).	Palmo-ulnar trapeziometacarpal ligament (PUTML).
Dorso-radial ligament (DRL).	Dorso-ulnar trapeziometacarpal ligament (DUTML).

New osteological definitions were noted, such as the distal border of the 1st MC facet, the distal and proximal ridge of the palmar surface of the1st MC, and eminences of the trapezial ridge of TM.

Overall, the results of my studies suggested that the importance of the PIML, DIML, and RTML should be considered when planning surgeries involving ligament reconstruction of the TMC joint.

Table of Contents

List of Figures

List of Tables

Author’s Declaration

I declare that the work presented in this thesis is entirely my own with all exceptions being clearly indicated or/ and properly cited in the context.

Signature.....

Yasser Al Harbi

The work has not been presented in part or alone for any other degree programme. Some of the work contained here has been submitted in part to be published:

Abbreviations

1st MC	First Metacarpal Bone
2nd MC	Second Metacarpal Bone
2D	Two-Dimensional Field
3rd MC	Third Metacarpal Bone
3D	Three-Dimensional Field
ADD	Adduction motion
AEL1	First Anterior Eminences Line
AEL2	Second Anterior Eminences Line
AOL	Anterior Oblique Ligament
APB	Abductor Pollicis Brevis Muscle
BMI	Body Mass Index
CMC	Carpometacarpal Joint
CT	Computed Tomography
CWL	Central Width Line
dAOL	Deep Anterior Oblique Ligament
DBL1	First Distal Border Line
DBL2	Second Distal Border Line
DIML	Dorsal Intermetacarpal Ligament
dPTML	Deep Palmar Trapeziometacarpal Ligament
DRL	Dorso-radial Ligament
DRTL1	First Dorso-radial Tubercle Line
DRTL2	Second Dorso-radial Tubercle Line
DUTML	Dorso-ulnar Trapeziometacarpal Ligament
EFIC	Episcopic Fluorescence Image Microscopy
ETL1	First Eminence Trpezial Line
ETL2	Second Eminence Trpezial Line
F	F Value of Regression Test
FPB	Flexor Pollicis Brevis Muscle
HREM	High Resolution episcopic Microscopy
IML	Intermetacarpal Ligament
IP	Interphalangeal Joint
MCP	Metacarpal Phalangeal Joint
MD1	First Metacarpal Dorsal Point
MD2	Second Metacarpal Dorsal Point
MD3	Third Metacarpal Dorsal Point

MD4	Fourth Metacarpal Dorsal Point
MD5	Fifth Metacarpal Dorsal Point
ME	Miller's Elastin Stain
MMT	Modified Masson's Trichrome Stain
MP1	First Metacarpal-Palmar Point
MP2	Second Metacarpal-Palmar Point
MP3	Third Metacarpal-Palmar Point
MP4	Fourth Metacarpal-Palmar Point
MP5	Fifth Metacarpal-Palmar Point
MPR1	First Metacarpal-Proximal Point
MPR2	Second Metacarpal-Proximal Point
MPR3	Third Metacarpal-Proximal Point
MPR4	Fourth Metacarpal-Proximal Point
MRI	Magnetic Resonance Image
N	Newton Unit
OA	Osteoarthritis Disease
OPP	Opposition Motion
PEG	Polyethylene Glycol
PEL1	First Posterior Eminences Line
PEL2	Second Posterior Eminences Line
PIML	Palmar Intermetacarpal Ligament
POL	Posterior Oblique Ligament
PTL1	First Palmar Tubercle Line
PTL2	Second Palmar Tubercle Line
PUTML	Palmo-ulnar Trapeziometacarpal Ligament
R^2	R Square of Regression Test
RBL1	First Radial Border Line
RBL2	Second Radial Border Line
RMS	Root- Mean-Square
RNA	Ribonucleic Acid
RTML	Radial Trapeziometacarpal Ligament
sAOL	Superficial Anterior Oblique Ligament
sPTML	Superficial Palmar Trapeziometacarpal Ligament
SSM	Statistical Shape Model
TCL	Transverse Carpal Ligament
TD1	First Trapezial-distal point
TD2	Second Trapezial-distal point

TD3	Third Trapezial-distal point
TD4	Fourth Trapezial-distal point
TM	Trapezium Bone
TMC	Trapeziometacarpal Joint
TPS	Thin-Plate Spline
TR1	First Trapezial- radial Point
TR2	Second Trapezial- radial Point
TR3	Third Trapezial- radial Point
TR4	Fourth Trapezial- radial Point
TR5	Fifth Trapezial- radial Point
TRP	Trapezoid Bone
UBL1	First Ulnar Border Line
UBL2	Second Ulnar Border Line
UCL	Ulnar Collateral Ligament
VG	Van Gieson Solution
X-Ray	X-ray Radiation

Old Name	New Name
Ulnar collateral ligament (UCL).	Radial trapeziometacarpal ligament (RTML).
Superficial anterior oblique ligament (sAOL).	Superficial palmar trapeziometacarpal ligament (sPTML).
Deep anterior oblique ligament (dAOL).	Deep palmar trapeziometacarpal ligament (dPTML).
Posterior oblique ligament (POL).	Palmo-ulnar trapeziometacarpal ligament (PUTML).
Dorso-radial ligament (DRL).	Dorso-ulnar trapeziometacarpal ligament (DUTML).

Table illustrates the old and new names of the TMC ligaments.

Chapter One

General Introduction

Many anatomists and clinicians have studied the anatomy of the basal joint of the thumb, known as the *trapeziometacarpal joint* (TMC). The pan-trapezial base joint of the thumb includes the unique TMC joint, also called the *first carpometacarpal* joint, and the scaphotrapeziotrapezoidal joint, also called the *triscaphe* joint. The TMC is formed by the proximal joint facet of the first metacarpal and the distal facet of the trapezium.

The morphological features of these facets, together with a lax but strong joint capsule, give the thumb great mobility and play a key role in the opposition of the thumb. The TMC articulation is a saddle-type joint that allows rotational movement in such a way that the tip of the thumb can oppose the tips of the other digits.

The prehensile functions of the hand are based on thumb-finger relationships, which are viewed as an essential element in various manipulations in our daily living activities.

The stability of the TMC is not guaranteed by joint surfaces and ligaments alone. The function of the muscles that cross the joint is essential (Kuczynski 1974). The analysis of motion patterns of the TMC is poorly linked with anatomically accurate models, thus creating disconnect between anatomic and physiologic investigations. The combination of structural and kinaesthetic data is most readily applied to the clinical management of joint subluxation and degenerative diseases. The mechanisms of failure may be better understood with more precise anatomical knowledge.

The kinematics of the thumb in relation to the trapezium and the first metacarpal remains poorly understood *(Kuo et al. 2004)*. Although considerable research has been conducted into the morphology of the trapezium, the importance of the morphology of the intervening joint is not so well understood. A better understanding of this region will provide an improved understanding of the kinematics of the trapezium, as well as of the TMC. In turn this will enhance the clinical management of a number of thumb dysfunctions. These discussions will

establish the current level of relevant knowledge, upon which further investigation can be built.

The morphology of the bones that comprise the TMC joint plays a very important role in increasing or decreasing the stabilisation of the TMC joint. In addition, the TMC joint's shape is related to the insertion of certain TMC ligaments, such as the dorso-radial (DRL) and the anterior oblique ligaments (AOL) (D'Agostino *et al.* 2014).

In addition, the attachments of the TMC ligaments have been the subject of several investigations; some of these have recorded the relation between the specific ligament of the TMC joint with the types of the entheses (Benjamin *et al.* 2002; Benjamin *et al.* 2006; Chung 2007; Claudepierre and Voisin 2005; Francois *et al.* 2001).

Because the flexor retinaculum of the hand has been shown to overlap with the DRL fascicles through histological investigation of the TMC ligaments, the current study will concentrate on the DRL ligament and other TMC ligaments to explain the mechanism of the attachment of the TMC ligaments, as well as the relation of these ligaments with the flexor retinaculum (Cobb *et al.* 1993; Goitz *et al.* 2014; Nigro 2001).

While the traditional histological procedures include embalming, embedding, sectioning, cutting, and staining, most histological research studies have focussed on the new concepts of the protocol procedures and on re-timing the section with embedding or staining. In addition, these studies have concentrated on new techniques to provide a good view of the tissue slides under the microscope (Asonova and Migalkin 1996; Carleton *et al.* 1980; Claudepierre and Voisin 2005; Goldner 1938; Isa and Hoo 1980; Li *et al.* 2005).

1.1 Ligaments and stability

1.1.1 Number of Ligaments

The numbers of TMC ligaments have varied from one study to another; Bettinger (1999) named four ligaments around the TMC joint, called the dorsal ligament complex, as follows (Figure 1.1):

1. Posterior oblique ligament (POL)
2. Dorso-radial ligament (DRL)
3. Anterior oblique ligament (AOL)
4. Intermetacarpal ligament (IML)

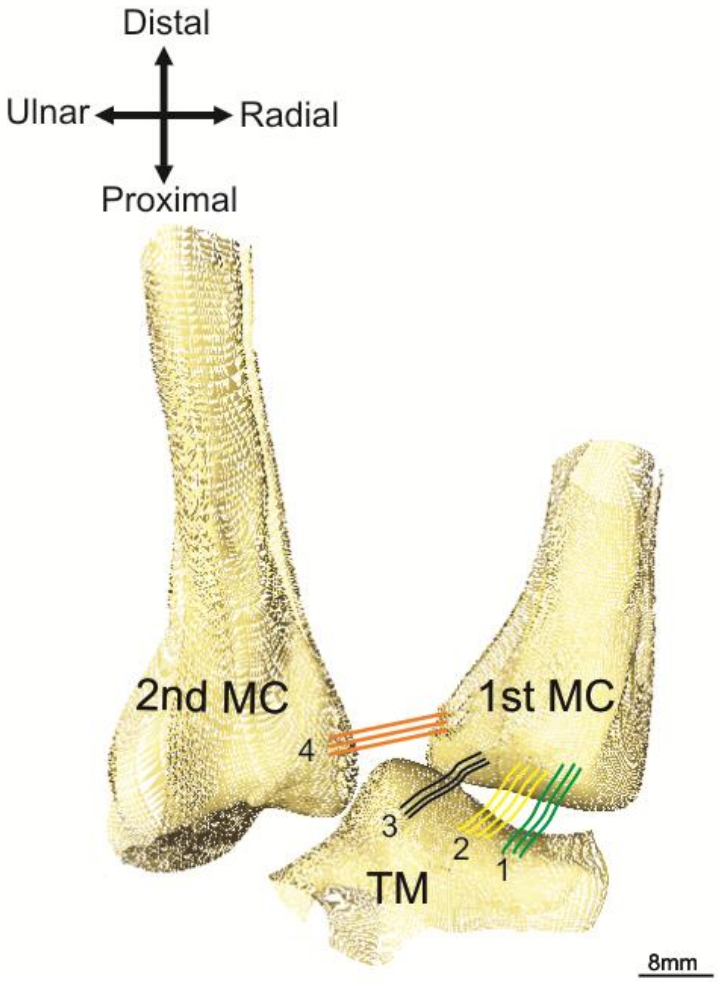

Figure 1.1: Anterior views of the trapeziometacarpal joint and its ligaments, from Bettinger (1999).
1. Anterior oblique ligament (AOL). 2. Posterior oblique ligament (POL). 3. Dorso-radial ligament (DRL). 4. Intermetacarpal ligament (IML).

Imaeda (1993) recorded five main ligamentous structures as follows (Figure 1.2):

1. Anterior oblique ligament (AOL)
2. Posterior oblique ligament (POL)
3. Ulnar collateral ligament (UCL)
4. First intermetacarpal ligament (IML)
5. Dorsoradial ligament (DRL)

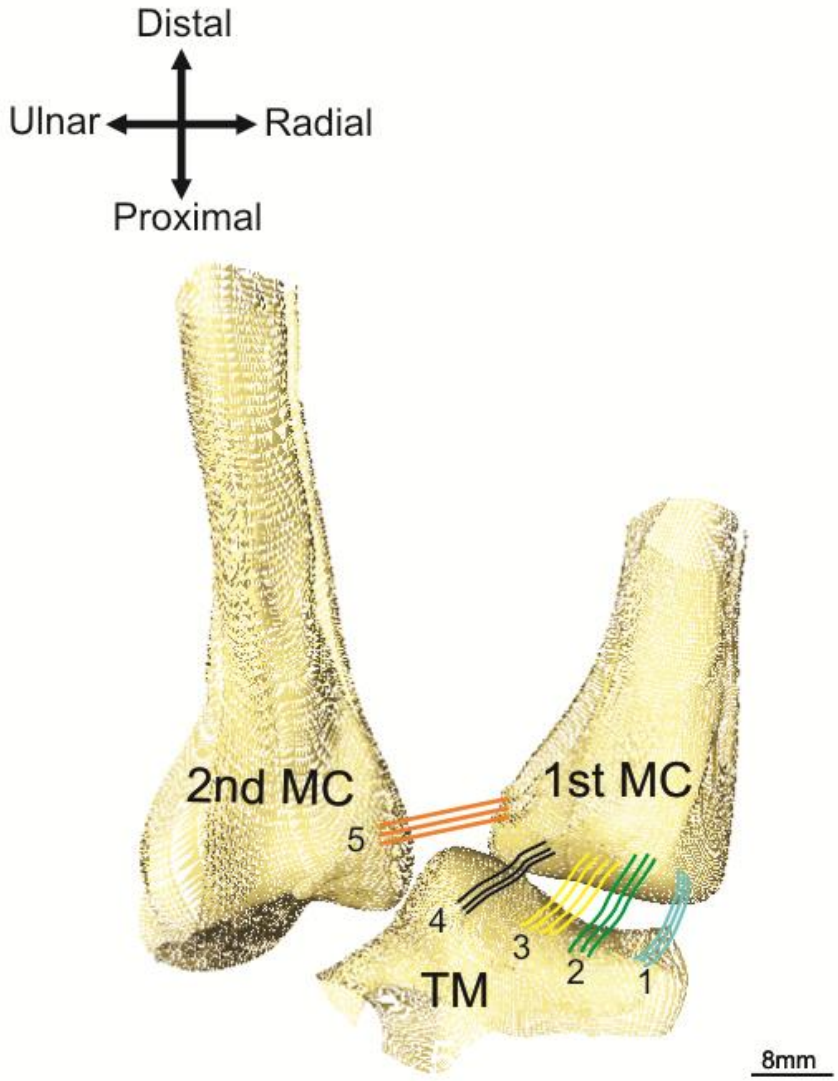

Figure 1.2: Anterior views of the trapeziometacarpal joint and its ligaments, from Imaeda (1993).
1. Ulnar collateral ligament (UCL). 2. Anterior oblique ligament (AOL). 3. Posterior oblique ligament (POL). 4. Dorso-radial ligament (DRL). 5. Intermetacarpal ligament (IML).

Rongieres (2004) and Lin (2013) classified the TMC ligaments into six ligaments around the TMC joint (Lin *et al.* 2013; Rongieres 2004) as follows (Figure 1.3):

1. Superficial anterior oblique ligament (sAOL)
2. Deep anterior oblique ligament (dAOL)
3. Posterior oblique ligament (POL)
4. First intermetacarpal ligament (IML)
5. Dorsoradial ligament (DRL)
6. Dorsal intermetacarpal ligament (DIML)

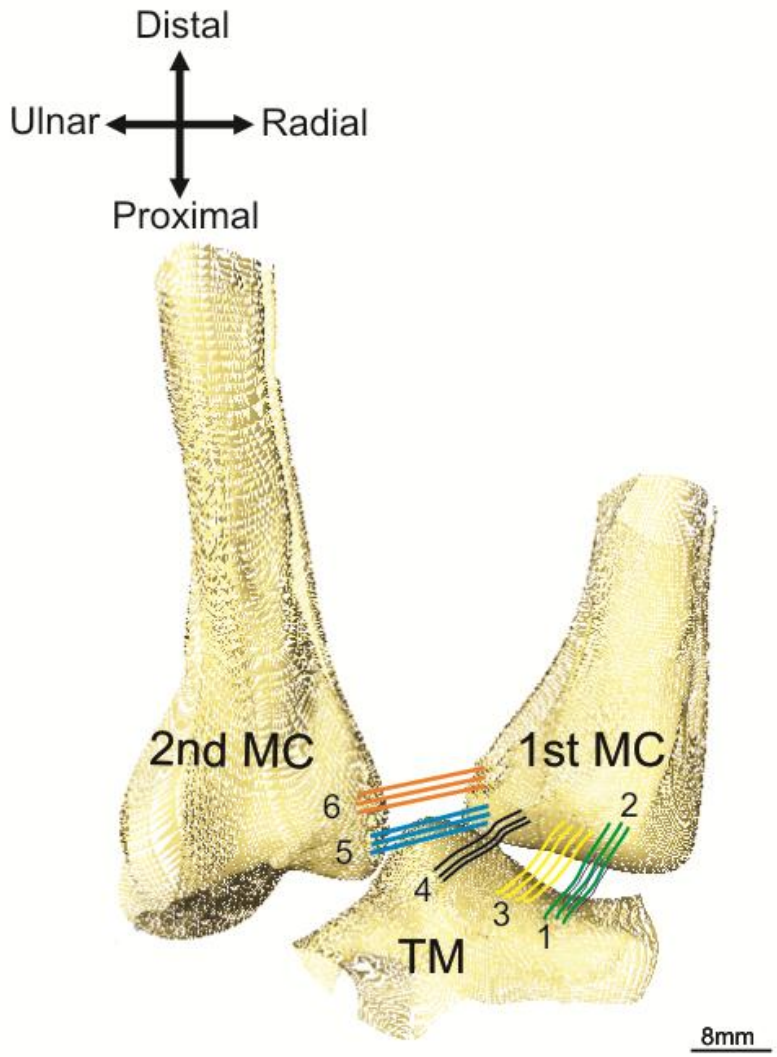

Figure 1.3: Anterior views of the trapeziometacarpal joint and its ligaments, from Rongieres (2004) and Lin (2013).
1. Sperficial anterior oblique ligament (sAOL). 2. Deep anterior oblique ligament (dAOL) 3. Posterior oblique ligament (POL). 4. Dorso-radial ligament (DRL). 5. Palmar intermetacarpal ligament (PIML). 6. Dorsal intermetacarpal ligament (DIML).

Bettinger (2000) have been identified seven ligaments around the TMC joint as follows (Figure 1.4):

1. Superficial anterior oblique ligament (sAOL)
2. Deep anterior oblique ligament (dAOL)
3. Dorsoradial ligament (DRL)
4. Posterior oblique ligament (POL)
5. Ulnar collateral ligament (UCL)
6. Intermetacarpal ligament (IML)
7. Dorsal intermetacarpal ligament (DIML)

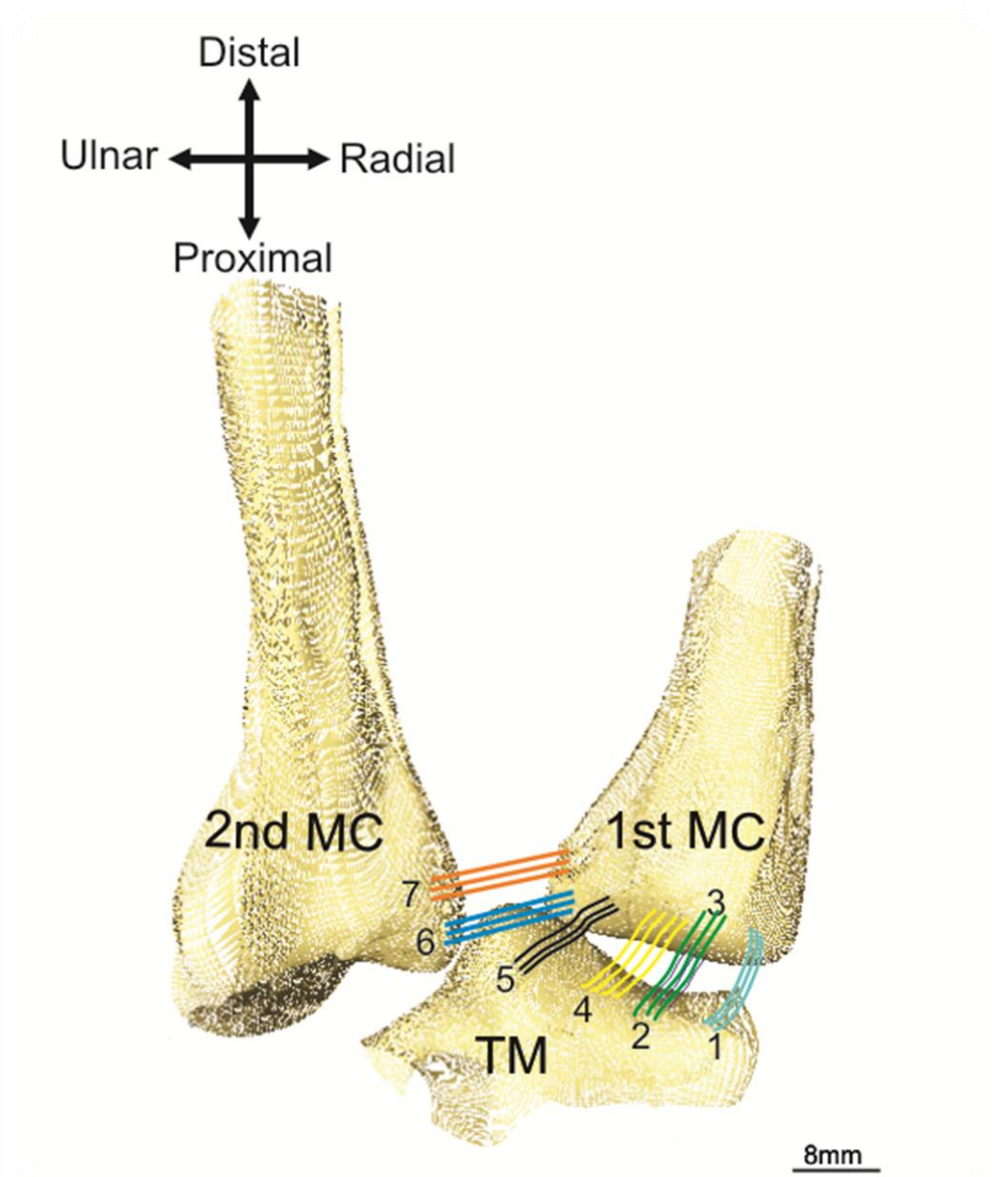

Figure 1.4: Anterior views of the trapeziometacarpal joint and its ligaments, from Bettinger (2000).
1. Ulnar collateral ligament (UCL). 2. Sperficial anterior oblique ligament (sAOL). 3. Deep anterior oblique ligament (dAOL) 4. Posterior oblique ligament (POL). 5. Dorso-radial ligament (DRL). 6. Palmar intermetacarpal ligament (PIML). 7. Dorsal intermetacarpal ligament (DIML).

Thus, the number of TMC ligaments are needed for clarify and precision based on dissections and 2D experiments.

According to previous studies, there were variations in the number of TMC ligaments. These findings are consistent throughout this thesis as seen by viewing the micro-dissection of the cadavers as well as the rendering of the TMC ligaments into a 2D reconstruction and 3D model in a 3D virtual environment.

1.1.2 Attachment of the ligaments

Others studies have provided more detailed information on individual ligaments (Chiavaras *et al.* 2010; Koff *et al.* 2003; Pieron 1973). The AOL arises from the palmar side of the first metacarpal and inserts on the palmar side of the trapezium (Koff *et al.* 2003). It is completely lax during the screw-home torque rotation and plays no part in the prevention of dorsal subluxation. It is tensed only when the thumb is placed in the ‘hitchhiker’ position.

The AOL extends from the palmar tubercle of the trapezium to the ulnopalmar aspect of the base of the first metacarpal. In this way, the fibres are obliquely directional from radial and proximal to ulnar and distal, and form an important part of the joint capsule at the palmar and ulnar sides of the joint (Chiavaras *et al.* 2010).

The sAOL originates from the palmar tubercle of the trapezium 0.5 mm proximal to the articular surface and inserts across the palmo-ulnar tubercle of the first metacarpal 2 mm distal to the articular margin of the palmar styloid process (Pieron 1973); Pieron described this ligament as running in a curtain-like fashion. It is superficial to dAOL and deep to the thenar muscles and capsular ligament, and thins at its edges to blend into the capsule itself. The course of the fibres runs in a slightly oblique direction from proximoradial to distal-ulnar. It becomes taut upon rotation, especially in pronation and extension; in addition, it limits palmar subluxation. dAOL inserts at the articular margins of the trapezium and originates just ulnar to the palmar styloid process at the base of the first metacarpal. Its intra-articular ligament is oriented obliquely from proximoradial to distal-ulnar and lies within the concavity of the trapezium. It serves as a pivot point for rotation, especially pronation, to produce opposition; it is shorter than sAOL and prevents

extreme ulnar subluxation of the base of the first metacarpal towards the second metacarpal. It also shares responsibility with the sAOL of stabilising palmar metacarpal subluxation; it is taut in pronation and full abduction (Figure 1.6).

The DRL is the widest and thickest ligament attached to the trapezium, and is also the shortest ligament spanning the TMC. It originates from the dorsoradial tubercle of the trapezium and inserts into the dorsal edge of the base of the first metacarpal, its capsular ligament, is a fan-shaped ligament. The fibres are oriented in both a longitudinal and oblique direction, depending on which side of the tubercle they originate from. The middle third of the fibres lies directly longitudinal, while the radial third spans from proximo-ulnar to distal-radial, and the ulnar third spans from proximoradial to distal-ulnar. It becomes taut with a dorsal or dorsoradial subluxating force in all positions of the TMC except full extension; DRL tightens in supination and also with pronation when the TMC is flexed (Koff *et al.* 2003). Moreover, the DRL originates at the dorso-ulnar tubercle of the trapezium and extends to the dorsal rim of the base of the first metacarpal (Chiavaras *et al.* 2010) (Figure 1.7).

The POL originates on the dorso-ulnar side of the trapezium and inserts onto the dorso-ulnar aspect of the first metacarpal and palmo-ulnar tubercle, along with IML. Its capsular ligament runs obliquely from proximoradial to distal-ulnar. It is covered superficially by the extensor pollicis longus tendon and is taut in full abduction (Oehmke *et al.* 2009) (Figure 1.8).

The UCL originates from the distal margin of the Transvers carpal ligament (TCL) ulnarly to the insertion of the TCL onto the trapezial ridge and inserts superficially and ulnarly to the sAOL on the palmar-ulnar tubercle of the first metacarpal along with IML. Its extra-capsular ligament is oriented obliquely from proximoradial to distal-ulnar, and becomes taut in extension, abduction, and pronation, which limits palmar subluxation of the first metacarpal along with the sAOL and the dAOL (Cooney *et al.* 1981) (Figure1.4).

The IML originates from the dorso-radial aspect of the second metacarpal radial to the extensor carpi radialis longus and inserts into the palmar-ulnar tubercle of the base of the first metacarpal with POL and UCL. It is extra-capsular and runs obliquely from the dorsoradial aspect of the second metacarpal onto the palmar-ulnar aspect of the first metacarpal. It becomes taut with abduction,

opposition, and supination, and also works to stabilise the metacarpal during radiopalmar subluxation of its base (Frazer and ed 1965) (Figure 1.5).

Finally, DIML originates from the dorsoradial tubercle of the second metacarpal superficial to the extensor carpi radialis longus insertion, and inserts onto the dorsum of the dorso-ulnar corner of the first metacarpal. The radial half of the ligament, however, splits off in a Y fashion. It is extra-capsular, and its fibres run in a transverse direction from the first metacarpal to the second metacarpal, and become taut in pronation and with dorsal and radial subluxation of the base of the first metacarpal (Frazer 1920) (Figure 1.4).

The experiment was performed 3D analysis of the ligamentous attachments of the TMC (Nanno *et al.* 2006a); the authors showed the ligament attachments, and measured the lengths, widths, and thickness of each ligament. The size of the ligament attachment areas on the first metacarpal bone in order from largest to smallest was POL > sAOL > DRL > DIML > dAOL > PIML > UCL. The size of ligament attachment areas on the trapezium, in order from largest to smallest, was sAOL > POL > DRL > dAOL. Also, Nanno and colleagues further reported that:

- the DRL originates from the dorsoradial tubercle of the trapezium to the dorsoradial edge of the first metacarpal;
- the POL originates from the dorso-ulnar edge of the trapezium to the dorso-ulnar edge of the first metacarpal;
- the sAOL originates from the palmar edge of the trapezium to the palmar edge of the first metacarpal;
- the dAOL originates from the ulnopalmar edge of the trapezium to the ulnopalmar edge of the first metacarpal;
- the UCL originates from the transvers carpal ligament (TCL) to the ulnopalmar edge of the first metacarpal;
- the DIML originates ulnarly to the dorsoradial tubercle of the second metacarpal and radially towards the dorso-ulnar of the first metacarpal; and
- the PIML originates ulnarly to the ulnopalmar of the second metacarpal and radially towards the radiopalmar of the first metacarpal.

Based on previous definitions of individual TMC joint ligaments, there were variations on the attachments of TMC ligaments to the first metacarpal, second

metacarpal, and trapezium bones. This thesis will address these issues by performing micro-dissections on each regular fascicle apart from the two attachments (Proximal and distal).

1.1.3 Ligament stabilization

A review of the literature reveals that the anatomic orientation of the ligaments of the TMC and their contributions to joint stability remain unclear (Ghavami and Oishi 2006). Several concepts have been suggested that propose the stabilising role of the ligaments of the TMC.

1.1.3.1 Intermetacarpal ligament (IML)

The stability of the TMC joint through the intermetacarpal ligament (IML) has been determined (Pagalidis *et al.* 1981). The first IML alone was found to be responsible for the development the subluxation in full abduction of the first metacarpal; the authors also found that spontaneous attenuation of the IML was demonstrated in advanced osteoarthritis. In addition, the IML was considered a secondary stabiliser of the TMC joint in some experiments (Imaeda *et al.* 1993; Tan *et al.* 2011). The IML also has the ability to act as the main stabiliser between the first and second metacarpal bones (Koff *et al.* 2003) (Figure 1.5).

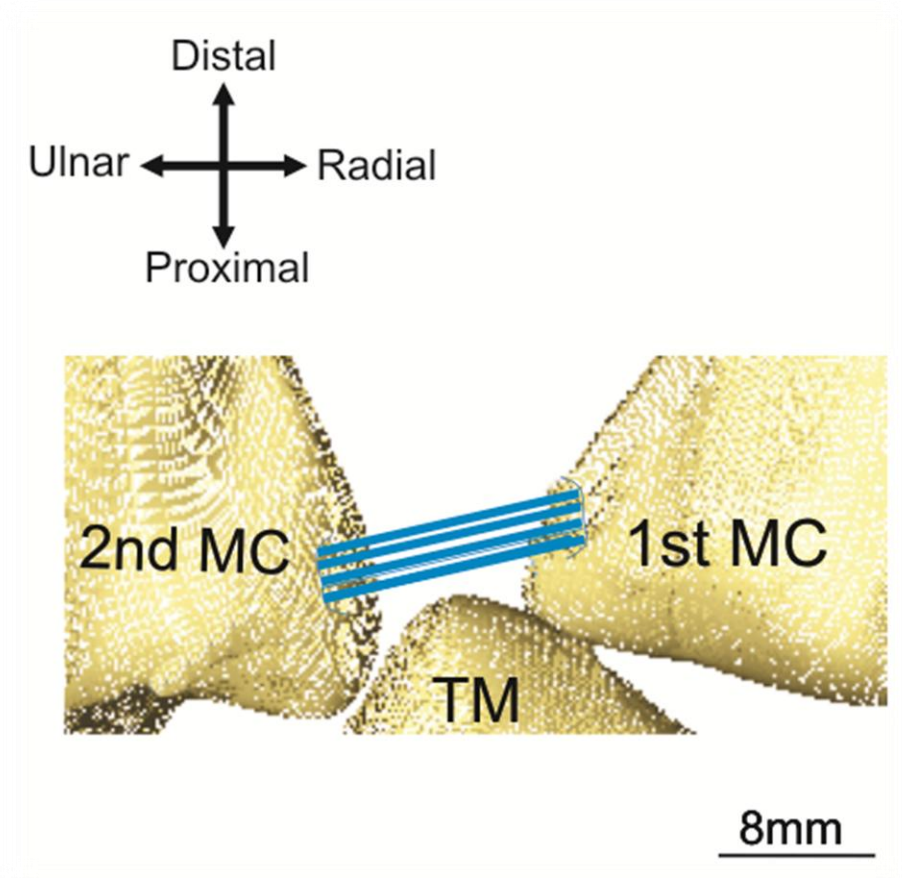

Figure 1.5: Anterior view of the trapeziometacarpal joint and its intermetacarpal ligament, from Pagalidis (1981). Blue lines illustrate the intermetacarpal ligament attachment between first and second metacarpal bones.

1.1.3.2 Anterior oblique ligament (AOL)

It has been suggested that the AOL is supported by the UCL (Pieron 1973). It has also been suggested that the AOL acts as a primary stabiliser assisted by the UCL (Connell *et al.* 2004), and that these are the most important stabilisers of the thumb (Eaton and Littler 1969). Also, the AOL was the primary stabiliser of the TMC (Imaeda *et al.* 1993), whilst the IML, UCL, and POL appeared to be secondary. Other studies of the anatomy have confirmed the idea that the AOL is necessary for stabilising the TMC (Bettinger *et al.* 1999; Bettinger *et al.* 2000; Imaeda *et al.* 1993; Lin *et al.* 2013; Rongieres 2004). Moreover, the two parts of the AOL, the superficial and deep parts, serve as a pivot point during thumb pronation, especially the dAOL, which becomes taut in abduction or extension to prevent ulnar subluxation of the thumb metacarpal (Ghavami and Oishi 2006) (Figure 1.6).

Also, Jantea et al (1994) experimented on the stability of the TMC by simulating two relevant mechanisms of full extension and full abduction. The result

was that the AOL of the TMC was ruptured mostly in full abduction, while POL, DRL, and IML were ruptured mostly in full extension. However, the comparsion between full extension and full abduction mechanisms, to explore which position lead to more severe injuries of the soft tissues of the thumb was reasonable.

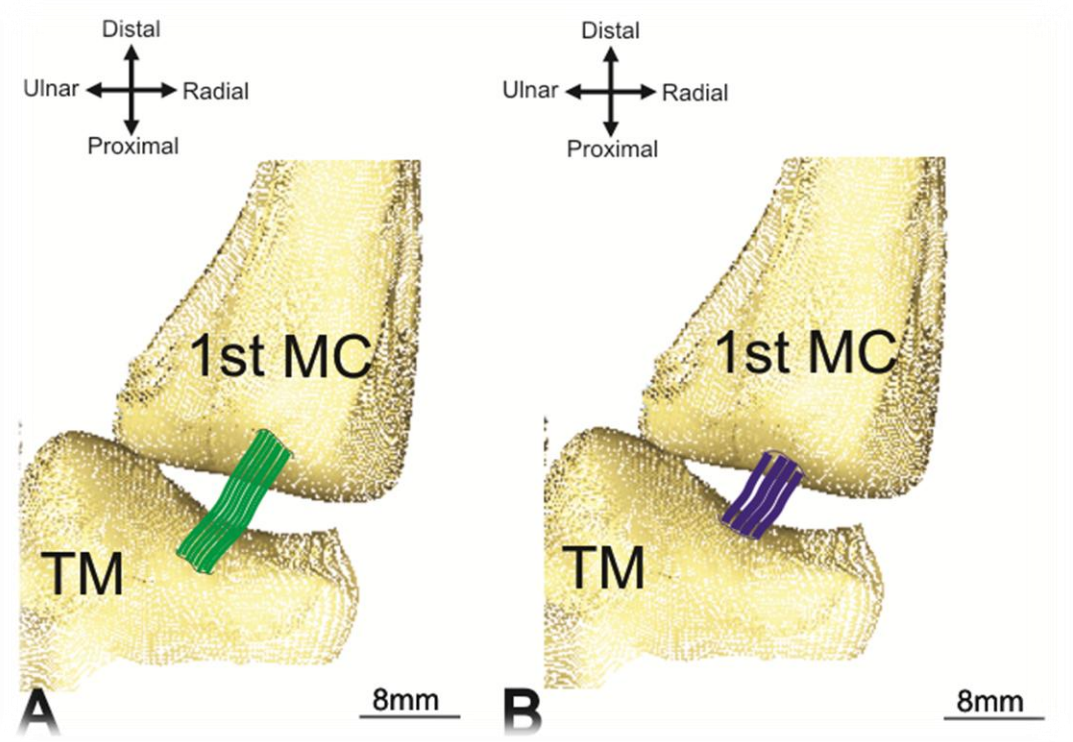

Figure 1.6: Anterior view of the trapeziometacarpal joint and its anterior oblique ligaments, from Eaton and Littler (1969).
A. The green lines illustrate the superficial part of anterior oblique ligament.
B. The purple lines illustrate the deep part of anterior oblique ligament.

1.1.3.3 Dorso-radial ligament (DRL)

The investigation of the DRL is related to osteoarthritis (OA) (Lin *et al.* 2013); stated that, over the past two decades, increasing evidence suggests that the DRL is the most important stabiliser of the TMC joint. However, it reflects the change of the shapes of bones and ligaments, and affects the properties of the ligaments, which decreases the percentage of the stabilisation of the affected TMC ligaments.

In addition, the relative contributions of the DRL and the dAOL to the stability of the TMC have been determined (Colman *et al.* 2007). The results showed that the DRL appears to be relatively more important than the dAOL in stabilising the

TMC. The authors believed that the most appropriate surgical intervention in patients with acquired ligament laxity is one that prioritises the reconstruction of both ligaments but also emphasises a full reconstruction of the DRL. Also, the DRL is considered to be an important ligament for stabilising the TMC (Tan *et al.* 2011). The DRL is reinforced by the abductor pollicis longus tendon and is the strongest ligament amongst the TMC ligaments (Connell *et al.* 2004); however, the anatomical position of this ligament may play a very important role in its place as the main stabiliser of the TMC ligament (Figure 1.7).

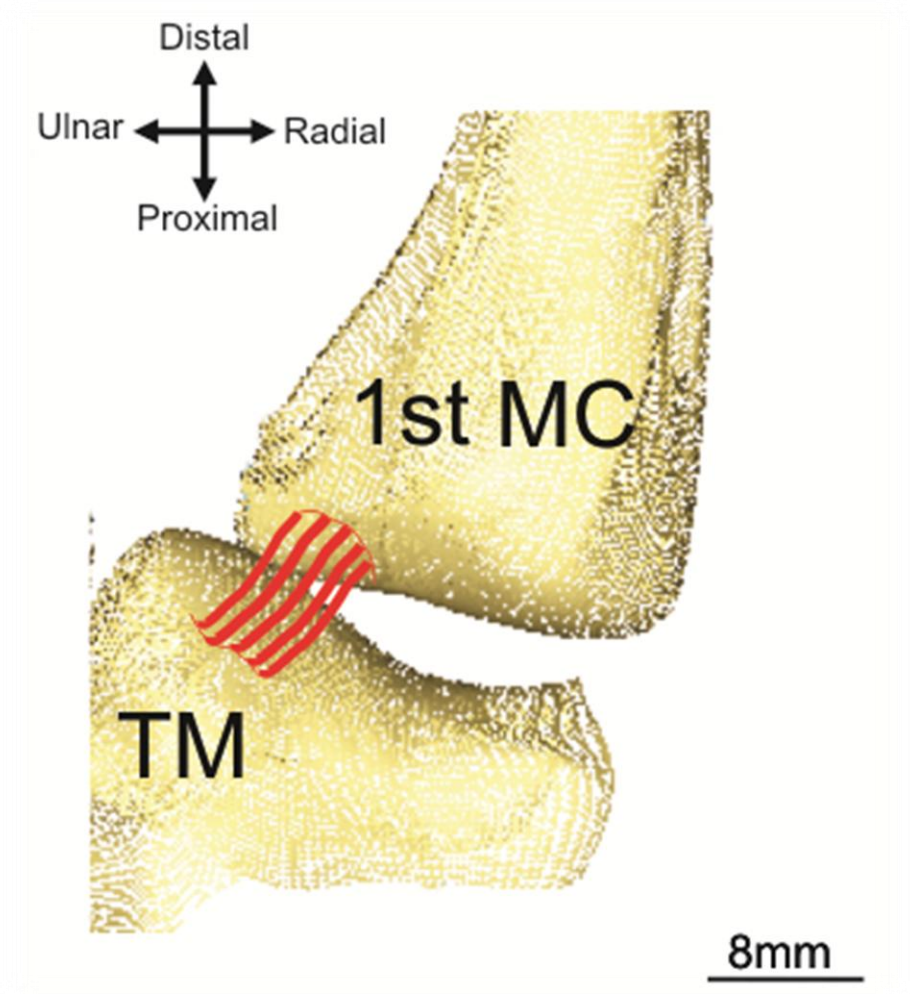

Figure 1.7: Anterior view of the trapeziometacarpal joint and its dorso-radial ligament, from Connell (2004). The red lines illustrate the dorso-radial ligament.

1.1.2.4 Dorsal complex ligaments

The dorsal complex ligaments consist of two ligaments: the POL and the DRL, which work together as one ligament to prevent TMC joint dislocation (Cardoso *et al.* 2009). The author considers the dorsal complex ligaments to be at least as important as the AOL in preventing dorsal subluxation.

Also, the dorsal complex ligaments have been discovered to be amongst the main ligaments that prevent dorsal subluxation and dislocation of the TMC (Strauch *et al.* 1994; Van Brenk *et al.* 1998). Moreover, the concept that the dorsal complex ligaments are more important than any other ligaments for stabilisation is supported by Koff (2003) (Figure 1.8).

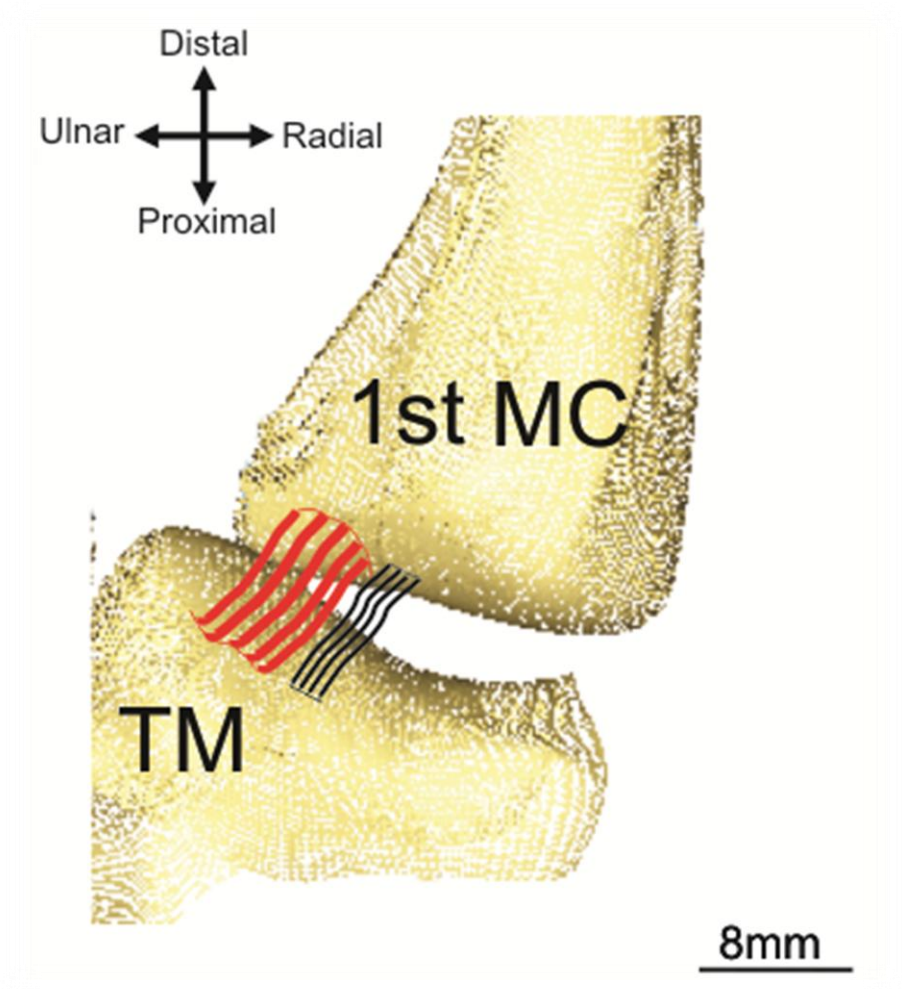

Figure 1.8: Anterior view of the trapeziometacarpal ligament and its dorsal complex ligaments, from Cardoso (2009).
Both red and black lines illustrate the dorsal complex ligaments, red lines for dorso-radial ligament and black lines for posterior oblique ligament.

The beginning of the account the TMC ligaments were back to the mid 18th century, the stabilization also have determined as a primary and secondary stabliziers. The following table will illustrate the historical review of TMC ligament stabilization:

Year	Study	Ligament study	Importance of ligaments
1944	(Haines 1944)	AOL,POL, anterior IML, posterior IML, radial ligament	AOL, POL, Posterior IML, and radial ligament are strong. Anterior IML is weak
1955	(Napier 1955)	AOL, POL, lateral ligament	No discussion regarding the importance
1969	(Eaton and Littler 1969)	Dorsal and palmar ligaments	Dorsal ligament is stabilizer
1973	(Pieron 1973)	AOL, DRL, POL, IML,UCL	AOL and DRL are strong
1976	(Harvey and Bye 1976)	POL, dorsal IML, radial ligament	Dorsal IML is stabilizer
1976	(Bojsen-Moller 1976b)	AOL, POL, DRL, IML	IML able to limit thumb motion
1981	(Pagalidis *et al.* 1981)	AOL, POL, DRL, IML, palmar ligament	IML is limiting dorsal displacement

1991	(Pellegrini 1991)	AOL	AOL has central role in causing TMC osteoarthritis
1993	(Pellegrini Jr *et al.* 1993)	AOL	AOL is vital static structure
1993	(Imaeda *et al.* 1993)	AOL, DRL, POL, IML, UCL	AOL is primary stabilizer, UCL and IML are important, DRL has no role in stability.
1994	(Imaeda *et al.* 1994)	AOL, IML, UCL	AOL and UCL are more important than IML
1994	(Strauch *et al.* 1994)	AOL, DRL, POL, IML	DRL is the restraint to dorsal dislocation
1997	(Imaeda *et al.* 1997)	AOL, DRL, POL, IML, UCL	AOL and IML are stabilizing TMC joint
1997	(Najima *et al.* 1997)	AOL, DRL, POL, IML, UCL	DRL is primary restraint to dorso-radial subluxation
1998	(Van Brenk *et al.* 1998)	AOL, DRL, IML	DRL is a stabilizer
1999	(Doerschuk *et al.* 1999)	Beak ligament	Beak ligament degenerate with osteoarthritis of TMC joint

1999	(Bettinger *et al.* 1999)	sAOL, dAOL, DRL, POL, IML, UCL	DRL is a primary stabilizer
2000	(Bettinger *et al.* 2000)	AOL, DRL	DRL is strongest and stiffest ligament
2006	(Lubahn *et al.* 2006)	Palmar oblique	Relaxin binds to the Palmar oblique ligament
2007	(Colman *et al.* 2007)	dAOL,DRL	DRL more important than dAOL
2011	(Tan *et al.* 2011)	dAOL, DRL, POL, IML, dorsal IML	DRL is maintaining joint stability
2012	(Hagert *et al.* 2012)	AOL, DRL, POL, UCL	DRL has density of innervations
2012	(Ladd *et al.* 2012)	AOL, DRL, POL, UCL, IML	Dorsal deltoid ligament complex are important
2013	(Ladd *et al.* 2013)	AOL, dorsal deltoid ligaments	Dorsal deltoid ligaments are strong stabilizer
2013	(Lin *et al.* 2013)	DRL	DRL play role for stabilizing TMC joint
2014	(D'Agostino *et al.* 2014)	AOL, DRL	AOL is preventing the dorso-radial subluxation, DRL

			stiffest and thickest ligament of TMC joint
2014	(Maes-Clavier *et al.* 2014)	DRL, POL, IML, UCL, AOL	Procedure of stabilization should be required to strengthen the dorsal ligamentary complex.

Table 1.1: Illustrate the historical review of the TMC ligament stabilization since 1944 – 2014.

It is clear that there was a large controversy regarding TMC ligament stabilization throughout many literature reviews. This thesis will work to address these variations by using kinematic procedures in 2D reconstruction and 3D modelling of the TMC ligament; in particular, to observe the stretching and relaxing of each TMC ligament in two positions (neutral and full abduction positions).

1.1.4 Ligament nomenclature

Part of the controversy surrounding the anatomy and function of these ligaments arises from the differing terminology that has been used by various authors (Bojsen-Moller 1976a; Kaplan 1965; Pieron 1973). AOL, POL, and IML are practically constant and known everywhere in the same way. Other ligaments are habitually described with variable names; the DRL is sometimes called the *radial ligament*, *lateral ligament*, or *light oblique ligament* (Pellegrini Jr *et al.* 1993). In addition, the UCL is sometimes named the *ulnar ligament*, the *volar ligament*, or the *ligament of Kaplan*, while the dAOL is also called the *beak ligament* or the *palmar beak ligament* (Imaeda *et al.* 1994). In addition, (Bettinger *et al.* 2000) used the word *volar* instead of *palmar*, and described the directions of the movement by the words *radially*, *ulnarly*, or *dorsoradially* instead of *medially*, *laterally*, and *posteriolaterally*. Further investigations on the TMC ligaments and bones would

create a new name for each ligament based on scientific procedures and reliable results.

The ligaments of the TMC joint require further investigation for clarity and consistency, especially in naming them. This thesis will use special 3D software to address this matter. This software will render each ligament into a 2D reconstruction (shape) in a 3D virtual environment in order to observe each ligament in three planes: coronal, sagittal, and transverse. The position of each TMC ligament will be shown clearly in these planes, and will make allow determination of their names and positions.

1.2 Ligament kinematics

The study of the workspace and range of motion between specific joints (trapezium and first metacarpal) has recently been directed towards gaining a more detailed understanding of the individual movements of carpal bones, such as the scaphoid, trapezium, and first metacarpal (Najima *et al.* 1997). Studies have used a variety of methods to calculate the range of motion of the TMC, such as:

- **1.2.1 Electromagnetic tracking devices**

Goubier et al (2009) compared the normal range of motion of the TMC to a range of motion database that was constituted from normal active TMC.The result was 41° for flexion-extension, 51° for abduction-adduction, and 21° for axial rotation and circumduction. Comparisons between females and males showed significant difference concerning flexion-extension, abduction-adduction, axial rotation, and circumduction. No significant differences were noted between right and left hands, except for abduction-adduction movement.

Also, Goubier et al (2011) studied patients after they had undergone trapezectomy and found the range of motion of the TMC to be 50° for flexion-extension, 47° for abduction-adduction, and 11° for axial rotation; they found no significant differences in flexion-extension, abduction-adduction, and axial rotation comparisons between patients and healthy subjects except that circumduction was reduced. In addition, no significant differences were noted between the operated side and the contralateral side.

In addition, Kuo et al (2004) used a quantitative method to measure maximal workspace of the TMC; they used an electromagnetic tracking device with the concept of 3D imagery and impairment of the TMC. The result demonstrated the accuracy of 3D imagery in TMC motion, with high statistical reliability and low variability of the maximal TMC workspace. Factors such as gender, age, dominance, and occupation have not been analysed as possible influences on the measurement of maximal TMC.

Kuo (2003) used surface markers for assessing the motion of the TMC; the researcher used an electromagnetic device to provide quantitative measurement and evaluation of the relationship between the skin and bony segment while moving the TMC in flexion-extension, abduction-adduction, and circumduction. The results also showed that using a spherical model to calculate the maximal workspace as an index for assessing TMC impairment is practical, although the skin motion creates artefacts in the thumb, especially in the area of the TMC. Therefore the question is to what extent analysis of the surface markers placed on the segments accurately represents the actual movements of the corresponding underlying bones.

Meanwhile, Kuo et al (2009a) studied the effects of age and gender on the range of motion of the TMC. They recorded the TMC motions using an electromagnetic tracking system through flexion-extension, adduction-abduction, and circumduction movements. They found that there is no significant effect between males and females when not regarding age as a factor, whereas there were significant differences between males and females when age was included as a factor.

The high percentage of decreased range of motion can affect older people more so than younger people. Younger females have been recorded to have a higher range of motion than younger males, while the range of motion is decreased in older females. The results could be not being accurately measured for complex movement, however, such as circumduction and the opposition of the TMC according to the effect of age and gender in the dominant hand, without any comparison with the non-dominant hand. Although, Zhang et al (2005) reported that gender does not significantly influence the movement ranges of thumb joints, only young adults were considered in their study.

In addition, the functional workspace of the thumb-finger grasp is considered to be the range of all possible positions in which the thumb-tip and each fingertip can simultaneously contact each other, Kuo et al (2009) used a video-capture system for calculating thumb-tip and fingertip motions via numerical methods based on maximal workspaces obtained. Therefore, the maximum workspace was between thumb tip and tip of the middle finger whereas, the minimum workspace was between tip of the thumb and tip of the index finger. However, the mechanisim for measuring the range of motion need more accurate process to find the precise results.

- **1.2.2 Fluoroscopy**

Kuo et al (2002) conducted an investigation using fluoroscopy on the surface markers to represent a thumb kinematic; they concluded that the application of a video-based motion analysis system with surface markers to thumb kinematics is warranted. The fluoroscopy images, however, were 2D representations; it is difficult to analyse these differences in 3D movements since axial rotation and circumduction of the TMC is not measured by a 2D fluoroscopic analysis.

A comparative *in vivo* kinematic analysis of normal and osteoarthritic TMC conducted by Miura et al (2004a) used a fluoroscope to determine the difference between normal and arthritic joints. They calculated the centre of rotation during abduction-adduction and flexion-extension by using the longitudinal line in the modular canal of the thumb metacarpal on the postero-anterior view, and the perpendicular bisector of the metacarpal facet of the TMC joint on the lateral view. In addition, they quantified the radial and dorsal translations of the centre of rotation as the distances from the centre of rotation to the perpendicular bisector of the trapezial facet of the TMC on the postero-anterior view and on the lateral view. They measured the volar tilt (which is the complementary angle between the two lines), the tangential line to the dorsal cortex of the thumb metacarpal, and the line connecting the two edges of the metacarpal facet of the TMC. However, the methods for measuring the articular surface were reseanable based on the irregular surface of shape.

- **1.2.3 MRI analysis.**

MRI analysis allows static study in different positions (Momose et al. 1999). Momose et al (1999) studies the postures of the thumb particullary at full

abduction position, used the MRI for analysis the thumb static range degree in full abduction position. Therefore, the full abduction postion degree was between 60° to 65°. However, the MRI analysis need to more procedures comparing with other devices to reveal the accurate measurements.

In addition, Punsola –lzard et al (2012) studied the TMC joint motions through the effects of the TMC joint with OA, especially in stability and hypermobility. The aim of their study was to detect the alignment of the metacarpal phalangeal (MCP) joint while the thumb is in lateral pinch in healthy volunteers. The results identified four different thumb postures during lateral pinch. Moreover, the centre of rotation in flexion-extension translated dorsally in the patient group compared to the healthy group, whereas the centre of rotation in abduction-adduction did not differ significantly between the patients and healthy groups. The average palmar tilt in the patients with osteoarthritis increased significantly compared with the healthy group. The excessive palmar tilt increases the dorsal vector of load at the metacarpal facet of the TMC, however, which attenuates the ligament strength with age and results in the dorsal translation of the centre of rotation in flexion-extension.

- **1.2.4 Goniometers**

The goniometer is a tool for measuring the degree of joint motion, which consists of movable arms, fixed arms, and pivot at middle with scale of degree. The special goniometer for thumb, it’s called thumb goniometer (Figure 1.9).

Conney et al (1981) used the thumb goniometer to measure the thumb tip to the distal palmar crease of the palm. The results were showed the flexion 45°, extension 80°, adduction 15°, and abduction 59°. However, still there was a little bit percentage of hand error, which would illustrate by variation with other studies results.

In addition, Ebskov and Boe (1966) also used thumb goniometer for comparsing the normal thumb range of motion and capture motion path of the thumb. Therefore, their study found that the thumb goniometer allows free movement within the normal range of motion and captures the motion path of the metacarpal bone and phalanx movement.

Cole and Abbs (1986) used electrogoniometers and a light-emitting diode to record angular and spatial positions of the joints of the index finger and thumb. Their study illustrated the relation between the positioning of the thumb and finger path endpoints at the point of contact. Although their study provided clear kinematics for the thumb and index finger during pinch activity, the results may indicate that prehensility occurs mainly on the thumb.

Kuo et al (2004) used a goniometer to measure most of the joint motion, including the thumb metacarpal (MP) and interphalangial (IP) joints. The result showed TMC joint flexion 45° with IP extended 170° whereas TMC joint flexion 55° with IP flexed 45°. However, it is impossible to measure TMC motion in any plane as a consequence of its location at the base of the hand.

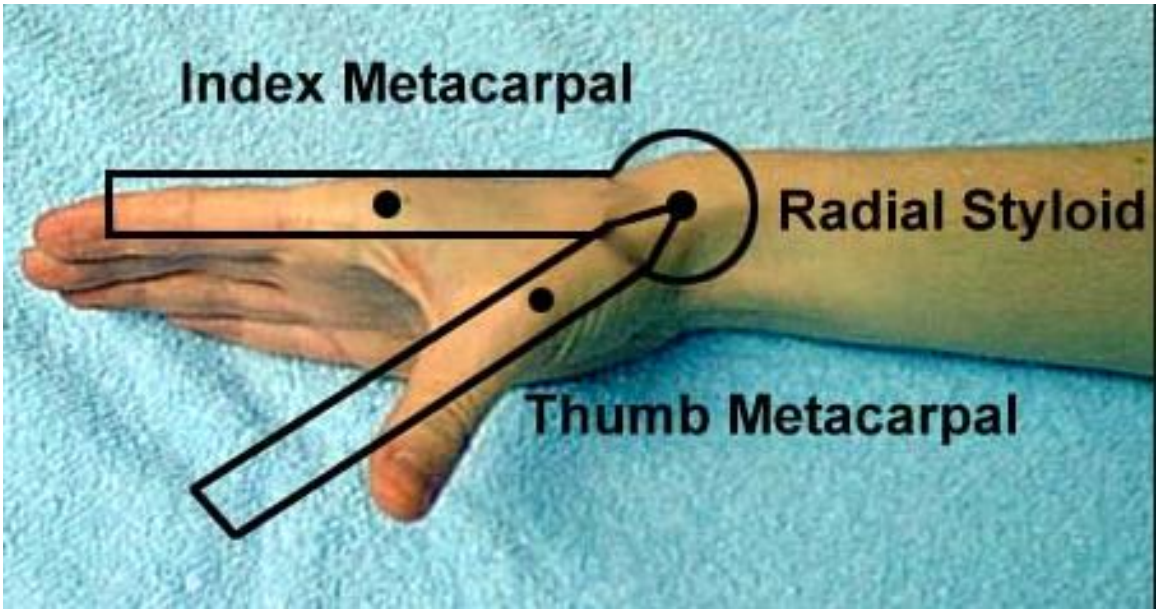

Figure 1.9: Thumb Goniometer, from www.scranton.edu

- **1.2.5 X-ray analysis**

The study of static postures or dynamic motion of the thumb by X-ray not common and rare use in experiment particulary at healthy volunteers, but its useful for cadaverics studies (Punsola-Izard *et al.* 2012). The X-ray analysis may be considered dangerous for the patient because of radiation exposure, as well as being limited to static studies (Ebskov and Boe 1966).

- **1.2.6 CT scan**

Buffi et al (2013) used a CT scan image to quantify the kinematics of the TMC joint through 3D methods; their study used 3D software to render and measure the axis between the fourth and fifth metacarpal bones. The results showed the equivalent angle that rotated the fourth metacarpal through the range of motion quantified from the CT data was approximately three times smaller than the equivalent angle for the fifth metacarpal. Such 3D procedures have the ability to give accurate measuring results for quantitative study.

- **1.2.7 Kapandji score measures**

Kapandji score measures in which the thumb opposition is measured as the maximal distance between the thumb tip and the fingertip and linear measurement (Kapandji 1989) (Figure 1.10) and (Table1.1). The opposition measured by score according the position of the tip of the thumb achieve as follows:

Score	Location achieved
1	Radial side of the proximal phalanx of the index finger.
2	Radial side of the middle phalanx of the index finger.
3	Tip of the index finger.
4	Tip of the middle finger.
5	Tip of the ring finger.
6	Tip of the little finger.
7	Distal interphalangeal joint crease of the little finger.

8	Proximal interphalangeal joint crease of the little finger.
9	Metacarpophalangeal joint crease of the little finger.
10	Distal palmar crease

Table 1.2: Score distribution of the Kapandiji score measures, from Kapandiji (1989).

However, a Kapandji score measures the entire thumb motion and gives no accurate data on range of motion of the TMC. In addition, the linear method is not fully reliable except for thumb abduction (Miura *et al.* 2004a).

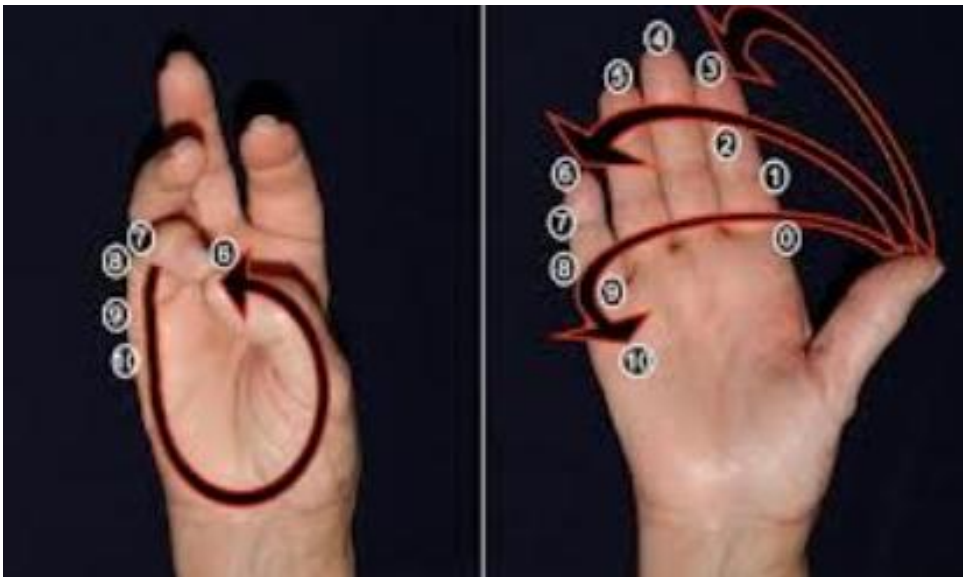

Figure 1.10: Kapandji score measurement, from Kapandji (1989). Is a tool useful for assessing the opposition of the thumb, based on where on their hand the patient is able to touch with tip of their thumb.

Many methods were used to measure TMC joint movement and to analyze motions such as flexion, extension, and opposition. Also, different devices were utilized to obtain precise results. This thesis will use the most modern and unique methods for measurement and analysis of thumb motions. The 3D Rhinoceros software will solve this issue because it has numerous ways to deal for the shape of the thumb and its motions.

- **1.2.8 Directions and Axes**

Ebskove and Boe (1966) defined two main axes for the primary movements of the TMC, as if the movements between the trapezium and the first metacarpal take place on a saddle joint. The axes run from lateral to medial and from anterior to posterior, at an angle approximately 45° to the frontal plane of the hand. In addition, Pearlman et al (2004) mentioned a third main axis perpendicular to the two previously described axes (Figure 1.11).

They stated that this is because the TMC is functionally comparable to a ball-socket joint; this third axis represents the active and passive rotation about the longitudinal axis of the first metacarpal. The performance of an axial rotation as obligate motion has been questioned, however. For instance, Steven (2009) used sections of the TMC held in the middle position, revealed markedly different shapes of the contact between the surfaces in subsequent planes. In lateral-medial sections, a striking correspondence of the curvature can be observed, whereas in the anterior- posterior sections, the curvatures differ in shape and in conformity.

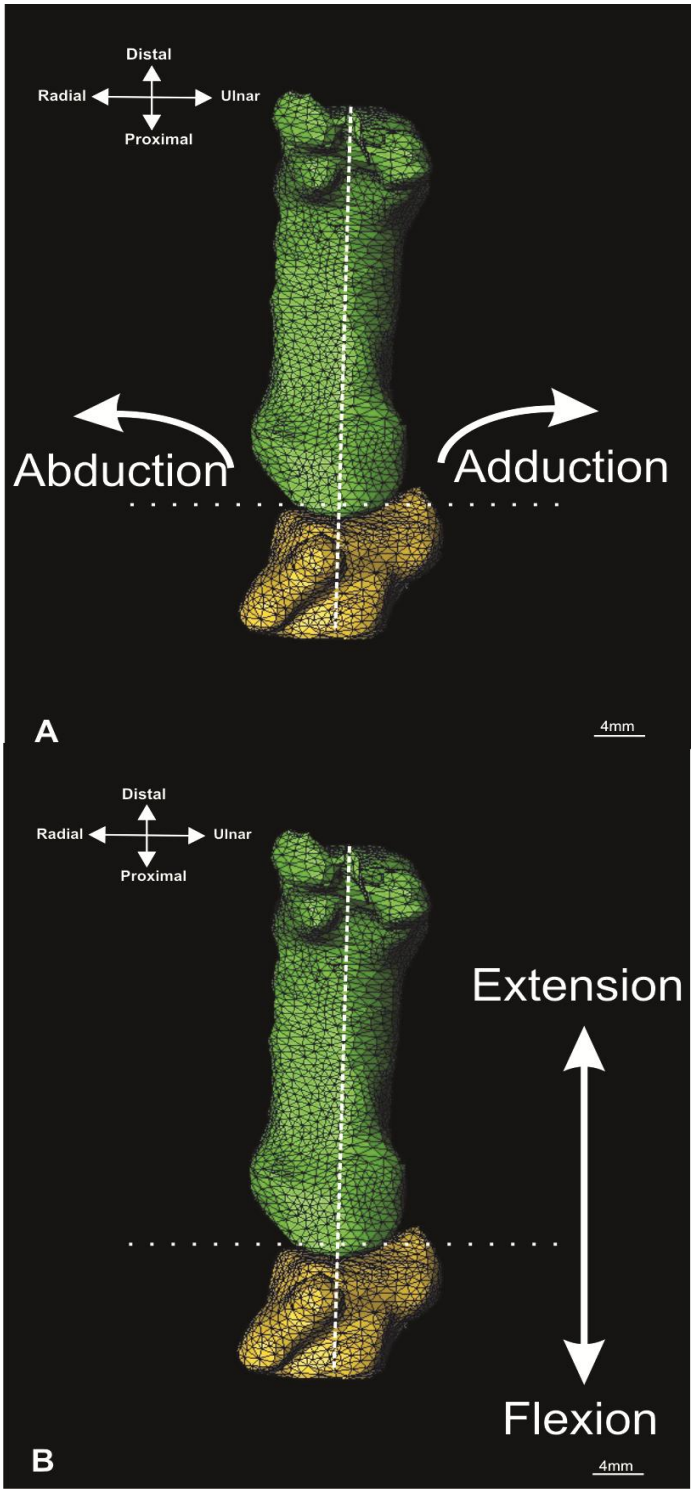

Figure1.11: Anterior view of the trapeziometacarpal joint, from Ebskove and Boe (1966). A. Illustrate the sagittal plane of TMC joint which is producing two motions adduction and abduction. B. Illustrate the coronal plane which is producing two motions flexion and extension.

Zancolli et al (1987) described that the biomechanics of the TMC depend on a few factors that affect the direction of the movements: muscle action, the shape of the joint during the motion, and ligament stability. In addition, they divided the motions into two main movements: 1) simple angular movement (non-rotational), which is represented by flexion, extension, adduction, and abduction, and which

occurs in the saddle-shaped part of the facet of the trapezium; (Figure 1.12) and 2) simultaneous angular movement (rotational), which is represented by circumduction with supination (retroposition) and circumduction with pronation (opposition); this occurs in the spherical part of the facet of the trapezium (Figure 1.12).

The head of the first metacarpal during circumduction of the thumb follows an oval course that has two parts: a radial (outer) curve, and an ulnar (inner) curve. These two curves are represented by two similar curves of joint contact during the displacement of the first metacarpal to the trapezium through circumduction. During the motion along the radial curve, the areas of contact in the TMC are mainly situated on the radial part of the trapezium surface, while motion along the ulnar curve shows areas of contact of more ulnar parts of the trapezium surface (Zhang *et al.* 2005). In addition, the movement of the circumduction is accompanied by an axial rotation of the first metacarpal to the trapezium in a clockwise or anti-clockwise direction, depending on the curve along which the first metacarpal moves (Pieron 1973).

Haines (1944) studied the mechanism of the rotation of the TMC joint through describing the ligaments associated with TMC bone; the study suggested that their function was mainly a guiding one, which was responsible for the axial rotation of the first metacarpal bone, specifically at the end movements of flexion and extension at TMC joint. The TMC ligaments, however, have regulating action on the bone concerned.

In addition, Napier (1955) studied the function of the TMC joint and its motion, concluding that when the TMC joint is in the mid-position, the articular surfaces are markedly incongruent and the ligaments are relaxed, the motion changes from mid-position to the full abduction or adduction positions.

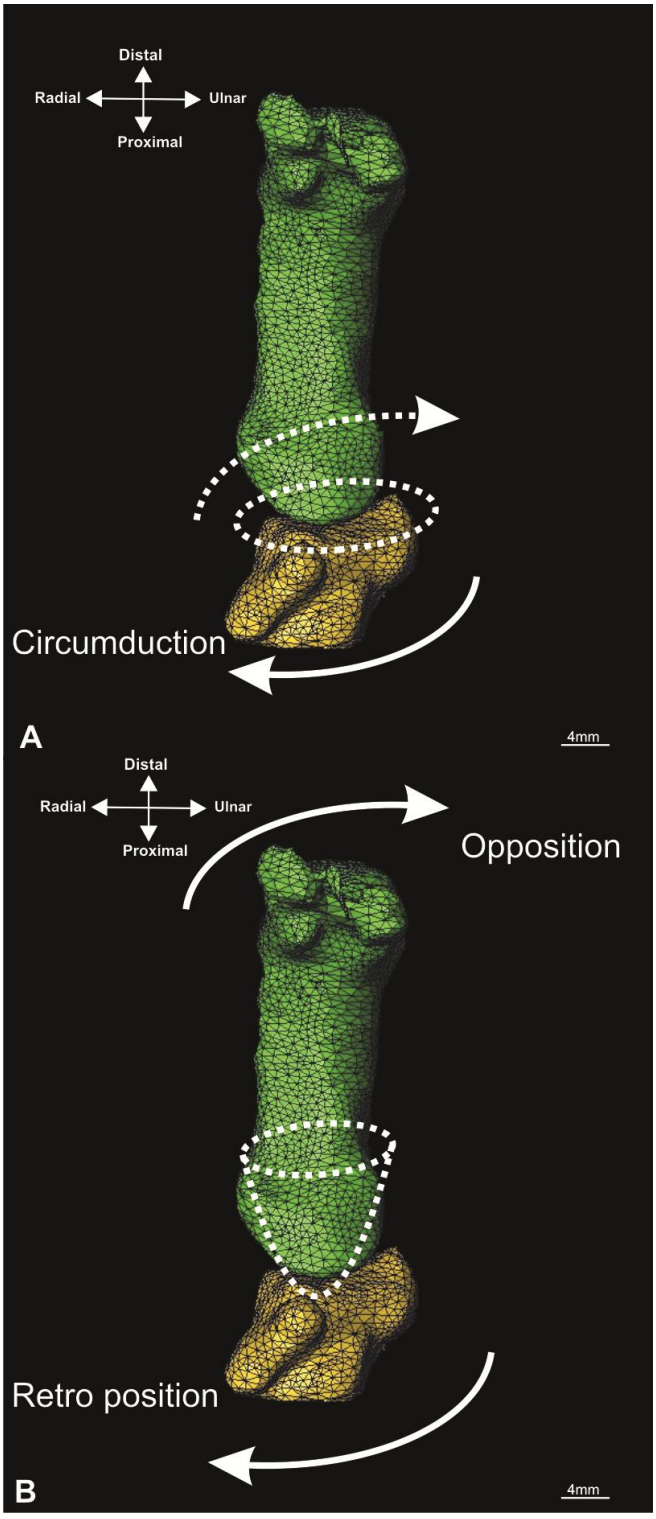

Figure1.12: Anterior view of the trapeziometacarpal joint, from Zancolli et al (1987). A and B illustrate simultaneous angular movement which is producing circumduction, opposition and retroposition motions.

Moreover, Lin et al (2010) conducted a kinematic study of the TMC joint related to the activities of daily living. The concept of this study was centred on the type of motions that occur in the thumb as a whole. The results showed that the metacarpophalangeal joint is active mainly in abduction and the cylinder grip; the

spherical grip has the largest angle. The TMC joint, the cylinder grip, and the spherical grip showed a relatively larger rotational range of motion, while the interphalangeal joint in the three thumb joints was primary active in flexion.

The directions of the thumb are complex and vast, and the decision to choose one or two movements is key to ensure the accuracy of the experiment. This thesis will use the most critical movements as a key. The neutral position is very important as a starting position and at same time illustrates the anatomical position of the thumb. Also, the full abduction position is ideal as the final target of the kinematic study, because it shows the critical degree when the thumb is positioned at full abduction. Most injuries have occurred as Bennet, Pseudo Bennet, and Rolandos fractures. The subluxations (dorsal-lateral) are mostly occurring after excessive full abduction of the thumb. Therefore, it is reasonable to use full abduction as the final key, and neutral position as the starting key. The static and dynamic procedures will illustrate this throughout these movements of the thumb.

- **1.2.9 Laxity, unstability and strength of TMC joint**

Many studies have concentrated on the relationship between thumb laxity and trapezium kinematics (Cheze *et al.* 2009; Crisco *et al.* 2005; Zancolli *et al.* 1987). The joint capsule in general is lax; every position of the thumb shows that one or more ligaments are tight. Only when a ligament is tight will it guide the motion of the metacarpal in a certain direction (Pearlman *et al.* 2004). According to this principle, the ligaments are the guiding elements that produce axial rotation during opposition of the thumb.

Cheze et al (2009) stated the the trapezium would be inherently unstable due to its anatomic location at the radial aspect of the wrist, with no bony radial stabilisers, without strong supporting ligaments. The lack of fixed axial base of support (the scaphoid mobile) contributes further to potential instability. One would predict that there should be a large number of ligaments attaching to the trapezium to provide stability to withstand the axial loads placed on it by the thumb.

Garcia-Elisas and Orsolini (2011) conducted an investigation to determine whether there is a relationship between thumb laxity, distal trapezial inclination, and trapezial motion during lateral- medial deviation. The result of their study

showed that the amount of trapezium bending is proportional to the degree of thumb laxity. Further, individuals with laxer thumbs do not necessarily have a trapezium with a more inclined distal articular surface, but the bone moves more relative to the second metacarpal during radio-ulnar deviations.

In addition, Nallakaruppan et al (2012) tested the abduction strength of the thumb through blocking full abduction in the normal population by using a vertical board, measuring the strength of the thumb with the dominant hand and non-dominant hand, and comparing between males and females in two positions: first, with a vertical board, and second without a vertical board. The study isolated the action of the abductor pollicis longus and the palmaris longus to keep the thumb in the palmar abduction position, as well as to measure the functions of the thenar muscles. The result was that males had greater abduction strength of the thumb than females, but there were no differences in abduction strength of the thumb between the dominant and non-dominant hands for both male and female when a vertical board was used. Without the board, the values were significantly greater in the dominant hand. The study had several limitations, however. First, using maximum effort may not be significant when healthy subjects are evaluated, but can become challenging when patients are evaluated. Second, it is difficult to ensure that the subject is not recruiting other muscles. Third, it is difficult to keep the direction, amount, and rate of force being applied constant.

Kapandji and Heim (2002) found evidence that the more inclined the joint, the higher the tendency for the TMC ligaments to attenuate in cases where anterolateral subluxation of the metacarpal base and secondary degenerative osteoarthritis of the TMC is induced. Indeed, if the joint is substantially inclined and the constraining ligaments are insufficient or stretched, significant subluxation of the metacarpal base occurs (Pellegrini 2001). Whether the increased subluxation tendency due to congenital passive hypermobility evokes higher risk of developing joint degeneration is controversial, however.

Although epidemiological data suggest that patients with increased passive mobility of the thumb have a higher incidence of degenerative TMC osteoarthritis (Jonsson *et al.* 1996). More recent epidemiological studies suggest the opposite. Hypermobility may instead be a protective factor for hand osteoarthritis (Kraus *et al.* 2004).

A powerful shearing and dorsal subluxing force compresses the TMC. A powerful grasp can generate up to a 120 N force in the TMC, which is force for a 70 Kg human (Cooney and Chao 1977). The compressive forces at the TMC can be 12 times the force in a lateral pinch at the tips of the thumb and index finger, and the shear stresses are 2.5 times the applied force. The dorsal ligament complex is the key ligament in stabilising these powerful dorsal subluxing forces in the power pinch and power grip (Smith *et al.* 1964).

Edmunds (2011) demonstrated the ligamentous stability and the resting position of TMC through screw-home torque rotation (the power of pinch and power of grip). In the resting position, the TMC is lax and subluxable, and the concavity and convexity of the trapezium and relatively large TMC joint space is reduced. The AOL disengages from its contact recess in the palmar aspect of the trapezial surface, and the dorsal ligament complex is lax. The screw-home torque rotation changes a lax, incongruous TMC to a rigidly stable, congruous joint for power grip and power grasp. The posterior ligament complex is made tense to drive the AOL into its recess in the trapezium for rigid stability. In addition, during the power pinch and grip, the abductor pollicis brevis, opponens pollicis, adductor pollicis, and flexor pollicis longus muscles drive the AOL into the recess of trapezium in the last phase of opposition for rigidity of the thumb. The reason for stabilising the TMC during change from the resting position to opposition movement, however, is to prevent subluxation of the TMC, with the dorsal ligament complex and the muscles guiding the motions.

Previous experiments explained the flexibility and strength of the TMC joint during the different types of forces (external-internal), these issues are considered throughout this thesis as an important factor of the joint stabilization.

1.3 Two-dimensional and three-dimensional investigation

Many studies have investigated the shape and architecture of muscles (Agur *et al.* 2003; Momersteeg *et al.* 1995; Song *et al.* 2004; Stark *et al.* 2012), yet regarding ligaments, the reviewed literature included no studies that state accurate data about the fascicles and the style of elongation and relaxation of ligaments, with the changed shape undergoing external force in specific positions.

Also, there are many references related to large ligaments, such as the anterior cruciate ligament (ACL) (Agur *et al.* 2003; Henning *et al.* 1985; Hirokawa and Tsuruno 1997; Hirokawa and Tsuruno 2000; Momersteeg *et al.* 1995; Pioletti *et al.* 1995; Song *et al.* 2004). However, there are a limited number of studies that have investigated small ligaments such as the TMC ligaments. Therefore, this study will investigate the TMC ligament, and will record the changes that could occur within each of the TMC ligaments and also observe the displacement that can occur during the various positions of the thumb.

Tan et al (2011) rendere the TMC ligament into 3D shape, the 3D structures of the bones of the thumb during flexion, abduction and opposition were reconstructed, showing the paths of the fibres of the five principle ligaments, dAOL, DRL, POL, IML and DIML, at each of the TMC positions. The results showed that the greatest change in virtual lengths of the ligaments was in flexion, except for the dAOL, which decreased. Thumb flexion caused the greatest changes in the length of the DRL. The greatest change in the virtual length of the POL was in abduction, while the DRL, IML and DIML recorded only small changes. Further, opposition caused a change in length for the dAOL and DRL.

Nanno et al (2006a) performed 3D analysis of the ligamentous attachments of the TMC joint. This study demonstrated the shape of TMC ligament attachment throughout 3D virtual enviorment. Therefore, the footprint showed in two places; one on the second metacarpal bone and the other showed on the trapezium bone. The greatest size of foorprint was measured for trapezium bone, while the leatest was for second metacarpal bone. However, its logical results due to the most of TMC ligament attached between trapezium and first metacarpal bones.

Both 2D and 3D rendering are very important to the investigation of the TMC ligaments and bones. This thesis will use these methods for illustrating the ligament attachments and bone descriptions.

1.4 Ligament tension

Quantitative *in vivo* data on the biomechanics of thumb ligament structures and their strain behaviours are essential for understanding thumb ligament injuries, for success in repair and reconstruction procedures, for rehabilitation programs following surgery and for the design of prosthetic ligaments. In order to study the detailed mechanics of the ligaments, especially of the trapeziometacarpal ligaments (TMC), strain measurements have been performed by means of strain gauges (Henning *et al.* 1985) and other types of displacement transducers (Hirokawa and Tsuruno 1997).

In addition, discrepancies among previous experiments on ligament strain are due to three factors. First, the apparatus which impinges on the ligament may change its geometry and cause measurement errors. Secondly, depending on the region being tested, highly variable deformations cannot be adequately quantified by localized measurements because specific bands of the ligament, and specific portions within the ligament, are considerably altered during thumb movement. Thirdly, conventional measurements of the longitudinal strains in ligaments under tension have been essentially one-dimensional measurements of deformation (Hirokawa and Tsuruno 1997).

Hirokawa and Tsurnuo (2000) explained that the TMC ligaments are so highly anisotropic, which were not empty from insdie (fascicles). Also, mentioned the strains that applied on the TMC ligament were by the motions of the thumb into full abduction, the cylindrical strains were deformeties the TMC ligaments espically PIML and DIML. However, these non-longitudinal strains are also essential to formulate constitutive models of the ligament.

Studies measuring the material properties of the ligament are extensive. However, when the ligament is studied in isolation, the exact loading conditions and the ligament geometry *in situ* remain unknown. The data on ligament properties vary, depending upon which ligament geometry is being measured (Song *et al.* 2004). One study has shown that the ligament's structural properties vary considerably as a consequence of changes in the configuration of the ligament. The study also reports that there is no such thing, functionally speaking, as “ligament stiffness” (Momersteeg *et al.* 1995).

The tension and strain analysis is very important for describing the properties of the ligament, the biomechanics of the thumb structures, and strain behaviours that are essential for understanding the TMC ligaments tears. This thesis will establish the nature of the ligaments through kinematic experiments, and will explain that tension may occur on the TMC ligaments during movement of the thumb from neutral position to full abduction position.

1.5 Comparison between frozen and embalmed specimens.

Human cadaveric specimens are widely used in studies analyzing the biomechanical properties and efficacy of orthopaedic and trauma devices, Storage of fresh human cadaveric ligaments at a temperature of –20°C is a commonly used and accepted method for preservation of ligament (Park *et al.* 2011). Many studies have shown that freezing does not alter the biomechanical properties of human ligaments (MacBride 1998; Park *et al.* 2011; Sterling *et al.* 2000). The cadavers have usually been embalmed with a formalin solution for at least 1 year before usage. Some studies have investigated the effects of embalming cadaveric ligaments and bones regarding their biomechanical properties (Burkhart *et al.* 2010; Linde and Sorensen 1993; MacBride 1998; McElhaney *et al.* 1964).

The classical embalming methods are based on fluids containing a high concentration of formaldehyde or glutaraldehyde. These methods have proven to be very effective to stop the degeneration process, to be strongly disinfectant and to preserve the overall histological properties of human tissue (Thiel 2002). Yet there are important drawbacks to this classical embalming technique: most studies suggest that aldehydes alter the properties of collagen tissue (Wilke *et al.* 1996). The embalmed tissue becomes stiffer and more brittle with respect to fresh or fresh frozen tissue (Burkhart *et al.* 2010; Park *et al.* 2011; Wilke *et al.* 1996), due to intermolecular cross-linking of proteoglycan monomers (e.g. of collagen) (Wilke *et al.* 1996).

The changing of both soft and hard tissues can occur in frozen cadavers that are ready to be embalmed. This change can also affect the accuracy of the results. However, this thesis will examine both fresh and embalmed cadavers using the same experiments to see if there are any effects.

1.6 Histology

1.6.1 Entheses

The entheses of the trapeziometacarpal ligaments are complex and varied (Benjamin *et al.* 2006; Chung 2007; Claudepierre and Voisin 2005). *Enthesis* is a word derived from ancient Greek to designate the structures that attach ligaments, tendons, and joint capsules to bone. These structures are transition zones between two tissues with widely differing histological features (Claudepierre and Voisin 2005). The entheses can also cover a vast surface area: for instance, at the site of the trapeziometacarpal ligaments' attachment to the trapezium, first metacarpal and second metacarpal bones.

In addition, the term *Sharpey fibres*, which relate to descriptions of the entheses, have been described by Sharpey and Ellis; these fibres penetrate directly into the compact bone (Benjamin *et al.* 2002; Francois *et al.* 2001). The Sharpey fibres are only present in fibrous entheses (Benjamin *et al.* 2002) (Figure 1.13).

This study has investigated entheses—particularly their histology, pathology, and pathophysiology—throughout the body, and explains the considerable clinical and radiological polymorphism of entheseal diseases. The results of this study have shown that the spondylo-arthropathies provide the most striking examples of entheseal involvement in inflammatory joint disease (Claudepierre and Voisin 2005).

Other studies have investigated the entheses for clinical purposes, such as tennis elbow, golfer's elbow, and jumper's knee. Because stress concentration is such an issue in entheses, the need for stress dissipation governs the anatomical structure of attachment sites. The understanding of basic principles of enthesis structure and function, however, can underpin a consideration of enthesopathies (Chung 2007).

The entheses in relation to exercise and mechanical load have also been studied at sites of stress concentration at the region where tendons and ligaments attach to bone. Benjamin et al (2006) stated that biomechanical factors contribute

to the development of enthesopathies such as increase tenions on the ligament during loading.

This thesis will observe the entheses to explain the nature of the relationship between the TMC ligaments in each attachment (proximal-distal), as well as to explain that loading could occur on the TMC ligaments during movement.

1.6.2 Type of entheses

The classification of entheses has been studied throughout the tendons at the site of skeleton attachment (Benjamin *et al.* 2002). Many other studies have investigated the entheses zone and have classified the entheses into two main groups—fibrous and fibrocartilaginous—according to the tissue present at the skeleton attachment site (Benjamin *et al.* 2002; Benjamin *et al.* 2006; Chung 2007; Claudepierre and Voisin 2005; Freemont 2002; Slobodin *et al.* 2007).

The fibrous entheses, also called *direct entheses*, are sites of attachment to metaphyseal or diaphyseal bone. In the fibrous connective tissue linking the ligament to the bone or periosteum, the role of this type of tissue in diseases has been limited (Chung 2007) (Figure 1.13). The fibrocartilaginous entheses (also called indirect entheses) are found on the epiphyses of long bones or on small bones such as the carpal bones. In this type, the connective tissue occurs in four zones, as follows (Benjamin *et al.* 2002; Benjamin *et al.* 2006; Chung 2007): In the first zone, which is the ‘pure dense fibrous connective tissue‘at the end of the ligament, the lamellar tissue is composed of longitudinally aligned collagen bundles separated by looser connective tissue that merges with the peritenon and contains a variable number of elastic fibres (Figure 1.14);

In the second zone, which is uncalcified, unmineralised fibrocartilage, the cells take on the chondrocyte phenotype, becoming rounded and arranging themselves in pairs within the lacunae in the extracellular matrix;

The third zone is composed of ‘calcified‘mineralised fibrocartilage;

The fourth zone is ‘bone‘, composed of compact bone.

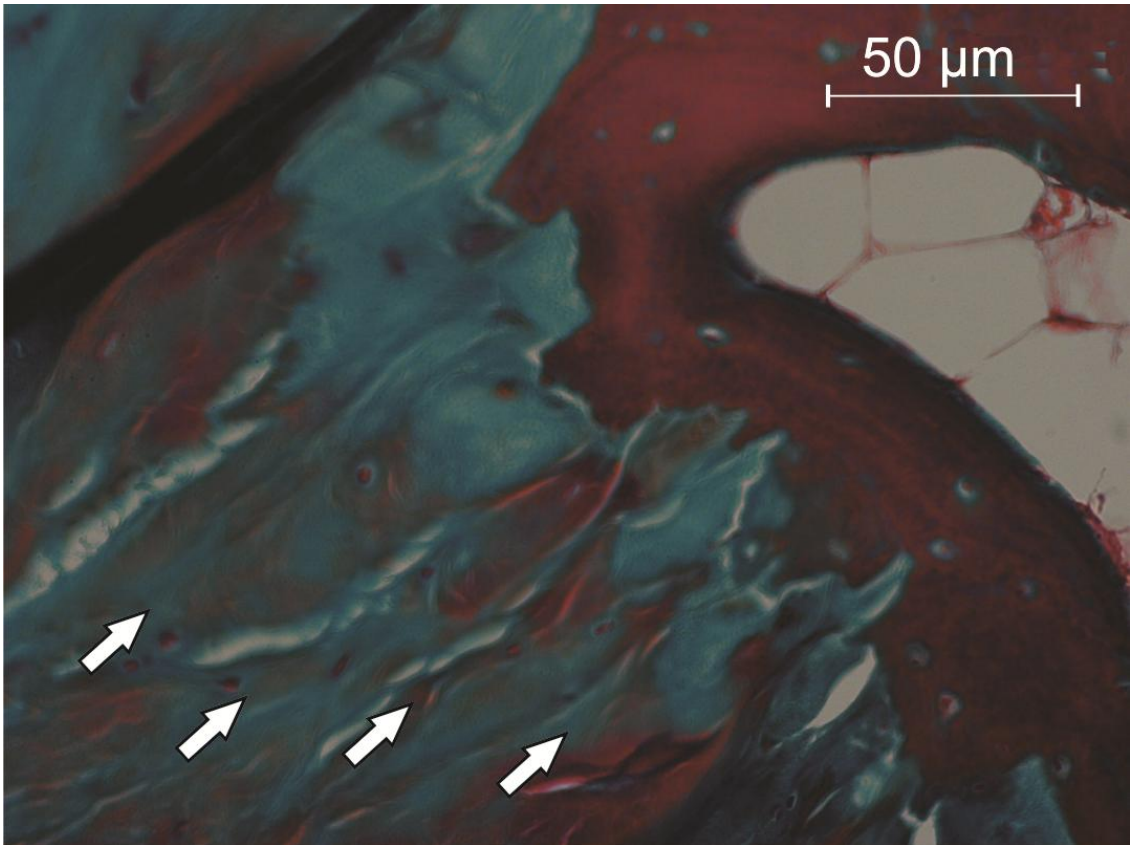

Figure 1.13: Histological sections of fibrous entheses from posterior oblique ligament of the TMC joint, with magnification × 10. Modified Masson's Trichrome.

Fibrous type of entheses which illustrate the sharpey fibers beside each other and penetrate directly into the compact bone without interruption. The white arrows present the tiny strings with green colour (sharpey fibers).

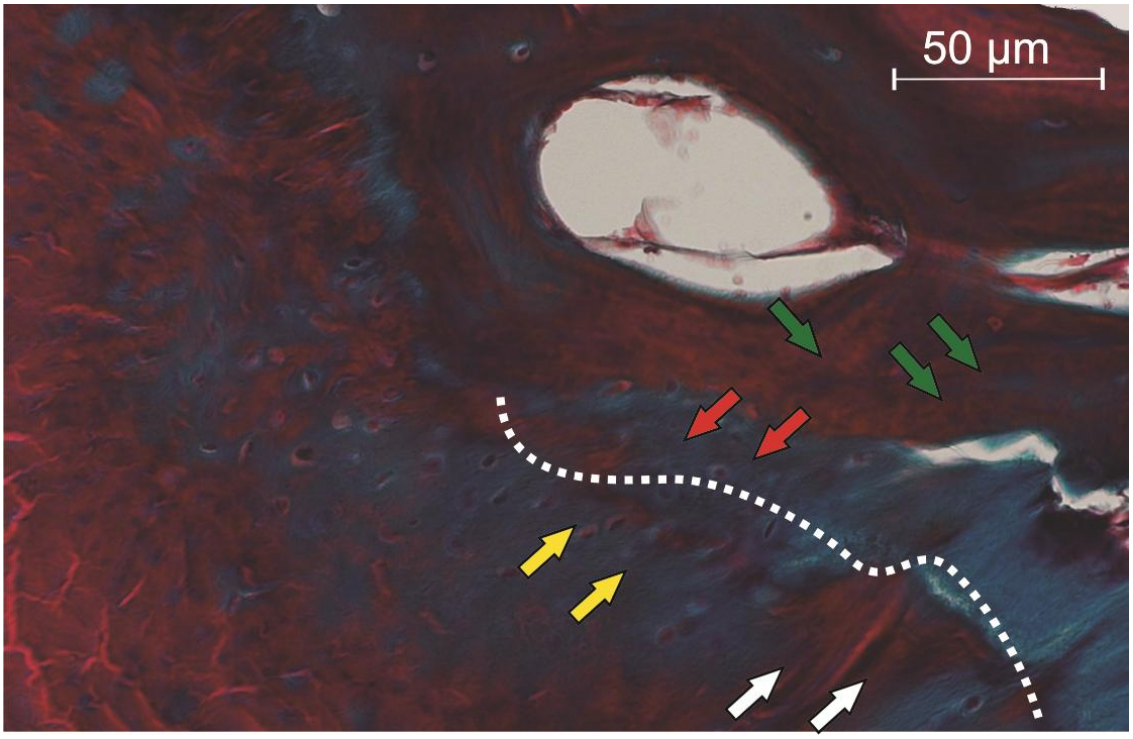

Figure 1.14: Histological sections of fibrocartilaginous entheses from posterior oblique ligament of the TMC joint, with magnification × 10. Modified Masson's Trichrome.

Fibrocartilaginous type of entheses which illustrate four zones; the white arrows presnt the pure dense fibrous connective tissue (dark green colour), the yellow arrows presnt the unmineralised fibrocartilage, the cells take on the chondrocyte phenotype, becoming rounded and arranging themselves in pairs within the lacunae in the extracellular matrix, the red arrows near to bone cell which presnt mineralised fibrocartilage zone, and the green arrows which is the bone zone.

The dotted white line presnt the tide mark line which separate between the second zone (unmineralised fibrocartilage) and third zone (mineralised fibrocartilage).

In addition, variations of the entheses have been noted in some parts of the attachment sites. For instance, some studies have shown that the fibrocartilaginous type is found not only at sites where the ligament, tendon, or capsules attach to bone, but also may be seen within tendons and bursae (Benjamin *et al.* 2002; Benjamin *et al.* 2006). The fibrocartilaginous type concentrates at the frication or pressure on the bone area, which provides a strong mechanical interaction function that protects both the bones and the tendon or ligament, which is also called the enthese-organ (Moriggl *et al.* 2003).

The fibrous entheses have been divided into two types: periosteal and bony. They are periosteal if the collagen fibres attach to the periosteum, which thus indirectly attaches the ligament to the bone, called periosteal fibrous entheses. In contrast, if the collagen fibres attach directly to the bone without any interruption, they are bony fibrous entheses (Ohtera *et al.* 2000; Patel and Buckland-Wright 1999).

1.6.3 The tidemark

The tidemark is the basophilic line separating the calcified and un-calcified fibrocartilagenous entheses; the tidemark also presents a mechanical boundary between soft and hard tissues (Patel and Buckland-Wright 1999). In addition, the tidemark may be duplicated; this has been interpreted in articular cartilage as a consequence of start-stop phases of calcification (Benjamin *et al.* 2002; Ohtera *et al.* 2000) (Figure 1.15).

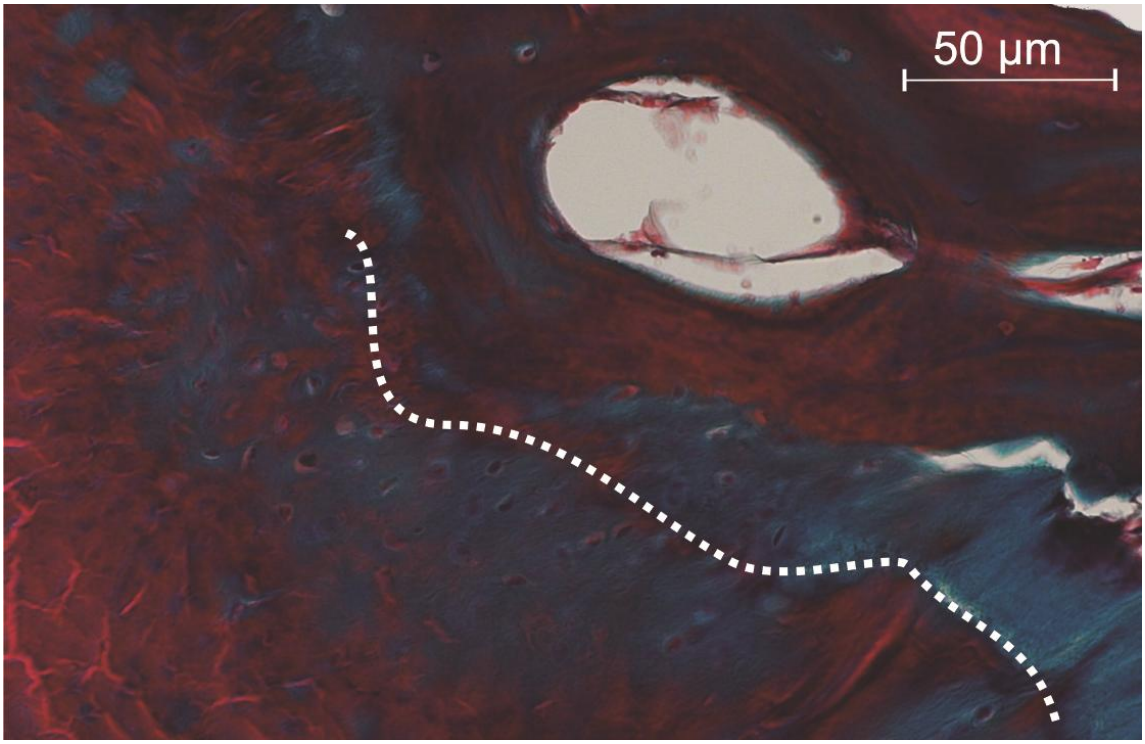

Figure 1.15: Histological sections of entheses from posterior oblique ligament of the TMC joint, with magnification × 10. Modified Masson's Trichrome.
The dotted white line presnt the tide mark line which separate between the second zone (unmineralised fibrocartilage) and third zone (mineralised fibrocartilage).

Benjamin et al (2002) studied the pattern of the tidemark; the study showed that the pattern was straight line between the uncalcified and calcified zones; in contrast, the tidemark between the calcified and subchondral bone was highly irregular.

The types of the entheses have importance and explain load conditions on the ligament and determine the healthy condition of the ligament. This thesis will consider these conditions during the experiments.

1.6.4 Staining

Modified Masson's Trichrome (MMT) and Miller Elastin (ME) staining have been used for illustrating collagen fibres and elastin fibres in tissues (Cobb *et al.* 1993; Fogg 2004; Freemont 2002), few studies have utilised a combination of both staining procedures when investigating such tissues.

A Modified Masson's Trichrome (MMD) is the best staining method to use for connective tissues such as muscle, ligament, tendon, and bone; histological researchers use this stain for distinguishing structures such as collagen fibre, bone, and articular cartilage in single tissue sections (Asonova and Migalkin 1996; Fogg 2004; Goldner 1938; Isa and Hoo 1980; Li *et al.* 2005).

Trichrome methods are widely used in pathology. The methods of the MMD were obtained by hematoxylins (Heidenhain's iron hematoxylin) with a reliable cytoplasmic stain that gives a wealth of detail (acid fuchsin with ponceau de xylidine), and a very selective stain for connective tissue (light green or aniline blue). This method requires mordanting with ammonio-ferric alum for 24 hours, followed by staining with Regaud's hematoxylin (the formula based on Heidenhain's) for a similar length of time (Goldner 1938).

Furthermore, these methods have been developed over many years to obtain the optimum clarity of the sections' structures; thus, the MMD has been used in un-decalcified tissues for staining decalcified bone sections. The methods are applied to staining of the calciphylaxis zones after their decalcification (Asonova and Migalkin 1996). The adapted Masson's method has different colours of stain, however, for mineralised bone (blue) and for osteoids (red).

In addition, many experiments have been conducted to combine MMD staining with other staining methods to see if any change occurs in the connective tissues or if any new colours appear that would increase the understanding of the connective tissue sections. A combination of Verhoeff's elastic and Masson's trichrome stain has been applied for routine histology (O'Connor and Valle 1982).

In addition, Movat's pentachrome staining has been adapted and modified as a stain for un-decalcified bone sections. After embedding in methyl methacrylate, this procedure yields consistently good results, with an excellent and colourful contrast between mineralised and unmineralised compartments of both cartilage and bone. In addition, osteoblasts, osteoclasts, and other cells and tissue components can easily be differentiated. The method is especially useful for the study of bone growth and bone repair, however, and as a stain for conventional histomorphometry and computer-assisted image analysis in bone biopsies (Olah *et al.* 1977).

Normally, the final results of the MMD staining have the same contrasts, which are black or blue colour for nuclei; red for the cytoplasm, muscle, and acidophil granules; and green for collagen fibres, cartilage, mucin, and basophil granules (Asonova and Migalkin 1996). But the effects of the embedding are related to the contrast of the colour in the final results; it may change the whole colour, or may decrease or increase the contrast of the colour under the microscope (Asonova and Migalkin 1996; Veuthey *et al.* 2014). A large numbers of experiments have utilised different chemical components; a combination of some staining of each would be a good way to get precise results.

The Miller Elastin (ME) staining method has also been studied by different protocols to achieve the best results for distinguishing the elastin fibres; Miller first proposed the method in 1971. The ME method is a result of modifications to earlier methods, such as Weigert's resorcein-fuchsin method in 1898; this method was then modified by French in 1929 through incorporating crystal violet into the resorcein-fuchsin stain (Miller 1971). The methods of the ME staining group of the aminotriarylmethanes dyes include the three dyes of Victoria blue, fuchsin, and crystal violet.

Although the resorcein-fuchsin mechanism is thought to occur by hydrogen bonding of the dye complex to the elastin fibrils (Miller 1971), the combination between MMD and ME has still not yet been studied.

Staining is essential to distinguish tiny structures in the ligaments, and the contrasting colours are important for clear visibility. Combination of the two stains is an ideal way to achieve clear results. Based on the previous experiments there are many examples of combining, such as haematoxylin with Eosin, Miller elastin with Van Gieson, and Verhoff elastic with Masson trichrome. This thesis will combine two stains to reach the optimal visibility of TMC ligament structures.

1.7 Anatomy of flexor retinaculum

The flexor retinaculum is the structure that connects or attaches to four bones: the pisiform, hook of the hamate, the tuberosity of the scaphoid, and the ridge of the trapezium (Nigro 2001). The term “flexor retinaculum” called “transverse carpal ligament” (TCL), and also called “antebrachial fascia”; this name was proposed because the layer of the fascia lies superficial to the flexor retinaculum (Pacek *et al.* 2010) (Figure 1.16).

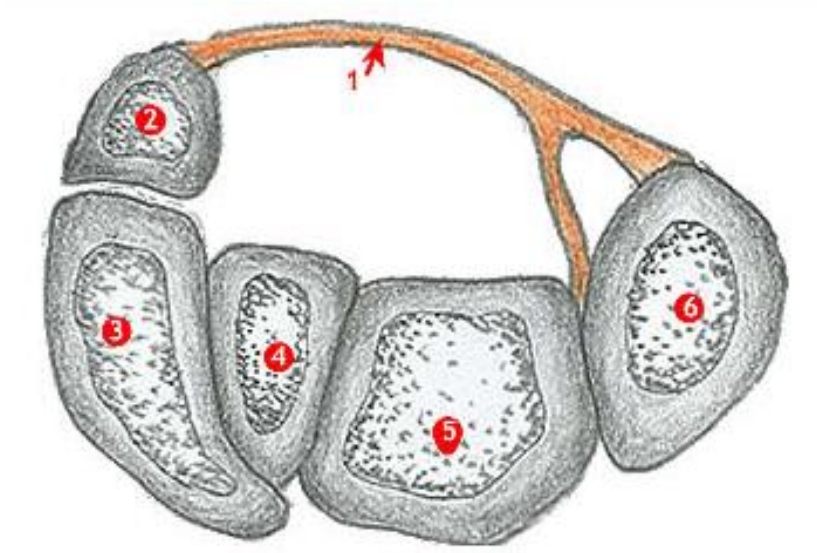

Figure 1.16: Illustrate the flexor retinaculum attachment throught carpal bones from Nigro (2001), 1.flexor retinaculum 2. Pisiform 3. Triquetral 4. Hamate 5. Lunate. 6. Scaphoid.

Anatomically, the flexor retinaculum has three distinct parts and extends from the distal part of the radius, to the level of the distal part of the base of the third

metacarpal, which is called the “proximal portion of the flexor retinaculum”. In addition, the fascia is continuous with deep fascia of the forearm. It also serves as a roof of the anatomic carpal tunnel. Although several studies have described the attachment of the flexor retinaculum, however, they did not mention a relation between the flexor retinaculum and the TMC ligaments (Goitz *et al.* 2014; Manley *et al.* 2013; Nigro 2001; Pacek *et al.* 2010; Presazzi *et al.* 2011).

Another study has noted the anatomical descriptions of the TCL; the TCL forms a retinacular bridge over the carpal tunnel, extending from the ulnar to the radial direction. Its main function is to protect the contained without a significant mechanical action in supporting the transverse carpal arch. Two muscles are related to TCL: the flexor carpi ulnaris and the palmaris longus, which present a distal attachment forming the superficial layer of the aponeurosis palmaris (Nigro 2001).

The boundaries of the carpal tunnel begin from the carpal bones, which are present in the floor, and flexor retinaculum (or TCL), which is present in the roof. The TCL consequently inserts into the pisiform, the hook of the hamate, the trapezium, and the tuberosity of the scaphoid. It divides into two layers: superficial and deep (Presazzi *et al.* 2011).

A quantitative study investigated the flexor retinaculum through the attachment into carpal bones, as follows (Manley *et al.* 2013):

Bones	**Insertion measurement (Proximal to distal × radial to ulnar maximum distance)**	**Area measurement**	**Perimeter of the insertion**
Scaphoid	6 × 6 mm	29 mm	21 mm
Pisiform	9 × 6 mm	38 mm	25 mm
Trapezium	13 × 6 mm,	42 mm	28 mm

Hamate	11 × 5 mm	40 mm	29 mm

Table 1.3: Illustrate the measurement area and perimeter of the TCL insertions with carpal bone.

In addition, the anatomical characteristics of TCL have recently been further clarified. Its bony attachment sites proximally to the scaphoid and pisiform are more round, whereas the distal attachment sites to the trapezium and hamate are more oblong, the measurement of the thickness of the TCL varies along the path of the median nerve, with the thickest portions distal ulnarly and proximal radially (Goitz *et al.* 2014).

A morphological analysis was necessary to recognise the nature of the TCL, to redefine the anatomical terminology concerning the TCL and its surrounding structures, and to evaluate any correlation with the external structures. The TCL was the thickest distally at the midline and ulnar segments, and the thickest proximally at the radial segment; in addition, the TCL thickness distribution is variable along the radioulnar axis; the study found that it was 2.1 ± 0.8 mm (Pacek *et al.* 2010).

The flexor retinaculum attachment descriptions are very important to explain the relationship between these structures and the TMC ligaments, especially the dorso-radial ligament since this ligament is closest to the flexor retinaculum attachments. This thesis will investigate this relationship.

1.8 High resolution episcopic microscopy

High resolution episcopic microscopy (HREM) is a technique used to render 2D photography into 3D images by using Amira 3D software. Several studies have used this technique for providing a comparison between 2D and 3D images (Geyer *et al.* 2009; Mohun and Weninger 2012; Rosenthal *et al.* 2004; Weninger *et al.* 2006). Entheses research studies have often been done by histological process; indeed, these 2D sections have a great deal of detail, but 3D models can provide precise data of the section, particularly if it uses the HREM technique for comparison study.

HREM is a technique in which a series of digital images are taken of the object in question. It includes taking images of consistent dimensions, exposure, and depth of field while cutting through the specimen. This results in a data set of images that are perfectly aligned. The images are then reconstructed by using dedicated computer software to give a clear and interactive 3D model (Geyer *et al.* 2009).

Geyer et al (2009) used the HREM method to visualise embryo anatomy and labelled gene product patterns; their study utilised a 3D computer model to evaluate the development of vertebrate embryos. The use of HREM also makes it feasible to generate episcopic fluorescence image capturing (EFIC) image stacks using cryo-embedded or polyethylene glycol (PEG)–embedded specimens, which allows for combining with 3D RNA or protein expression profiling. It is thus possible to view different features in a specimen, which is invaluable for analysing dynamic changes in tissue structure in the developing embryo (Rosenthal *et al.* 2004).

Comparisons between the two techniques of EFIC and HREM have been done for generating digital volume data and creating 3D images. While EFIC detects autofluorescence emitted from the embedded tissue, HREM requires the tissue to be stained with a fluorescent dye such as eosin. Different procedures are therefore necessary for embedding tissues for EFIC or HREM imaging (Mohun and Weninger 2012).

When descriptions of rapid 2D and 3D computer analysis and visualisation of gene expression and gene product pattern in the context of anatomy and tissue architecture are used by HREM technique for embryos, the quality of the HREM images resembles the quality of digital images of true histological sections with respect to resolution and contrast (Weninger *et al.* 2006).

HREM technique had varied use throughout the literature reviews. This thesis will use this technique to explain the relationship between the dorso-radial ligament and the flexor retinaculum of the hand.

1.9 Osteology

1.9.1 Trapezium bone (TM)

Most studies on the morphology of the carpal bones are not detailed enough for clear understanding (Kuczynski 1974). In these studies, the osteologic disruptions of the trapezium and first metacarpal bones are inadequate and difficult to reproduce when present. The etymologic derivation of the trapezium is from the Greek trapezion (a quadrilateral with two parallel sides) and trapeza (a table, altar) (Ateshian et al. 1992). (Drake 2010; Frazer 1965) used standard texts, concentrating mainly on the articular surfaces or facets, whereas the International Anatomical Nomenclature Committee's (1989a) only named landmark of the trapezium is the tuberculum ossis trapezii. (A 'landmark' is the point of correspondence on each object that matches across and within populations. The same part was also named the ridge by (Humes et al. 2004) and a crest by (Tocheri et al. 2005). The lack of a detailed anatomical description of the bone creates difficulties in both diagnosis and treatment of injuries of the trapezium and the thumb.

The trapezium has six surfaces (Frazer 1965). Four are articular facets, and the remaining two are non-articular palmar and dorsal surfaces. The body of the trapezium lies from the junction of the trapezoid and scaphoid articular facets proximally and distally to the first metacarpal facet. It projects between the base of the first and second metacarpal bones most distally, and carries a small facet, which articulates with the base of the second metacarpal. The trapezium also has medial tubercle and groove on its rough palmar surface that is more medial and contains the tendon of the flexor carpi radialis muscle; two layers of the flexor retinaculum are attached to margins of tubercle. The tubercle of the trapezium is obscured by the thenar muscles (opponens pollicis, flexor pollicis brevis, and abductor pollicis brevis muscles). The dorsal surface of the trapezium is related to the radial artery. Its lateral surface is rough for the attachment of the radial collateral ligament and the capsular ligament of the TMC (Figures 1.17-1.18).

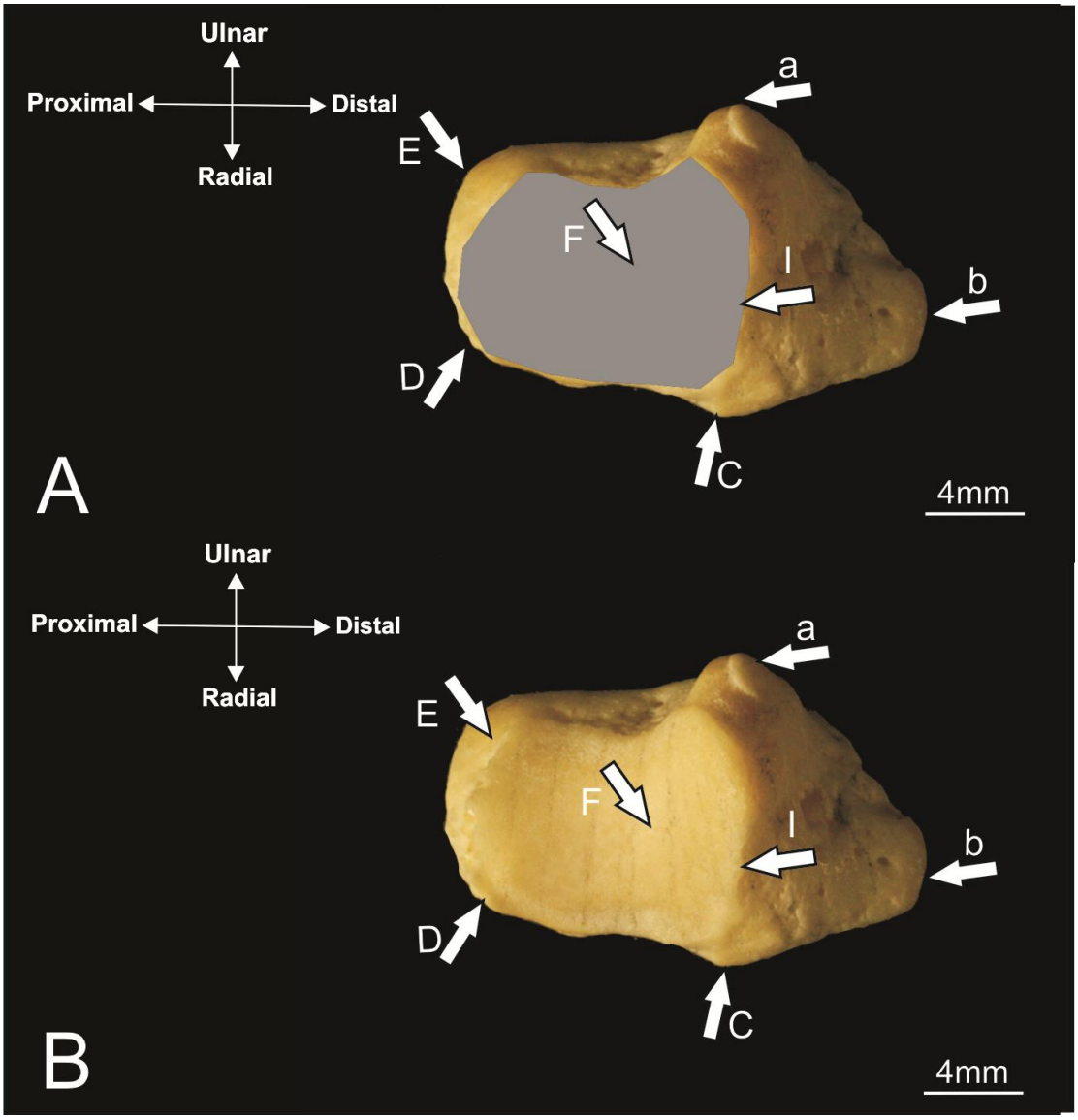

Figure 1.17: Radial view of the TM bone, fom Frazer (1965). a: eminence of the trapezial ridge, b: radial tubercle, C: dorso-ulnar tubercle, D: dorso-radial tubercle, E: palmar tubercle, F: facet of 1st MC of TM bone, I: distal border of 1st MC.

A. Dry TM bone, the articular surface with first metacarpal bone coloured by Grey coloure to illustrate a whole facet area.
B. Dry TM bone.

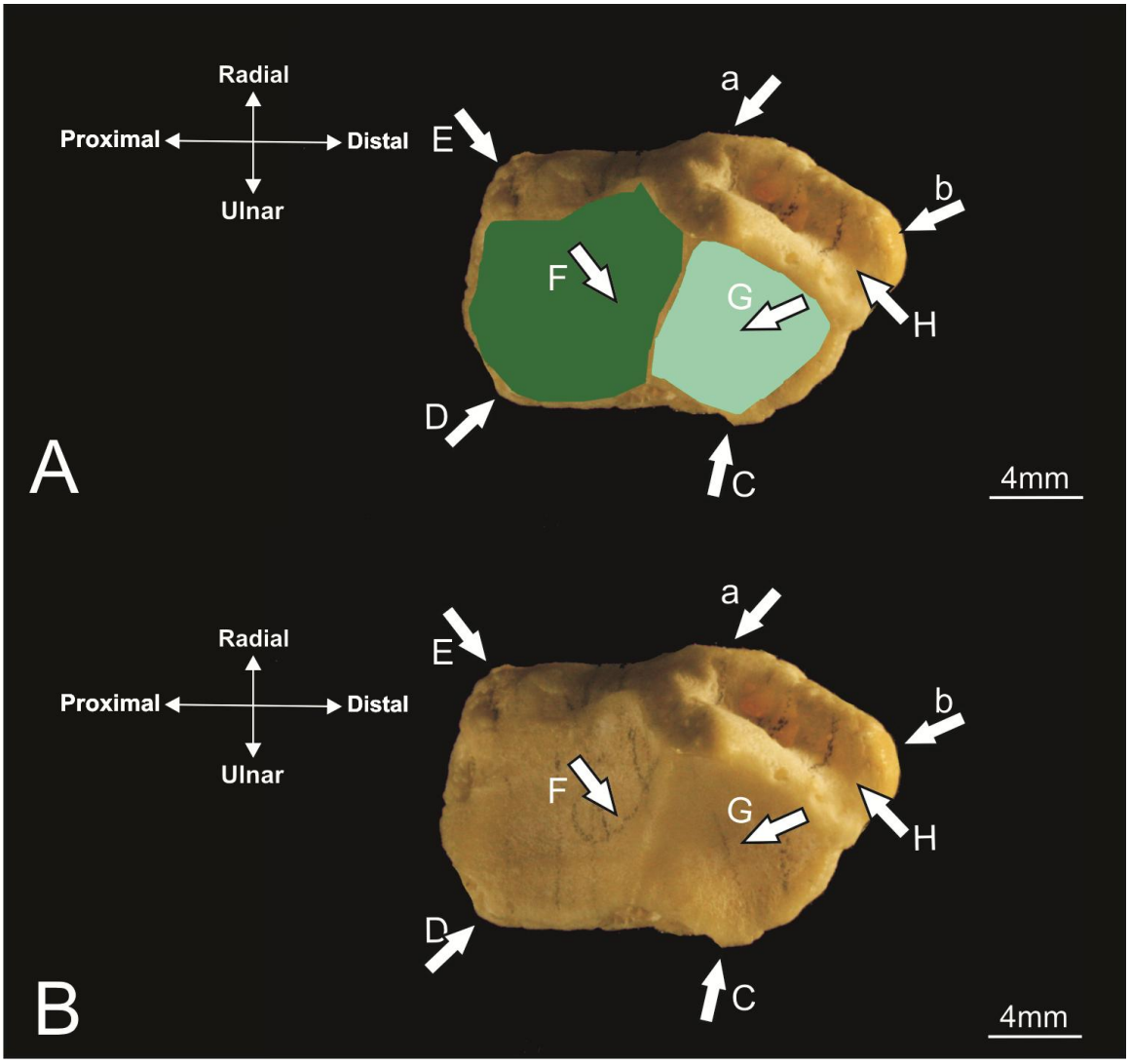

Figure 1.18: Ulnar view of the TM bone, fom Frazer (1965). a: eminence of the trapezial ridge, b: radial tubercle, C: dorso-ulnar tubercle, D: dorso-radial tubercle, E: palmar tubercle, F: facet of trapezoid bone, G: facet of the scaphoid bone, H: groove of the palmar surface for flexor carpi radialis tendon.

A. Dry TM bone, the articular surface with trapezoid bone coloured by dark green colour. And the articular surface with scaphoid bone coloured by light green colour to illustrate a whole facet area.
B. Dry TM bone.

Schild et al (1981) conducted a radiological demonstration and pointed out aspects of traumatology of the trapezium bone. The authors considered the trapezium as one of the pentagonal bodies with seven surfaces; it is articulated with four bones. It is distal with the first metacarpal, proximal with the scaphoid, ulnar proximal with the trapezoid, and distal ulnar with the second metacarpal. In addition, the surfaces are distal: the bigger joint surface is articulated with the base of the first metacarpal, and the surface is concave from the mediolateral and

convex from the anterioposterior direction. The medial surface is divided into the large proximal, which is a concave surface articulated with the trapezoid, and the small distal, which is a narrow surface articulated with the base of the second metacarpal. The proximal surface is smooth and slightly concave in the middle part and rough in the lateral part; it is articulated with the scaphoid. The lateral surface is rough, while the dorsal surface is rough and larger than the palmar surface. A small part of the abductor pollicis longus muscle passes through it and the radial head of the first dorsal interosseus muscle, which covers the dorsal area of the trapezium. In addition, the palmar surface has a tubercle and groove for the flexor carpi radialis tendon, and a tubercle for originating some of the TMC ligaments, muscles of the adductor group, and thenar muscles.

In addition, Humes et al (2004) described new landmarks in their study for the tubercle of the trapezium. The largest articular surface is the first metacarpal facet; it is concave mediolateraly and convex anterioposteriorly. The trapezoid facet, which is the second largest of the articular facets, is elongated and concave. The scaphoid facet is rounded, and the proximal facet is articulated with the tubercle of the scaphoid. In addition, the index metacarpal facet is the smallest and most distal of the articular surfaces. The most palmar surface is a bony ridge (the trapezial ridge). The tubercle of the trapezial ridge is known as the *tubercle of trapezium*; the lateral side of the trapezial ridge is concave and roughened, while the medial side of the trapezial ridge is a groove that contains the tendon of the flexor carpi radialis muscle. On the dorsal surface there are two tubercles: the dorso-ulnar tubercle and the dorsoradial tubercle. The dorsoradial tubercle is more prominent than the dorso-ulnar tubercle.

Also, Humes et al (2004) found the new osteological landmarks were the index metacarpal facet, the dorsoradial tubercle, and the dorso-ulnar tubercle on the dorsal surface of the trapezium. Further, when the tubercle of trapezium is described as the tubercle of the trapezial ridge, this provides a clearer understanding of the anatomy of the trapezium (Drake 2010).

The palmar trapezial surface is irregularly curved, and shows an oblique running ridge crossing the surface at its greatest diameter. The ridge runs from the small facet of the second metacarpal to the lateral margin of the joint surfaces, thus dividing the trapezium surface into a radial part, which is the more palmarly

situated part, and an ulnar part, which is the more dorsally situated part; both are slightly concave. The two parts are connected by a groove crossing the ridge nearly perpendicularly. In adduction of the thumb, the most convex part of the ridge on the trapezium surface matches the most concave part of the groove on the first metacarpal. Abduction of the thumb will move the most concave part of the groove on the first metacarpal to the flatter palmar lateral part of the trapezium surface (Steven 2009). This change from a more congruent to a more incongruent situation, however, can partly explain the increase of the mobility in the joint in certain positions (Figures 1.19-1.20).

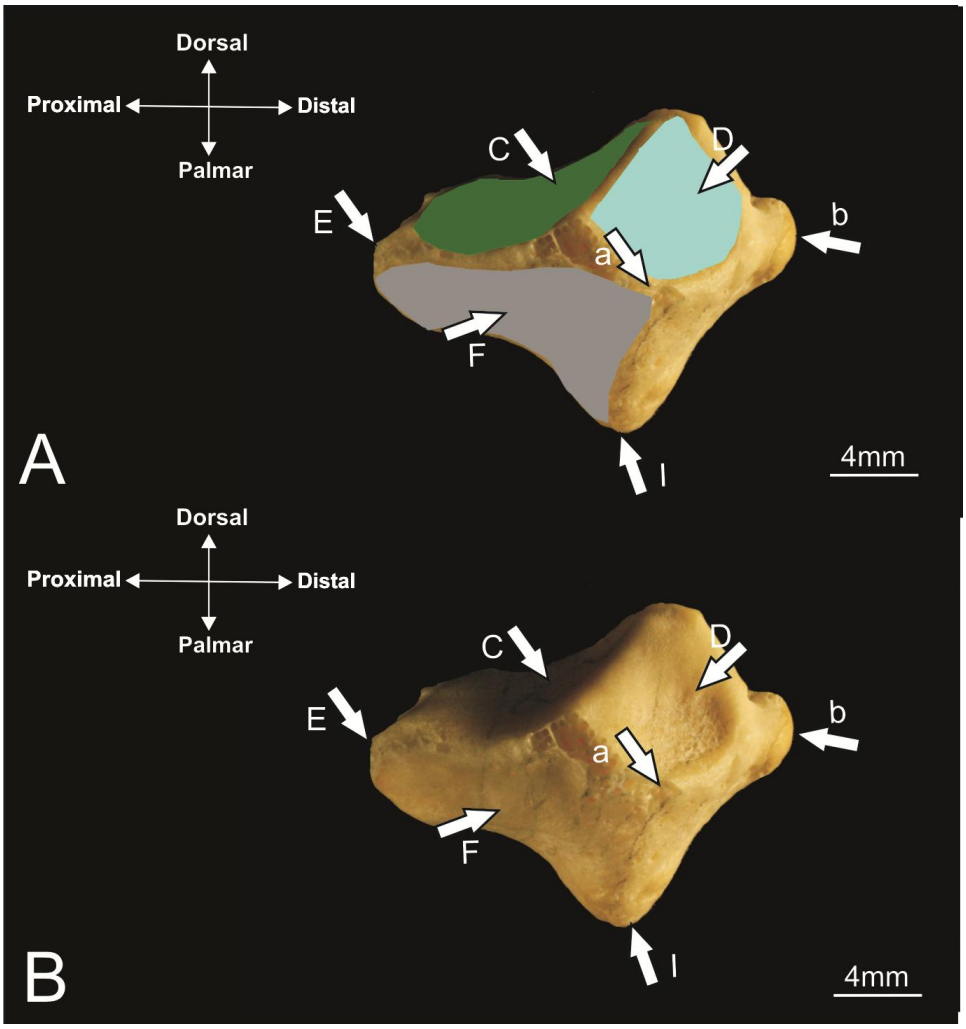

Figure 1.19**:** Dorsal view of the TM bone, from Steven (2009). a: eminence of the trapezial ridge, b: radial tubercle, C: facet of trapezoid bone, D: facet of the scaphoid bone, E: palmar tubercle, F: facet of 1st MC of TM bone, I: distal border of the 1st MC facet of the TM bone.

A. Dry TM bone, the articular surface with trapezoid bone coloured by dark green colour. And the articular surface with scaphoid bone coloured by light green colour, the articular surface with first metacarpal bone coloured by Grey colour to illustrate a whole facet area.
B. Dry TM bone.

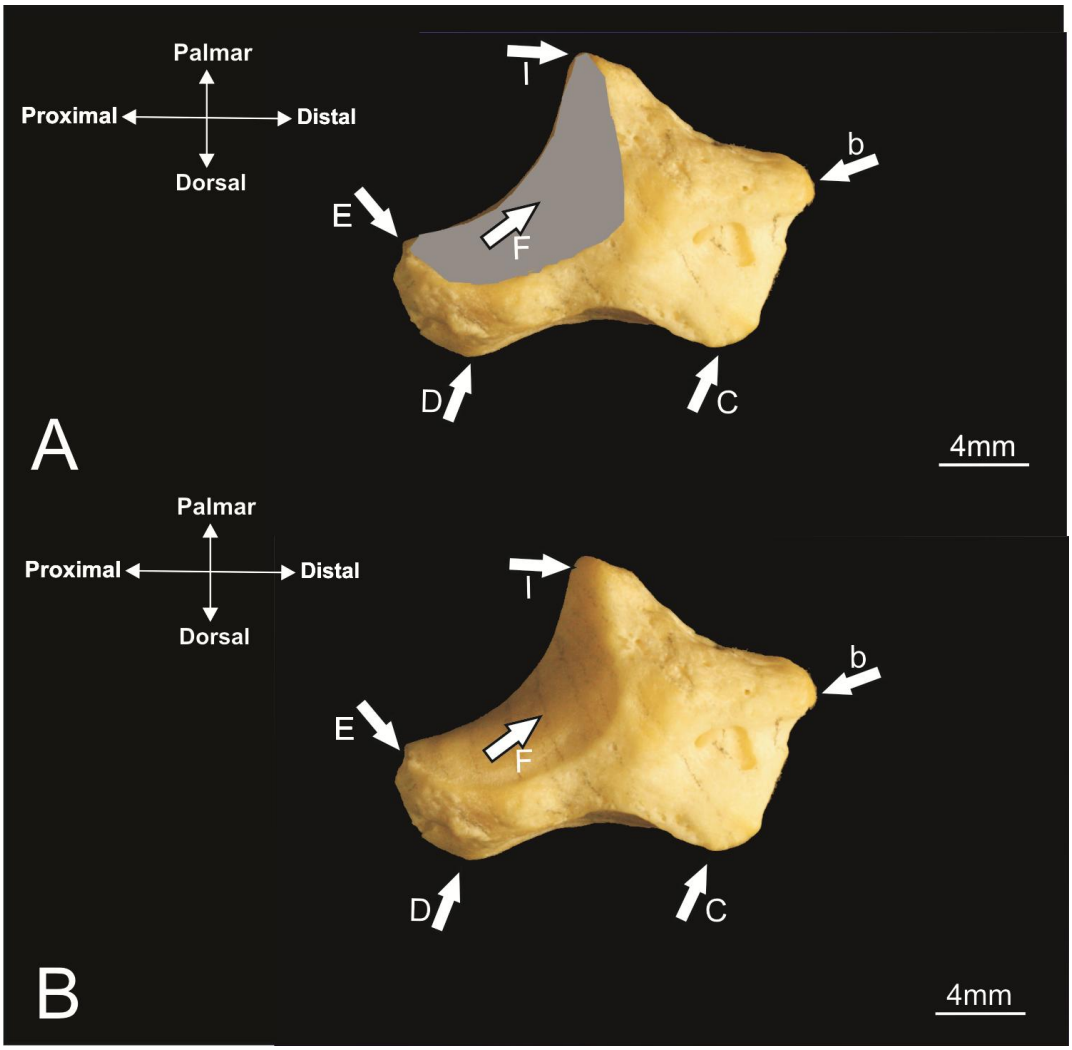

Figure 1.20: Palmar view of the TM bone, from Steven (2009). b: radial tubercle, C: dorso-ulnar tubercle, D: dorso-radial tubercle, E: palmar tubercle, F: facet of 1st MC of TM bone, I: distal border of the 1st MC facet of the TM bone.

A. Dry TM bone, the articular surface with first metacarpal bone colourd by Grey colour to illustrate a whole facet area.
B. Dry TM bone.

The trapezium is articulated with the thumb metacarpal, index metacarpal, scaphoid, and trapezoid. The trapezium has a recess that is adjacent to the AOL insertion; it plays a very important role as a pivot through the screw-home torque rotation from the resting position of the thumb to final opposition, the change from laxity to rigidity, and from incongruousness to congruousness. The trapezium also contains a deep groove for the flexor carpi radialis tendon, which is at risk during trapezioectomy. The TCL partially inserts into the trapezium, trapezoid, and scaphoid; therefore, during trapezioectomy procedures the TCL enters and releases the carpal tunnel (Edmunds 2011).

The trapezium bone is an irregularly sided bone of medium size; it is distinguished by the largest facet, a saddle-shaped articular surface for the TMC, and by a long, raised, narrow tubercle or crest. The trapezial ridge (crest or tubercle) on the palmar surface is elongated proximodistally, and projects for attachment to the flexor retinaculum. The facet for the first metacarpal bone is considered the largest one; the facet for the second metacarpal bone is the smallest facet found on the distal apex of the trapezium. The facet for the trapezoid is sandwiched between the facet of the second metacarpal bone and the facet of the scaphoid; the facet for the scaphoid is the most proximal facet. The anatomical siding is the trapezial ridge; it is palmar medial towards the centre of the hand. The positional siding places the bone on the flat surface, with the tubercle on top and away from the body, and the concave facets on either side (Drake 2010). It is still not clear how to distinguish the palm surface and the dorsal surface, however, as well as the anterior and posterior face of the trapezium.

Some studies have been concerned with the articular surfaces of the trapezium. The articular surface is saddle shaped, and allows thumb motion in the medial-lateral and anterior- posterior directions, as well as some rotation. The trapezial surface is concave in the medial-lateral plane and convex in the anterior-posterior plane; the concave surface may be likened to a valley, and the convex surface to a hill. The hill of the trapezium articulates with the valley of the metacarpal, and the trapezial valley articulates with the metacarpal hill (North and Rutledge 1983).

1.9.2 First metacarpal (1st MC)

The first metacarpal (1st MC) is one of the very important metacarpal bones. Approximately 90% of hand functions, such as grasping, opposition and hitchhiker position depend on 1st MC. The 1st MC is more anterior relative to the other metacarpals, and is rotated medially on its axis through 90º, so that its morphologically dorsal surface is lateral, its radial border is palmar, its palmar surface is medial and its ulnar border is dorsal. Hence, the thumb flexes medially across the palm and can be rotated into opposition with each metacarpal (Snell 2004) (Figure 1.21)

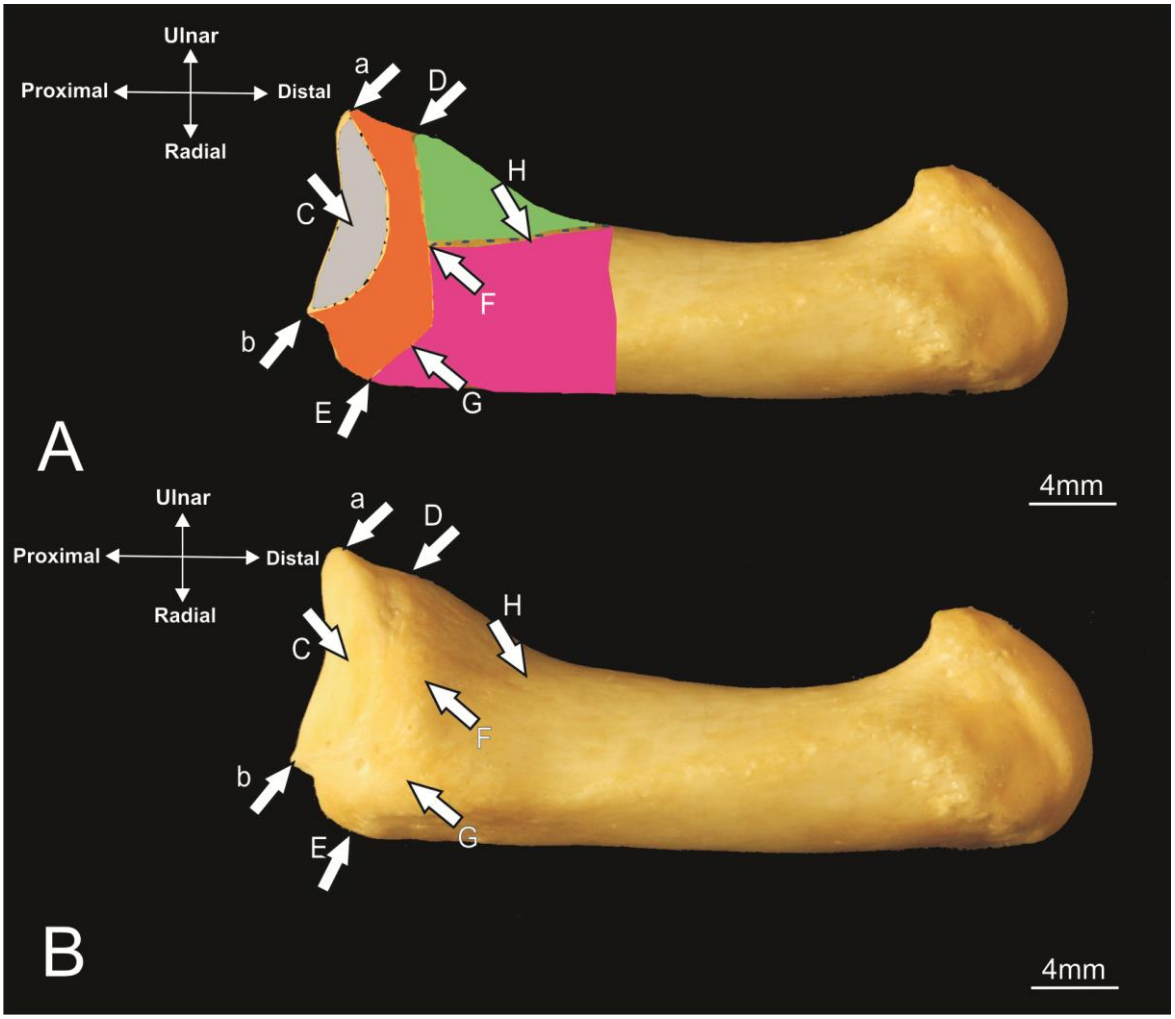

Figure 1.21: Radial view of the right 1st MC bone, from (Snell 2004). a: anterior eminence, b: posterior eminence, C: facet of the TM bone of the 1st MC bone, D: palmo-ulnar tubercle, E: palmo-radial tubercle, F: proximal ridge of palmar surface, G: dorso-ulnar tubercle, H: distal ridge of palmar surface.

A. Dry 1st MC bone, the articular surface coloured by grey colour represents the articular area with TM facet of the 1st MC bone. Orange colour represents the area between the facet of the TM of the 1st MC bone and palmar surface. Green colour represents the area of the small part of ulnar area of the palmar surface of the 1st MC bone. Pink colour represents the area of a large part of the radial area of the palmar surface of the 1st MC bone.
B. Dry 1st MC bone.

The 1st MC is short and thick. Its dorsal surface can be felt to face laterally; its long axis diverges disto-laterally from its neighbour. The shaft is flattened, dorsally broad and transversely convex. The palmar surface is longitudinally concave and divided by a ridge into a larger lateral (anterior) and smaller ulnar (posterior) part. The opponens pollicis muscle is attached to the radial border and the adjoining palmar surface; the first dorsal interosseous muscle (radial head) is attached to its ulnar border and adjacent palmar surface. The base is concavo-

convex and articulates with the trapezium. The abductor pollicis longus is attached on its lateral side. The first palmar interosseous muscle is attached to its ulnar side. The head is less convex than the other metacarpals and is transversely broad. Sesamoid bones glide on radial and ulnar articular eminences on its palmar aspect (Snell 1995) (Figure 1.22).

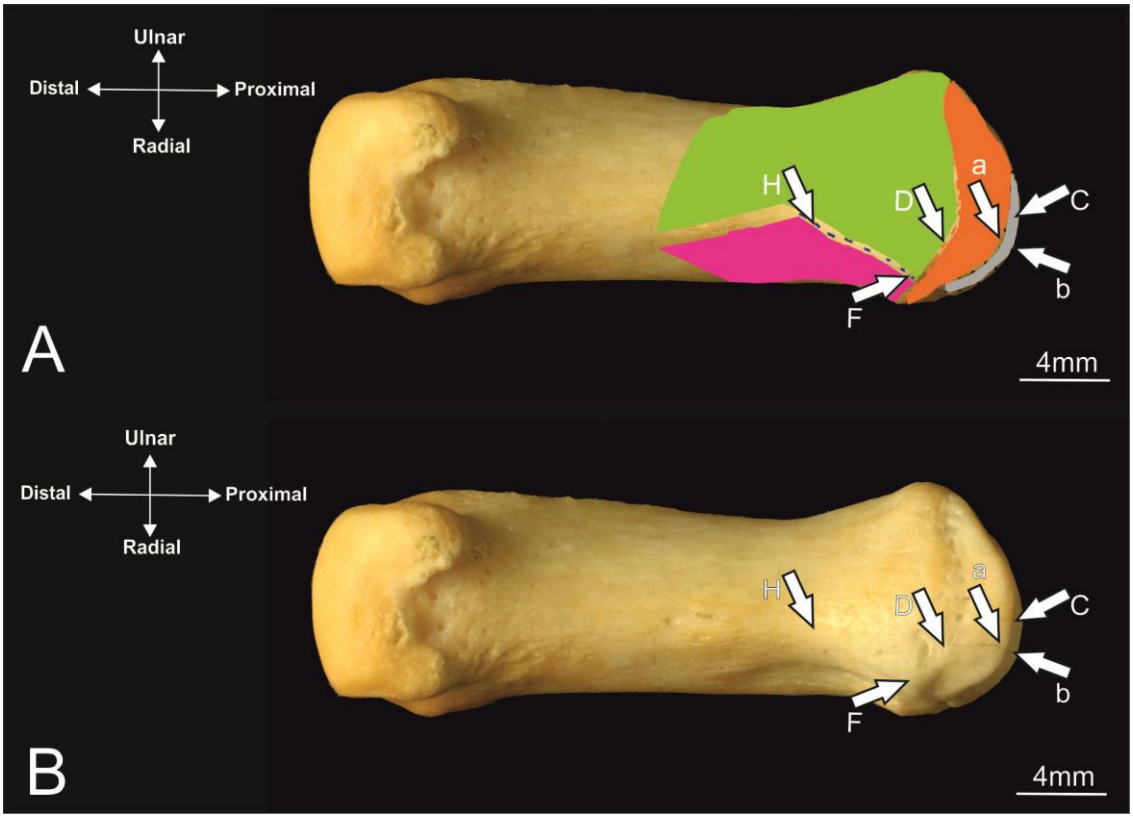

Figure 1.22: Palmar view of the right 1st MC bone, from (Snell 2004). a: anterior eminence, b: Posterior eminence, C: Facet of the TM bone of the 1st MC bone, D: Palmo-ulnar tubercle, F: Proximal ridge of palmar surface, H: Distal ridge of palmar surface.

A. Dry 1st MC bone, the articular surface coloured by grey colour represents the articular area with TM facet of the 1st MC bone. Orange colour represents the area between the facet of the TM of the 1st MC bone and palmar surface. Green colour represents the area of the small part of ulnar area of the palmar surface of the 1st MC bone. Pink colour represents the area of a large part of the radial area of the palmar surface of the 1st MC bone.
B. Dry 1st MC bone.

Nanno et al (2006a) has modelled the 1st MC in 3D study of the attachments of the TMC ligaments. A superimposing outline of the attachment drew on the base of the 1st MC. Therefore, the base was divided into anterior and posterior surfaces, with a main ridge across the two surfaces, lateral and medial.

However, the concept to use 3D technique for modelling the first metacarpal was reasonable.

Based on the literature reviews there were deficiencies in the descriptions of the trapezium and first metacarpal bones, this thesis will investigate each bone as individually, noting each ridge, decline, and prominence on the surface of the bones as well as study the relationship of these features to the TMC ligaments attachments using 3D software (Amira-Landmark-Rhinoceros).

1.9.3 History of landmark procedures

Body shape was a difficult, but important, trait to quantify. Researchers have traditionally used multivariate analysis of several linear measures (‘trusses’) across the body form to quantify shape. Newer geometric morphometric methods claim to estimate shape better because they analyze the geometry of the locations of all landmarks simultaneously, rather than the linear distances between pairs of landmarks. A landmark was the point of correspondence on each object that matches across and within populations (Williams and Richtsmeier 2003). This study compared the results of several traditional morphometric analyses against a newer geometric analysis involving thin-plate splines (TPS). These analyses were applied to a common data set of morphologically variable New World cichlids, *Amphilophus citrinellus* and *A. zaliosus*. The results indicated that geometric morphometrics can be a more effective way to analyze and interpret body form, but also that traditional methods can be relied upon to provide statistical evidence of shape differences, although not necessarily accurate information about the nature of variation in shape (Parsons *et al.* 2003).

Complex variation associated with body form was one of the most difficult types of variation to quantify, and the methods used to assess it are collectively referred to as morphometrics. These methods are concerned with quantifying shape variation within and among samples, usually to address developmental and evolutionary questions related to shape change during growth, across experimental treatments or among different populations (James Rohlf and Marcus 1993). Methods for comparing biological forms range from classic verbal and pictorial representations to methods involving the tracing of outlines and lists of measured linear distances between pairs of identifiable landmarks on an organism (Bookstein 1997; Loy *et al.* 2000).

Newer methods involving the geometric locations of landmarks have been developed (Kume *et al.* 2007; Parsons *et al.* 2003; Rudemo 2000; Williams and Richtsmeier 2003). The most common approaches, referred to as 'traditional' morphometrics, are only a few decades old (James Rohlf and Marcus 1993), and typically apply multivariate statistical methods. Examples include principal components analysis, canonical variate analysis, discriminant function analysis and multivariate analysis of variance to a set of variables measured on each individual.

Frequently, the variables are linear distances, often called 'trusses' (Bookstein 1997), measured between pairs of landmarks on the body or body parts, or angles described by sets of three landmarks.

Five basic limitations drove the most recent morphometric revolution. First, linear truss lengths are generally strongly positively related to individual body size, rather than a standard size (Bookstein 1997). The size problem was inherent to any data derived from landmarks, including the newer geometric approaches because the geometric coordinates of landmarks are influenced by body size.

Second, variation among samples becomes more difficult to assess when homologous landmarks do not define trusses. The problem of missing data or absent landmarks was also a persistent problem in morphometric studies.

Third, different shapes can yield identical sets of truss lengths because the locations of trusses relative to each other are not quantified.

Fourth, the exclusion of potentially important geometric shape information suggests that there can be reduced statistical power to distinguish variation among samples.

Fifth, the only quantitative visual representations of shape involve multiple scatter plots or histograms of either numerous univariate measures or statistically derived multivariate measures (Parsons *et al.* 2003).

Finally, the osteological study is needed to explain the features of the TM and the first MC bones, and to give accurate details related to the TMC ligaments' attachment.

It is clear that there were a number of limitations when using Landmark software. This thesis will attempt to avoid these limitations by increasing number of dry bones, decreasing the distance of measurement, and decreasing the number of single coordination points on the surface of the bones, as well as by using other software to measure the articular surface of each bone.

1.10 Aims of the proposed research

The proposed research has the following goals:

- To determine the number of the TMC ligaments;
- To describe the TMC ligaments' attachments;
- To understand the relationship between the TMC ligaments and their stabilisation;
- To determinate variations in the ligaments of the TMC, and how this influences joint kinematics;
- To understand the kinematics of the TMC;
- To explain the entheses and its type of the TMC ligaments;
- To obtain a good visibility of the TMC ligaments structures;
- To examine the trapezium / first metacarpal morphology and their variations;
- To describe the relationship between the trapezium and the first metacarpal and their associated joints.
- To understand the clinical injuries that occurs on the TMC joint especially its ligaments.

Chapter Two

2D reconstructions of the Trapeziometacarpal Ligaments

2.1 Introduction

The ligaments of the trapeziometacarpal joint (TMC) are complex and highly varied. Various studies report different patterns of the ligament (Cole and Abbs 1986; Cooney *et al.* 1981; Kapandji and Heim 2002). The naming of the TMC ligaments is inconsistent throughout the literature (Ebskov and Boe 1966; Goubier *et al.* 2011; Jantea *et al.* 1994). A number of articles discuss the anatomy and function of the ligaments of the trapeziometacarpal joint (Garcia-Elias and Orsolini 2011; Kauer 1987; Nallakaruppan *et al.* 2012).

A review of the literature reveals that the anatomic orientation of the ligaments of the TMC and their contribution to joint stability remains unclear (Ghavami and Oishi 2006; Goubier *et al.* 2009; Haines 1944).

The literatures reviews in the chapter one (pages 34-49) discussed in details the experiments and studies related to this chapter.

The aims of this study are to (1) explore the TMC ligament around TMC joint by micro-dissection, (2) quantify the shape and orientation of the TMC ligaments throughout 2D reconstructing shape in 3D virtual environment, (3) quantify the changes of measurement (length, with and surface area) of the TMC ligaments during the neural and full abduction positions of the thumb, and (4) create a consistent terminology based on these anatomical findings, (5) comparison between frozen and embalmed specimen to observe the variation could be happen.

This information could improve knowledge and understanding of normal anatomy, show its impact on the mechanics of the trapeziometacarpal (TMC) joint, and help in the assessment and treatment of the various injuries and degenerative changes seen in the TMC joint.

2.2 Material and Methods

2.2.1 Distinguishing Between the Ligamentous Attachments

Fifty embalmed cadaveric specimens (26 male specimens, 24 female specimens; 13 pairs; age range, 72±8 years) and ten fresh frozen cadaveric specimens (5 males, 5 females; age range, 68±6) were dissected. The trapeziometacarpal joint of all 60 specimens was meticulously dissected by palmar and dorsal approaches using loupe microscopic magnification (with 6× magnification).

The main propose of dissecting the thumb is to expose the TMC ligaments. During the first time dissecting the thumb to see the TMC ligaments, the dissector must follow the regular fascicles from the bone-to-bone (proximal-distal) attachment, which preserve these fascicles without cutting. In contrast, cutting any irregular tissue overlaps with the fascicles and cleans the edge of fascicles. All these procedures must be done under the microscope to be sure the visibility of the irregular and regular fascicles. Finally, the regular fascicles will appear around the TMC joint parallel to and beside each other, covering the whole articulate area of TMC joint (Figures 2.3-2.4).

Dorsal side of specimen, the extensor pollicis longus, extensor pollicis brevis and extensor carpi radialis longus tendons were reflected distally. The radial artery was excised as it emerged dorsally in the anatomic snuff-box to the level of the first dorsal interosseous muscle. The proximal half of the first dorsal interosseous muscle was also removed to expose the intermetacarpal region. All other structures were then excised from the surface of the trapezium, trapezoid, and first and second metacarpals to reveal the underlying interosseous ligaments. Two ligaments were identified from this exposure: the palmar intermetacarpal ligament (PIML) and DIML (Figures 2.3-2.4).

Palmar side of specimen, the abductor pollicis brevis, superficial head of flexor pollicis brevis and opponens pollicis muscles were reflected distally off the radial-most portion of the transverse carpal ligament (TCL) and the first metacarpal, thus revealing the underlying TMC joint and ligaments. A blunt-tipped probe was used to delineate adjacent ligaments, especially along the palmar side of the TMC joint

intermetacarpal region. Five additional ligaments were identified at this point: the sAOL, deep anterior oblique ligament (dAOL), UCL, POL, and DRL (Figures 2.5-2.6).

A superficial layer of the anterior oblique ligament (sAOL) was pulled off from the deep layer. The proximal site of the sAOL and dAOL remained attached to the trapezium bone. Finally, the TMC joint with ligaments was hinged open like a book on the dorsal side (hingeing on the palmar side) to be ready for reconstruction.

The two positions have chosen as keys of the kinamtics procedures (Kuo *et al.* 2009a);

- Neutral positions (35°) which is the anatomical position of the hand, the thumb in lateral pinch position; the pad is perpendicular to the palm, the TMC joint flexed (25°) from the middle of palm of hand (Figure 2.1).

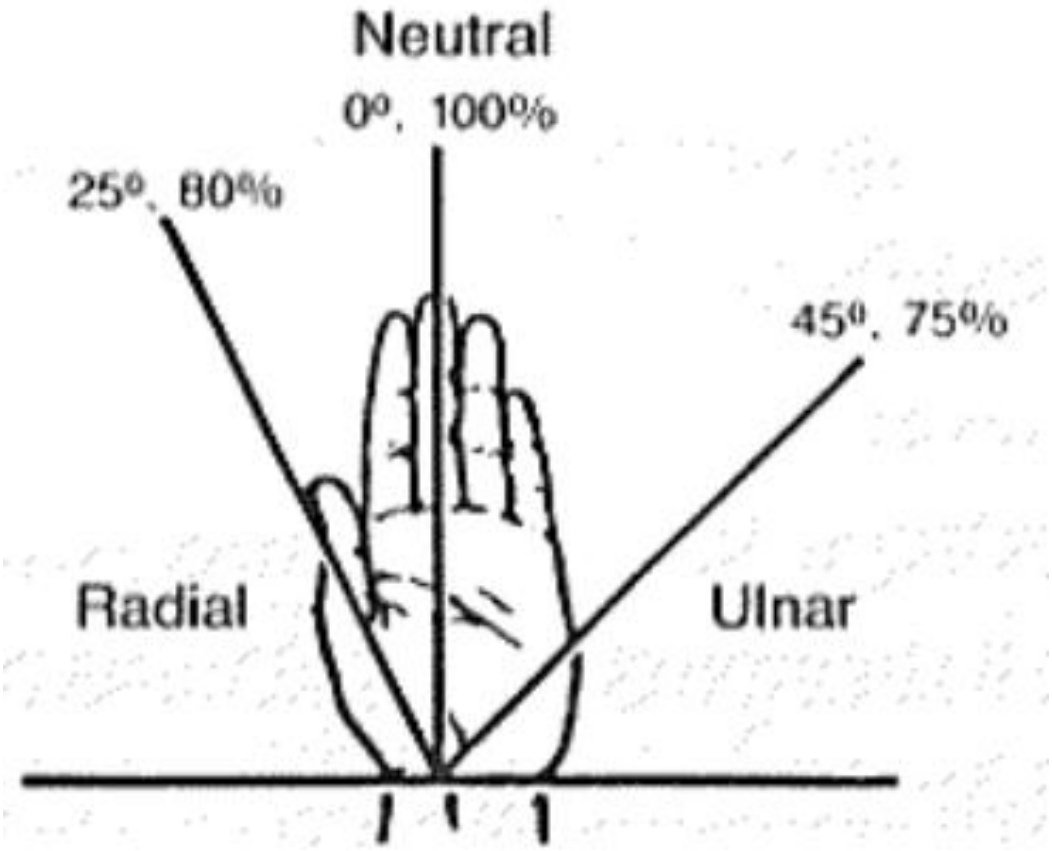

Figure 2.1: Illustrate the neutral position of the thumb, from Kuo et al (2009a).

- The full abduction (60°) which is the maximum a stretch of the thumb in the plane which was perpendicular to the palm of the hand (Figure 2.2).

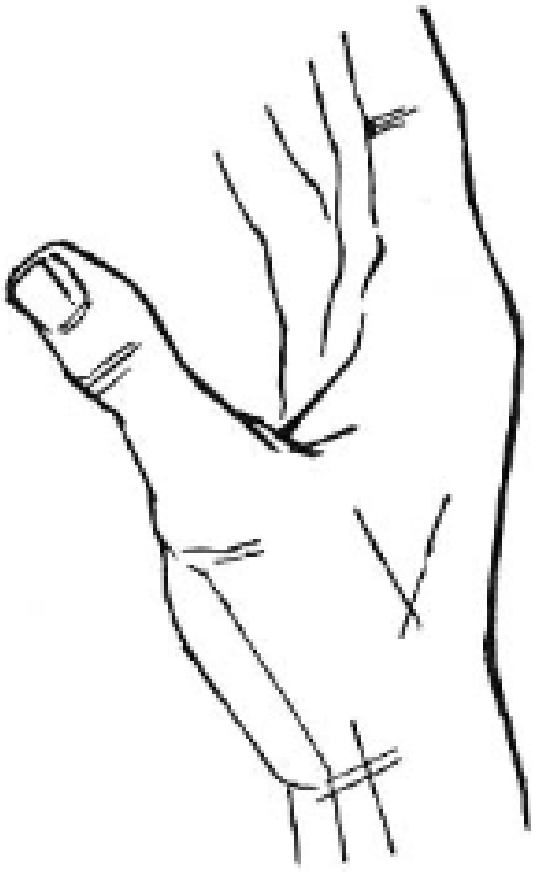

Figure 2.2: Illustrate the full abduction position of the thumb, from Kuo et al (2009a).

A thumb goniometer was used to calculate the angle between the first metacarpal and second metacarpal from neutral to full abduction positions, and then the thumb was fixed in a neutral position; the reading of the goniometer was 35˚and fixed again when the thumb moved towards a full abduction position at 60˚. Three 1.5 mm pins were inserted into the first metacarpal, second metacarpal and hamate bones to ensure it was firmly fixed to the digitizing platform.

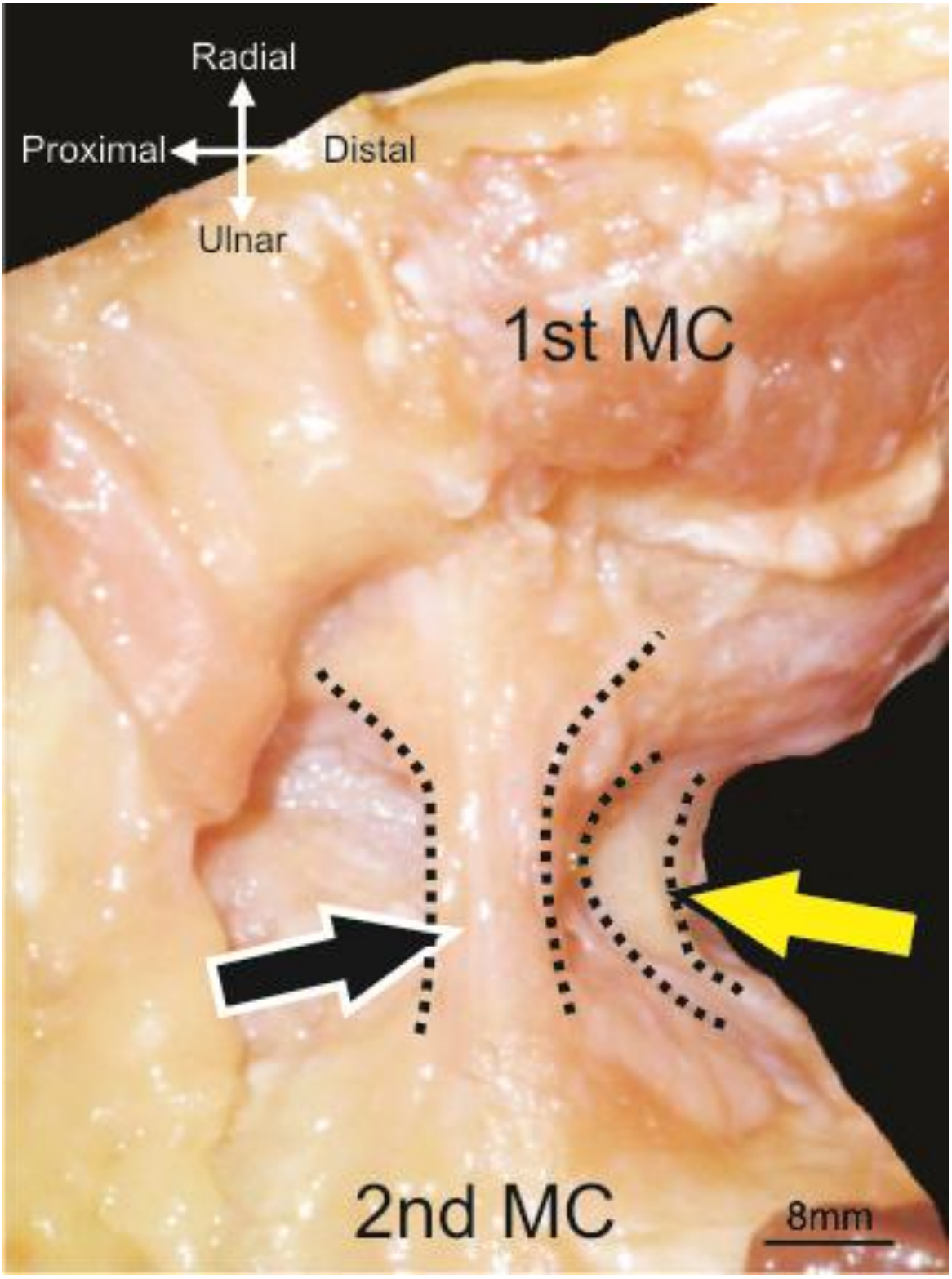

Figure 2.3: Posterior view of the unembalmed donor TMC ligaments. (Black Arrow) the dorsal intermetacarpal ligament (DIML) and (Yellow Arrow) palmar intermetacarpal ligament (PIML).Dotted lines depicted at the ligament borders indicate the course and limit of the ligaments from and to the bones.

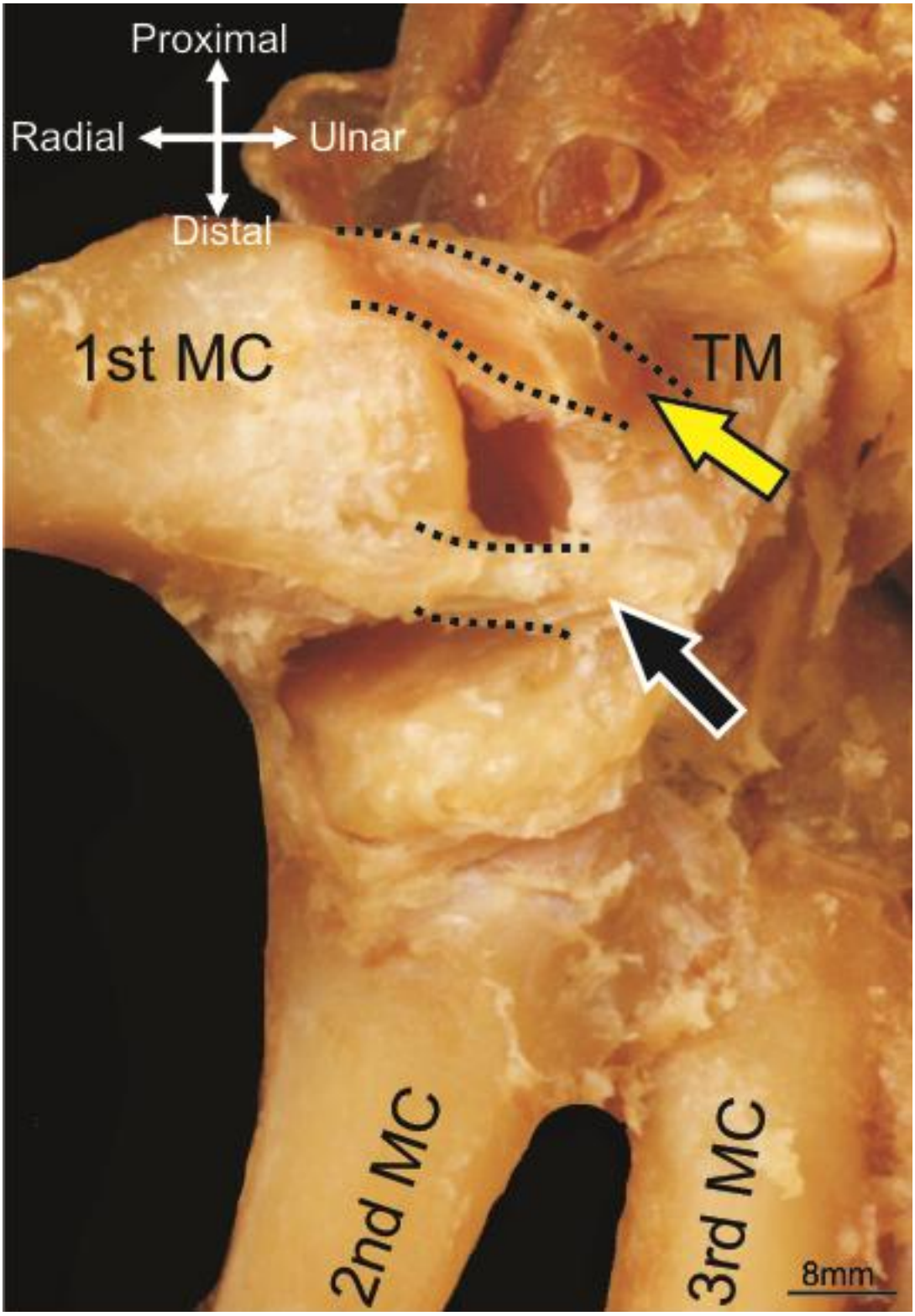

Figure 2.4: Lateral view of the embalmed donor TMC ligaments.
(Black Arrow) the dorsal intermetacarpal ligament (DIML) and (Yellow Arrow) palmar intermetacarpal ligament (PIML). Dotted lines depicted at the ligament borders indicate the course and limit of the ligaments from and to the bones.

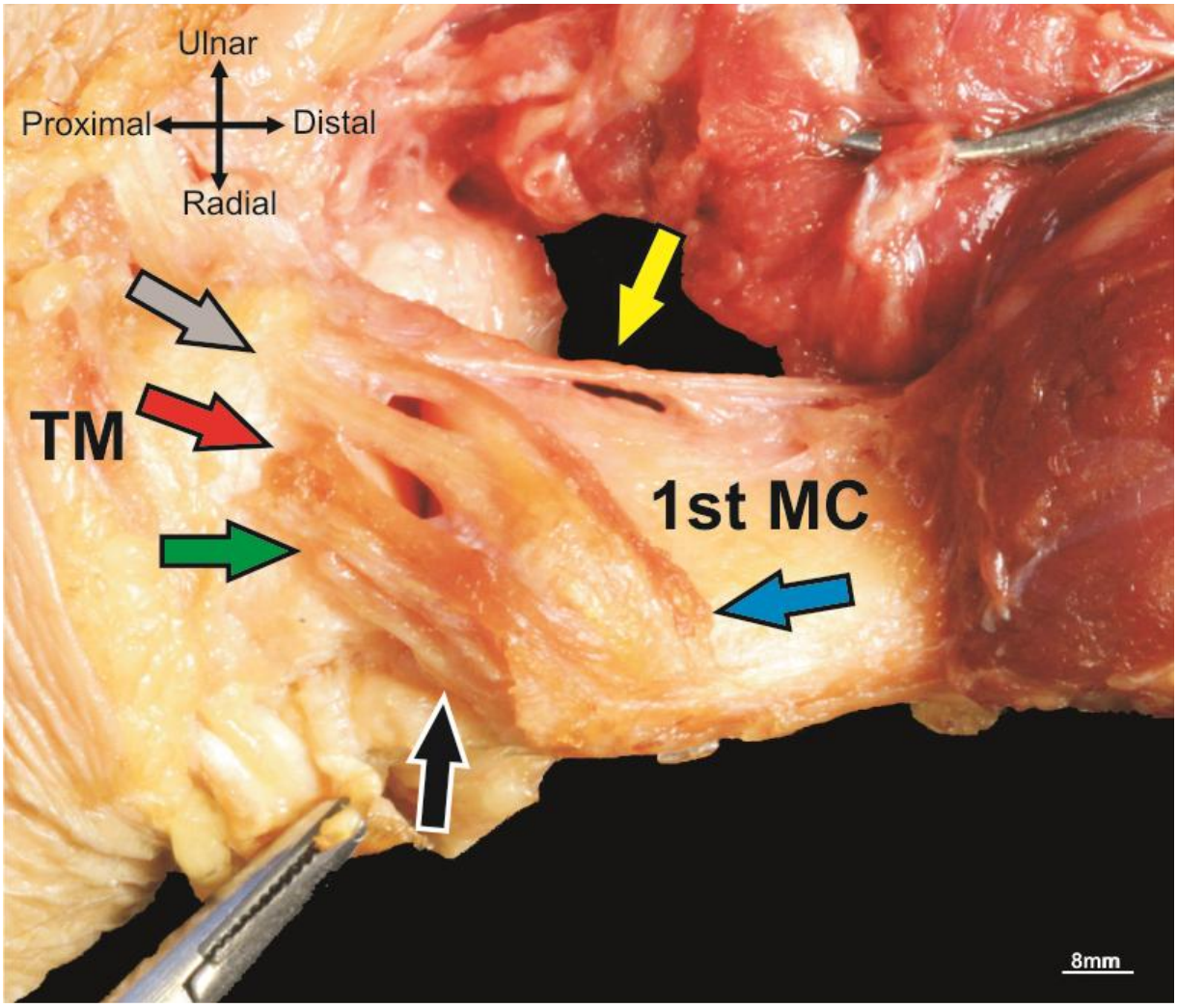

Figure 2.5: Anterior view of the unembalmed donor TMC ligaments.
(Black Arrow) the ulnar collateral ligament (UCL), (Red Arrow) superficial part of the anterior oblique ligament (sAOL), (Green Arrow) deep part of the anterior oblique ligament (dAOL), (Grey Arrow) posterior oblique ligament (POL), (Blue Arrow) dorsoradial ligament (DRL), and (Yellow Arrow) palmar intermetacarpal ligament (PIML).

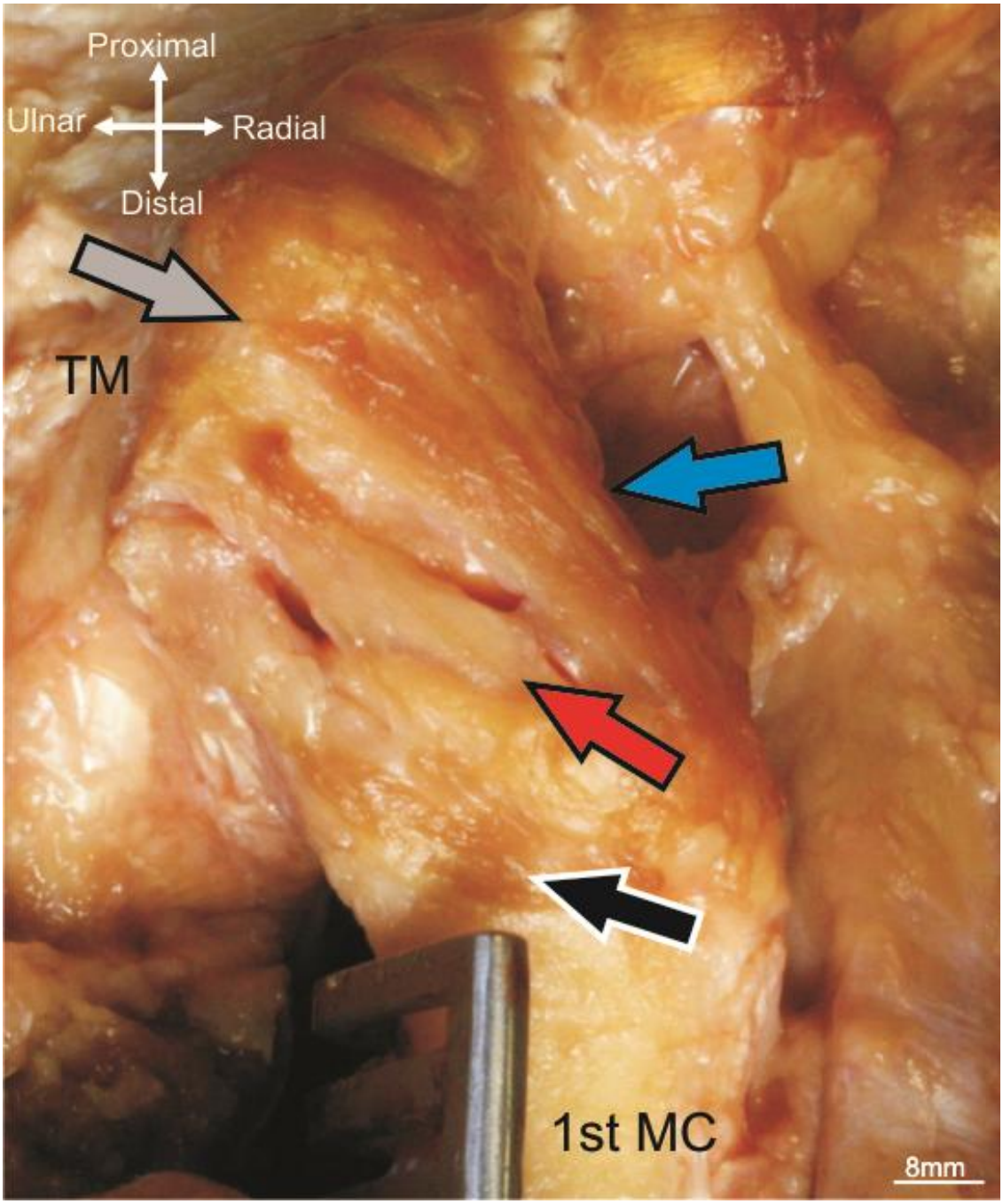

Figure 2.6: Anterior view of the unembalmed donor TMC ligaments.
(Black Arrow) the ulnar collateral ligament (UCL), (Red Arrow) superficial part of the anterior oblique ligament (sAOL),(Grey Arrow) posterior oblique ligament (POL), and (Blue Arrow) dorsoradial ligament (DRL).

2.2.2 Making the Three-Dimensional Digitized Surface and Models with Bone

A digitizer (Microscribe-3DX Digitizer) and 3D surface reconstruction software (Rhinoceros Version 5) were used to digitize manually the ligamentous attachments and their bones: the trapezium, first metacarpal and second metacarpal (Figure 2.7). The microscribe digitizer pen collects the coordinates of single points in 3D space. Multiple points can be connected in a formal line. The multiple lines create a scaffold over which a virtual surface can be lofted. This lofted structure is a virtual model of the actual object (Figure 2.8).

Figure 2.7: A digitizer (Microscribe-3DX Digitizer).
http://microscribe.ghost3d.com/gt_microscribe.htm

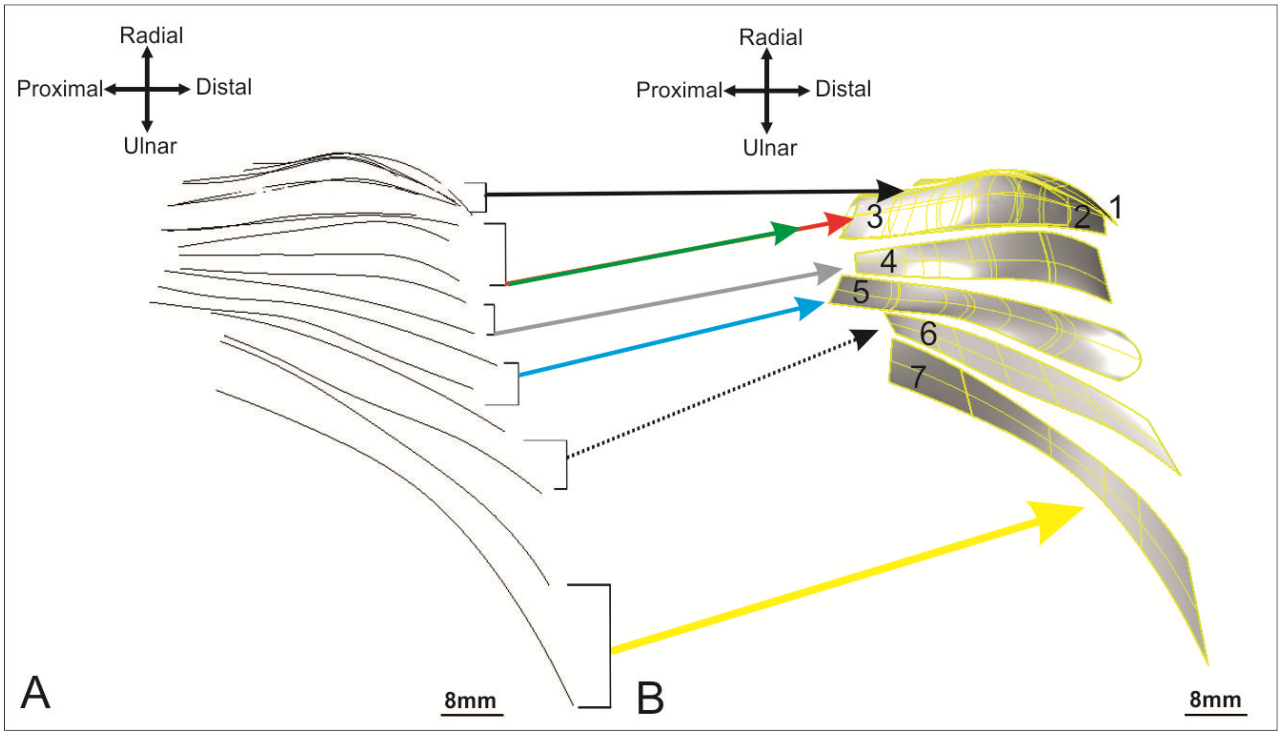

Figure 2.8: (A) Virtual lines of the TMC ligaments lofted to be two-dimensional, (B) two-dimensional reconstruction in a three-dimensional virtual environment.

(1) The Ulnar collateral ligament (UCL), (2 and 3) superficial and deep parts of the Anterior oblique ligament (sAOL, dAOL), (4) Posterior oblique ligament (POL), (5) dorso-radial ligament (DRL), (6) palmar intermetacarpal ligament (PIML) and (7) dorsal intermetacarpal ligament (DIML).

2.2.3 Measurement of TMC Ligaments

All TMC ligaments were identified and categorized. The length, width and area of each ligament were measured in the neutral and full abduction positions. The neutral position of the thumb was defined as the thumb in lateral pinch position. The full abduction position was defined as a maximum a stretch of the thumb in the plane which was perpendicular to the palm of the hand (Kuo *et al.* 2009b). The gender of the specimens was recorded. Surface areas for each ligament were determined and calculated in square millimetres (mean ± SD). The ligaments of the TMC joint are small and have an irregular shape; three lines have been depicted along the anterior surface of each ligament for length and width measurement by (Image J) software (Figures 2.9-2.10).

The line descriptions are a follows:

- Ulnar line which is along the ulnar border of the ligament.
- Middle line which is at the middle between the ulnar and radial lines (the distance between two lines are equal together).
- Radial line which is along the radial border of the ligament.
- Proximal line which is located at the proximal attachment of the ligament.
- Mid-portion line which is located between the proximal and distal lines (the distance between two lines are equal together).
- Distal line which is located at the distal attachment of the ligament.

The length of each ligament was calculated by taking the average of corresponding horizontal lines, and the width was calculated by taking the average of the vertical lines, respectively. After measurement, the capsule and the periosteum on each bone were excised to distinguish the sites of the ligamentous attachments.

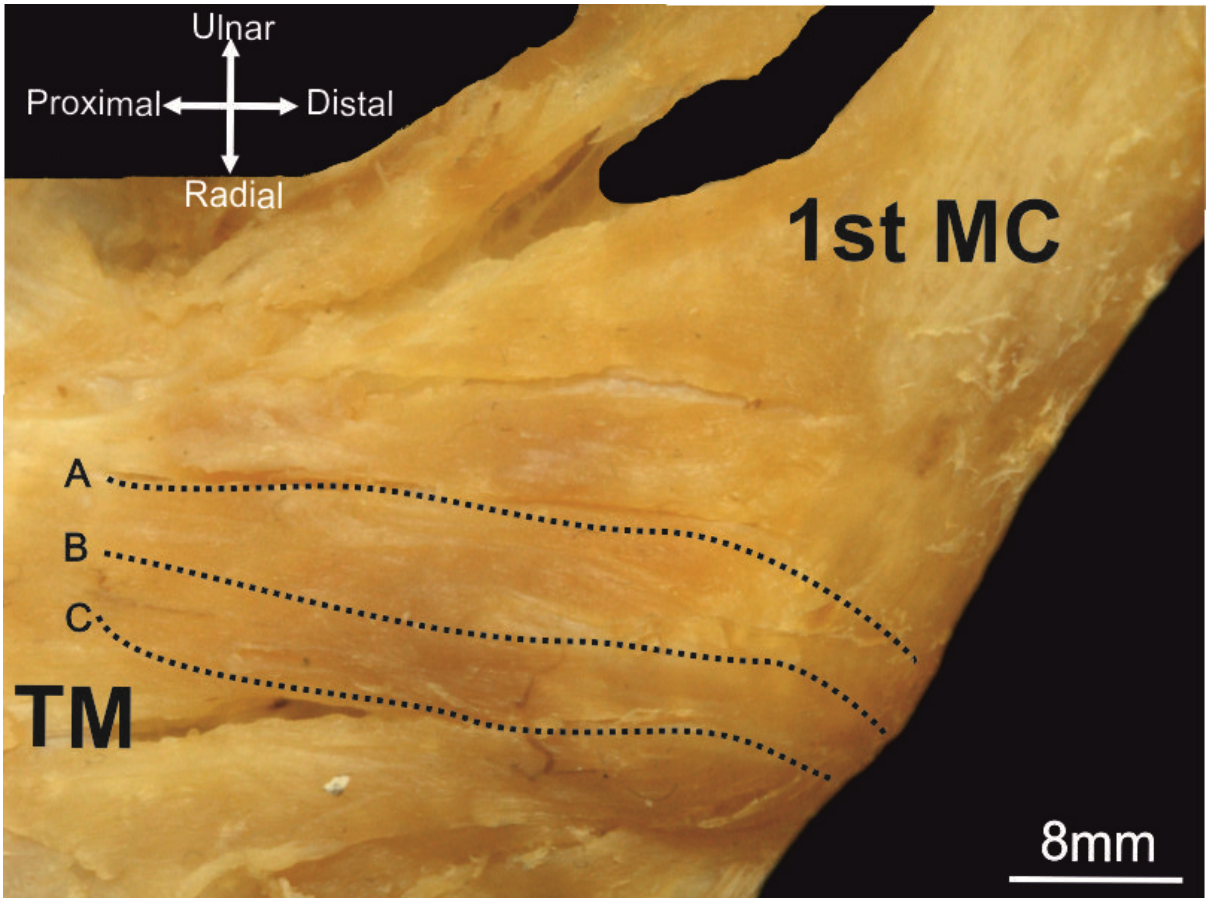

Figure 2.9: Anterior view of the posterior oblique ligament (POL). Embalmed donor.
Three lines were drawn horizontally to measure the length of the ligament; (A) ulnar line in the border of the ligament on the ulnar side, (B) middle line was drawn in the middle between both the border lines and (C) radial line is on the border of the ligament on the radial side.

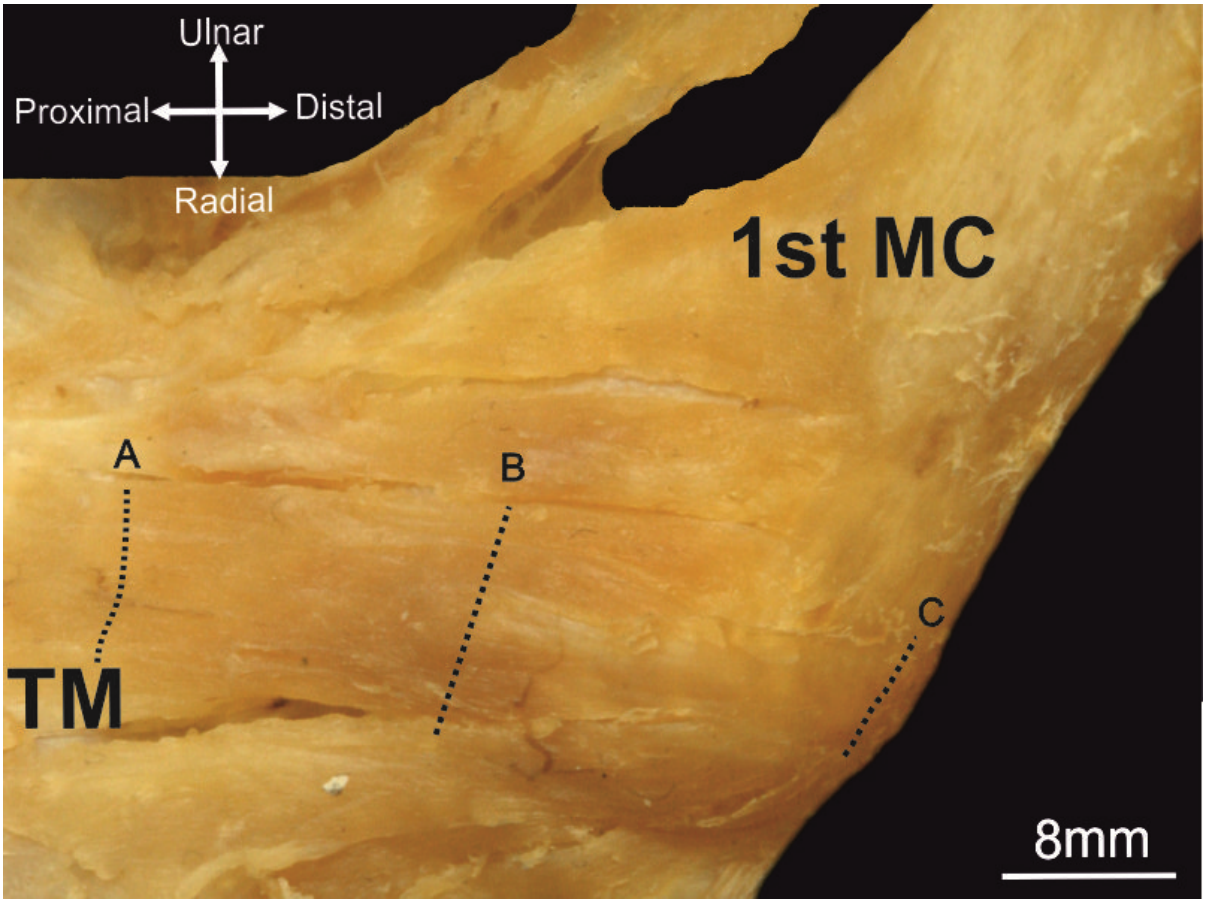

Figure 2.10: Anterior view of the posterior oblique ligament (POL). Embalmed donor.
Three lines were drawn vertically to measure the width of the ligament: (A) proximal line in the proximal attachment of the ligament, (B) mid-portion line was drawn in the middle between both lines (A, C) and (C) distal line is in the distal attachment of the ligament.

2.2.4 Photographic procedures

The specimens were placed on the fixed table under the camera (CANON) with their wrist and fingers immobilized by a fixation instrument, as mentioned previously. To obtain the neutral position, the pin between the first metacarpal and second metacarpal was removed, with the angle kept at 35˚. Furthermore, to obtain the full abduction position, the pin was inserted between the first metacarpal and second metacarpal at 60˚.

2.2.5 Statistical Analysis

For statistical analysis, 2 tailed paired *t*- test was used for comparisons between the length, width and area of the TMC ligaments through neutral 35˚and full abduction 60˚positions. The Student's *t* test (p> 0.5) was used to compare the

mean values between right- and left-hand specimens. Also, *t* tests were used to compare male and female groups. Four experiments were investigated for each specimen. A *t* test was applied for experiments on each specimen. There was no significant difference ($p > 0.05$, 0.89) between the four experiments in neutral and full abduction positions. Significance was set at *P of 0.05.*

The manual calliper was used to measure the 3rd MC and to index the measurement against hand size (Figure 2.11) (Munoz *et al.* 2001; Musgrave and Harneja 1978). The equation used for this procedure was

$$Index\ Ligament = \frac{\text{Raw Ligament}}{\text{Index Value (61.16)}}$$

Raw Ligament is the actual measuring of one of the TMC ligaments. *Index value* which is the mean of 3rd MC length was (61.16). The result of the equation presents by *index ligament* which is the accurate reading of each TMC ligaments against a variety of hand specimen sizes. The equation was applied in all TMC joint measurements (area, length and width) to confirm the result accurancy against different hands size.

In addition, intra-observer variation were recorded; this method is believed to give a more accurate, precise and reproducible measurement. One of the averages of the four experiments was then arbitrarily selected for further analysis.

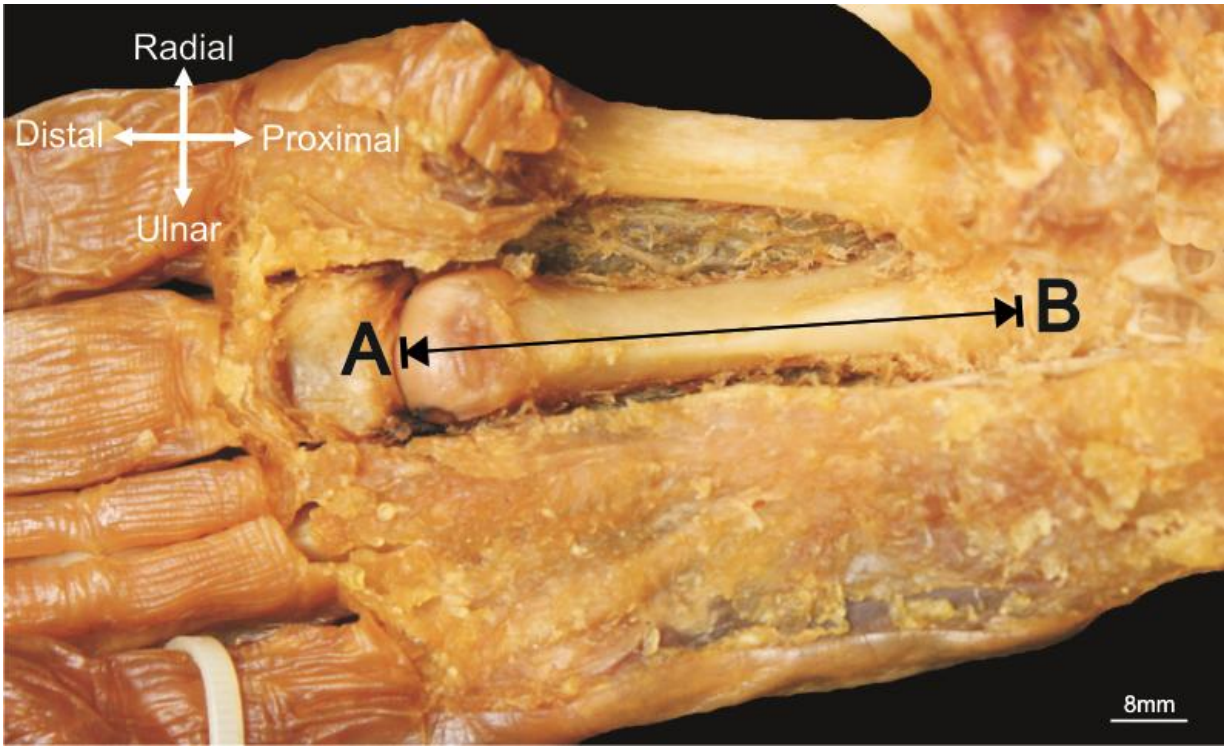

Figure 2.11: Anterior view of the 3rd MC bone of right hand. Embalmed donor. Showed the 3rd MC bone after removing; skin, muscles, blood vessels, and ligaments. (A) Head of the 3rd MC bone, (B) base of the 3rd MC bone, the line between head and base of 3rd MC bone presented the length of the bone which measured by manual calliper.

2.3 Results

2.3.1 Naming of the TMC ligaments

The naming of the TMC ligaments was investigated according to, firstly, the anatomical positions of the TMC ligaments throughout the planned 2D reconstruction in a three-dimensional virtual environment, which was achieved by Rhinoceros Version 5 software. The three planes X, Y and Z digitized, and the images of each ligament were rolled in a 3D format to obtain the accurate and precise placement of TMC ligaments through the TMC joint. Also, the distributions of the TMC ligaments in the coronal and transverse planes, around the first metacarpal, second metacarpal and trapezium bones, illustrated the directions of the ligament fibres and their attachments (Figures 2.12-2.13-2.14).

Secondly, the orientations of the attachment between the first metacarpal, second metacarpal and the trapezium bones were investigated by gross dissection, and the elongation of the TMC ligament fibres between the origin and the insertion was noted. Specifically, the ligaments were attached between the first metacarpal and trapezium bones because these ligaments have small length, width and thickness collected in narrow areas.

Thirdly, TMC ligaments were divided into two groups. The first group consist of the five ligaments attached between the first metacarpal and trapezium bones: the sAOL, deep anterior oblique ligament (dAOL), POL, UCL and DRL. The second group consist of the two ligaments attached between the first metacarpal and second metacarpal: the palmar intermetacarpal ligament (PIML) and DIML.

Fourthly, terminology was added, such as *palmar* and *trapeziometacarpal*, for some of the ligaments to be more precise and accurate. Some terminology was changed, such as *ulnar collateral ligament* (UCL) to *radial trapeziometacarpal ligament* (RTML). Other terminology was not changed, such as *the dorsal intermetacarpal ligament* (DIML) and *palmar intermetacarpal ligament* (PIML).

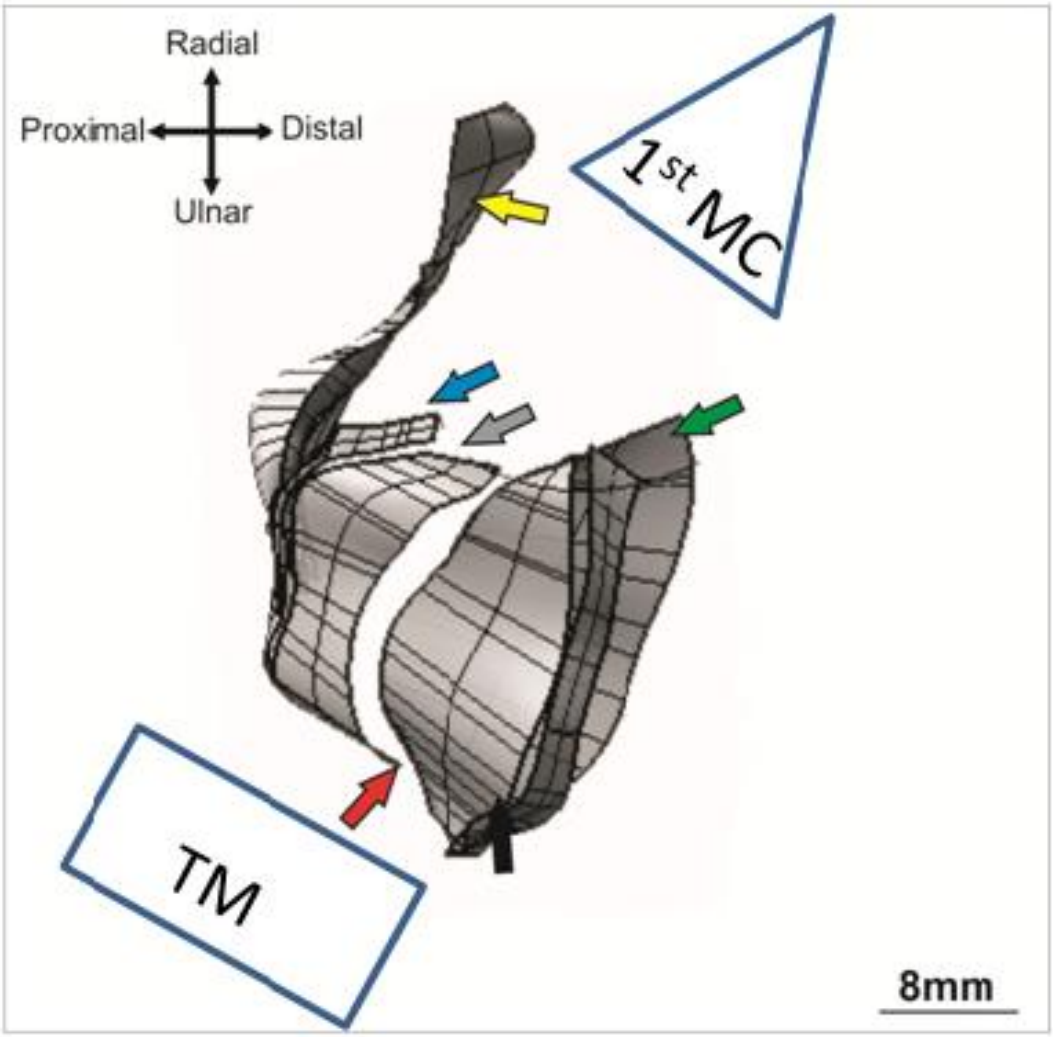

Figure 2.12: 2D reconstruction of the TMC ligaments in 3D virtual environment.

The figure illustrates the seven ligaments of the TMC joint crossing a coronal plane, the coloured arrows identifies the ligament; (Black Arrow) the radial trapeziometacarpal ligament (RTML), (Red Arrow) superficial part of the palmar trapeziometacarpal ligament (sPTML), (Green Arrow) deep part of the palmar trapeziometacarpal ligament ligament (dPTML), (Grey Arrow) palmo-ulnar trapeziometacarpal ligament (PUTML), (Blue Arrow) dorso-ulnar trapeziometacarpal ligament (DUTML), and (Yellow Arrow) dorsal intermetacarpal ligament (DIML). The orientation of the ligaments is 3D, the printing as 2D, so can be confusing to determine the actual plane.

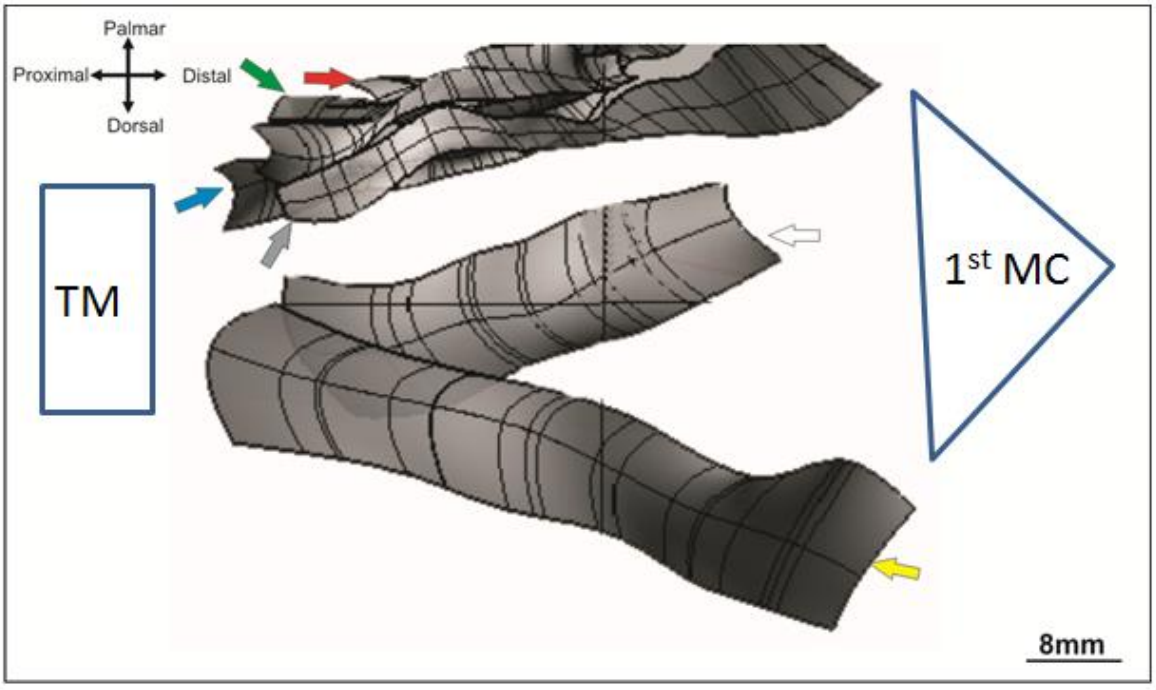

Figure 2.13: 2D reconstruction of the TMC ligaments in 3D virtual environment.

The figure illustrates the seven ligaments of the TMC joint crossing saggital plane, the coloured arrows identifies the ligament; (White Arrow) the palmar intermetacarpal ligament (PIML), (Red Arrow) superficial part of the palmar trapeziometacarpal ligament (sPTML), (Green Arrow) deep part of the palmar trapeziometacarpal ligament ligament (dPTML), (Grey Arrow) palmo-ulnar trapeziometacarpal ligament (PUTML), (Blue Arrow) dorso-ulnar trapeziometacarpal ligament (DUTML), and (Yellow Arrow) dorsal intermetacarpal ligament (DIML). The orientation of the ligaments is 3D, the printing as 2D, so can be confusing to determine the actual plane.

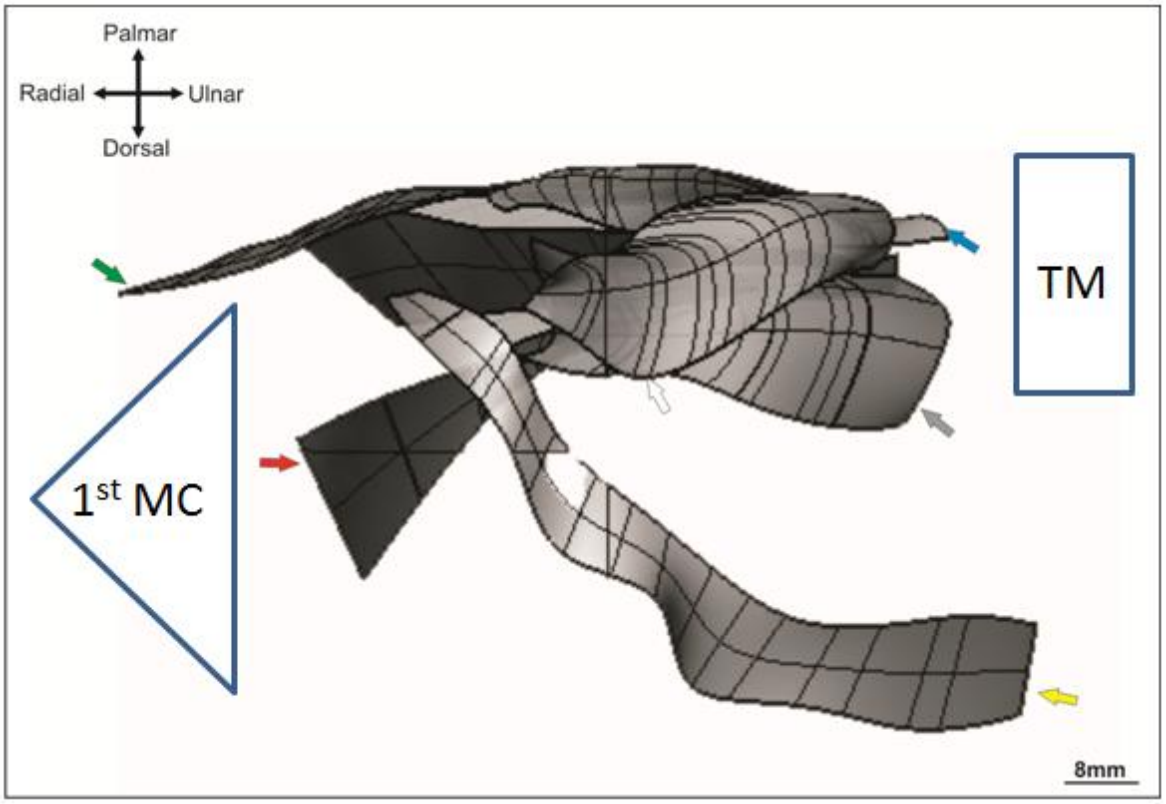

Figure 2.14: 2D reconstruction of the TMC ligaments in 3D virtual environment.

The figure illustrates the seven ligaments of the TMC joint crossing transverse plane, the coloured arrows identifies the ligament; (White Arrow) the palmar intermetacarpal ligament (PIML), (Red Arrow) superficial part of the palmar trapeziometacarpal ligament (sPTML), (Green Arrow) deep part of the palmar trapeziometacarpal ligament ligament (dPTML), (Grey Arrow) palmo-ulnar trapeziometacarpal ligament (PUTML), (Blue Arrow) dorso-ulnar trapeziometacarpal ligament (DUTML), and (Yellow Arrow) dorsal intermetacarpal ligament (DIML). The orientation of the ligaments is 3D, the printing as 2D, so can be confusing to determine the actual plane.

Old Name	New Name
Ulnar collateral ligament (UCL).	Radial trapeziometacarpal ligament (RTML).
Superficial anterior oblique ligament (sAOL).	Superficial palmar trapeziometacarpal ligament (sPTML).
Deep anterior oblique ligament (dAOL).	Deep palmar trapeziometacarpal ligament (dPTML).
Posterior oblique ligament (POL).	Palmo-ulnar trapeziometacarpal ligament (PUTML).
Dorso-radial ligament (DRL).	Dorso-ulnar trapeziometacarpal ligament (DUTML).

Table 2.1: Illustrate the old and new names of the TMC ligaments. Remaining two ligaments have not changed; palmar intermetacarpal ligament (PIML), and dorsal intermetacarpal ligament (DIML).

2.3.1.1 The radial trapeziometacarpal ligament (RTML)

2.3.1.1.1 Terminology description

RTML is the new name for the ulnar collateral ligament (UCL). R indicates the radio-palmar side of the first metacarpal bone, which is radial to the palmar trapeziometacarpal ligament (PTML), and radial to all TMC ligaments. Furthermore, it has a radial position through the coronal and transverse planes. TM indicates the attachment of this ligament, which is between the first metacarpal and trapezium bones. L is the abbreviation for the word *ligament*.

2.3.1.1.2 Attachment and fibre orientation

The radial trapeziometacarpal ligament (RTML) originates proximally from the distal edge of the transverse collateral ligament (TCL) and the trapezial ridge. This ligament, which forms a J- shaped pattern, attaches distally on the radio-palmar

side of the first metacarpal bone. It is located superficial and radial to the palmar trapeziometacarpal ligament (PTML). The fibre orientations of the RTML are oriented slightly oblique from proximo-radial to disto-radial.

2.3.1.1.3 The position producing ligament tension

The RTML is taut in a neutral position and may play a very important role in preventing dorsal subluxation of the first metacarpal.

2.3.1.2 The palmar trapeziometacarpal ligament (PTML)

The palmar trapeziometacarpal ligament (PTML) has two layers: superficial and deep.

2.3.1.2.1 The superficial palmar trapeziometacarpal ligament (sPTML)

2.3.1.2.1.1 Terminology description

The sPTML is the new name for the superficial anterior oblique ligament (sAOL). The s indicates the superficial layer of the (PTML). P indicates the palmar side of the TMC joint and palmar edge of the trapezium bone. TM indicates the attachment of this ligament, which is between the first metacarpal and trapezium bones. L is the abbreviation for the word *ligament*.

2.3.1.2.1.2 Attachment and fibre orientation

The superficial palmar trapeziometacarpal ligament (sPTML) has a large attachment proximal to the palmar edge of the trapezium bone. This ligament attaches distal to the palmar edge of the first metacarpal base. According to the position of this ligament, it has a very important role to play as a pivot for motion from any direction. Specifically, it involves the motion from the distal to proximal, such as flexion-extension and adduction-abduction of the TMC joint. The sPTML thins down at its edges to blend into the capsule itself, especially at its radial edge. The fibres of this ligament are oriented to run in a slightly oblique direction from proximo-radial to disto-ulnar.

2.3.1.2.1.3 The position producing ligament tension

The sPTML is taut in a neutral position, and it limits palmar subluxation with the deep palmar trapeziometacarpal ligament (dPTML).

2.3.1.3 The deep palmar trapeziometacarpal ligament (dPTML)

2.3.1.3.1.1 Terminology description

The new name, dPTML, is used for the deep anterior oblique ligament (dAOL). The d indicates the deep layer of the PTML. P indicates the palmar side of the TMC joint and palmar edge of the trapezium bone. TM indicates the attachment of this ligament, which is between the first metacarpal and trapezium bones. L is the abbreviation for the word *ligament*.

2.3.1.3.2 Attachment and fibre orientation

The dPTML originates proximally on the ulno-palmar edge of the trapezium bone. This ligament attaches distally on the ulno-palmar edge of the base of the first metacarpal. It is situated deep to the superficial palmar trapeziometacarpal ligament (sPTML) and is shorter than the sPTML. Also, it has been referred to as a beak, thicker and wider than the RTML. In addition, the dPTML fibre is oriented obliquely from proximo-radial to disto-ulnar and elongated within the concavity of the trapezium.

2.3.1.3.1.3 The position producing ligament tension

The dPTML is taut in a neutral position, and it assists the sPTML in preventing palmar subluxation.

2.3.1.4 The palmo-ulnar trapeziometacarpal ligament (PUTML)

2.3.1.4.1 Terminology description

PUTML is the new name for the posterior oblique ligament (POL). PU indicates the palmo-ulnar side of the TMC joint and the palmar edge of the first metacarpal and trapezium bones. TM indicates the attachment of this ligament,

which is between the first metacarpal and trapezium bones. L is the abbreviation for the word *ligament*.

2.3.1.4.2 Attachment and fibre orientation

The palmo-ulnar trapeziometacarpal ligament (PUTML) is proximal to the palmar and ulnar edge of the trapezium bone. This ligament attaches distally to the palmo-ulnar edge of the first metacarpal base and proximal to the dorso-ulnar trapeziometacarpal ligament (DUTML). The fibres of the PUTML run obliquely from the ulnar side of the trapezium to the ulnar base of the first metacarpal bones.

2.3.1.4.3 The position producing ligament tension

The PUTML is taut in the full abduction position.

2.3.1.5 The dorso-ulnar trapeziometacarpal ligament (DUTML)

2.3.1.5.1 Terminology description

DUTML is the new name for the dorso-radial ligament (DRL). DU indicates the dorsal side of the TMC joint and the dorso-ulnar edge of first trapezium bone.TM indicates the attachment of this ligament, which is between the first metacarpal and trapezium bones. L is the abbreviation for the word *ligament*.

2.3.1.5.2 Attachment and fibre orientation

The DUTML originates proximal to the dorso-radial tubercle of the trapezium bone and is attached to the dorso-ulnar edge of the first metacarpal bone. It is the thickest ligament attached to the trapezium bone and is on the radial side of the PUTML.

2.3.1.5.3 The position producing ligament tension

The DUTML is taut in full abduction.

2.3.1.6 The palmar intermetacarpal ligament (PIML)

2.3.1.6.1 Attachment and fibre orientation

The palmar intermetacarpal ligament (PIML) originates ulnar to the radio-palmar base of the second metacarpal and inserts on the radial side of the radio-palmar base of the first metacarpal. The PIML runs obliquely from the first metacarpal and second metacarpal bones.

2.3.1.6.2 The position producing ligament tension

The PIML is taut in full abduction, and it has a strong connection with the DIML between the first metacarpal and second metacarpal bones.

2.3.1.7 The dorsal intermetacarpal ligament (DIML)

2.3.1.7.1 Attachment and fibre orientation

The DIML originates ulnar to the dorso-radial tubercle of the second metacarpal bone and inserts radial to the dorso-ulnar side of the first metacarpal bone. This ligament is immediately adjacent to the palmar side of the extensor carpi radialis longus attachment. The dorsal first intermetacarpal artery, which is a branch of the radial artery, runs superficially to the DIML.

2.3.1.7.2 The position producing ligament tension

The DIML is taut when the TMC joint tenses towards the full abduction.

2.3.2 Ligamentous measurements

2.3.2.1 Areas

The differences in the area of the TMC ligaments between the neutral and full abduction positions were significant ($p < 0.05$). RTML $t = 6.81$, $df = 4$, $p = 0.002$, sPTML $t = 9.43$, $df = 4$, $p = 0.0001$, d PTML $t = 8.86$, $df = 5$, $p = 0.0003$, PIML $t = 7.4$, $df = 5$, $p = 0.0004$, PUTML $t = 10.07$, $df = 5$, $p = 0.0001$. The changes in the surface areas of the TMC ligaments decreased in the full abduction position, except the DUTML and DIML were not significantly different ($p > 0.05$). The sPTML, dPTML and PUTML increased in surface area in a full abduction position (Table 2.2).

As a consequence, most of the TMC ligaments changed significantly ($p < 0.05$) in the full abduction direction – specifically, the ligaments which are attached between the first metacarpal and trapezium bones – except for the DUTML did not change significantly ($p > 0.05$) (Figure 2.15). The surface areas of some ligaments, such as the RTML, DUTML, PIML and DIML, decreased in some cases. Furthermore, both ligaments which are attached between the first metacarpal and second metacarpal bones decreased in surface area.

The percentages of the decrease areas in order of largest to smallest ranked as follows: DIML > PIML > RTML > dPTML > DUTML (Figure 2.16). The percentages of the increase areas in order of largest to smallest ranked as follows: sPTML > PUTML (Figure 2.17).

The comparison between right and left specimens is shown in Figure (2.18-2.19). They were not significantly different ($p > 0.05$) in full abduction positions in all 13 pairs of embalmed specimens (Table 2.3), while there were significant differences ($p < 0.05$) between the male and female specimens, specifically in the DUTML $t = 9.41$, $df = 5$, $p = 0.002$, sPTML $t = 7.34$, $df = 4$, $p = 0.0001$, dPTML $t = 10.02$, $df = 5$, $p = 0.0003$ and PIML $t = 9.47$, $df = 4$, $p = 0.006$ (Figure 2.20-2.21 and Table 2.4).

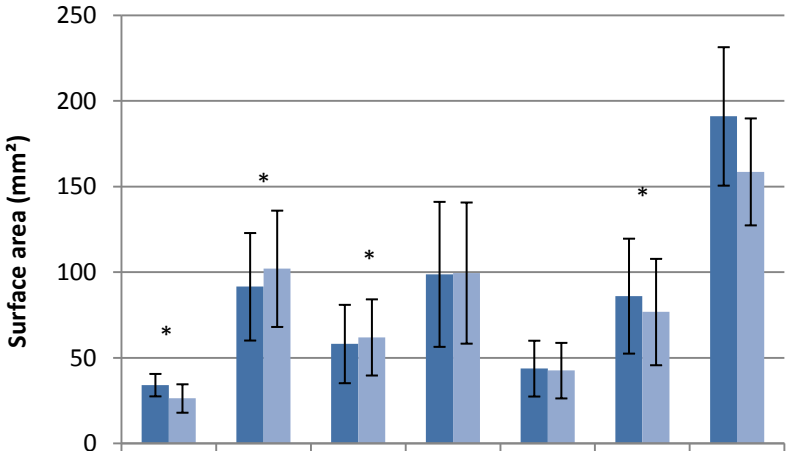

	RTML	sPTML	dPTML	PUTML	DUTML	PIML	DIML
Neutral position	34.16	91.59	58.18	98.84	43.81	86.13	191.05
Full abduction position	26.36	102.09	62.02	99.59	42.62	76.83	158.66

Figure 2.15: Average of the surface area of the TMC ligaments, described in millimetres squared (mean ± SD). The figure illustrates that DUTML and DIML did not change significantly ($p > 0.05$, 0.081) from neutral to full abduction positions. Unite: mm², N=50.

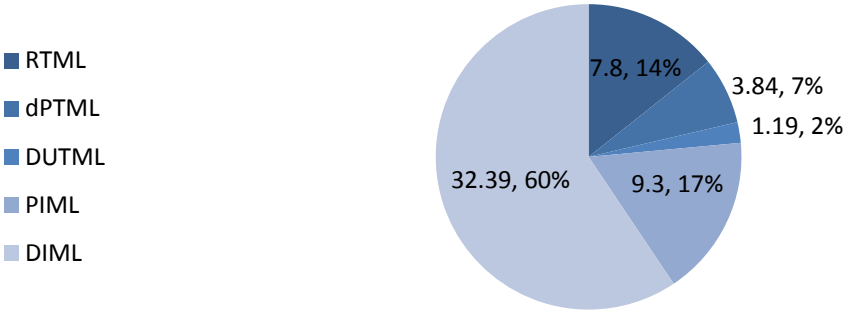

Figure 2.16: Percentages of the decrease in area of the RTML, dPTML, DUTML, PIML, and DIML in the full abduction position. The figure illustrates the maximum percentage was DIML, while the minimum percentage was DUTML 60%. Unit: mm², N=50.

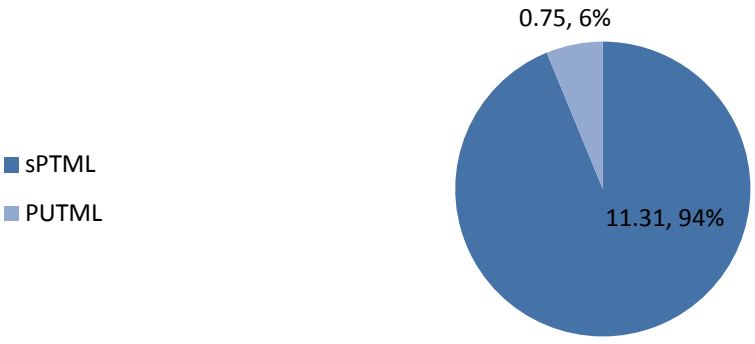

Figure 2.17: Percentages of the increase in area of the sPTML and PUTML in the full abduction position. The figure illustrates the maximum percentage was sPTML, while the minimum percentage was PUTML 6%. Unit: mm², N=50.

Ligaments	Neutral position mm²	SD of Neutral position	Full abduction position mm²	SD of Full abduction position	p value
RTML	34.16	± 6.5	26.36	± 8.3	0.002
sPTML	91.59	± 31.39	102.9	± 33.01	0.0001
dPTML	58.18	± 22.87	62.02	± 22.23	0.0003
PUTML	98.84	± 42.3	99.59	± 41.21	0.0001
DUTML	43.81	± 16.29	42.62	± 16.21	0.081
PIML	86.13	± 33.55	76.83	± 31.05	0.0004
DIML	191.05	± 40.42	158.66	±31.22	0.09

Table 2.2: Mean of the change in area of TMC ligaments and their standard deviation, p value, unit: mm², N=50.

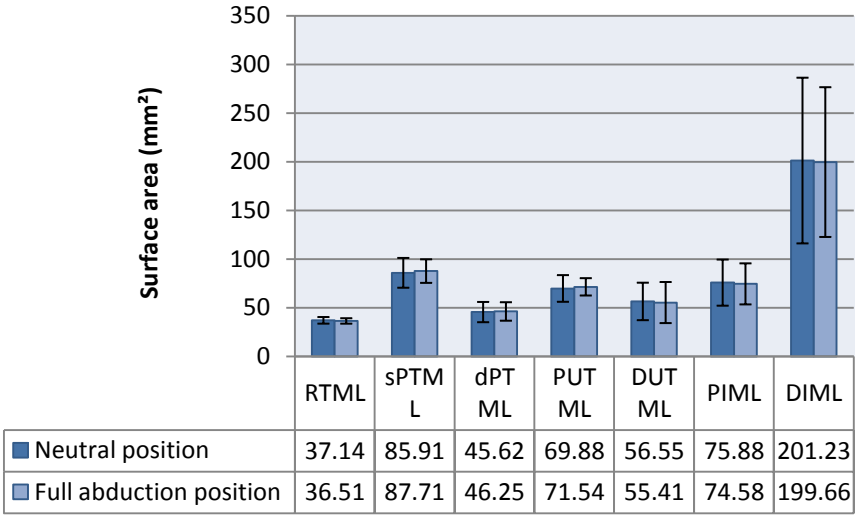

Figure 2.18: Average of the surface area of the TMC ligaments of right specimens, described in millimetres squared (mean ± SD). The figure illustrates that were not significantly different (p > 0.05) between the neutral and full abduction positions of right TMC ligaments. Unite: mm², N=13 pairs, 26 specimens.

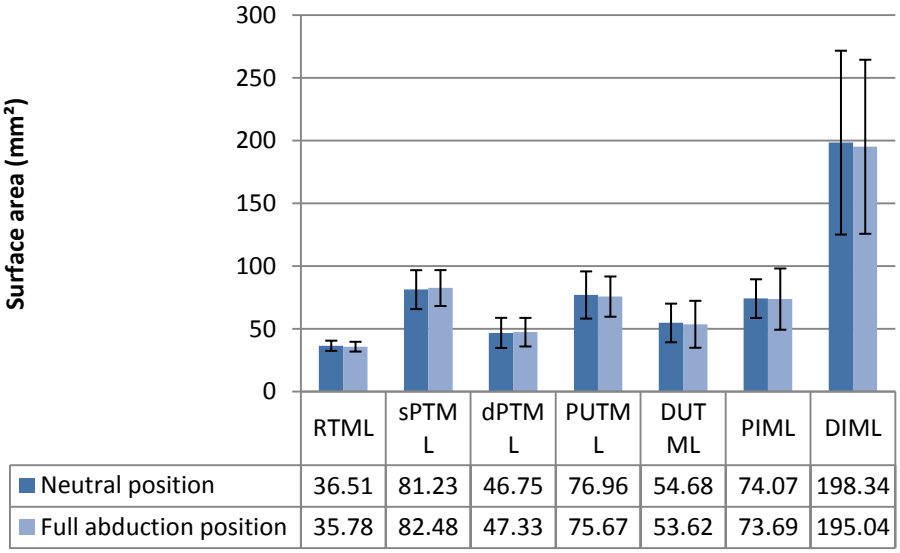

Figure 2.19: Average of the surface area of the TMC ligaments of left specimens, described in millimetres squared (mean ± SD). The figure illustrates that were not significantly different (p > 0.05) between the neutral and full abduction positions of left TMC ligaments. Unite: mm², N=13 pairs, 26 specimens.

Ligaments	Right specimens mm²		P value	Left specimens mm ²		P value
	Neutral position	Full abduction position		Neutral position	Full abduction position	
RTML	37.14 ±3.4	36.51 ± 4.07	0.06	36.51 ± 2.8	35.78 ± 3.9	0.08
sPTML	85.91 ± 15.3	87.23 ± 15.5	0.055	81.71 ±12.1	82.48 ± 14.3	0.06
dPTML	45.62 ± 10.4	46.75 ±12.01	0.074	46.25 ±9.5	47.33 ± 11.4	0.061
PUTML	69.88 ±13.7	71.96 ± 18.8	0.1	76.54 ± 8.9	75.67 ± 16.04	0.054
DUTML	56.55 ± 19.25	55.68 ± 15.4	0.095	54.41 ±21.1	53.62 ± 18.7	0.057
PIML	75.88 ± 23.7	74.07 ± 15.4	0.066	74.58 ± 21.08	70.69 ± 24.4	0.085
DIML	201.23 ± 85.07	199.34 ± 73.24	1.01	198.66 ± 76.9	195.04 ± 69.33	0.076

Table 2.3: Mean of the change in area of the TMC ligaments and their standard deviation in right and left specimens, p value, unit: mm², N=13 pairs, 26 specimens.

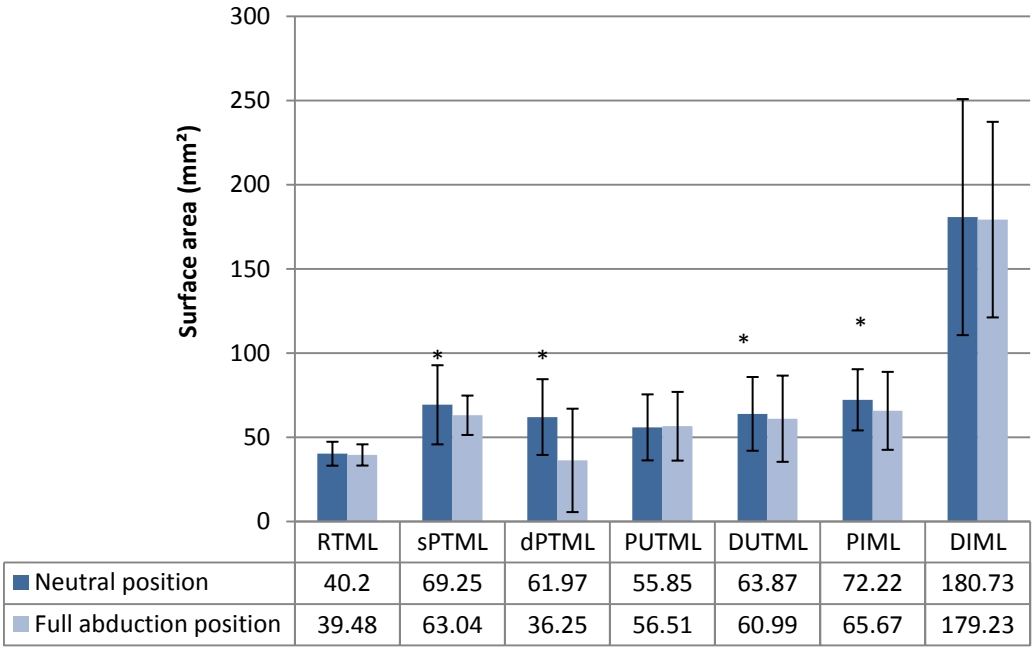

Figure 2.20: Average of the surface area of the TMC ligaments of male specimens, described in millimetres squared (mean ± SD). The figure illustrates that were significant differences ($p < 0.05$) between the neutral and full abduction positions, specifically in the DUTML, sPTML, dPTML and PIML. Unit: mm², N= 26.

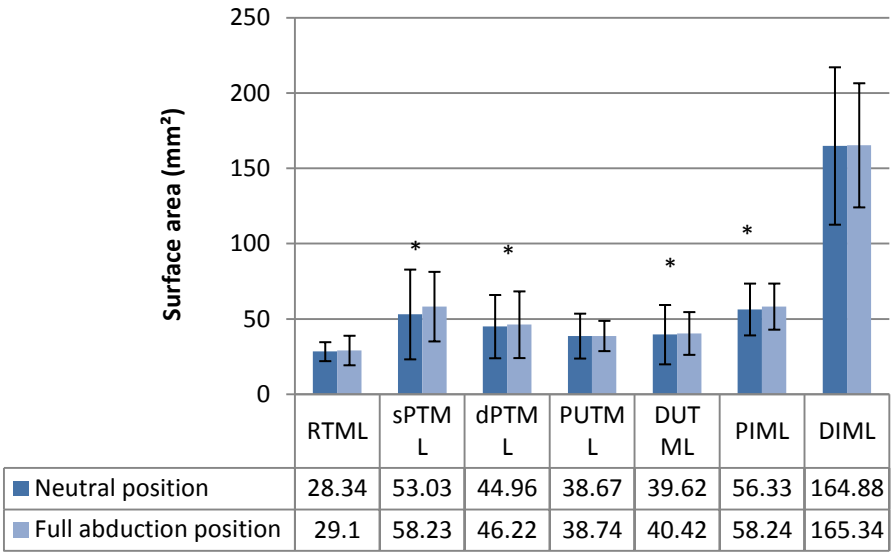

Figure 2.21: Average of the surface area of the TMC ligaments of female specimens, described in millimetres squared (mean ± SD). The figure illustrates that were significant differences ($p < 0.05$) between the neutral and full abduction positions, specifically in the DUTML, sPTML, dPTML and PIML. Unit: mm², N= 24.

Ligaments	Male specimens mm²		P value	Female specimens mm ²		P value
	Neutral position	Full abduction position		Neutral position	Full abduction position	
RTML	40.2 ±7.1	39.48 ± 6.3	1.02	28.34 ± 9.8	29.1 ± 6.3	0.08
sPTML	69.25 ± 23.5	63.04 ±11.07	0.0001	53.03 ± 23.1	58.23 ± 29.8	0.011
dPTML	61.97 ± 22.5	63.25 ±30.7	0.0003	44.96 ± 22.14	46.22 ±21.01	0.017
PUTML	55.85 ±19.6	56.51 ± 20.4	0.12	38.67 ± 10.04	38.74 ± 14.9	0.07
DUTML	63.87 ± 21.9	60.99 ±25.6	0.002	39.62 ± 14.2	40.42 ± 19.7	0.02
PIML	72.22 ± 18.18	65.67 ± 23.15	0.006	56.33 ± 15.3	58.24 ± 17.2	0.019
DIML	180.73 ± 70.1	179.23 ± 58.08	1.01	164.34 ± 52.25	165.88 ± 41.21	0.097

Table 2.4: Mean of the change in area of the TMC ligaments and their standard deviation in male and female specimens, p value, unit: mm², N= 50, 26 male and 24 female specimens.

2.3.2.2 Lengths

There were significant differences ($p < 0.05$) in the sPTML $t = 6.3$, $df = 4$, $p = 0.01$, PUTML $t = 8.8$, $df = 5$, $p = 0.03$ and DUTML $t = 6.7$, $df = 4$, $p = 0.07$ in the full abduction position, while there were no significant differences ($p > 0.05$) in the RTML, dPTML, PIML and DIML (Figure 2.22 and Table 2.5). The RTML

decreased in length in the full abduction position, which means the ligament had relaxed in this position. In contrast, the PUTML, DUTML, PIML and DIML had streched in length (taut) in the full abduction position.

The percentages of the elongation in order of largest to smallest were as follows: DIML > PIML > DUTML > PUTML (Figure 2.23). The percentages of the relaxation in order of largest to smallest were as follows: RTML > sPTML > dPTML (Figure 2.24).

The comparison between right and left shown in (Figure 2.25-2.26), and significant differences ($p < 0.05$) were shown in only two ligaments, the PIML $t = 5.1$, $df = 6$, $p = 0.002$ and DIML $t = 7.04$, $df = 6$, $p = 0.004$, whereas significant differences ($p > 0.05$) were not noted in the remaining TMC ligaments (Table 2.6). Moreover, the comparison between genders indicated no significant differences ($p > 0.05$) (Figure 2.27-2.28 and Table 2.7).

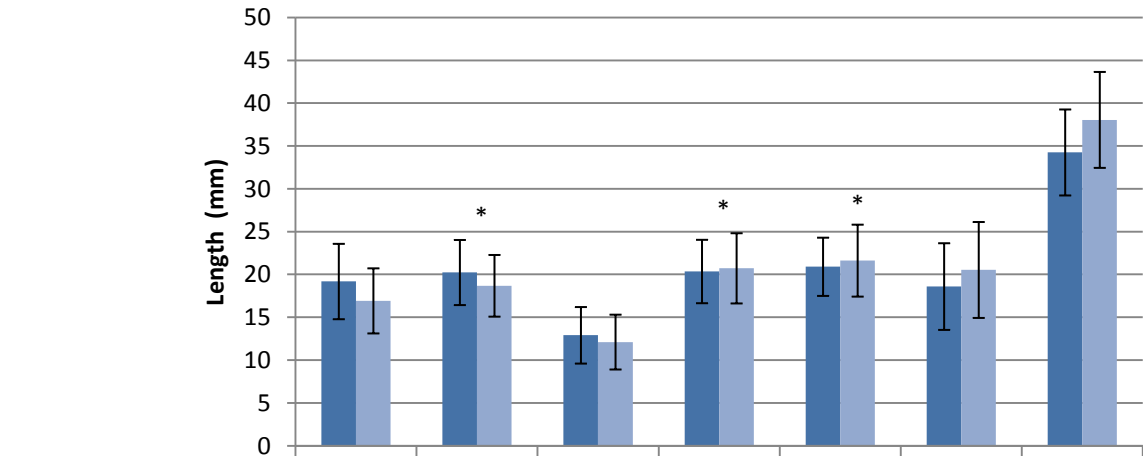

	RTML	sPTML	dPTML	PUTML	DUTML	PIML	DIML
Neutral position	19.18	20.23	12.9	20.35	20.9	18.59	34.25
Full abduction position	16.92	18.68	12.11	20.72	21.62	20.53	38.05

Figure 2.22: Length measurement of the TMC ligaments with their standard deviation. The figure illustrates that the RTML and sPTML relaxed (length decreased) from neutral to full abduction positions, while dPTML, PUTML, DUTML, PIML, and DIML stretched (length increased) from neutral to full abduction positions. Unite: mm, N=50.

Ligaments	Neutral position mm	SD of Neutral position	Full abduction position mm	SD of Full abduction position	P value
RTML	19.18	± 4.4	16.92	±3.8	0.07
sPTML	20.23	± 3.8	18.68	± 3.6	0.01
dPTML	12.9	± 3.3	12.11	± 3.2	0.084
PUTML	20.35	± 3.7	20.72	± 4.1	0.03
DUTML	20.09	± 3.4	21.62	± 4.2	0.07
PIML	18.59	± 5.06	20.53	± 5.6	0.098
DIML	34.25	± 5.02	38.05	± 5.6	0.061

Table 2.5: Mean of the taut and relaxed state of the TMC ligaments and their standard deviation, p value, unit: mm, N= 50.

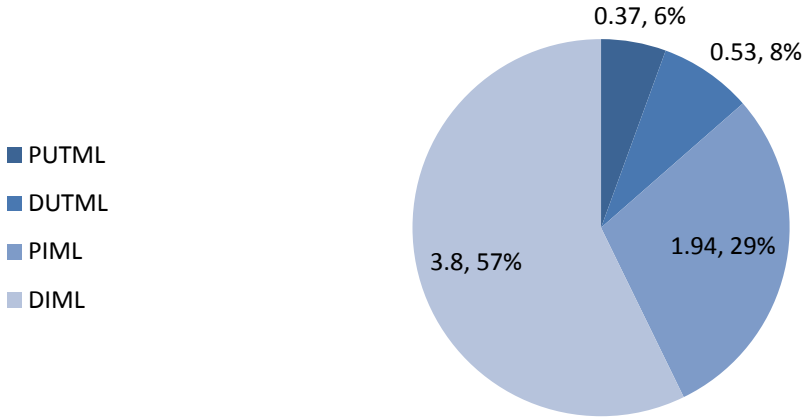

Figure 2.23: Percentages of the elongation of the PUTML, DUTML, PIML and DIML in the full abduction position. The figure illustrates the maximum percentage was DIML 57%, while the minimum percentage was PUTML 6%. Unit: mm,N=50.

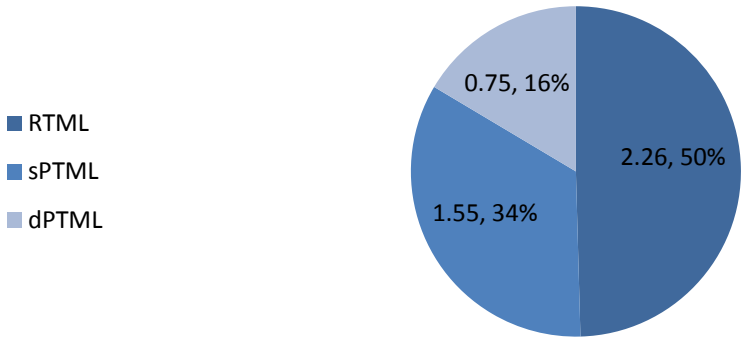

Figure 2.24: The percentages the relaxation of the RTML, sPTML and dPTML in the full abduction position. The figure illustrates the maximum percentage was RTML 50%, while the minimum percentage was dPTML 16%. Unit: mm, N=50.

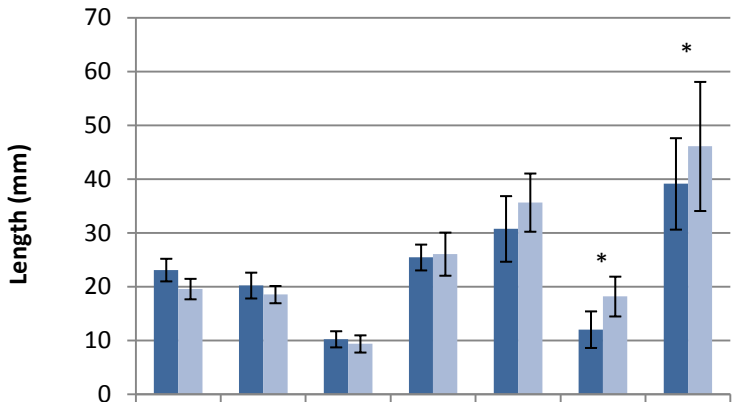

	RTML	sPTML	dPTML	PUTML	DUTML	PIML	DIML
Neutral position	23.1	20.22	10.23	25.44	30.75	12.023	39.12
Full abduction position	19.57	18.54	9.37	26.06	35.64	18.18	46.08

Figure 2.25: Comparison of right specimens in length measurement of the TMC ligaments with their standard deviation. The figure illustrates that there were significant differences ($p < 0.05$) shown in only two ligaments, the PIML and DIML, whereas there were not significant differences ($p > 0.05$) noted in the remaining TMC ligaments. Unite: mm, N=13 pairs, 26 specimens.

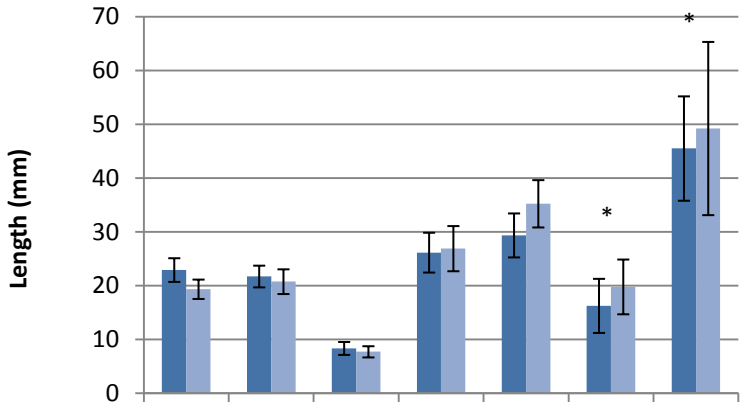

	RTML	sPTML	dPTML	PUTML	DUTML	PIML	DIML
Neutral position	22.9	21.7	8.33	26.14	29.34	16.24	45.49
Full abduction position	19.33	20.74	7.7	26.88	35.22	19.77	49.21

Figure 2.26: Comparison of left specimens in length measurement of the TMC ligaments with their standard deviation. The figure illustrates that there were significant differences ($p < 0.05$) shown in only two ligaments, the PIML and DIML, whereas there were not significant differences ($p > 0.05$) noted in the remaining TMC ligaments. Unite: mm, N=13 pairs, 26 specimens.

Ligaments	Right specimens mm		P value	Left specimens mm		P value
	Neutral position	Full abduction position		Right specimens	Full abduction position	
RTML	23.1 ± 2.1	19.57 ± 1.9	0.076	22.9 ± 2.2	19.33 ± 1.8	0.062
sPTML	20.22 ± 2.4	18.54 ± 1.6	0.098	21.7 ± 2.02	20.74 ± 2.3	0.09
dPTML	10.23 ± 1.5	9.37 ± 1.6	0.23	8.33 ± 1.2	7.7 ± 1.04	0.98
PUTML	25.44 ± 2.4	26.06 ± 4.01	0.21	26.14 ± 3.7	26.88 ± 4.2	0.10
DUTML	30.75 ± 6.1	35.64 ± 5.41	0.1	29.34 ± 4.09	35.22 ± 4.4	0.10
PIML	12.23 ± 3.4	18.18 ± 3.7	0.002	16.24 ± 5.03	19.77 ± 5.09	0.024
DIML	39.12 ± 8.5	46.08 ± 12.0	0.004	45.49 ± 9.7	49.21 ± 16.1	0.003

Table 2.6: Mean of the taut and relaxed state between right and left specimens of the TMC ligaments and their standard deviation. Unite: mm, N=13 pairs, 26 specimens.

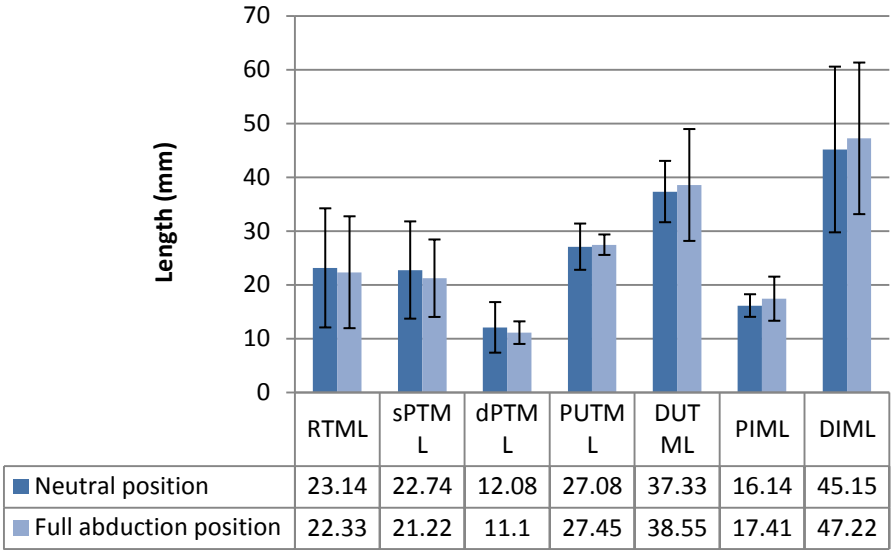

Figure 2.27: Comparison between neutral and full abduction position of male specimens in length measurement of the TMC ligaments with their standard deviation. The figure illustrates that there were not significant differences ($p < 0.05$) between the male and female specimens. Unit: mm, N=26.

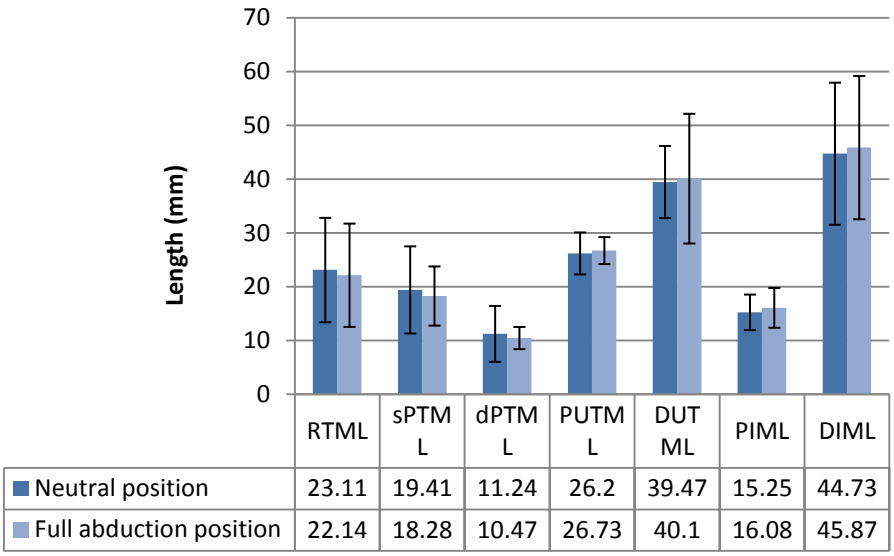

Figure 2.28: Comparison between neutral and full abduction position of female specimens in length measurement of the TMC ligaments with their standard deviation. The figure illustrates that there were not significant differences ($p < 0.05$) between the male and female specimens. Unit: mm, N= 24.

Ligaments	Male specimens mm		p value	Female specimens mm		p value
	Neutral position	Full abduction position		Neutral position	Full abduction position	
RTML	23.14 ± 11.07	22.33 ± 10.4	0.09	23.11 ± 9.7	22.14 ± 9.6	0.076
sPTML	22.74 ± 9.04	21.22 ± 7.2	0.08	19.41 ± 8.1	18.28 ± 5.5	0.098
dPTML	12.18 ± 4.7	11.1 ± 2.1	0.1	11.24 ± 5.2	10.47 ± 2.06	0.063
PUTML	27.08 ± 4.3	27.45 ± 1.9	0.064	26.2 ± 3.9	26.73 ± 2.5	0.072
DUTML	37.33 ± 5.7	38.55 ± 10.4	0.097	39.47± 6.7	40.1 ± 12.06	0.081
PIML	16.14 ± 2.1	17.41 ± 4.1	0.07	15.25 ± 3.3	16.08 ± 3.7	0.077
DIML	45.15 ± 15.4	47.22 ± 14.09	0.087	44.73 ± 13.21	45.87 ± 13.32	0.064

Table 2.7: Mean of the taut and relaxed state between male and female specimens of the TMC ligaments and their standard deviation, p value, unit: mm, N= 50, 26 male and 24 female specimens.

2.3.2.3 Width

There were significant differences ($p < 0.05$) in PUTML $t = 10.8$, $df = 6$, $p = 0.009$, DUTML $t = 9.45$, $df = 5$, $p = 0.0023$, PIML $t = 10.01$, $df = 5$, $p = 0.02$ and DIML $t = 9.9$, $df = 6$, $p = 0.035$, while the RTML, sPTML, and dPTML were not significantly different ($p > 0.05$) (Figure 2.29 and Table 2.8). The percentages of

widening in order of largest to smallest ranked as follows: d PTML > sPTML > RTML (Figure 2.30). The percentages of thinning in order of largest to smallest ranked as follows: PIML > DIML > PUTML > DUTML (Figure 2.31).

Also , the comparison between right and left specimens showed no significant differences (p > 0.05) in all TMC ligaments (Figure 2.32-2.33 and Table 2.9), while comparing between males and females indicated that some TMC ligaments, such as the PIML t = 10.2, df = 4, p = 0.002, DIML t = 9.74, df = 5, p = 0.004 , PUTML t = 9.47, df = 5, p = 0.008 and RTML t = 6.14, df = 4, 0.003 were significantly different (p< 0.05) (Figure 2.34-2.35 and Table 2.10).

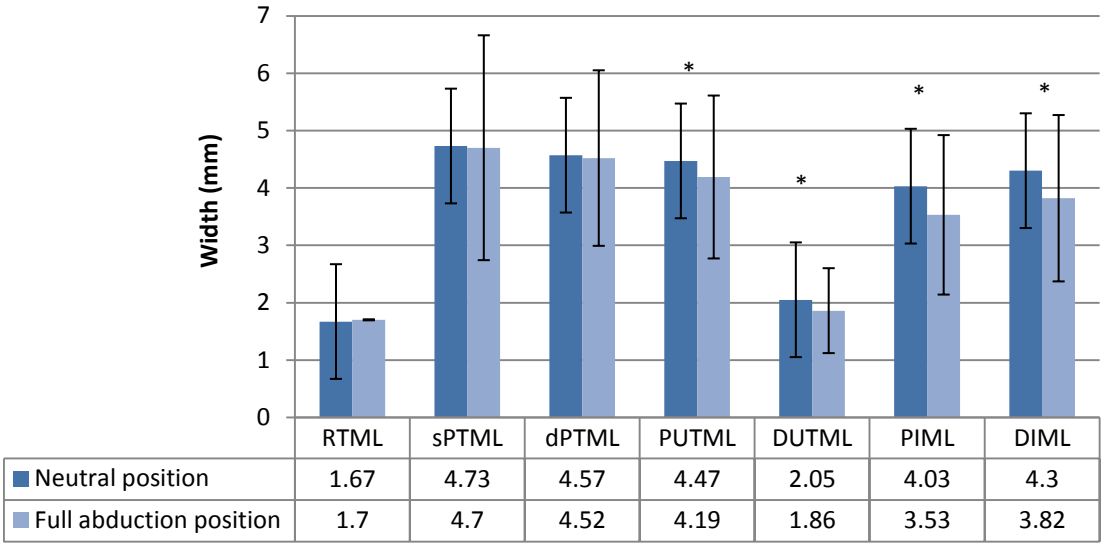

Figure 2.29: Width measurement of the TMC ligaments with their standard deviation. The figure illustrates that the PUTML, DUTML, PIML and DIML thined (width decreased) from neutral to full abduction positions, while the RTML, sPTML, and dPTML were not changed from neutral to full abduction positions. Unite: mm, N=50.

Ligaments	Neutral position mm	SD of neutral position	Full abduction position mm	SD of Full abduction position	p value
RTML	1.67	± 0.68	1.7	± 0.094	0.088
sPTML	4.73	± 1.88	4.8	84 ±1.53	0.079
dPTML	4.57	± 1.37	4.	± 1.96	0.058
PUTML	4.47	± 1.6	4.19	± 1.42	0.009
DUTML	2.06	± 0.89	1.86	± 0.74	0.023
PIML	4.03	± 1.38	3.52	± 1.39	0.020
DIML	4.3	± 1.48	3.82	± 1.45	0.035

Table 2.8: Mean of thinning and widening of the TMC ligaments and their standard deviation, p value, Unite: mm, N=50.

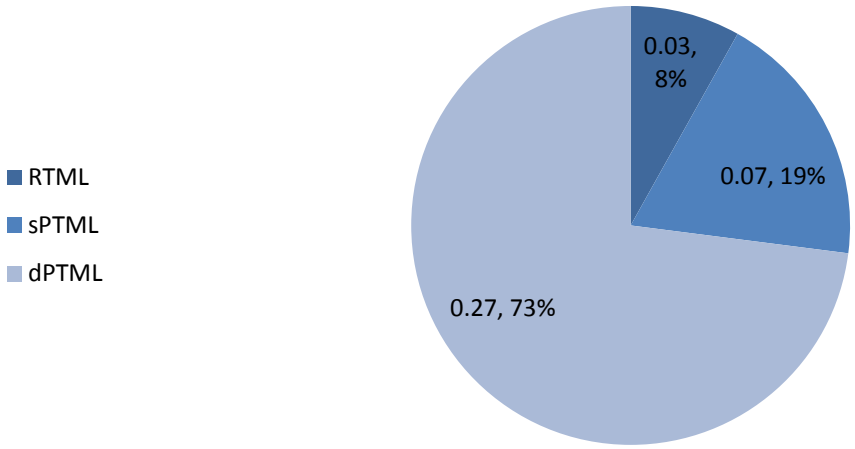

Figure 2.30: Percentages of widening of the RTML, sPTML and dPTML in the full abduction position. The figure illustrates the maximum percentage was dPTML 73%, while the minimum percentage was RTML 8%. Unit: mm, N=50.

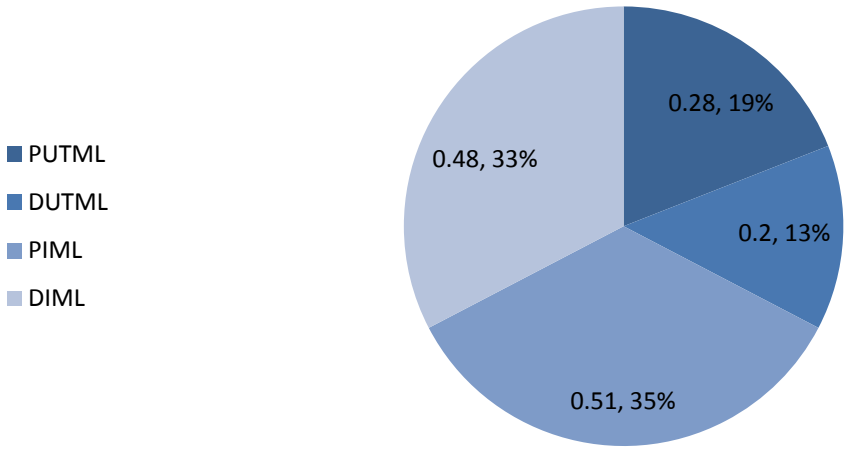

Figure 2.31: Percentages of thinning of the PUTML, DUTML, PIML and DIML in the full abduction position. The figure illustrates the maximum percentage was PIML 35%, while the minimum percentage was DUTML 13%. Unit: mm, N=50.

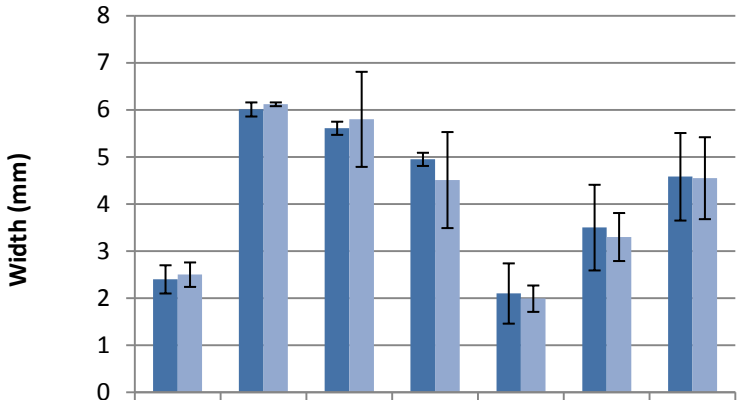

	RTML	sPTML	dPTML	PUTML	DUTML	PIML	DIML
Neutral position	2.4	6.01	5.61	4.95	2.1	3.5	4.58
Full abduction position	2.5	6.12	5.8	4.51	1.99	3.3	4.55

Figure 2.32: Comparison between neutral and full abduction positions of right specimens in width measurements of the TMC ligaments with their standard deviation. The figure illustrates that there were not significantly different ($p > 0.05$) of right specimens in full abduction positions of TMC ligaments. Unite: mm, N=13 pairs, 26 specimens.

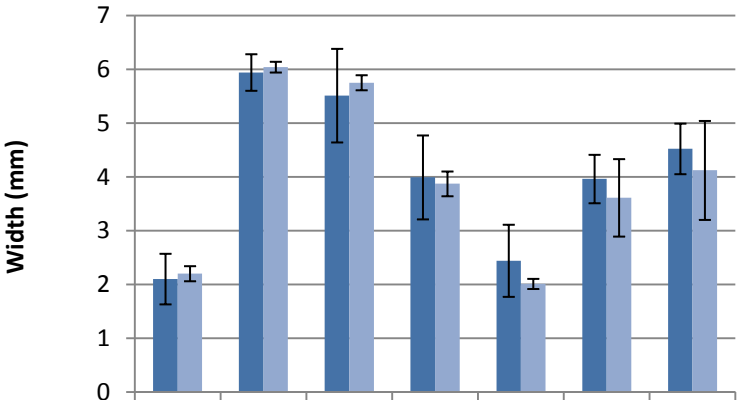

	RTML	sPTML	dPTML	PUTML	DUTML	PIML	DIML
Neutral position	2.1	5.94	5.51	3.99	2.44	3.96	4.52
Full abduction position	2.2	6.04	5.75	3.87	2.01	3.61	4.12

Figure 2.33: Comparison between neutral and full abduction positions of left specimens in width measurements of the TMC ligaments with their standard deviation. The figure illustrates that there were not significantly different ($p > 0.05$) of left specimens in full abduction positions of TMC ligaments. Unite: mm, N=13 pairs, 26 specimens.

Ligaments	Right specimens mm		p value	Left specimens mm		p value
	Neutral position	Full abduction position		Neutral position	Full abduction position	
RTML	2.4 ± 0.3	2.5 ± 0.26	0.061	2.1 ± 0.47	2.2 ± 0.41	0.054
sPTML	6.01 ± 0.15	6.12 ± 0.04	0.057	5.94 ± 0.34	6.04 ±0.1	0.059
dPTML	5.61 ± 0.14	5.8 ± 1.01	0.098	5.51 ± 0.87	5.75 ± 0.14	0.060
PUTML	4.95 ± 0.74	4.51 ± 1.02	0.064	3.99 ± .087	3.87 ± 0.23	0.072
DUTML	2.1 ± 0.64	1.99 ± 0.28	0.074	2.44 ± 0.67	2.01 ± .094	0.097
PIML	3.5 ± 0.91	3.3 ± 0.51	0.10	3.96 ± 0.45	3.61 ± 0.72	0.088
DIML	4.58 ± 0.93	4.55 ± 0.87	0.12	4.52 ± 0.47	4.12 ± 0.96	0.064

Table 2.9: Mean of thinning and widening between right and left specimens of the TMC ligaments and their standard deviation, p value, Unite: mm, N=13 pairs, 26 specimens.

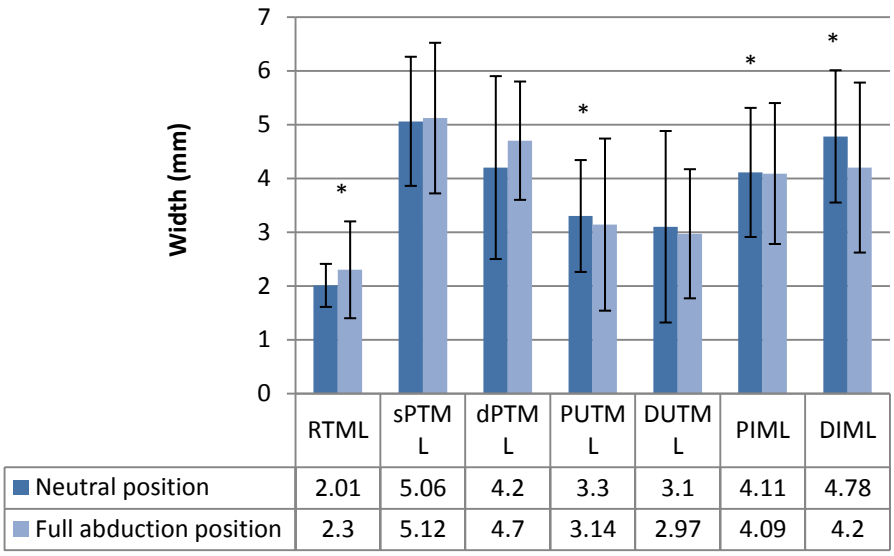

Figure 2.34: Comparison between neutral and full abduction position of male specimens in width measurements of the TMC ligaments with their standard deviation. The figure illustrates that the PIML, DIML, PUTML and RTML were significantly different ($p < 0.05$), while sPTML, dPTML, and DUTML were not changed siginficantly ($p>0.05$). Unit: mm, N= 26.

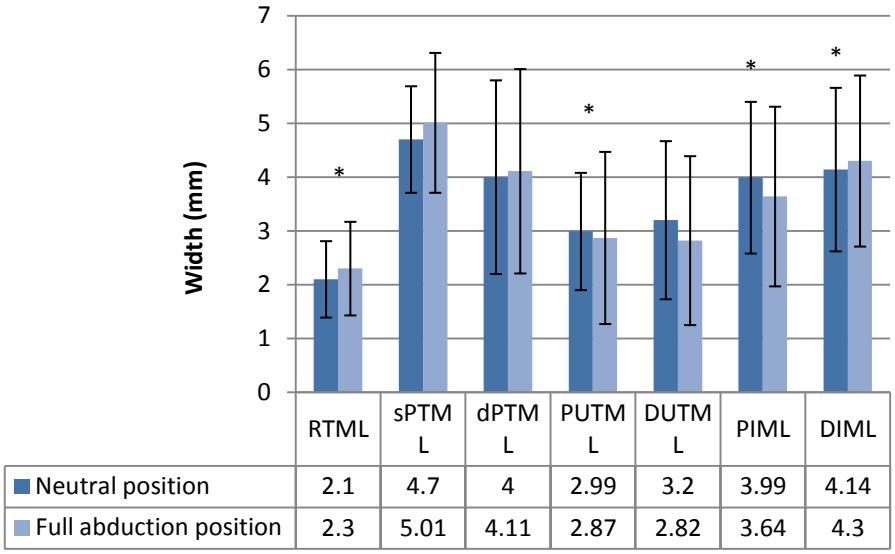

Figure 2.35: Comparison between neutral and full abduction position of female specimens in width measurements of the TMC ligaments with their standard deviation. The figure illustrates that the PIML, DIML, PUTML and RTML were significantly different ($p < 0.05$), while sPTML, dPTML, and DUTML were not changed siginficantly ($p>0.05$). Unit: mm, N= 24.

Ligaments	**Male specimens mm**		**p value**	**Female specimens mm**		**p value**
	Neutral position	**Full abduction position**		**Neutral position**	**Full abduction position**	
RTML	2.01 ± 0.4	2.3 ± 0.9	0.003	2. 1 ± 0.71	2.3 ± 0.87	0.004
sPTML	5.06 ± 1.2	5.12 ± 1.4	0.057	4.7 ± 0.99	5.01 ±1.3	0.054
dPTML	4.2 ± 1.7	4.7 ± 1.1	0.1	4 ± 1.8	4.11 ± 1.9	0.061
PUTML	3.3 ± 1.04	3.14 ± 1.6	0.023	2.99 ±1.09	2.87 ± 1.6	0.008
DUTML	3.1 ± 1.78	2.97 ± 1.2	0.09	3.2 ± 1.47	2.82 ± 1.57	0.078
PIML	4.11 ± 1.2	4.09 ± 1.31	0.03	3.99 ±1.14	3.64 ± 1.67	0.002
DIML	4.78 ± 1.23	4.2 ± 1.58	0.043	4.14 ±1.52	4.30 ± 1.59	0.004

Table 2.10: Mean of thinning and widening between male and female specimens of the TMC ligaments and their standard deviation. Unit: mm, N= 50, 26 male and 24 female specimens.

2.3.3 Index measurement producers

2.3.3.1 Area

Statistical analysis of the data shown no significant difference between Raw and Index ligaments ($p > 0.05$, 0.35) in neutral and full abduction positions (Figures 2.36-2.37).

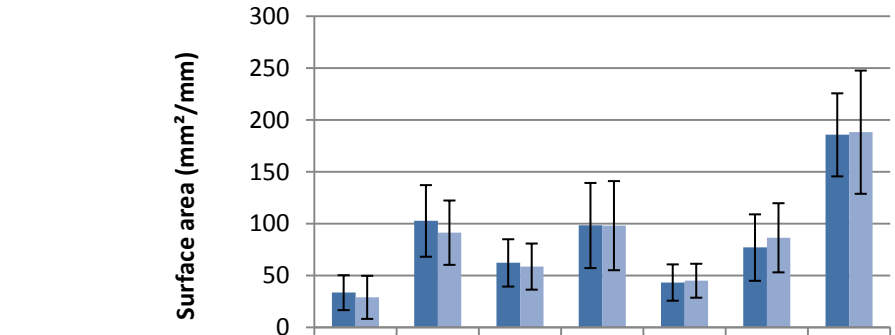

	RTML	sPTML	dPTML	PUTML	DUTML	PIML	DIML
Raw Ligament in Neutral position	33.65	102.77	62.33	98.35	43.42	77.1	185.69
Raw Ligament in Full abduction position	29.16	91.45	58.78	98.21	45.16	86.54	188.25

Figure 2.36: Raw ligament of area in neutral and full abduction positions with their standard deviation. The actual reading of area (mm²) in neutral position of all TMC ligaments. Unit: mm², N=50.

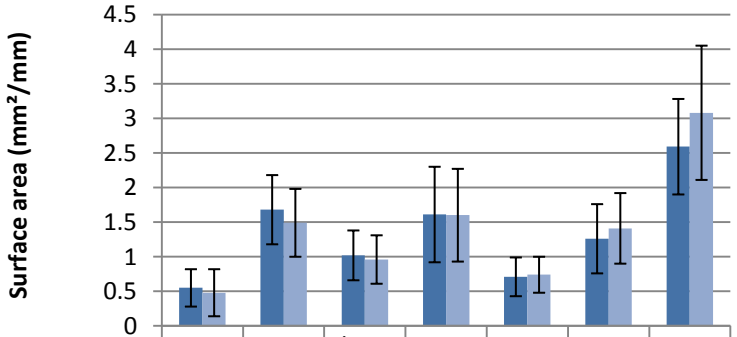

	RTML	sPTML	dPTML	PUTML	DUTML	PIML	DIML
IndexLigament in Neutral position	0.55	1.68	1.02	1.61	0.71	1.26	2.59
Index Ligament in Full abduction position	0.48	1.49	0.96	1.6	0.74	1.41	3.08

Figure 2.37: Index ligament of area in neutral and full abduction positions with their standard deviation. The index ligament was indexed against the length (mm) of the third metacarpal. Unit: mm², N=50.

2.3.3.2 Length

Statistical analysis of the data shown no significant difference between Raw and Index ligaments ($p > 0.05$, 0.37) in neutral and full abduction positions (Figures 2.38-2.39).

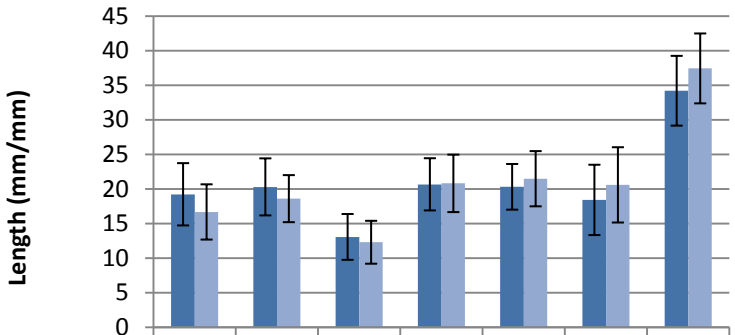

	RTML	sPTML	dPTML	PUTML	DUTML	PIML	DIML
Raw Ligament in Neutral position	19.23	20.3	13.07	20.67	20.31	18.42	34.19
Raw Ligament in Full abduction position	16.68	18.6	12.3	20.81	21.48	20.59	37.42

Figure 2.38: Raw ligament of length in neutral and full abduction positions with their standard deviation. The actual reading of length (mm) in neutral position of all TMC ligaments. Unit: mm, N=50.

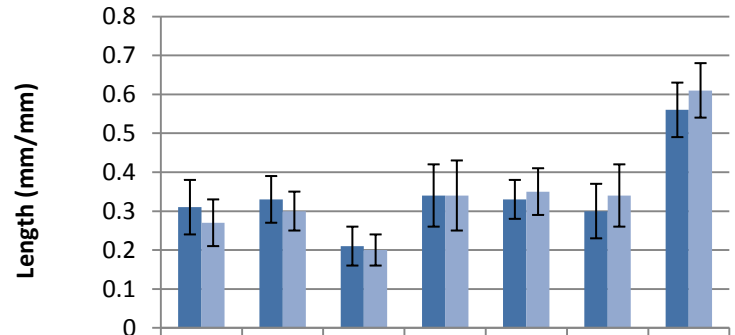

	RTML	sPTML	dPTML	PUTML	DUTML	PIML	DIML
IndexLigament in Neutral position	0.31	0.33	0.21	0.34	0.33	0.3	0.56
Index Ligament in Full abduction position	0.27	0.3	0.2	0.34	0.35	0.34	0.61

Figure 2.39: Index ligament of length in neutral and full abduction positions with their standard deviation. The index ligament was indexed against the length (mm) of the third metacarpal. Unit: mm, N=50.

2.3.3.3 Width

Statistical analysis of the data shown no significant difference between Ligaments data and value data ($p > 0.05$, 0.41) in neutral and full abduction positions (Figures 2.40-2.41).

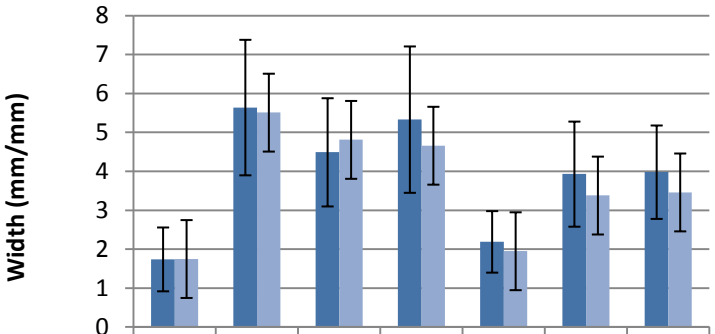

	RTML	sPTML	dPTML	PUTML	DUTML	PIML	DIML
Raw Ligament in Neutral position	1.74	5.64	4.49	5.33	2.19	3.93	3.98
Raw Ligament in Full abduction position	1.75	5.51	4.81	4.66	1.95	3.38	3.46

Figure 2.40: Raw ligament of width in neutral and full baduction positions with their standard deviation. The actual reading of width (mm) in neutral position of all TMC ligaments. Unit: mm, N=50.

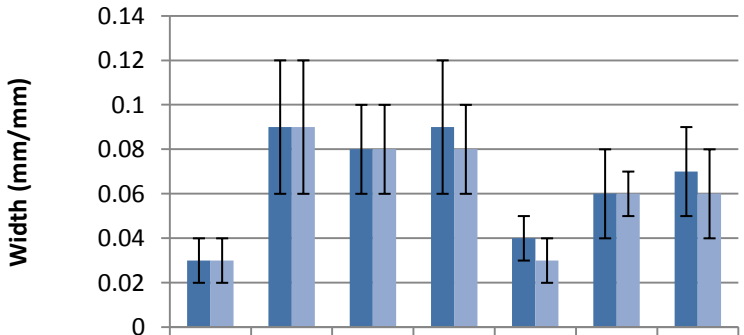

	RTML	sPTML	dPTML	PUTML	DUTML	PIML	DIML
IndexLigament in Neutral position	0.03	0.09	0.08	0.09	0.04	0.06	0.07
Index Ligament in Full abduction position	0.03	0.09	0.08	0.08	0.03	0.06	0.06

Figure 2.41: Index ligament of width in neutral and full abduction positions with their standard deviation. The index ligament was indexed against the length (mm) of the third metacarpal. Unit: mm, N=50.

2.3.4 Comparison between embalmed and fresh specimens

The t *test* was applied for all TMC ligament measurements; areas, length and width. The results showed there were no significant differences ($p > 0.05$) in neutral and full abduction positions between embalmed and fresh specimens (Figures 2.42-2.43-2.44-2.45-2.46-2.47), (Tables 2.11-2.12-2.13).

Ligaments	Neutral position of Embalmed Specimens mm²	Full abduction position of Embalmed Specimens mm²	Neutral position of Fresh Specimens mm²	Full abduction position of Fresh Specimens mm²
RTML	27.16 ± 6.5	26.36 ± 8.3	24.8 ± 3.5	23.05 ± 3.3
sPTML	100.59 ± 31.39	102.9 ± 33.01	102.45 ± 17.31	103.41 ± 20.11
dPTML	60.18 ± 22.87	62.02 ± 22.23	59.33 ± 13.02	60.12 ± 15.62
PUTML	98.84 ± 42.3	99.59 ± 41.21	101.86 ± 36.71	102.55 ± 32.18
DUTML	43.81 ± 16.29	42.62 ± 16.21	38.11 ± 9.74	37.47 ± 9.94
PIML	86.13 ± 33.55	85.83 ± 31.05	81.45 ± 18.71	79.36 ± 17.33
DIML	191.05 ± 40.42	190.66 ±31.22	191.46 ± 31.01	190.39 ± 26.14

Table 2.11: Mean of the area of the TMC ligaments and their standard deviation in embalmed and fresh specimens, p value, unit:mm², N=60 (50 embalmed, 10 fresh) specimens.

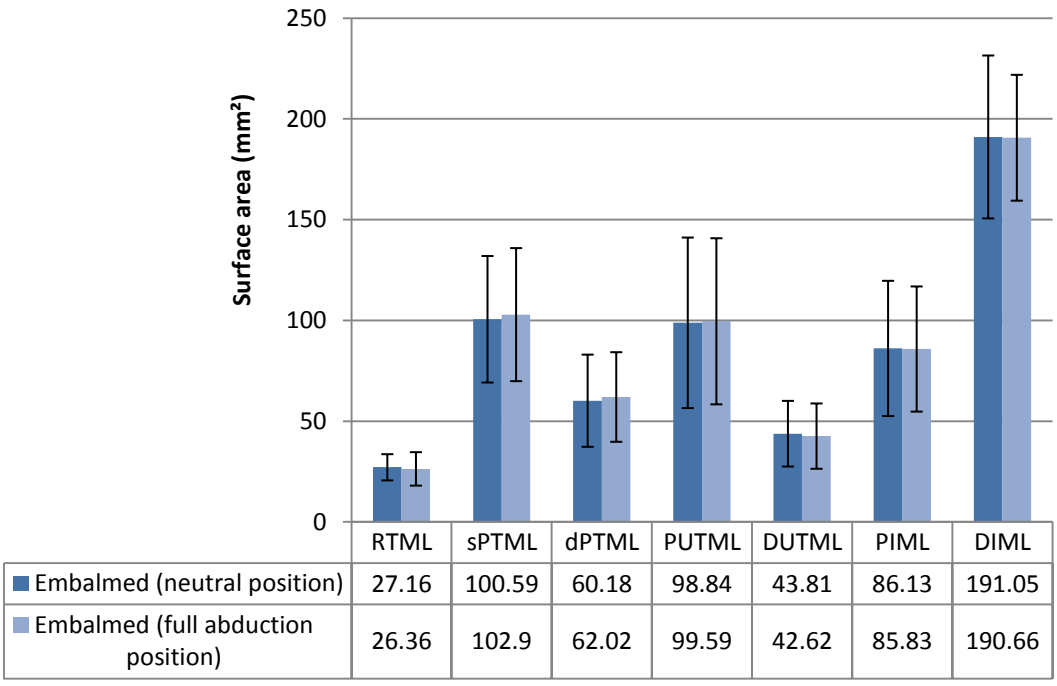

Figure 2.42: Comparison of embalmed specimens in area measurement of the TMC ligaments with their standard deviation. The figure illustrates that there were no significant differences ($p>0.05$) of all TMC ligaments, in both neutral and full abduction positions. Unit:mm², N=50.

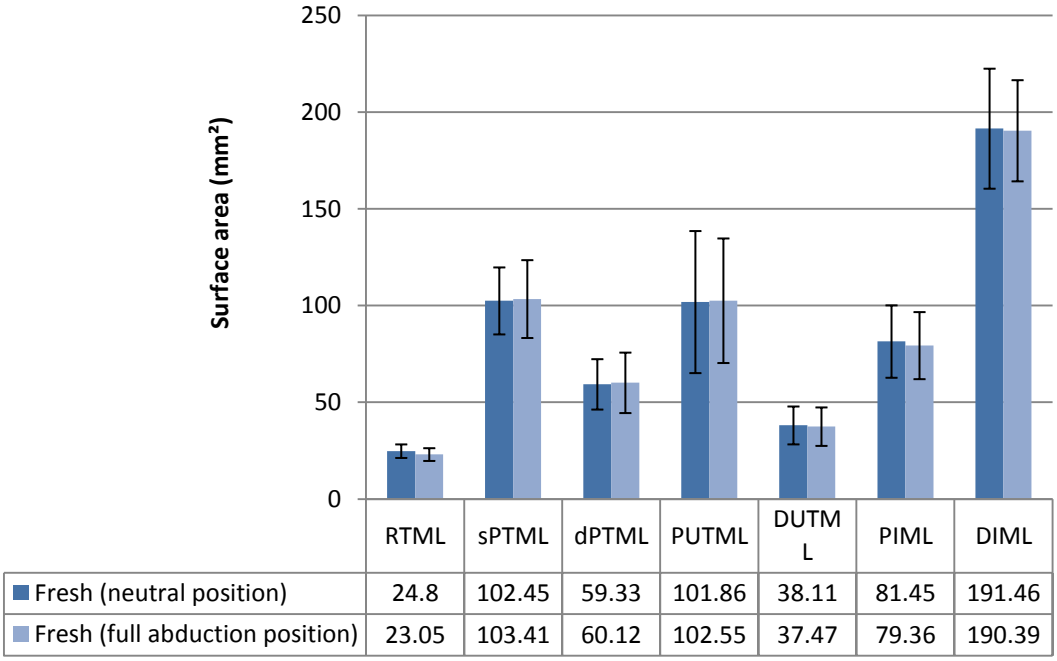

Figure 2.43: Comparison of fresh specimens in area measurement of the TMC ligaments with their standard deviation. The figure illustrates that there were no significant differences ($p>0.05$) of all TMC ligaments, in both neutral and full abduction positions. Unit:mm², N=10.

Ligaments	**Neutral position of Embalmed Specimens mm**	**Full abduction position of Embalmed Specimens mm**	**Neutral position of Fresh Specimens mm**	**Full abduction position of Fresh Specimens mm**
RTML	19.18 ± 4.4	18.92 ±3.8	14.95 ± 3.1	14.28 ± 3.08
sPTML	20.23 ± 3.8	19.68 ± 3.6	22.04 ± 2.14	21.63 ± 2.6
dPTML	12.9 ± 3.3	12.11 ± 3.2	10.97 ± 2.3	10.02 ± 2.2
PUTML	20.35 ± 3.7	20.72 ± 4.1	21.45± 3.2	22.17 ± 1.9
DUTML	20.09 ± 3.4	21.62 ± 4.2	19.64 ± 2.9	20.11 ± 1.8
PIML	19.59 ± 5.06	20.53 ± 5.6	18.21 ± 2.06	19.78± 1.6
DIML	34.25 ± 5.02	35.05 ± 5.6	34.14± 2.02	35.62 ± 2.6

Table 2.12: Mean of the length of the TMC ligaments and their standard deviation in embalmed and fresh specimens, p value, unit:mm, N=60 (50 embalmed, 10 fresh) specimens.

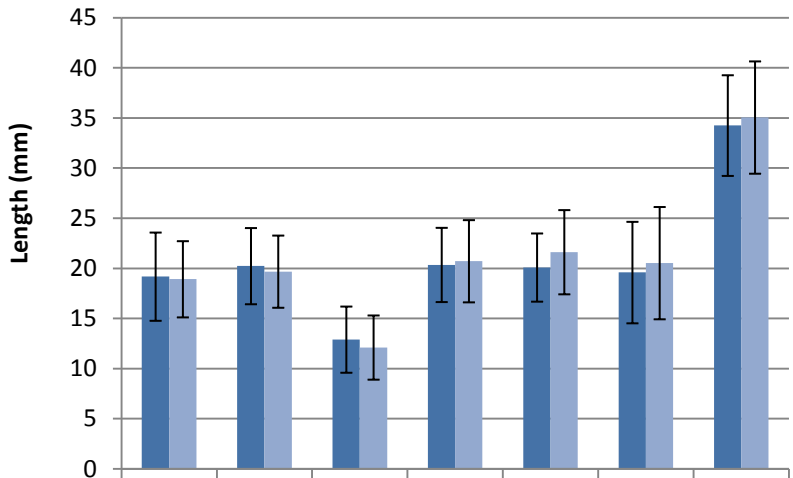

	RTML	sPTML	dPTML	PUTML	DUTML	PIML	DIML
Embalmed (neutral position)	19.18	20.23	12.9	20.35	20.09	19.59	34.25
Embalmed (full abduction position)	18.92	19.68	12.11	20.72	21.62	20.53	35.05

Figure 2.44: Comparison of embalmed in length measurement of the TMC ligaments with their standard deviation. The figure illustrates that there were no significant differences (p>0.05) of all TMC ligaments, in both neutral and full abduction positions. Unit:mm, N=50.

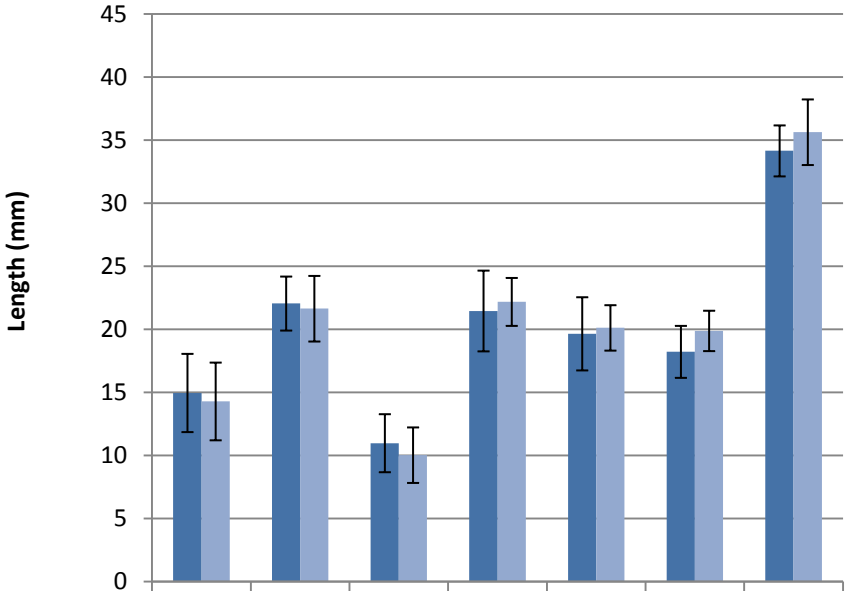

	RTML	sPTML	dPTML	PUTML	DUTML	PIML	DIML
Fresh (neutral position)	14.95	22.04	10.97	21.45	19.64	18.21	34.14
Fresh (full abduction position)	14.28	21.63	10.02	22.17	20.11	19.87	35.62

Figure 2.45: Comparison of fresh in length measurement of the TMC ligaments with their standard deviation. The figure illustrates that there were no significant differences (p>0.05) of all TMC ligaments, in both neutral and full abduction positions. Unit:mm, N=10.

Ligaments	Neutral position of Embalmed Specimens mm	Full abduction position of Embalmed Specimens mm	Neutral position of Fresh Specimens mm	Full abduction position of Fresh Specimens mm
RTML	1.67 ± 0.68	1.7 ± 0.094	1.95 ± 0.22	1.48 ± 0.8
sPTML	4.73 ± 1.88	4.8 ± 1.96	3.21 ± 0.87	3.29 ± 0.47
dPTML	4.57 ± 1.37	4.84 ± 1.53	3.22 ± 0.98	3.31 ± 1.02
PUTML	4.47 ± 1.6	4.19 ± 1.42	5.45 ± 0.45	5.12 ± 0.25
DUTML	2.06 ± 0.89	1.86 ± 0.74	1.88 ± 1.09	1.51 ± 0.09
PIML	4.03 ± 1.38	3.52 ± 1.39	3.83 ± 1.19	3.01 ± 1.01
DIML	4.3 ± 1.48	3.82 ± 1.45	4.31 ± 0.48	3.22 ± 0.95

Table 2.13: Mean of the width of the TMC ligaments and their standard deviation in embalmed and fresh specimens, p value, unit:mm, N=60 (50 embalmed, 10 fresh) specimens.

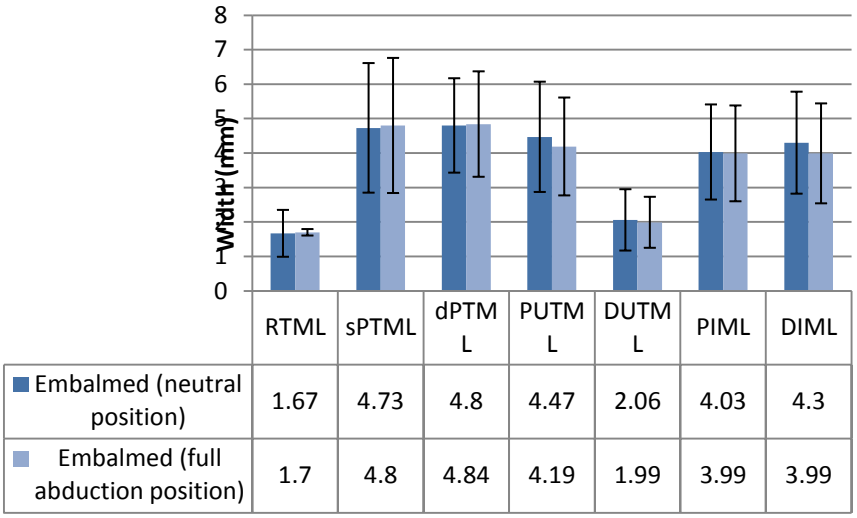

Figure 2.46: Comparison of embalmed specimens in width measurement of the TMC ligaments with their standard deviation. The figure illustrates that there were no significant differences (p>0.05) of all TMC ligaments, in both neutral and full abduction positions. Unit:mm, N= 50.

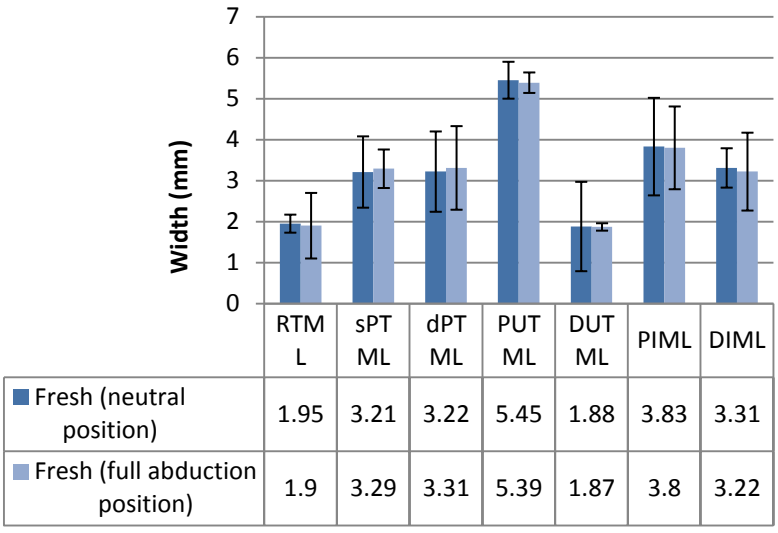

Figure 2.47: Comparison of fresh specimens in width measurement of the TMC ligaments with their standard deviation. The figure illustrates that there were no significant differences (p>0.05) of all TMC ligaments, in both neutral and full abduction positions. Unit:mm, N= 10.

2.4 Discussion

The most controversial topic with regard to the trapeziometacarpal, or TMC, joint is which ligament is the primary stabilizer of this articulation. The measurement of TMC ligaments to obtain stabilization changes markedly with the thumb in full abduction compared with the neutral position in vivo. The length, width and area changes of these principle ligaments stabilizing the joint and also differ in the full abduction position. The TMC joint is of paramount importance to the function of the hand (Bettinger *et al.* 1999; Eaton and Littler 1969; Imaeda *et al.* 1997).Previous biomechanical studies have identified the roles of various ligaments in stabilizing the TMC joint (Bettinger *et al.* 2000; Van Brenk *et al.* 1998).

A number of TMC ligaments are taut in the full abduction position to prevent excessive motion of the thumb and to achieve stabilization (Agur *et al.* 2003; Chiavaras *et al.* 2010; Dumas *et al.* 2008). The group that is attached between the first metacarpal and trapezium bones strongly resists the motion against palmar subluxation (Su *et al.* 2003). In addition, the RTML resists only against lateral subluxation. This depends upon its fibre distribution and the anatomical position of this ligament between the TMC ligaments. On the other hand, the ligaments which are connected between the first metacarpal and second metacarpal play necessary roles in stabilizing the TMC joint in full abduction. However, it is difficult to consider a ligament by itself to limit the individual action. Most of the TMC ligaments work as a group.

Therefore, previous investigations have only measured the length, width and area of relatively long ligaments using this method (Goubier *et al.* 2011). In the current study, this method is extended to measure the relatively short ligaments (Marzke *et al.* 2012). The change in shape of the TMC ligaments may not represent the elasticity of the ligament fibres because the ligaments of the small joints are generally thinner, and some ligaments tend to be lax or even folded when they are shortened. Thus, there is a need to understand which ligaments should be augmented or reconstructed when treating this complex joint. Based on the literature, the dPTML is the chief stabilizer of the TMC joint. The results of the current study do not support this hypothesis because the DUTML, PIML and DIML are more important for preventing dorsal subluxation. The DUTML, PIML and

DIML are significantly longer and thinner than the dPTML in the full abduction position (Figures 2.15-2.22-2.27).

The DIML and PIML are of the largest and broadest ligaments in the TMC joint; their function is to prevent dorso-radial subluxation of the metacarpal (Watt and Hooper 1987). The present study shows that the length of these ligaments increases markedly with the TMC joint in full abduction. The anatomical positions of these ligaments in the dorso-ulnar aspect of the TMC joint, which elongates (stretches) based on reconstructed in 2D, were 57% and 29% (Figure 2.23) with the TMC joint in full abduction position. Furthermore, the widths were thinned 33% and 35% (Figure 2.29), which may indicate substantial stretching of these ligaments between the first and second metacarpal bones in the full abduction position, which further points to the critical role of these ligaments in maintaining TMC joint stability.

The DUTML is very important for stabilizing the TMC joint (Bettinger *et al.* 1999; Colman *et al.* 2007; D'Agostino *et al.* 2014; Ladd *et al.* 2013; Van Brenk *et al.* 1998). The percentage of elongation for this ligament was approximately near to that of the percentage of the DIML and PIML. The percentages of elongation and relaxation were 8% and 13% (Figures 2.23-2.24), respectively, which may indicate that this ligament works as an assistant to the DIML and PIML during the motion from neutral toward full abduction positions. The DUTML stabilizes the TMC joint with the last two ligaments. This finding supports the concept that the ligaments of the TMC joint work together to maintain the stabilization of the TMC joint.

As mentioned previously, the RTML serves to restrain lateral subluxation of the metacarpal (Su *et al.* 2003). A unique pattern was found in the changes in length and width of this ligament. Unlike other ligaments, this ligament stretches in a neutral position and relaxes in the full abduction position. Also, the sPTML and dPTML had the same action throughout the motions; this indicates that these ligaments may be relatively tense when in a neutral position, but tension decreases with the TMC in the full abduction position. However, the thumb motions involve flexion of the TMC joint anteriorly, decreasing the distance between the two attachments of these ligaments (Tan *et al.* 2011). The measurement based on both 3D images and cadaveric dissection showed that the

lengths of the RTML, sPTML and dPTML decrease. The percentages of the relaxation of these ligaments were 50%, 34% and 16% (Figures 2.24), respectively. According these results, the hypothesis that the ligaments of the TMC joint work as one group is supported.

The PUTML in combination with the DUTML, PIML and DIML, prevents the dorsal subluxation of the TMC joint. The elongating and thinning of the PUTML is similar in direction to the PIML, DIML and DUTML. In addition, it should further be noted that the changes in the PUTML are variable (Lin *et al.* 2013; Nanno *et al.* 2006b). The percentage of elongation was 6%, while the percentage of thinning was 19%, which indicates that the percentage of the stretch is smaller than for the PIML, DIML and DUTML. This suggests that this ligament has little to do with preventing dorsal subluxation (Figure 2.48).

The area measurements investigated in this study indicate that the sPTML had the largest increase in area (94%) in the full abduction position (Figure 2.17). Therefore, the shape of this ligament is shown to be wider than when in a neutral position. The DIML had the largest decrease in area (60%) in the full abduction position (Figure 2.16), and the ligament was shown to be thinner than in the neutral position.

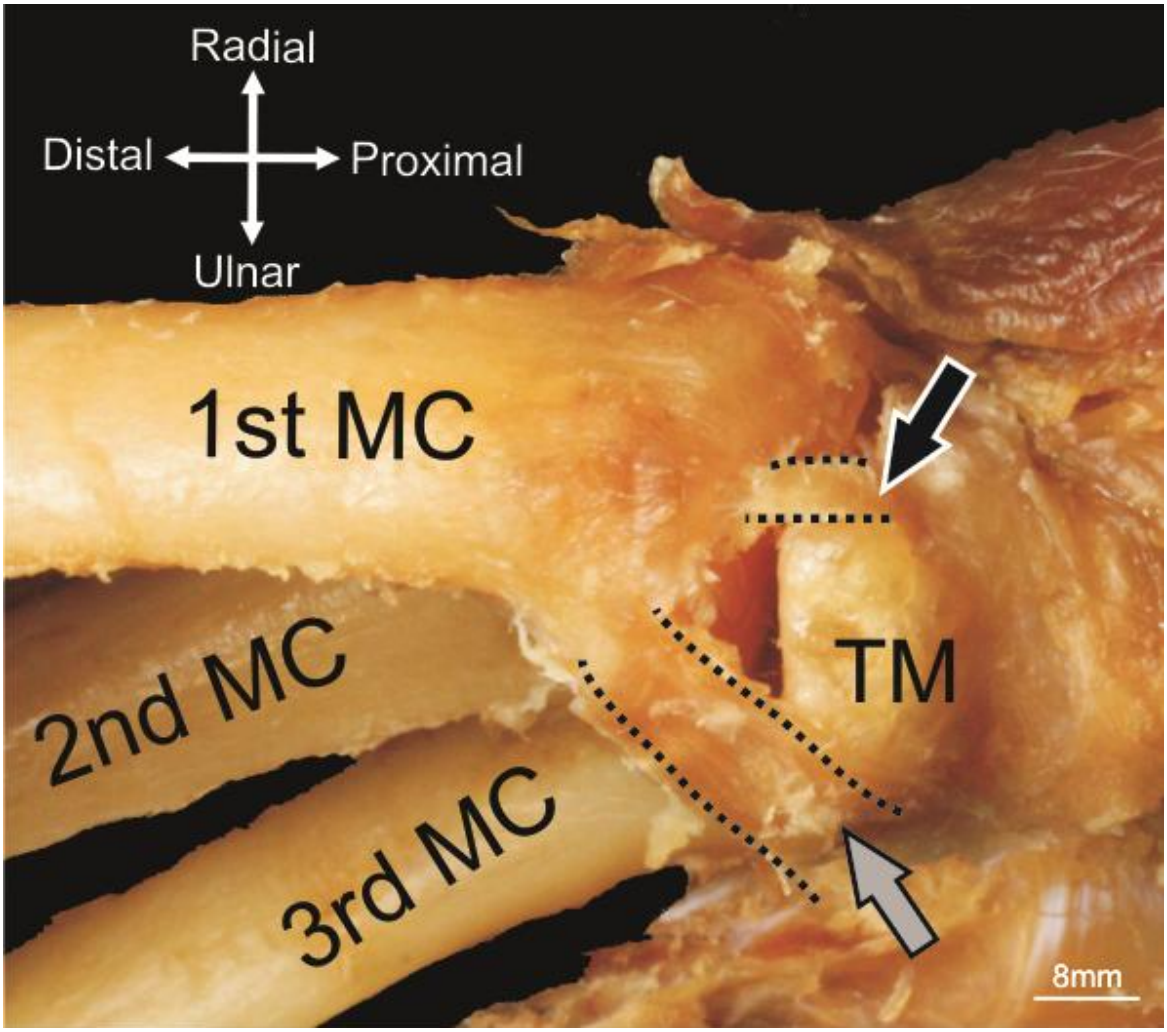

Figure 2.48: Anterior view of the TMC ligaments. Donor embalmed.

The figure illustrates the changes in the shape of the dorsal intermetacarpal ligament (DIML) and the palmo-ulnar trapeziometacarpal ligament (PUTML). The black arrow shows the elongation of the DIML, and the Grey arrow shows the elongation of the PUTML in full abduction position. Dotted lines depicted at the ligaments borders indicate to the course and limit of the ligaments from and to the bones.

The shape of the TMC ligaments may change by the internal force that comes from the muscle action to produce the motion, but the laxity of the ligament prevents tearing from the extreme movement. However, the ability of the ligament to absorb excessive force depends on the percentage of the surfaces area of the ligament, which plays a role in determining which ligament has more laxity and greater ability to be the primary stabilizer of the TMC joint. Although ligament laxity has long been known to be important to the pathomechanics of TMC joint osteoarthritis (Batra and Kanvinde 2007), this may include abnormally shallow

TMC joint contours, thumbs that tend to remain in reposition, premature cartilage aging or hormonal differences (Ateshian *et al.* 1992).

The results from the comparison between right and left specimens showed that the widths and areas did not change significantly in the full abduction position, while the length measurements of the PIML and DIML changed in the full abduction position (Figures 2.18-2.23-2.28). Moreover, the comparison between males and females was recorded in all geometric measurements (length, width and area) in the full abduction position. The variety of the length, width and area measurements of the TMC ligaments may reflect the size of the cadaver's hands, as male hands are typically larger than female hands in the metacarpal and trapezium bones (Cerveri *et al.* 2008).

To simulate physiological conditions in vivo, fresh ligament would be the best testing material. For biomechanical testing, high numbers of ligaments are needed, and testing has to be performed often over several days, which requires ligament preservation. Changes in biomechanical properties after preservation have been discussed in the literature (page 64), and they are the subject of some controversy (Park *et al.* 2011).

Besides fresh frozen ligaments, embalmed human specimen ligaments are common in biomechanical studies. There are also varied and contradictory opinions in the literature as to whether embalmed bone reflects realistic physiological conditions. In experiments with embalmed specimens, (Currey *et al.* 1995) reported a decrease in impact strength of bovine bone after fixation with formaldehyde without any change in the connective tissues. In contrast, (van Haaren *et al.* 2008) showed that fixation with formalin had no effect on the biomechanical properties of goat bones and surrounding tissues after a fixation period of up to one year, and they suggested that embalmed bones can be safely used for biomechanical testing purposes.

In the current study, when comparing embalmed specimen ligaments to fresh frozen specimen ligaments in neutral and full abduction positions for all geometrical measurements such as areas, length, and width, there was a slight numerical change in the measurement reading of TMC ligaments in the fresh specimen from that of the embalmed specimen. For example, the area of the

RTML of the embalmed specimen when in neutral position 35º was 34.16 mm², and after stretching the thumb toward full abduction 60º it became 26.36 mm². Alternatively, the area in the frozen specimen changed from 36.8 mm² in neutral position 35º to 23.05 mm² in full abduction position 60º (Table 2.11). The degree of position was very important to preserve the differences in angle between the embalmed and fresh specimens and also between the embalmed specimens themselves. Thus, the limitation of the neutral in the 35º position and full abduction in the 60º position helped to decrease the percentage of errors. The result had no statistically significant differences (Figures 2.42-2.43-2.44-2.45-2.46-2.47) , but the difference between both readings may be the result of the effect of formalin on the elasticity of the tissue (Thiel 2002). However, in this study the result depends on the motion and direction without considering the biological properties of the ligament.

In addition, a large number of specimens with different hand sizes was dissected and investigated in the current study, and the variation in results from one specimen to another was a big challenge. After dissecting the 50 specimens, we recorded the length of the 3rd MC, which was the *index value* 61.16 mm. The comparison between raw ligament and index ligament defined the accuracy of each ligament measurement. For example, the raw ligament of the length in neutral position for RTML was 19.23 mm, but the index data for the same ligament in the same position was 0.31mm (Figures 2.38-2.39). The index ligament was used as a baseline result for the same ligament in a large number of specimens, while raw ligament have used on same ligament in one specimen.

From the current study, it can be concluded that there is no single ligament that provides the sole stabilization in a normal TMC joint and the previous studies supported that (Hirokawa and Tsuruno 2000; Nanno *et al.* 2006a; Tan *et al.* 2011). The PIML and DIML appear to be the more important ligaments and are commonly stretched in the full abduction position, in contrast, the others studies supported the concept that the AOL (PTML) had the main stabilizer of TMC joint (Benjamin *et al.* 2002; Buffi *et al.* 2013; Edmunds 2011; Napier 1955). The DUTML and PUTML are secondary stabilizers that are stretched less than the PIML and DIML. The RTML acts as a restrain for gross radial subluxation but probably does not play a major role in the initial stages of TMC joint stability. The sPTML and dPTML act as

a pivot for movement of the TMC joint and may assist in preventing palmar subluxation.

Nevertheless, some limitations of this study must be acknowledged. No clinical and dominant hand history was available. The advanced age of the cadavers could be responsible for making visualization of attenuated ligaments more difficult through the full abduction motion. Finally, this study fosters a better understanding of the function of each ligament supporting the TMC joint and could play a key role in successful ligament reconstruction of this joint. Further biomechanical study is in progress to determine more precisely the function of individual ligaments and their roles in TMC joint stability.

Chapter Three

3D Modelling of the Trapeziometacarpal Ligaments

3.1 Introduction

Stability and mobility represent the paradoxical demands of the trapeziometacarpal (TMC) joint, yet the structural origin of each functional demand is poorly defined (Agur *et al.* 2003). The shape of external configuration and internal arrangement of the ligament fascicles have only been recorded two-dimensionally. Three-dimensional modelling presents an exciting innovation because it makes it feasible to document and visualise each fascicle (Stark *et al.* 2012).

The literatures review of experiments and studies relate to this chapter explained in details in chapter one (pages 50-66)

The aims of this current study are to (1) improve the two-dimensional reconstruction study of the TMC ligament to modulation shape of 3D, (2) quantify the 3D shape of TMC ligaments through various static positions (neutral static, full abduction static), (3) quantify the displacements of each of the TMC ligaments by dynamic displacement, (4) add a new measurements rather than previuse chapter such as thickness, volume, and cross- sectional area to explain the change that will occur on the TMC ligaments during neutral and full abduction position, (5) create ligament stretcher device for modelling the TMC ligaments a way from TMC joint, and (6) make a comparison between two-dimensional reconstruction and three-dimensional modelling to support the concept of the stabliziation.

This study is essential for understanding thumb ligament injuries, for success in repair and reconstruction procedures, for rehabilitation programs following surgery and for the design of prosthetic ligaments.

3.2 Material and methods

3.2.1 TMC ligament dissections

Ten embalmed cadaveric specimens (5 male specimens, 5 female specimens; age range, 68± 4.1years) were dissected. The trapeziometacarpal joint of all specimens was meticulously dissected through the palmar and dorsal approaches using loupe microscopic magnification (with 6× magnification).

Posterior side of specimen, the extensor pollicis longus, extensor pollicis brevis and extensor carpi radialis longus tendons were reflected distally. The radial artery was excised as it emerged dorsally in the anatomic snuff-box to the level of the first dorsal interosseous muscle. The proximal half of the first dorsal interosseous muscle was also removed to expose the intermetacarpal region. All other structures were then excised from the surface of the trapezium, trapezoid and 1st and 2nd metacarpals to reveal the underlying interosseous ligaments. Two ligaments were identified from this exposure: the palmar intermetacarpal ligament (PIML) and the DIML ligament (Figure 3.1).

Anterior side of specimen, the abductor pollicis brevis, the superficial head of flexor pollicis brevis and opponens pollicis muscles were reflected distally off the radial-most portion of the transverse carpal ligament (TCL) and the 1st metacarpal, thus revealing the underlying TMC joint and ligaments. A blunt-tipped probe was used to delineate adjacent ligaments, especially along the palmar side of the TMC joint intermetacarpal region. Five additional ligaments were identified at this point: the sPTML, dPTML, RTML, PUTML and DUTML (Figure 3.2).

The superficial layer of the palmar trapeziometacarpal ligament (sPTML) was pulled off from the deep layer. The proximal site of the sPTML and dPTML remained attached to the trapezium bone. Finally, the TMC joint with ligaments was hinged open like a book on the dorsal side (hinging on the palmar side) to be ready for reconstruction.

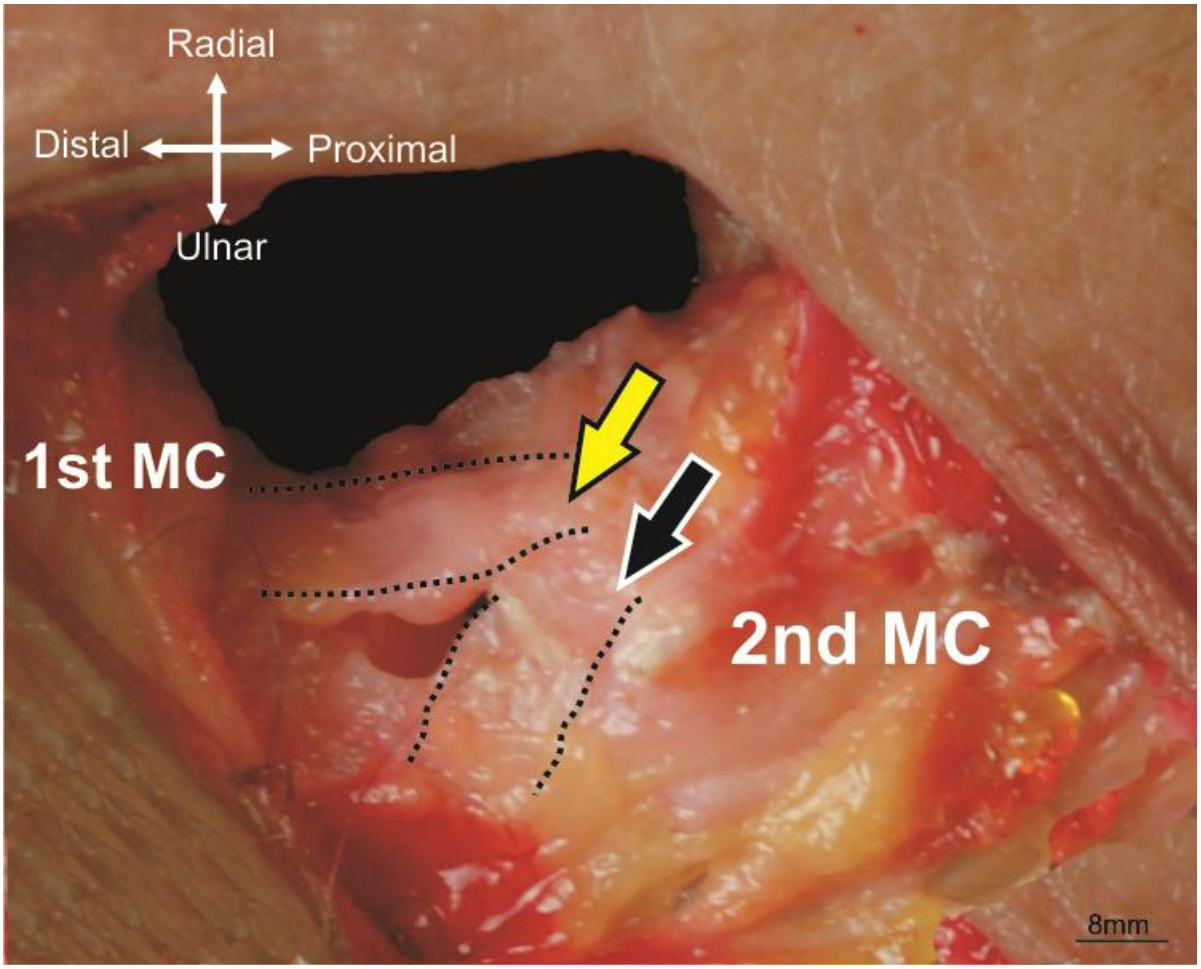

Figure 3.1: Lateral view of the TMC joint with its ligaments. Unembalmed donor.

(Black arrow) shows the dorsal intermetacarpal ligament DIML and (Yellow arrow) shows the palmar intermetacarpal ligament PIML. The DIML shows ulnarly related to the PIML and other TMC ligamens, and it is more distal ligament. The PIML is more radially related to DIML, and more ulnarly related to the other TMC ligaments. Dotted lines depicted at the ligaments borders indicate the course and limit of the ligaments from and to the bones.

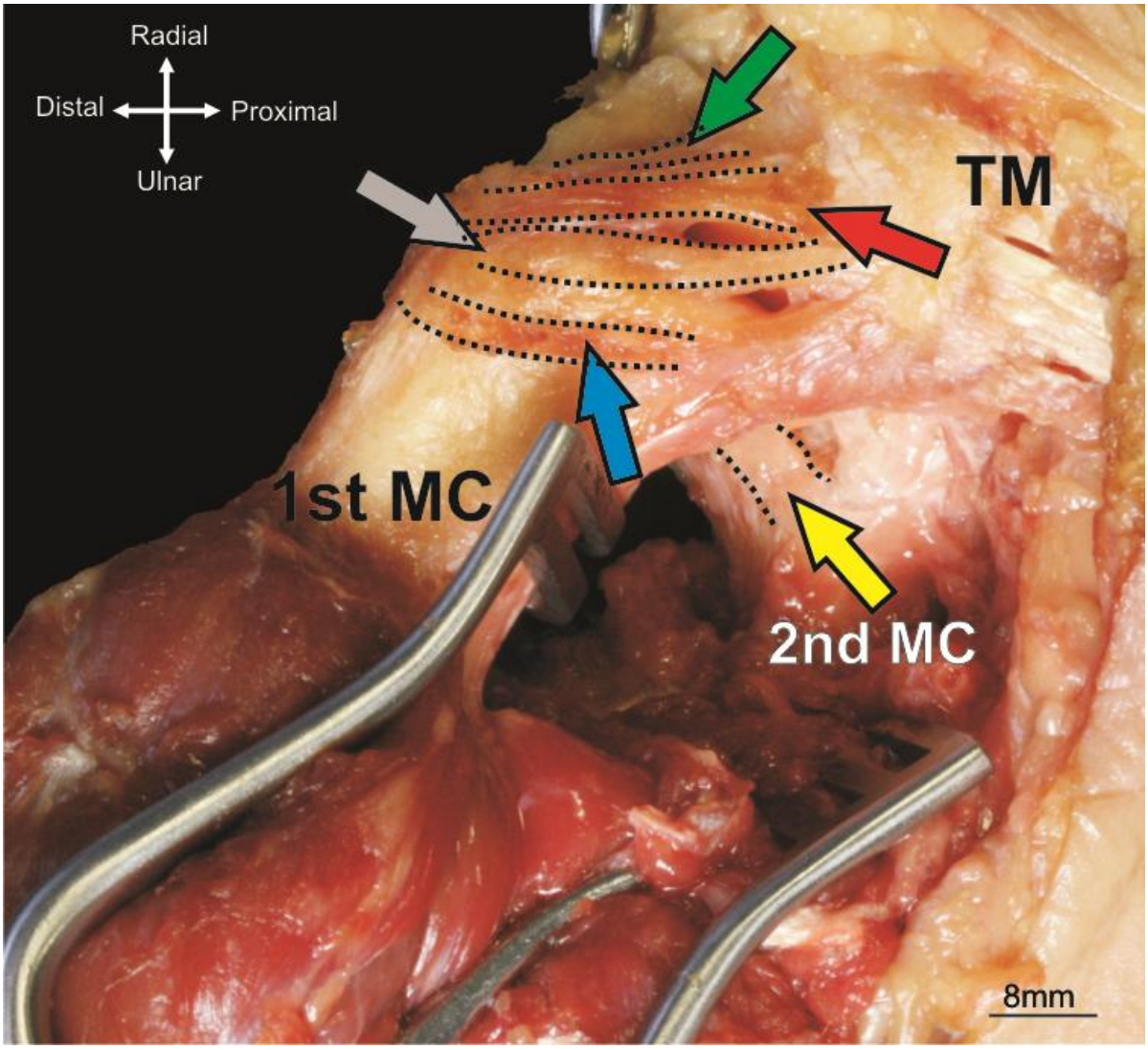

Figure 3.2: Anterior view of the TMC joints with their ligaments. Unembalmed donor

(Green arrow) shows the deep layer of the palmar trapeziometacarpal ligament dPTML, (Red arrow) shows the superficial layer of the palmar trapeziometacarapl ligament sPTML, both of these layers set radially to the PUTML and ulnarly to the RTML. (Grey arrow) shows the palmo-ulnar trapeziometacarpal ligament PUTML, this ligament has a huge fascicles set in between PTML radially, and DUTML ulnarly. (Blue arrow) shows the dorso-ulnar trapeziometacarpal ligament DUTML, this ligament shows as a half moon connection between 1st MC and TM bones, set at the end border of the TM bone, radially to both PIML and DIML, ulnarly to all TMC ligaments except PIML and DIML. (Yellow arrow) shows the palmar intermetacarpal ligament PIML. It is fascicels enlongate from 1st MC to 2nd MC bones. Dotted lines depicted at the ligament's borders indicate the course and limit of the ligaments from and to the bones.

3.2.2 Fixation instruments and devices

Normal anatomical instruments were used for preparing the specimen as follows:

1- A digitizer (Microscribe-3DX) Digitizer and 3D surface reconstruction software (Rhinoceros Version 5) were used to manually digitize the ligaments (Figure 2.7).

2- Two 1.5 mm pins were inserted into the 1st metacarpal and 2nd metacarpal bones to ensure they were firmly fixed to the digitizing platform (Figure 3.3).

3- A long dissection scissor was used to stabilize and control the direction of the ligament (Figure 3.3).

4- Two woods were used, triangular and flat, to stabilize the specimen and the scissor (Figure 3.3).

5- A 3CCD Ultra-Compact ® Digital Palmcorder® MultiCam™ Camcorder with 2.3 Megapixel Still Picture Recording was used to transfer the picture to a big screen (32 Inch, F5300 Series 5 Smart HD TV) during the modelling of the ligaments and to magnify the ligaments so that they were clear and would show the fascicles of the ligaments that allowed the pen of the microscribe to follow the fascicles (Figure 3.4).

6- An external load (80 mg) was used to increase the stabilization of the ligament throughout modelling procedures (Figure 3.4).

7- A new design fixation instrument called (Ligament Stretcher) and designed by workshop Lab of Life Science and Veterinary College was used. This ligament stretcher has five parts: (1) fixed arm;, (2) movable arm; (3) ligament hanging, which allows the fixing of the ligament through attachment of a pin; (4) dragging hand and (5) solid base. It also has a scale for reading the elongation of the ligament (Figures 3.5-3.6).

3.2.3 Three-dimensional modelling of the TMC ligaments

3.2.3.1 Procedures on the ligament still connected with the TMC joint

After dissecting the specimen, we put the thumb or TMC joint at the neutral position (35º) to record the elongation or relaxation measurements (length) of the ligament using the digital microscribe and then put the TMC joint at full abduction (60º) and recorded the elongation or relaxation measurements using the digital microscribe.

Therefore, we used the results of the measurements of the neutral (35º) and full abduction (60º) positions of each TMC ligament for the ligament stretcher device. We used the scale of the ligament stretcher device to reach the optimal elongation or relaxation of the ligament before we began the modulation the ligament three-dimensionally (Figure3.3).

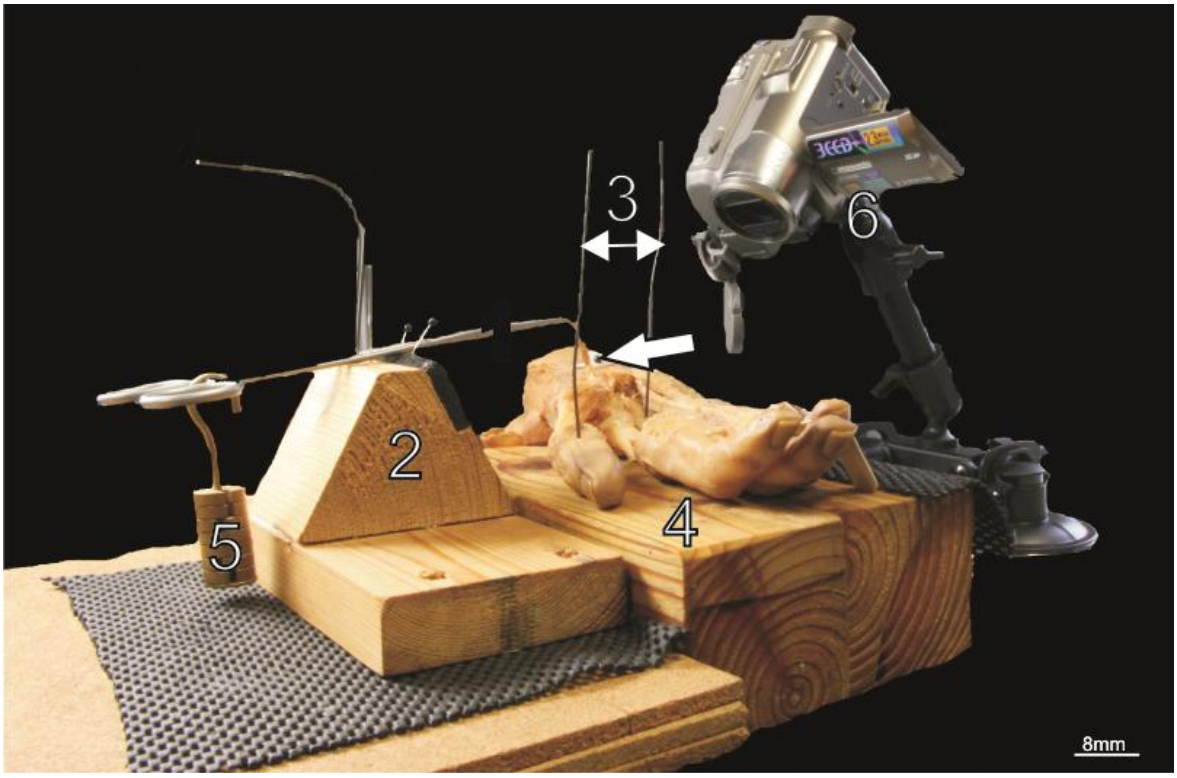

Figure 3.3: Lateral view of palmo-ulnar trapeziometacarpal ligament (PUTML), right cadaveric hand with fixation instruments.

Illustration of the materials of the fixation that were applied on the specimens during the three-dimensional modelling. (2) Triangular design wood to stabilize the long dissection scissor and control the direction of the ligament through the modelling procedure, (3) Two 1.5 mm pins inserted into the 1st metacarpal and 2nd metacarpal bones to ensure they were firmly fixed to the digitizing platform, (4) Fixed flat wood to stabilize the specimen, (5) External load with 80 mg to increase the stabilization through modelling procedure and (6) 3CCD Ultra-Compact® Digital Palmcorder® MultiCam™ Camcorder with 2.3 Megapixel Still Picture Recording. The arrow shows the ligament.

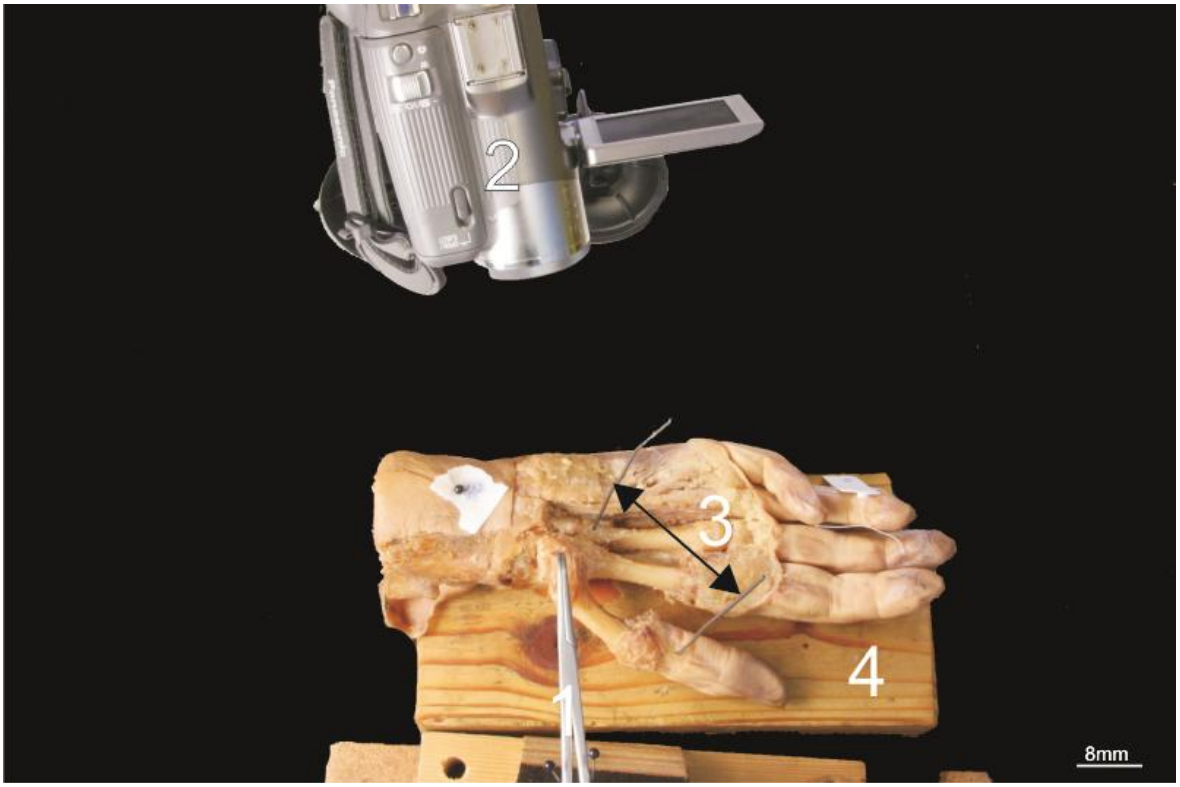

Figure 3.4: Overhead view of palmo-ulnar trapeziometacarpal ligament (PUTML), right cadaveric hand with fixation instruments.

Illustration of the materials of the fixation applied on the specimens during the three-dimensional modelling. (2) 3CCD Ultra-Compact® Digital Palmcorder® MultiCam™ Camcorder with 2.3 Megapixel Still Picture Recording , (3) Two 1.5 mm pins inserted into the 1st metacarpal and 2nd metacarpal bones to ensure they were firmly fixed to the digitizing platform and (4) Fixed flat wood to stabilize the specimen.

3.2.3.2 Procedures on the ligament after removal from the TMC joint

We removed the ligament from the TMC joint with the proximal and distal attachments of the ligament attached (the remaining small parts of the trapezium and 1st MC bones) and then hung the ligament between two arms of the ligament stretcher and used two pins to fix the ligament on the ligament stretcher device (Figures 3.4-3.5).

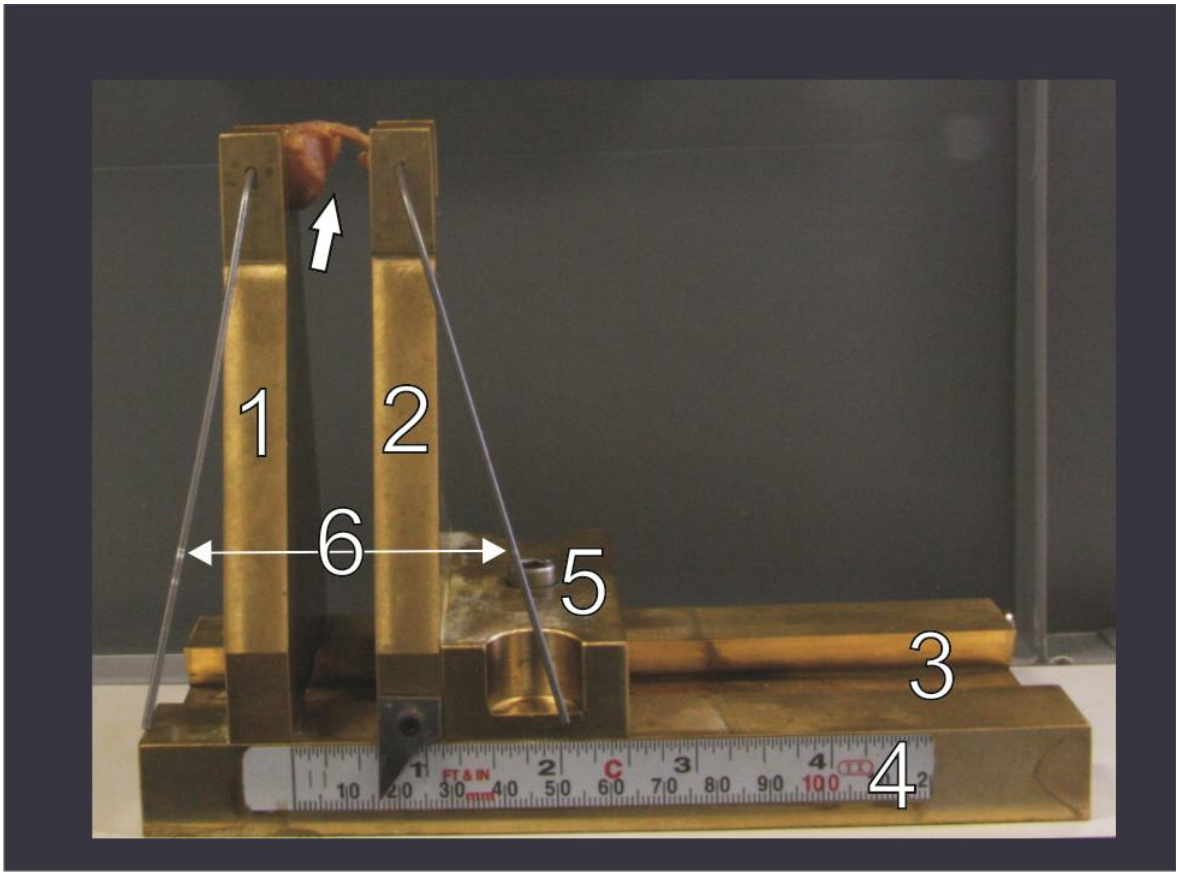

Figure 3.5: Custom-designed ligament stretcher. (Al Harbi and Fogg, MVLS mechanical workshop)

Ligament stretcher designed by the workshop at the Life Sciences and Veterinary College. Used to fixed the ligament when the ligament outside the joint during the full abduction static procedure of ligament modulation. (1) Fixed arm, (2) Movable arm, (3) Solid base, (4) Scale, (5) Dragging hand and (6) two pins inserted into the hanging for fixing the ligament. The figure shows the ligament fixed between two arms of the ligament stretcher.

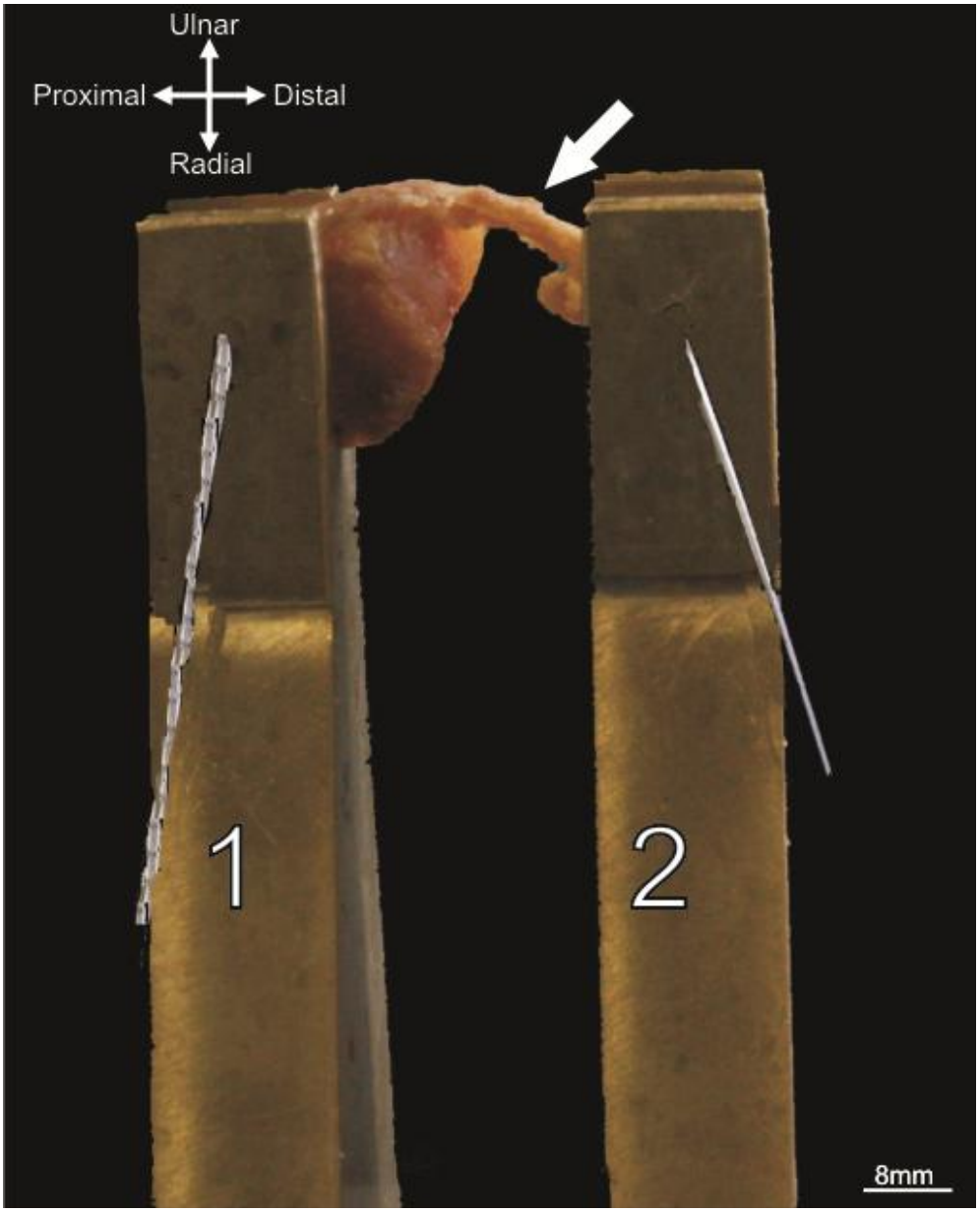

Figure 3.6: Custom-designed ligament stretcher. (Al Harbi and Fogg, MVLS mechanical workshop)

Figure showing the ligament fixed between the two arms of the ligament stretcher. (1) Fixed arm and (2) Movable arm. The arrow shows how the ligament exposes the two anterior and posterior surfaces, respectively, for modelling using the pin of the microscribe device.

3.2.4 Making the three-dimensional surface

A digitizer (Microscribe-3DX) Digitizer and 3D surface reconstruction software (Rhinoceros Version 5) (Figure 3.6) were used to manually digitize the ligamentous attachments and their bones: the trapezium, the 1st metacarpal and the 2nd metacarpal.

For the modulation, we divided the ligament into two surfaces, the anterior surface and posterior surface, defined as follows:

1- Anterior surface: fascicle bundles span from proximal attachment on trapezium bone to distal attachment to the 1st or 2nd MC bone on the anterior aspect of the ligament.

2- Posterior surface: fascicle bundles span from proximal attachment on trapezium bone to distal attachment to the 1st or 2nd MC bones on the posterior aspect of the ligament.

The microscribe digitizer pen collects the coordinates of single points in 3D space. Multiple points can be connected in a formal line. The multiple lines create a scaffold over which a virtual surface can be lofted. This lofted structure is a virtual model of the actual object (Figure 3.7). Three-dimensional coordinates at the beginning and the end of each fascicle's origin and attachment were collected. These data were sorted on a computer for further processing. To prevent drying, the specimen was kept moist and covered with damp cloths.

3.2.5 Modelling technique

Firstly, a tube created from all directions of the ligament by surrounding the microscribe pen along the anterior and posterior surfaces of the ligament. Secondly, the two borders matched of each surface corresponding together.

Thirdly, the computer model allowed full reconstruction of all parts of the ligament's tube from the digitized data. The three-dimensional model is fully manipulatable, allowing visualization of the ligament tube from any angle (Figure 3.8)

Fourthly, the computer model contains a B-spline solid that was built using a continuous volume sample function (Ng-Thow-Hing 2001). The B-spline solid can capture details of the ligament three-dimensionally. Once the original digitized data have been entered into the model, additional fascicles (streamlines) can be generated. Because the streamlines have an analytical expression, the physical dimensions of the new fascicles can be computed, added to the B-spline solid, and

visualized. The design of ligament fascicles generation techniques is based on Sobol sequences (Ng-Thow-Hing 2001) to evenly distribute the fascicles throughout the volume of the ligament (Figures 3.9-3.10).

The ligament fascicles are displayed throughout the volume of the ligament and can be animated to show the sequential arrangement of ligament fascicles; the diameter of all fascicles (as diameter-specific tubes) was limited to 0.158 mm for a more anisotropic shape.

Fifthly, we removed the proximal and distal attachments of the ligament from the bones to reconstruct the bone and, after reconstructing the bone, merged two models (tube with fascicles and bones) together to one three-dimensional model (Figure 3.11).

3.2.6 Visualization of TMC ligaments using a B-spline solid model

Three-dimensional modelling of ligaments has not been documented throughout the literature. The visualization of ligaments has been limited to two-dimensional planes (Maes-Clavier *et al.* 2014; Nanno *et al.* 2006a; Punsola-Izard *et al.* 2012; Su *et al.* 2014; Tan *et al.* 2011). Anatomical photogrammetry, in conjunction with B-spline modelling, has enabled the creation of a three-dimensional manipulatable model of an entire TMC ligament from one cadaver. The TMC ligament can be viewed in its entirety; as marginal, anterior, and posterior surfaces or as individual rows/layers of fascicles with the attachment zones.

One of the advantages of using B- spline modelling is that it can mathematically interpolate the original data set (template) to create any number of fascicles as a tube (Agur *et al.* 2003). The characteristics of B-spline functions make them ideal for representing the smooth, geometric component of ligaments. The three-dimensional parameterization of the solid allows us to reference any point within the volume of the ligament.

The internal contents present by ligament fascicles aids in calculating the volume measurements of each TMC ligament. (Henning *et al.* 1985; Hirokawa and Tsuruno 1997; Humphrey *et al.* 1989; Ng-Thow-Hing 2001).

The anistropic is the ability of the geometrical shape to be rigid (solid), the following equation which is describing the anistropic mathematicly (Henning *et al.* 1985; Hirokawa and Tsuruno 2000).

0 _____ $anisotropic$_____ 1

If the result is near to zero, the geometrical shape has rigidity. If the result is close to one, that means the geometrical shape has flexibility (Figures 3.8-3.9)

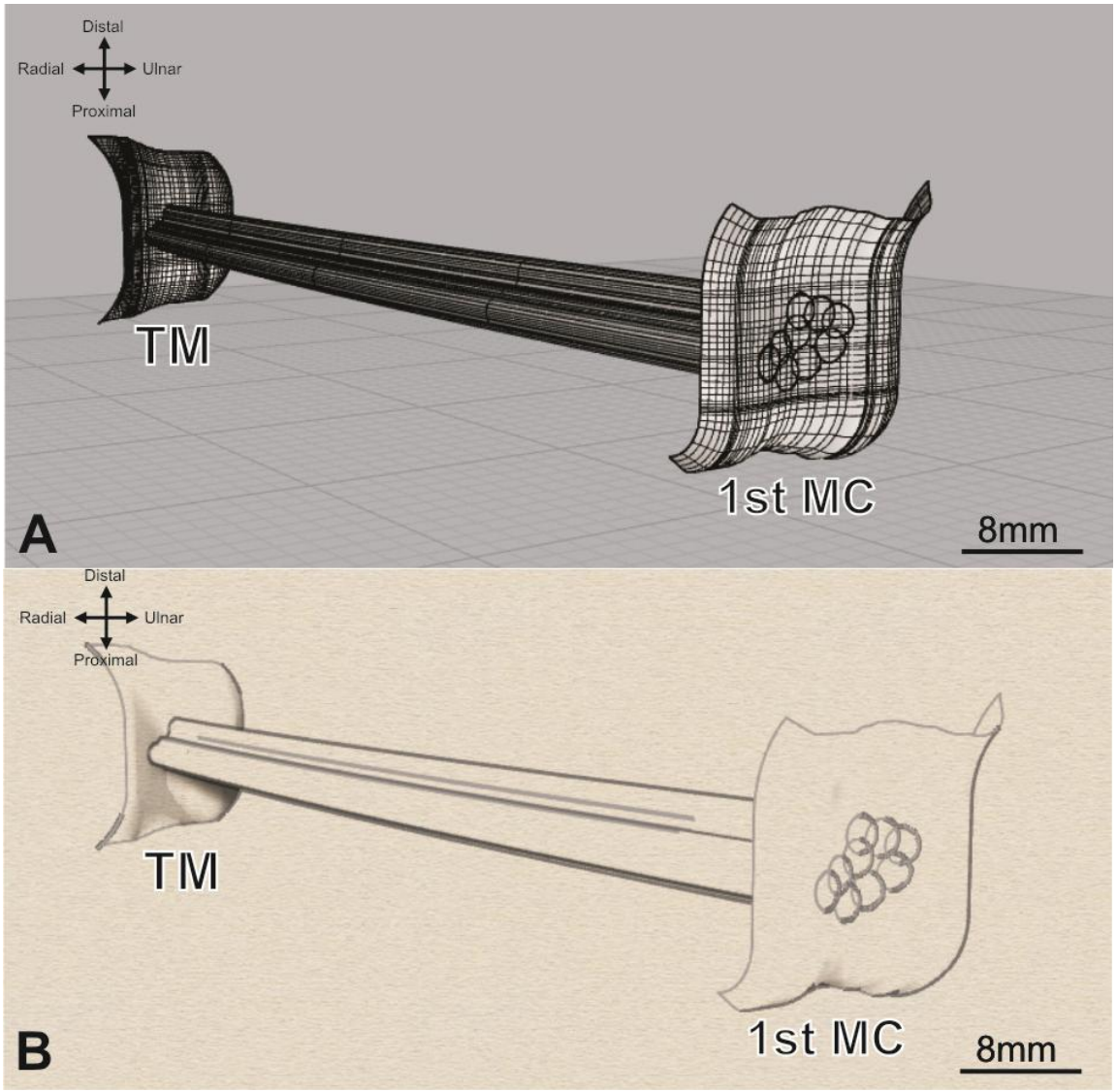

Figure 3.7: True three-dimension modelling of the PUTML ligament.

(A) 3D modelling with grid virtual environment. (B) Alternative view of 3D modelling with artist virtual environment. The microscribe digitizer pen collects the coordinates of single points in 3D space. Multiple points can be connected in a formal line. The multiple lines create a scaffold over which a virtual surface can be lofted. This lofted structure is a virtual model of the actual object. Sequential arrangement of fascicles of the anterior, posterior and marginal surfaces with covering tube. The figure shows the alignment of ligament with bone connection, particularly at sites of attachments

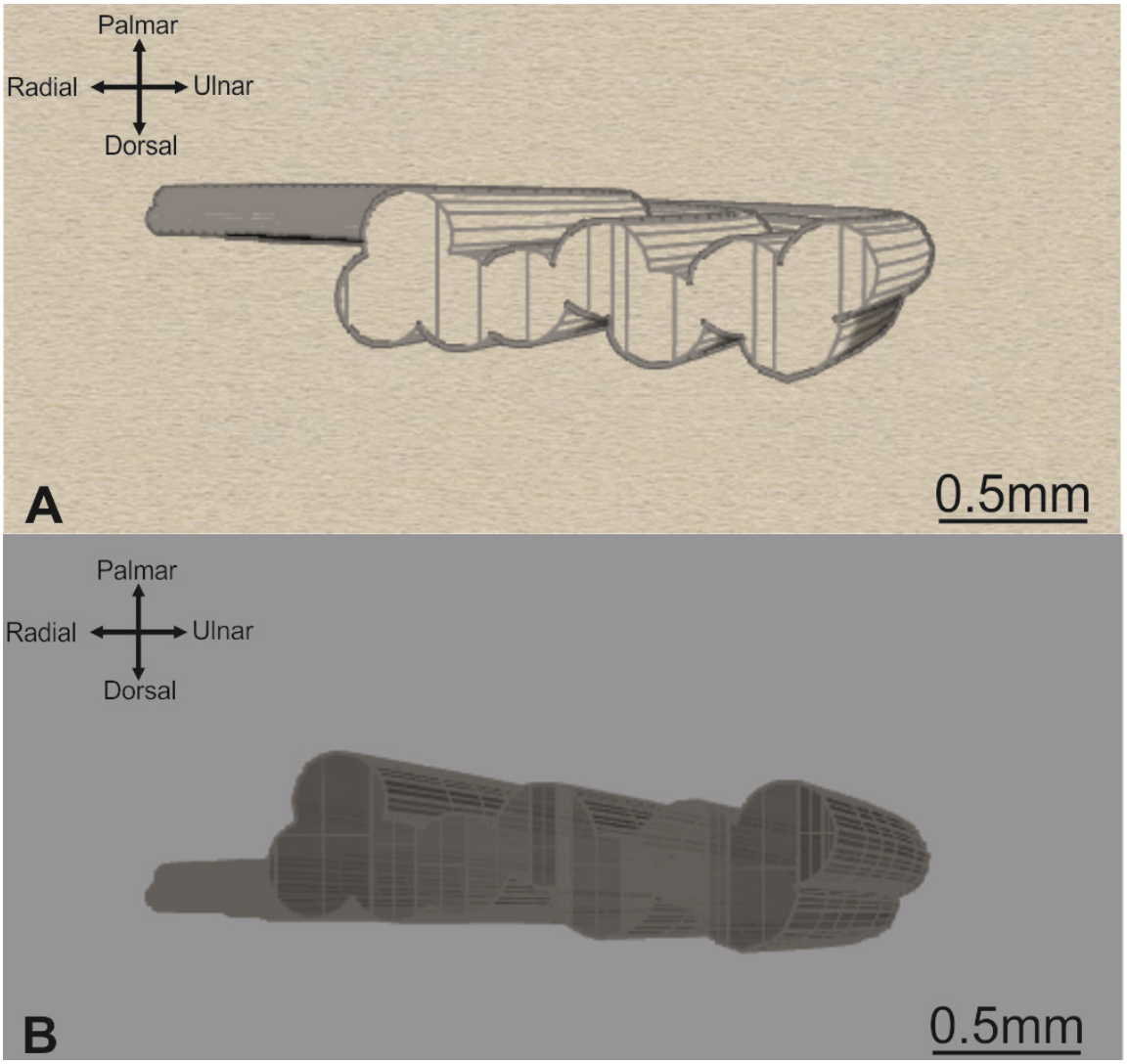

Figure 3.8: Peripheral tube/surface encompassing all the fascicles.

3D model of the dorso-ulnar trapeziometacarapal ligament (DUTML). The tube is empty from inside before merging with the B-spline model to create a final 3D model with individual fascicles.

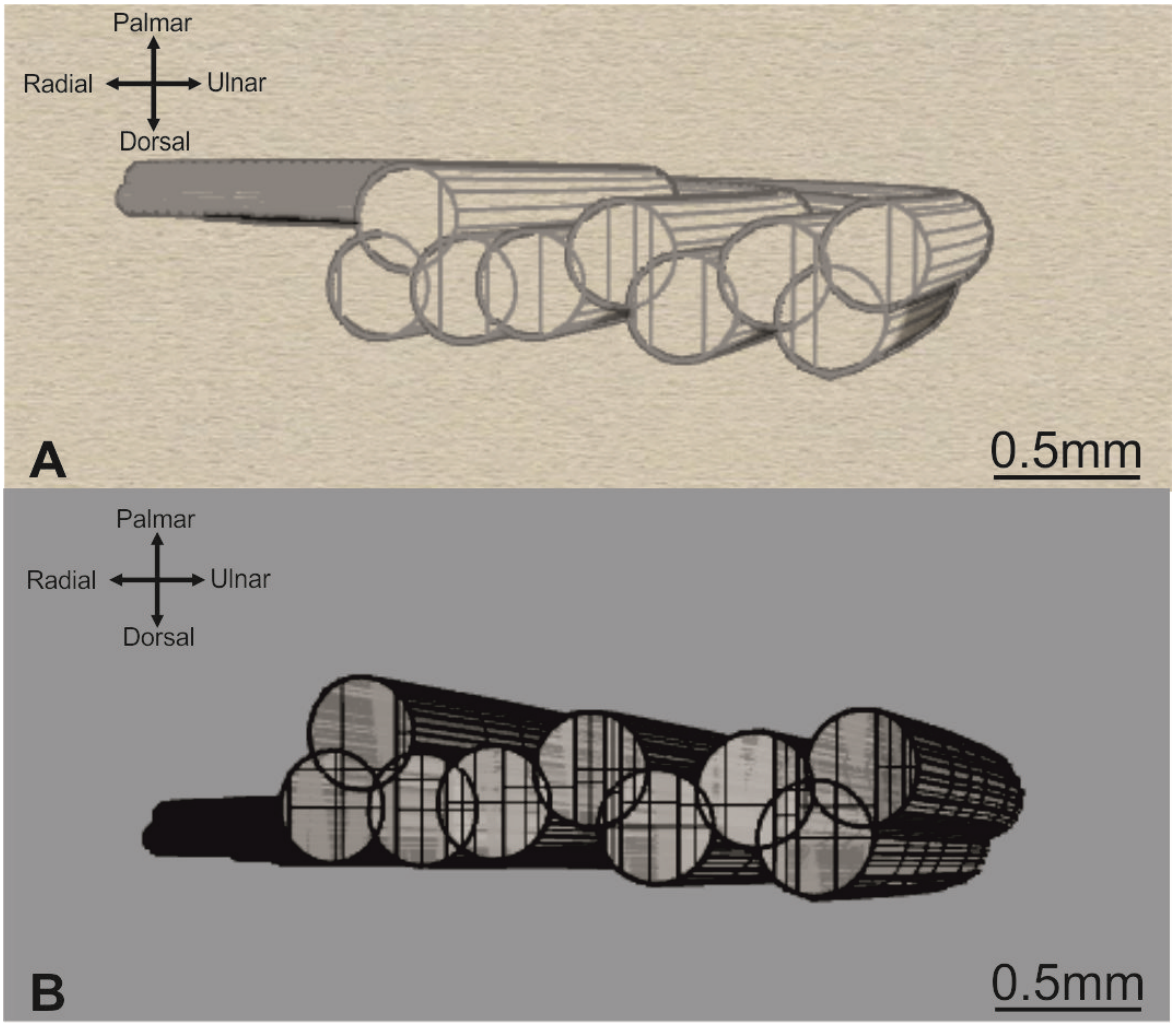

Figure 3.9: Individual fascicles modelled as diameter-specific tubes.

Three-dimensional model of the dorso-ulnar trapeziometacarpal ligament (DUTML). Individual fascicles were traced and assigned a single diameter (0.158mm) to allow consistent modelling. The external borders were verified by the modelling of the single tube, forcing all virtual “fascicles” to be contained within the “tube” created by the tube.

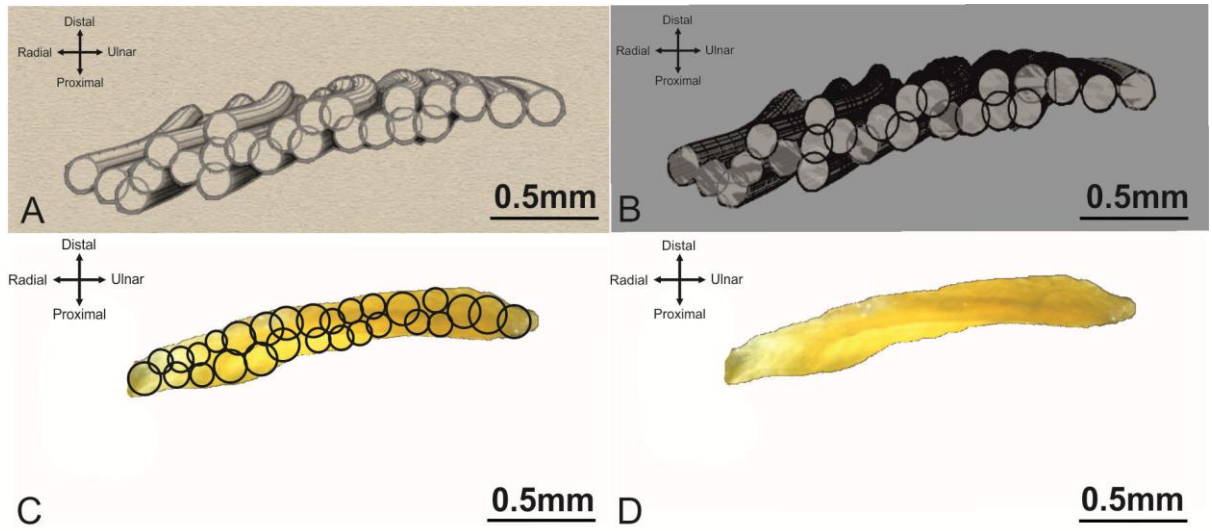

Figure 3.10: Creation the fascicles of the PIML.

(A) Alternative view of 3D modelling with artist virtual environment. (B) 3D modelling with grid virtual environment. Both figures have several tubes presented as the fascicels of the ligament, each tube has a single diameter 0.158mm, to measure the volume of a whole tube by summing the volume of all tubes. (C) Tubes with a single dimeter created on the ligament fascicels, this stage has done under the microscope (with 6 × magnifications) (D) cross- section of the ligament without tubes.

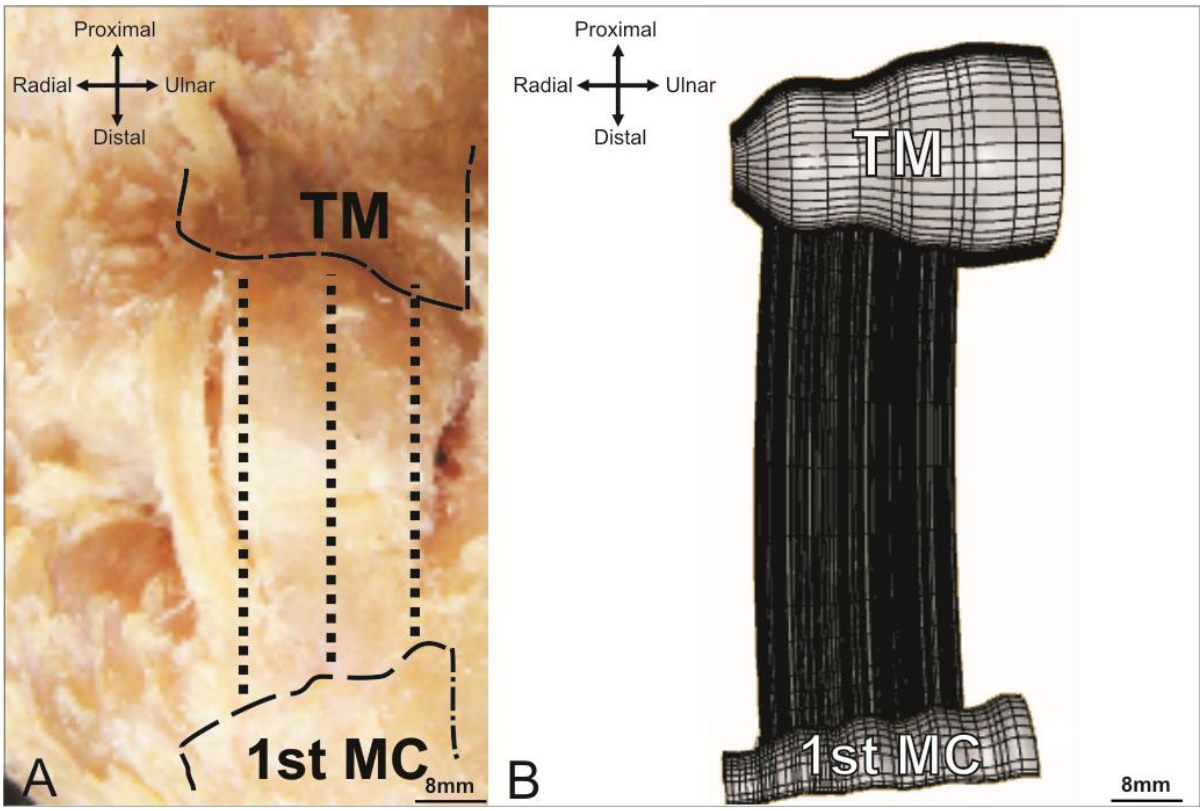

Figure 3.11: Anterior view of the palmo-ulnar trapeziometacarpal ligament (PUTML).

(A)The dissected specimen with the radial and ulnar margins of the ligament demarcated (dotted lines); dashed lines at the border of the attachment between TM and 1st MC bones to the ligament (the bone cut and removed with ligament to provide a stable base for stretching.

(B) Virtual model of the PUTML built by tracing individual fascicles with a digital microscribe. Partial surfaces of the trapezium (TM) and 1st metacarpal (1st MC) were included in the manual modelling.

3.2.7 Measurement procedures of the TMC ligaments

The measurements in this study were divided into the following:

1. Static neutral position 35º, which the ligament is measured both; when connected with the TMC joint (previous study), and when using the ligament stretcher device (current study).

2. Static full abduction position 60º, which the ligament is measured both; when connected with TMC joint in (previous study), and when using ligament stretcher device (current study).

3. Dynamic measurements, which is the difference between both the static neutral position 35º and the full abduction position 60º measurements. The results of these measurements show the displacement of each ligament in different positions.

All TMC ligaments were identified and categorized. The length, width and thickness of each ligament were measured. Cross-sectional areas for each ligament were determined and calculated in square millimetres (mean ± SD).The cross-sectional area was divided into a proximal cross-sectional area, which is at the proximal attachment of the ligament; a middle cross-sectional area, which is at the middle of the ligament and a distal cross-sectional area, which is at the distal attachment of the ligament. The shape of the ligament attachments were investigated in both neutral positions 35º and after stretching in full abduction position 60º (Figure 3.12).

Also, the volumes of each ligament were recorded in cubic millimetres (mean ± SD). The ligaments of the TMC joint are small and have an irregular shape; three lines were depicted along the anterior surface of each ligament for length and width measurement.

The length of each ligament was calculated by summing the average of corresponding horizontal lines, the width was calculated by summing the average of the vertical lines and the thickness was calculated by summing the three perpendicular lines, respectively (Figures 3.13-3.14-3.15).

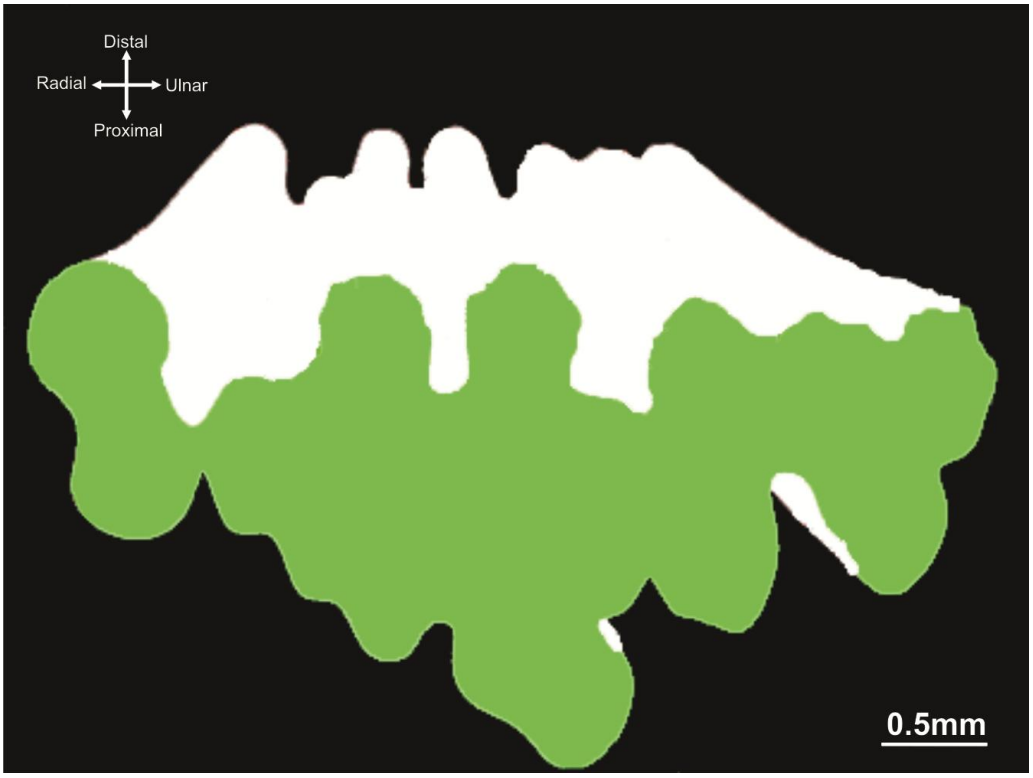

Figure 3.12: 3D shape of a ligament.
The green surface shows the cross-sectional area of the ligament and the shape of the attachment.

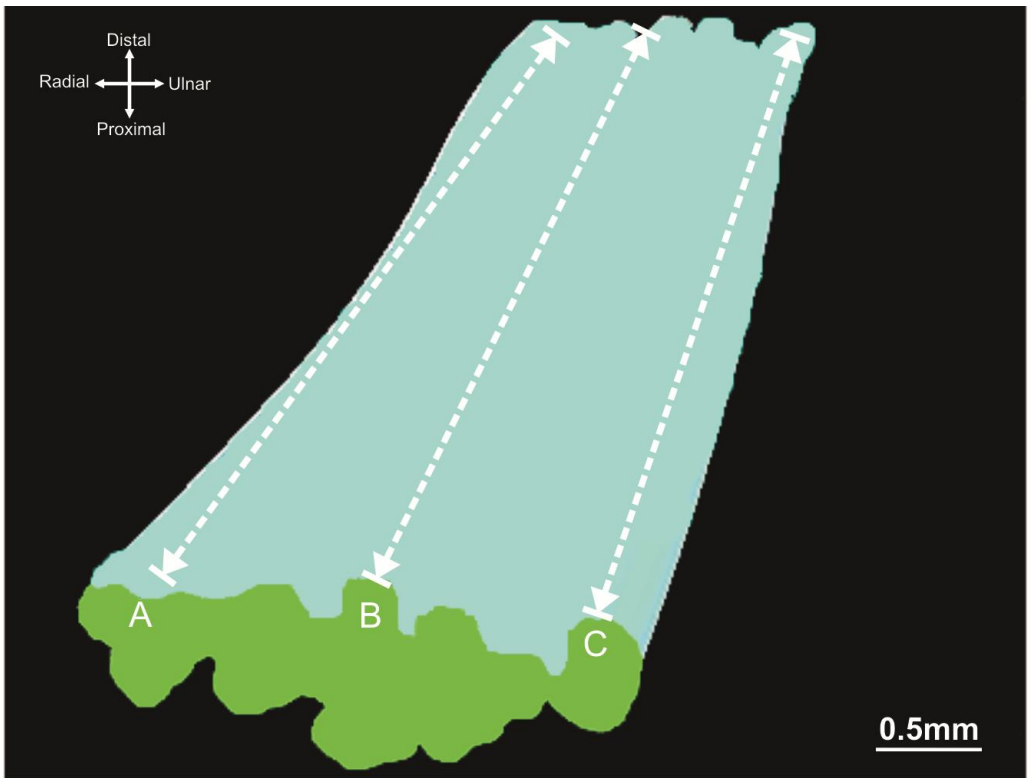

Figure 3.13: 3D shape of a ligament with three length lines.
Three lines were drawn horizontally to measure the length of the ligament: (A) a radial line was drawn in the border of the ligament on the radial side, (B) a middle line was drawn in the middle between both the border lines and (C) an ulnar line was drawn on the border of the ligament on the ulnar side.

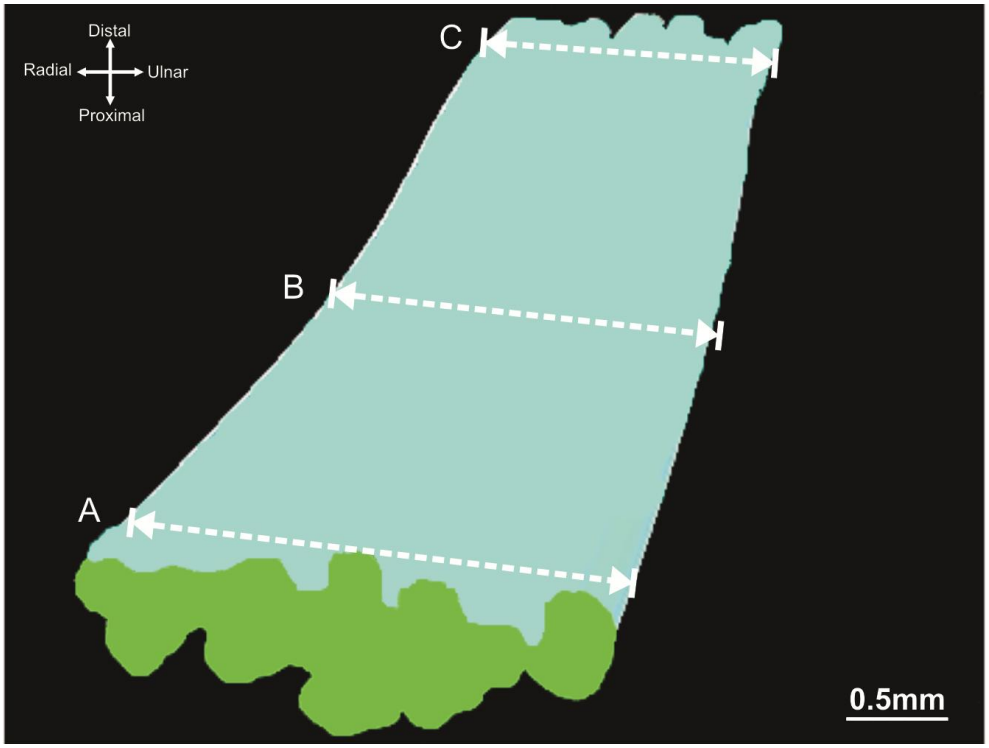

Figure 3.14: 3D shape of a ligament with three width lines.
Three lines were drawn vertically to measure the width of the ligament: (A) a proximal line was drawn in the proximal attachment of the ligament, (B) a mid-portion line was drawn in the middle between both lines (A, C) and (C) a distal line was drawn in the distal attachment of the ligament.

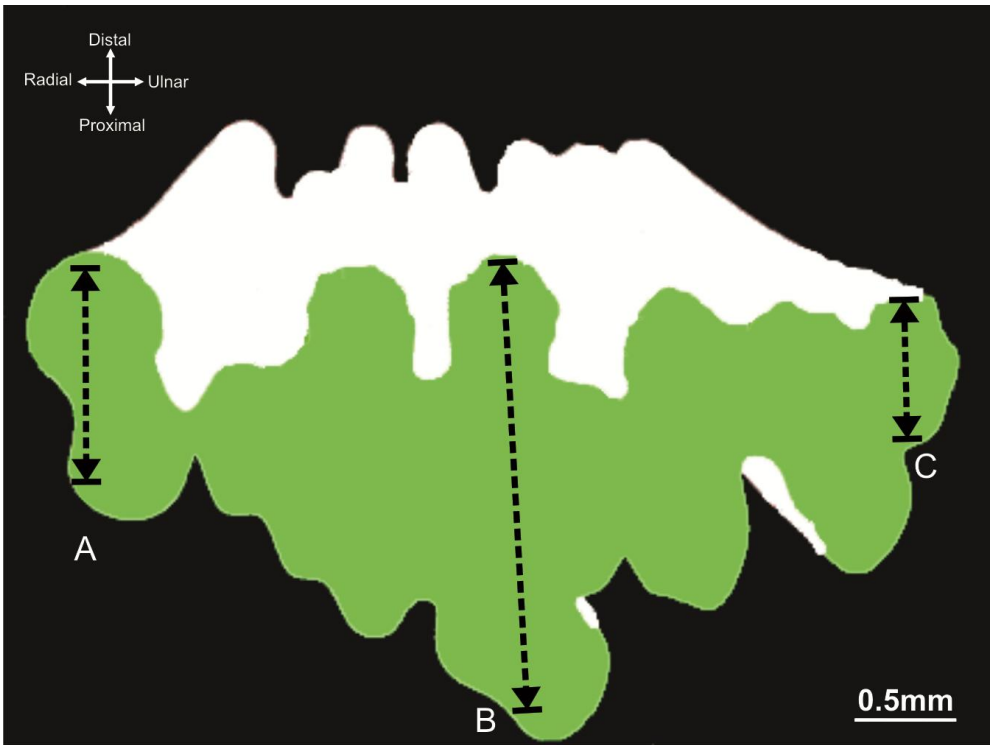

Figure 3.15: 3D of a ligament with three thickness lines.
Three lines were drawn perpendicularly to measure the thickness of the ligament: (A) a radial thickness line was drawn in the radial side of the ligament, (B) a mid-portion thickness line was drawn in the middle between both lines (A, C) and (C) an ulnar thickness line was drawn in the ulnar side of the ligament.

The three thickness lines were named according to the anatomical position, which is followed by:

1. A radial thickness line, which is the line that comes perpendicularly to the ligament at the radial side, and it begins from the highest point of the fascicle to the lowest point of the same fascicle.

2. An ulnar thickness line, which is the line that comes perpendicularly to the ligament at the ulnar side, and it begins from the highest point of the fascicle to the lowest point of the same fascicle.

3. A mid-portion thickness line, which is the line that comes perpendicularly to the ligament at the mid-portion between both radial and ulnar thickness lines, and it begins from the highest point of the fascicle to the lowest point of the same fascicle (Figure 3.15).

The dynamic displacements percentage was calculated for all geometrical measurements of the ligament during the static neutral and full abduction positions by summing the individual measurements for all TMC ligaments, such as a length, and dividing the results of the specific measuring of specific ligament and then multiplying by one hundred:

$$the\ dynamic\ displacement\ percentage = \frac{\text{specific measuring}}{\text{total measuring}} \times 100$$

For statistical analysis, 2 tailed paired *t*- test was used for comparisons between the length, width and area of the TMC ligaments through static neutral 35° and static full abduction 60° positions. The Student's *t* test was used to compare the mean values between the two-dimensional reconstruction in the previous study and the three-dimensional modelling in the current study.

A manual calliper was used to measure the 3rd MC and to index the measurement against hand size (Munoz *et al.* 2001; Musgrave and Harneja 1978). (Figure 2.11); the equation used for this procedure was:

$$Index\ Ligament = \frac{\text{Raw Ligament}}{\text{Index Value (61.16)}}$$

Raw Ligament is the actual measuring of one of the TMC ligaments. *Index value* which is the mean of 3rd MC length was (61.16). The result of the equation presents by *index ligament* which is the accurate reading of each TMC ligaments against a variety of hand specimen sizes. The equation was applied in all TMC joint measurements (area, length, and width) to confirm the result accurancy against different hands size.

In addition, intra-observer data were recorded; this method is believed to give a more accurate, precise and reproducible measurement. One of the averages of the four experiments was then arbitrarily selected for further analysis.

3.2.8 Ligament curvatures and tension analysis

The curvatures of the TMC ligaments were observed throughout (Rhinoceros software V5). The process of using this procedure by managing the three-dimensional shape of the TMC ligament and converting it to three-dimensional with default dynamic shape. The three-dimensional default dynamic shape has three colours demonstrated by: red represents the relaxed area or the area without potential tension, blue represents forces or tensions acting upon the fascicles and green represents the curvatures of the fascicles throughout static neutral and full abduction positions (Figure 3.16). The curvatures and tensions were applied on the fascicles by dividing the surface of the ligament fascicles into three surface zones: the proximal surface zone, which is the area on the surface of the ligament fascicles elongated from the middle surface zone to the proximal edge at the proximal attachment; the middle surface zone, which is the restricted area between both proximal and distal surface zones; and the distal surface zone, which is the remaining area, beginning from the middle surface zone to the distal edge at the distal attachment (Figure 3.17).

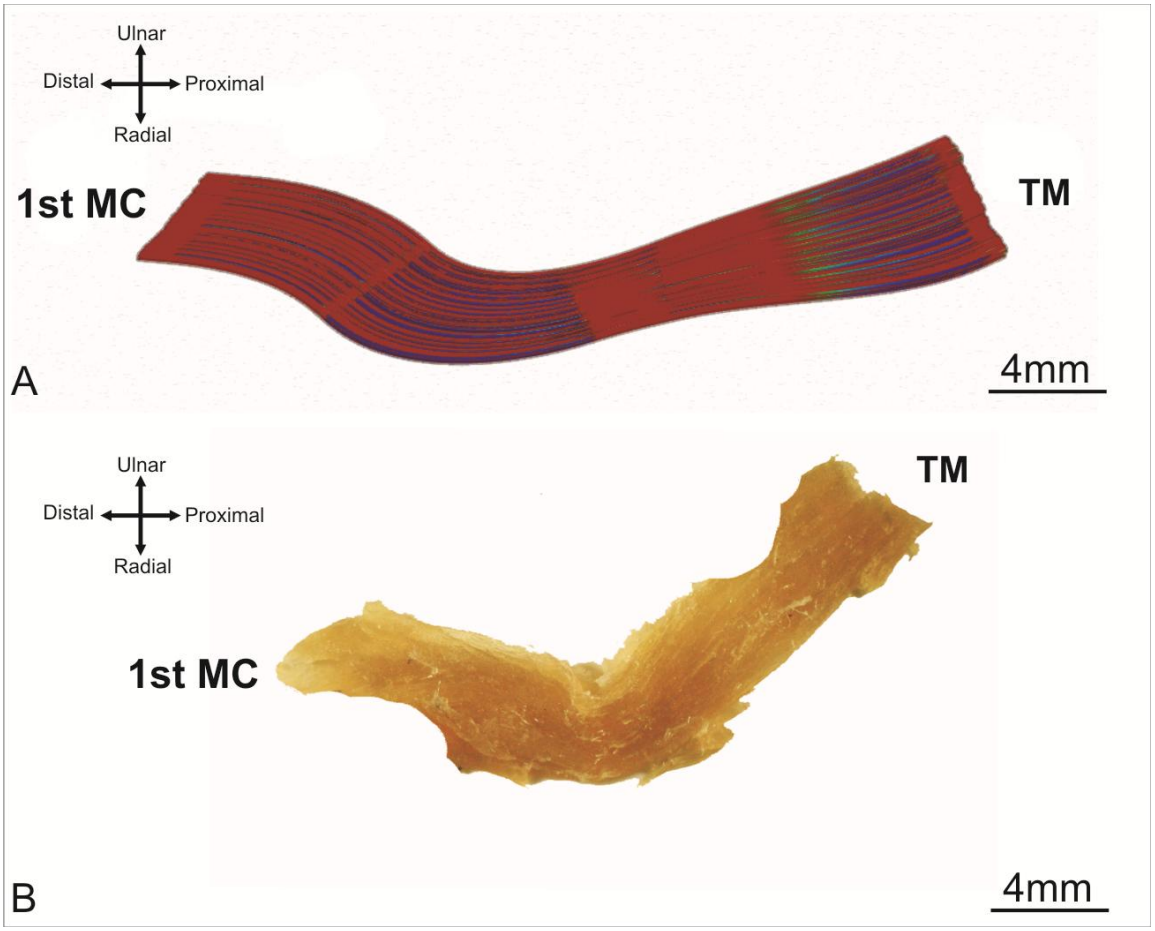

Figure 3.16: Surface curvature and tensions analysis of the PUTML.

(A) 3D model of the ligament, the figure illustrates the curvature and tension, the red colour represents a lack of tension upon the fascicles. The blue colour represents potential tension on the fascicles. The green colour represents the curvature of the fascicles. (TM) trapezium bone. (1^{st} MC) first metacarpal bone. (B) Actual shape of the PUTML after the bone connections was removed.

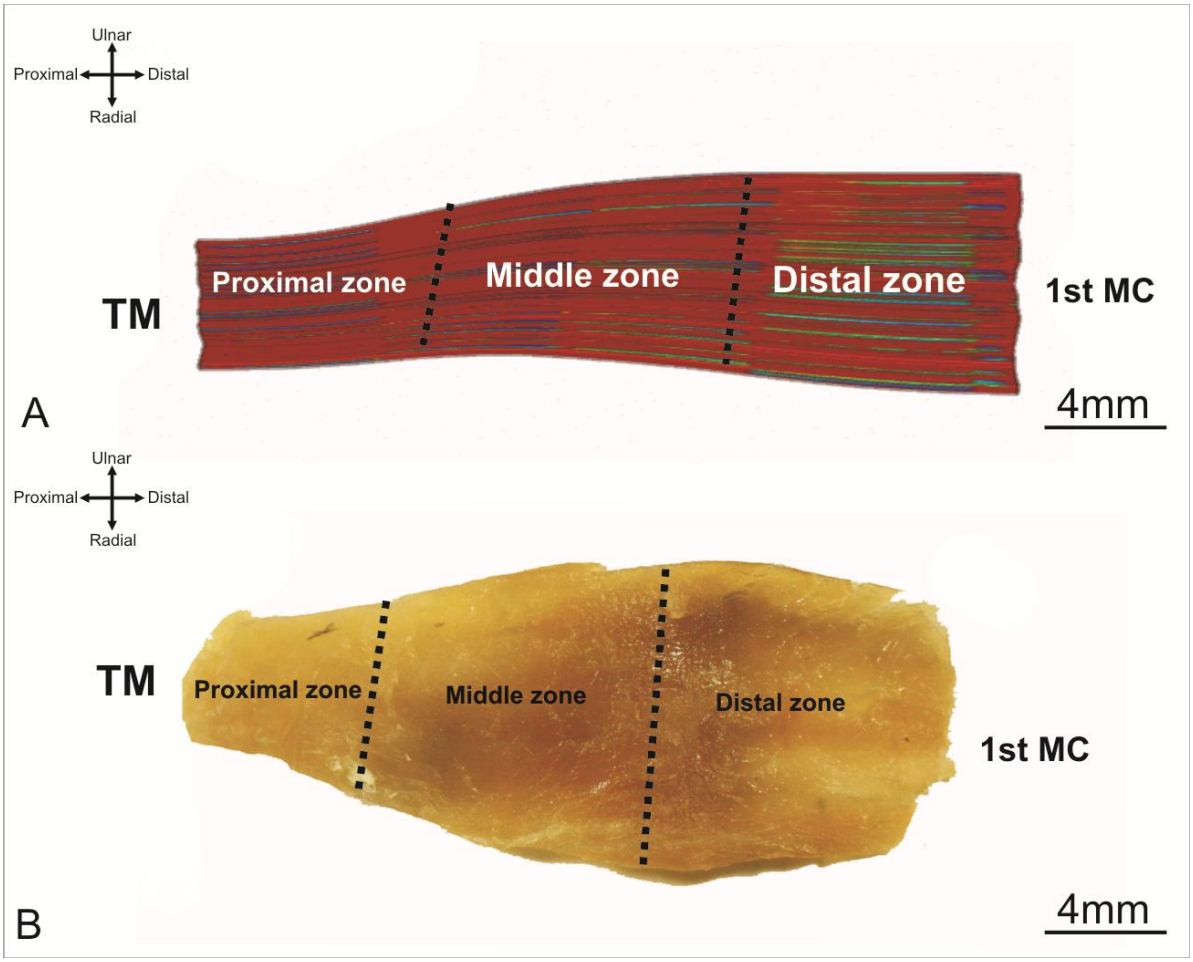

Figure 3.17: Surface curvature and tensions analysis of the PIML.

(A) 3D model of the ligament, the figure illustrates the curvatures and tensions were applied on the fascicles by dividing the surface of the ligament fascicles into three surface zones: the proximal surface zone, which is the area on the surface of the ligament fascicles elongated from the middle surface zone to the proximal edge at the proximal attachment; the middle surface zone, which is the restricted area between both proximal and distal surface zones and the distal surface zone, which is the remaining area, beginning from the middle surface zone to the distal edge at the distal attachment.
(B) Actual shape of the PIML after the bone connections was removed.

3.2.9 Ligament edge analysis

The shape of the fascicles entering the bone was observed in the current study – both edges of the ligament: proximal edge and distal edge – which illustrated how the mechanism of the ligament fascicles entered (attachment zone) inside the bone. The edge was divided into three attachments zones: the radial attachment zone, which was the area elongated from the middle zone to the radial border of the ligament fascicles at the radial side; the middle attachment zone, which was the area restricted between both radial and ulnar attachments zones;

and the ulnar attachment zone, which was the area beginning from the middle attachment zone to the ulnar border of the ligament fascicles at the ulnar side (Figures 3.18-3.19).

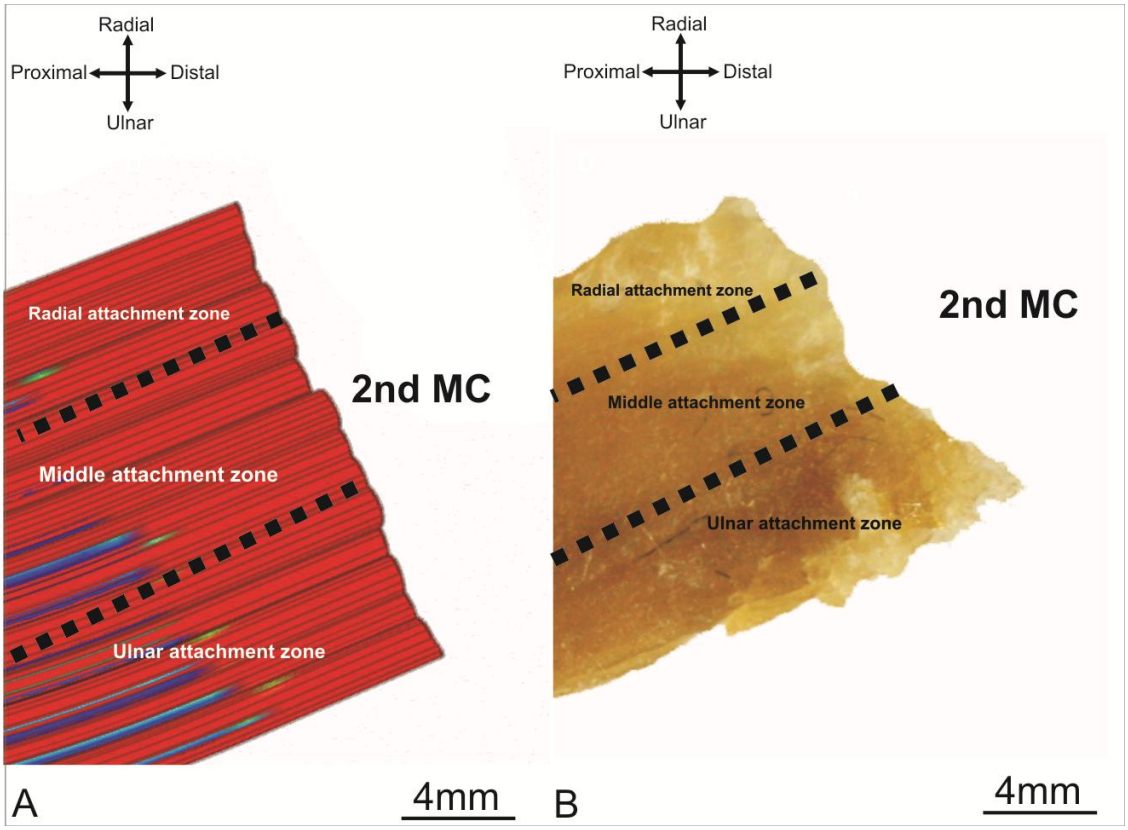

Figure 3.18: Edge analysis of the PIML in distal attachment (proximal zone).

(A) 3D model of the ligament, the figure illustrates the edge which divided into three attachments zones: the radial attachment zone, which was the area elongated from the middle zone to the radial border of the ligament fascicles at the radial side; the middle attachment zone, which was the area restricted between both radial and ulnar attachments zones and the ulnar attachment zone, which was the area beginning from the middle attachment zone to the ulnar border of the ligament fascicles at the ulnar side.
(B) Actual edge of the PIML after the bone connections was removed.

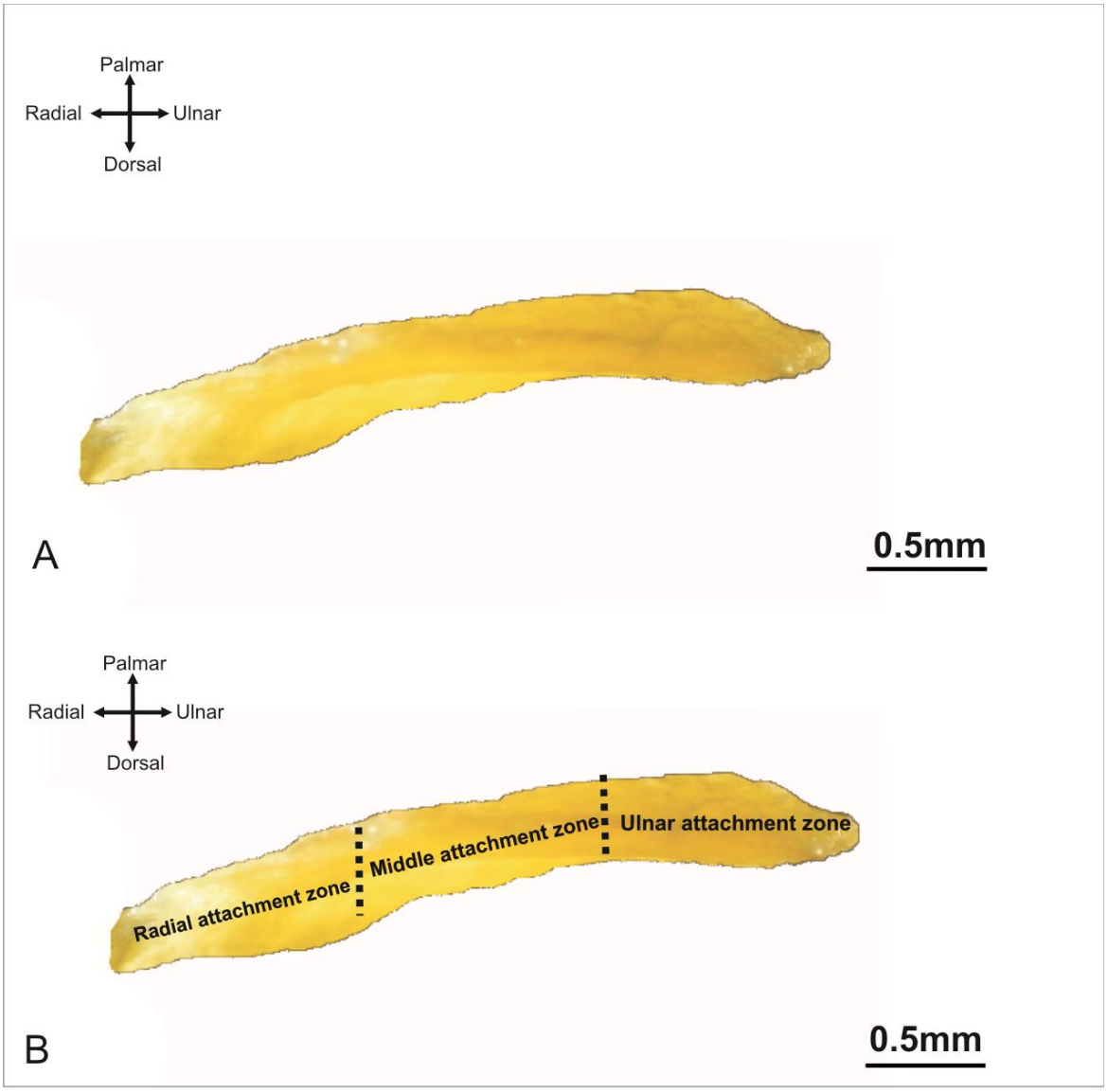

Figure 3.19: Proximal cross-sectional attachment view of PIML.

(A) A cross section of the ligament without identification the attachment zones.
(B) A cross section of the ligament with the attachment zones; radial attachment zone, middle attachment zone and ulnar attachment zone.

3.3 Results

3.3.1 Thickness

The results of the thickness measurements for all TMC ligaments were recorded; there were significant differences ($p<0.05$); sPTML $t = 2.3$, $df = 17$, $p = 0.0033$, PUTML $t = 1.99$, $df = 18$, $p = 0.0048$, DUTML $t = 2.38$, $df = 16$, $p = 0.0029$, PIML $t = 2.04$, $df = 16$, $p = 0.0047$, DIML $t = 2.36$, $df = 17$, $p = 0.03$ between all TMC ligaments except RTML and dPTML, which were recorded with no significant differences ($p>0.05$) during tension on the TMC ligaments from the static neutral toward static full abduction positions (Figure 3.20, Table 3.1).

Also, there were no significant differences ($p>0.05$) in the index procedures between thickness measurements in the static neutral and full abduction positions (Figure 3.21).

Dynamic displacement of the TMC ligament also recorded that PIML has the largest percentage (25%) of total TMC ligament displacement, while dPTML has smallest percentage (6%) of total TMC ligament displacement (Figures 3.22-3.23).

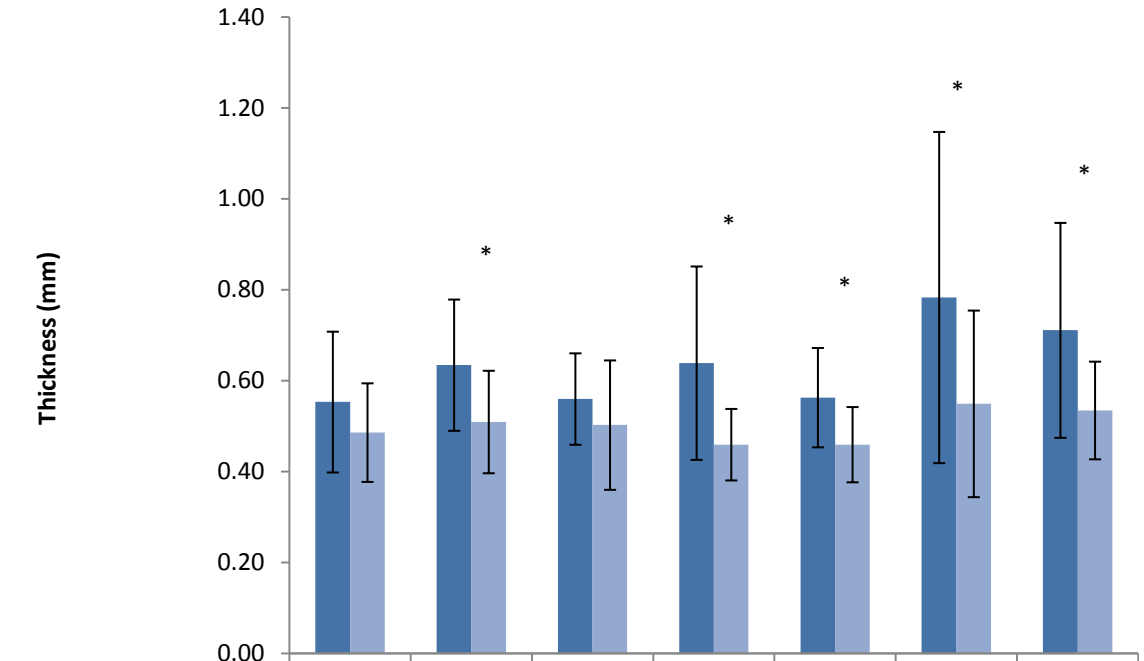

	RTML	sPTML	dPTML	PUTML	DUTML	PIML	DIML
Neutral position	0.55	0.63	0.56	0.64	0.56	0.78	0.71
Full abduction position	0.49	0.51	0.50	0.46	0.46	0.55	0.53

Figure 3.20: Thickness measurements in the static neutral and full abduction positions of the TMC ligaments with their standard deviation. The figure illustrates that there were significant differences ($p<0.05$) between all TMC ligaments except RTML and dPTML during tension on the TMC ligaments from the static neutral toward static full abduction positions. Unit: mm, N=10.

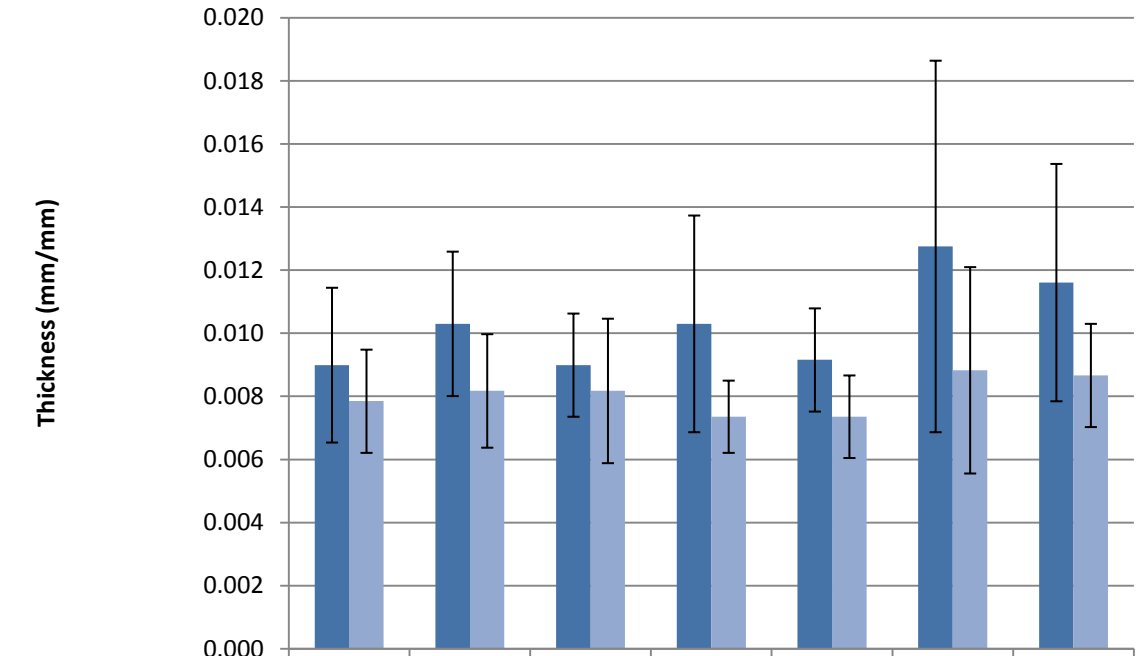

	RTML	sPTML	dPTML	PUTML	DUTML	PIML	DIML
Neutral position	0.009	0.010	0.009	0.010	0.009	0.013	0.012
Full abduction position	0.008	0.008	0.008	0.007	0.007	0.009	0.009

Figure 3.21: Index measurements of thickness in the static neutral and full abduction positions of the TMC ligaments with their standard deviation. The index ligament was indexd against the length (mm) of the third metacarpal. The figure illustrates that there were no significant differences ($p>0.05$) in the index procedures between thickness measurements in the static neutral and full abduction positions. The index ligament was indexed against the length (mm) of the third metacarpal. Unit: mm/mm, N=10.

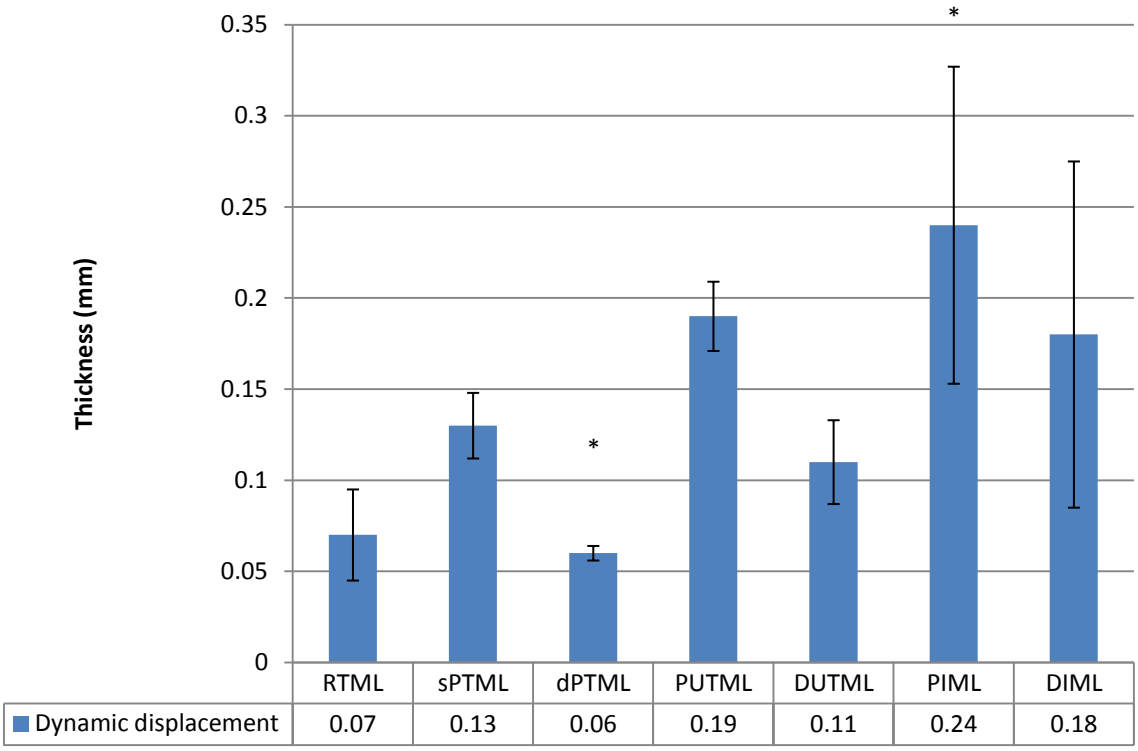

Figure 3.22: Thickness measurements in the dynamic displacement of the TMC ligaments. The figure illustrates that the PIML has the largest of total TMC ligament displacement, while dPTML has smallest of total TMC ligament displacement. Unit: mm, N=10.

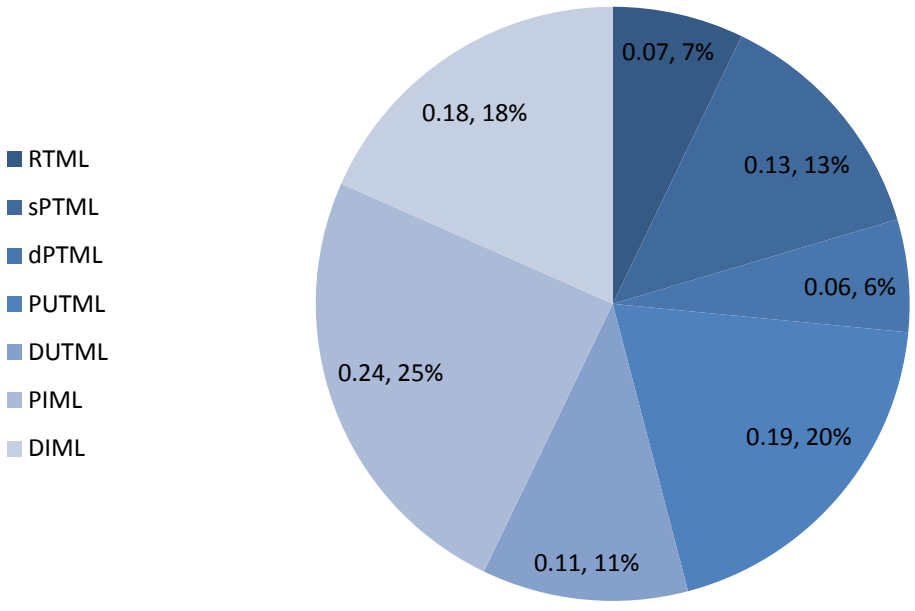

Figure 3.23: Percentages of dynamic displacement in thickness of all TMC ligaments. The figure illustrates that the PIML has the largest percentage (25%) of total TMC ligament displacement, while dPTML has smallest percentage (6%) of total TMC ligament displacement. Unit: mm, N=10.

Ligaments	Static neutral position mm	Static full abduction position mm	Dynamic displacement mm	Percentage of displacement	P value
RTML	0.55 ± 0.15	0.48 ± 0.10	0.07	7%	0.1
sPTML	0.63 ± 0.14	0.50 ± 0.11	0.13	13%	0.0033
dPTML	0.56 ± 0.10	0.50 ± 0.14	0.06	6%	0.085
PUTML	0.64 ± 0.21	0.45 ± 0.07	0.19	19%	0.0048
DUTML	0.56 ± 0.11	0.45 ± 0.08	0.11	11%	0.0029
PML	0.78 ± 0.36	0.54 ± 0.20	0.24	24%	0.0047
DIML	0.71 ± 0.24	0.53 ± 0.10	0.18	18%	0.0030

Table 3.1: Mean of the change in thickness of the TMC ligaments and their standard deviation. p value,unit: mm, N=10.

3.3.2 Length

The results of the length measurements for all TMC ligaments were recorded; there were significant differences ($p<0.05$) in sPTML $t = 1.86$, $df = 10$, $p = 0.049$, PUTML $t = 1.72$, $df = 11$, $p = 0.048$ and DUTML $t = 1.68$, $df = 11$, $p = 0.049$, while RTML, dPTML, PIML and DIML were recorded with no significant differences ($p>0.05$) during tension on the TMC ligaments from the static neutral toward static full abduction positions (Figure 3.24, Table 3.2).

Also, there were no significant differences ($p>0.05$) in the index procedures between length measurements in the static neutral and full abduction positions (Figure 3.25).

Dynamic displacement of the TMC ligament also recorded that DIML has the largest percentage (64%) of total TMC ligament displacement, while dPTML has the smallest percentage (1%) of total TMC ligament displacement (Figures 3.26-3.27).

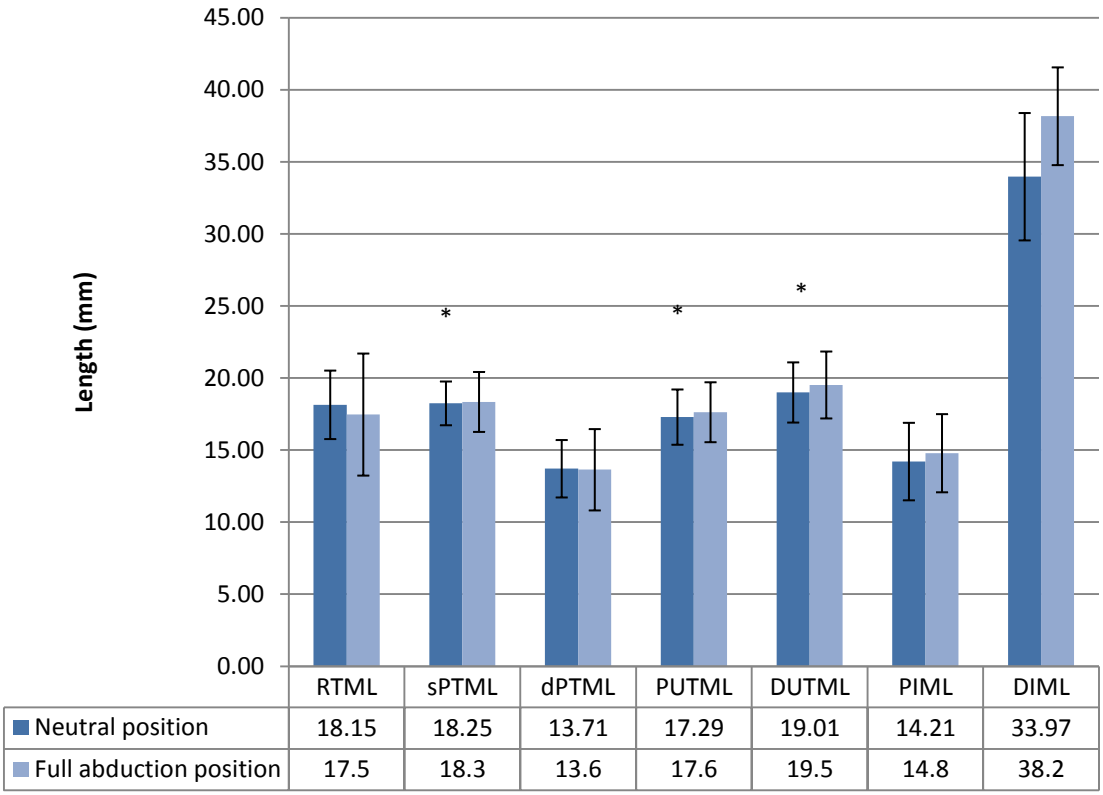

	RTML	sPTML	dPTML	PUTML	DUTML	PIML	DIML
Neutral position	18.15	18.25	13.71	17.29	19.01	14.21	33.97
Full abduction position	17.5	18.3	13.6	17.6	19.5	14.8	38.2

Figure 3.24: Length measurements in the static neutral and full abduction positions of the TMC ligaments with their standard deviation.The figure illustrates that there were significant differences ($p<0.05$) in sPTML, PUTML and DUTML, while RTML, dPTML, PIML and DIML were recorded with no significant differences ($p>0.05$) during tension on the TMC ligaments from the static neutral toward static full abduction positions. Unit: mm, N=10.

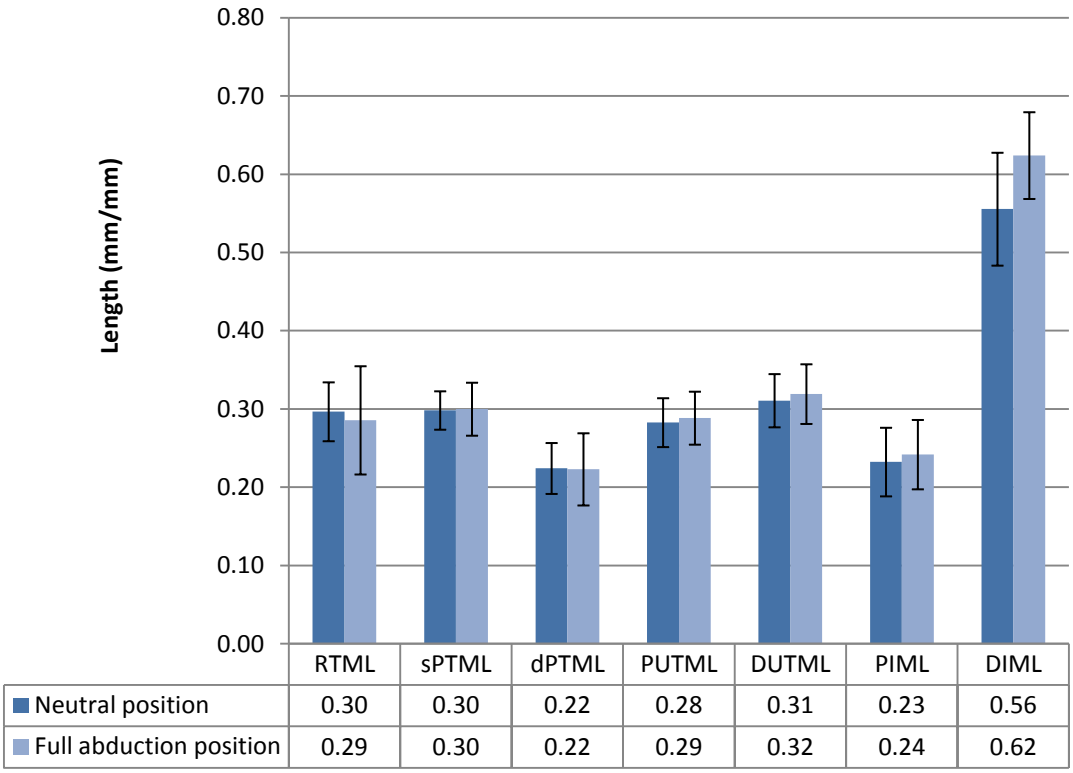

	RTML	sPTML	dPTML	PUTML	DUTML	PIML	DIML
Neutral position	0.30	0.30	0.22	0.28	0.31	0.23	0.56
Full abduction position	0.29	0.30	0.22	0.29	0.32	0.24	0.62

Figure 3.25: Index measurements of the length in static neutral and full abduction positions of the TMC ligaments with their standard deviation. The figure illustrates that there were no significant differences ($p>0.05$) in the index procedures between length measurements in the static neutral and full abduction positions.The index ligament was indexed against the length (mm) of the third metacarpal. Unit: mm/mm, N=10.

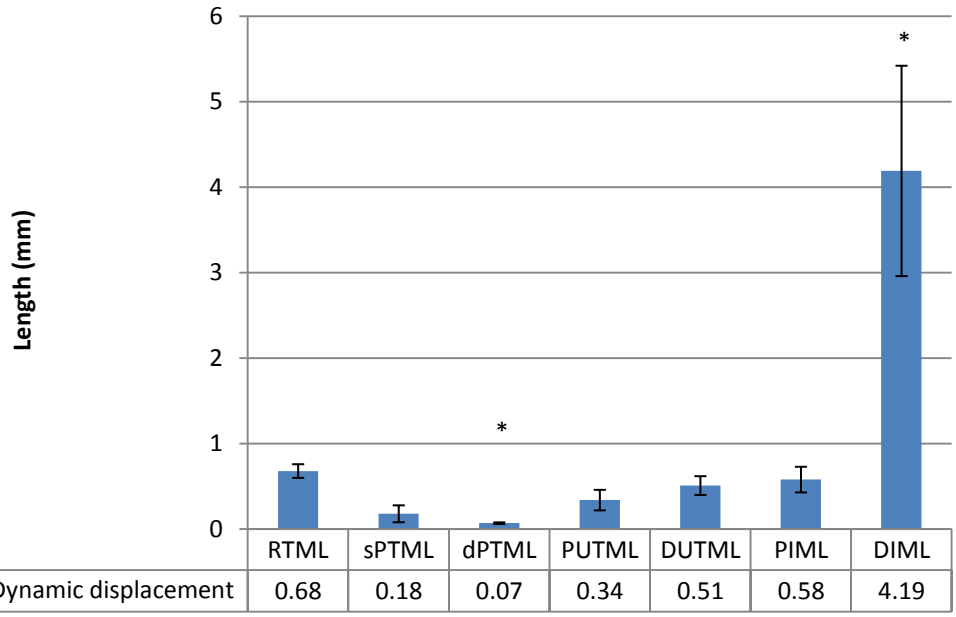

	RTML	sPTML	dPTML	PUTML	DUTML	PIML	DIML
Dynamic displacement	0.68	0.18	0.07	0.34	0.51	0.58	4.19

Figure 3.26: Length measurements in dynamic displacement of the TMC ligaments. The figure illustrates that recorded that DIML has the largest of total TMC ligament displacement, while dPTML has the smallest of total TMC ligament displacement. Unit: mm, N=10.

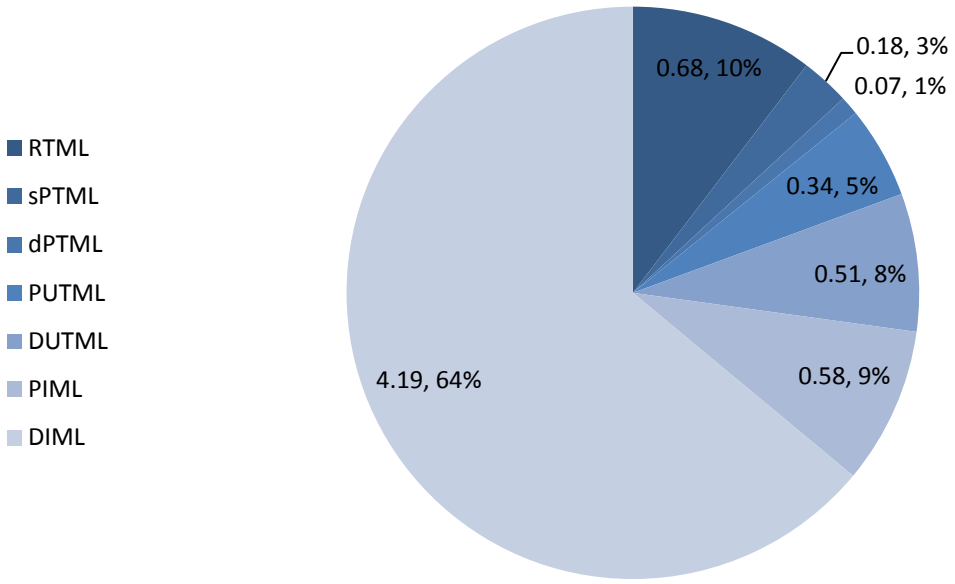

Figure 3.27: Percentages of dynamic displacement in length of all TMC ligaments. The figure illustrates that the DIML has the largest percentage (64%) of total TMC ligament displacement, while dPTML has the smallest percentage (1%) of total TMC ligament displacement. Unit: mm, N=10.

Ligaments	Static neutral position mm	Static full abduction position mm	Dynamic displacement mm	Percentage of displacement	p value
RTML	18.15 ± 2.38	17.47 ± 4.23	0.68	10%	0.16
sPTML	18.25 ± 1.51	18.34 ± 2.07	0.18	3%	0.049
dPTML	13.71 ± 1.99	13.641 ± 2.82	0.07	1%	0.089
PUTML	17.29 ± 1.92	17.63 ± 2.07	0.34	5%	0.048
DUTML	19.01 ± 2.09	19.52 ± 2.32	0.51	8%	0.049
PIML	14.21 ± 2.68	14.79 ± 2.71	0.58	9%	0.69
DIML	33.97 ± 4.41	38.16 ± 3.39	4.19	64%	0.71

Table 3.2: Mean of the change in length of the TMC ligaments and their standard deviation. p value,unit: mm, N=10.

3.3.3 Width

The results of the width measurements for all TMC ligaments were recorded; there were significant differences ($p<0.05$) in sPTML $t = 3.6$, $df = 14$, $p = 0.002$, PUTML $t = 1.88$, $df = 13$, $p = 0.027$, DUTML $t = 1.9$, $df = 15$, $p = 0.049$, PIML $t = 1.68$, $df = 12$, $p = 0.041$, DIML $t = 1.84$, $df = 15$, $p = 0.037$, except RTML and dPTML recorded with no significant differences ($p>0.05$) during tension on the TMC ligaments from the static neutral toward static full abduction positions (Figure 3.28, Table 3.3).

Also, there were no significant differences ($p>0.05$) in the index procedures between width measurements in the static neutral and full abduction positions (Figure 3.29).

Dynamic displacement of the TMC ligament also recorded that sPTML has the largest percentage (43%) of total TMC ligament displacement, while RTML and DUTML have the smallest percentage (2%) of total TMC ligament displacement (Figures 3.30-3.31).

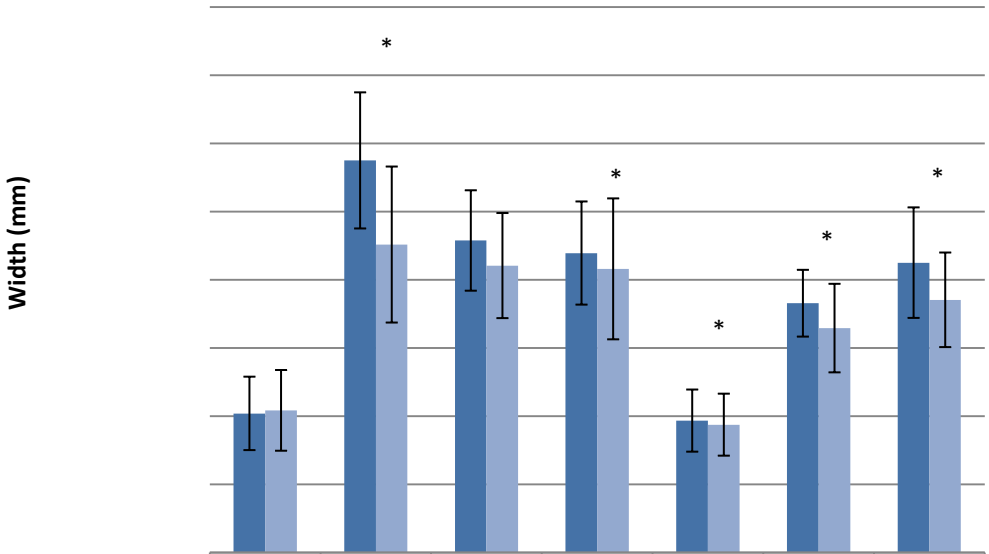

	RTML	sPTML	dPTML	PUTML	DUTML	PIML	DIML
Neutral position	2.04	5.75	4.57	4.39	1.93	3.65	4.25
Full abduction position	2.08	4.52	4.21	4.16	1.87	3.29	3.70

Figure 3.28: Width measurements in the static neutral and full abduction positions of the TMC ligaments with their standard deviation.The figure illustrates that there were significant differences ($p<0.05$) in all TMC ligaments, except RTML and dPTML during tension on the TMC ligaments from the static neutral toward static full abduction positions. Unit: mm, N=10.

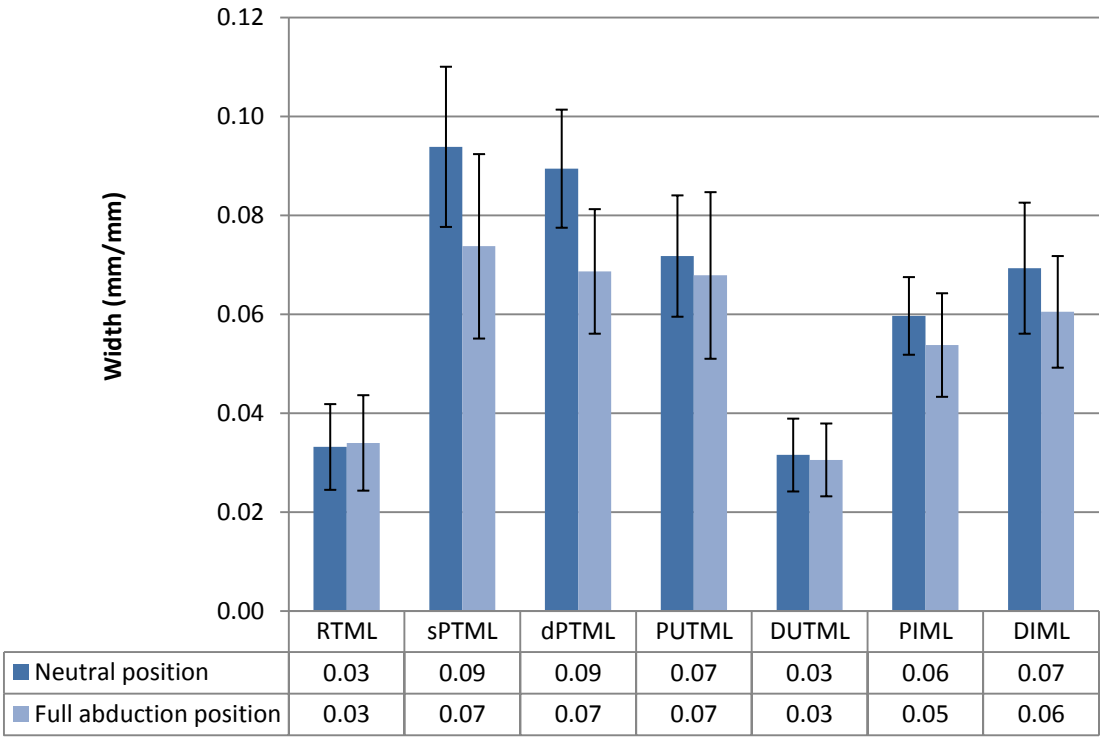

	RTML	sPTML	dPTML	PUTML	DUTML	PIML	DIML
Neutral position	0.03	0.09	0.09	0.07	0.03	0.06	0.07
Full abduction position	0.03	0.07	0.07	0.07	0.03	0.05	0.06

Figure 3.29: Index measurements of the width in static neutral and full abduction positions of the TMC ligaments with their standard deviation. The figure illustrates that there were no significant differences ($p>0.05$) in the index procedures between width measurements in the static neutral and full abduction positions. The index ligament was indexed against the length (mm) of the third metacarpal. Unit: mm/mm, N=10.

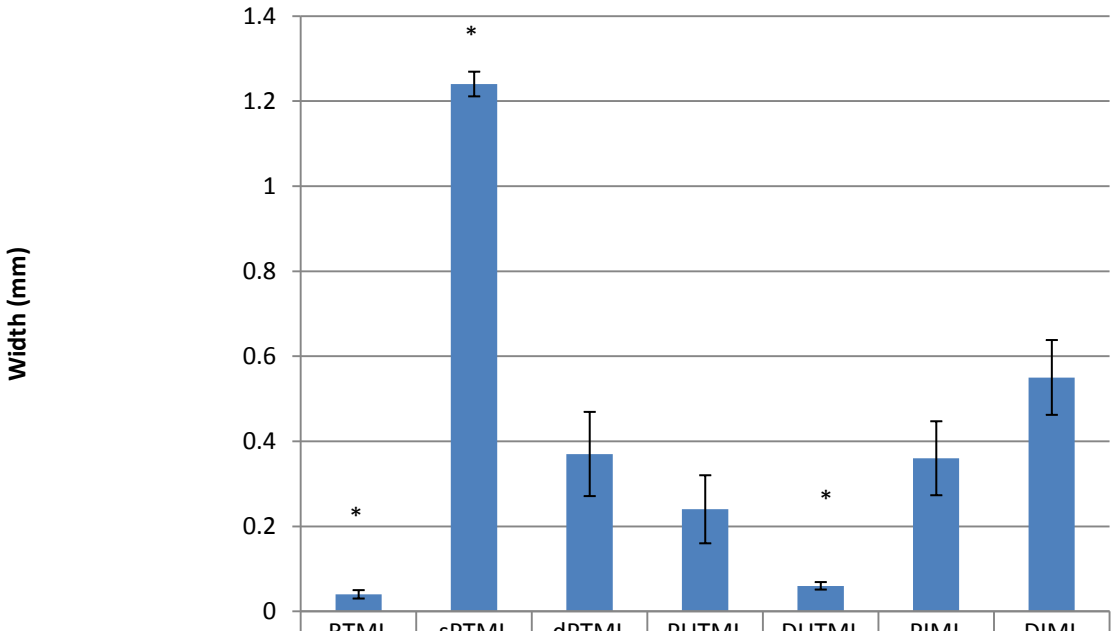

	RTML	sPTML	dPTML	PUTML	DUTML	PIML	DIML
Dynamic displacement	0.04	1.24	0.37	0.24	0.06	0.36	0.55

Figure 3.30: Width measurements in dynamic displacement of the TMC ligaments. The figure illustrates that the sPTML has the largest of total TMC ligament displacement, while RTML and DUTML have the smallest of total TMC ligament displacement. Unit: mm/mm, N=10.

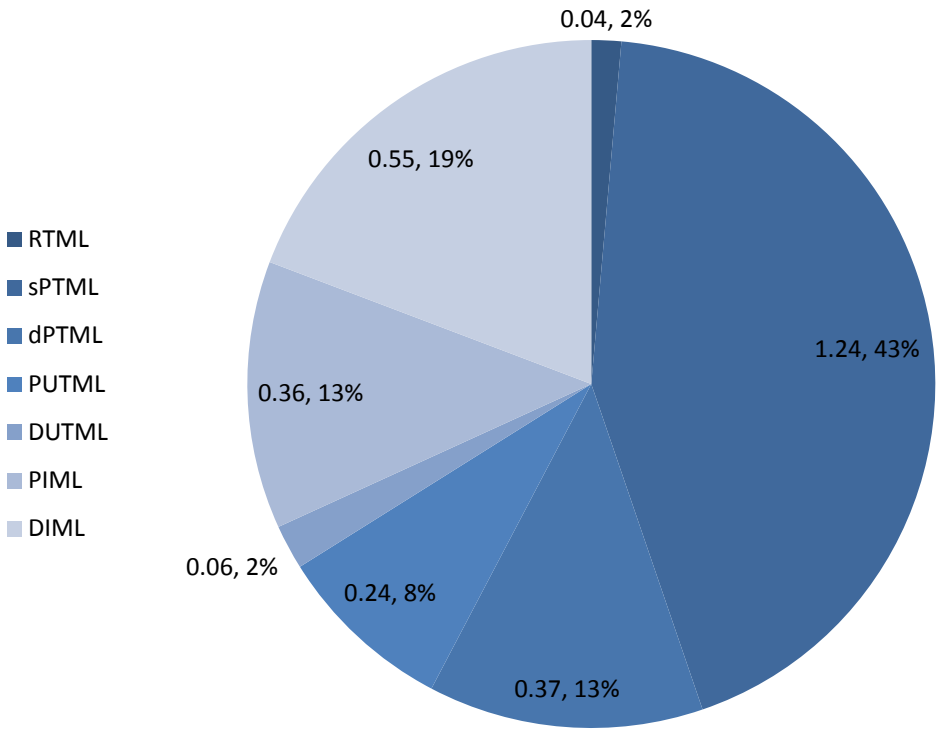

Figure 3.31: Percentages of dynamic displacement in width of all TMC ligaments. The figure illustrates that the sPTML has the largest percentage (43%) of total TMC ligament displacement, while RTML and DUTML have the smallest percentage (2%) of total TMC ligament displacement. Unit: mm/mm, N=10.

Ligaments	Static neutral position mm	Static full abduction position mm	Dynamic displacement mm	Percentage of displacement	p value
RTML	2.04 ± 0.54	2.08 ± 0.59	0.04	2%	0.099
sPTML	5.75 ± 0.99	4.51 ± 1.14	1.24	19%	0.002
dPTML	4.57 ± 0.74	4.20 ± 0.77	0.37	13%	0.074
PUTML	4.39 ± 0.76	4.15 ± 1.03	0.24	2%	0.027
DUTML	1.93 ± 0.45	1.87 ± 0.45	0.06	8%	0.049
PIML	3.65 ± 0.49	3.29 ± 0.64	0.36	13%	0.041
DIML	4.25 ± 0.81	3.70 ± 0.69	0.55	43%	0.037

Table 3.3: Mean of the change in width of the TMC ligaments and their standard deviation. p value, unit: mm/mm, N=10.

3.3.4 Volume

The results of the volume measurements for all TMC ligaments were recorded; there were no significant differences ($p>0.05$) in all TMC ligaments during tension on the TMC ligaments from the static neutral toward static full abduction positions (Figures 3.32, Table 3.4).

Also, there were no significant differences ($p>0.05$) in the index procedures between volume measurements in the static neutral and full abduction positions (Figure 3.33).

Dynamic displacement of the TMC ligament also recorded that DIML has the largest percentage (29%) of total TMC ligament displacement, while RTML and DUTML have the smallest percentage (1%) of total TMC ligament displacement (Figures 3.34-3.35).

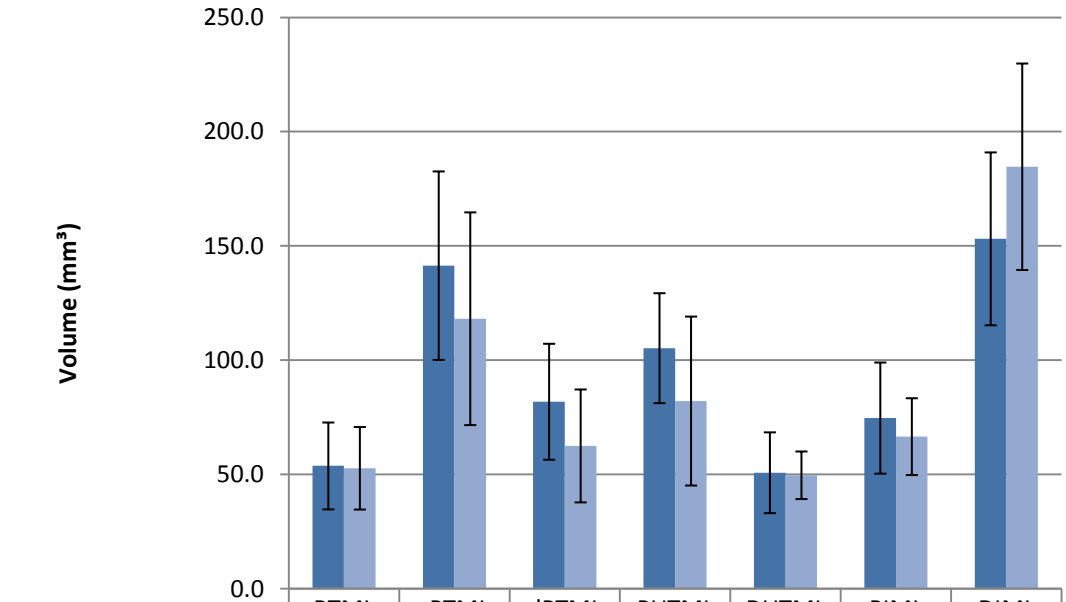

	RTML	sPTML	dPTML	PUTML	DUTML	PIML	DIML
Neutral position	53.7	141.4	81.8	105.3	50.8	74.7	153.1
Full abduction position	52.7	118.2	62.5	82.1	49.7	66.6	184.7

Figure 3.32: Volume measurements in the static neutral and full abduction positions of the TMC ligaments with their standard deviation. The figure illustrates that there were no significant differences ($p>0.05$) in all TMC ligaments during tension on the TMC ligaments from the static neutral toward static full abduction positions. Unit: mm^3, N=10.

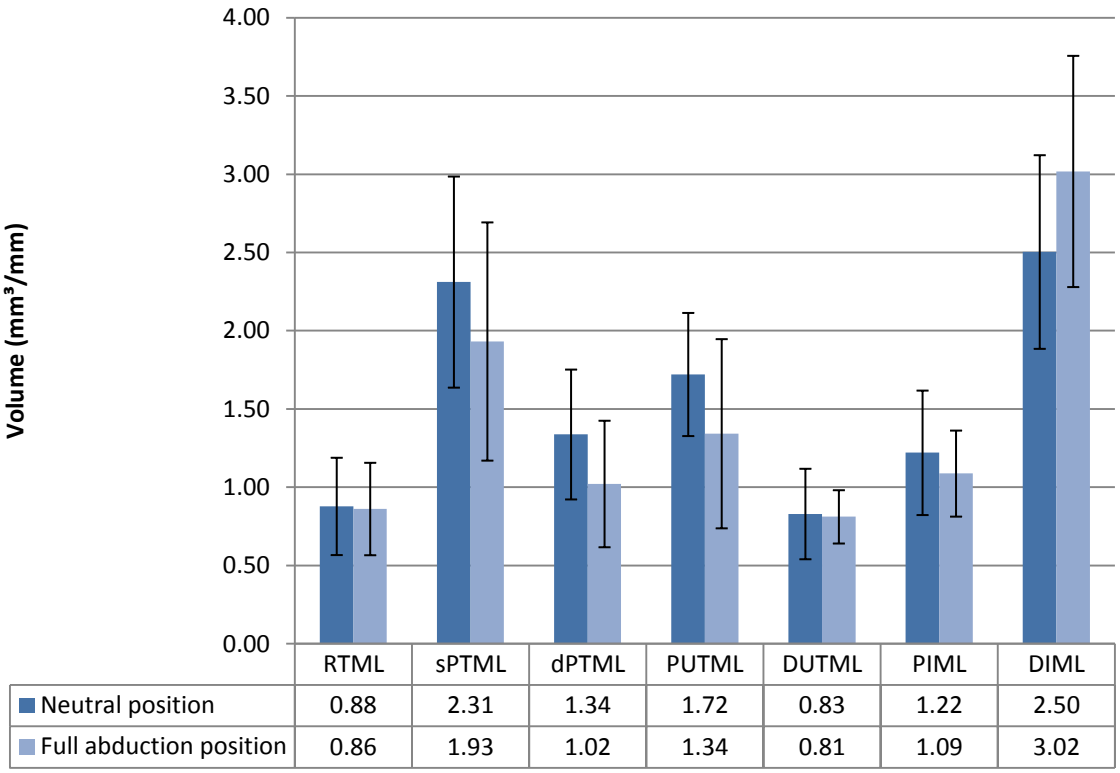

	RTML	sPTML	dPTML	PUTML	DUTML	PIML	DIML
Neutral position	0.88	2.31	1.34	1.72	0.83	1.22	2.50
Full abduction position	0.86	1.93	1.02	1.34	0.81	1.09	3.02

Figure 3.33: Index measurements of the volume in static neutral and full abduction positions of the TMC ligaments with their standard deviation. The figure illustrates that there were no significant differences ($p>0.05$) in the index procedures between volume measurements in the static neutral and full abduction positions. The index ligament was indexed against the length (mm) of the third metacarpal. Unit: mm³, N=10.

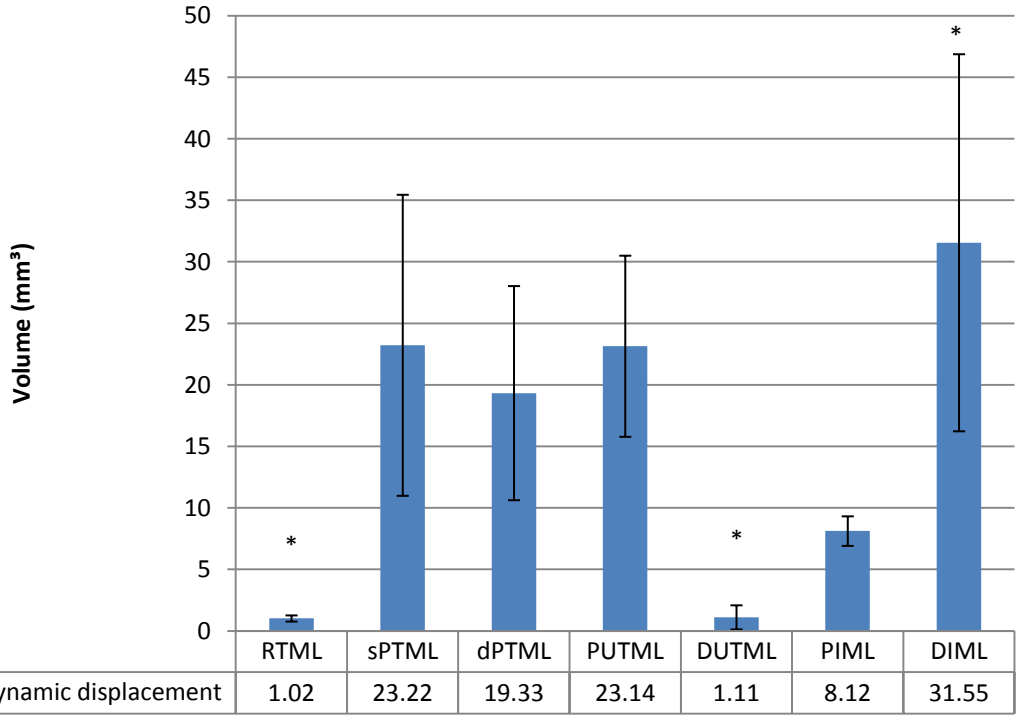

	RTML	sPTML	dPTML	PUTML	DUTML	PIML	DIML
Dynamic displacement	1.02	23.22	19.33	23.14	1.11	8.12	31.55

Figure 3.34: Volume measurements in dynamic displacement of the TMC ligaments. The figure illustrates that the DIML has the largest of total TMC ligament displacement, while RTML and DUTML have the smallest of total TMC ligament displacement. Unit: mm³, N=10.

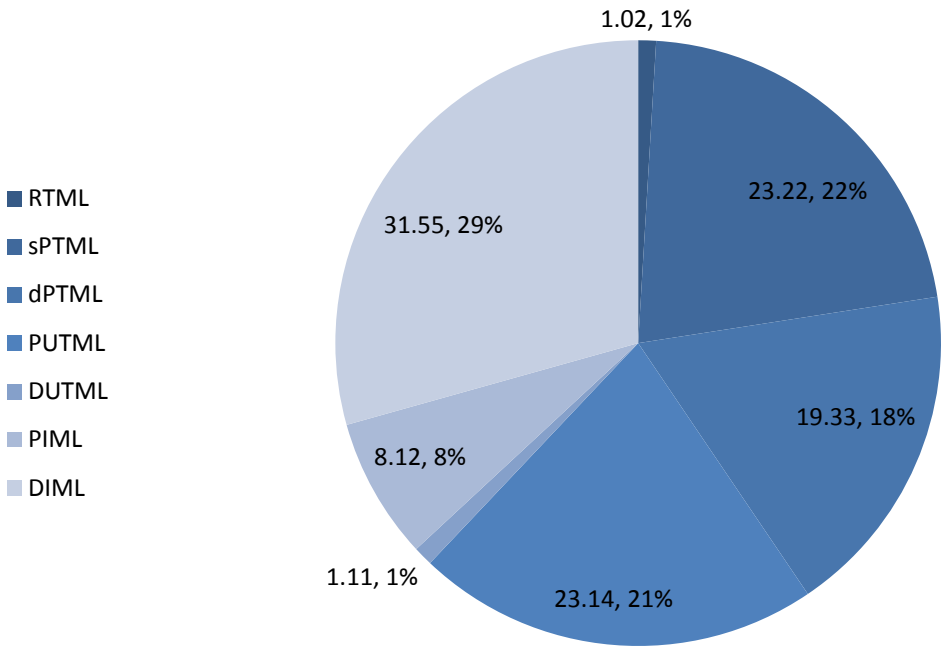

Figure 3.35: Percentages of dynamic displacement in volume of all TMC ligaments. The figure illustrates that the DIML has the largest percentage (29%) of total TMC ligament displacement, while RTML and DUTML have the smallest percentage (1%) of total TMC ligament displacement. Unit: mm³, N=10.

Ligaments	Static neutral position mm³	Static full abduction position mm³	Dynamic displacement mm³	Percentage of displacement
RTML	53.73 ± 19.00	52.71 ± 18.04	1.02	1%
sPTML	141.38 ± 41.24	118.16 ± 46.54	23.22	22%
dPTML	81.82 ± 25.37	62.49 ± 24.71	19.33	18%
PUTML	105.27 ± 24.05	82.13 ± 36.96	23.14	21%
DUTML	50.76 ± 17.67	49.65 ± 10.41	1.11	1%
PIML	74.67 ± 24.31	66.55 ± 16.81	8.12	8%
DIML	153.12 ± 37.83	184.67 ± 45.17	31.55	29%

Table 3.4: Mean of the change in volume of the TMC ligaments and their standard deviation. p value, unit: mm³, N=10.

3.3.5 Proximal cross-sectional area

The results of the proximal cross-sectional area measurement for all TMC ligaments were recorded; there were significant differences ($p<0.05$) in RTML $t = 2.15$, $df = 17$, $p = 0.045$, sPTML $t = 2.19$, $df = 18$, $p = 0.007$, dPTML $t = 2.58$, $df = 16$, $p = 0.019$, PUTML $t = 2.27$, $df = 17$, $p = 0.036$, DUTML $t = 3.49$, $df = 15$, $p = 0.003$, PIML $t = 3.88$, $df = 17$, $p = 0.001$, DIML, 2.42, $df = 15$, p - 0.028 during tension on the TMC ligaments from the static neutral toward static full abduction positions (Figures 3.36, Table 3.5).

Also, there were no significant differences ($p>0.05$) in the index procedures between proximal cross-sectional area measurements in the static neutral and full abduction positions (Figure 3.37).

Dynamic displacement of the TMC ligament also recorded that PIML has the largest percentage (23%) of total TMC ligament displacement, while RTML and DUTML have the smallest percentage (6%) of total TMC ligament displacement (Figures 3.38-3.39).

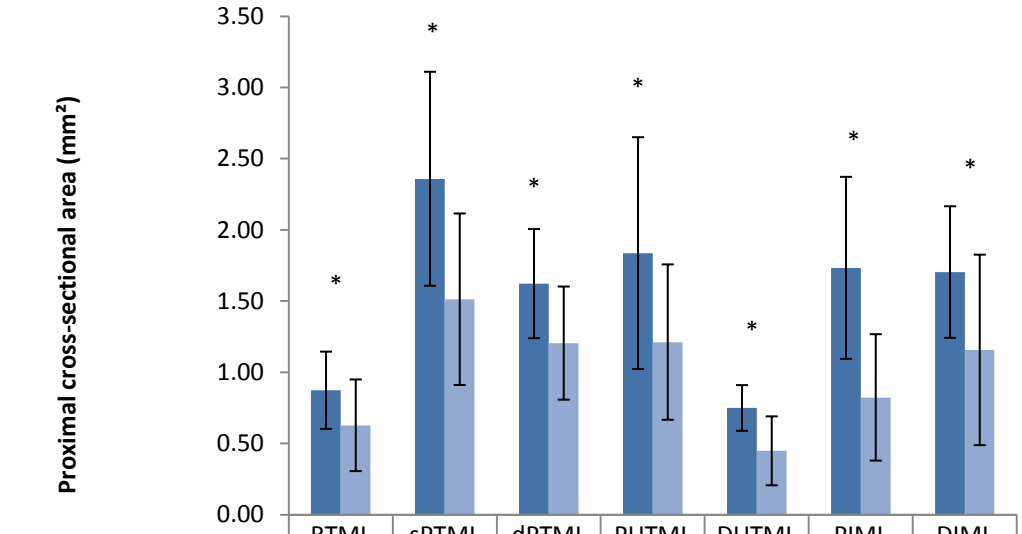

	RTML	sPTML	dPTML	PUTML	DUTML	PIML	DIML
Neutral position	0.87	2.36	1.62	1.84	0.75	1.73	1.70
Full abduction position	0.63	1.51	1.20	1.21	0.45	0.82	1.16

Figure 3.36: Proximal cross-sectional area measurements in the static neutral and full abduction positions of the TMC ligaments with their standard deviation. The figure illustrates that there were significant differences ($p<0.05$) in all TMC ligaments during tension on the TMC ligaments from the static neutral toward static full abduction positions. Unit: mm², N=10.

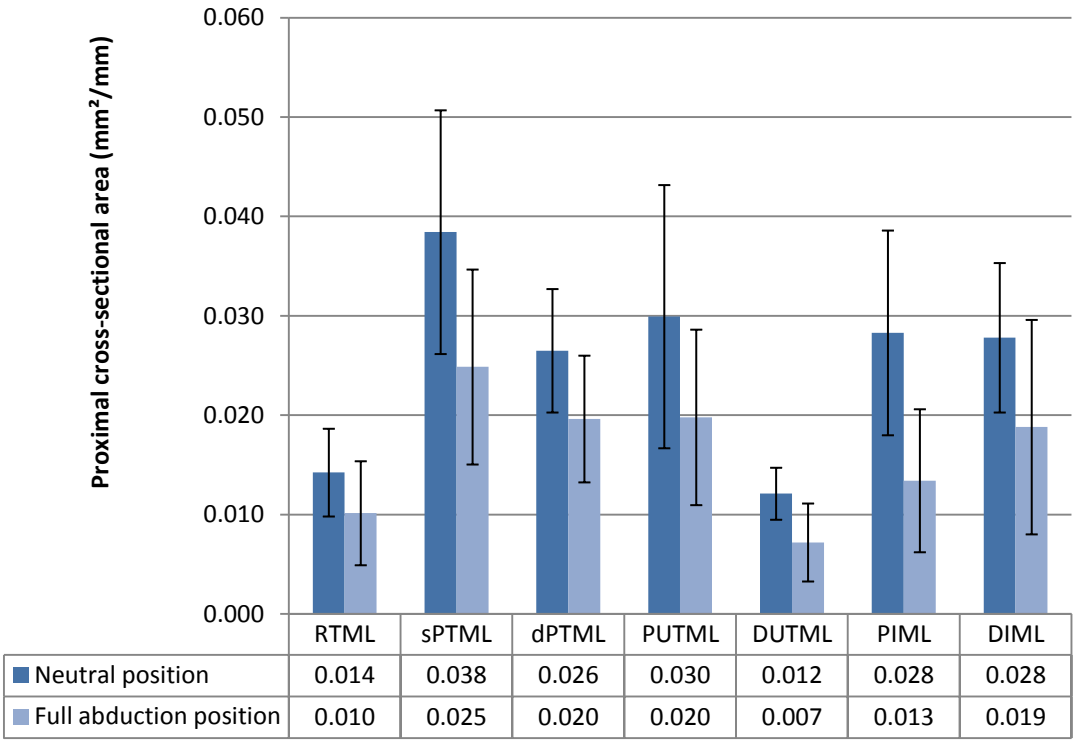

	RTML	sPTML	dPTML	PUTML	DUTML	PIML	DIML
Neutral position	0.014	0.038	0.026	0.030	0.012	0.028	0.028
Full abduction position	0.010	0.025	0.020	0.020	0.007	0.013	0.019

Figure 3.37: Index measurements of proximal cross-sectional area in the static neutral and full abduction positions of the TMC ligaments with their standard deviation. The figure illustrates that were no significant differences ($p>0.05$) in the index procedures between proximal cross-sectional area measurements in the static neutral and full abduction positions. The index ligament was indexed against the length (mm) of the third metacarpal. Unit: mm², N=10.

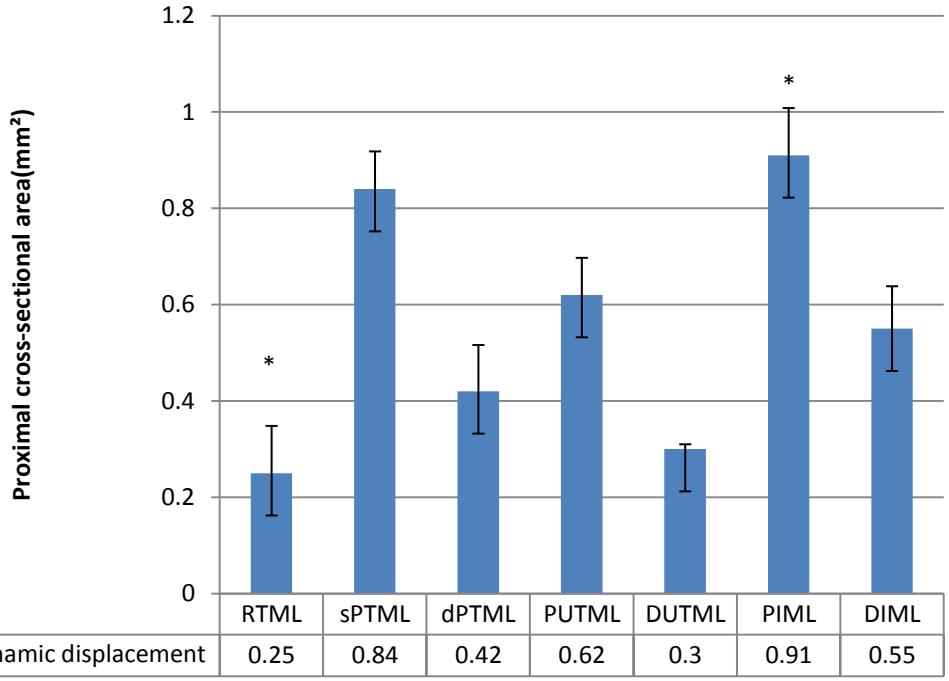

	RTML	sPTML	dPTML	PUTML	DUTML	PIML	DIML
Dynamic displacement	0.25	0.84	0.42	0.62	0.3	0.91	0.55

Figure 3.38: Proximal cross-sectional area measurements in dynamic displacement of the TMC ligaments. The figure illustrates that the PIML has the largest of total TMC ligament displacement, while RTML and DUTML have the smallest of total TMC ligament displacement. Unit: mm², N=10.

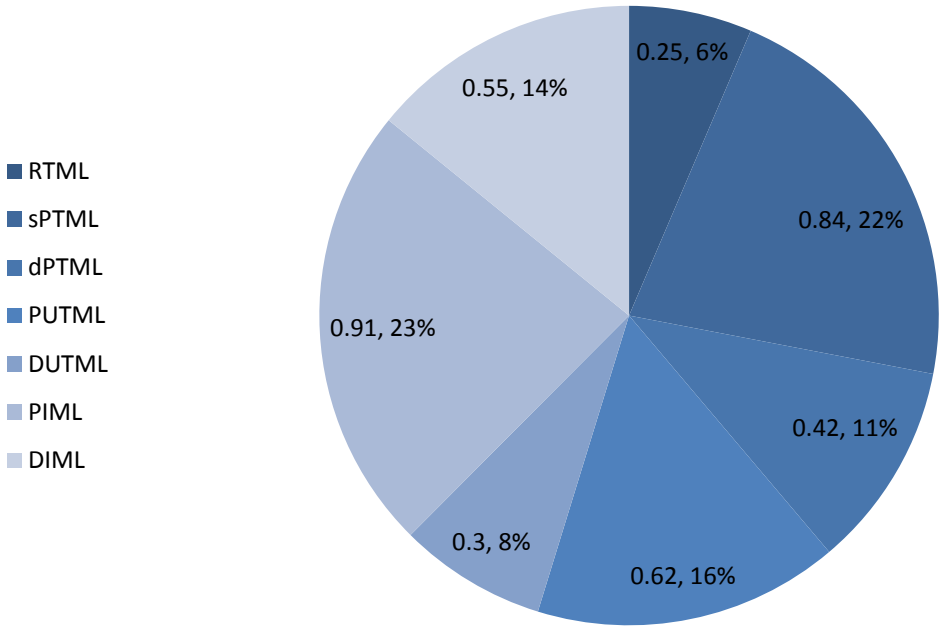

Figure 3.39: Percentages of dynamic displacement in proximal cross-sectional area of all TMC ligaments. The figure illustrates that the PIML has the largest percentage (23%) of total TMC ligament displacement, while RTML and DUTML have the smallest percentage (6%) of total TMC ligament displacement. Unit: mm², N=10.

Ligaments	**Static neutral position mm²**	**Static full abduction position mm²**	**Dynamic displacement mm²**	**Percentage of displacement**	**p value**
RTML	0.87 ± 0.27	0.62 ± 0.32	0.25	6%	0.045
sPTML	2.35 ± 0.75	1.51 ± 0.60	0.84	22%	0.007
dPTML	1.62 ± 0.38	1.20 ± 0.39	0.42	11%	0.019
PUTML	1.83 ± 0.81	1.21 ± 0.54	0.62	16%	0.036
DUTML	0.74 ± 0.16	0.44 ± 0.24	0.3	8%	0.003
PIML	1.73 ± 0.63	0.82 ± 0.44	0.91	23%	0.001
DIML	1.70 ± 0.46	1.15 ± 0.66	0.55	14%	0.028

Table 3.5: Mean of the change in proximal cross-sectional area of the TMC ligaments and their standard deviation. p value, unit: mm², N=10.

3.3.6 Middle cross-sectional area

The results of the middle cross-sectional area measurements for all TMC ligaments were recorded; there were significant differences ($p<0.05$) in sPTML $t = 2.6$, $df = 14$, $p = 0.02$, dPTML $t = 2.11$, $df = 18$, $p = 0.048$, PIML $t = 4$, $df = 15$, $p = 0.001$ and DIML $t = 2.21$, $df = 18$, $p = 0.04$, while there were no significant differences ($p>0.05$) in RTML, PUTML and DUTML during tension on the TMC ligaments from the static neutral toward static full abduction positions (Figure 3.40, Table 3.6).

Also, there were no significant differences ($p>0.05$) in the index procedures between middle cross-sectional area measurements in the static neutral and full abduction positions (Figure 3.41).

Dynamic displacement of the TMC ligament also recorded that PIML has the largest percentage (26%) of total TMC ligament displacement while RTML and DUTML have the smallest percentage (5%) of total TMC ligament displacement (Figures 3.42-3.43).

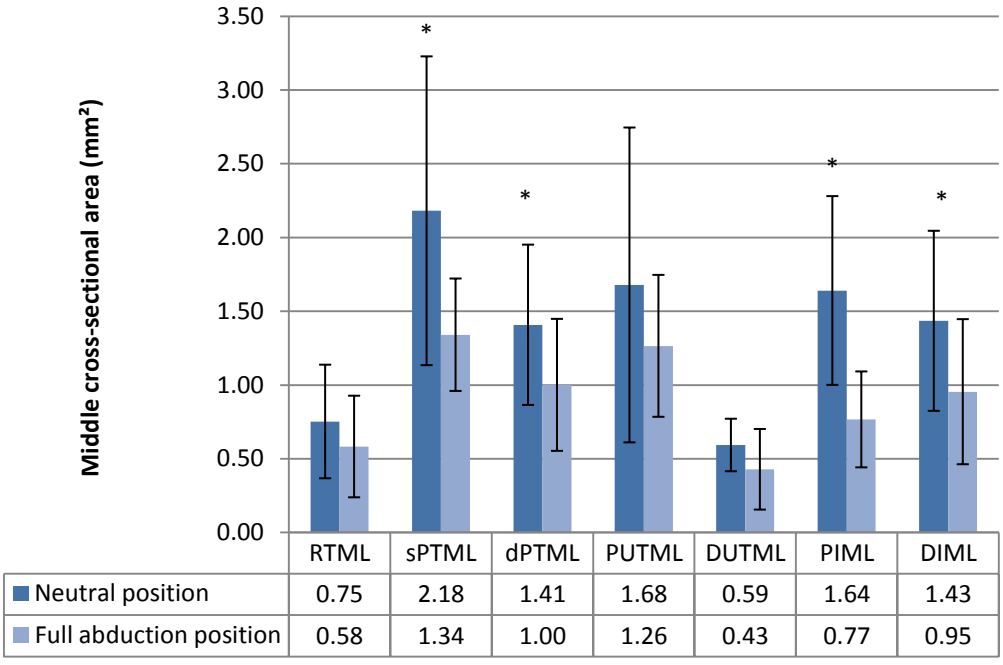

	RTML	sPTML	dPTML	PUTML	DUTML	PIML	DIML
Neutral position	0.75	2.18	1.41	1.68	0.59	1.64	1.43
Full abduction position	0.58	1.34	1.00	1.26	0.43	0.77	0.95

Figure 3.40: Middle cross-sectional area measurements in the static neutral and full abduction positions of the TMC ligaments with their standard deviation.The figure illustrates that there were significant differences ($p<0.05$) in sPTML, dPTML, PIML and DIML, while there were no significant differences ($p>0.05$) in RTML, PUTML and DUTML during tension on the TMC ligaments from the static neutral toward static full abduction positions. Unit: mm², N=10.

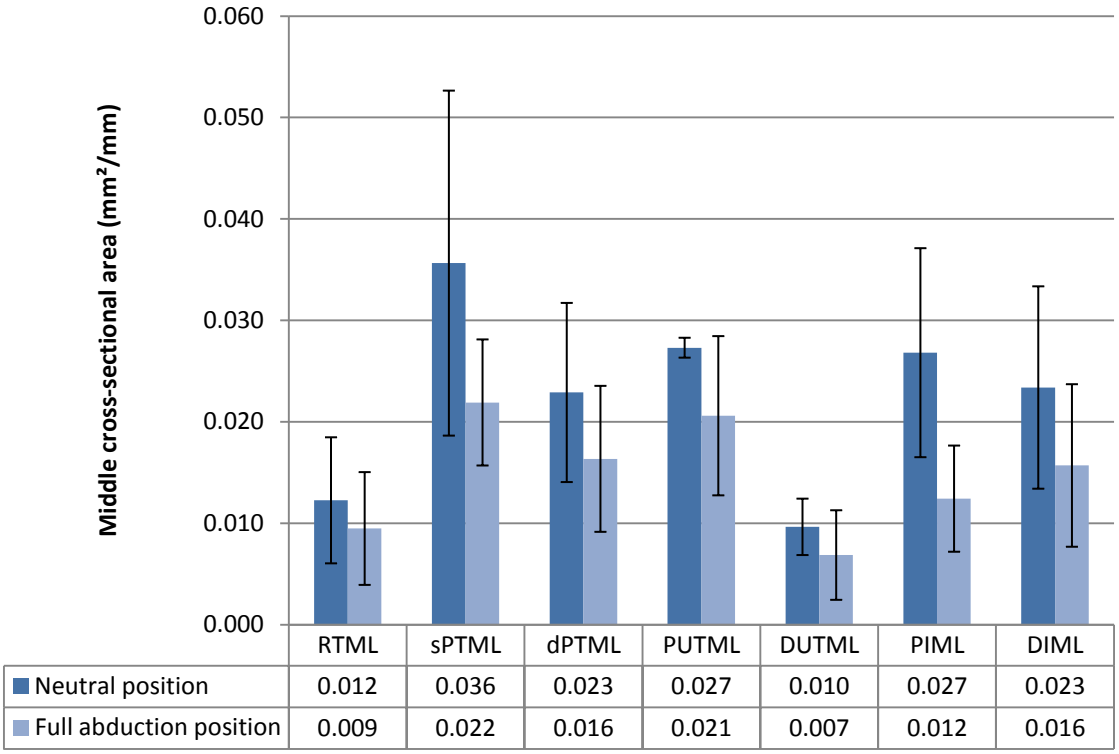

	RTML	sPTML	dPTML	PUTML	DUTML	PIML	DIML
Neutral position	0.012	0.036	0.023	0.027	0.010	0.027	0.023
Full abduction position	0.009	0.022	0.016	0.021	0.007	0.012	0.016

Figure 3.41: Index measurements of middle cross-sectional area in the static neutral and full abduction positions of the TMC ligaments with their standard deviation. The figure illustrates that there were no significant differences ($p>0.05$) in the index procedures between middle cross-sectional area measurements in the static neutral and full abduction positions. The index ligament was indexd against the length (mm) of the third metacarpal. Unit: mm², N=10.

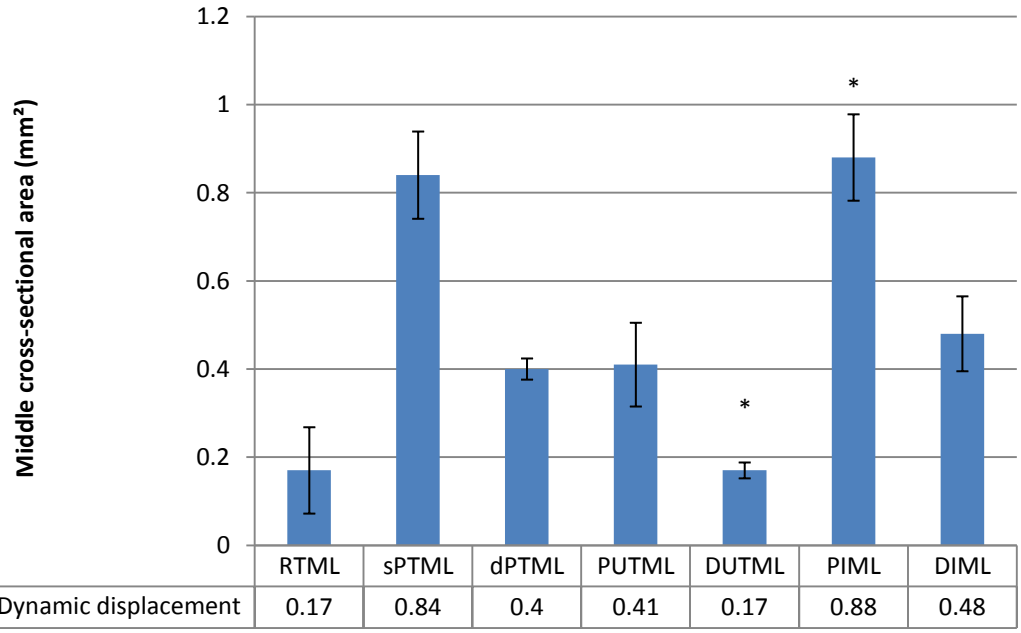

	RTML	sPTML	dPTML	PUTML	DUTML	PIML	DIML
Dynamic displacement	0.17	0.84	0.4	0.41	0.17	0.88	0.48

Figure 3.42: Middle cross-sectional area measurements in dynamic displacement of the TMC ligaments. The figure illustrates that the PIML has the largest of total TMC ligament displacement while RTML and DUTML have the smallest of total TMC ligament displacement. Unit: mm², N=10.

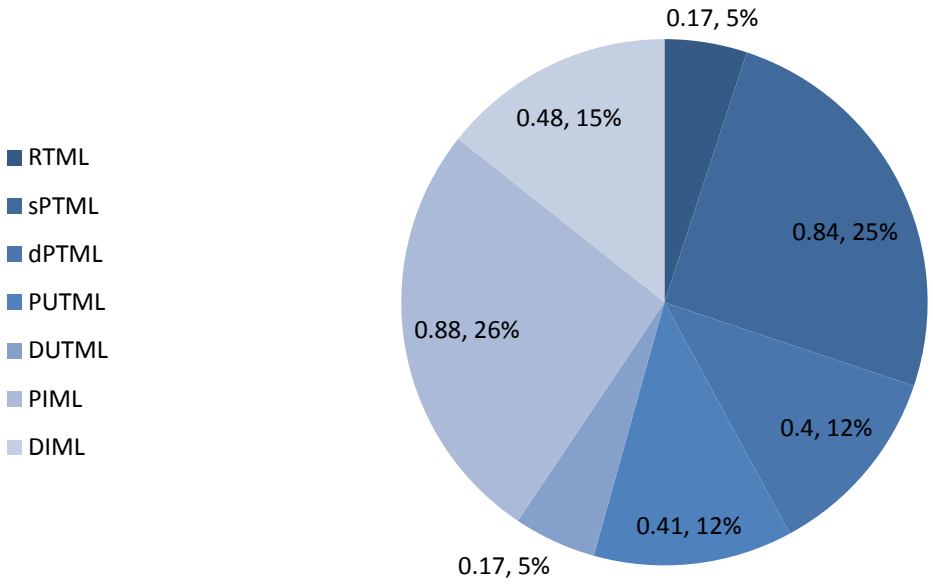

Figure 3.43: Percentages of dynamic displacement in middle cross-sectional area of all TMC ligaments. The figure illustrates that the PIML has the largest percentage (26%) of total TMC ligament displacement while RTML and DUTML have the smallest percentage (5%) of total TMC ligament displacement. Unit: mm², N=10.

Ligaments	Static neutral position mm²	Static full abduction position mm²	Dynamic displacement mm²	Percentage of displacement	p value
RTML	0.75 ± 0.38	0.58 ± 0.34	0.17	5%	0.65
sPTML	2.18 ± 1.04	1.34 ± 0.38	0.84	25%	0.02
dPTML	1.40 ± 0.54	1.00 ± 0.44	0.4	12%	0.048
PUTML	1.67 ± 1.06	1.26 ± 0.48	0.41	12%	0.85
DUTML	0.59 ± 0.17	0.42 ± 0.27	0.17	5%	0.98
PIML	1.64 ± 0.63	0.76 ± 0.32	0.88	26%	0.001
DIML	1.43 ± 0.61	0.95 ± 0.49	0.48	15%	0.04

Table 3.6: Mean of the change in middle cross-sectional area of the TMC ligaments and their standard deviation. p value, unit: mm², N=10.

3.3.7 Distal cross-sectional area

The results of the distal cross-sectional area measurements for all TMC ligaments were recorded; there were no a significant differences (p>0.05) in all

TMC ligaments, except PIML t = 3.10, df = 14, p = 0.007 and DIML t = 2.9, df = 18, p = 0.008 had significant differences (p<0.05) during tension on the TMC ligaments from the static neutral toward static full abduction positions (Figure 3.44, Table 3.7).

Also, there were no significant differences (p>0.05) in the index procedures between distal cross-sectional area measurements in the static neutral and full abduction positions (Figure 3.45).

Dynamic displacement of the TMC ligament also recorded that PIML has the largest percentage (26%) of total TMC ligament displacement while RTML has the smallest percentage (2%) of total TMC ligament displacement (Figures 3.46-3.47).

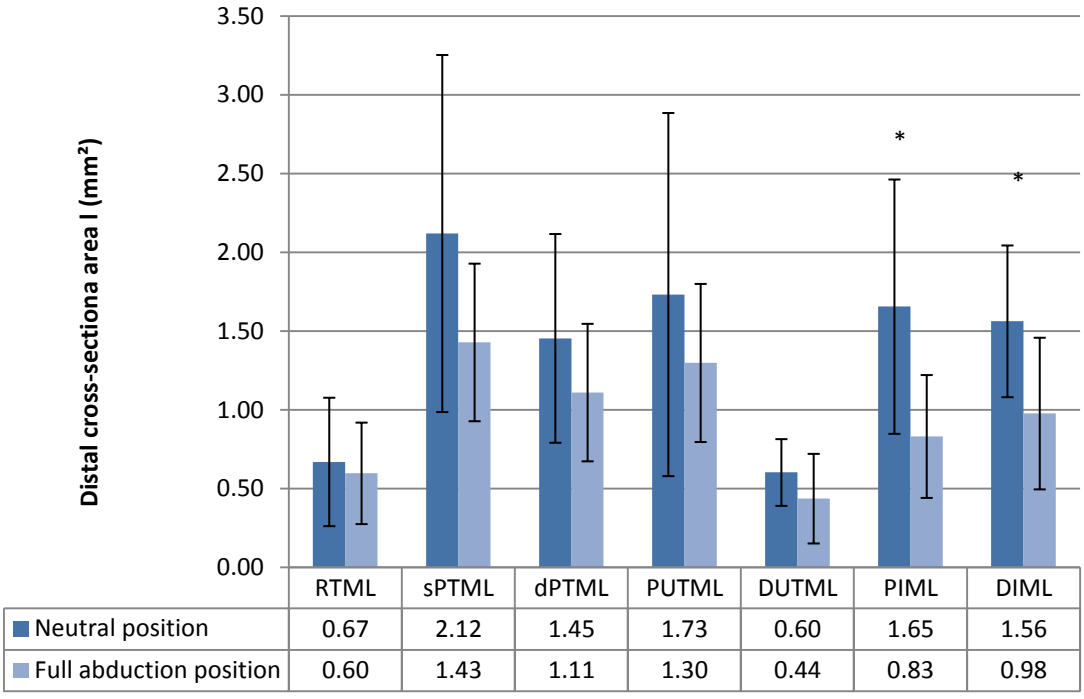

	RTML	sPTML	dPTML	PUTML	DUTML	PIML	DIML
Neutral position	0.67	2.12	1.45	1.73	0.60	1.65	1.56
Full abduction position	0.60	1.43	1.11	1.30	0.44	0.83	0.98

Figure 3.44: Distal cross-sectional area measurements in the static neutral and full abduction positions of the TMC ligaments with their standard deviation. The figure illustrates that there were no a significant differences (p>0.05) in all TMC ligaments, except PIML and DIML had significant differences (p<0.05) during tension on the TMC ligaments from the static neutral toward static full abduction positions. Unit: mm², N=10.

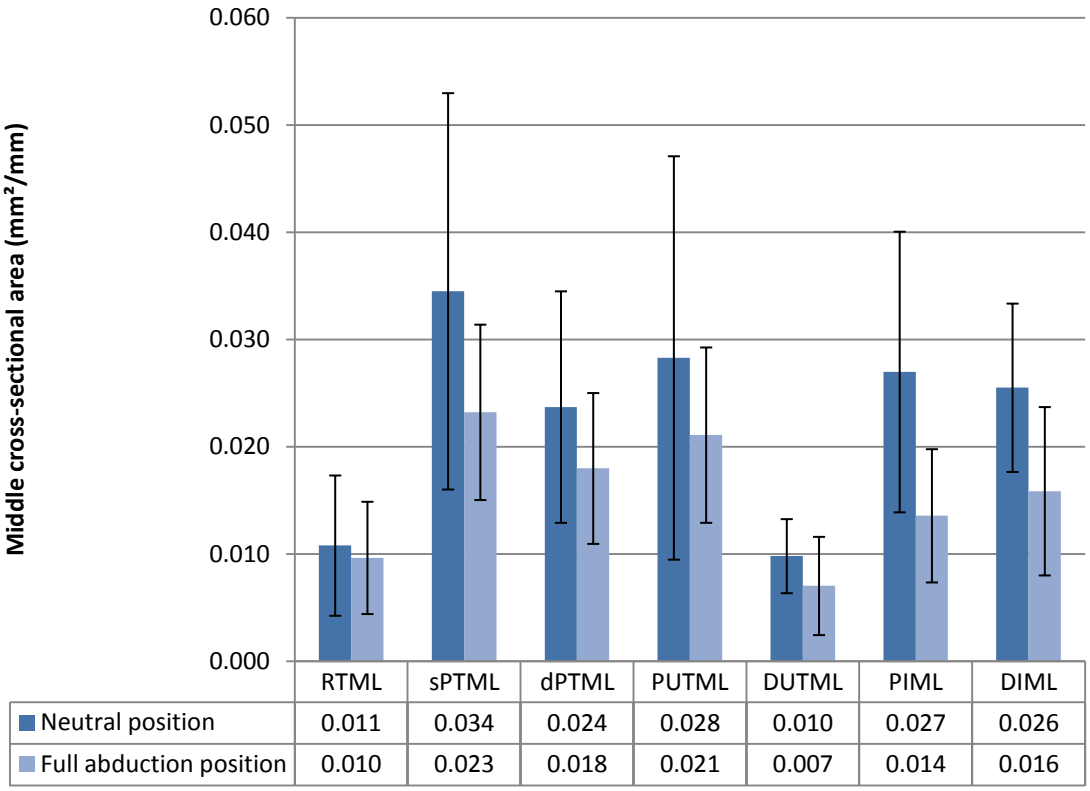

	RTML	sPTML	dPTML	PUTML	DUTML	PIML	DIML
Neutral position	0.011	0.034	0.024	0.028	0.010	0.027	0.026
Full abduction position	0.010	0.023	0.018	0.021	0.007	0.014	0.016

Figure 3.45: Index measurements of distal cross-sectional area in the static neutral and full abduction positions of the TMC ligaments with their standard deviation. The figure illustrates that there were no significant differences ($p>0.05$) in the index procedures between distal cross-sectional area measurements in the static neutral and full abduction positions. The index ligament was indexed against the length (mm) of the third metacarpal. Unit: mm², N=10.

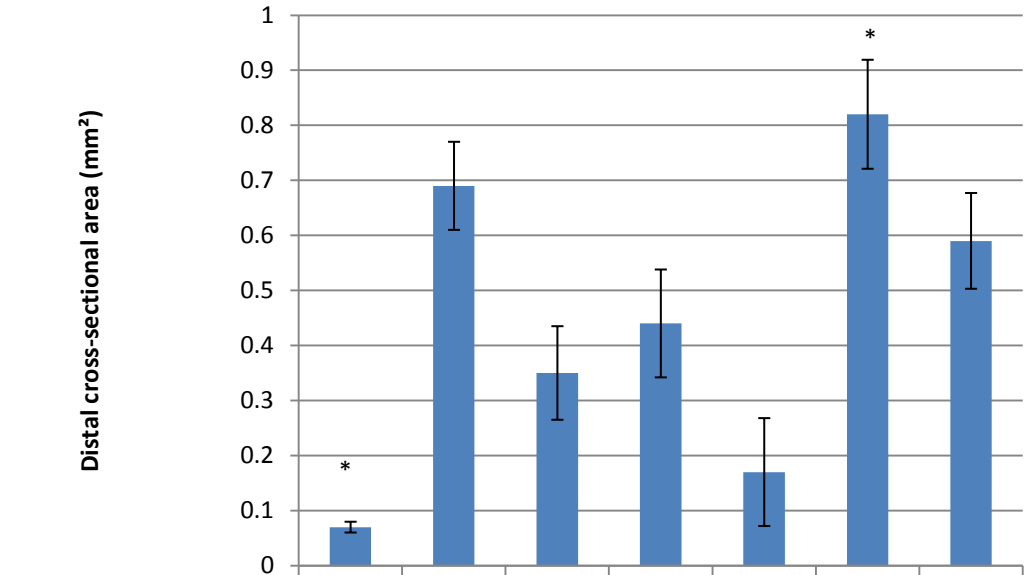

	RTML	sPTML	dPTML	PUTML	DUTML	PIML	DIML
Dynamic displacement	0.07	0.69	0.35	0.44	0.17	0.82	0.59

Figure 3.46: Distal cross-sectional area measurements in dynamic displacement of the TMC ligaments. The figure illustrates that the PIML has the largest of total TMC ligament displacement, while RTML has the smallest of total TMC ligament displacement. Unit: mm², N=10.

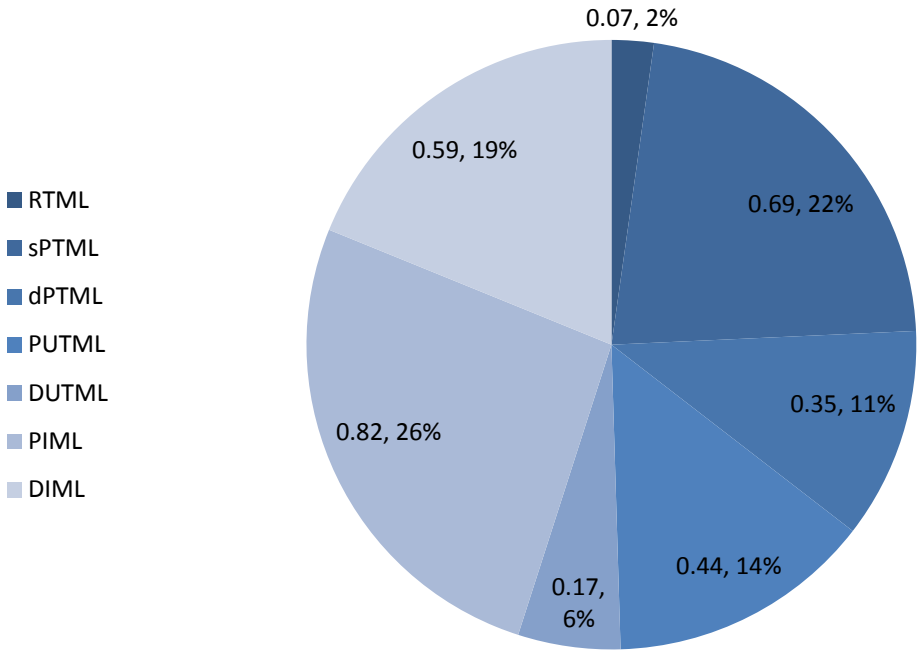

Figure 3.47: Percentages of dynamic displacement in distal cross-sectional area of all TMC ligaments. The figure illustrates that the PIML has the largest percentage (26%) of total TMC ligament displacement while RTML has the smallest percentage (2%) of total TMC ligament displacement. Unit: mm², N=10.

Ligaments	Static neutral position mm²	Static full abduction position mm²	Dynamic displacement mm²	Percentage of displacement	p value
RTML	0.66 ± 0.40	0.59 ± 0.32	0.07	2%	0.36
sPTML	2.11 ± 1.13	1.42 ± 0.50	0.69	22%	0.14
dPTML	1.45 ± 0.66	1.10 ± 0.43	0.35	11%	0.23
PUTML	1.73 ± 1.15	1.29 ± 0.50	0.44	14%	0.11
DUTML	0.60 ± 0.21	0.43 ± 0.28	0.17	6%	0.088
PIML	1.65 ± 0.80	0.83 ± 0.39	0.82	26%	0.007
DIML	1.56 ± 0.48	0.97 ± 0.48	0.59	19%	0.008

Table 3.7: Mean of the change in distal cross-sectional area of the TMC ligaments and their standard deviation. p value, unit: mm², N=10.

3.3 8 Ligaments shape analysis

3.3.8.1 Radial trapeziometacarpal ligament (RTML)

3.3.8.1.1 Surface curvature and tension analysis

The shape of the RTML mostly had no change from the static neutral position to the static full abduction position in all measurements except the proximal surface zone. Therefore, the fascicles of this ligament stretch at the proximal surface zone throughout the change from the static neutral toward static full abduction positions, while most zones mentioned above, such as the middle surface and distal surface zones, had no change, which means these zones relax or bend the fascicles together when ligament goes toward the static full abduction position of the TMC joint (Figures 3.48-3.49).

The results of RTML are shown by three colours: red represents the relaxed zone or the zone without potential tension. In the static full abduction position the tensions showed at mostly RTML surface except a little at zones elongated at the surface. The proximal zone of RTML had appeared in a blue colour, which means there was a little tension placed upon the fascicles in this position. In addition, the green colour showed at the middle zone near to the distal zone of the 1st MC attachment, which means the RTML fascicles' alignment had curved distally during the static full abduction position (Figure 3.49). Moreover, in the static neutral position, the red colour, or the relaxation of the fascicles, decreased, except the small zones distributed along the fascicles. Due to the occurrence of tension, the tensions appeared upon the fascicles partially at the distal zone of the RTML fascicles, the curvatures in this stage had appeared also (Figure 3.48).

3.3.8.1.2 Edge analysis (attachment zone)

The shape of the fascicles, which entering to the bone is observed in the current study. Both edge of the ligament; proximal edge and distal edge, which is illustrating how the mechanism of the fascicles of RTML enter (attachment zone) to the bone. The proximal edge is like (saw tooth), and its irregular ends of fascicles entering to the bone, the radial and ulnar zones of the attachment distinguishe by prominent and longest fascicles, while the middle zone fascicles

are shrunk and shortest fascicles.The distal edge is concavely ending to the bone and has approximately symmetrical fascicles endings (Figures 3.50-3.51).

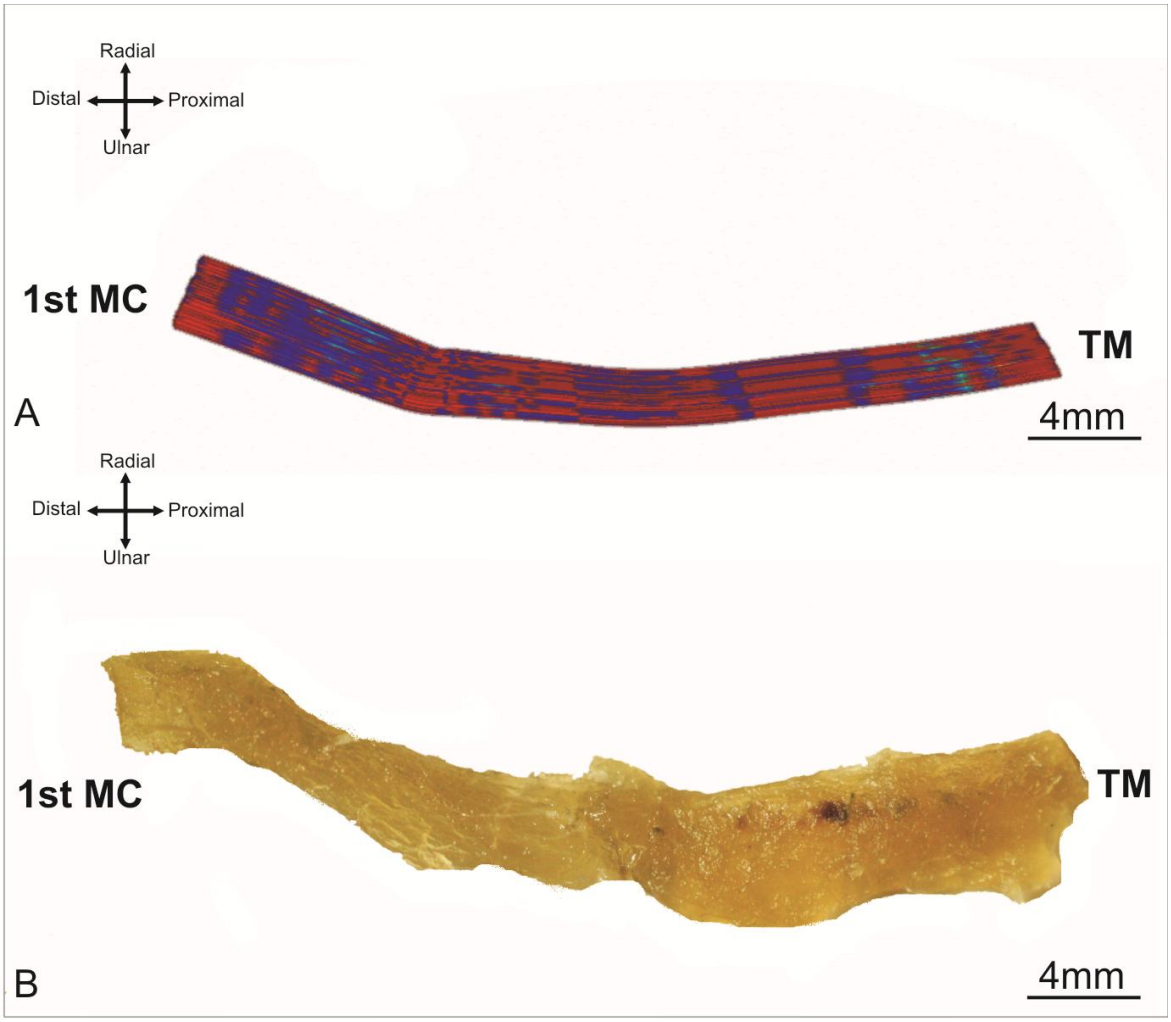

Figure 3.48: Surface curvature and tensions analysis of the RTML in the static neutral position.

(A) 3D model of the ligament's fascicles in the static neutral position. The red colour represents a relaxed state or lack of tension of the fascicles. The blue colour represents a potential tension of the fascicles. The green colour represents the curvature of the fascicles.
The tensions of the fascicles were decreased, except the small zones distributed along the fascicles. Also, the tensions appeared on the fascicles were partially at the distal zone of the RTML fascicles, the curvatures in this stage had appeared.
(B) Actual shape of the RTML after the bone connections was removed.

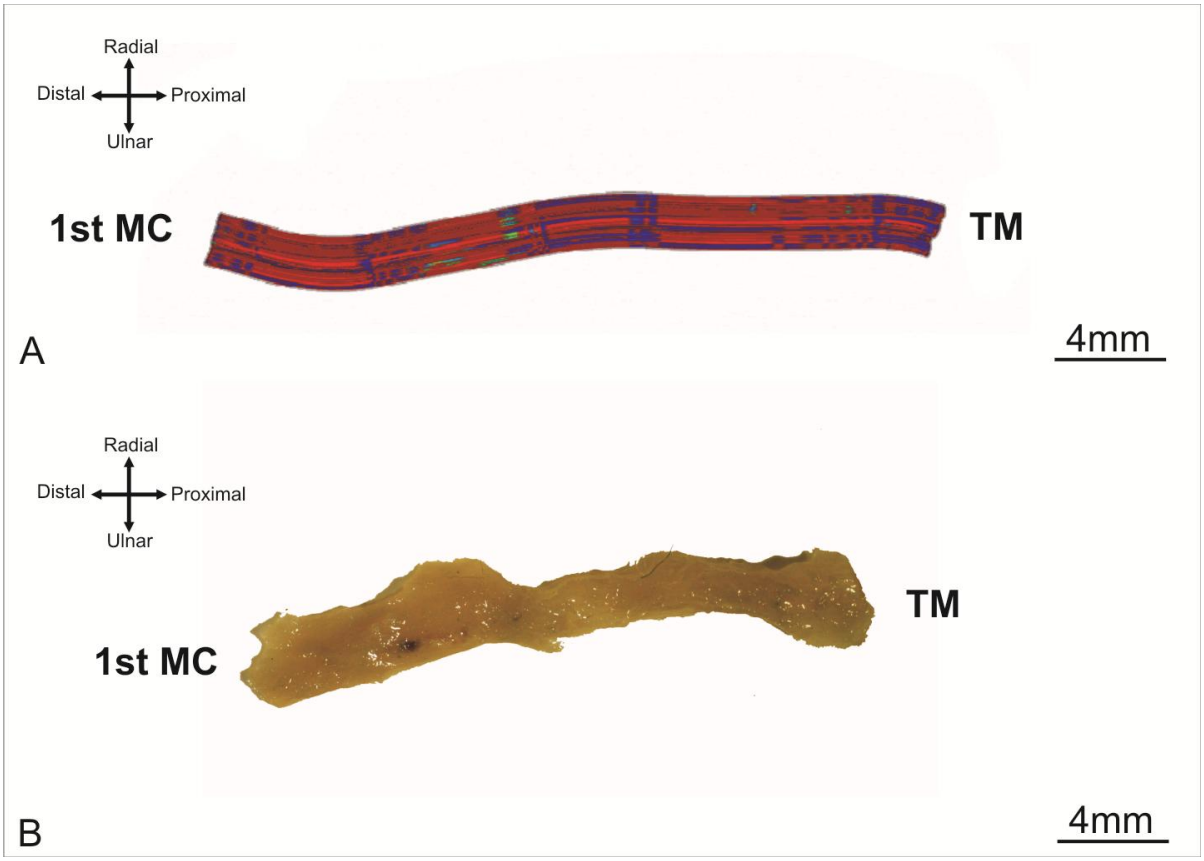

Figure 3.49: Surface curvature and tensions analysis of the RTML in the static full abduction position.

(A) 3D model of the ligament‘s fascicles in the static full abduction position. The red colour represents a relaxed state or lack of tension of the fascicles. The blue colour represents a potential tension of the fascicles. The green colour represents the curvature of the fascicles.
There was a little tension applied on the proximal zone of the RTML fascicles in this position. In addition, the curvatures showed at the middle zone near to the distal zone of the 1st MC attachment, which means the RTML fascicles’ alignment had curved distally during the static full abduction position.
(B) Actual shape of the RTML after the bone connections was removed.

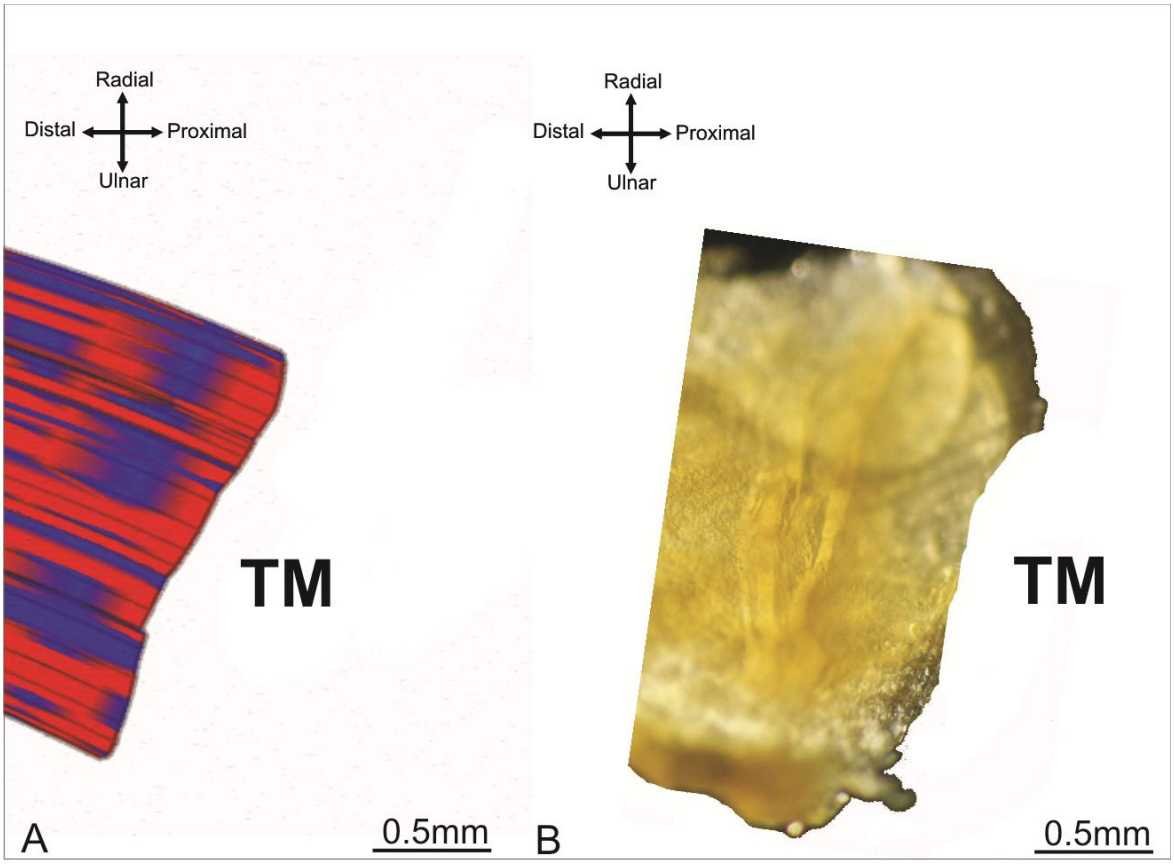

Figure 3.50: Edge analysis of the RTML in proximal attachment (proximal zone).

(A) 3D model of the ligament, which presents the edge of the ligament like (saw tooth), its irregular ends of fascicles which is entering to the bone, the radial and ulnar zones of the attachment distinguished by prominent and longest fascicles, while the middle zone fascicles were shrunk and shortest fascicles.
(B) Actual edge of the RTML after the bone connections was removed.

.

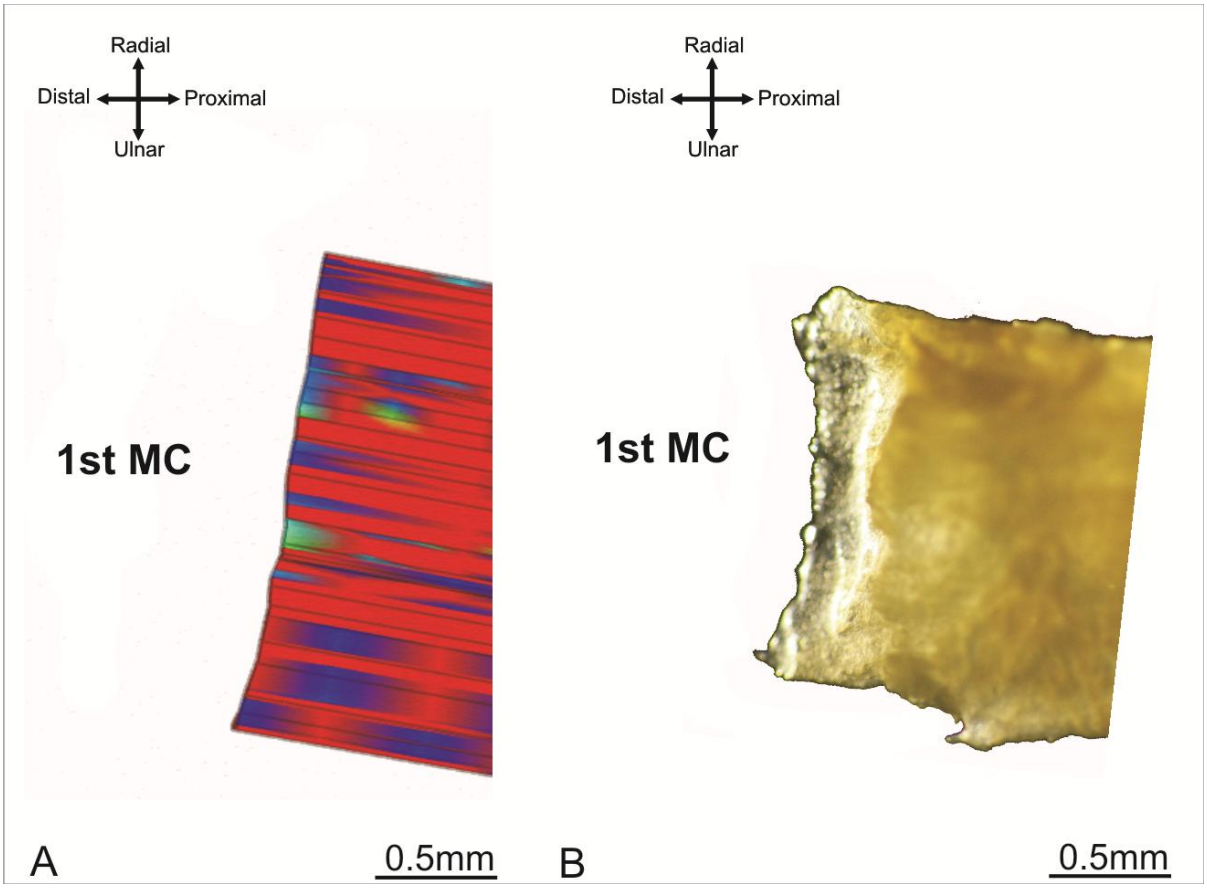

Figure 3.51: Edge analysis of the RTML in distal attachment (distal zone).

(A) 3D model of the ligament, which presents the edge of the ligament has concavely ending to the bone and approximately has a symmetrical fascicle endings.
(B) Actual edge of the RTML after the bone connections was removed.

3.3.8.2 Superfical palmar trapeziometacarpal ligament (sPTML)

3.3.8.2.1 Surface curvature and tension analysis

The shape of the sPTML changed from the static neutral position to the static full abduction position in all measurements except in the distal surface zone. Therefore, the fascicles of this ligament stretching or lengthening at the proximal and middle surface zones throughout the change from the static neutral toward static full abduction positions also appeared thicker and wider. The distal surface zone, which attaches with the 1st MC, had relaxed fascicles during the ligament's movement toward the static full abduction position of TMC joint (Figures 3.52-3.53).

In the static full abduction position, relaxation presented particularly at the proximal and distal zones, and elongation presented on the radial side of the sPTML fascicles, while tension or stress appeared particularly at the middle and ulnar attachment zones of the sPTML fascicles. The curvature showed at the middle surface zone near the ulnar attachment zone of this ligament, which means the sPTML fascicles' alignment had curved ulnarly during the static full abduction position (Figure 3.53). Moreover, in the static neutral position, the relaxation of the fascicles increased at the middle surface zone of fascicles, while it decreased at the proximal and distal surface zones, which means the stress or tension occurred in these zones. Also, the curvature of the sPTML fascicles decreased but still curved near the proximal zone (Figure 3.52).

3.3.8.2.2 Edge analysis (attachment zone)

The proximal edge had smooth ends of fascicles entering to the bone, the radial attachment zone distinguished by prominent and longest fascicles, while in the middle attachment zone the fascicles were at the same level with the radial attachment zone, the ulnar attachment zone was shrunk with a sharp angle. The distal edge mainly had more prominence than the proximal edge; it was most prominent at the middle attachment zone of the fascicles of this ligament (Figures 3.54-3.55).

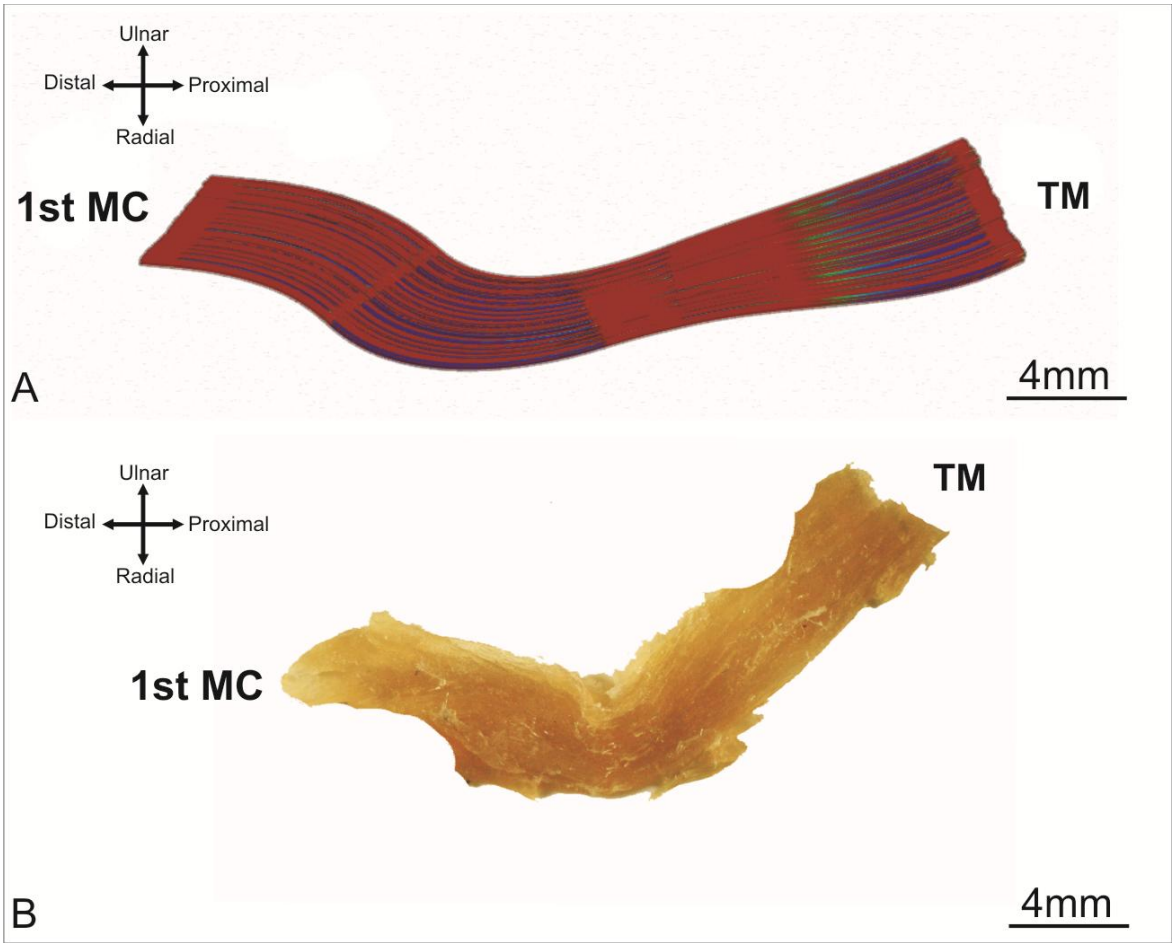

Figure 3.52: Surface curvature and tension analysis of the sPTML in the static neutral position.

(A) 3D model of the ligament's fascicles in the static neutral position.
The relaxation of the fascicles increased at the middle surface zone of fascicles, while it decreased at the proximal and distal surface zones, which means the stress or tension occurred in these zones. Also, the curvature of the sPTML fascicles decreased but still curved near the proximal zone.
(B) Actual shape of the sPTML after the bone connections was removed.

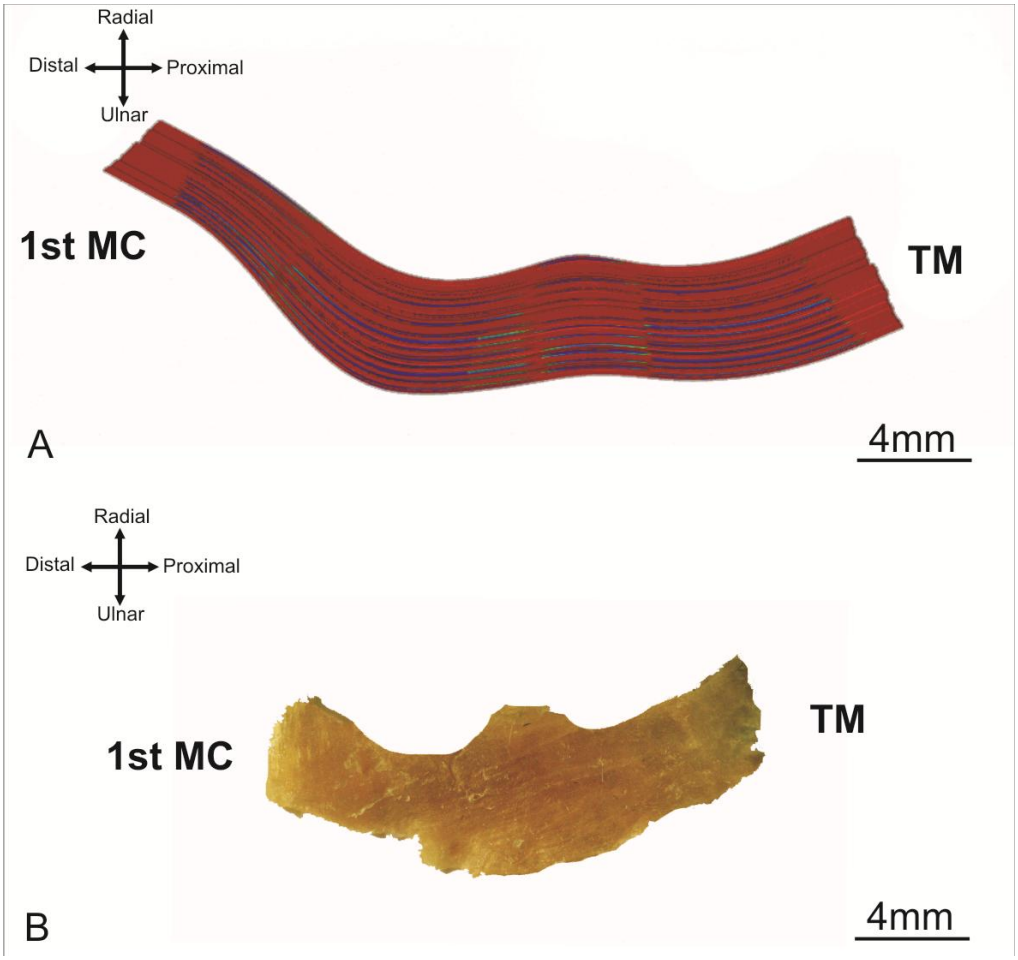

Figure 3.53: Surface curvature and tension analysis of the sPTML in the static full abduction position.

(A) 3D model of the ligament's fascicles in the static full abduction position. The relaxation presented particularly at the proximal and distal zones, and elongation presented on the radial side of the sPTML fascicles, while tension or stress appeared particularly at the middle and ulnar attachment zones of the sPTML fascicles. The curvature showed at the middle surface zone near the ulnar attachment zone of this ligament, which means the sPTML fascicles' alignment had curved ulnarly during the static full abduction position.
(B) Actual shape of the sPTML after the bone connections was removed.

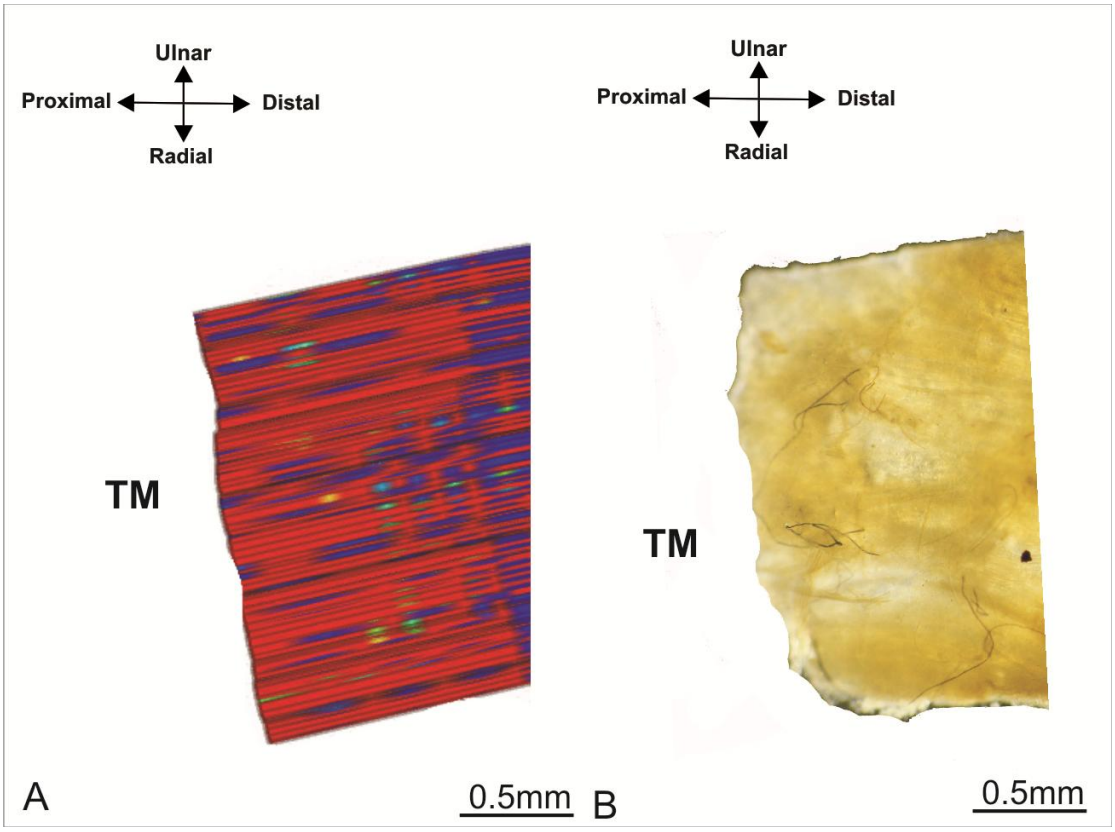

Figure 3.54: Edge analysis of the sPTML in proximal attachment (proximal zone).

(A) 3D model of the ligament which presents the proximal edge had smooth ends of fascicles entering to the bone, the radial attachment zone distinguished by prominent and longest fascicles, while in the middle attachment zone the fascicles were at the same level with the radial attachment zone, the ulnar attachment zone was shrunk with a sharp angle.
(B) Actual edge of the sPTML after the bone connections was removed.

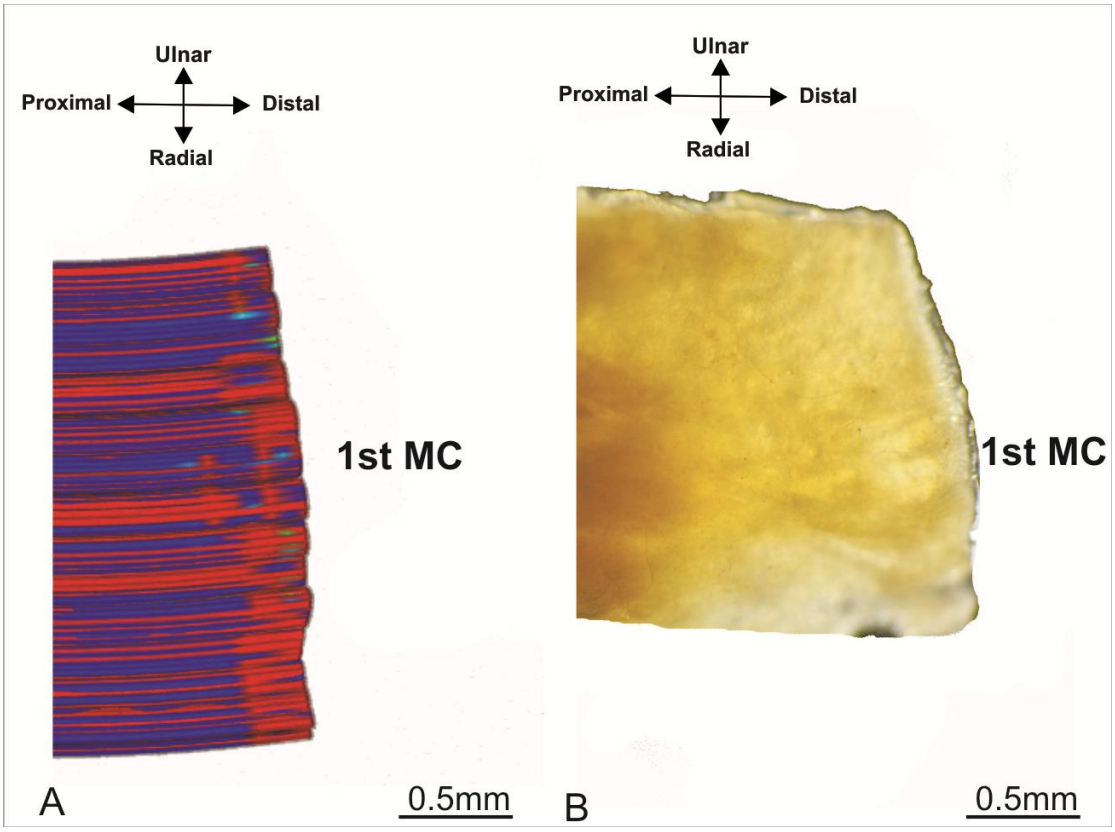

Figure 3.55: Edge analysis of the sPTML in distal attachment (distal zone).

(A) 3D model of the ligament, which presents the distal edge mainly, had more prominence than the proximal edge; it was most prominent at the middle attachment zone of the fascicles of this ligament, its asymetrical edge.
(B) Actual edge of the sPTML after removed the bone connections.

3.3.8.3 Deep palmar trapeziometacarpal ligament (dPTML)

3.3.8.3.1 Surface curvature and tension analysis

The shape of the dPTML showed no change from the static neutral position to the static full abduction position in all measurements except in the middle surface and distal surface zones. Therefore, the fascicles of this ligament stretch or lengthen at the middle and distal surface zones throughout the change from the static neutral toward the static full abduction positions and also appear thicker and wider. The proximal surface zone, which attaches with the 1st MC, had relaxed fascicles or fascicles that bent together during the ligament's movement toward the static full abduction position of TMC joint. The dPTML has same properties as the sPTML in being mostly relaxed, and the fascicles of these ligaments folded during static full abduction. Both ligaments stretched mainly when the TMC was in

the static neutral position, which means that both ligaments have a major role in stabilizing the thumb in this position (Figures 3.56-3.57).

In the static full abduction position, relaxation presented particularly at the proximal surface zone, and elongation presented on both the radial and ulnar attachment zones of the dPTML fascicles, while the tension or stress presented particularly at the middle surface zone of the sPTML fascicles. The curvature presented at the middle surface zone near the proximal surface zone of this ligament, which means the dPTML fascicles' alignment had curved proximally during the static full abduction position (Figure 3.57). Moreover, in the static neutral position, the relaxation of the fascicles presented in the proximal attachment zone of the fascicles, while the tension was restricted at the middle surface zone of the fascicles. Also, the curvature of the dPTML fascicles decreased but still curved near the proximal surface zone (Figure 3.56).

3.3.8.3.2 Edge analysis (attachment zone)

The proximal edge had small prominence ends, the radial and middle attachment zones were distinguished by symmetrical prominences, while the ulnar attachment zone was asymmetrical and had long ends entering to the bone. The distal edge had an oblique style (Figures 3.58-3.59).

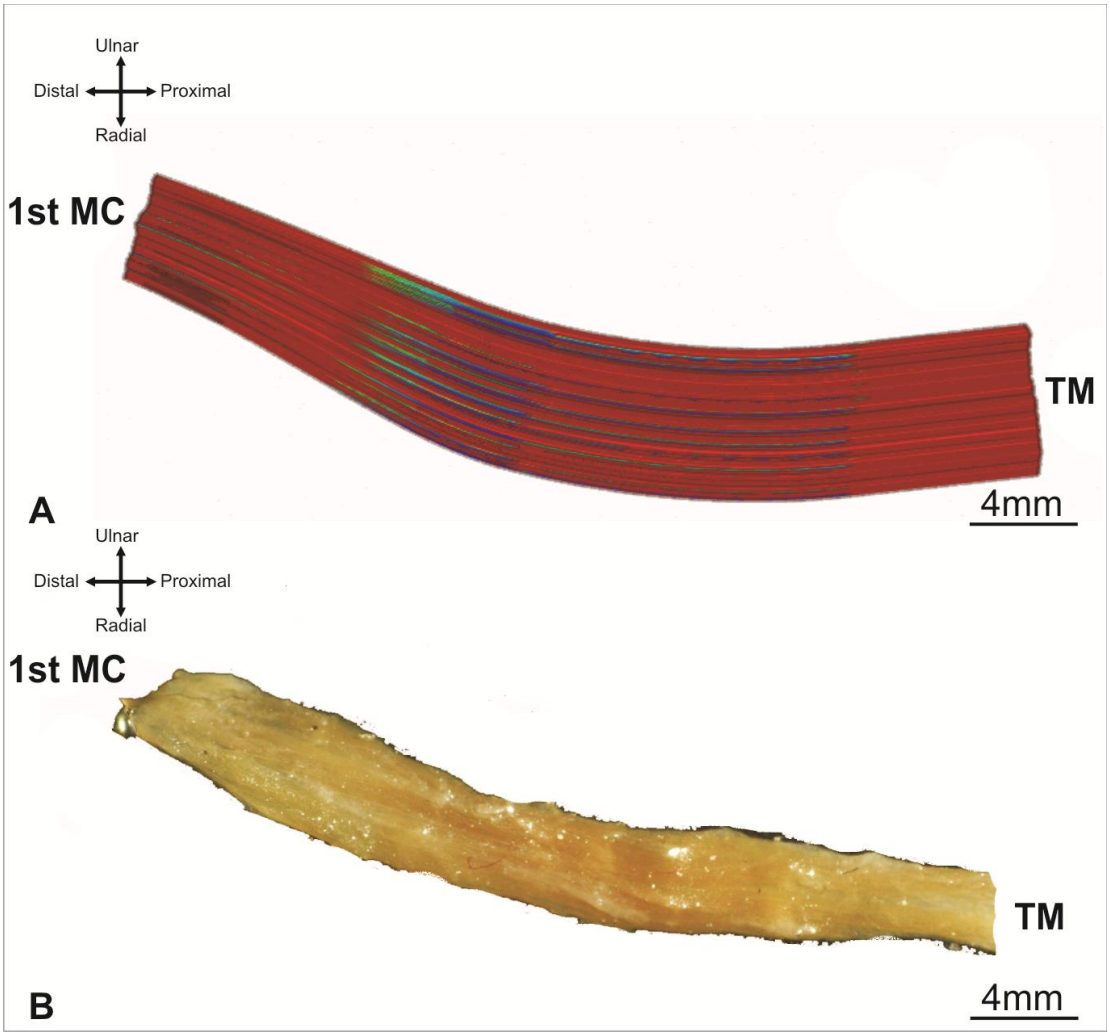

Figure 3.56: Surface curvature and tension analysis of the dPTML in the static neutral position.

(A) 3D model of the ligament's fascicles in the static neutral position. The relaxation of the fascicles presented in the proximal attachment zone of the fascicles, while the tension was restricted at the middle surface zone of the fascicles. Also, the curvature of the dPTML fascicles decreased but still curved near the proximal surface zone.

(B) Actual shape of the dPTML after the bone connections was removed.

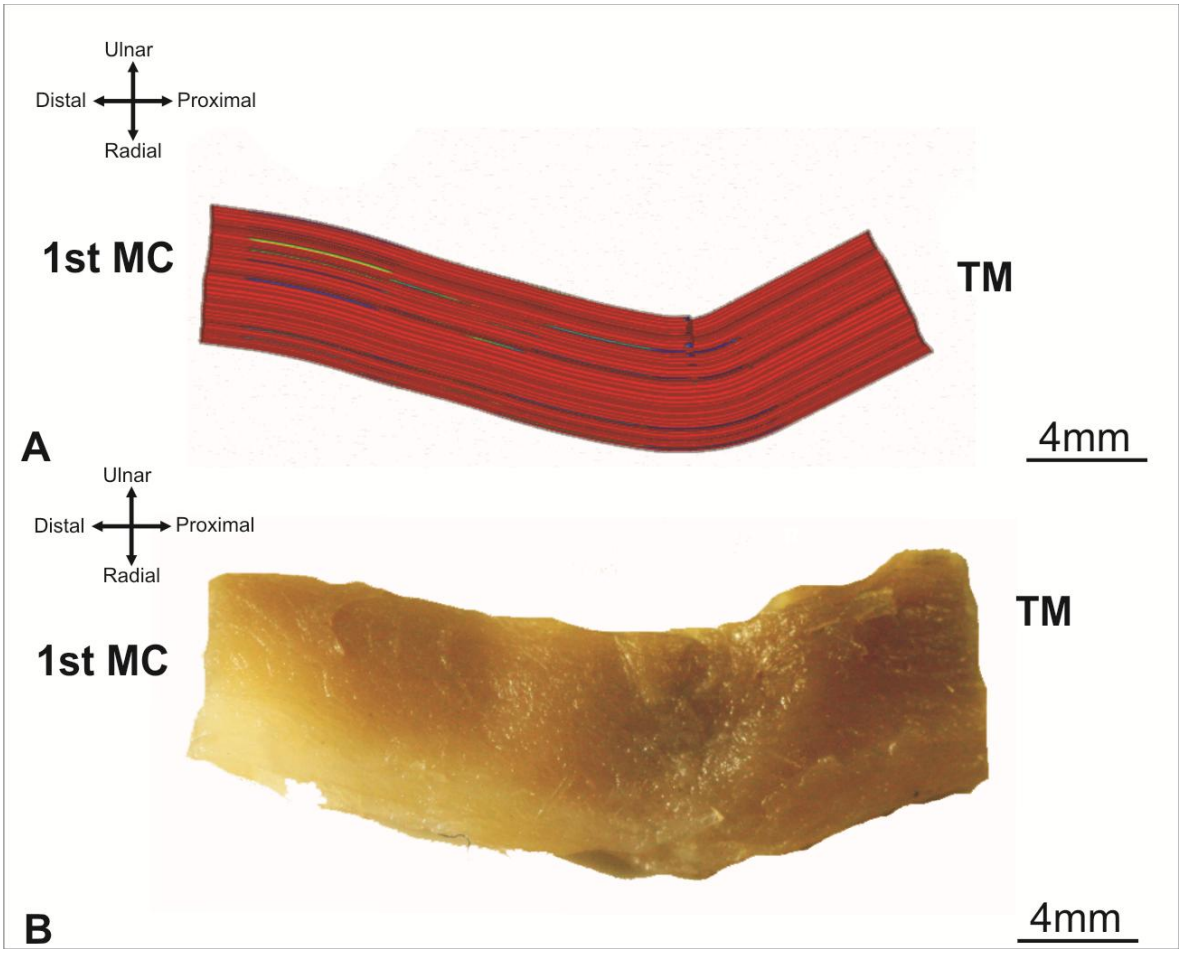

Figure 3.57: Surface curvature and tension analysis of the dPTML in the static full abduction position.

(A) 3D model of the ligament's fascicles in the static full abduction position. The relaxation presented particularly at the proximal surface zone, and elongation presented on both the radial and ulnar attachment zones of the dPTML fascicles, while the tension or stress presented particularly at the middle surface zone of the dPTML fascicles. The curvature presented at the middle surface zone near the proximal surface zone of this ligament, which means the dPTML fascicles' alignment had curved proximally during the static full abduction position.
(B) Actual shape of the dPTML after the bone connections was removed.

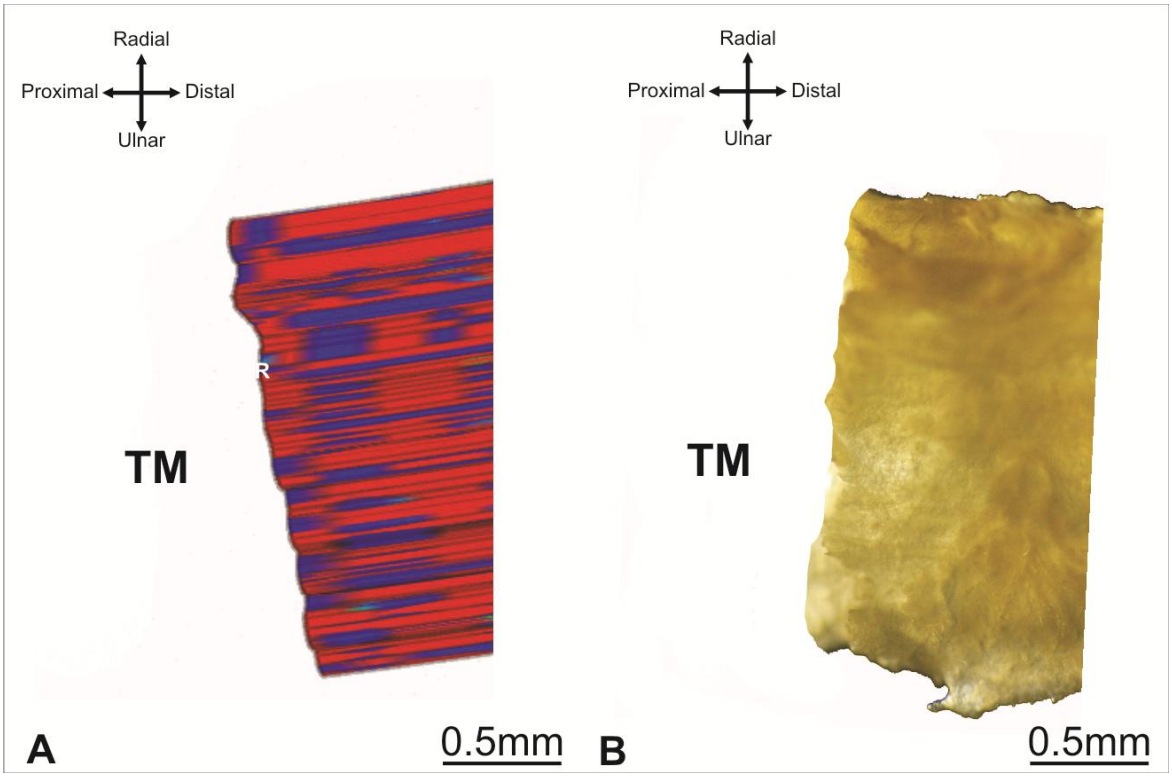

Figure 3.58: Edge analysis of the dPTML in proximal attachment (proximal zone).

(A) 3D model of the ligament which presents the proximal edge had small prominence ends, the radial and middle attachment zones were distinguished by symmetrical prominences, while the ulnar attachment zone was asymmetrical and had long ends entering to the bone.
(B) Actual edge of the dPTML after the bone connections was removed.

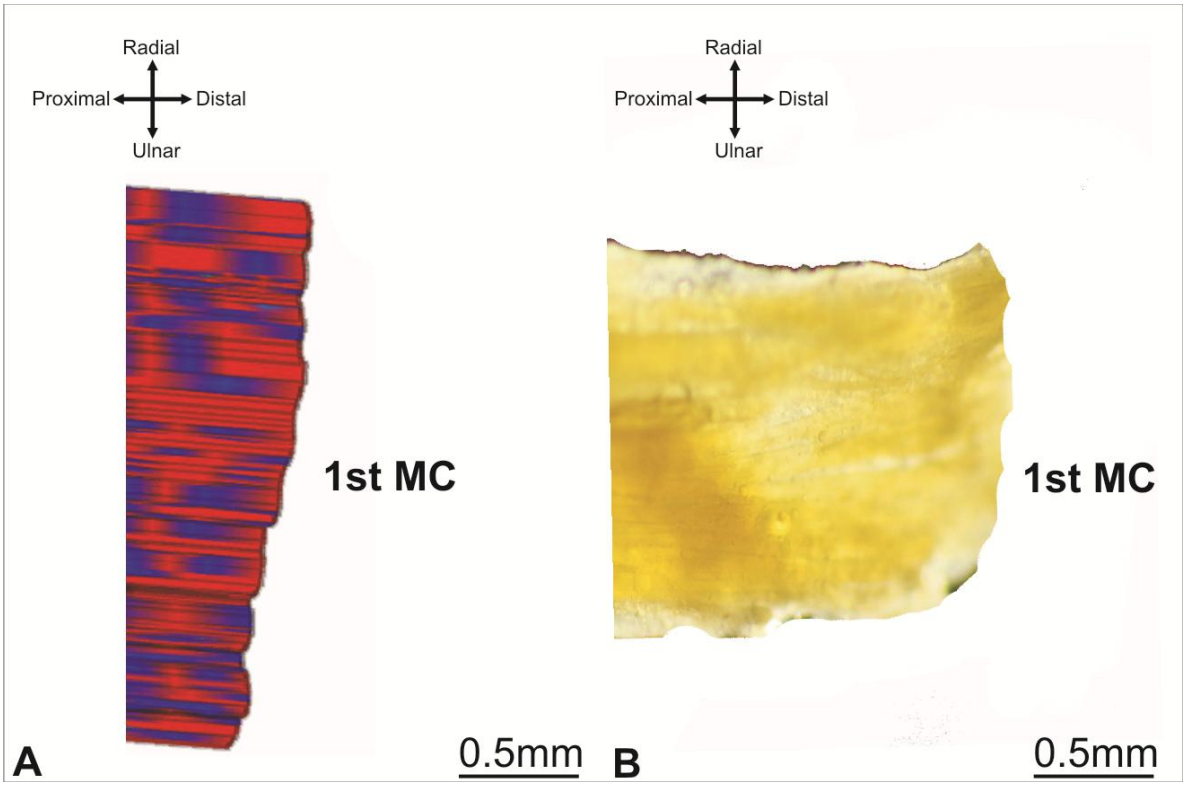

Figure 3.59: Edge analysis of the dPTML in distal attachment (distal zone).

(A) 3D model of the ligament which presents the distal edge had an oblique style with symmetrical fascicles ends.
(B) Actual edge of the dPTML after the bone connections was removed.

3.3.8.4 Palmo-ulnar trapeziometacarpal ligament (PUTML)

3.3.8.4.1 Surface curvature and tensions analysis

The PUTML changed in thickness, length and width from the static neutral position to the static full abduction position. Also, the proximal surface zone showed no change, but the middle and distal surface zones had changed. In general, the shape of the PUTML fascicles changed in all regions except the proximal surface zone, which indicates relaxation and a decreased percentage of stress or tension in this zone. Therefore, the fascicles of this ligament stretch or lengthen in the middle and distal zones throughout the change from the static neutral toward the static full abduction positions and also appear thinner and more elongated. The proximal cross-sectional area had relaxed fascicles during the ligament going toward the static full abduction position of the TMC joint. The properties of PUTML are the same as those of the dPTML in that they elongate in

the middle and distal zones and relax or shorten in the proximal zone (Figures 3.60-3.61).

In the static full abduction position, relaxation presented particularly at the proximal surface zone, and distributed along both the radial and ulnar attachment zones of PUTML fascicles, while the tension or stress presented particularly at the distal surface zone of the PUTML fascicles. The curvature showed at the middle and distal surface zones of this ligament, which means the PUTML fascicles alignment curved distally during the static full abduction position (Figure 3.61). Moreover, in the static neutral position, the relaxation of the fascicles presented in the proximal surface zone of the fascicles, while the tensions were restricted at both the radial and ulnar attachment zones' sequences (Figure 3.60).

3.3.8.4.2 Edge analysis (attachment zone)

The proximal edge had short prominence ends, the ulnar and middle attachment zones of the attachment were distinguished by symmetrical prominences, while the radial attachment zone was asymmetrical and long end entering to the bone, with a sharp angle at the radial border. The distal edge had large concavity ending at the middle attachment zone, while the radial and ulnar attachment zones had convexly ending fascicles (Figures 3.62-3.63).

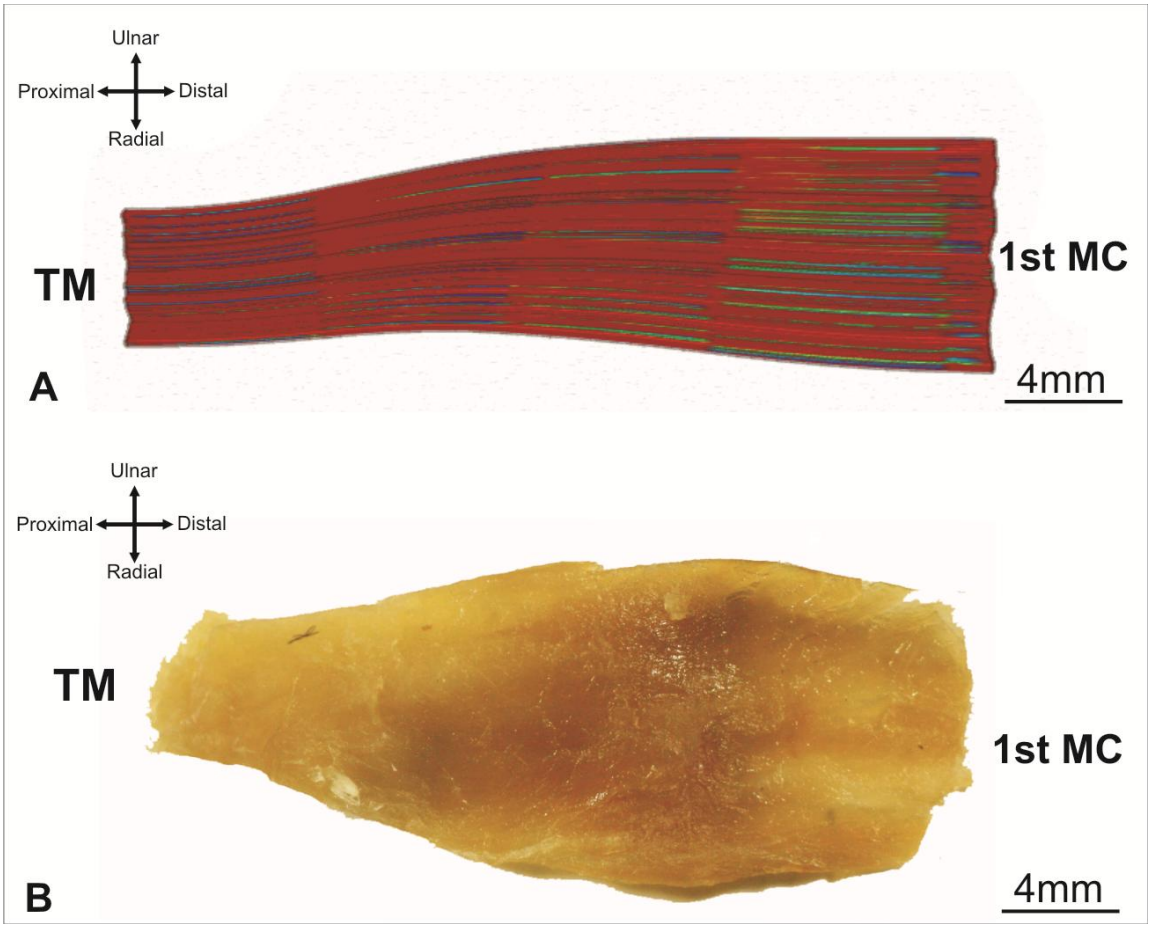

Figure 3.60: Surface curvature and tension analysis of the PUTML in the static neutral position.

(A) 3D model of the ligament's fascicles in the static neutral position.
The relaxation of the fascicles presented in the proximal surface zone of the fascicles, while the tensions were restricted at both the radial and ulnar attachment zones' sequences.
(B) Actual shape of the PUTML after the bone connections was removed.

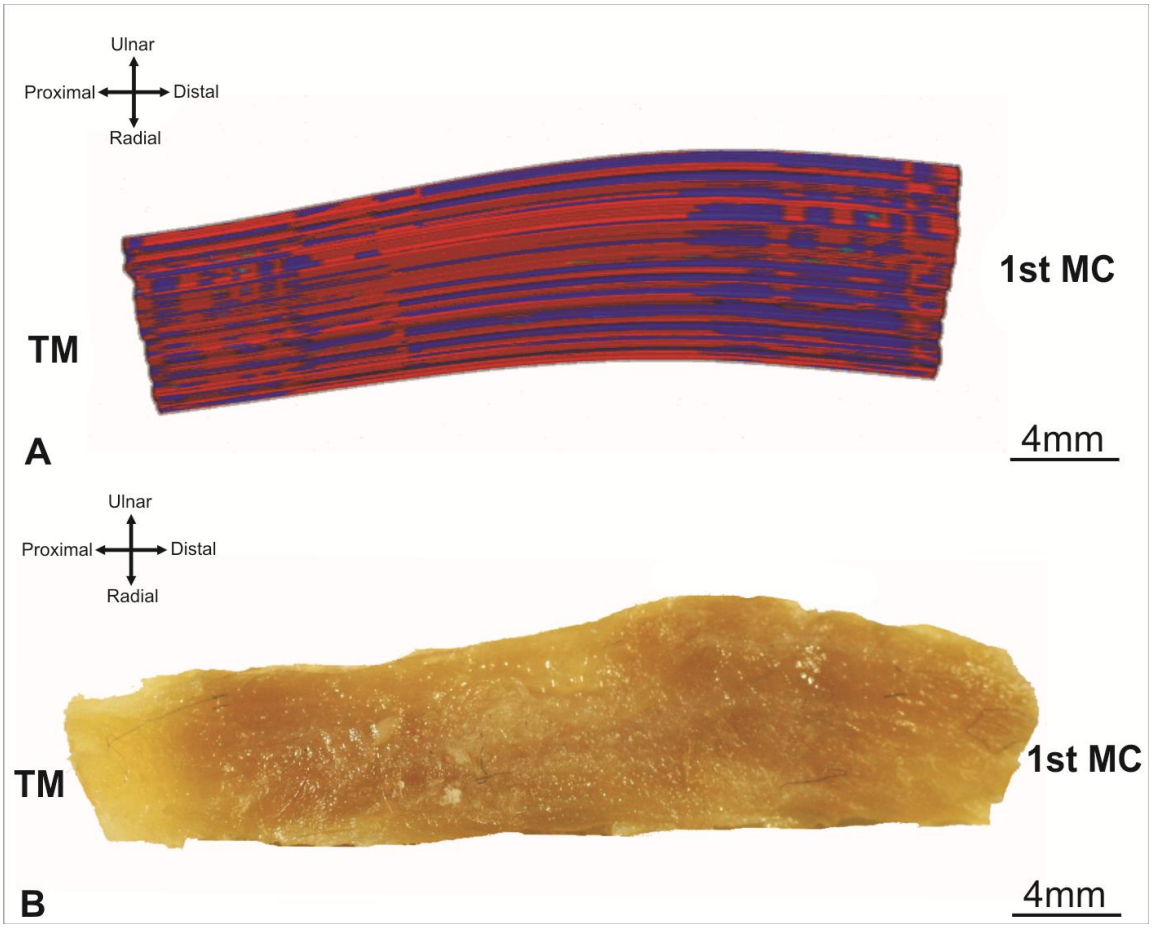

Figure 3.61: Surface curvature and tension analysis of the PUTML in the static full abduction position.

(A) 3D model of the ligament's fascicles in the static full abduction position. The relaxation presented particularly at the proximal surface zone, and distributed along both the radial and ulnar attachment zones of PUTML fascicles, while the tension or stress presented particularly at the distal surface zone of the PUTML fascicles. The curvature showed at the middle and distal surface zones of this ligament, which means the PUTML fascicles alignment curved distally during the static full abduction position.
(B) Actual shape of the PUTML after the bone connections was removed.

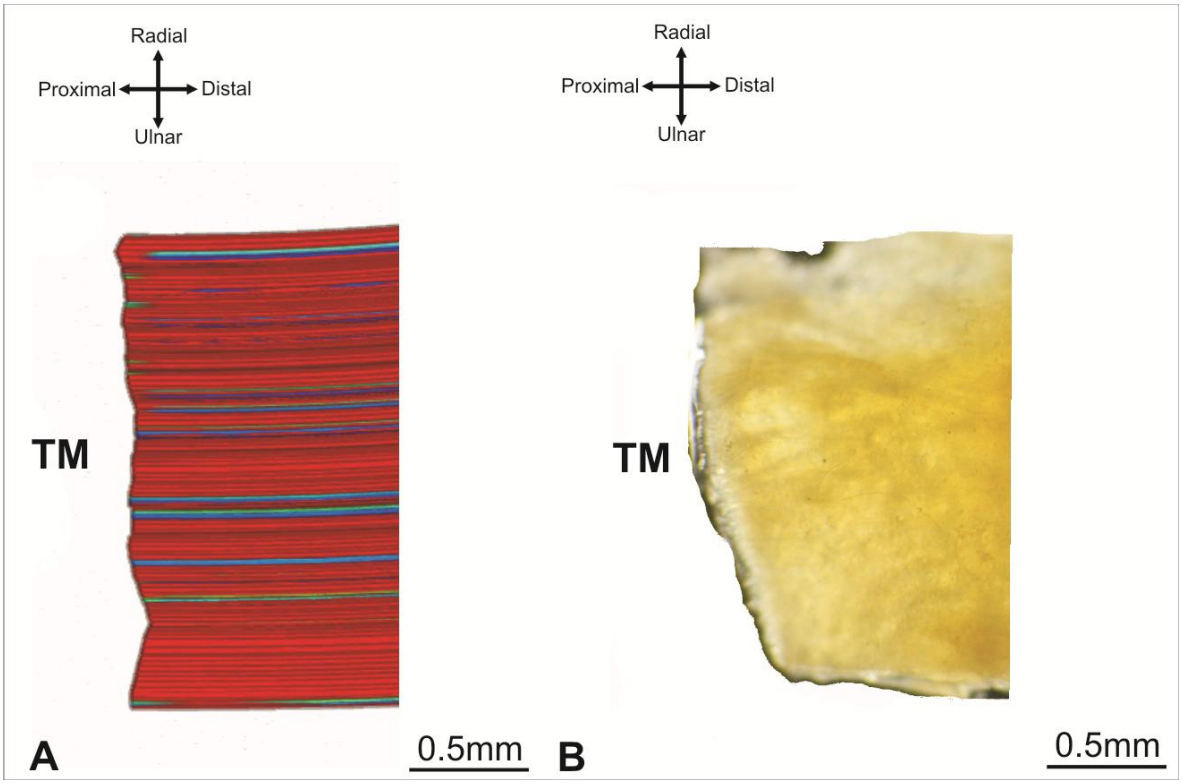

Figure 3.62: Edge analysis of the PUTML in proximal attachment (proximal zone).

(A) 3D model of the ligament which presents the proximal edge had short prominence ends, the ulnar and middle attachment zones of the attachment were distinguished by symmetrical prominences, while the radial attachment zone was asymmetrical and long end entering to the bone, with a sharp angle at the radial border.
(B) Actual edge of the PUTML after the bone connections was removed.

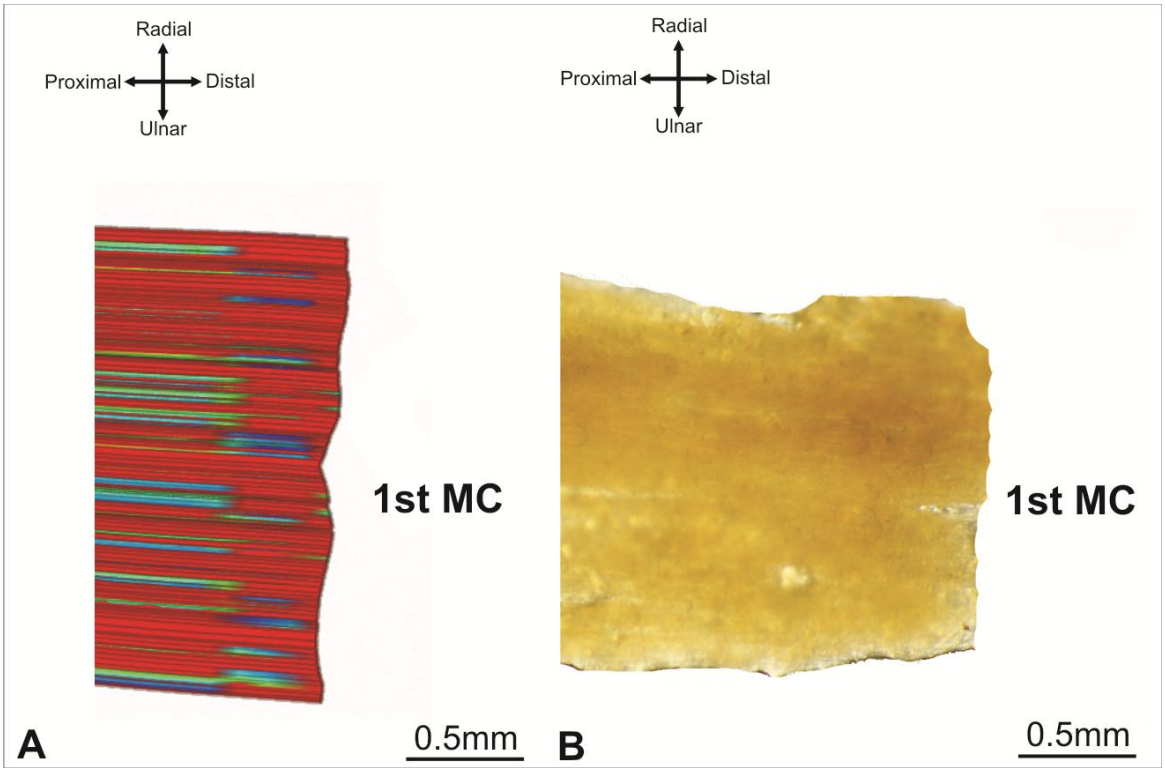

Figure 3.63: Edge analysis of the PUTML in distal attachment (distal zone).

(A) 3D model of the ligament which presents the distal edge had large concavity ending at the middle attachment zone, while the radial and ulnar attachment zones had convexly ending fascicles.
(B) Actual edge of the PUTML after the bone connections was removed.

3.3.8.5 Dorso-ulnar trapeziometacarpal ligament (DUTML)

3.3.8.5.1 Surface curvature and tension analysis

The DUTML changed in thickness, length and width from the static neutral position to the static full abduction position. Also, the middle and distal surface zones showed no change, but the proximal surface zone had changed. The shape of the DUTML fascicles changed in all surface zones except the middle and distal surface zones, which indicates relaxation and a decrease percentage of stress or tension in this zone. Therefore, the fascicles of this ligament stretch or lengthen at the proximal surface zone throughout the change from the static neutral toward static full abduction positions and also appeared thinner and more elongated. The middle and distal surface zones had relaxed fascicles during the ligament going toward the static full abduction position of the TMC joint. The property of the

DUTML is mainly curved ligaments, its takes elongation from the middle surface zone to distal surface zone like (half arch) (Figures 3.64-3.65).

In the static full abduction position, relaxation presented particularly at the middle surface zone of the DUTML fascicles, while the tension or stress appeared particularly at the distal surface zone of the PUTML fascicles. The curvature showed particularly at the middle and distal surface zones of this ligament, which means the DUTML fascicles curved radial-distally during the static full abduction position (Figure 3.65). Moreover, in the static neutral position, the relaxation of the fascicles presented in the proximal surface zone of the fascicles, while the tension was restricted to a small area of the distal surface zone (Figure 3.64).

3.3.8.5.2 Edge analysis (attachment zone)

The proximal edge had an irregular prominence end, the ulnar and radial attachment zones were distinguished by tapered head, while the middle attachment zone was asymmetrical with a long end entering to the bone. The distal edge had large concavity ending at the ulnar attachment zone, while the middle and radial attachment zones had obliquely ending fascicles (Figures 3.65-3.66).

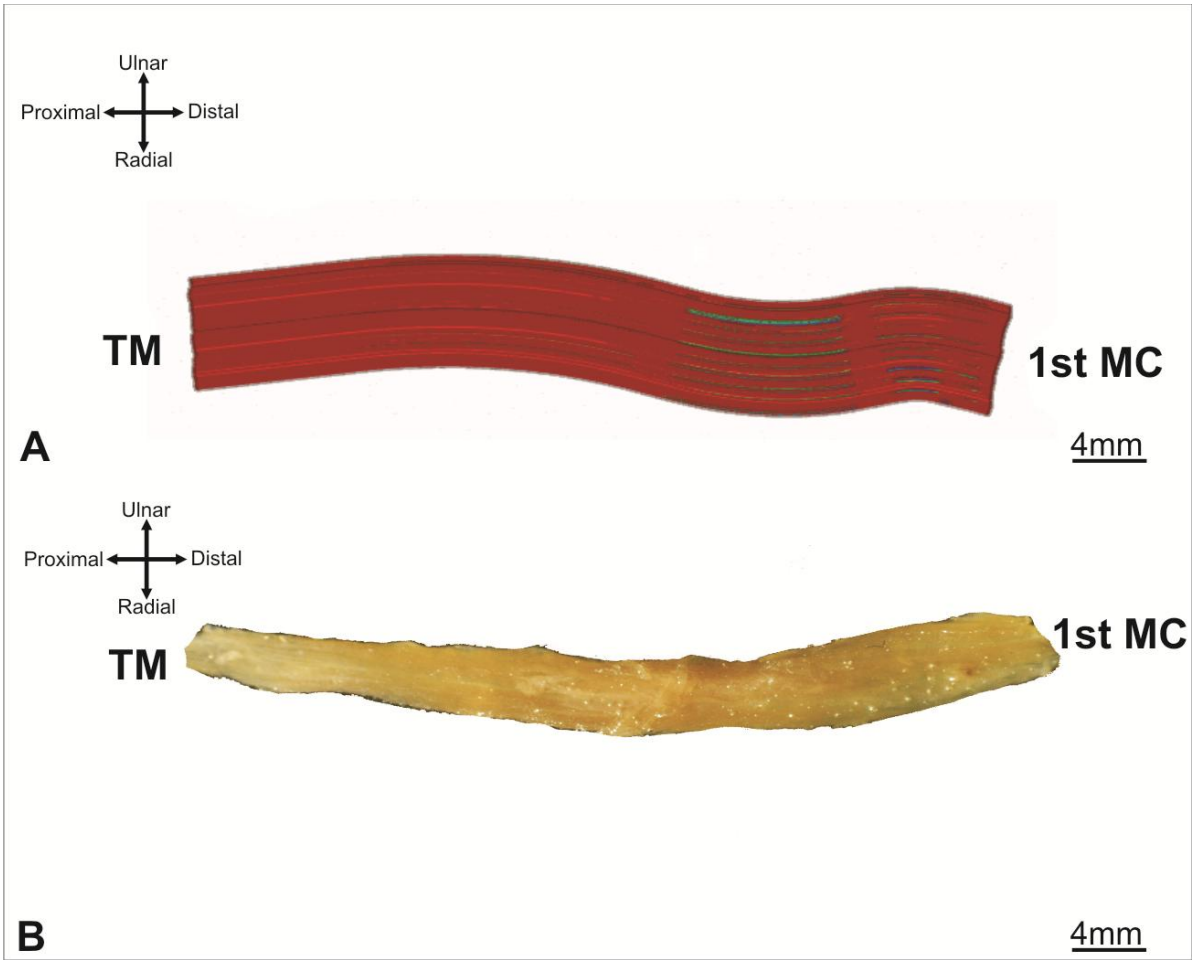

Figure 3.64: Surface curvature and tension analysis of the DUTML in the static neutral position.

(A) 3D model of the ligament's fascicles in the static neutral position. The relaxation of the fascicles presented in the proximal surface zone of the fascicles, while the tension was restricted to a small area of the distal surface zone
(B) Actual shape of the DUTML after the bone connections was removed.

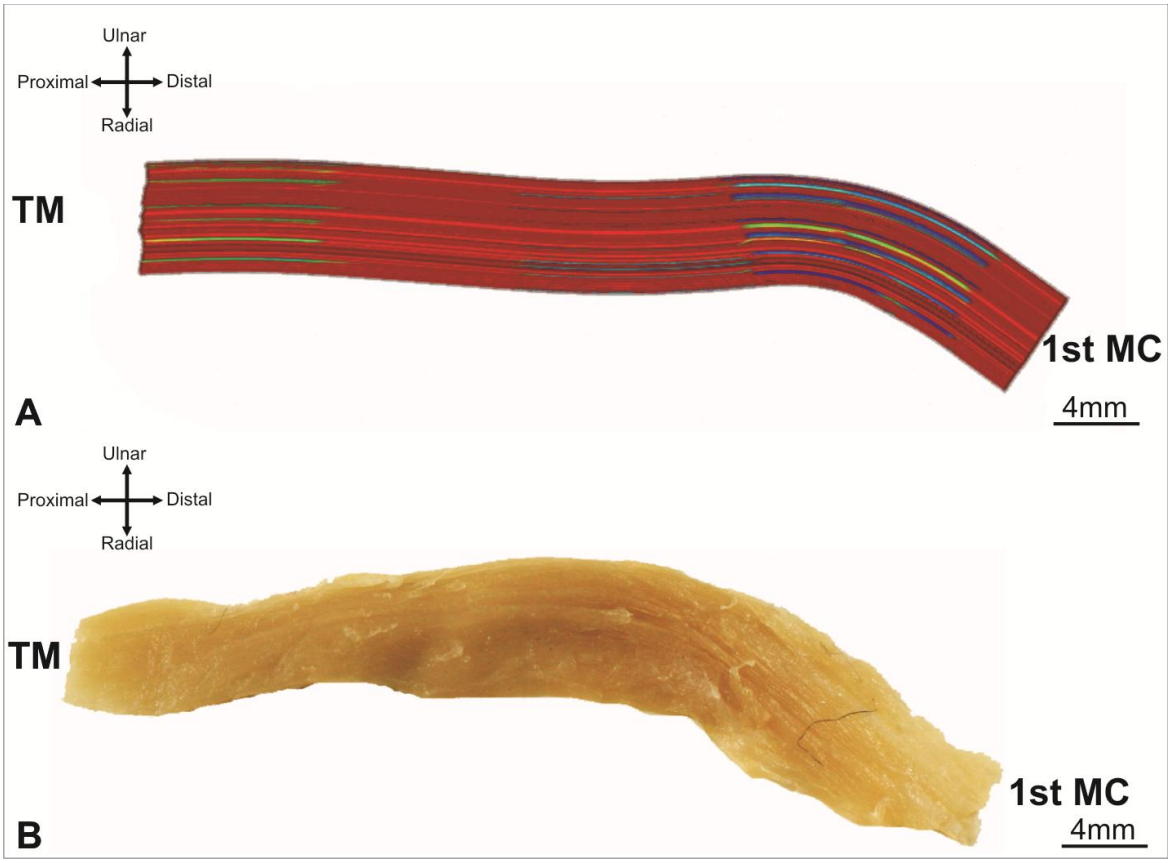

Figure 3.65: Surface curvature and tension analysis of the DUTML in the static full abduction position.

(A) 3D model of the ligament's fascicles in the static full abduction position. The relaxation presented particularly at the middle surface zone of the DUTML fascicles, while the tension or stress appeared particularly at the distal surface zone of the PUTML fascicles. The curvature showed particularly at the middle and distal surface zones of this ligament, which means the DUTML fascicles curved radial-distally during the static full abduction position.
(B) Actual shape of the DUTML after the bone connections was removed.

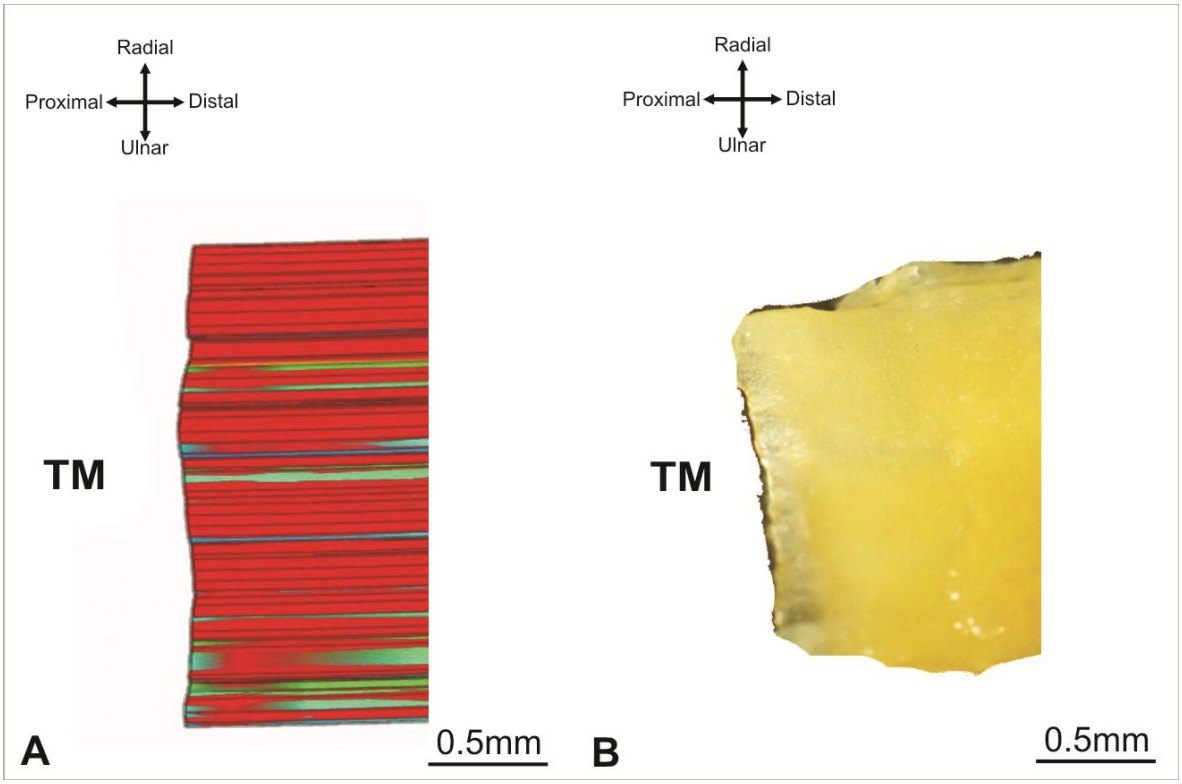

Figure 3.66: Edge analysis of the DUTML in proximal attachment (proximal zone).

(A) 3D model of the ligament which presents the proximal edge had an irregular prominence end, the ulnar and radial attachment zones were distinguished by tapered head, while the middle attachment zone was asymmetrical with a long end entering to the bone.
(B) Actual edge of the DUTML after the bone connections was removed.

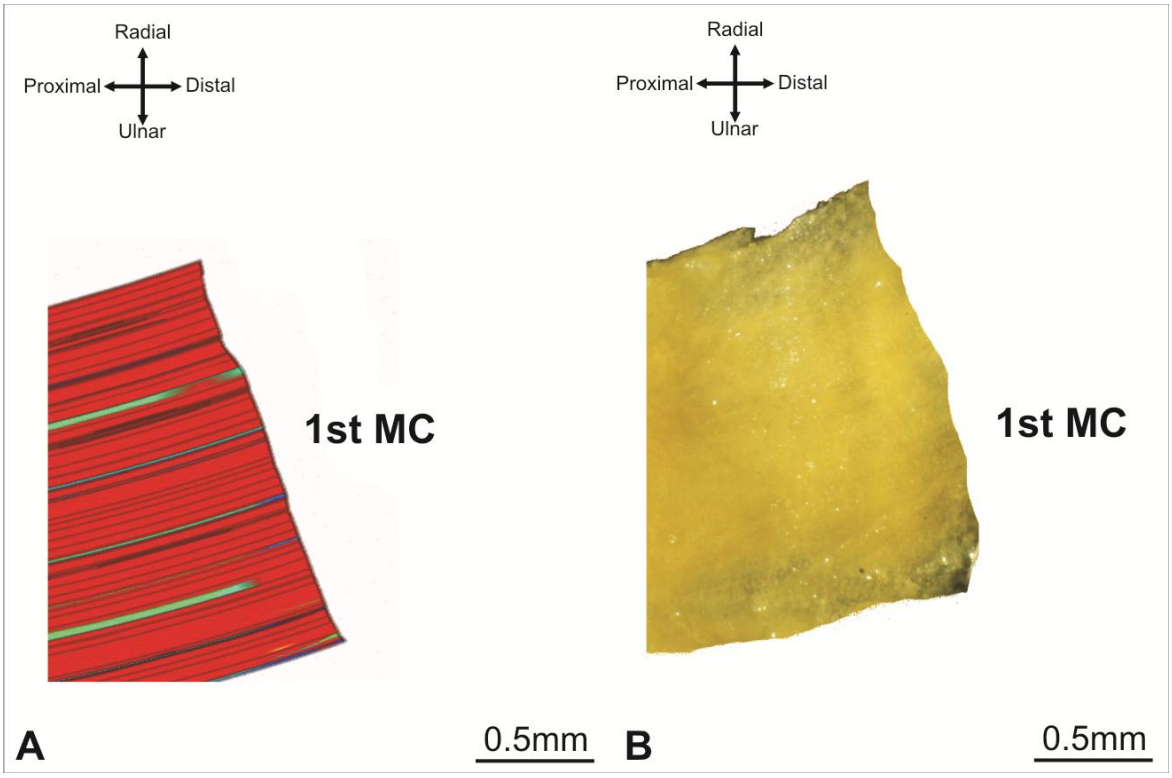

Figure 3.67: Edge analysis of the DUTML in distal attachment (distal zone).
(A) 3D model of the ligament which presents the distal edge had large concavity ending at the ulnar attachment zone, while the middle and radial attachment zones had obliquely ending fascicles.
(B) Actual edge of the DUTML after the bone connections was removed.

3.3.8.6 Palmar intermetacarpal ligament (PIML)

3.3.8.6.1 Surface curvature and tension analysis

The PIML had no change in all measurements, except the thickness, width, and length changed. The proximal, middle and distal surface zones showed extreme change. The fascicles of the PIML relaxed partially in the middle surface zone. Therefore, the fascicles of this ligament stretch or lengthen at the proximal and distal surface zones throughout the change from the static neutral toward static full abduction positions and also appeared thinner and more elongated. The properties of the PIML fascicles were under stress during the static neutral and static full abduction positions (Figures 3.68-3.69).

In the static full abduction position, extreme tension presented in all surface zones of the PIML fascicles. The curvature showed partially at the proximal and middle surface zones of this ligament, which means that the PIML fascicles' alignment had curved ulnar-proximally during the static full abduction position

(Figure 3.69). Moreover, in the static neutral position, the tension of the fascicles presented in the proximal, middle and distal surface zones. The tensions effection on this ligament was partially in the middle surface zone (Figure 3.68).

3.3.8.6.2 Edge analysis (attachment zone)

The proximal edge had an irregular prominence ending; the middle zone was distinguished by a sharp head, while the other attachment zones were asymmetrical. The distal edge had smoothly symmetrical fascicles ends with no sharpness and angles prominent (Figures 3.70-3.71).

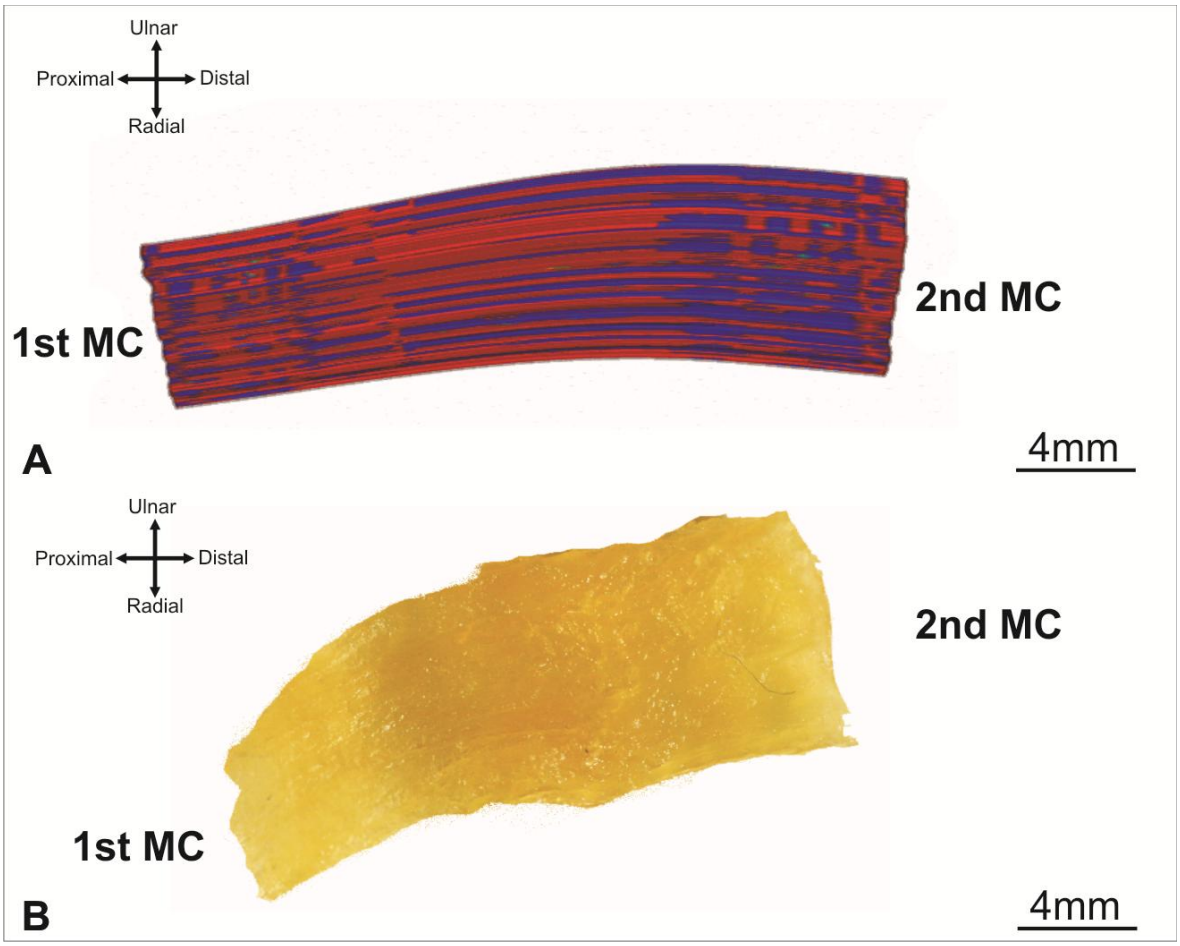

Figure 3.68: Surface curvature and tension analysis of the PIML in the static neutral position.

(A) 3D model of the ligament's fascicles in the static neutral position.
The tension of the fascicles presented in the proximal, middle, and distal surface zones. The tension effection on this ligament was partially in the middle surface zone.
(B) Actual shape of the PIML after the bone connections was removed.

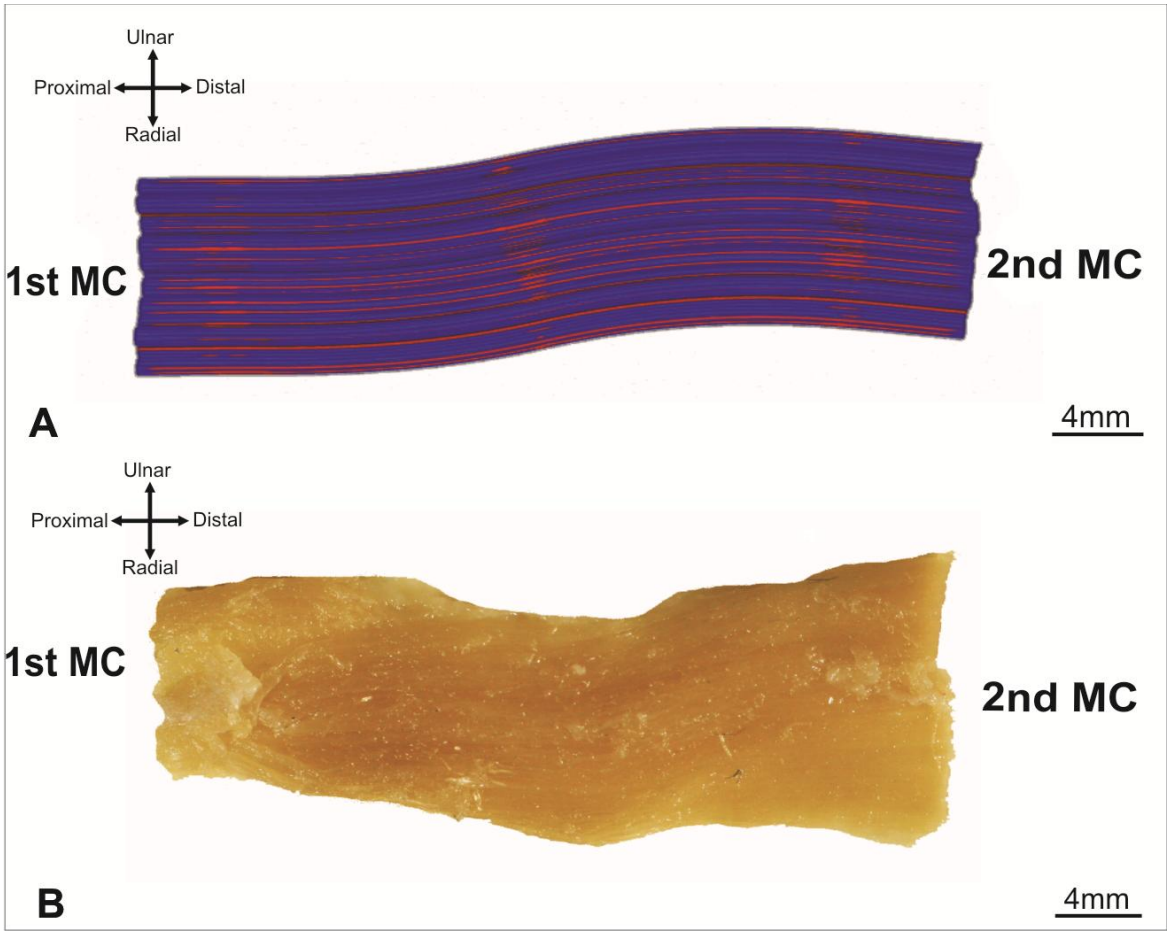

Figure 3.69: Surface curvature and tension analysis of the PIML in the static full abduction position.

(A) 3D model of the ligament illustrate the fascicles in the static full abduction position. The extremely tension presented in all surface zones of the PIML fascicles. The curvature showed partially at the proximal and middle surface zones of this ligament, which means that the PIML fascicles' alignment had curved ulnar-proximally during the static full abduction position.
(B) Actual shape of the PIML after the bone connections was removed.

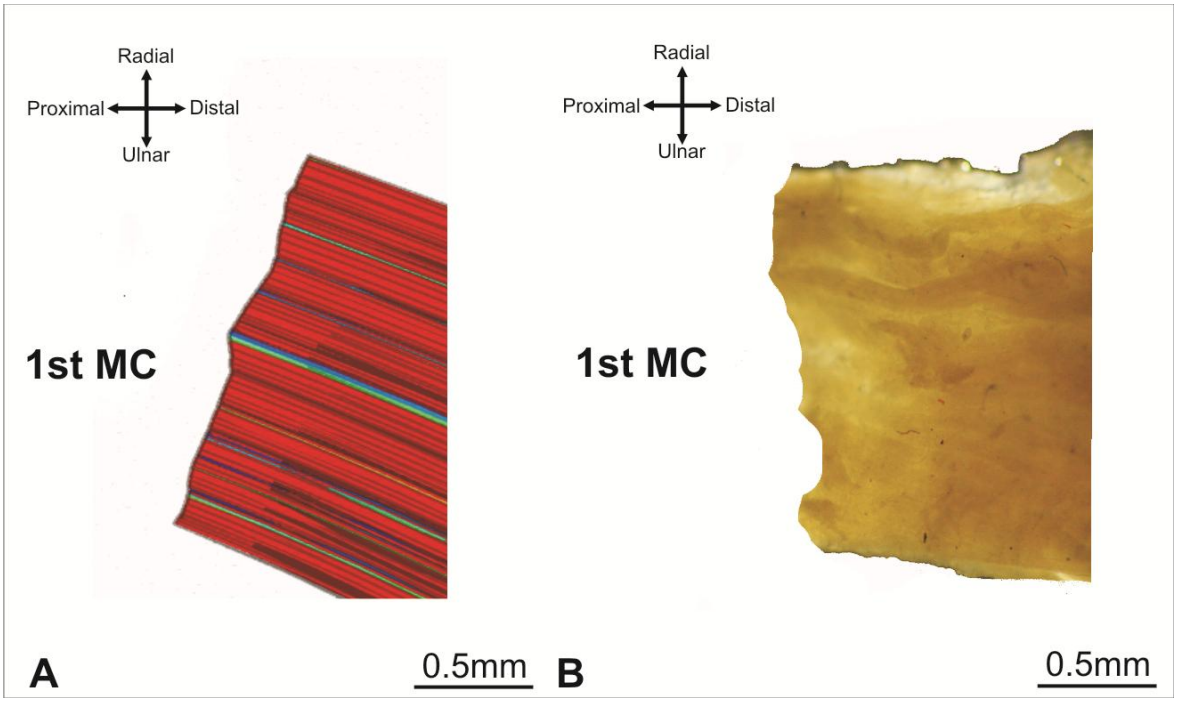

Figure 3.70: Edge analysis of the PIML in proximal attachment (proximal zone).

(A) 3D model of the ligament which presents the proximal edge had an irregular prominence ending; the middle zone was distinguished by a sharp head, while the other attachment zones were asymmetrical.
(B) Actual edge of the PIML after the bone connections was removed.

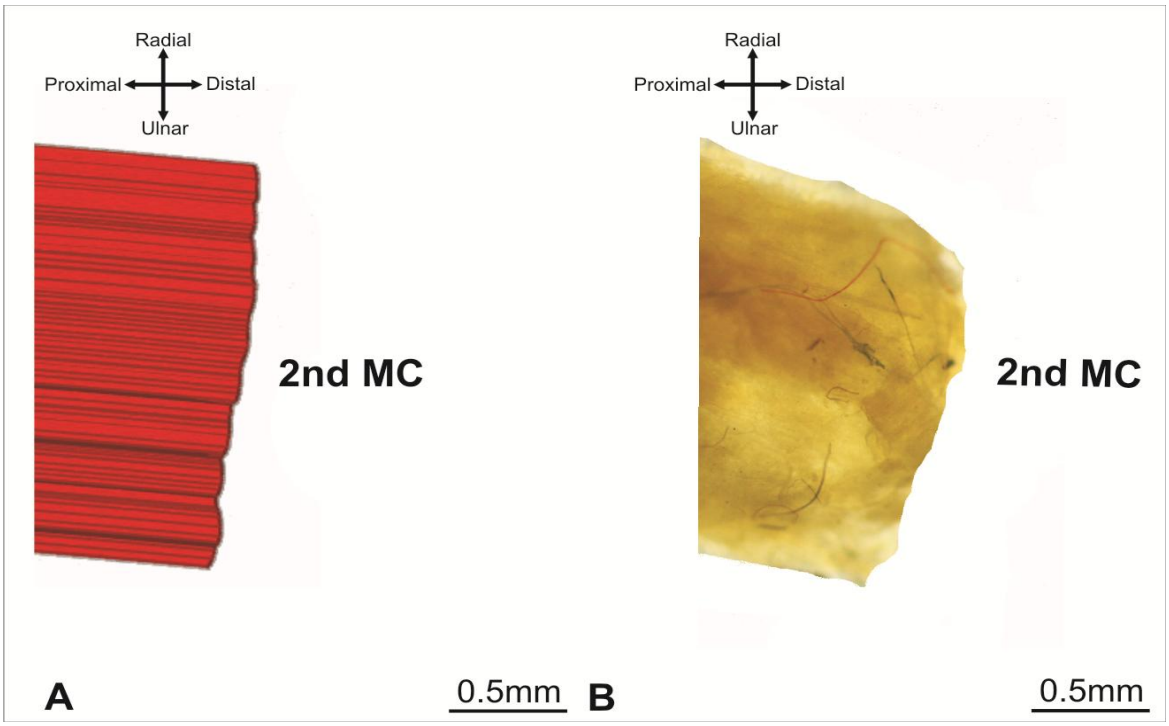

Figure 3.71: Edge analysis of the PIML in distal attachment (distal zone).

(A) 3D model of the ligament which presents the distal edge had smoothly symmetrical fascicles ends with no sharpness and angles prominent.
(B) Actual edge of the PIML after the bone connections was removed.

3.3.8.7 Dorsal intermetacarpal ligament (DIML)

3.3.8.7.1 Surface curvature and tension analysis

The DIML showed no change in all geometrical measurements except in thickness, width and length. The proximal, middle and distal surface zones showed extreme change. The fascicles of the DIML relaxed partially in the proximal zone. Therefore, the fascicles of this ligament stretch or lengthen at the middle and distal surface zones throughout the change from the static neutral toward static full abduction positions and also appeared thicker and wider in middle and distal surface zones. The properties of the PIML fascicles were under stress during the static neutral and static full abduction positions. The DIML and PIML have the same properties in that they stretch at the same surface zones, and both have tension during the static neutral and full abduction positions. The difference between them presents only in the shape of the fascicles: those of the PIML are thinner than those of the DIML in both positions, and the DIML fascicles have shown the (dove wing) in the distal surface zone (Figures 3.72-3.73).

In the static full abduction position, extreme tension presented in all surface zones of the DIML fascicles, and disturbed along the ulnar and radial attachment zones. The ulnar border has a high percentage of the tension upon the DIML fascicles. The curvature showed particularly at the middle and distal surface zones of this ligament, which means the DIML fascicles curved ulnar-distally during the static full abduction position (Figure 3.73). Moreover, in the static neutral position, the tension of the fascicles presented in the proximal, middle and distal surface zones. The tension effection was partially on the middle surface zone (Figure 3.72).

3.3.8.7.2 Edge analysis (attachment zone)

The proximal edge had an irregular prominence ending; the ulnar zone of the attachment was distinguished by sharp angle, while the other attachment zones were asymmetrical.The distal edge was distinguished by tapered head fascicles, and unequally arranged fascicles (Figures 3.74-3.75).

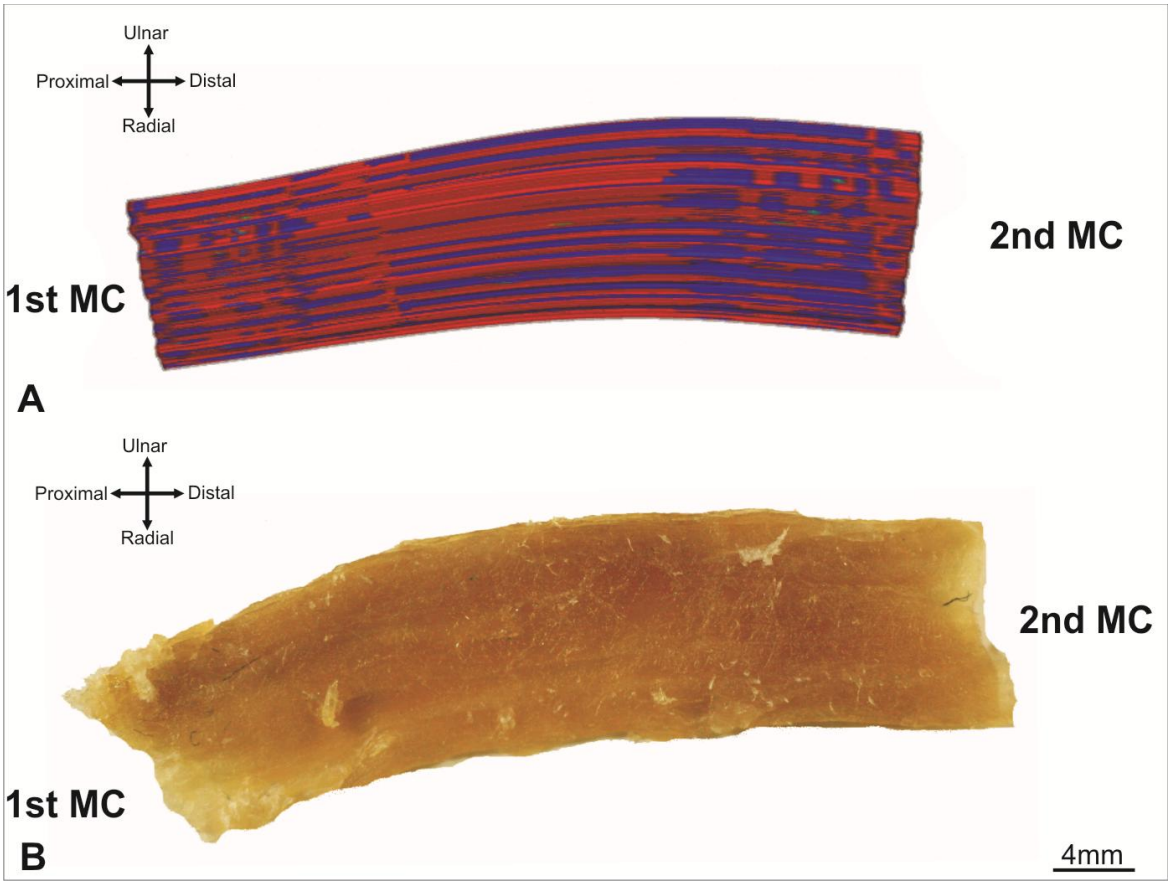

Figure 3.72: Surface curvature and tension analysis of the DIML in the static neutral position.

(A) 3D model of the ligament's fascicles in the static neutral position.
The tension of the fascicles presented in the proximal, middle, and distal surface zones. The tension effection was partially on the middle surface zone
(B) Actual shape of the DIML after the bone connections was removed.

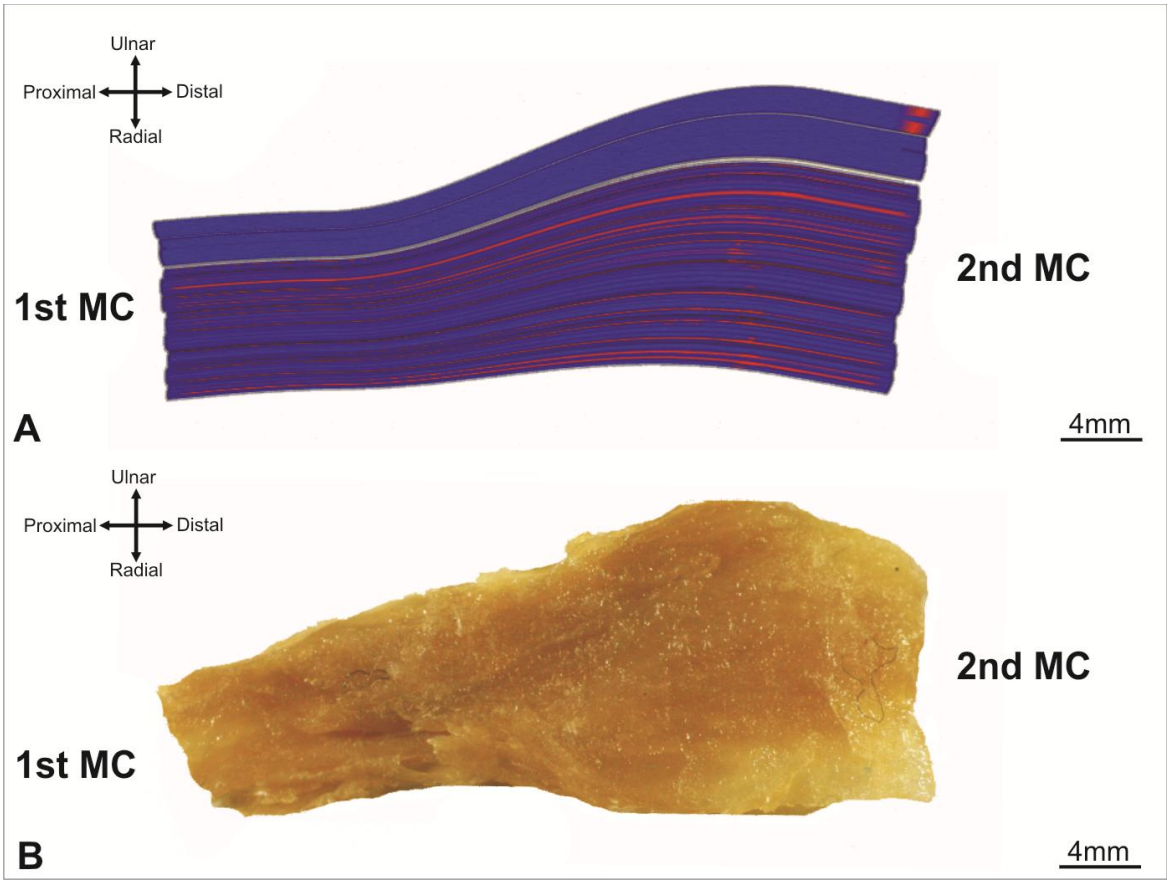

Figure 3.73: Surface curvature and tension analysis of the DIML in the static full abduction position.

(A) 3D model of the ligament's fascicles in the static full abduction position. The extremely tension presented in all surface zones of the DIML fascicles, and disturbed along the ulnar and radial attachment zones. The ulnar border has a high percentage of the tension upon the DIML fascicles. The curvature showed particularly at the middle and distal surface zones of this ligament, which means the DIML fascicles curved ulnar-distally during the static full abduction position (B) Actual shape of the DIML after the bone connections was removed.

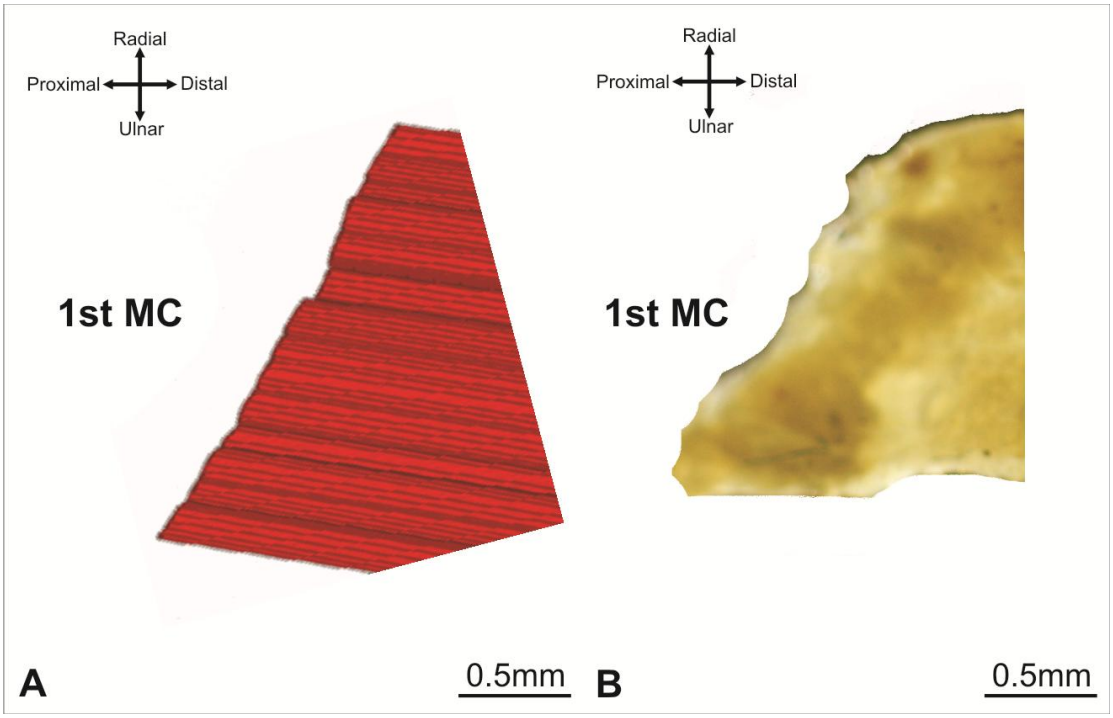

Figure 3.74: Edge analysis of the DIML in proximal attachment (proximal zone).

(A) 3D model of the ligament which presents the proximal edge had an irregular prominence ending; the ulnar zone of the attachment was distinguished by sharp angle, while the other attachment zones were asymmetrical.
(B) Actual edge of the DIML after the bone connections was removed.

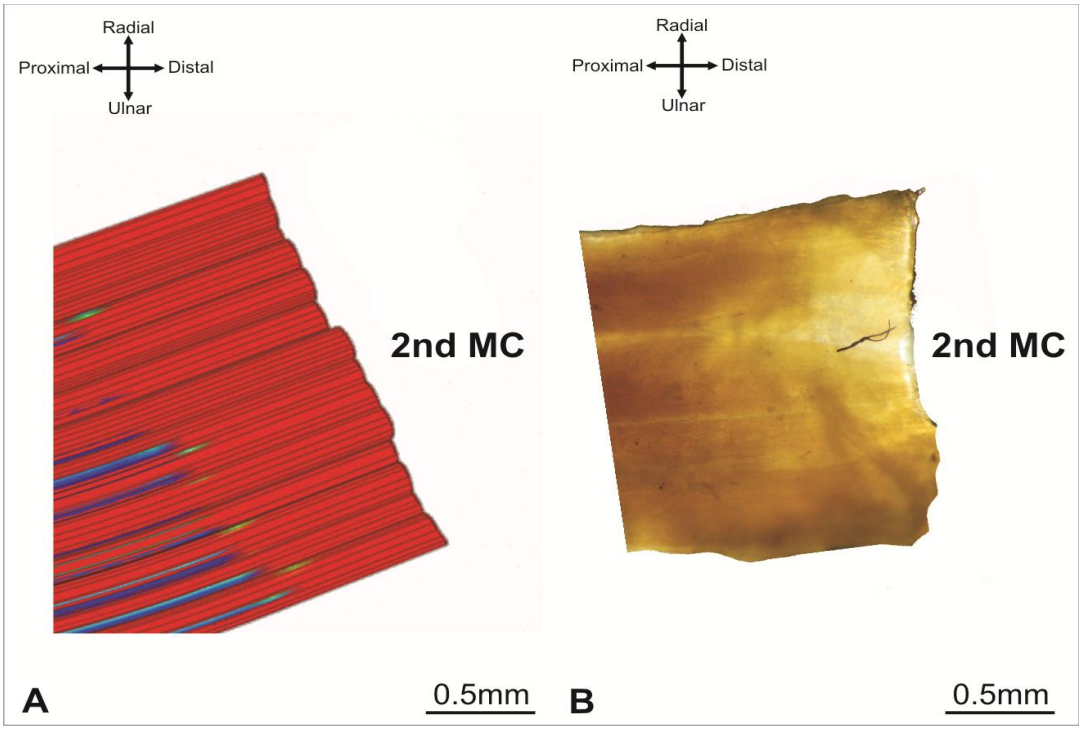

Figure 3.75: Edge analysis of the DIML in distal attachment (distal zone).

(A) 3D model of the ligament which presents the distal edge was distinguished by tapered head fascicles, and unequally arranged fascicles.
(B) Actual edge of the DIML after the bone connections was removed.

3.4 Discussion

Ligaments differ from musculotendons in that the former are passively elastic while the latter can actively contract (Benjamin *et al.* 2006). Although both tendons and ligaments contain collagen, elastic ligaments can contain twice as much elastin than collagen, giving them spring-like properties (Geyer *et al.* 2009). Functionally, ligaments are used to guide joint movement and maintain the stability of joints during movement. Visually, they are cord-like in appearance and can twist along their lengths. They tend to be shorter than musculotendons because they connect closely adjacent portions of bone.

The mathematics can involve developing geometric models of their shapes and computer graphics to visualize these models (Lin *et al.* 2010). Mathematical boundary representations are primarily used to represent these objects. This is usually an adequate representation since there is often no need to generate the internal contents of an object. However, when modelling ligament architecture, it is important to visualize internal features such as fascicle arrangements.

The geometrical measurements applied in this study, length, width, volume, thickness and cross-sectional area, were compared with those in previous study (two-dimensional), except the volume and cross-sectional area. The B- spline three-dimensional shape of the ligament gives the ability to visualize and calculate the shape in a three-plane space, and this was not possible in the previous study (Hirokawa and Tsuruno 1997). In addition, the thickness measurement provided very important data about the ability of the TMC ligament displacement – if the ligament has a high thickness measurement, it also has a great ability to stretch throughout the motions of the thumb. These issues have not been discussed in two-dimensional reconstruction.

3.4.1 Comparison between the two-dimensional reconstruction and three-dimensional modelling

The following table illustrates the differences and similarities of the TMC ligament measurements throughout the static neutral and full abduction positions in two-dimensional reconstruction and three-dimensional modelling:

Measurements		RTML	sPTML	dPTML	PUTML	DUTML	PIML	DIML
3D	Thickness	RTML and dPTML changed from the neutral to full abduction positions.						
2D & 3D	Length	RTML, dPTML, PIML, and DIML have no difference between the neutral to full abduction positions except sPTML, PUTML and DUTML.						
2D & 3D	Width	RTML and dPTML changed from the neutral to full abduction positions.						
3D	Volume	There are no changes in any of the TMC ligaments from the neutral to full abduction positions.						
3D	Proximal cross-sectional area	All the TMC ligaments change from the neutral to full abduction positions.						
3D	Middle cross-sectional	RTML, DUTML, and PUTML changed from the neutral to full abduction positions.						

	area	
3D	Distal cross-sectional area	sPTML, dPTML, PIML and DIML changed from the neutral to full abduction positions.

Table 3.8: The table illustrates the the differences and similarities of the TMC ligament measurements throughout the static neutral and full abduction positions in 2D reconstruction and 3Dmodelling.

The following table illustrates the differences and similarities of the TMC ligament measurements throughout dynamic displacements in two-dimensional reconstruction and three-dimensional modelling:

Measurements		RTML	sPTML	dPTML	PUTML	DUTML	PIML	DIML
3D	Thickness	RTML has a high dynamic displacement of 25%, while dPTML has a low dynamic displacement of 6% of the TMC ligaments.						
2D & 3D	Length	DIML has a high dynamic displacement of 64%, while dPTML has a low dynamic displacement of 1% of the TMC ligaments.						
2D & 3D	Width	sPTML has a high dynamic displacement of 43%, while RTML at 2% and DUTML at 2% have low dynamic displacements of the TMC ligaments.						
3D	Volume	DIML has a high dynamic displacement of 29%, while DUTML at 1% and RTML at 12% have low dynamic displacements of the						

		TMC ligaments.
3D	Proximal cross-sectional area	PIML has a high dynamic displacement of 23%, while RTML has a low dynamic displacement at 6% of the TMC ligaments.
3D	Middle cross-sectional area	PIML has a high dynamic displacement of 26%, while DUTML at 5% and RTML at 5% have low dynamic displacements of the TMC ligaments.
3D	Distal cross-sectional area	PIML has a high dynamic displacement of 26%, while RTML has a low dynamic displacement of 2% of the TMC ligaments.

Table 3.9: The table illustrates the the differences and similarities of the TMC ligament measurements throughout dynamic displacements in 2Dreconstruction and 3D modelling:

Both of the above tables demonstrate the cases of the TMC ligament during the neutral and full abduction positions and clarify the measurements of these ligaments in both two-dimensional reconstruction and three-dimensional modelling. In the current study, the thickness of the ligament has been measured only in three-dimensional modelling, and where the TMC ligaments have the differences in the neutral and full abduction position was recorded. Therefore, only the RTML and dPTML TMC ligaments changed statistically and dynamically, which clarifies the number of ligament fascicles that may have related to the thickness of these ligaments.

The number of the internal contents (ligament fascicles) directly correlates with the thickness of the ligament: the larger the number of fascicles the thicker the ligament. But this thesis is not accurate – the arrangement of the ligament’s

fascicles also plays a very important role in thickening the ligament. Therefore, the layers or rows of the ligament's fascicles inside the ligament's tube and the number of the ligament fascicles together constitute the main factor for thickening the ligament. The length and width have been compared in two-dimensional reconstruction and three-dimensional modelling, and the results of both are similar, which means both techniques were precise.

The measuring of volume does not vary statistically from both positions: The volume results have a strong influence on the other measurements, for instance, if the volume for a specific ligament varies from neutral to full abduction, this means the ligament's shape has changed in terms of its internal contents (the ligament's fascicles), which then affect the other measurements of the ligament.

In addition, the version five Rhinoceros software has the ability to cut the shape from anywhere. The current study used this option to record and observe a cross-sectional area of the ligament from the proximal, middle, and distal areas, respectively. The advantages of this procedure are precise results on the specific area and particularly the ability to visualize the cross sectional area at the attachment with the trapezium and first metacarpal bones. Also, the cross-sectional areas, especially proximal and distal, present the (footprint) or the edge of the attachment between the ligament and bone. The middle cross-sectional area observes only the state of the ligament in the stretching and relaxing positions, or widening and thinning. The differentiation between the neutral and full abduction positions of the middle cross-sectional area, which reflected the dynamic displacement act on the ligament. For instance, PIML, DUTML, and RTML have the highest and lowest percentages of the dynamic displacement among the TMC ligaments. Therefore, these ligaments have more ability to stretch or relax according to the thumb motions. Also, the PIML and RTML have the ability to change their shape, particularly at the attachment site during the thumb motion, because they have highest and lowest percentage of the dynamic displacement in both attachments area (proximal and distal). The results in the current study support the results from the previous study that the DIML and PIML are the main stabilizers of the TMC joint during the full abduction position. Moreover, the RTML has the ability to reduce radial subluxation throughout the full abduction motion because it has the lowest dynamic displacement in the proximal, middle, and distal cross-sectional areas. However, the measurements of the TMC ligaments in the

previous and current studies have a lot of data, to identify which ligament of TMC joint acts as a main stabilizer and which ligament does not have any roles during the thumb motion from the neutral toward full abduction position. Both two-dimensional reconstruction and three-dimensional modelling, with static and dynamic data, give more precise data to determine the stabilization between TMC ligaments.

3.4.2 Surface curvature, tension, and edge of the ligaments

The thumb ligament structures and their strain behaviours are essential for understanding thumb ligament injuries and for success in repair and reconstruction procedures. Strain measurements have been performed by means of strain gauges (Henning *et al.* 1985) and other types of displacement transducers (Hirokawa and Tsuruno 1997).

In the current study, it was necessary to identify the change that acted on the ligaments by tension. Therefore, the ligament was divided into three surface zones to depict which zones had a strong concentration of the tensions, and at the same time to observe the change that happens to the geometrical measurements, which reflects a change in the shape of the ligament. Also, the three attachment zones assist in describing the edge of the ligament, particularly at the attachment points with both bones (trapezium and first metacarpal). .

Normally, the ligament curvature comes after tension stream moving throughout the ligament fascicles, and the directions of the force depend on the thumb motion direction. In the current study, the direction of the force presents as tension inside the ligament fascicles toward full abduction.

In addition, the curvature of the ligaments depends on the thumb motion direction and shape of the bones. Some part of the ligament anatomically may be lying on the bone, if the bone has bridges or prominences at specific areas that reflect on the curvature of the ligament.

The anatomical description of a ligament edge would be a more deeply histological investigation. But the attachment shape in the current study was divided into three attachment zones to give more detail and create the ability to

visualize the ligament fascicles' ending. However, the edge of the ligament gave the precise data to describe the TMC ligament and with histological investigation would also give more accurate data for each of TMC ligaments.

The RTML, sPTML and dPTML were distinguished by relaxing during the full abduction position and stretching in the neutral position. The RTML was mostly curved ligament especially at the neutral position. The RTML was a main stabilizer to restrict excessive lateral displacement. However, both the sPTML and dPTML had a peak shape which helped to work as an axial of the TMC joint throughout the motion from neutral toward full abduction positions.

The shape of the sPTML curved near the proximal surface zone in the neutral position, and the curvature which changed in the full abduction position was concentrated at the middle surface zone near the ulnar attachment zone. Based on the position of dPTML, it must be curved with sPTML. But the dPTML curved in the full abduction position at the middle between middle and proximal surface zones. However, this ligament worked mostly with sPTML as one ligament.

The PUTML and DUTML are anatomically placed beside each other, but the DUTML has a half arch at the middle and distal surface zones. Both ligaments have the same characteristics of curving during the full abduction position, curving from the middle and distal surface zones. However, the affect of the tensions of both ligaments assisted the TMC joint to be balanced, which also happened with the morphological characteristics of the first metacarpal and trapezium bones.

Extreme tension and curvature were shown for PIML and DIML in the results of the current study; both ligaments had extreme tension during the neutral and full abduction positions. Therefore, the roles of these ligaments were very important in the stabilization of the TMC joint during the motion from the neutral toward full abduction position. According to the anatomical position of the PIML, the curvatures acted at the proximal and middle surface zones, because the PIML was placed between the first and second metacarpal bones palmarly, and the insertion of the PIML was located near to the transverse carpal ligament (TCL). Therefore, the PIML ligament curved prximo-ulnarly. The DIML curved disto-ulnarly with tension upon the ligament during the full abduction position. Also, the tension of both ligaments increased somewhat in the full abduction position, and no

relaxation potentially affecting the status of these ligaments, except PIML relaxed a little at the middle surface zone. However, both ligaments play a role as a primary stabilizer of the TMC joint.

Nevertheless, some limitations of this study must be acknowledged. No clinical and dominant hand history was available. The advanced age of the cadavers could be responsible for making visualization of the attenuated ligaments more difficult through the full abduction motion. Also, there was no comparsion between the right and left hand, gender was not considered, and the number of specimens was low.

Finally, the current study has shown the value of this combined approach of detail measurements, tension and curvature analysis and digitization to determine the specific locations and areas of ligament attachments on the metacarpal and carpal bones. This information offers further knowledge on the shape of the TMC ligaments, including new information on the three-dimensional locations and attachments. This information is also displayed visually by three-dimensional bone images, which adds an additional means of understanding ligament anatomy. This detailed shape can assist in a better understanding of the motion and mechanics of the normal TMC joint. It can also help improve diagnostic image analysis of ligament repair, and/or reconstruction of the TMC joint, and can perhaps even offer better insight into the pathomechanics of degenerative changes seen so often in the thumb TMC joint.

Chapter Four

Technique Development for Histological Staining of Trapeziometacarpal Ligament Attachments

4.1 Introduction

The entheses of the trapeziometacarpal ligaments are complex and varied (Benjamin *et al.* 2006; Chung 2007; Claudepierre and Voisin 2005). While Modified Masson's Trichrome (MMT) and Miller Elastin (ME) staining have been used for illustrating collagen fibres and elastin fibres in tissues (Cobb *et al.* 1993; Fogg 2004; Freemont 2002), few studies have utilised a combination of both staining procedures when investigating such tissues.

The literatures review of experiments and studies relate to this chapter explained in details in chapter one (pages 67-77).

The aims of this current study are to (1) use histological sections of key trapeziometacarpal ligaments to more accurately describe their attachments; (2) describe the two layers of the palmar trapeziometacarpal ligament (PTML); (3) observe the attachment of the dorso-ulnar trapeziometacarpal ligament (DUTML), and investigate if there are any relationships with the flexor retinaculum by using the HREM technique; (4) develop a better staining protocol by combining MMT and ME staining to define the individual TMC ligaments more precisely; and (5) to re-time the ME staining protocol specifically (Miller's Elastin stain and Van Gieson solutions).

The development of the staining protocols and combining the two stainings with each other would provide new techniques that would help to investigate and analyse entheses. This will also help to better understand the structure and function of entheseal tissue in order to relate these findings to medical issues in diagnosing and treating enthesis-related injuries and diseases.

4.2 Materials and methods

4.2.1 Sample preparation

Eight embalmed cadaveric specimens were used, with ages ranging from 67±4.04 (58 blocks of each TMC ligaments). Hand dissection was performed carefully to obtain the required ligament of the TMC joint without damaging it, and with desired attachment and origin attachment (entheses) of TMC ligaments. Each ligament of the TMC joint with their ligamentous attachment (entheses) have been distinguished and removed then used a small K-wire to drill through all the attached bones to fix the ligament throughout the tissue preparation process.

The procedures of the decalcification, dehydration, cleaning, and embedding of the tissues were performed as shown in (Figures 4.1-4.2) (Appendix 1).

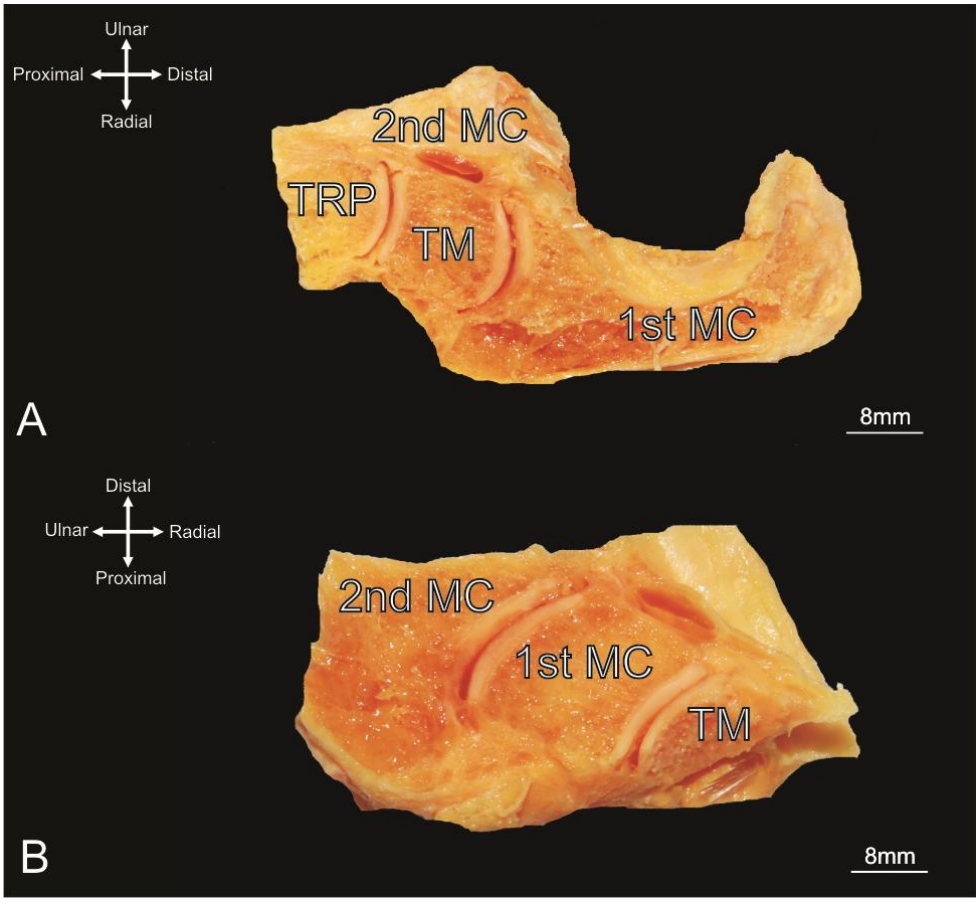

Figure 4.1: Multiple view of the TMC ligament sample preparation.
This shows the specimens' cutting, decalcification, dehydration, and embedding. (TM) trapezium bone, (1st MC) first metacarpal bone, (2nd MC) second metacarfpal bone, and (TRP) trapezoid bone.

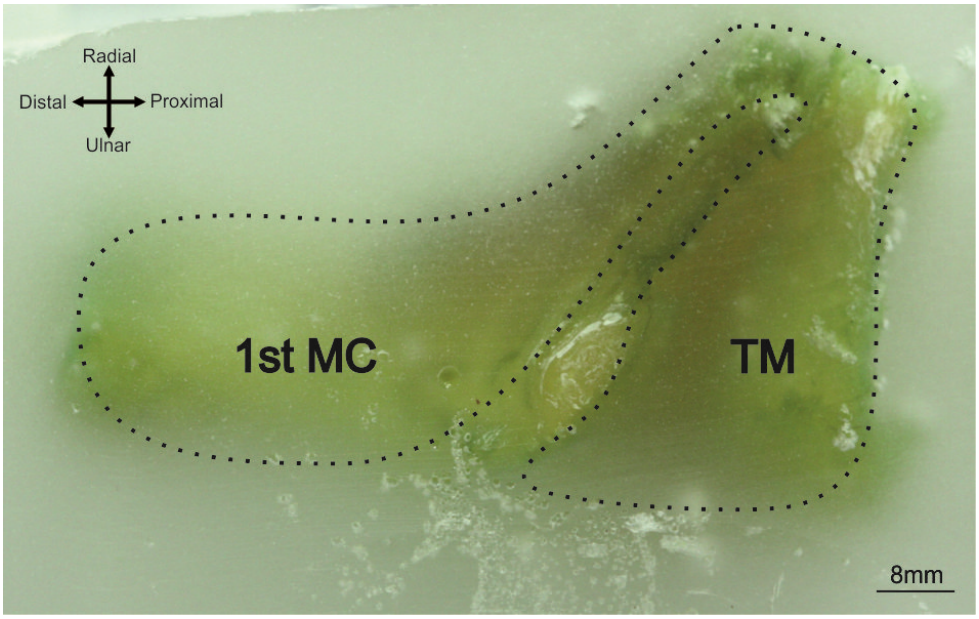

Figure 4.2: Double embedding of the TMC ligaments.
This shows the final end of the double embedding procedure, in which the tissue is mounted in blocks for cutting. (TM) trapezium bone and (1st MC) first metacarpal bone.

4.2.2 Sectioning and cutting

The microtome (Leica RM2235) was utilised to cut the blocks into many thin sections (10 µm); the blades of the microtome must be high-quality and sharp, and the angle of the blades must be optimised to avoid specimen trauma and cross-contamination. After the tissues were cut, we placed the sections firmly and carefully in slides, and kept them there for 15 minutes for drying; then the slides were ready for staining.

4.2.3 Staining procedures

This study used two main types of histological staining protocols: a Modified Masson's Trichrome (MMT) and Miller's Elastin (ME) staining protocol (Appendix 2-3). A combination protocol between the two main types was obtained; the combining started with MMT then was followed by ME (Appendix 4); then, in contrast, we started with ME then followed by MMT (Appendix 5).

For the combination staining started with MMT, the steps as following:

- Hydration sequenced of the slides.

- Then completed the MMT stain steps (Appendix 2), just before the slides started into the dehydration stage, switched to ME stain (Appendix 3), and continued all steps of the EM stain protocol.

- Dehydration steps of the ME stain continued, and mounted the slides in Histomount/DPX (Appendix 4).

For the combination staining that started with ME, the steps as following:

- Hydration of the slides.

- Then stains with ME staining (except Van Gieson) sequenced (Appendix 3), switched the slides into MMT stain (Appendix 2), and continued all steps of MMT stain.

- Dehydration steps of the MMT stain, and mounted the slides in Histomount/DPX continued (Appendix 5).

4.2.4 Re-timing the Miller's Elastin (ME) staining

The concept of the procedure is to increase and decrease the time the slides are in the container of the Miller's Elastin (ME) and Van Gieson (VG) stains, respectively. The procedure is divided into five experiments. In the first experiment, the slides are put into Me E stain for 2 hours and the VG stain for 30 seconds. The second experiment keeps the time of ME stain at 2 hours but decreases the time in the VG stain to 15 seconds. The third experiment increases the time in the ME stain to 2.5 hours and keeps the VG stain at 15 seconds. The fourth experiment keeps the ME stain at 2.5 hours and decreases the VG stain to 10 seconds. The fifth experiment increases the ME stain to 3 hours and keeps the VG stain at 10 seconds (Appendix 6).

4.2.5 Photography of slides

After the slides were stained and ready for photographing, we stitched multiple overlapped images that were taken under 2.5× magnifications and thus created a panorama image. We used 10× and 40× magnifications specifically for entheseal

images. Each TMC ligament has 4 images of different protocols of staining. The retiming protocol used DUTML.

4.2.6 Palmar trapeziometacarpal ligament (PTML) layers

Based on the literature review, there is controversy about the layers of the PTML; some studies have stated that the PTML has only one layer, while others that there are two layers: superficial and deep.

The histological finding is very important to solve this question. The investigation of the PTML layers was performed by four stains: MMT, ME, combination started with MMT, and combination started with ME. The procedure of block cutting of the PTML was by cross-section cutting.

4.2.7 High resolution episcopic microscopy (HREM) procedure

The current study used this technique to discover if there is any relationship between the flexor retinaculum and the attachment of the DUTML. As such, we applied HREM only for DUTML.

The instruments and devices used for the HREM study are as follows:

1. A stable setup had to be used to ensure alignment of images;

2. A table tripod (Manfrotto PIXI) to hold a digital camera (Canon 6D), which has 20.2 megapixel resolution and macro lens with 100 mm focal length (Canon Macro 100mm f/2.8);

3. A remote shutter release to avoid shaking and to improve the sharpness of pictures;

4. Microtome (Leica RM2235) was used to cut (10 µm).

The modelling of the tissues was performed by Amira 3D software; the dataset was uploaded to the software as JPEG files. In addition, the software automated the images, and corrected any unexpected alignment issues. The selection of the tissues was done manually: because the accuracy of the automatic section of the

Amira 3D software was weak, the process of the selection tissues was done slide by slide. The adjacent resolution power was also regulated manually, after complete sections of the regarded tissues. The software rendered into 3D modelling through the Gensurface option; the 3D model at this stage needed to decrease the roughness. We decreased this roughness by decreasing the face surface of the model by using the “smooth surface” option.

4.3 Results

4.3.1 Entheses of the TMC ligament (attachments)

Histological referencing and comparisons between different TMC ligaments were obtained by a modified Masson’s Trichrome staining; the slides showed clearly the trapezium (TM), first metacarpal (1st MC), and second metacarpal (2nd MC) bones. The pattern of the fasciculi within the fibrous matrix of each TMC ligament was also clear; the types of the entheses were investigated in both attachments: proximal and distal (from or to) the bone.

In addition, the tidemark was shown in some slides, such as palmar trapeziometacarpal ligament (PTML), palmo-ulnar trapeziometacarpal ligament (PUTML), dorso-ulnar trapeziometacarpal ligament (DUTML), palmar intermetacarpal ligament (PIML), and dorsal intermetacarpal ligament (DIML) (Figures 249-254).

Furthermore, based on the slides investigated, all the TMC ligaments entheses were type two (which is fibrocartilagenous entheses); the calcification of the collagen fibres were clear with its tidemark, which showed a large fasciculi within a fibrous matrix rows beside each other and merged with the bone cell (osteon). The fasciculi are within the fibrous matrix in the fibrocartilagenous type before attached to the bone for fixing the ligament had three zones. The first zone that appeared uncalcified was the fasciculi; the second zone was the tidemark line, which separeted both zones (uncalcified and calcified); the third zone was replaced into calcification of the fasciculi immediately before the fibres attached to the bone (Figures 4.3-4.4-4.5-4.6-4.7-.4.8).

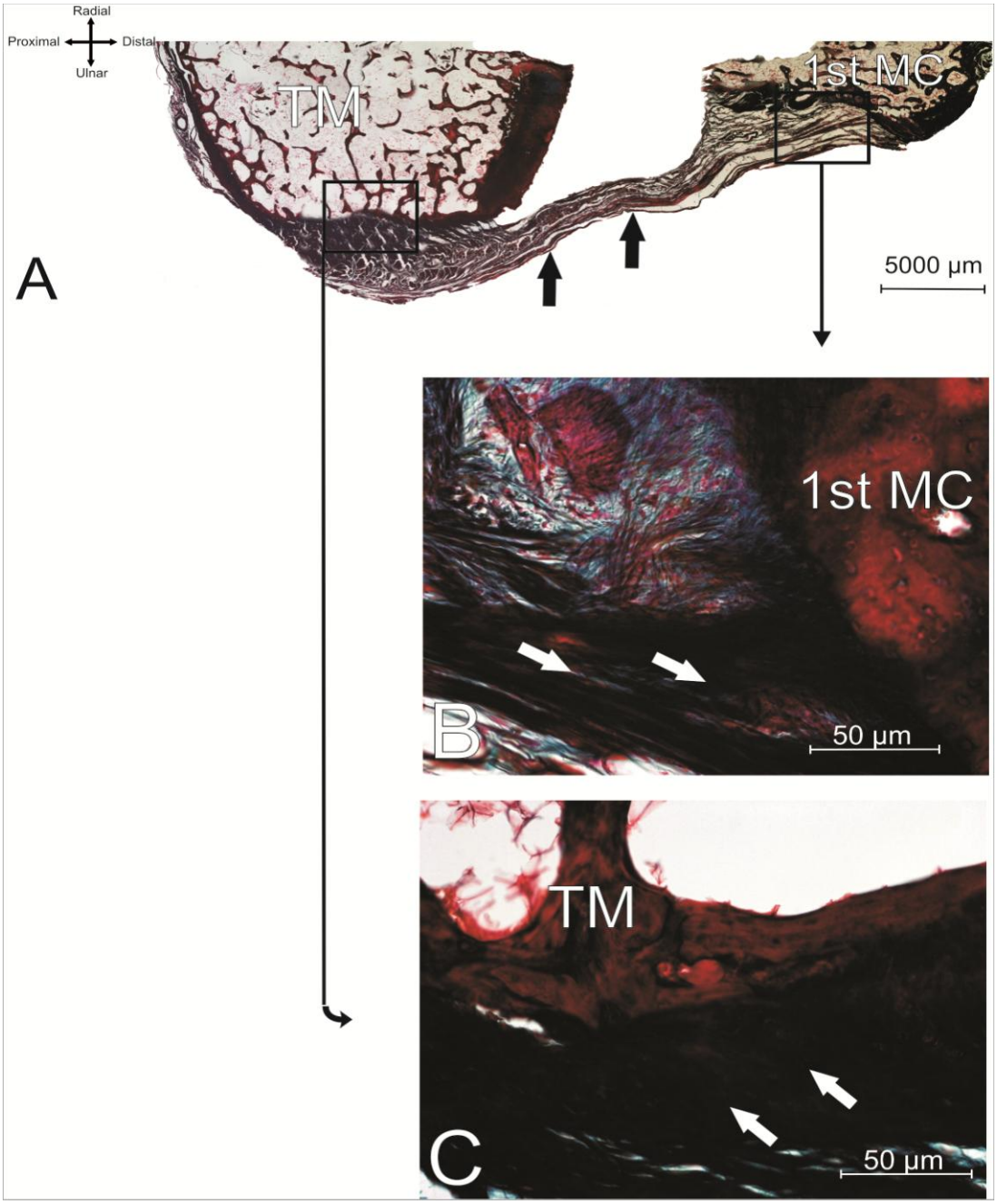

Figure 4.3: Section through the radial trapeziometacarpal ligament (RTML).

A. Panorama image of the RTML, with (magnification × 2.5).

B. Distal attachment; the RTML attached to first metacarpal (1st MC) bone. Zoomed-in section also showing true entheseal attachment; the arrows show the fibrocartilagenous type of the entheses. The tidemark in the section was not clear enough. The fasciculi was presented as strings beside each other with dark green colour, the bony tissues presented as big lacuna with dark red, and articular cartilage of the bones was as a small lacuna within a fibrous matrix with deeply dark green colour, with (magnification × 10).
C. Proximal attachment; the RTML attached to trapezium (TM) bone. Zoomed-in section showing true entheseal attachment (mechanically specific) over the trapezium bone. The arrows show the fasciculi configuration is gradually replaced by uncalcified fibrocartilage followed by calcified fibrocartilage that is directly attached to the bone, with (magnification × 10). Modified Masson's Trichrome.

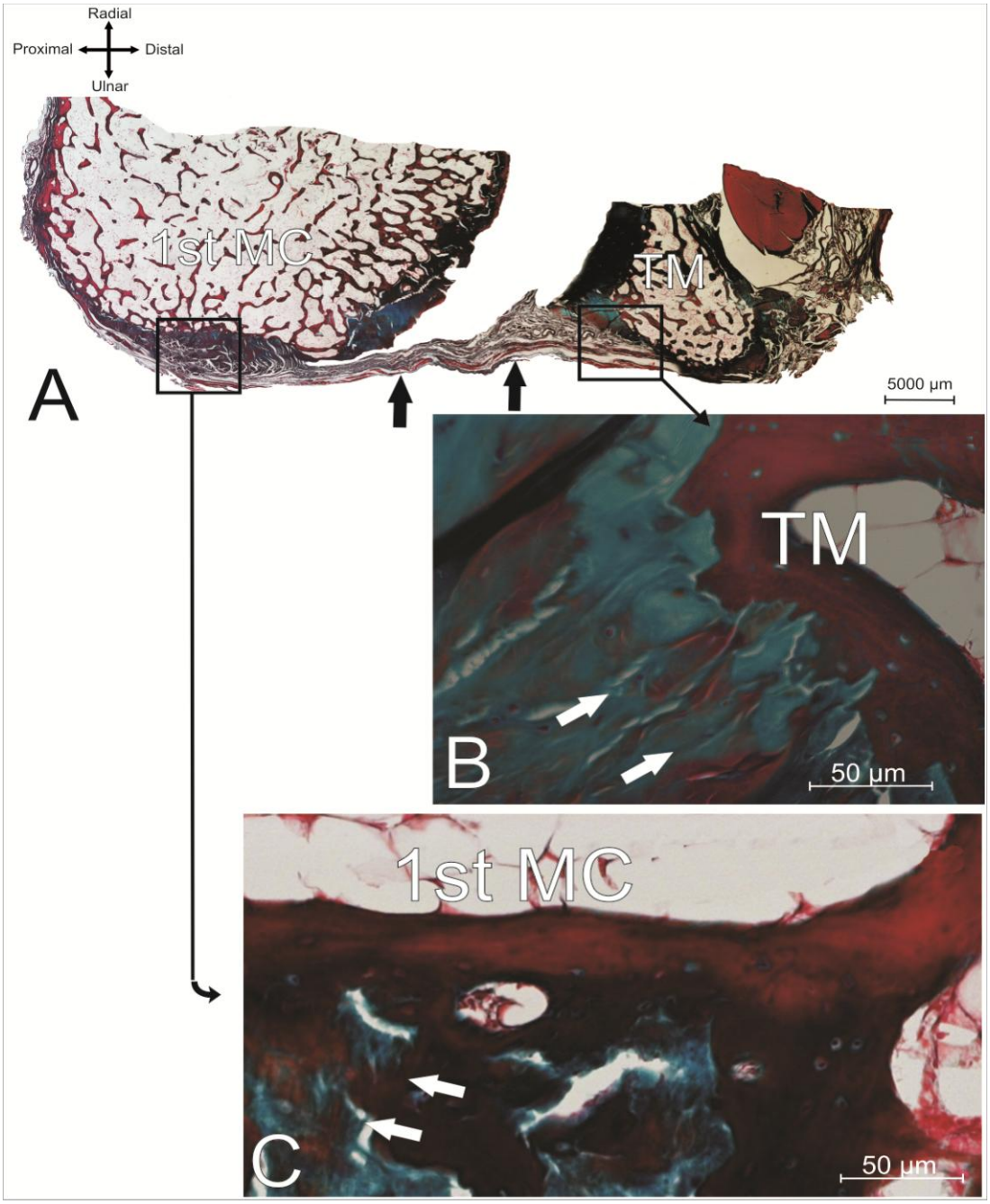

Figure 4.4: Section through the palmar trapeziometacarpal ligament (PTML).

A. Panorama image of the PTML, with (magnification × 2.5).

B. Proximal attachment; the PTML attached to trapezium (TM) bone. Zoomed-in section also showing true entheseal attachment; the arrows show the fibrocartilagenous type of the entheses. The tidemark in the section was clear, particularly in proximal attachment. The fasciculi was presented as strings beside each other with dark green colour, the bony tissues presented as big lacuna with dark red, and articular cartilage of the bones was as a small lacuna within a fibrous matrix with deeply dark green colour, with (magnification × 10).
C. Distal attachment; the PTML attached to first metacarpal (1st MC) bone. Zoomed-in section showing true entheseal attachment (mechanically specific) over the 1st MC bone. The arrows show the fasciculi configuration is gradually replaced by uncalcified fibrocartilage followed by calcified fibrocartilage that is directly attached to the bone, with (magnification × 10). Modified Masson's Trichrome

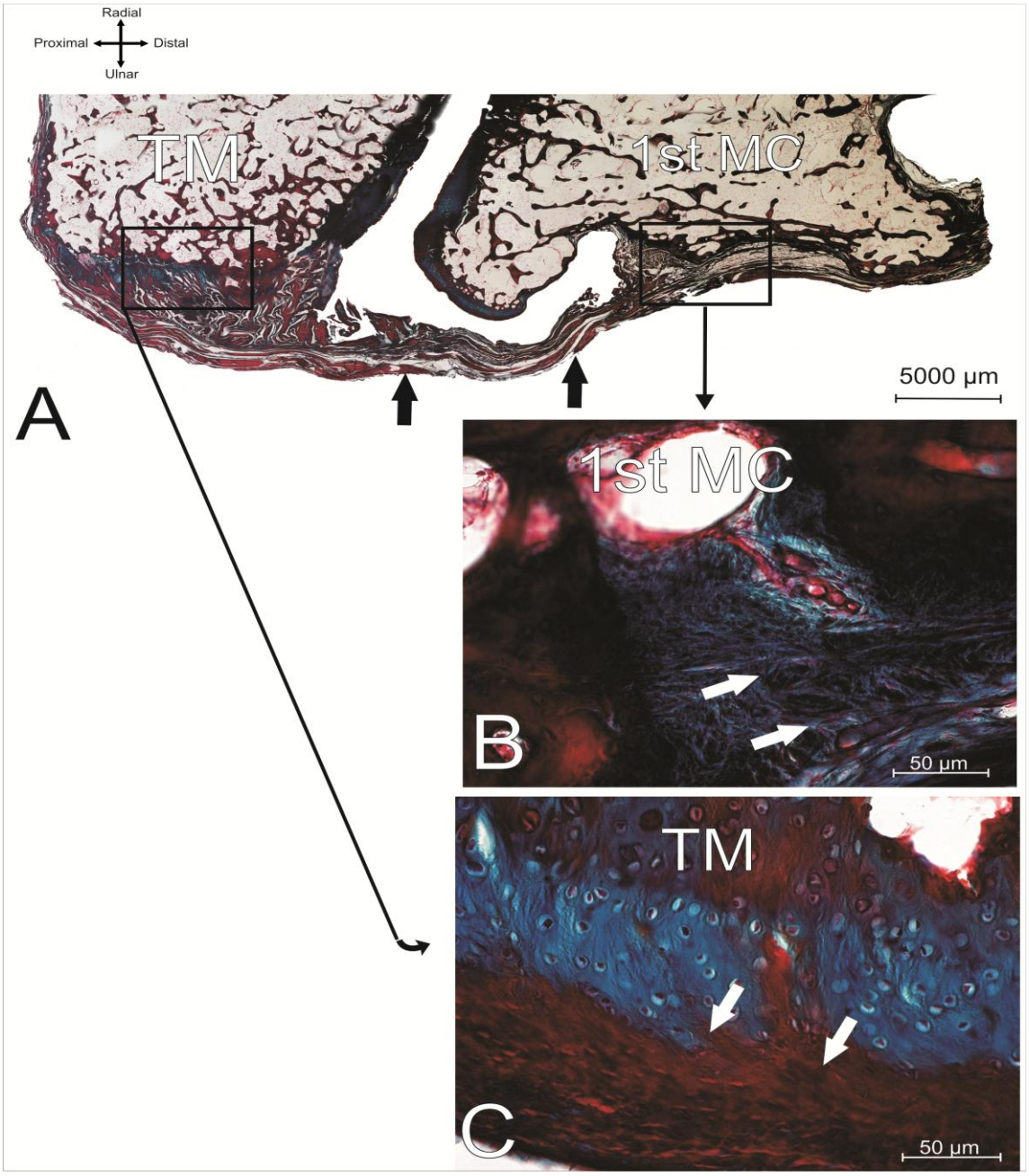

Figure 4.5: Section through the palmo-ulnar trapeziometacarpal ligament (PUTML).

A. Panorama image of the PUTML, with (magnification × 2.5).

B. Distal attachment; the PUTML attached to first metacarpal (1st MC) bone. Zoomed-in section also showing true entheseal attachment; the arrows show the fibrocartilagenous type of the entheses. The tidemark in the section was clear, particularly in proximal attachment. The fasciculi was presented as strings beside each other with dark green colour, the bony tissues presented as big lacuna with dark red, and articular cartilage of the bones was as a small lacuna within a fibrous matrix with deeply dark green colour, with (magnification × 10).
C. Proximal attachment; the PUTML attached to trapezium (TM) bone. Zoomed-in section showing true entheseal attachment (mechanically specific) over the trapezium bone. The arrows show the fasciculi configuration is gradually replaced by uncalcified fibrocartilage followed by calcified fibrocartilage that is directly attached to the bone, with (magnification × 10). Modified Masson's Trichrome.

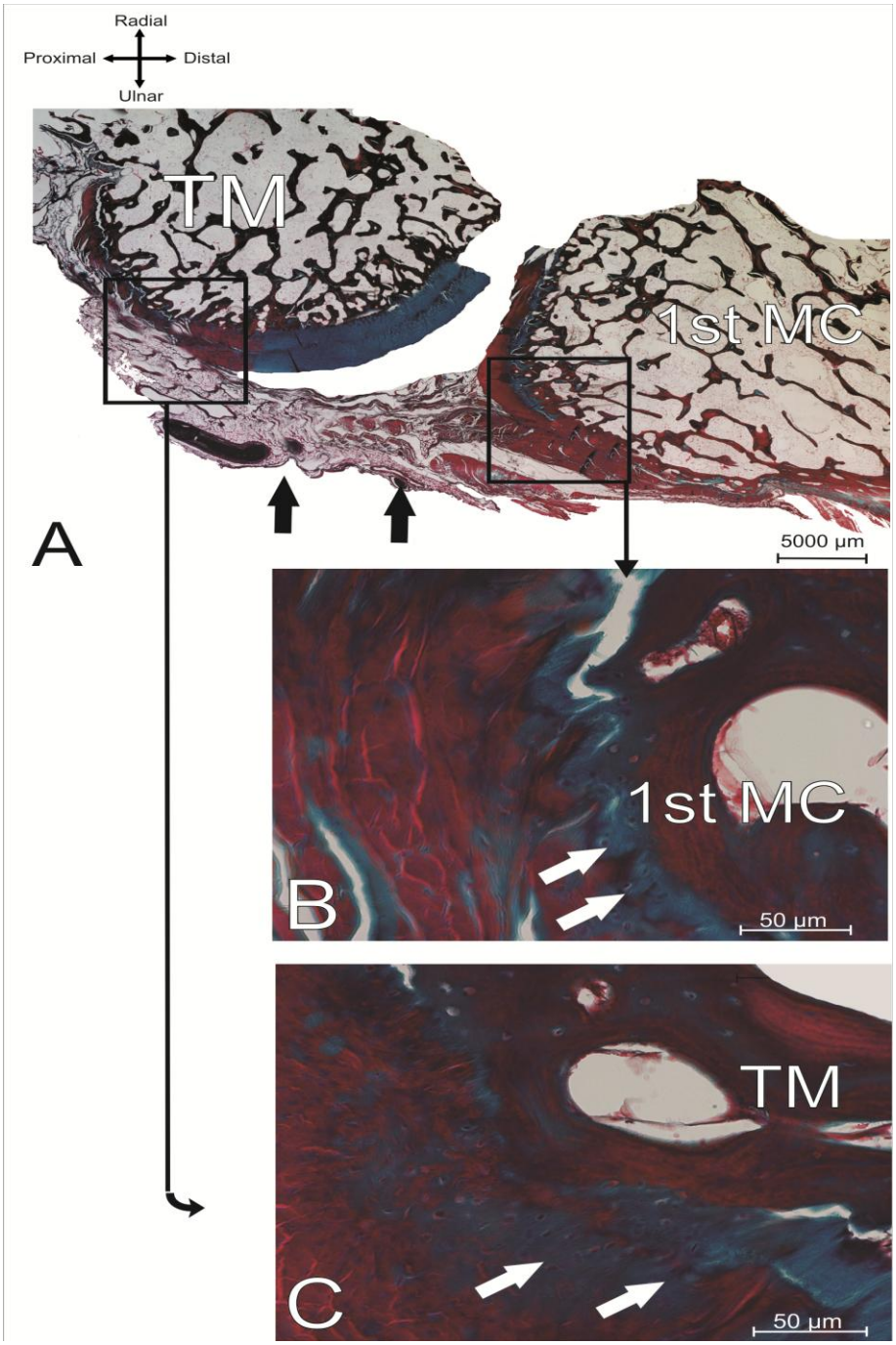

Figure 4.6: Section through the dorso-ulnar trapeziometacarpal ligament (DUTML).

A. Panorama image of the DUTML, with (magnification × 2.5).

B. Distal attachment; the DUTML attached to first metacarpal (1st MC) bone. Zoomed-in section also showing true entheseal attachment; the arrows show the fibrocartilagenous type of the entheses. The tidemark in the section was clear in both attachments. The fasciculi was presented as strings beside each other with dark green colour, the bony tissues presented as big lacuna with dark red, and articular cartilage of the bones was as a small lacuna within a fibrous matrix with deeply dark green colour, with (magnification × 10).
C. Proximal attachment; the DUTML attached to trapezium (TM) bone. Zoomed-in section showing true entheseal attachment (mechanically specific) over the trapezium bone. The arrows show the fasciculi configuration is gradually replaced by uncalcified fibrocartilage followed by calcified fibrocartilage that is directly attached to the bone, with (magnification × 10). Modified Masson's Trichrome.

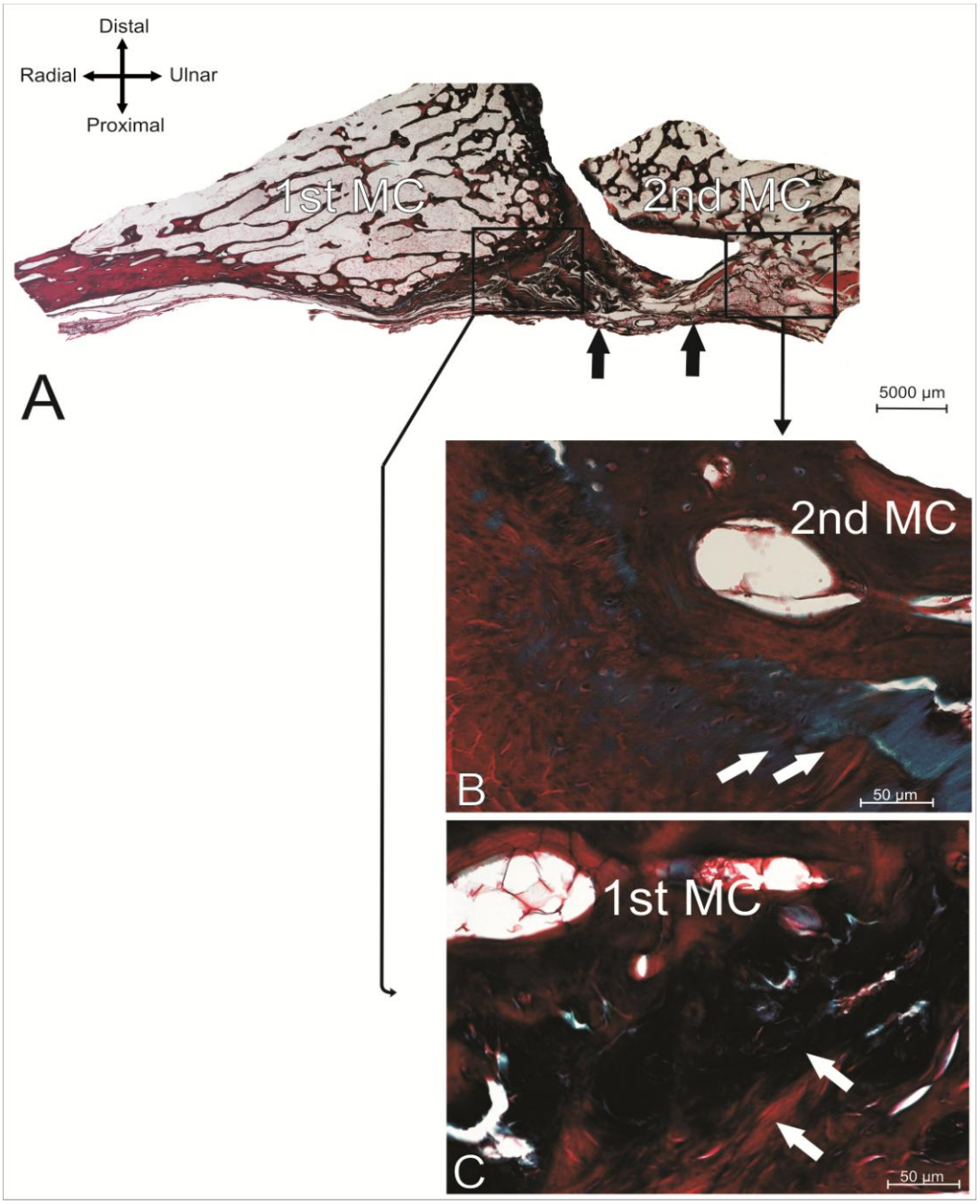

Figure 4.7: Section through the palmar intermetacarpal ligament (PIML).

A. Panorama image of the PIML, with (magnification × 2.5).

B. Distal attachment; the PIML attached to second metacarpal (2nd MC) bone. Zoomed-in section also showing true entheseal attachment; the arrows show the fibrocartilagenous type of the entheses. The tidemark in the section was clear in both attachments. The fasciculi was presented as strings beside each other with dark green colour, the bony tissues presented as big lacuna with dark red, and articular cartilage of the bones was as a small lacuna within a fibrous matrix with deeply dark green colour, with (magnification × 10).
C. Proximal attachment; the PIML attached to first metacarpal (1st MC) bone. Zoomed-in section showing true entheseal attachment (mechanically specific) over the 1st MC bone. The arrows show the fasciculi configuration is gradually replaced by uncalcified fibrocartilage followed by calcified fibrocartilage that is directly attached to the bone, with (magnification × 10). Modified Masson's Trichrome.

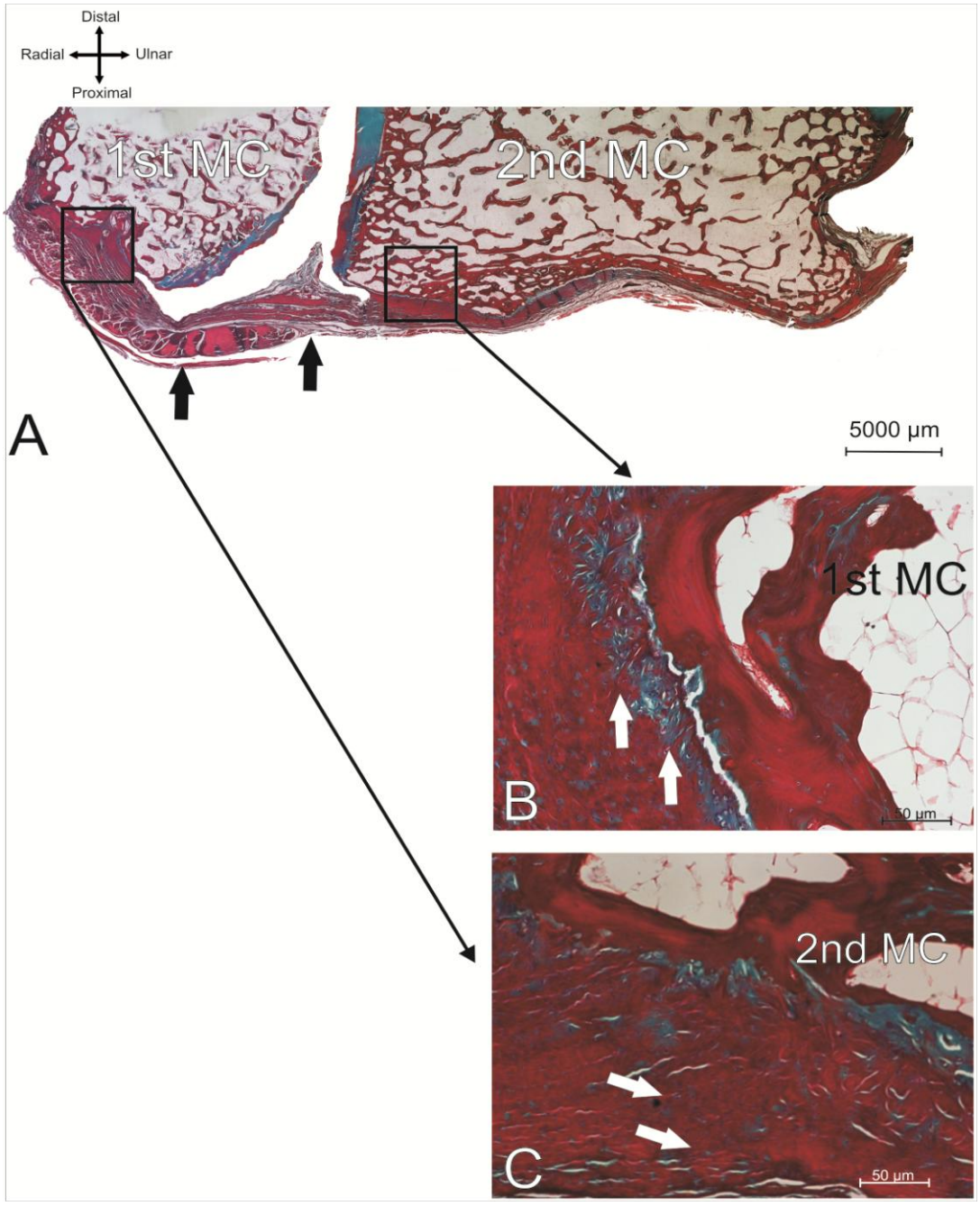

Figure 4.8: Section through the dorsal intermetacarpal ligament (DIML).

A. Panorama image of the DIML, with (magnification × 2.5).

B. Distal attachment; the DIML attached to second metacarpal (2nd MC) bone. Zoomed-in section also showing true entheseal attachment; the arrows show the fibrocartilagenous type of the entheses. The tidemark in the section was clear in both attachments. The fasciculi was presented as strings beside each other with dark green colour, the bony tissues presented as big lacuna with dark red, and articular cartilage of the bones was as a small lacuna within a fibrous matrix with deeply dark green colour, with (magnification × 10).
C. Proximal attachment; the DIML attached to first metacarpal (1st MC) bone. Zoomed-in section showing true entheseal attachment (mechanically specific) over the 1st MC bone. The arrows show the fasciculi configuration is gradually replaced by uncalcified fibrocartilage followed by calcified fibrocartilage that is directly attached to the bone, with (magnification × 10). Modified Masson's Trichrome

4.3.2 Descriptions of the palmar trapeziometacarpal ligament (PTML) layers

The results determined that the PTML has two layers—superficial and deep—as clarified in the images (Figures 4.9-4.10-4.11-4.12). The study used more than one stain to clarify the PTML and its structures.

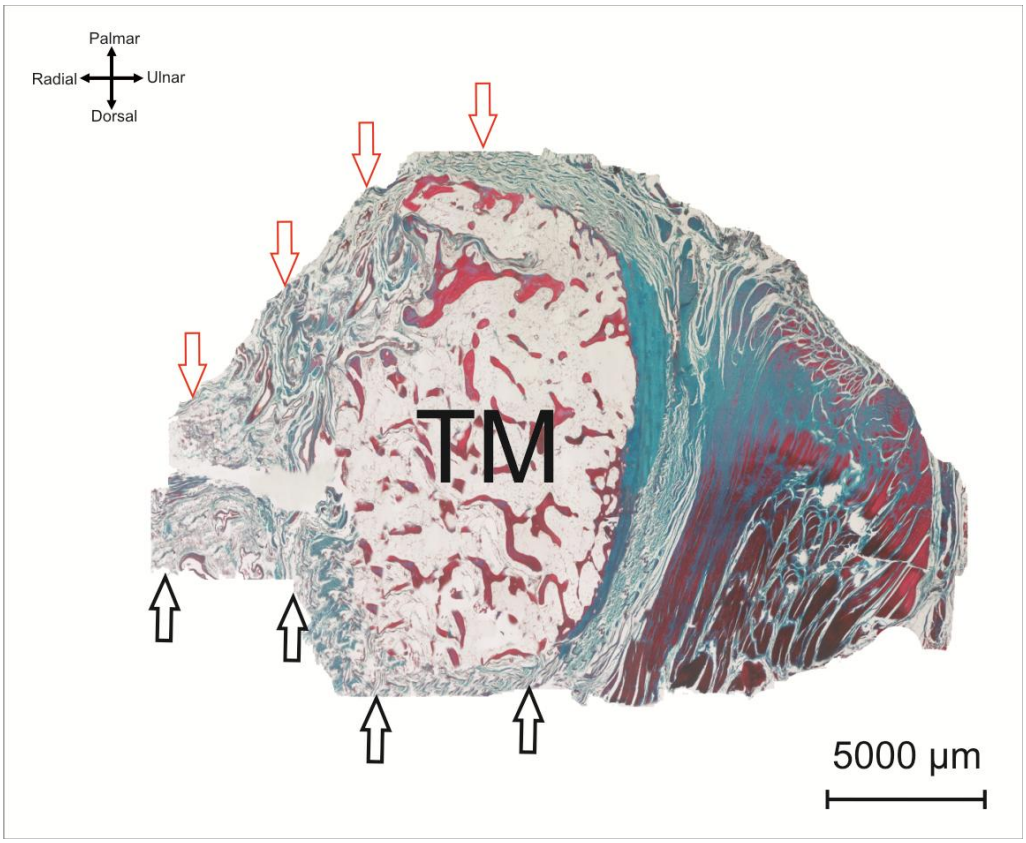

Figure 4.9: Cross-section through palmar trapeziometacarpal ligament (PTML).

Red arrows show the superficial layer of the PTML, which was the fasciculi pattern superficially to the deep layer. Black arrows show the deep layer of the PTML, which was the fasciculi pattern deeply to the superficial layer. TM. Trapezium bone. Modified Masson's Trichrome.

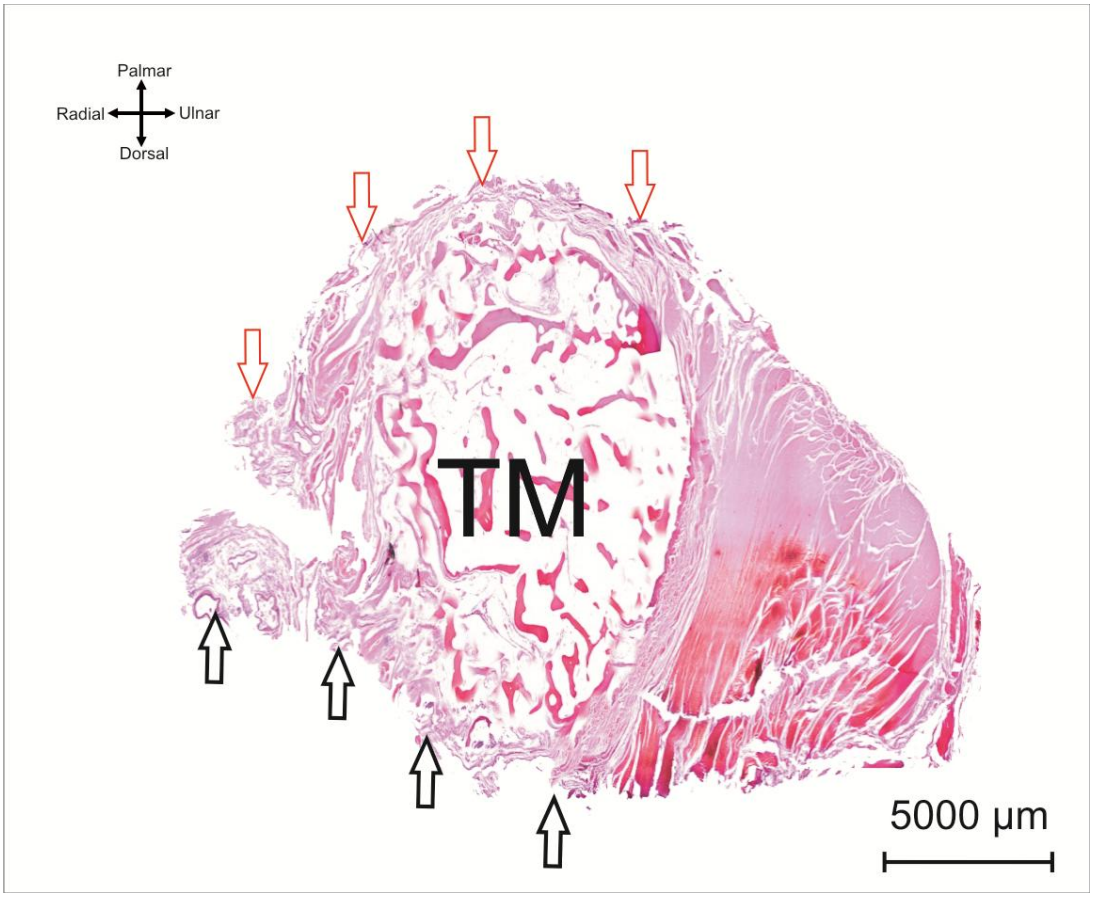

Figure 4.10: Cross-section through palmar trapeziometacarpal ligament (PTML).

Red arrows show the superficial layer of the PTML, which was the fasciculi pattern superficially to the deep layer. Black arrows show the deep layer of the PTML, which was the fasciculi pattern deeply to the superficial layer. TM. Trapezium bone. Miller's Elastin.

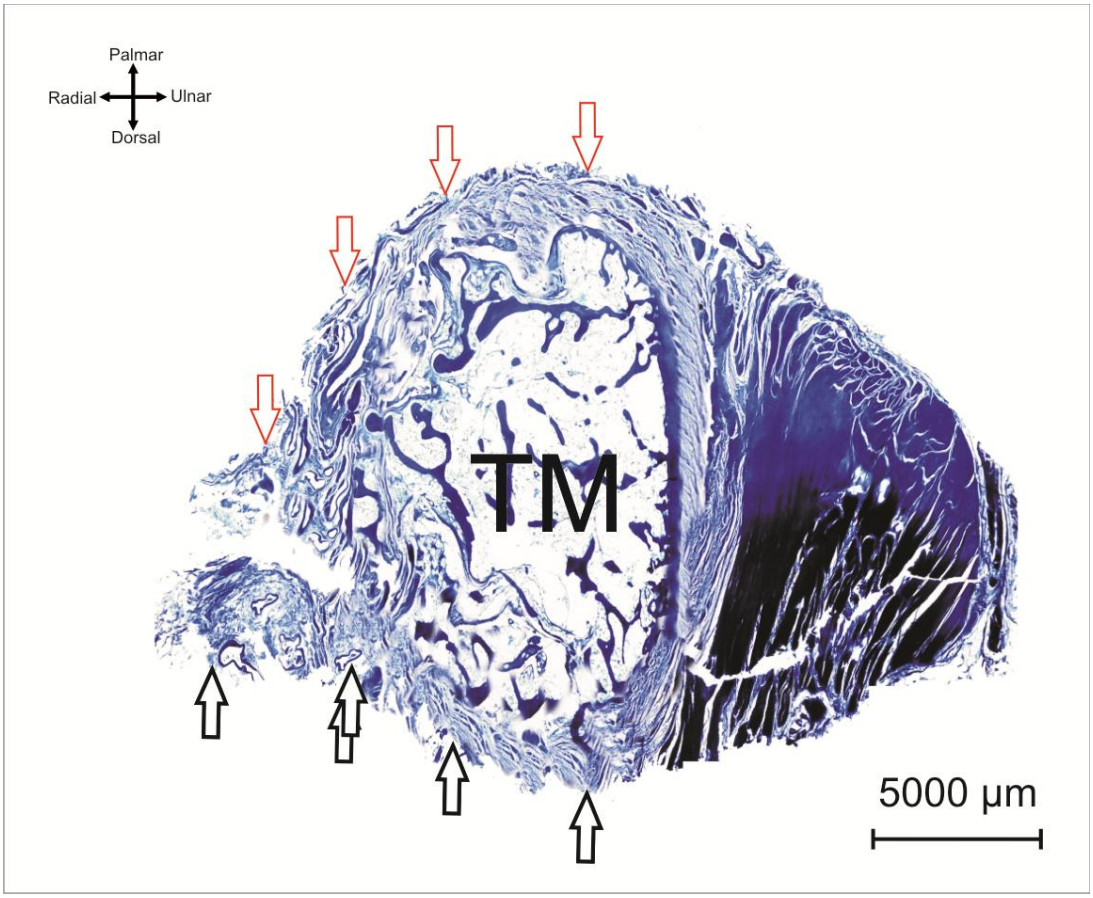

Figure 4.11: Cross-section through palmar trapeziometacarpal ligament (PTML).

Red arrows show the superficial layer of the PTML, which was the fasciculi pattern superficially to the deep layer. Black arrows show the deep layer of the PTML, which was the fasciculi pattern deeply to the superficial layer. TM. Trapezium bone. Combination Modified Masson's Trichrome and Miller's Elastin started with Modified Masson's Trichrome.

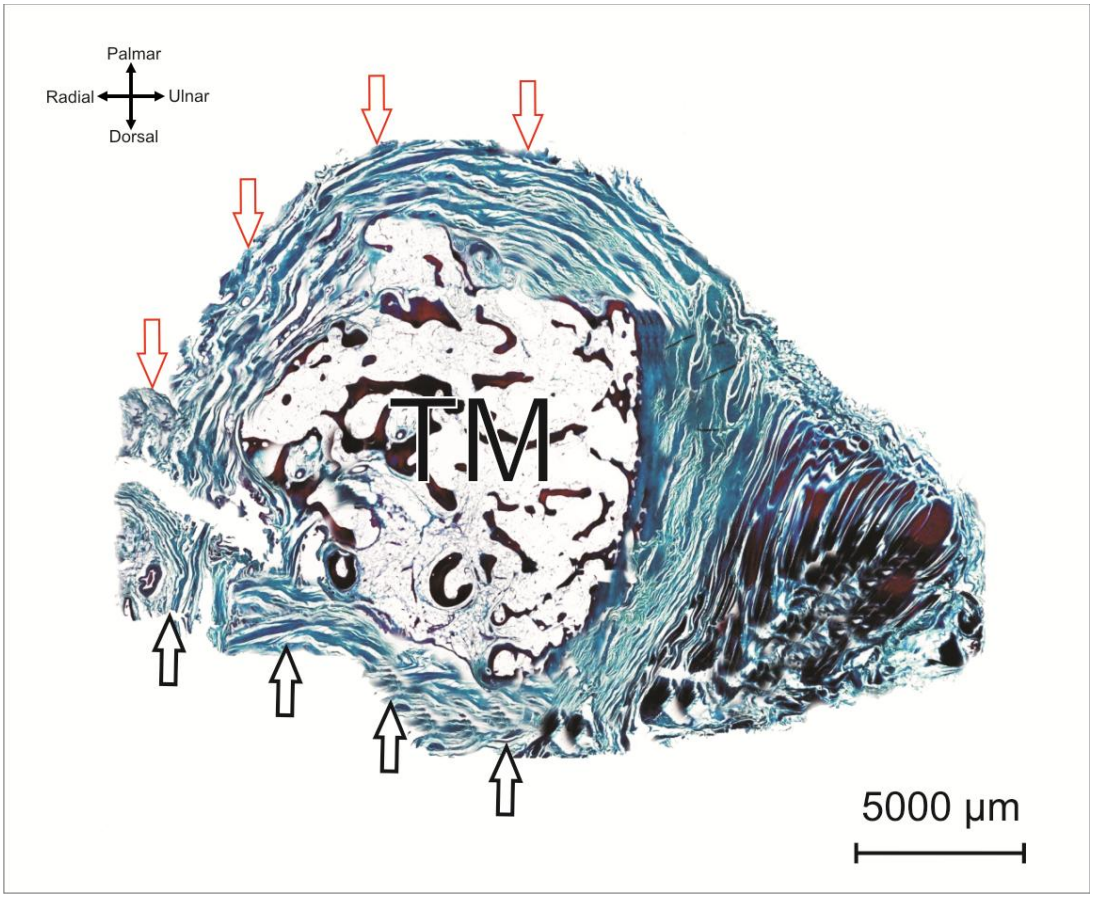

Figure 4.12: Cross-section through palmar trapeziometacarpal ligament (PTML).

Red arrows show the superficial layer of the PTML, which was the fasciculi pattern superficially to the deep layer. Black arrows show the deep layer of the PTML, which was the fasciculi pattern deeply to the superficial layer. TM. Trapezium bone. Combination Modified Masson's Trichrome and Miller's Elastin started with Miller's Elastin.

4.3.3 Miller's Elastin stain (ME)

The elastic fibres show as a bundle of elastin in an extracellular matrix of connective tissues; the function of these fibres is to stretch and relax during the lengthening and shortening of the individual TMC ligament. The elastin fibres show also the limitation of the fascicles and determine the ligaments throughout it. The results show the elastin fibres to be clearly identified in all soft tissues such as ligaments, capsules, and blood vessels (Figures 4.13-4.14-4.15-4.16-4.17-4.18).

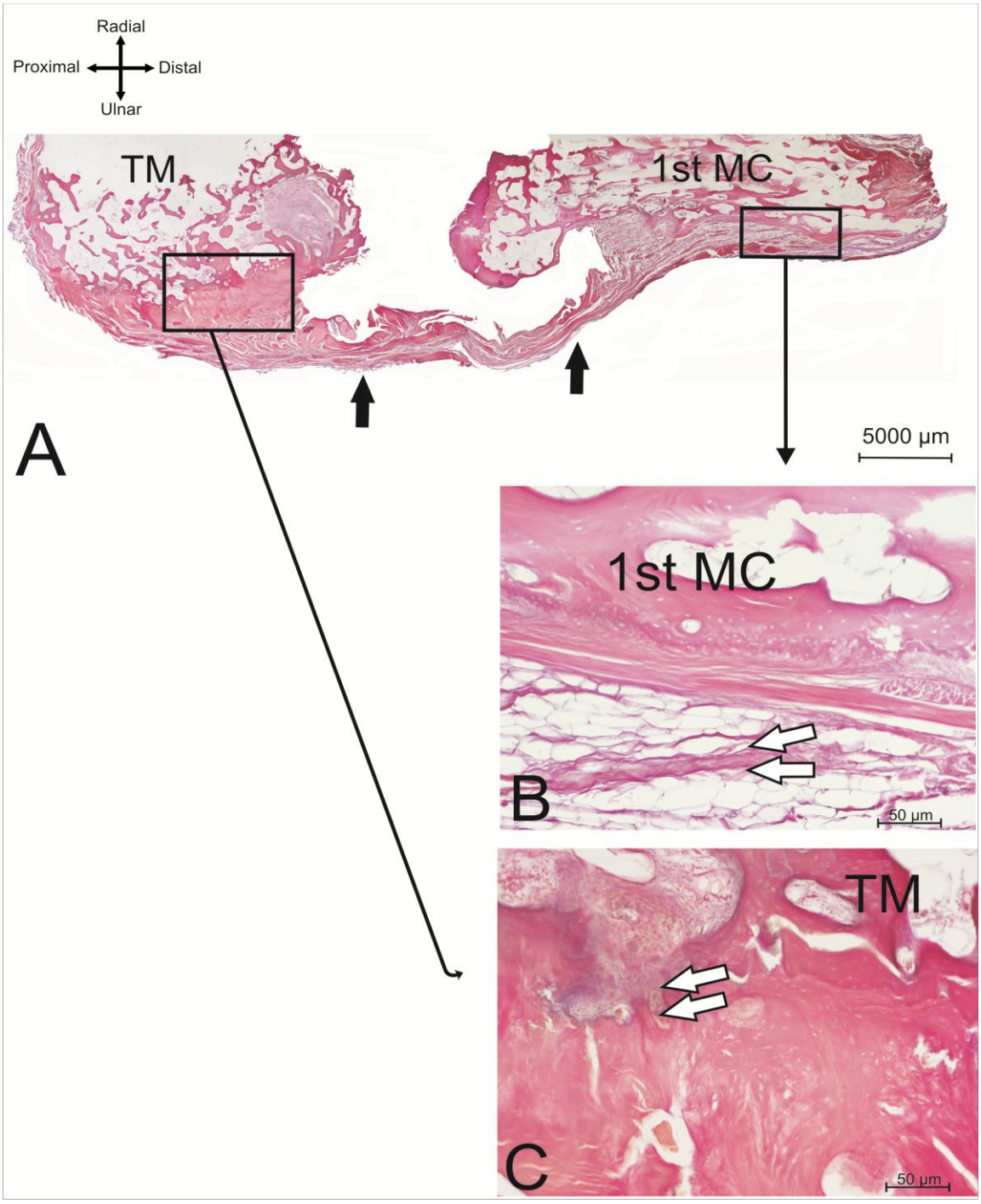

Figure 4.13: Section through radial trapeziometacarpal ligament (RTML) in Miller's Elastin stain.

A. Panorama image of the RTML, with (magnification × 2.5).

B. Distal attachment; the RTML attached to first metacarpal (1st MC) bone. Zoomed-in section also showing elastin fibres in extracellular matrix of the ligament; the arrows clearly show the bundle of elastin fibres. The elastin fibres are presented by black colour, the collagen presented by deep red colour, and blood vessels presented by yellow colour, with (magnification × 10).
C. Proximal attachment; the RTML attached to trapezium (TM) bone. Zoomed-in section showing elastin fibres in extracellular matrix of the ligament. The arrows show the bundle of elastin fibres surrounded by vein, with (magnification × 10). Miller's Elastin stain.

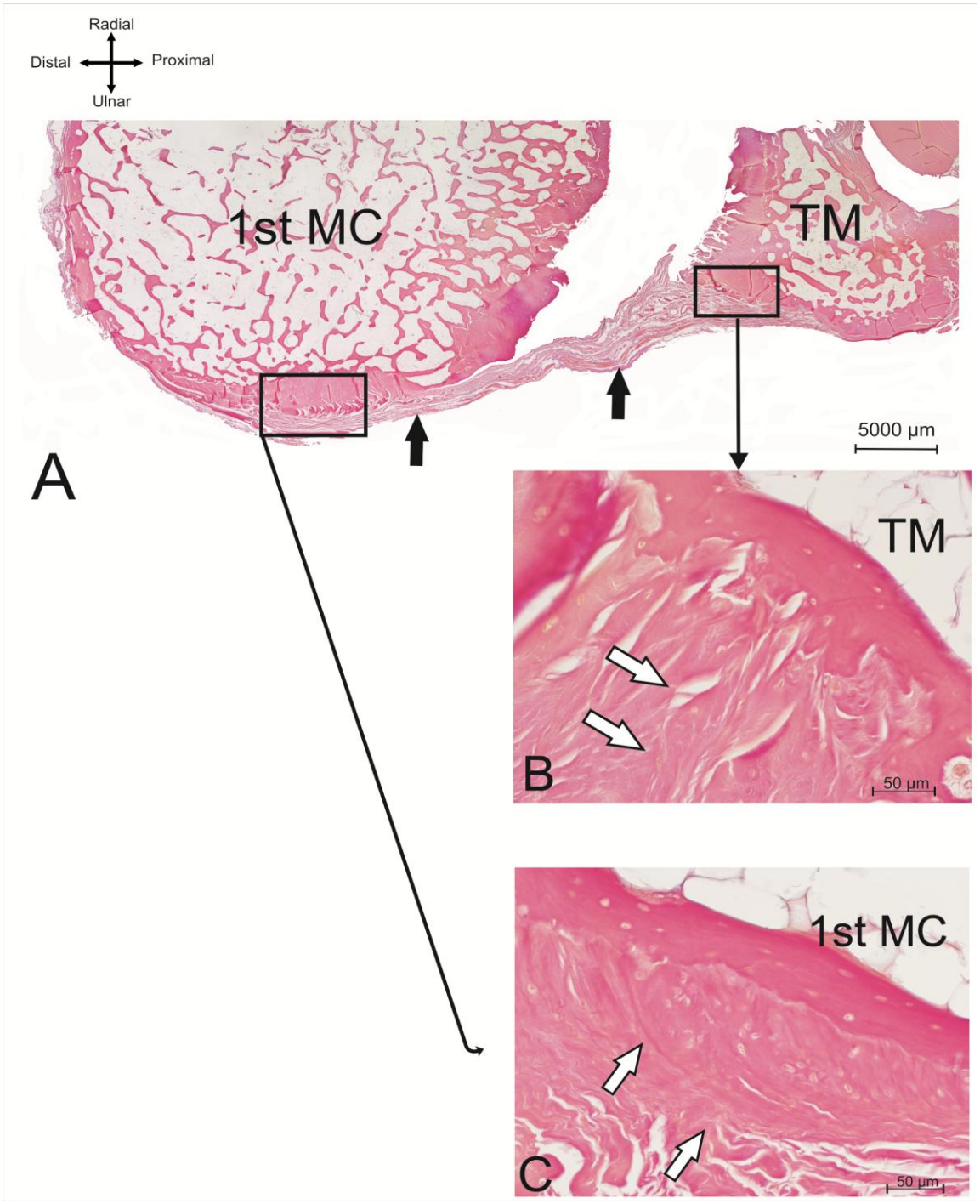

Figure 4.14: Section through palmar trapeziometacarpal ligament (PTML) in Miller's Elastin stain.

A. Panorama image of the PTML, with (magnification × 2.5).

B. Proximal attachment; the PTML attached to trapezium (TM) bone. Zoomed-in section also showing elastin fibres in extracellular matrix of the ligament; the arrows clearly show the bundle of elastin fibres. The elastin fibres are presented by black colour, the collagen presented by deep red colour, and blood vessels presented by yellow colour, with (magnification × 10).
C. Distal attachment; the PTML attached to first metacarpal (1st MC) bone. Zoomed-in section showing elastin fibres in extracellular matrix of the ligament, articular cartilage, collagen, and bone cell. The arrows show the bundle of elastin fibres, with (magnification × 10). Miller's Elastin stain.

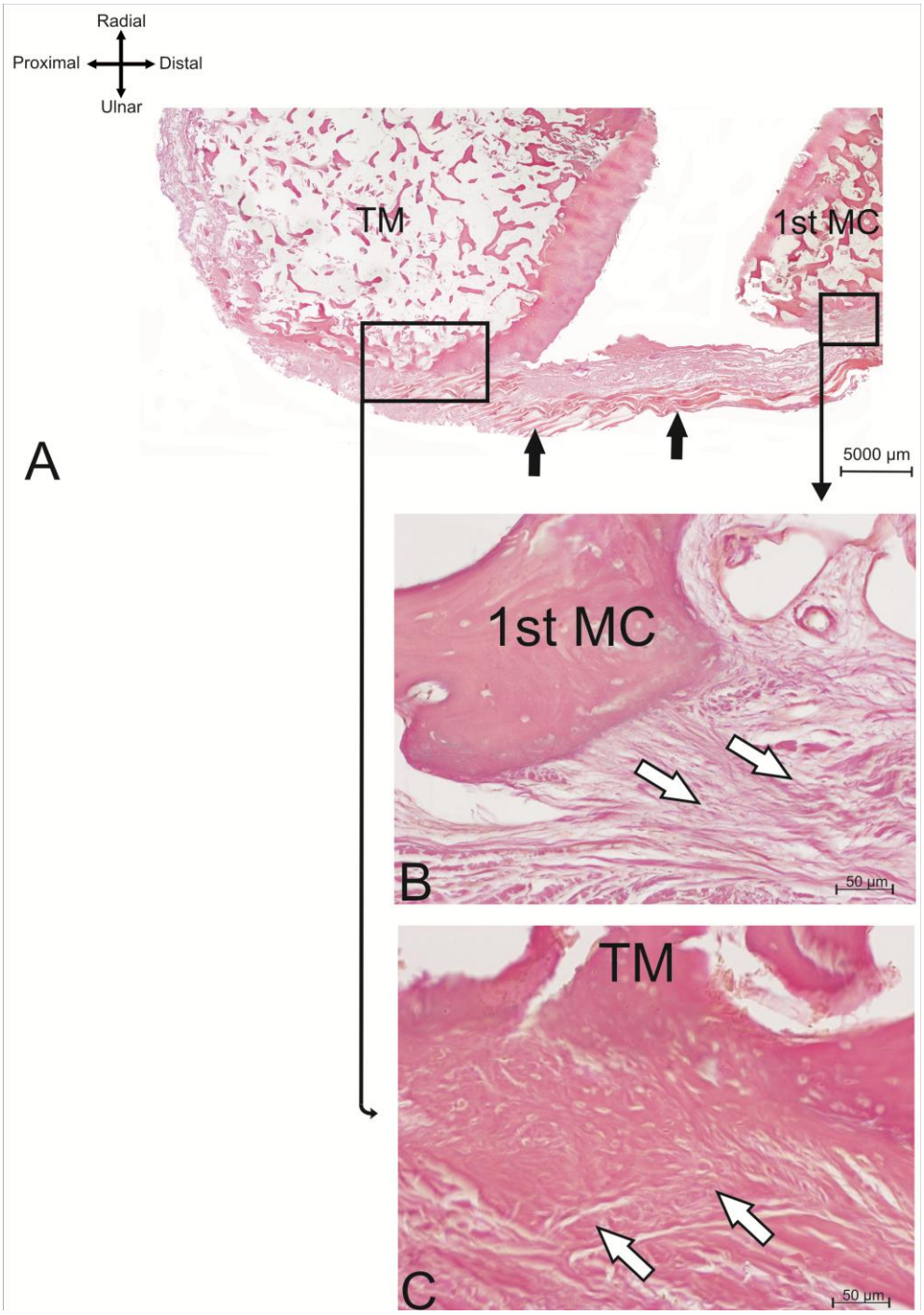

Figure 4.15: Section through palmo-ulnar trapeziometacarpal ligament (PUTML) in Miller's Elastin stain.

A. Panorama image of the PUTML, with (magnification × 2.5).

B. Distal attachment; the PUTML attached to first metacarpal (1st MC) bone. Zoomed-in section also showing elastin fibres in extracellular matrix of the ligament; the arrows clearly show the bundle of elastin fibres. The elastin fibres are presented by black colour, the collagen presented by deep red colour, and blood vessels presented by yellow colour, with (magnification × 10).
C. Proximal attachment; the PUTML attached to trapezium (TM) bone. Zoomed-in section showing elastin fibres in extracellular matrix of the ligament. The arrows show the bundle of elastin fibres, with (magnification × 10). Miller's Elastin stain.

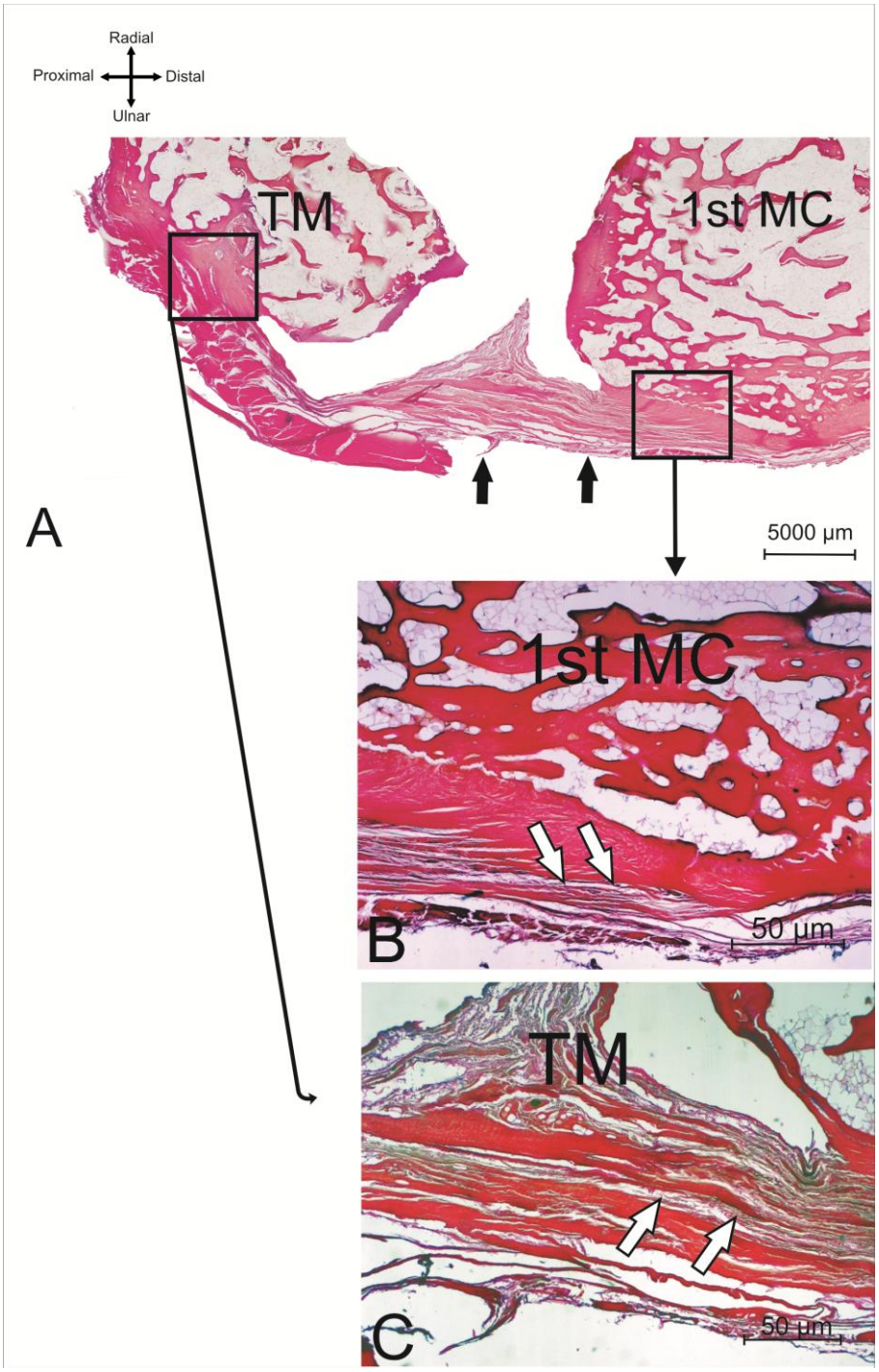

Figure 4.16: Section through dorso-ulnar trapeziometacarpal ligament (DUTML) in Miller's Elastin stain.

A. Panorama image of the DUTML, with (magnification × 2.5).

B. Distal attachment; the DUTML attached to first metacarpal (1st MC) bone. Zoomed-in section also showing elastin fibres in extracellular matrix of the ligament; the arrows clearly show the bundle of elastin fibres. The elastin fibres are presented by black colour, the collagen presented by deep red colour, and blood vessels presented by yellow colour, with (magnification × 10).
C. Proximal attachment; the DUTML attached to trapezium (TM) bone. Zoomed-in section showing elastin fibres in extracellular matrix of the ligament, articular cartilage, collagen, and bone cell. The arrows show the bundle of elastin fibres, with (magnification × 10). Miller's Elastin stain.

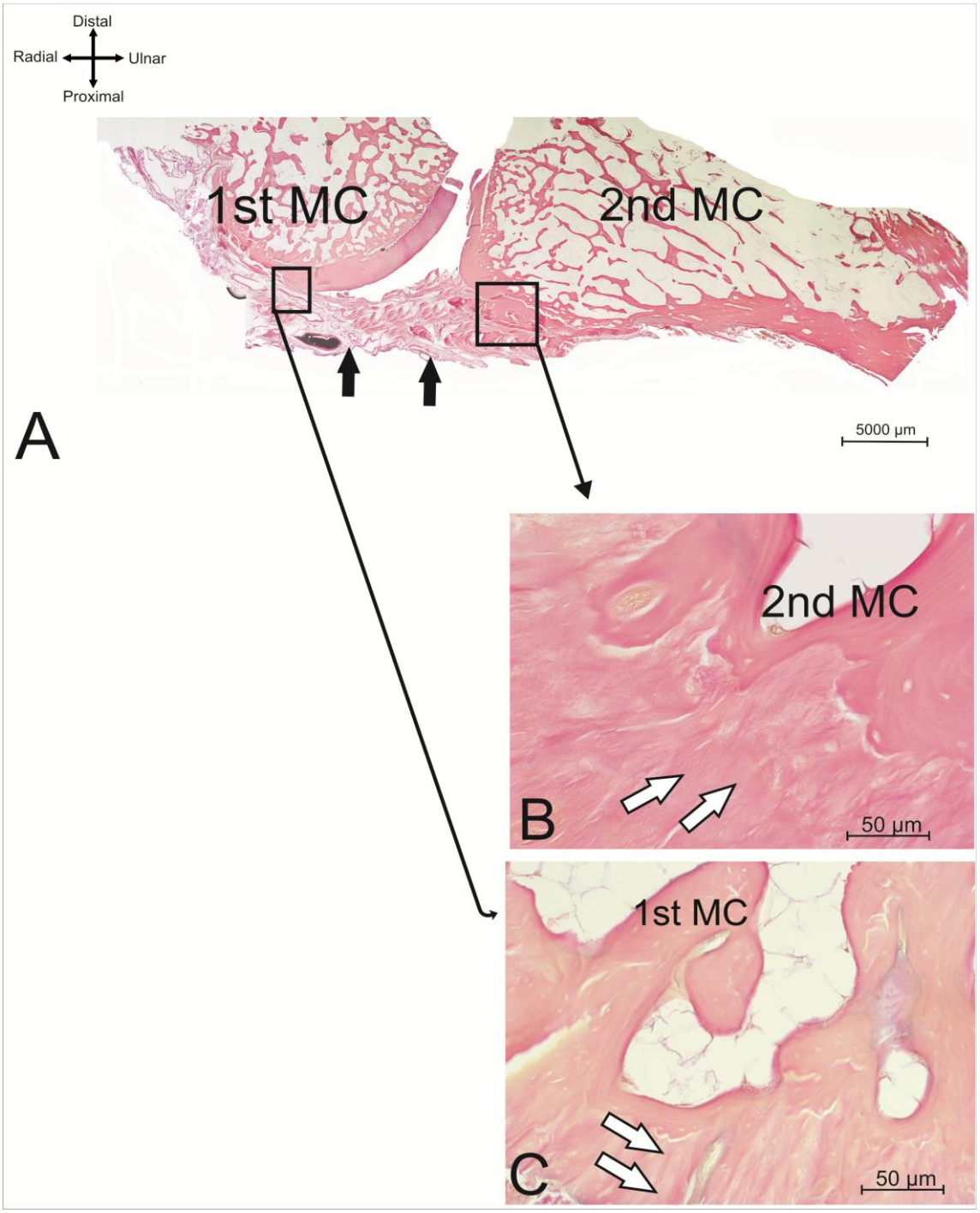

Figure 4.17: Section through palmar intermetacarpal ligament (PIML) in Miller's Elastin stain.

A. Panorama image of the PIML, with (magnification × 2.5).

B. Distal attachment; the PIML attached to second metacarpal (2nd MC) bone. Zoomed-in section also showing elastin fibres in extracellular matrix of the ligament; the arrows clearly show the bundle of elastin fibres. The elastin fibres are presented by black colour, the collagen presented by deep red colour, and blood vessels presented by yellow colour, with (magnification × 10).
C. Proximal attachment; the PIML attached to first metacarpal (1st MC) bone. Zoomed-in section showing elastin fibres in extracellular matrix of the ligament, articular cartilage, collagen, and bone cell. The arrows show the bundle of elastin fibres, with (magnification × 10). Miller's Elastin stain.

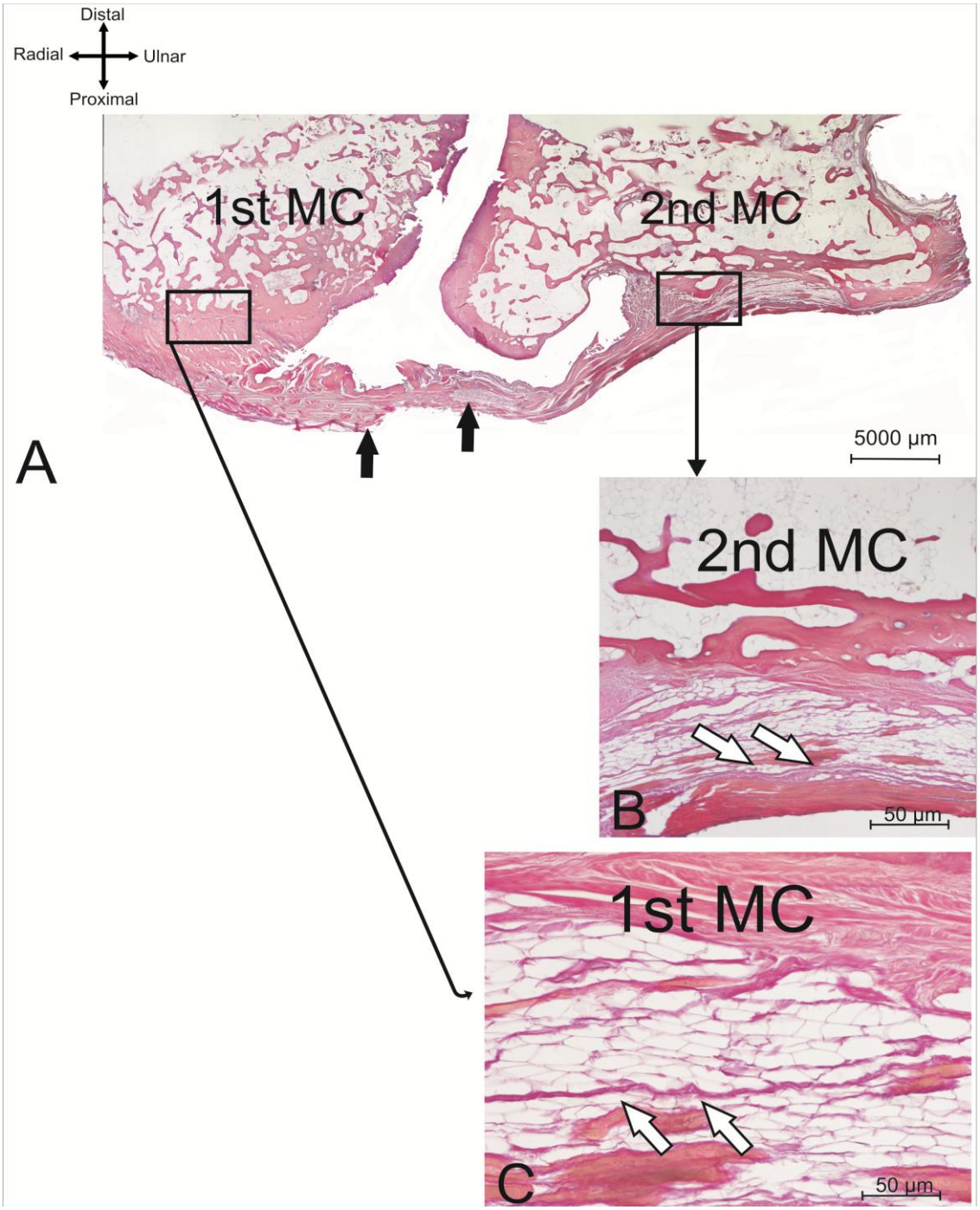

Figure 4.18: Section through dorsal intermetacarpal ligament (DIML) in Miller's Elastin stain.

A. Panorama image of the DIML, with (magnification × 2.5).

B. Distal attachment; the DIML attached to second metacarpal (2nd MC) bone. Zoomed-in section also showing elastin fibres in extracellular matrix of the ligament; the arrows clearly show the bundle of elastin fibres. The elastin fibres are presented by black colour, the collagen presented by deep red colour, and blood vessels presented by yellow colour, with (magnification × 10).
C. Proximal attachment; the DIML attached to first metacarpal (1st MC) bone. Zoomed-in section showing elastin fibres in extracellular matrix of the ligament, articular cartilage, collagen, and bone cell. The arrows show the bundle of elastin fibres, with (magnification × 10). Miller's Elastin stain.

4.3.4 Development of staining protocols

4.3.4.1 Combination staining between Modified Masson's Trichrome (MMT) and Miller's Elastin (ME) stains

MMT stain alone has been effective in demonstrating soft tissue differences and entheseal types; the ME alone has a good alternative view of some of the tissues of interest, such as elastin fibres. But more contrast between organised and disorganised tissues was wanted.

4.3.4.1.1 Starting with MMT

The combination protocol starting with ME allowed for only rough discrimination between dense and loose soft tissues, and lost much finer details (Figures 4.19-4.20-4.21-4.22-4.23-4.24).

The new colours of tissues have shown as followed:

1. Nuclei—Black
2. Cytoplasm, muscle and acidophil granules—Blue
3. Collagen, cartilage, mucin, and basophil granules—Deep blue

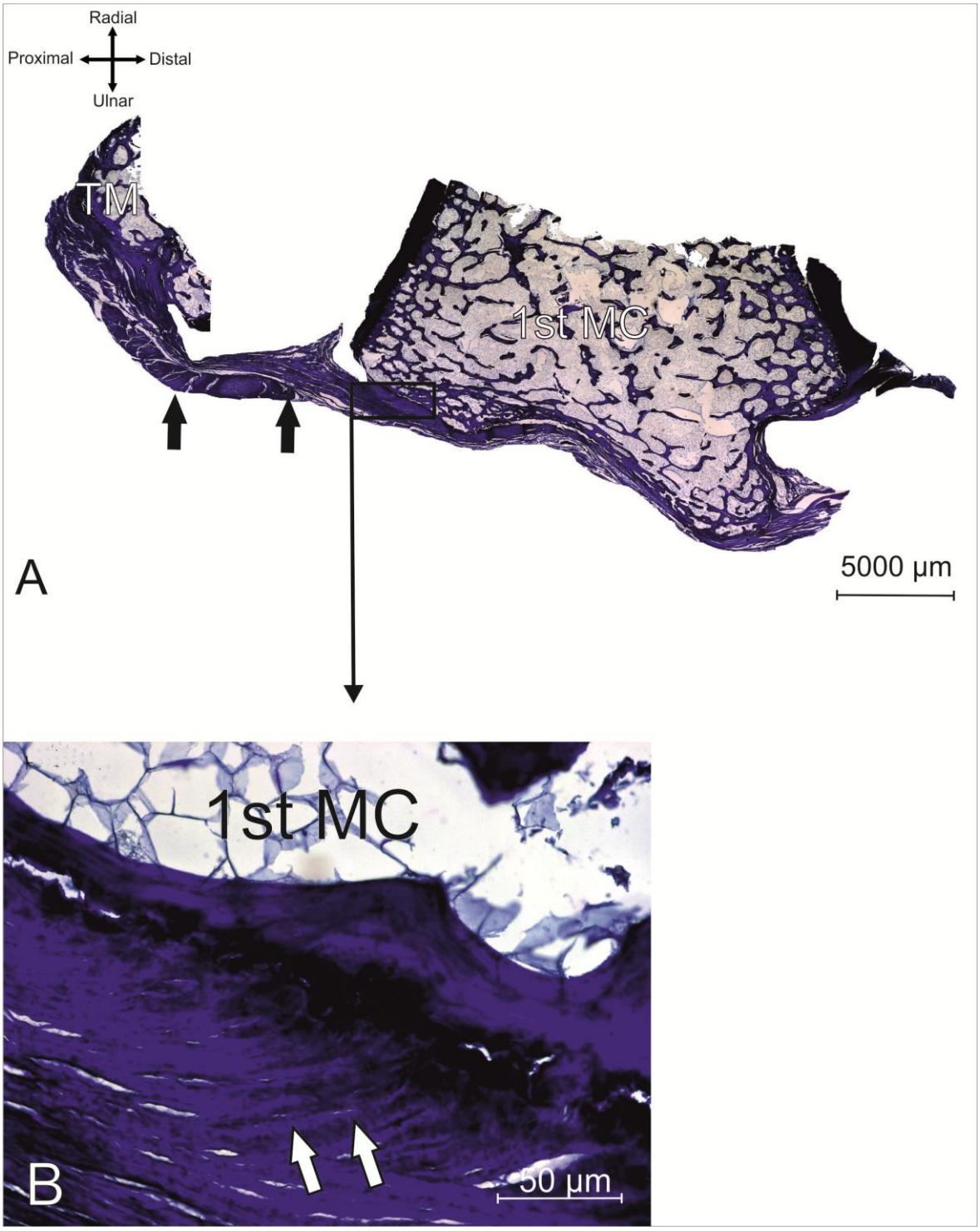

Figure 4.19: Section through radial trapeziometacarpal ligament (RTML) in combination starting with MMT stain.

A. Panorama image of the RTML, with (magnification × 2.5).
B. Distal attachment; the RTML attached to first metacarpal (1st MC) bone. Zoomed-in section showing the bone cell, articular cartilage, and entheseal. The entheseal zone is not clear enough to recognise the type, and also the tidemark is not clear; the contrast of the colours merge together in the blue colour. Distinguishing between the specific structures is difficult. The large lacuna with white colour presented bony tissues, the string bundle with deep blue colour presented fascicles, with (magnification × 10). Combination staining starting with MMT.

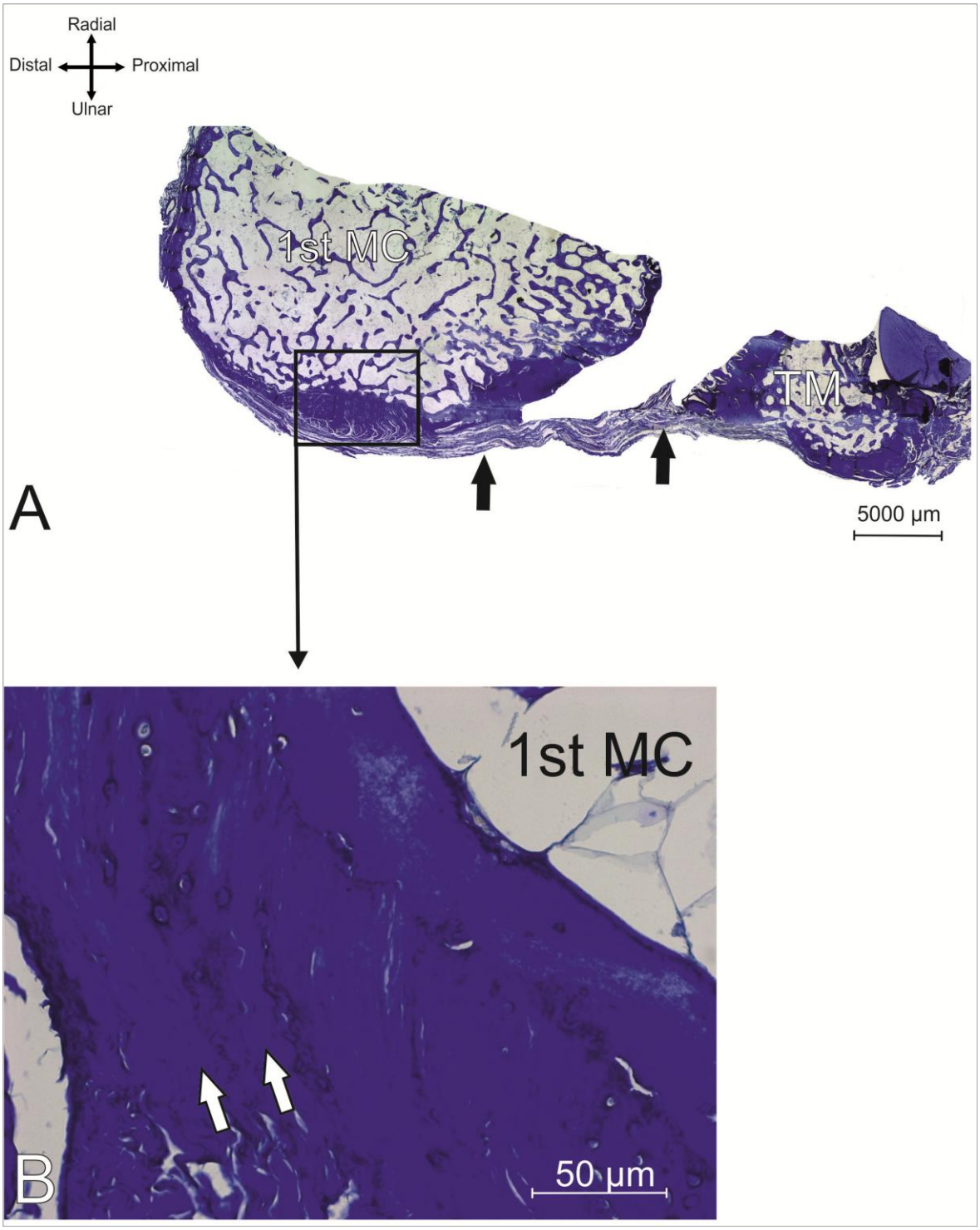

Figure 4.20: Section through palmar trapeziometacarpal ligament (PTML) in combination starting with MMT stain.

A. Panorama image of the PTML, with (magnification × 2.5).
B. Distal attachment; the PTML attached to first metacarpal (1st MC) bone. Zoomed-in section showing the bone cell, articular cartilage, and entheseal. The entheseal zone is not clear enough to recognise the type, and also the tidemark is not clear; the contrast of the colours merge together in the blue colour. Distinguishing between the specific structures is difficult. The large lacuna with white colour presented bony tissues, the string bundle with deep blue colour presented fascicles, with (magnification × 10). Combination staining starting with MMT.

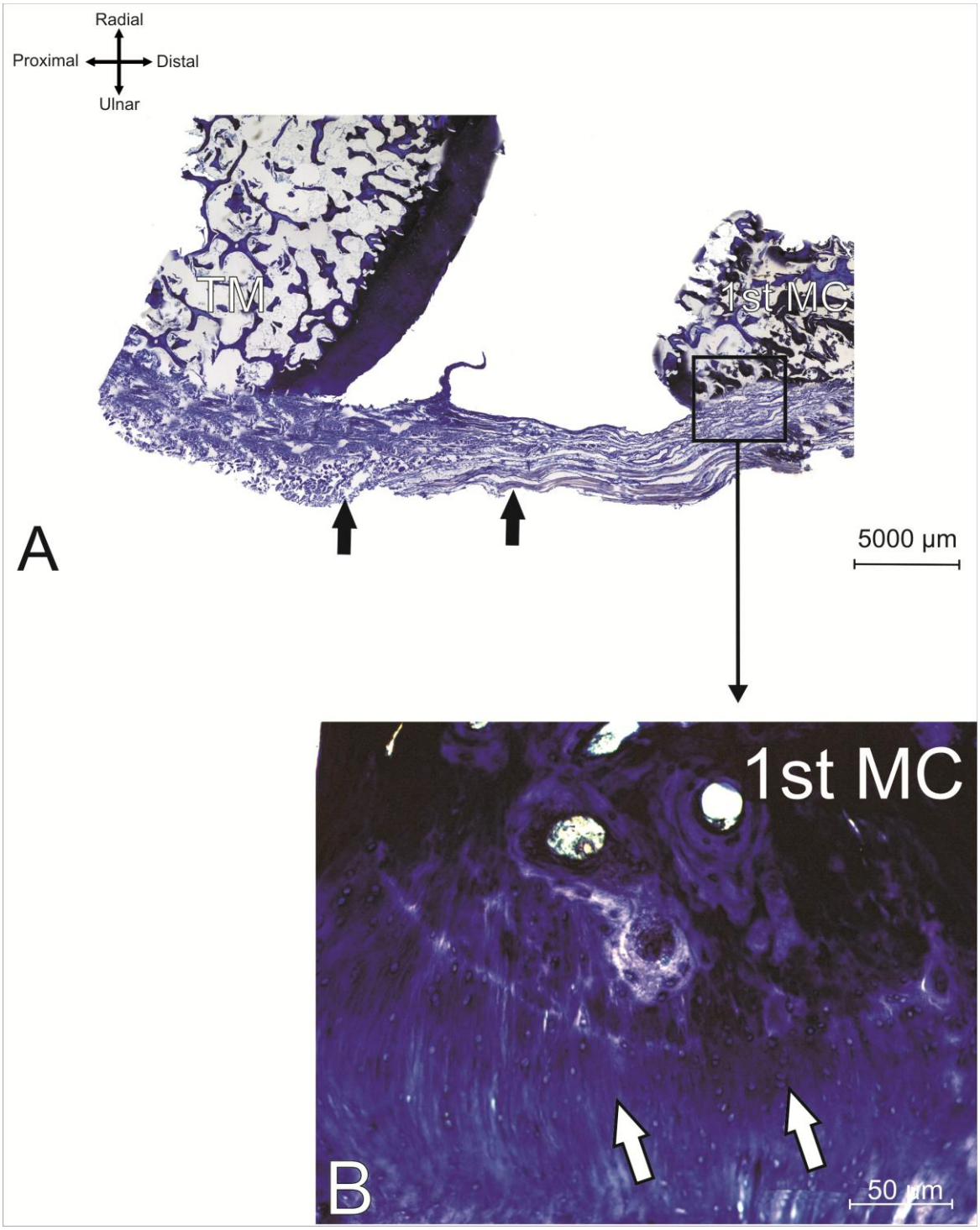

Figure 4.21: Section through palmo-ulnar trapeziometacarpal ligament (PUTML) in combination starting with MMT stain.

A. Panorama image of the PUTML, with (magnification × 2.5).
B. Distal attachment; the PUTML attached to first metacarpal (1st MC) bone. Zoomed-in section showing the bone cell, articular cartilage, and entheseal. The entheseal zone is not clear enough to recognise the type, and also the tidemark is not clear; the contrast of the colours merge together in the blue colour. Distinguishing between the specific structures is difficult. The large lacuna with white colour presented bony tissues, the string bundle with deep blue colour presented fascicles, with (magnification × 10). Combination staining starting with MMT.

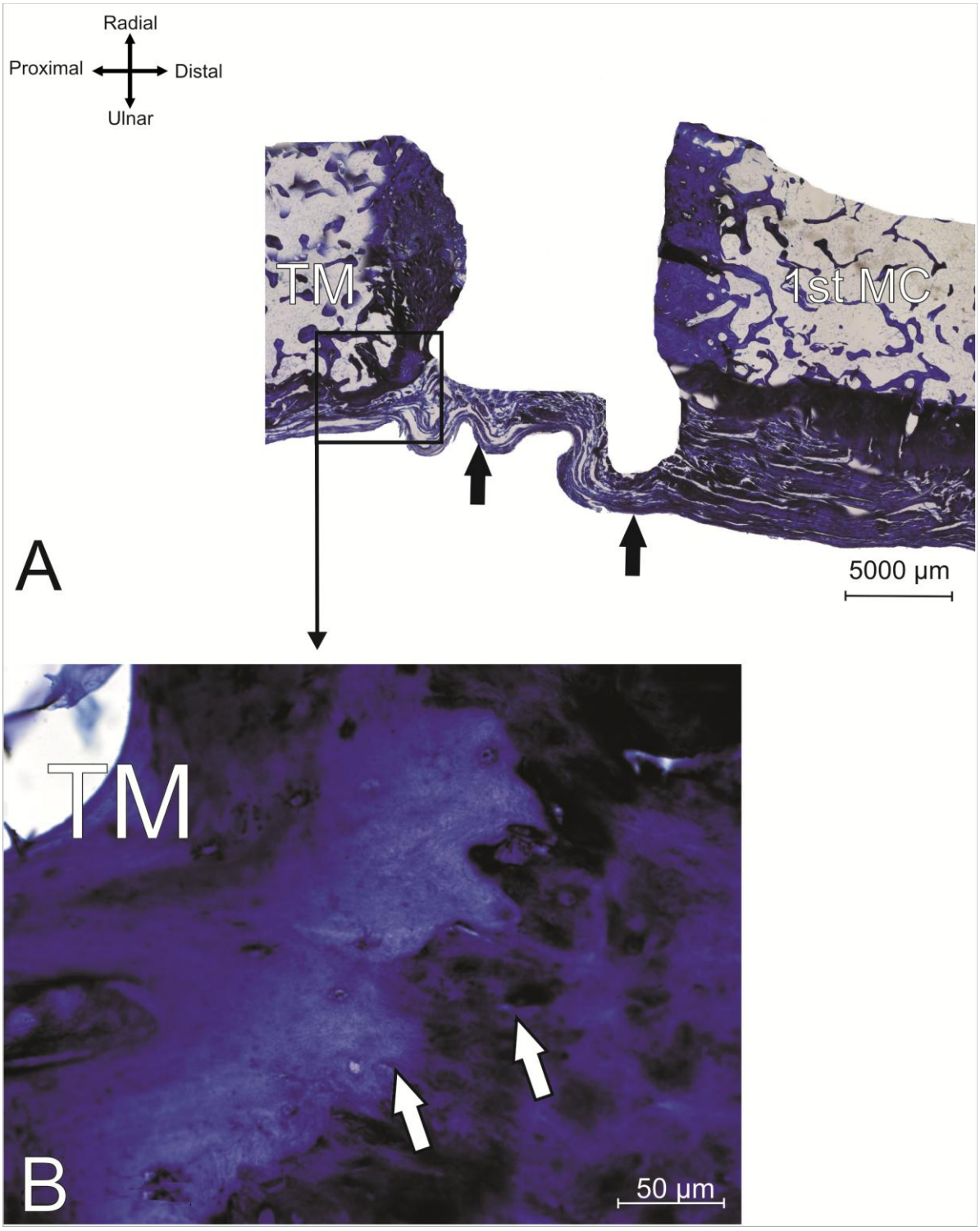

Figure 4.22: Section through Dorso-ulnar trapeziometacarpal ligament (DUTML) in combination starting with MMT stain.

A. Panorama image of the DUTML, with (magnification × 2.5).
B. Proximal attachment, the DUTML attached to trapezium (TM) bone. Zoomed in section showing the bone cell, articular cartilage, and enthesial. The enthesial zone not clear enough to recognize the type, and also the tidemark not clear, the contrast of the colour merge together in blue colour. The distinguishing between the specific structures too difficult. The large lacuna with white colour presented bony tissues, the string bundle with deep blue colour presented fascicles, with (magnification × 10). Combination staining starting with MMT.

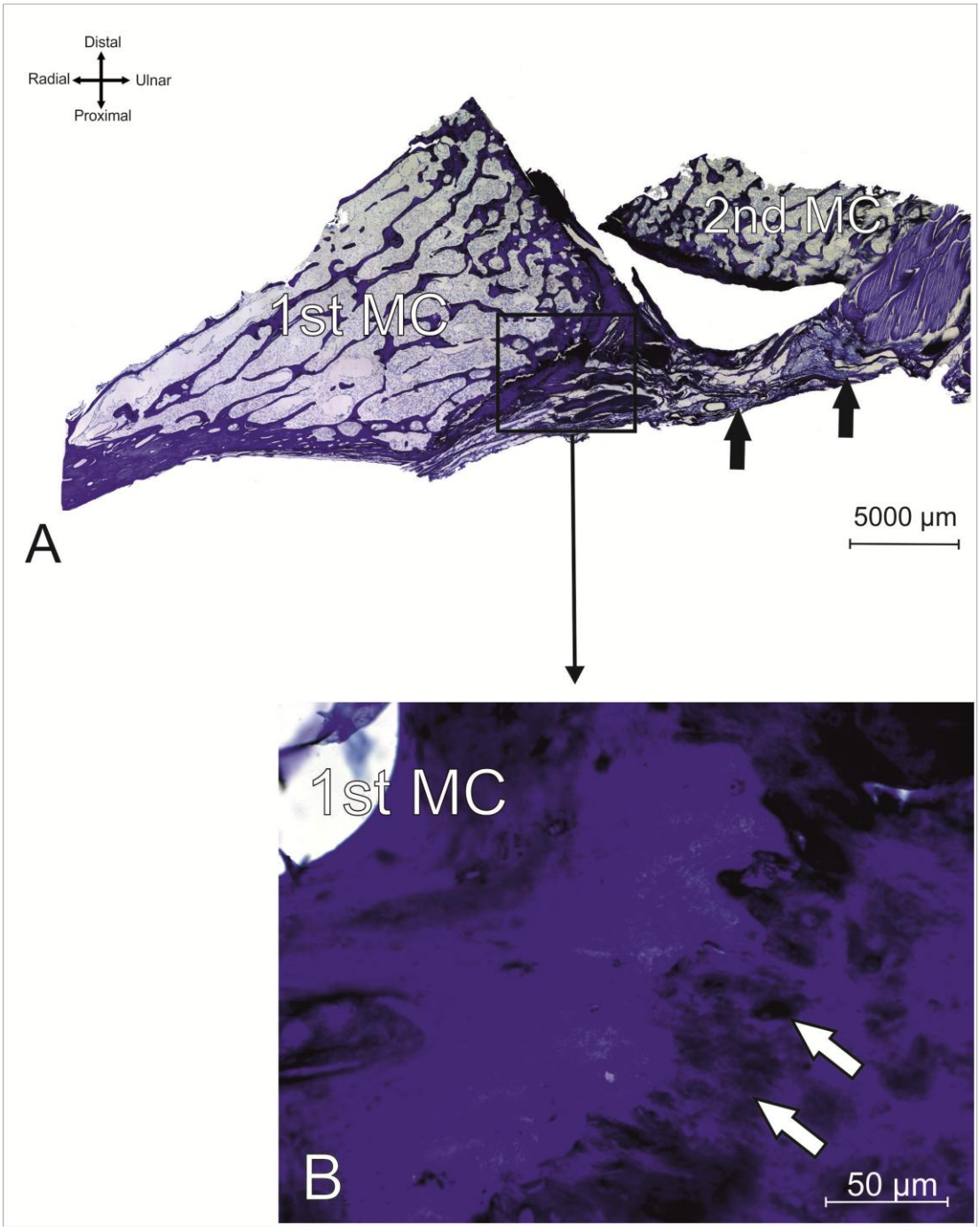

Figure 4.23: Section through Palmar intermetacarpal ligament (PIML) in combination starting with MMT stain.

A. Panorama image of the PIML, with (magnification × 2.5).
B. Proximal attachment, the PIML attached to first metacarpal (1st MC) bone. Zoomed in section showing the bone cell, articular cartilage, and enthesial. The enthesial zone not clear enough to recognize the type, and also the tidemark not clear, the contrast of the colour merge together in blue colour. The large lacuna with white colour presented bony tissues, the string bundle with deep blue colour presented fascicles, with (magnification × 10). Combination staining starting with MMT.

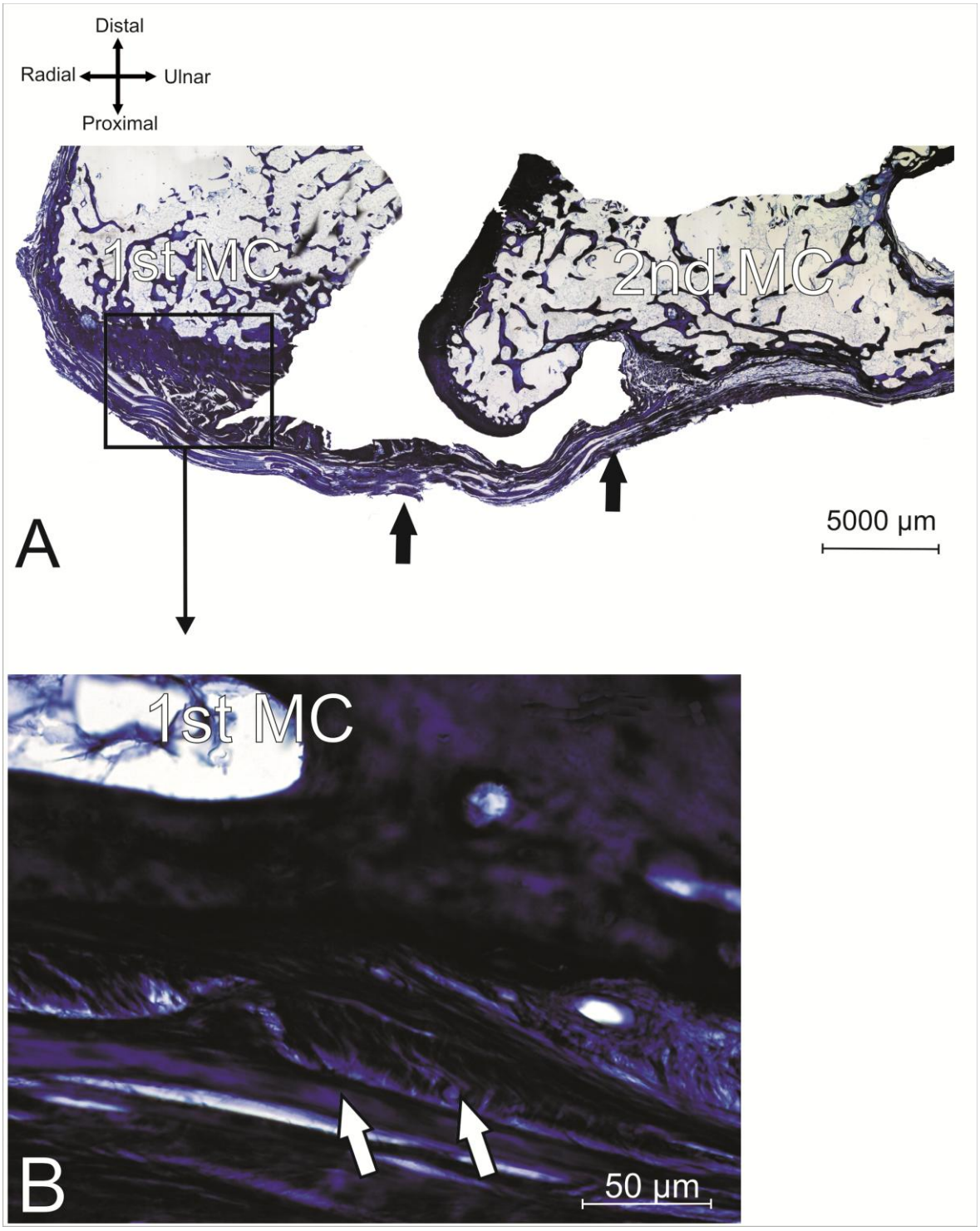

Figure 4.24: Section through dorsal intermetacarpal ligament (DIML) in combination starting with MMT stain.

A. Panorama image of the DIML, with (magnification × 2.5).
B. Proximal attachment; the DIML attached to first metacarpal (1st MC) bone. Zoomed-in section showing the bone cell, articular cartilage, and entheseal. The entheseal zone is not clear enough to recognise the type, and also the tidemark is not clear; the contrast of the colours merge together in the blue colour. Distinguishing between the specific structures is difficult. The large lacuna with white colour presented bony tissues, the string bundle with deep blue colour presented fascicles, with (magnification × 10). Combination staining starting with MMT.

4.3.4.1.2 Starting with ME

A combination protocol starting with MMT allowed for discrimination between dense and loose soft tissue, but obscured finer structures (Figures 4.25-4.26-4.27-4.28-4.29-4.30). The new colours of the tissues are as follows:

1. Nuclei—Blue / Black
2. Cytoplasm, muscle, and acidophil granules—Deep red
3. Collagen, cartilage, mucin, and basophil granules—Deep green

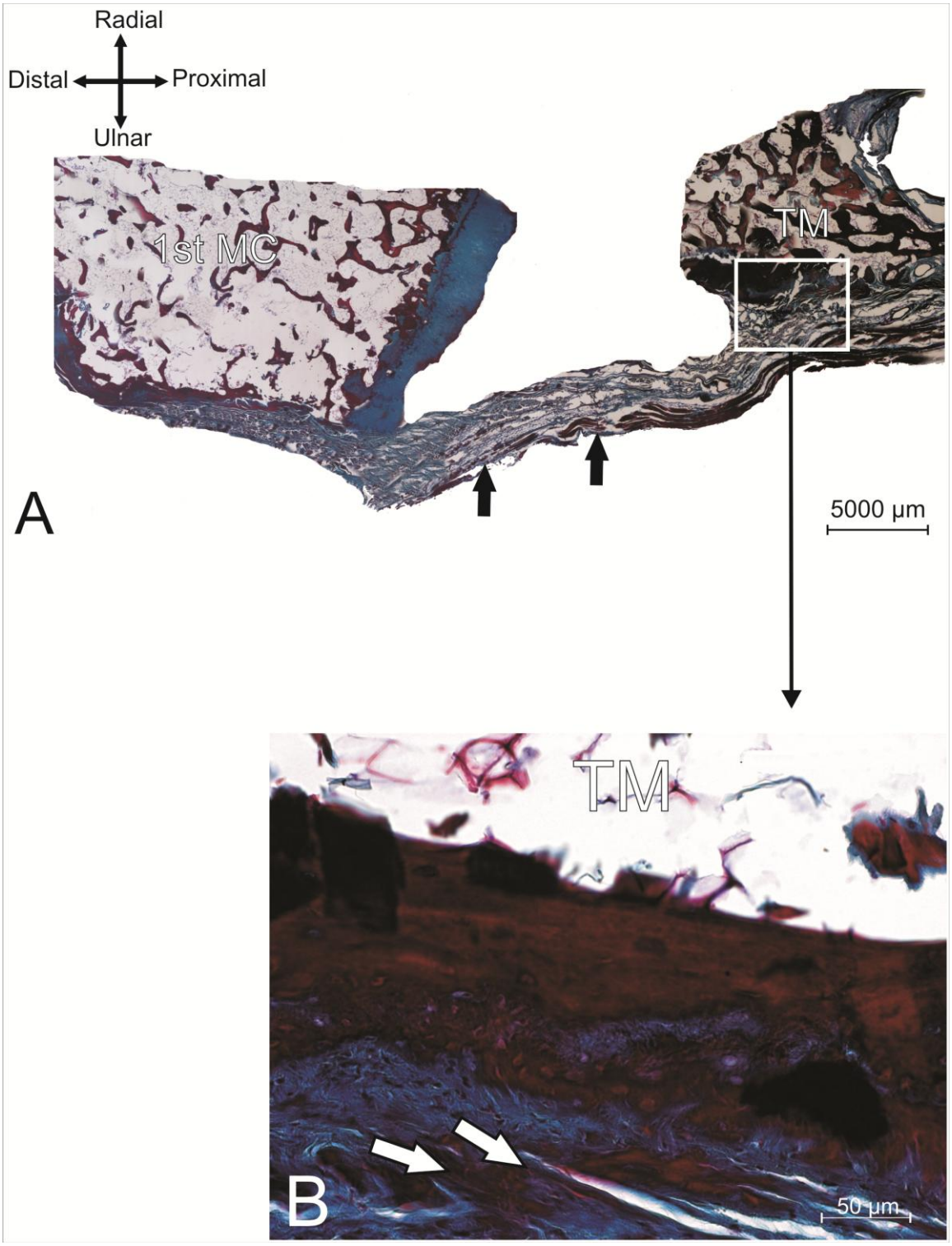

Figure 4.25: Section through radial trapeziometacarpal ligament (RTML) in combination starting with ME stain.

A. Panorama image of the RTML, with (magnification × 2.5).
B. Proximal attachment; the RTML attached to trapezium (TM) bone. Zoomed-in section showing the bone cell, articular cartilage, and entheseal. The entheseal zone is not clear enough to recognise the type; the distinction between the specific structures is not clear enough. The tidemark is hazy in this stain. The large lacuna with white colour presented bony tissues, the string bundle with green colour presented fascicles.with (magnification × 10). Combination staining starting with ME.

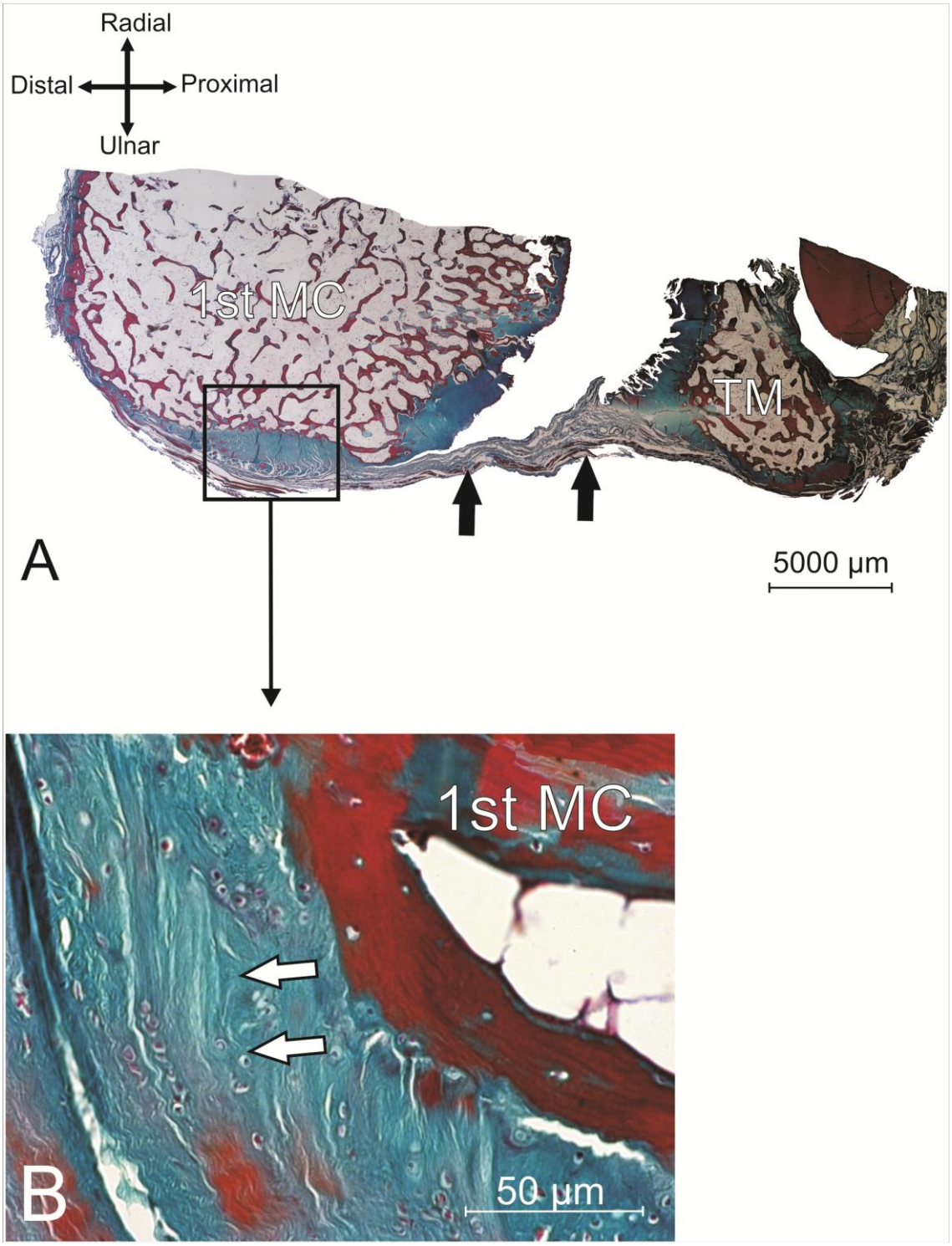

Figure 4.26: Section through palmar trapeziometacarpal ligament (PTML) in combination starting with ME stain.

A. Panorama image of the PTML, with (magnification × 2.5).
B. Distal attachment; the PTML attached to first metacarpal (1st MC) bone. Zoomed-in section showing the bone cell, articular cartilage, and entheseal. The entheseal zone is not clear enough to recognise the type; the contrast of the colours merges together in the blue colour. The large lacuna with white colour presented bony tissues, the string bundle with green colour presented fascicles, with (magnification × 10). Combination staining starting with ME.

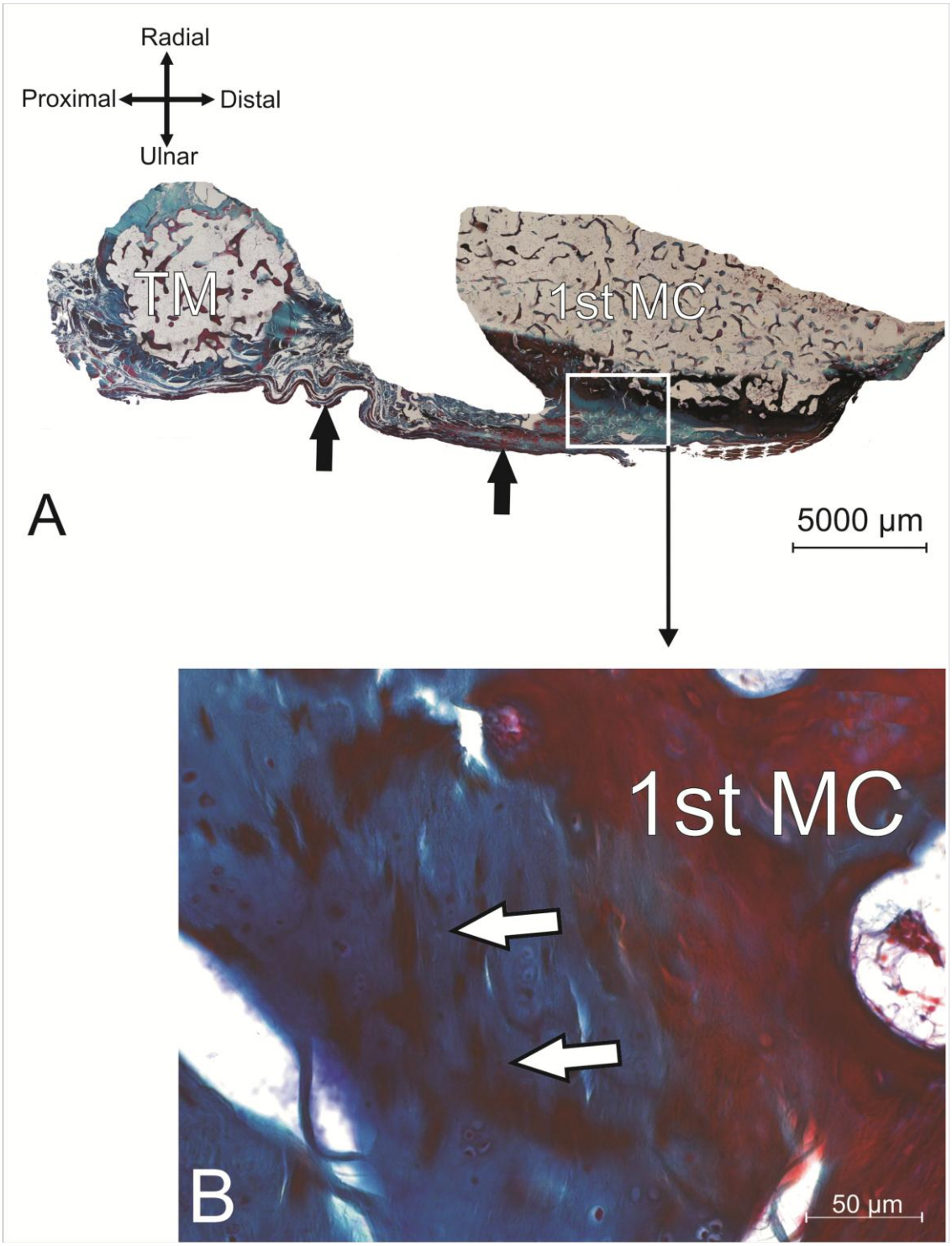

Figure 4.27: Section through palmo-ulnar trapeziometacarpal ligament (PUTML) in combination starting with ME stain.

A. Panorama image of the PUTML, with (magnification × 2.5).
B. Distal attachment; the PUTML attached to first metacarpal (1st MC) bone. Zoomed-in section showing the bone cell, articular cartilage, and entheseal. The entheseal zone is not clear enough to recognise the type; the contrast of the colours merges together in the blue colour. The large lacuna with white colour presented bony tissues, the string bundle with green colour presented fascicles, with (magnification × 10). Combination staining starting with ME.

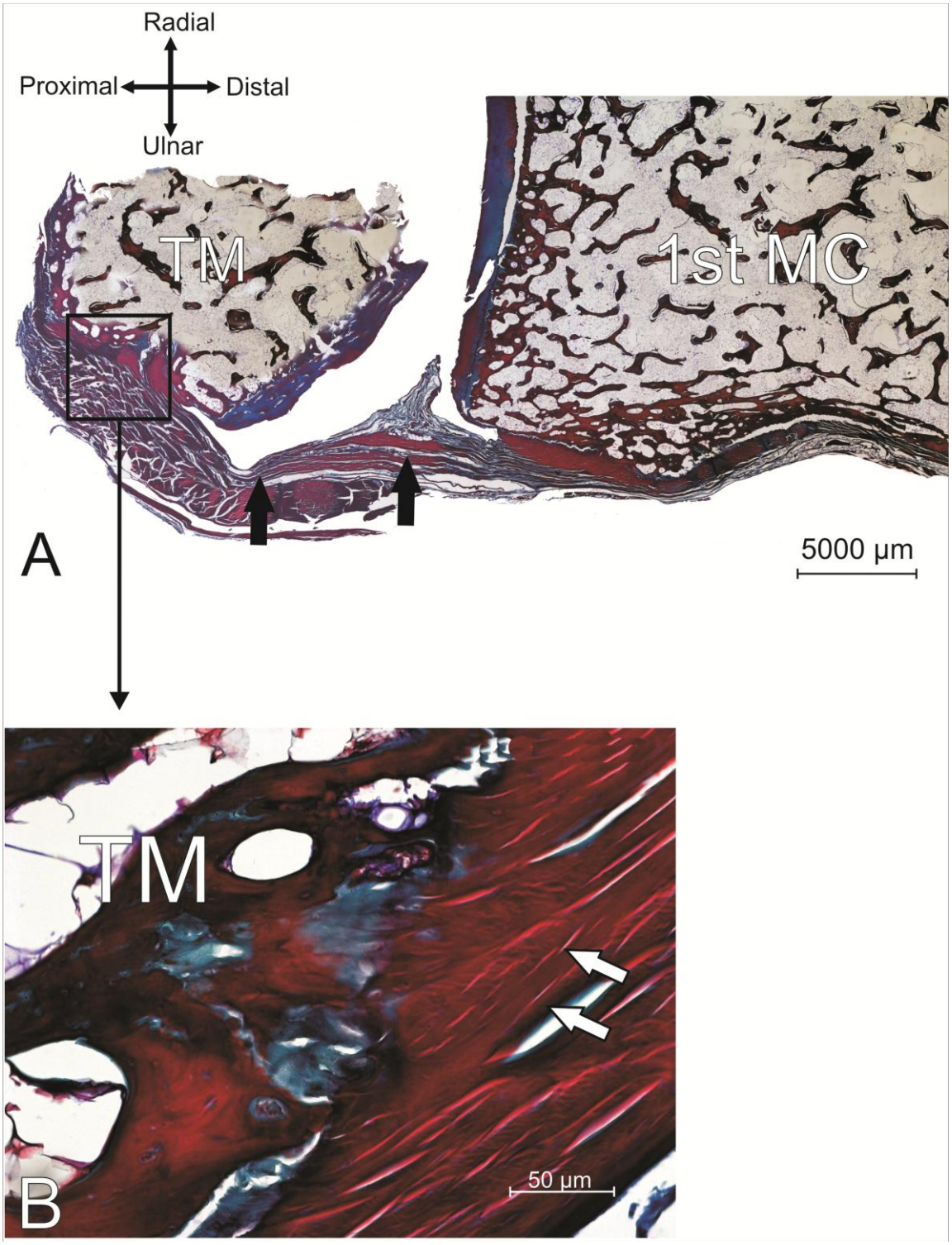

Figure 4.28: Section through dorso-ulnar trapeziometacarpal ligament (DUTML) in combination starting with ME stain.

A. Panorama image of the DUTML, with (magnification × 2.5).
B. Proximal attachment; the DUTML attached to trapezium (TM) bone. Zoomed-in section showing the bone cell, articular cartilage, and entheseal. The entheseal zone is not clear enough to recognise the type; the contrast of the colours merges together in the blue colour; the large lacuna with white colour presented bony tissues, the string bundle with green colour presented fascicles, with (magnification × 10). Combination staining starting with ME.

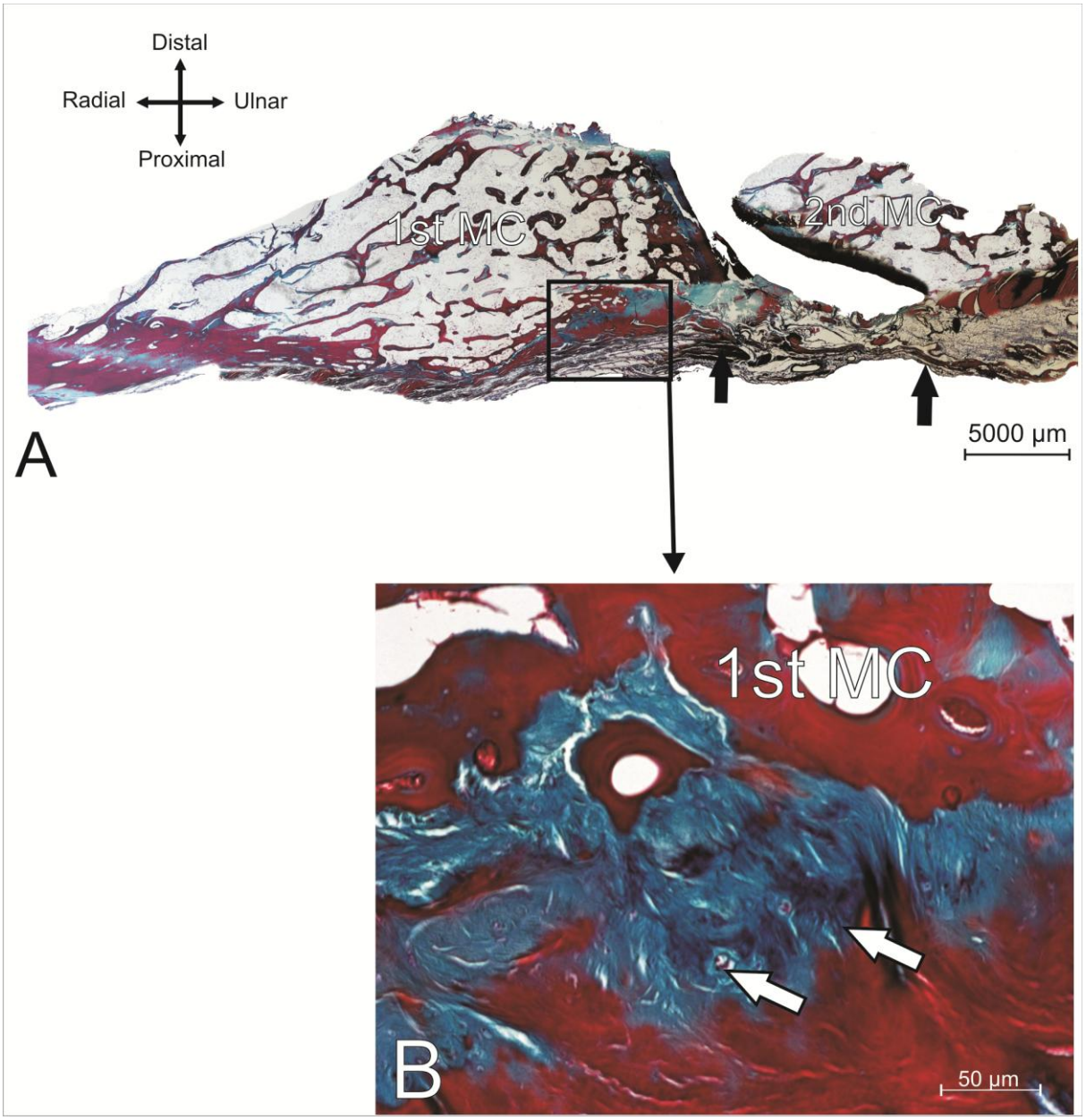

Figure 4.29: Section through palmar intermetacarpal ligament (PIML) in combination starting with ME stain.

A. Panorama image of the PIML, with (magnification × 2.5).
B. Proximal attachment; the PIML attached to first metacarpal (1st MC) bone. Zoomed-in section showing the bone cell, articular cartilage, and entheseal. The entheseal zone is not clear enough to recognise the type; the contrast of the colours merges together in the blue colour; the tidemark is hazy in this stain. The large lacuna with white colour presented bony tissues, the string bundle with green colour presented fascicles, with (magnification × 10). Combination staining starting with ME.

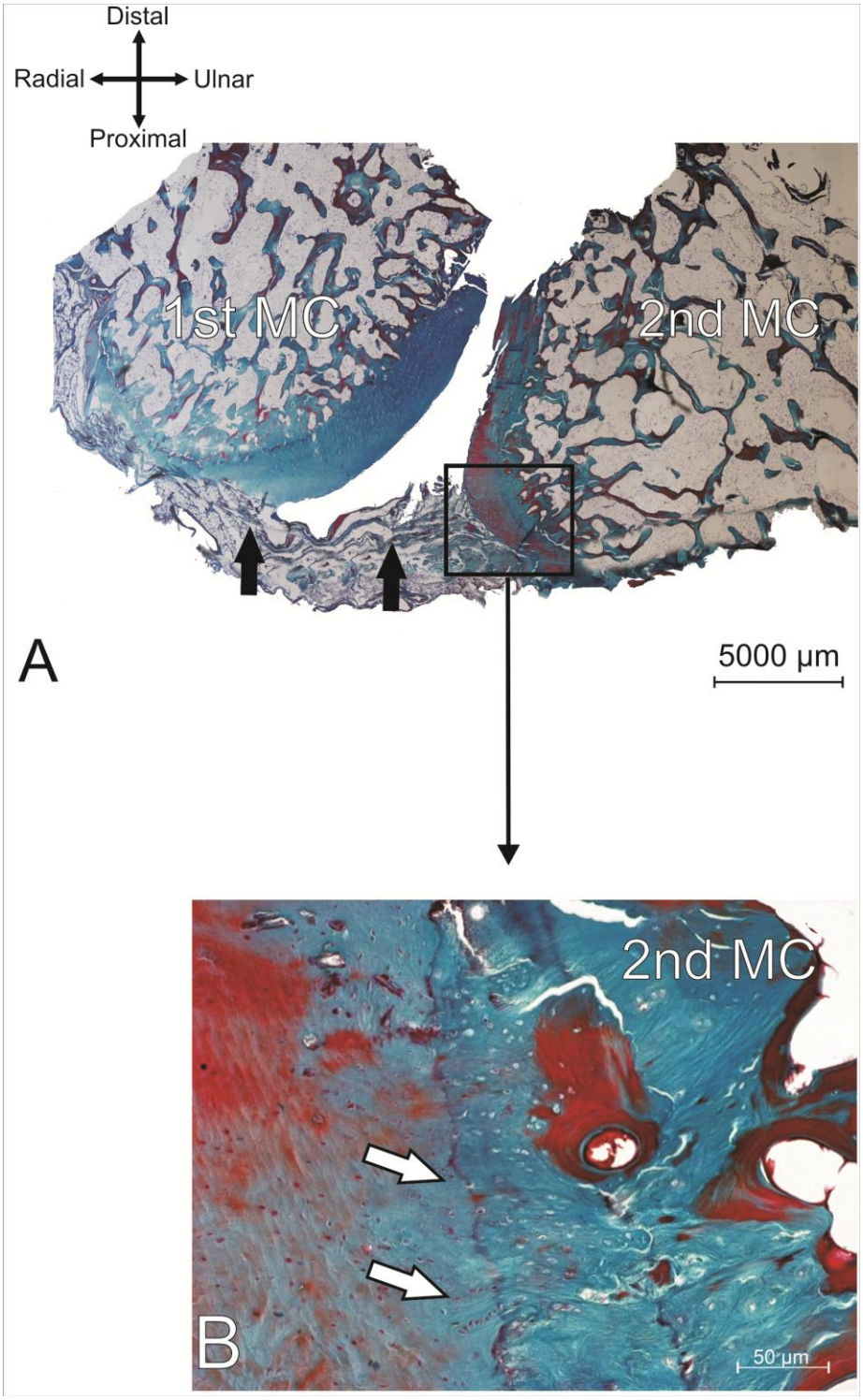

Figure 4.30: Section through dorsal intermetacarpal ligament (DIML) in combination starting with ME stain.

A. Panorama image of the DIML, with (magnification × 2.5).
B. Distal attachment; the DIML attached to second metacarpal (2nd MC) bone. Zoomed-in section showing the bone cell, articular cartilage, and entheseal. The entheseal zone is not clear enough to recognise the type; the contrast of the colours merges together in the blue colour; the tidemark is hazy in this stain. The large lacuna with white colour presented bony tissues, the string bundle with green colour presented fascicles. A small varieties lacuna with deep red presented articular cartilage, with (magnification × 10). Combination staining starting with ME.

4.3.5 Miller’s Elastin re-timing

The discrimination of the ligament from the capsule was not done by ME alone; the ligaments had greater density and organisation of elastic fibres. The percentage of the contrast can change the appearance of the elastic fibres throughout the section. The process to change this protocol basically depends on two main stains: Miller’s Elastin and Van Gieson (VG) stains. The Miller’s Elastin stain is responsible for staining the specific elastic fibres in the connective fibrous matrix, whereas the VG stain is responsible for giving a good background dark colour, which reflects a precise view of the elastin fibres. In addition, both stains are needed to complete the work of the other. In the current study, the development of the protocol restricted the duration of keeping the slides in the stain container.

The time of the staining increased and decreased alternately in the five experiments, as follows:

Experiment	Time of Miller's Elastin stain (ME)	Time of Van Gieson stain (VG)	Appearance of Elastic fibre	Appearance of other structures
1 (Figure 4.31)	2 Hours	30 Seconds	Good appearance; the clarity of differentiation was good, the colour was mild black nearly to pink	Good distinguishing of blood vessels presented by yellow colour nearly to orange; the collagen was also clear in the fibrous matrix presented by light red nearly to pink; the bony tissue was also red, but it had large lacuna stains by white colour; the articular cartilage had deep red colour.
2 (Figure 4.32)	2 Hours	15 Seconds	Very good appearance; the clarity of differentiation was very good; the colour was mild black nearly to grey. In general this experiment was better than the first experiment, especially in the clarity of elastin fibres.	Very good distinguishing of blood vessels presented by yellow colour nearly to orange; the collagen was also clear in the fibrous matrix presented by mild deep red; the bony tissue was also red but it had large lacuna stains by white colour; the articular cartilage had deep red colour;

				the bone cell in this experiment had better visibility than the first experiment.
3 (Figure 4.33)	2.5 Hours	15 Seconds	Excellent appearance; the clarity of differentiation was excellent, the colour was mild black nearly to pink. In general, this experiment was better than the first and second experiments, especially in clarity of elastin fibres.	Excellent distinguishing of blood vessels presented by yellow colour nearly to orange; the collagen was also clear in the fibrous matrix presented by mild deep red nearly to orange; the bony tissue was also red but it had large lacuna stains by white colour; the articular cartilage had deep red colour; the bone cell in this experiment had better visibility than the second experiment.
4 (Figure 4.34)	2.5 Hours	10 Seconds	Excellent appearance; the clarity of differentiation was excellent, the colour was mild black nearly to pink. In general this experiment was better than the first and second experiments, especially in clarity of elastin fibres, but there was no significant change between the third and fourth experiments.	Good distinguishing of blood vessels presented by yellow colour nearly to orange; the collagen was also visible in the fibrous matrix presented by mild deep red colour; the bony tissue also light red but it had large lacuna stains by white colour; the articular cartilage had light red colour; the bone cell in this experiment had a worse view than the third experiment.

5 (Figure 4.35)	3 Hours	10 seconds	Excellent appearance; the clarity of differentiation was excellent, the colour was mild black nearly to pink. The colour of this experiment was nearly as good as the fourth experiment. There was not a big change.	Bad distinguishing of blood vessels presented by yellow colour nearly to orange; the collagen was also visible in the fibrous matrix presented by mild deep red colour, the bony tissue also light red but it had large lacuna stains by white colour; the articular cartilage had light red colour. In general this experiment had worse results than previous experiments

Table4.1: Five experiments of the re-timing Miller elastin stain.

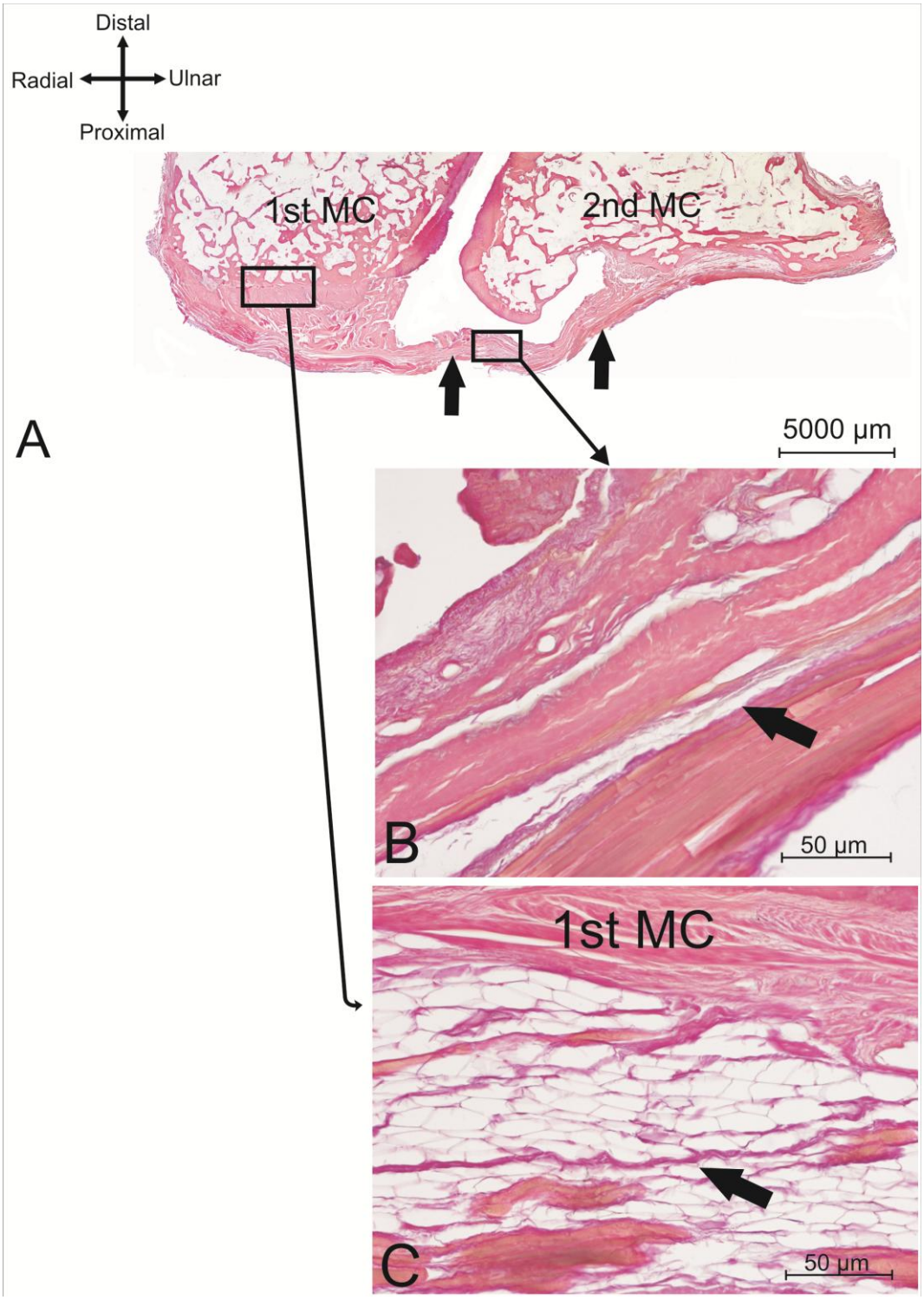

Figure 4.31: Section of the dorsal intermetacarpal ligament (DIML) in 2 hours ME, 30 seconds VG.

A. Panorama image of the DIML, with (magnification × 2.5). **B**. Middle section of the DIML. The arrows show good appearance of elastin fibres, the clarity of differentiation of elastin fibres was good, the colour was mild black nearly to pink. Good distinguishing of blood vessels presented by yellow colour nearly to orange; the collagen was also visible in the fibrous matrix presented by light red nearly to pink; the bony tissue was also red but it had large lacuna stains by white colour; the articular cartilage had deep red colour, with (magnification × 10). **C.** Proximal attachment, with (magnification × 10). Miller's Elastin re-timing (2 hours ME, 30 sec VG).

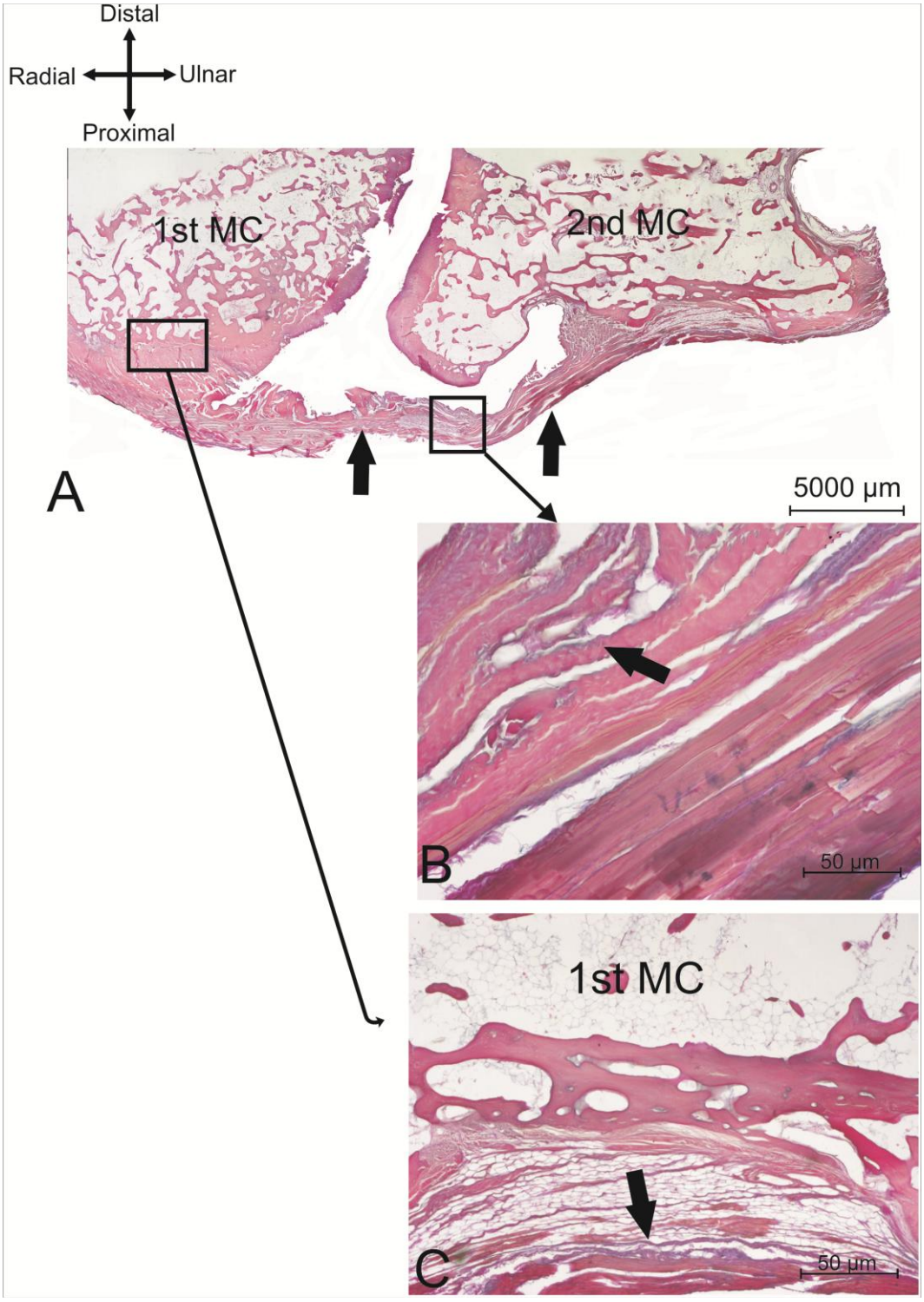

Figure 4.32: Section of the dorsal intermetacarpal ligament (DIML) in 2 hours ME, 15 seconds VG.

A. Panorama image of the DIML, with (magnification × 2.5). **B.** Middle section of the DIML; the arrows show very good appearance of elastin fibres, the clarity of differentiation of elastin fibres were very good, the colour was mild black nearly to grey. Very good distinguishing of blood vessels presented by yellow colour nearly to orange; the collagen was also visible in the fibrous matrix presented by mild deep red, the bony tissue was also red but it had large lacuna stains by white colour; the articular cartilage had deep red colour, with (magnification × 10). **C**. Proximal attachment, with (magnification × 10). Miller's Elastin re-timing (2 hours ME, 15 sec VG).

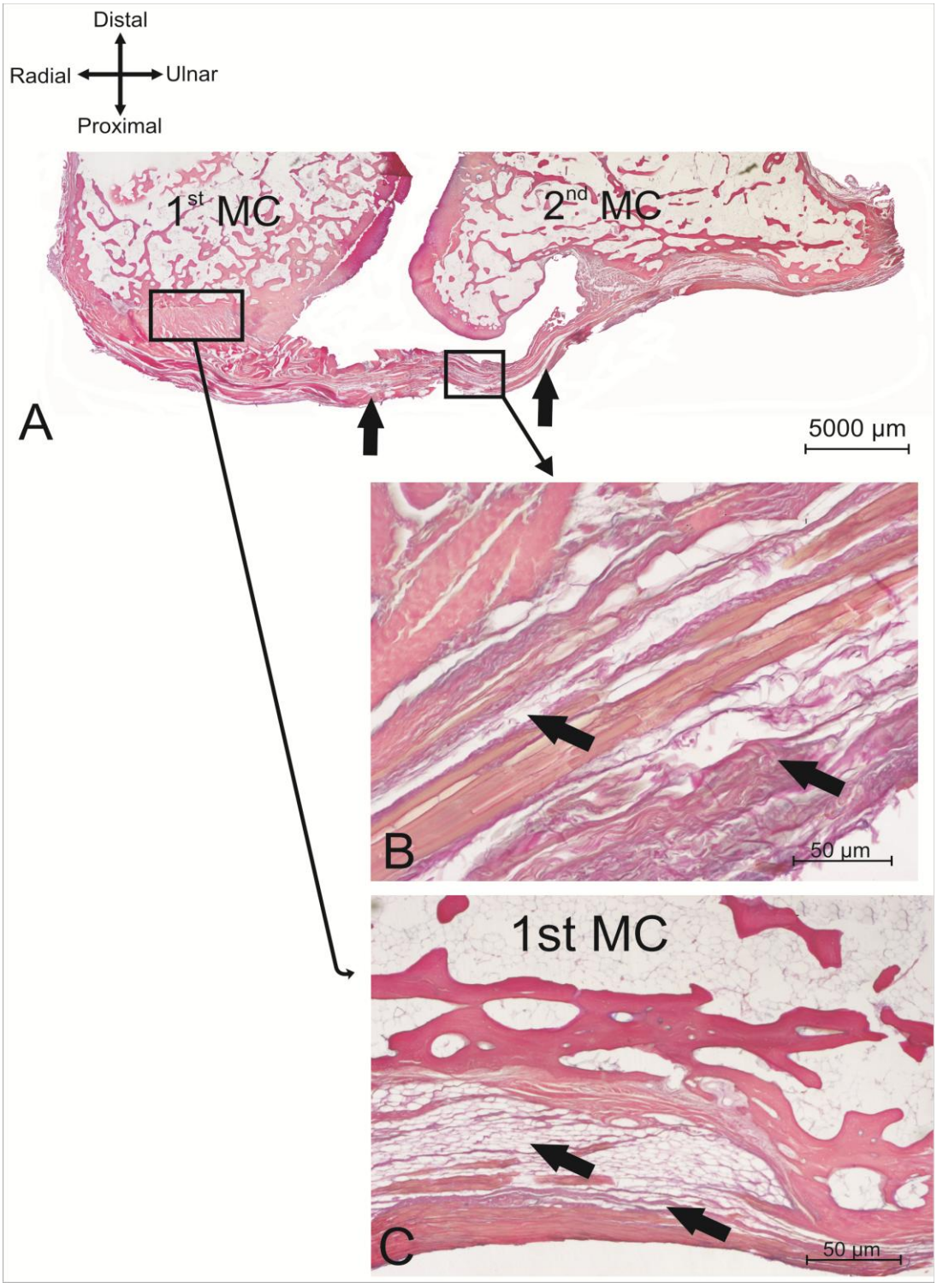

Figure 4.33: Section of the dorsal intermetacarpal ligament (DIML) in 2.5 hours ME, 15 seconds VG.

A. Panorama image of the DIML, with (magnification × 2.5).**B.** Middle section of the DIML. The arrows show excellent appearance of elastin fibres, the clarity of differentiation of elastin fibres were excellent, the colour was mild black nearly to pink. Excellent distinguishing of blood vessels presented by yellow colour nearly to orange; the collagen was also visible in the fibrous matrix presented by mild deep red nearly to orange, the bony tissue was also red but it had large lacuna stains by white colour; the articular cartilage had deep red colour, with (magnification × 10). **C.** Proximal attachment, with (magnification × 10). Miller's Elastin re-timing (2.5 hours ME, 15 sec VG).

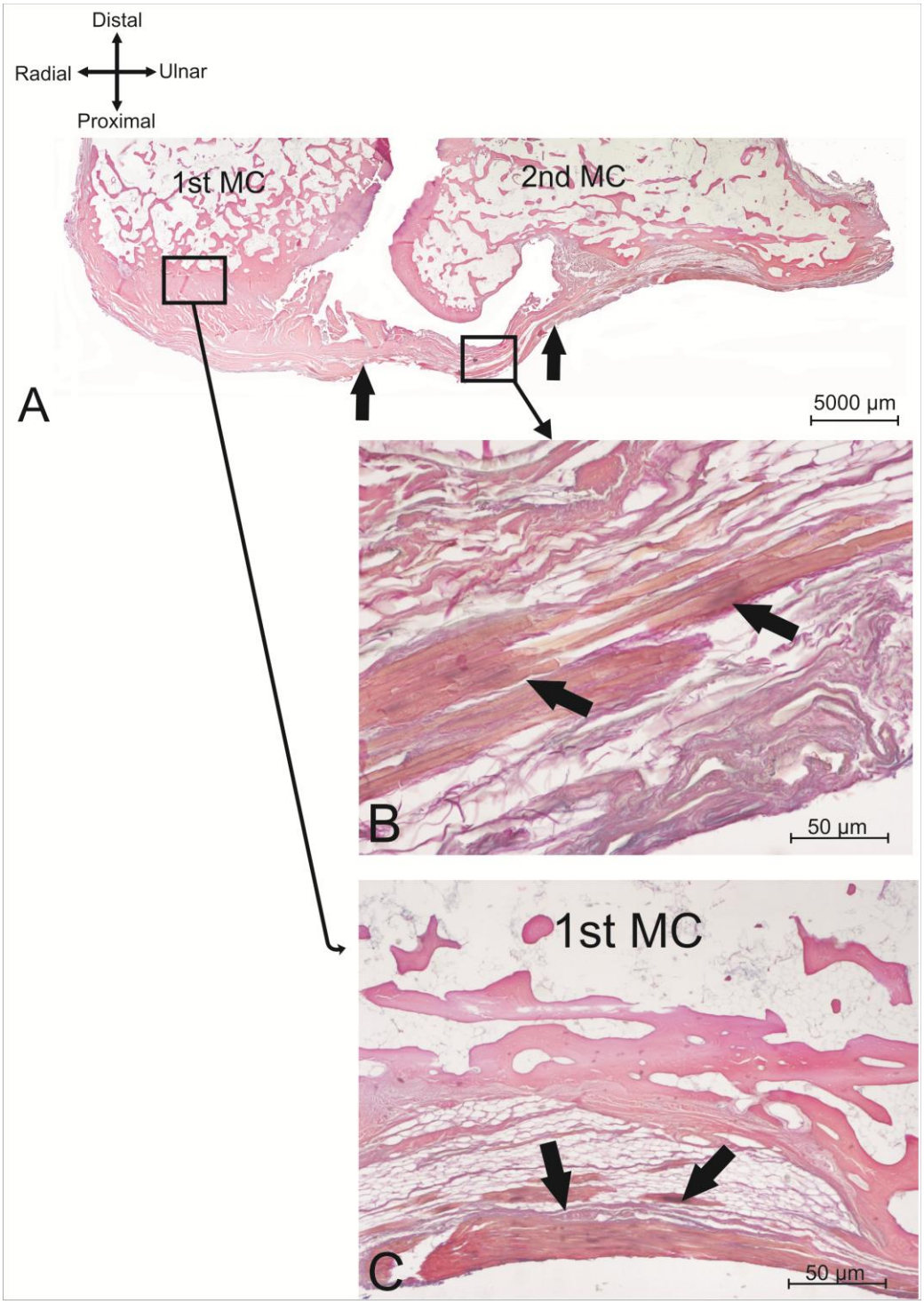

Figure 4.34: Section of the dorsal intermetacarpal ligament (DIML) in 2.5 hours ME, 10 seconds VG.

A. Panorama image of the DIML, with (magnification × 2.5). **B.** Middle section of the DIML. The arrows show excellent appearance of elastin fibres, the clarity of differentiation of elastin fibres were excellent, the colour was mild black nearly to pink. Good distinguishing of blood vessels presented by yellow colour nearly to orange; the collagen was also visible in the fibrous matrix presented by mild deep red colour, the bony tissue also light red but it had large lacuna stains by white colour; the articular cartilage had light red colour, with (magnification × 10). **C.** Proximal attachment, with (magnification × 10). Miller's Elastin re-timing (2.5 hours ME, 10 sec VG).

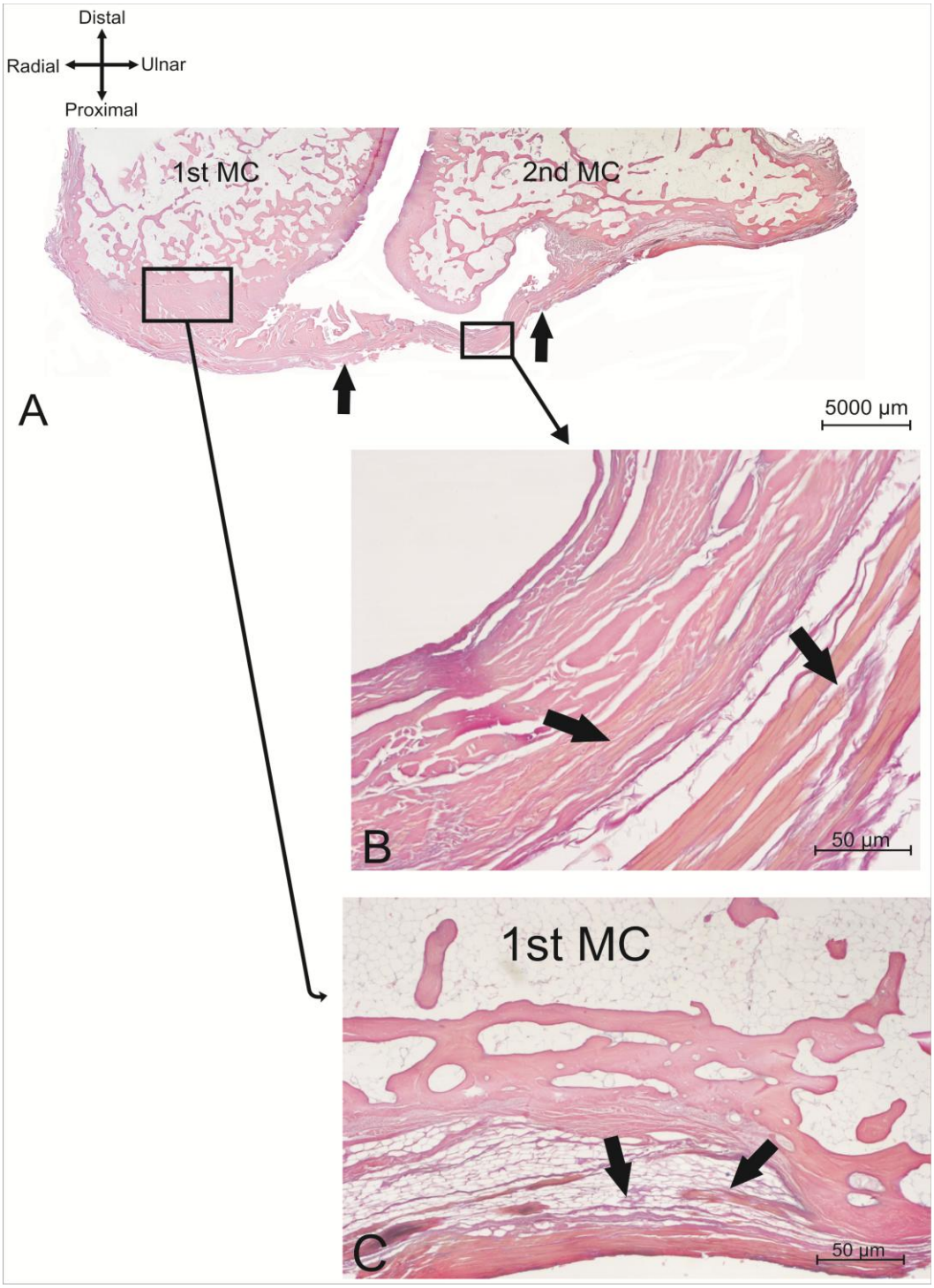

Figure 4.35: Section of the dorsal intermetacarpal ligament (DIML) in 3 hours ME, 10 seconds VG.

A. Panorama image of the DIML, with (magnification × 2.5). **B.** Middle section of the DIML. The arrows show excellent appearance of elastin fibres, the clarity of differentiation of elastin fibres were excellent, the colour was mild black nearly to pink. Bad distinguishing of blood vessels presented by yellow colour nearly to orange; the collagen was also visible in the fibrous matrix presented by mild deep red colour, the bony tissue also light red but it had large lacuna stains by white colour; the articular cartilage had light red colour. In general this experiment had worse results than previous experiments, with (magnification × 10). **C**. Proximal attachment, with (magnification × 10). Miller's Elastin re-timing (3 hours ME, 10 sec VG).

4.3.6 HREM

The result of this experiment proved that there is no relation between flexor retinaculum and doro-ulnar trapeziometacarpal ligament (DUTML). The 2D images rendered into 3D model by using Amira 3D software, the process of applied the software explained previously in this chapter. The fascicles and bone margin were determined, the pattern of the ligament also showed in 3D, the enthesial tissue could not be represented (Figures 4.36-4.37-4.38-4.39-4.40).

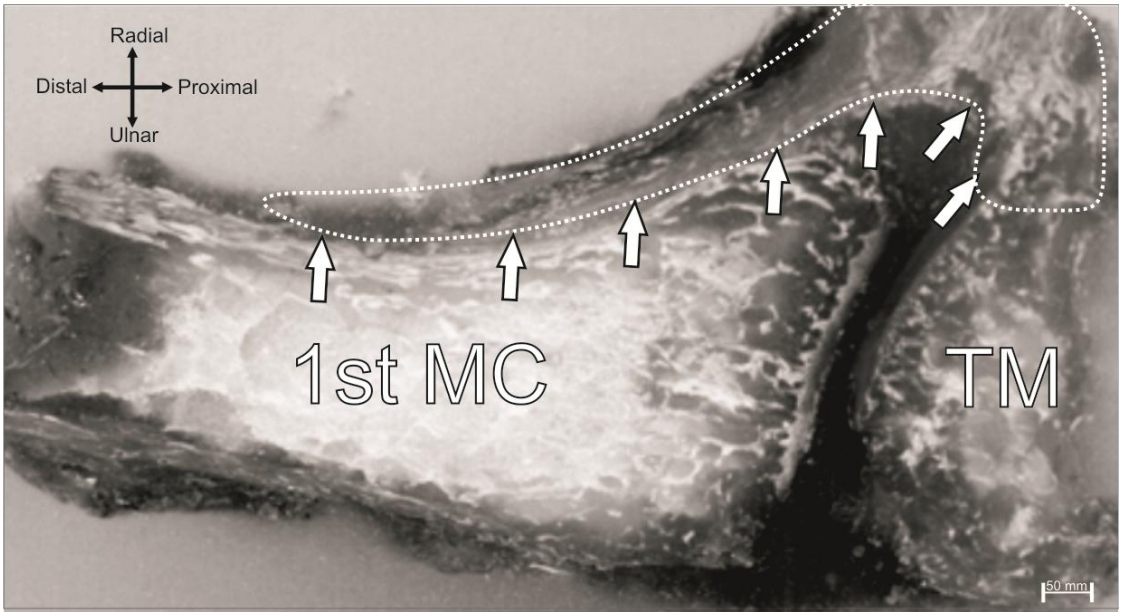

Figure 4.36: Highly detailed section of the specimen showed the entheses of dorso-ulnar trapeziometacarpal ligament DUTML.
The arrows illustrate the pattern of the DUTML. An undesired shadowing of deeper tissue is also visible. Dotted lines depicted at the ligaments borders indicates to the course and limit of the ligaments from and to the bones. 1st MC. First metacarpal bone. TM. Trapezium bone.

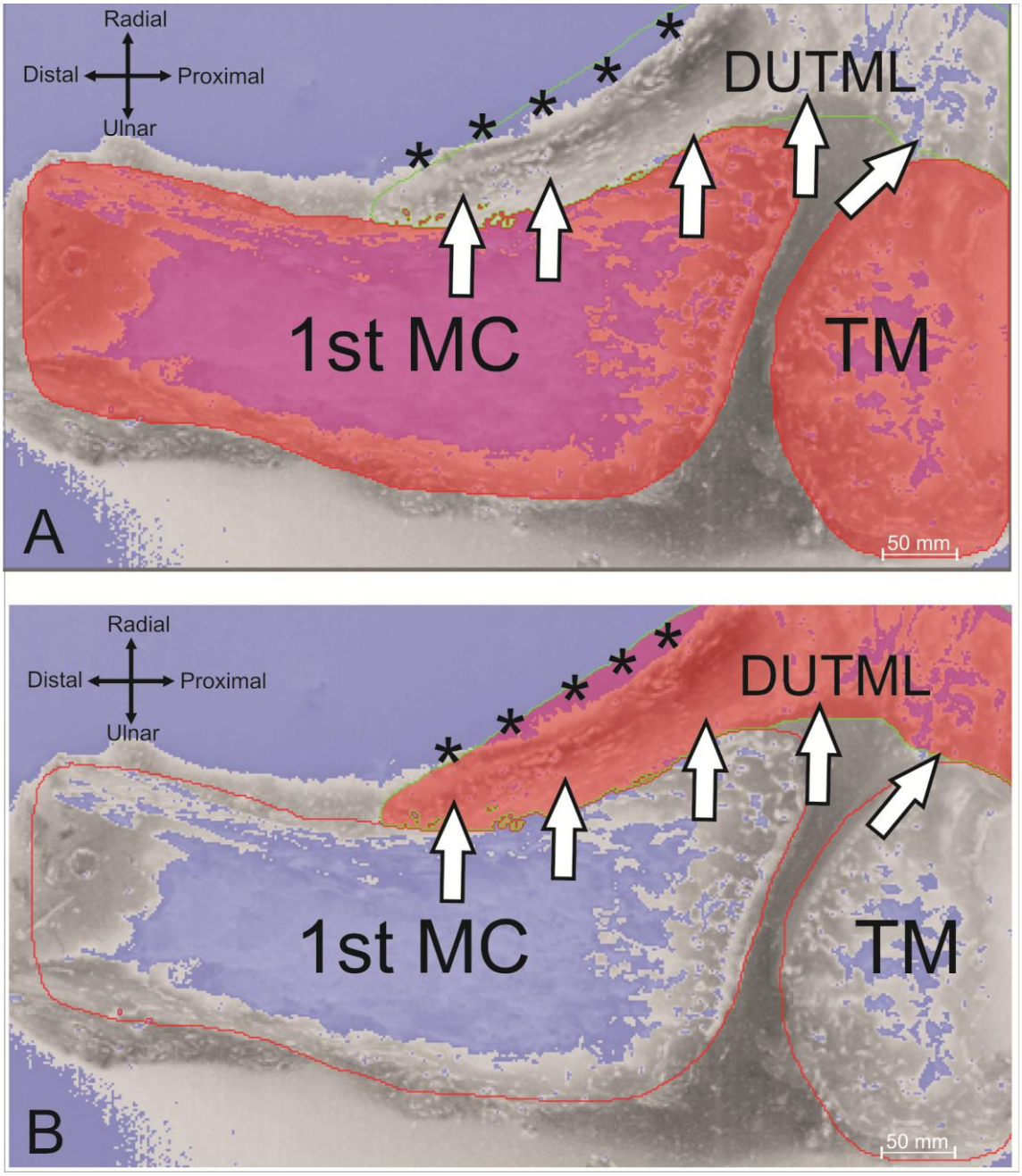

Figure 4.37: Manual selection of different tissue process on Amira 3D software.
A. Red restricted circle presents bony tissue of (TM) trapezium bone, and (1st MC) first metacarpal bone.The arrows show the ligament course from and to both two bones.
B. Red restricted circle presents ligament tissue of (DUTML) dorso-ulnar trapeziometacarpal ligament. The arrows show the ligament course from and to both two bones.This process is done slide by slide.
(*******) indicate to the maximum area of ligament a cross all sections –slides.

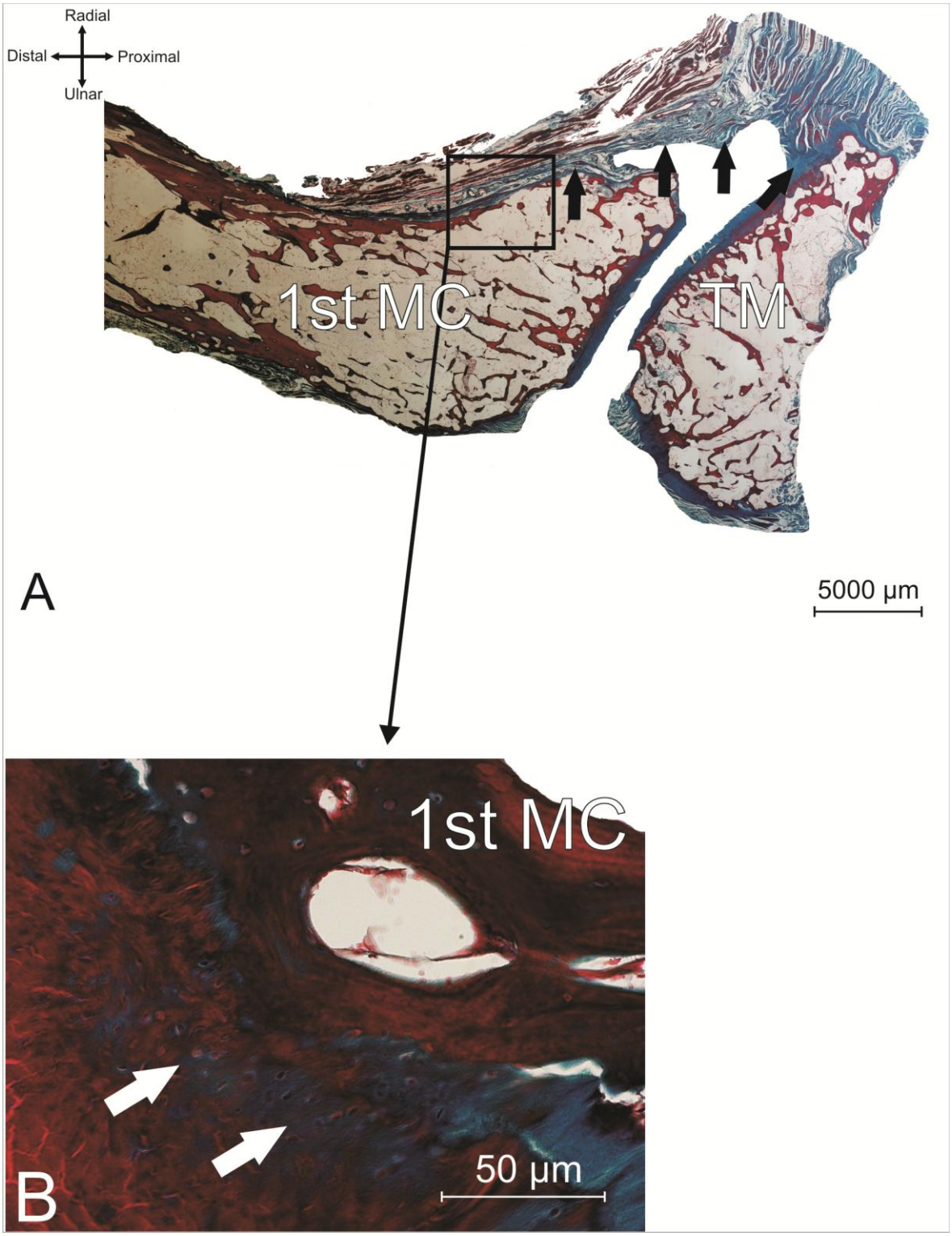

.
Figure 4.38: Section through dorso-ulnar trapeziometacarpal ligament (DUTML) satins by Modified Masson's Trichrome.

A. Panorama image of the DUTML, with (magnification × 2.5).
B. High magnification of enthesial zone, with (magnification × 10). The arrows show the calcified tissue and tidemark, the bony tissue also showed as big lacuna stains by white colour, the articular cartilage presented by deep red with a small varieties lacuna. There was no connection of the DUTML with flexor retinaculum fibre. The green colour presented the bundle of fascicles like "string" beside each others. Modified Masson's Trichrome.

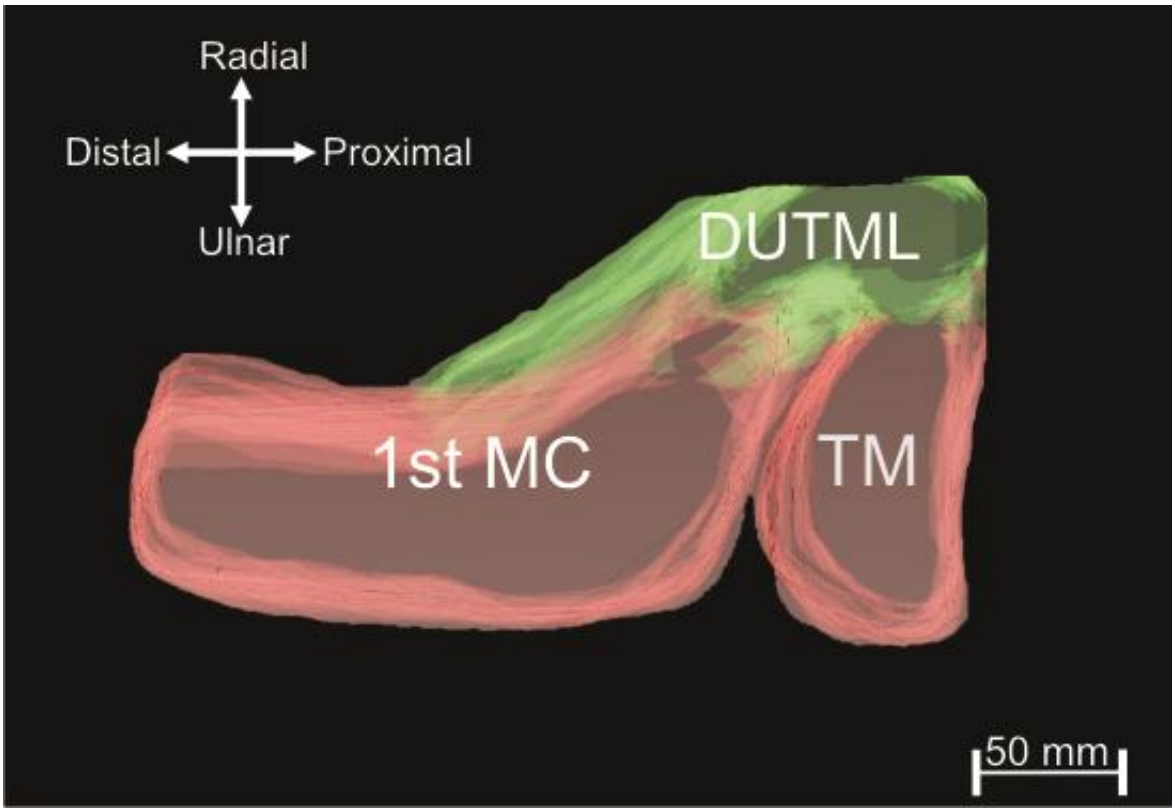

Figure 4.39: Virtual view of the dorso-ulnar trapeziometacarpal ligament (DUTML) rendered into 3D image.

The red colour presents bony tissue of both (TM) trapezium bone and (1st MC) first metacarpal bone. The green colour presents (DUTML) dorso-ulnar trapeziometacarpal ligament, and its fascicles pattern.

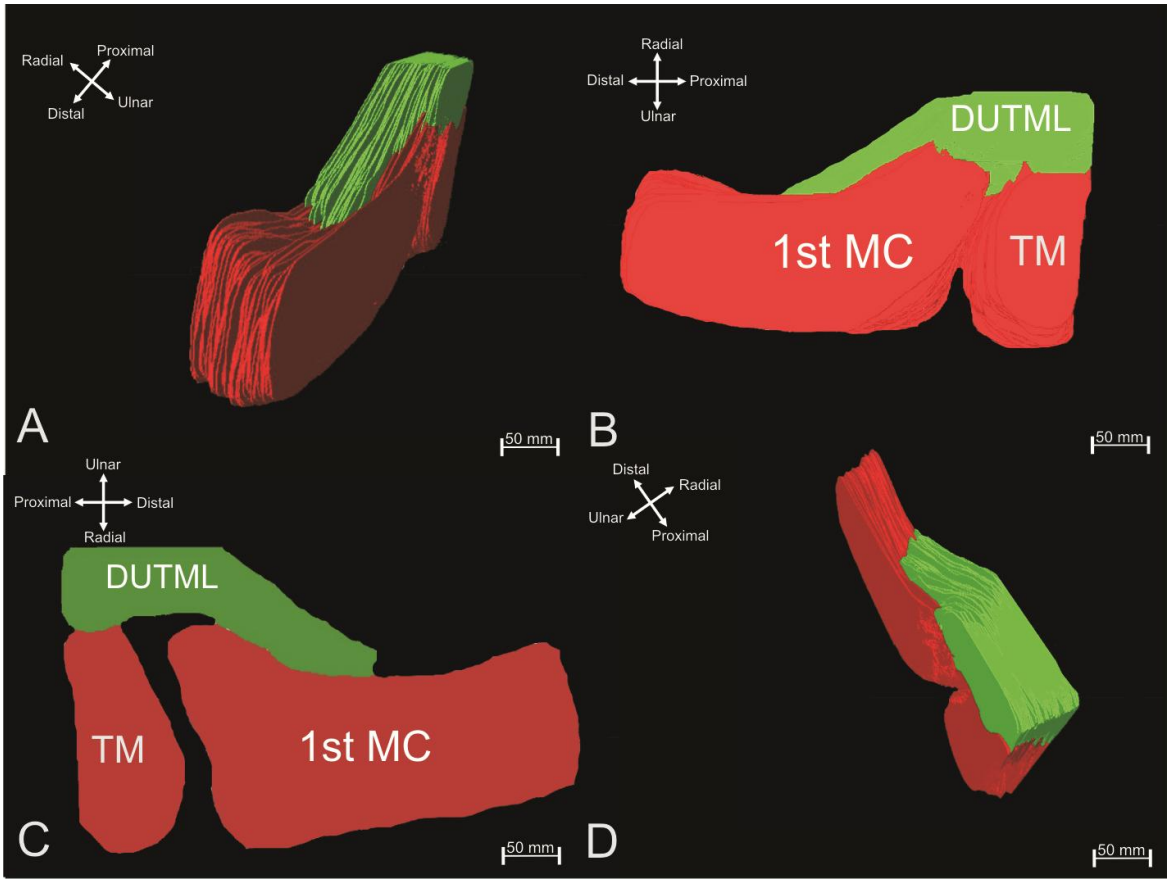

Figure 4.40: Using different planes of the dorso-ulnar trapeziometacarpal ligament (DUTML) rendered into 3D image.

The red colour presents bony tissue of both (TM) trapezium bone and (1st MC) first metacarpal bone. The green colour presents (DUTML) dorso-ulnar trapeziometacarpal ligament, and its fascicles pattern. Show many layers collected together to confirm 3D model.

A. Oblique view. B. Radial view. C. Ulnar view. D. Superior view.

4.4 Discussion

4.4.1 Type of the entheses

Basically, there are two types of the enthesis based on the mechanical process of the fascicles entry to the bone cell, which contains the link between both structures (ligament and bone). This link should be strong and flexible in the same time. Actually, this concept is impossible to achieve, because strengthening is needed for stability, and flexibility for laxity. In addition, direct connections between the ligament and bone, called fibrous entheses, whereas indirect connections are called fibrocartilagenous (Chung 2007; Claudepierre and Voisin 2005; Francois *et al.* 2001). Both types describe the changes that occur on the connective tissue.

The fibrous type is considered as a healthy connection, as it rarely occurs with disease (Slobodin *et al.* 2007). Unfortunately this type has not been seen in the current study. The fibrocartilagenous type has processes consisting of three zones as mentioned previously in this chapter (Francois *et al.* 2001), also the fibrocartilagenous type indicates an unhealthy or ageing change. The current study finds the fibrocartilagenous type to occur in the TMC ligament, and in both proximal and distal attachments. However, the ageing of the cadaveric and the disease conditions may have a role in the fibrocartilagenous type.

The current study used the MMT stains to see the structures of the ligament clearly. According the protocol used, the nuclei stain a black colour, muscle and cytoplasm stain red, and collagen and cartilage stain a green. Based on the slides in the current study, the colour observed is not like the protocol (Appendix 2); the nuclei stain mild black, the cytoplasm and muscle stain deep red, and the collagen and cartilage stain dark green (Figures 4.3-4.4-4.5-4.6-4.7-4.8). Moreover, the contrast of the main colour has changed. In the current study the embedding protocol (Appendix 1) was possibly affecting the cadaveric tissue during the embedding process, or maybe the solutions that were used in embedding the specimen reacted with the staining solutions.

In the current study, the results showed the calcified and uncalcified zones, separated by tidemark line, the fascicles showed within the fibrous matrix, the

pattern of the fascicles were considered as string bundles beside each other, and have a wavy shape surrounded by blood vessels and nerve supply. In addition, the articular cartilage with many small lacuna composed together, the bony tissue were very clear and presented with a big lacuna near to the articular cartilage (Figures 4.3-4.4-4.5-4.6-4.7-4.8). However, the MMT stain helped to define the structures of the ligament under microscope clearly.

4.4.2 PTML Layers

The layers of the PTML were controversial in many studies (Bojsen-Moller 1976a; Kaplan 1965; Pieron 1973). The current study investigated the PTML ligament by a “cross-sectional” cutting of the specimen. Therefore, in the image of the PTML it was clear that the PTML has two layers, superficial and deep layers, and the anatomical explanation of these layers was mentioned in the first chapter. However, the cross-sectional cutting of the specimen was able to reveal the section of the PTML with its layers, and also the images showed one of the layers superficially to the other. This is called the superficial palmar trapeziometacarpal ligament (sPTML), whereas the other is called the deep palmar trapeziometacarpal ligament (dPTML).

The classification of the PTML into superficial and deep layers by histological findings is providing a more detailed understanding of the anatomy, especially the tiny ligament. However, the histological investigations particularly in the small ligament are difficult, due to the fixing and embedding of the small ligament, which needs more precise work under the microscope.

In the current study, we explored the variations of staining PTML by MMT alone, ME alone, combination stain start with MMT, and combination stain start with ME (Figures 4.9-4.10-4.11-4.12). Therefore, the images gave a multi-coloured view of the same ligament, in the same section. Indeed, the MMT was a better stain for this task, due to the the contrast of the colours

4.4.3 Descriptions of the entheses

The entheses is the area of the attachment between the collagen fibres of the ligament and the bone (Benjamin *et al.* 2002; Benjamin *et al.* 2006). However, this

description provides a good vision especially for the anatomists, and helps to explain the mechanism of the attachment between the fascicles and the bone cell.

Moreover, the functional role of the entheses has been investigated to test the concept of the “development enthesis” (Claudepierre and Voisin 2005). This is described by the hyaline cartilage undergoing endochondral ossification, replacing it by bony trabeculae, and the fascicles of the ligament undergoing metaplasia into cartilage cell, which lay down a layer of fibrocartilage. However, the final step of these processes is the enthesis, composed of ligament, then fibrocartilage, and bone with no hyaline cartilage. Also, the entheses reflect the pathological changes that happen in the tissue, especially at the dense connective tissues such as ligament, tendon, and bone (Claudepierre and Voisin 2005; Francois *et al.* 2001).

Moreover, the descriptions of pathological disorders depend on several factors that play a very important role in changing the properties of the entheses. Firstly, the biochemistry of the matrix enthesis, that is, the composition found across the four zones of the enthesis; collagen types one to five were expressed both in tendon and in the fibrocartilage, whereas, collagen type two was expressed mainly within the fibrocartilage. These findings shed light on the pathophysiology of Spondyloarthropathies (Claudepierre and Voisin 2005; Francois *et al.* 2001; Freemont 2002)

Secondly, aging is associated with an increased prevalence of asymptomatic radiological enthesopathy. In addition, sporting activities and other repeated strenuous physical activities are cause of symptomatic enthesopathy (Patel and Buckland-Wright 1999; Slobodin *et al.* 2007). Thirdly, diffuse idiopathic spinal hyperostosis (DISH) is a cause of enthesopathy, and there are many metabolic diseases that can cause abnormalities of the entheses. However, the mechanism of the metabolic disease involvement is unknown (Benjamin *et al.* 2006; Chung 2007; Claudepierre and Voisin 2005).

Finally, there is a relationship between inflammatory disease and the enthesopathy (Chidgey *et al.* 1991). However, the entheses area have many descriptions according to the results seen under the microscope, the pathological descriptions are one of the most studied in the entheses area, and reflect the natural changes that occur in connective tissues.

4.4.4 Miller's Elastin development

ME stain is a product that stains connective tissue and especially elastic fibres (Doschak *et al.* 2005). The value of this stain comes from the distinctive colour produced during the process of staining. The ME and VG stains work together to present the structures of the section in different colours, and a key factor in the popularity of this stain is the short time needed to stain samples (Miller 1971). Since time is very important in maximising the contrast of the colour specifically in the elastic fibres (Miller 1971), the current study changed the staining protocol in terms of time of staining only in order tog et the best images possible.

In the current study of the elastic fibres of the TMC ligament, the results showed that there was a lot of extracellular matrix comprising an elastin core (Figures 4.13-4.14-4.15-4.16-4.17-4.18). The biology of elastic fibres is complex because they have multiple components (Veuthey *et al.* 2014). However, the function of the elastic fibres was not directly investigated in the current study, the ability to distinguish the elastic fibres' colours was very important in depicting the pattern of the fascicles, and to allow us to trace the collagen fibres from the proximal and distal attachment sites precisely.

Re-timing was performed on DIML, which was chosen randomly. The first experiment followed the original protocol in the Appendix 3, and the result illustrated mild black for elastic fibres, the blood vessels were yellow nearly to orange, and the bony tissue and articular cartilage were light red nearly to pink. However, the result of this experiment gave a good view of the elastic fibres but a lack of visibility of the other structures.

The second experiment gave the same results s the first experiment, except there was a little bit of improvement in the viewing of the elastic fibres, and the background of the image was lighter which made visualising the other structures easier.

The third experiment gave the best resolution of all experiments, due to the image having excellent colours, and with the elastic fibres much more clearly defined. Also, the blood vessels were highlighted through the section. This experiment allowed an excellent viewing of the elastic fibres and other structures.

The time of ME stain was 2.5 hours, and for the VG was 15 seconds. The fourth and fifth experiments gave the same results regarding the elastic fibres, but the others structures were less evident in the fifth experiment, suggesting the ME stain needs a more time to stain the elastic fibres perfectly.

In the current study, based on the results of the five experiments of the ME retimed staining, the third experiment was the best and gave a good viewing of the elastic fibres and other structures. The optimum time for the ME stain was 2.5 hours, which means the ME stains needs more time to react with section components. In addition, increasing the time of ME staining by more than 2.5 hours had no further benefit in enhancing the contrast of darkness in the image. However, decreasing the VG stain to less than 15 seconds badly affected the image background. The optimum time for the VG was 15 seconds (Appendix 6).

4.4.5 Combination stains

The concept of combining stains was originally seen by combining the Verholeff's elastic and Masson's Trichrome stains (O'Connor and Valle 1982), and this concept enhanced the development of the staining. Moreover, the Miller's stain in 1971 tried both stains Miller's Elastin and Van Gieson stains (Miller 1971), the Weigert's elastic stain was made by combining of resorceinol and fuchsine stains (Carleton *et al.* 1980).

The aim of applying both stains in one section in histological procedures, is to maximise the information about the structures of the histological section. For instance, some structures such as fascicles and blood vessels are too tiny, so the visualisation and distinguishing of these structures are needed. Also, the pattern or (course) of the fascicles needs to be visualised to permit analysis of the style of the fascicles and for measuring the length, or enthesial area of ligament. However, the combination of the chemical products of staining can help to produce new colours that assisting distinguishing between the section's structures.

The current study used two main stains, MMT and ME, and the protocols for combining these stains progressed according to the first stain used. The combining of stains started with MMT, which meant the protocols of hydration of slides and staining started with the MMT protocol (Appendix 4), while the

dehydration of slides followed the ME protocol (Appendix 3). The results of this combination were; Nuclei presented black, Cytoplasm, muscle and acidophil granules presented blue, and collagen, cartilage, mucin and basophil granules presented deep blue (Figures 4.19-4.20-4.21-4.22-4.23-4.24). However, the main reasons of combining these two stains was to visualize organised and disorganised structures more clearly throughout the section, and this was not achieved by this combination.

When combining stains started with ME, which meant the protocols of hydration of slides and staining started with the ME protocol (Appendix 5), the stain did not utilise the VG stain, because the VG stain has a high background staining , which affects the contrast on the slides. Moreover, the main structures usually identified by the VG stain are elastin fibres, but this combination did not distinguish elastin fibres. So thus, the protocol omitted the VG stain (Appendix 5). The features of the images were; Nuclei were black, the cytoplasm, muscle and acidophil granules were deep red, and the collagen, cartilage, mucin and basophil granules were deep green (Figures 4.25-4.26-4.27-4.28-4.29-4.30). However, this combination gave a better clarity of image that the previous stain combination.

4.4.6 HREM

One of the goals of histological studies was the ability to render 2D images into a 3D model (Geyer *et al.* 2009; Mohun and Weninger 2012; Rosenthal *et al.* 2004; Weninger *et al.* 2006). There are many software packages available to do this work, such as Amira 3D, Rhinoceros V5, and Avizo 3D. The preparation of the block needs to mount the specimens to be ready for producing a 2D image, which can then be imported as a series of sequential images as a dataset into the 3D software. The preparation of the block must overcome the obstacles of the slight transport embedding, in which the deeper tissues form shadows on the surface of image (Figure 4.2), and optimise distinguishing the fascicles of the ligaments and other components of the structures in the 2D image.

In addition, we rendered a 3D model of the DUTML to detect if there was any relationship between flexor retinaculum and DUTML fascicles (Cobb *et al.* 1993; Goitz *et al.* 2014; Manley *et al.* 2013; Nigro 2001; Pacek *et al.* 2010), or if there was any overlapping within the individual tissues. In the current study, we used

HREM technique for only one ligament of TMC ligament, to view the changes may have occurred in the transitional area between bone and enthesial tissue. HREM may also be useful for comparison between the structures achieved by rendering a 2D image to a 3D model, or with MRI images (Mohun and Weninger 2012), or CT scan images rendered into a 3D model. Moreover, the resolution of the 3D model helps us to advance the anatomical analysis of structures.

The current study found the fascicles of the DUTML attachment was from trapezium to first metacarpal bones, without any interference from other structures, particularly the flexor retinaculum. However, the optimisation of the new technique of HREM requires the best model and viewing.

The studies were interesting in developing a better understanding of how different stains interact within joint tissues. It has strengthened the opinion that a MMT stain is the best option for clearly describing the majority of joint and enthesis-related tissues. Moreover, this information may lead to better selection of ligaments for surgical restoration, augmentation, or more appropriate sites for tissue transfers.

This study has some limitations due to ageing of the specimen affecting on the results since most of the entheses type was fibrocartilagenous. No gender information was mentioned through the study, and no clinical history of the specimens was available, which might have identified reasons for enthesial type. Also, no statistical investigation was performed on the enthesial area. The embedding protocol might also have affected the colour contrast throughout the staining procedures with MMT and ME, or during combination staining. More experiments are needed for the re-timing of ME staining, and the HREM technique should be applied to more than one ligament, as it gives more detailed anatomical information. Using the HREM technique in conjunction with CT scan and / or MR images may provide critical alternate view that aids to interpret of 2D sections.

Chapter Five

Osteological and Statistical Description of the Trapeziometacarpal Joint

5.1 Introduction

Most studies of the morphology of the carpal bones are not detailed enough to provide a clear understanding of their anatomy (Humes *et al.* 2004; Kuczynski 1974; Nanno *et al.* 2006b; Schild *et al.* 1981). In those studies, the osteologic disruptions of the trapezium and first metacarpal bones are inadequate and difficult to reproduce when present.

The etymologic derivation of the trapezium was from the Greek trapezion (a quadrilateral with two parallel sides) and trapeza (a table, altar) (Ateshian *et al.* 1992). (Drake 2005; Frazer 1965; Gray 2005) used standard texts concentrating mainly on the articular surfaces or facets. The International Anatomical Nomenclature Committee's (1989b) only named landmark of the trapezium was the tuberculum ossis trapezii. That same part was named as a ridge by (Humes *et al.* 2004) and as a crest by (Tocheri *et al.* 2005). The lack of a detailed anatomical description of the bone creates difficulties in both diagnosis and treatment of injuries of the trapezium and thumb.

The most details experiments and studies releate to this chapter explained in the first chapter (pages78-89).

The aims of this study are to (1) explain the features of the trapezium and first metacarpal bones, (2) quantify the shape and orientation of the trapezium and first metacarpal bones throughout 3D modelling in 3D virtual environment, (3) quantify the changes of measurement (length, with and surface area) of the trapezium and first metacarpal bones, and (4) compose two bones of (trapezium, first metacarpal) in one shape by Landmark software to observe the change could occur on the specific features on the surface of (trapezium- first metacarpal) bones., and (5) compare between the accurancy of the software especially in measurement procedures.

5.2 Material and methods

5.2.1 Sample population and programs use

Ninety-two dry cadaver trapezium (TM) and 1st metacarpal (1st MC) bones of unknown age and sex were used. Three-dimensional modelling was rendered in a virtual space using a digital microscribe and modelled/analysed using three programmes: three-dimensional modelling was rendered in a virtual space using a digital microscribe and modelled/analysed using three programmes:

1. Rhinoceros 5.0: software that renders the 2D shape into 3D model in a 3D virtual environment. The mechanism for rendering uses the micro scribe device (pen) which places dots along the surface of the shape. Then the dots are converted automatically into lines by specific software tools. Finally, the lines merge together to create the 3D model. The investigations, such as the length, width, and area of the models also have special tools to measure (Figures 5.1-5.2-5.3).

2. Amira 3D software: also renders the shape into a 3D model through a 3D virtual environment. The difference between Amira and Rhinoceros is in importing data. Rhinoceros depends on the microscribe device to import the data inside the software, while Amira depends on a CT scan file (DICOM) to import the data inside the software. The Amira software uses these files to convert the 2D shape into a 3D model. It also has special tools to render and measure the model (Figures 5.4-5.5-5.6-5.7-5.8-5.9).

3. Landmark: software that uses the (PLY) files from Rhinoceros to merge two models together in order to make the combined shape between both models. The software uses the single coordination points system to merge the two models together into one model. The mechanism puts the points on surfaces and matches the points on different surfaces with each other. The final 3D model is produced from two models which each have the most important features to create the new model from (Figures 5.10-5.11-5.12).

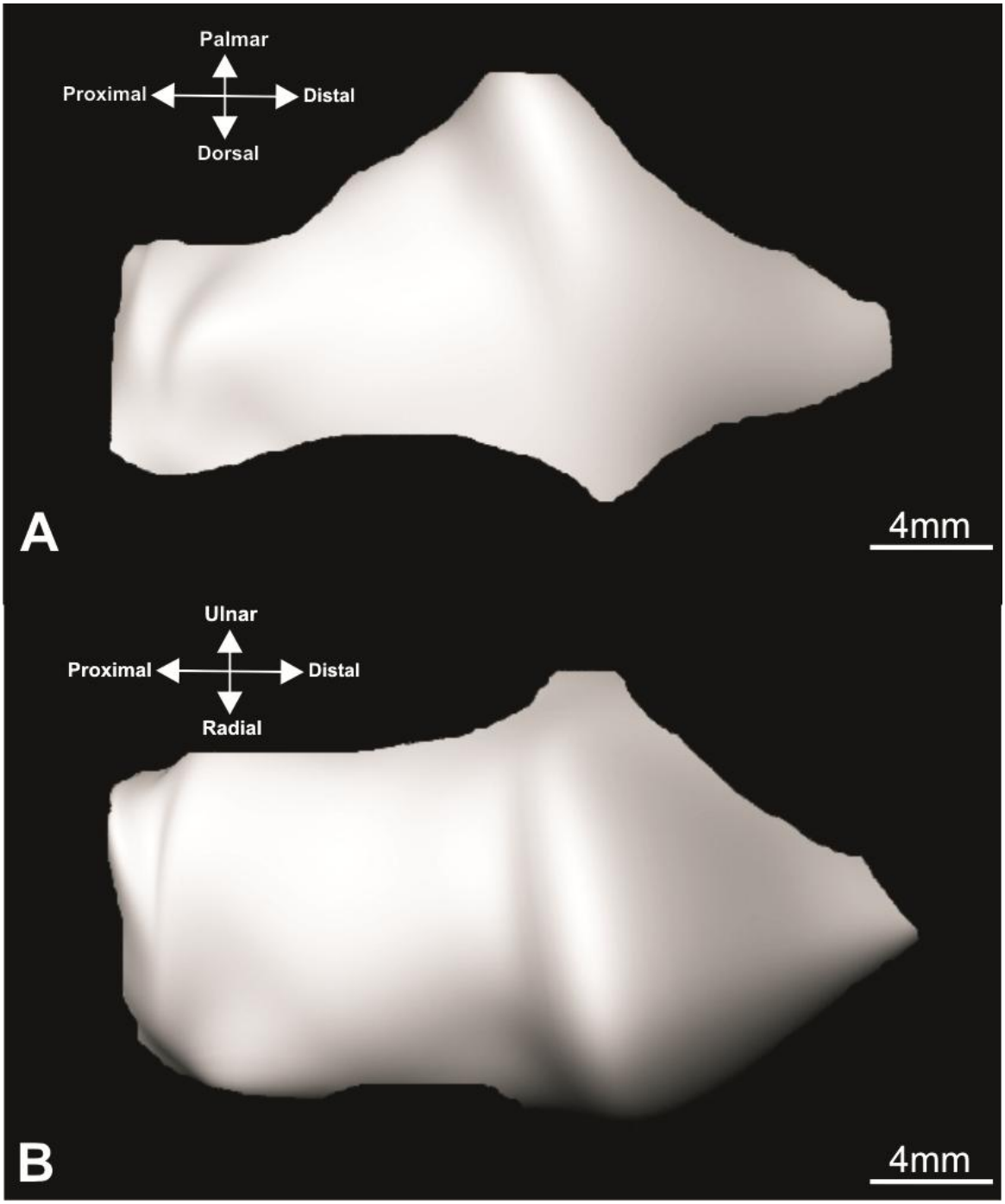

Figure 5.1: Radial and facet views of the trapezium (TM) bone rendered in a virtual space using a digital microscribe with the Rhinoceros 5.0 program.

A. Radial view of the TM bone which moves from the radial side to the ulnar side of the bone. This view illustrates the radial shape and curvature of its edge.
B. Facet view of the TM bone in which the direction moves from the distal side to the proximal side (top view) of the bone. This view illustrates the nature of the articular surface, prominences, and declines.

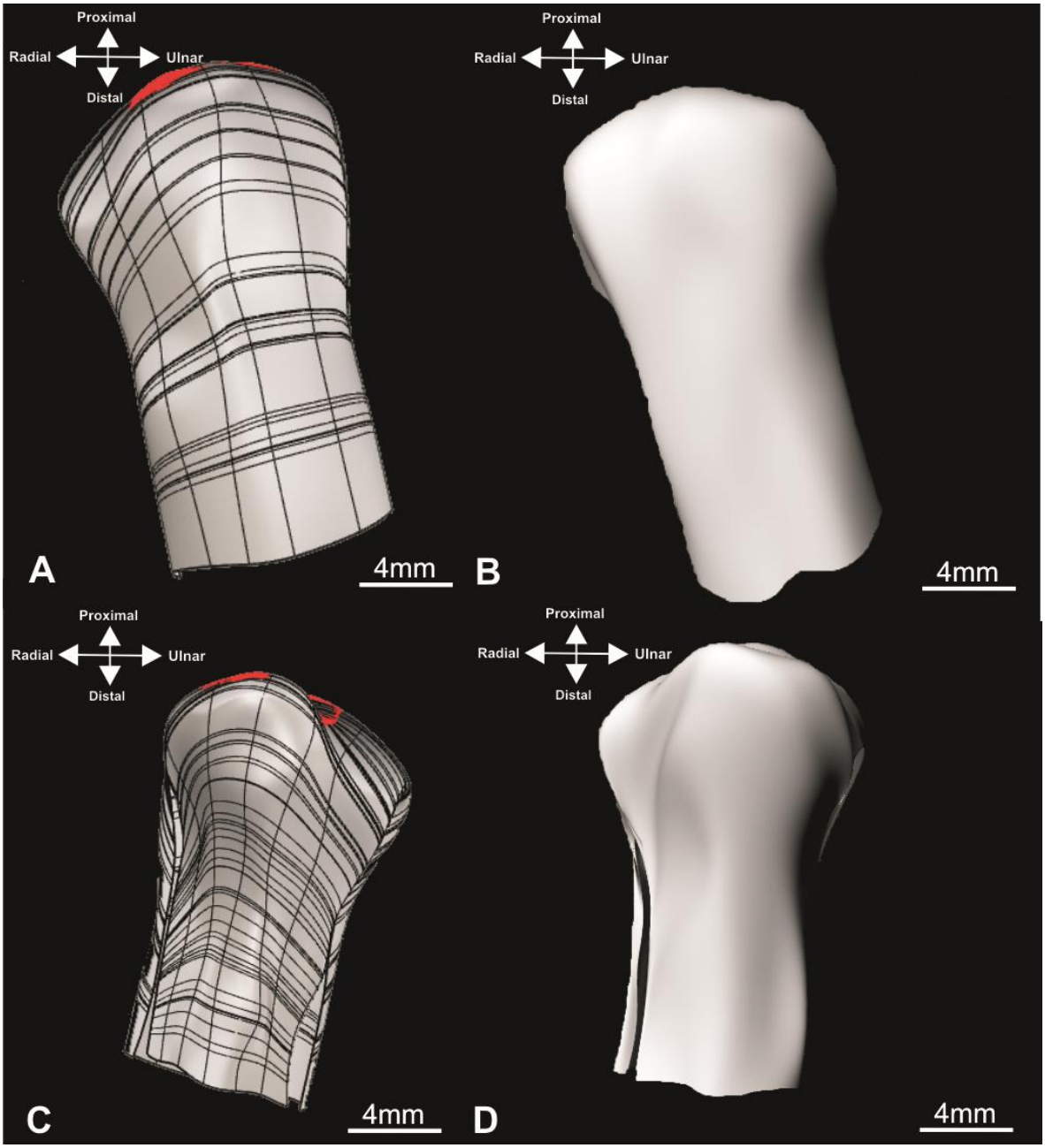

Figure 5.2: Dorsal and palmar sides of the 1st metacarpal bone (1st MC) of the trapeziometacarpal (TMC) joint rendered in a virtual space using a digital microscribe with the Rhinoceros 5.0 program.

A. Dorsal view of the 1st MC bone with lines, which illustrates the virtual shape process used by (Rhinoceros 5.2) program.
B. Dorsal view of 1st MC bone illustrates the bone without the lines.
C. Palmar view of the 1st MC bone with lines, which illustrates the virtual shape process used by (Rhinoceros 5.2) program.
D. Palmar view of 1st MC bone illustrates the bone without the lines. .

Figure 5.3: The trapeziometacarpal (TMC) joint rendered in a virtual space using a digital microscribe with the Rhinoceros 5.0 program.
1st MC. First metacarpal bone. 2 nd MC . Second metacarpal bone. TM. Trapezium bone.
The red colour illustrates the articular surface between two bones.
(*) indicate to articular surface with second metacarpal bone not visible on the trapezium bone.

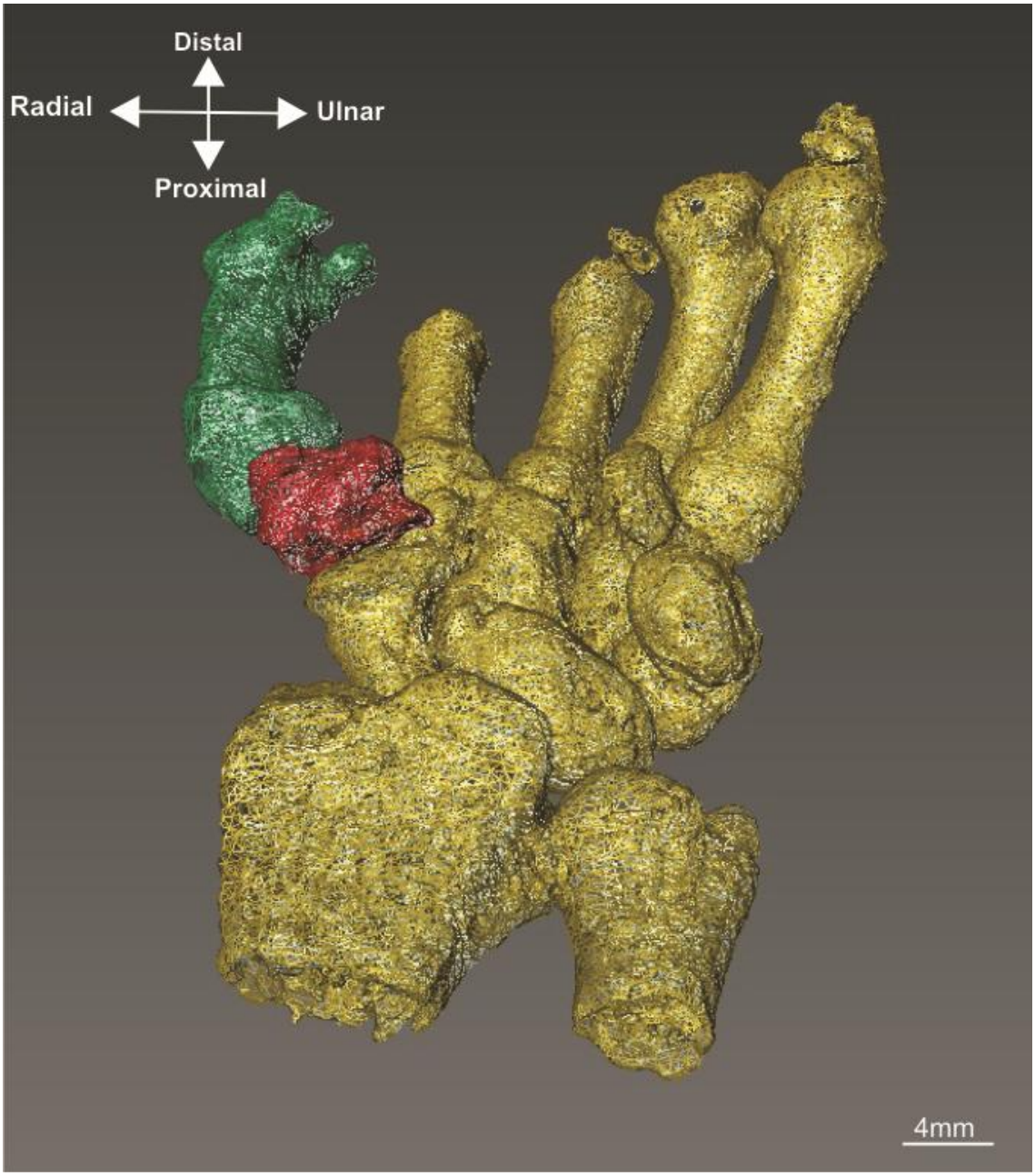

Figure 5.4: 3D palmar view of the left hand rendered in a virtual space by Amira 3D software.The figure illustrates the 1st MC bones in green and TM bone in red.

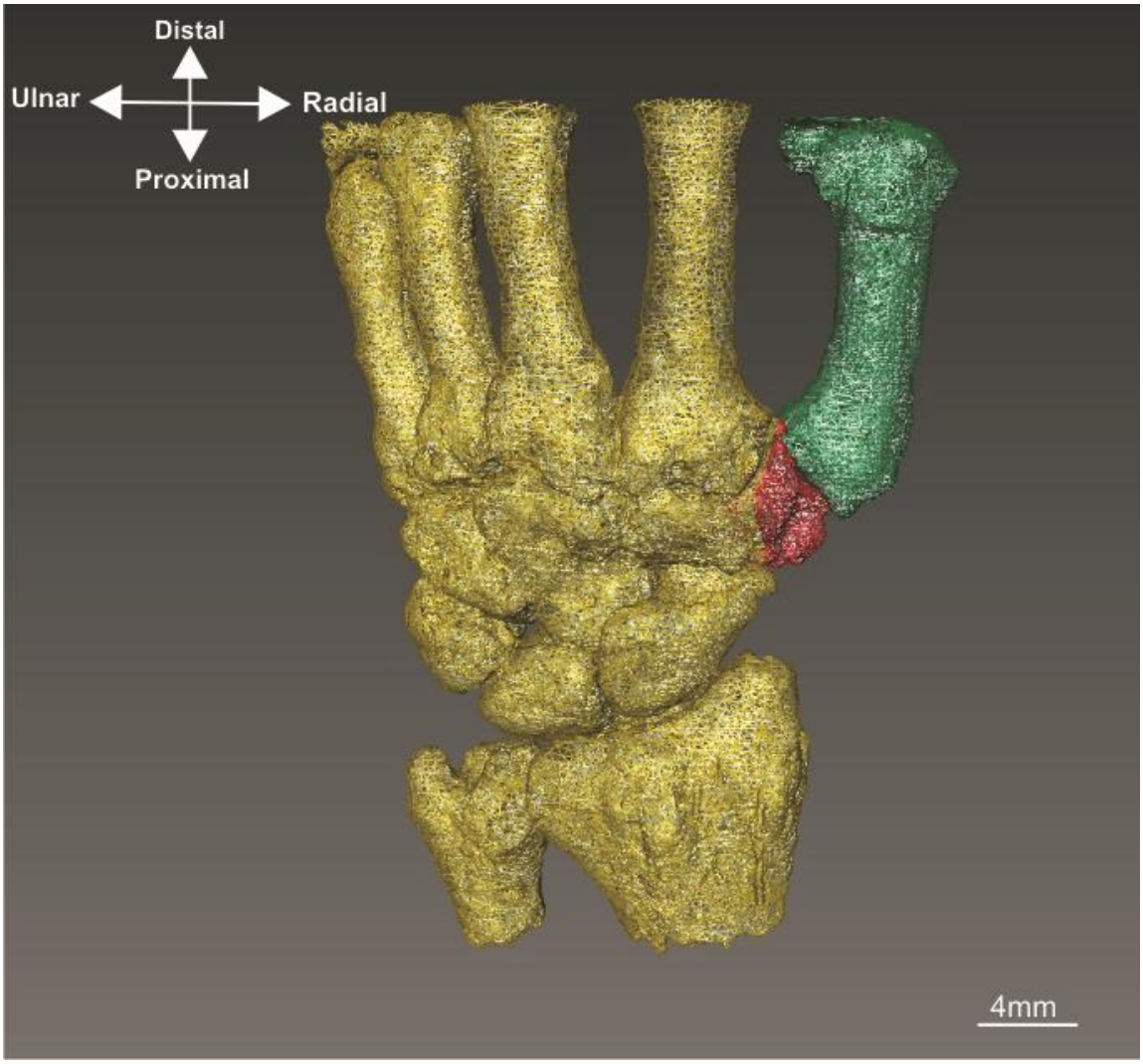

Figure 5.5: 3D dorsal view of the left hand rendered in a virtual space by Amira 3D software. The figure illustrates the 1st MC bones in green and the TM bone in red.

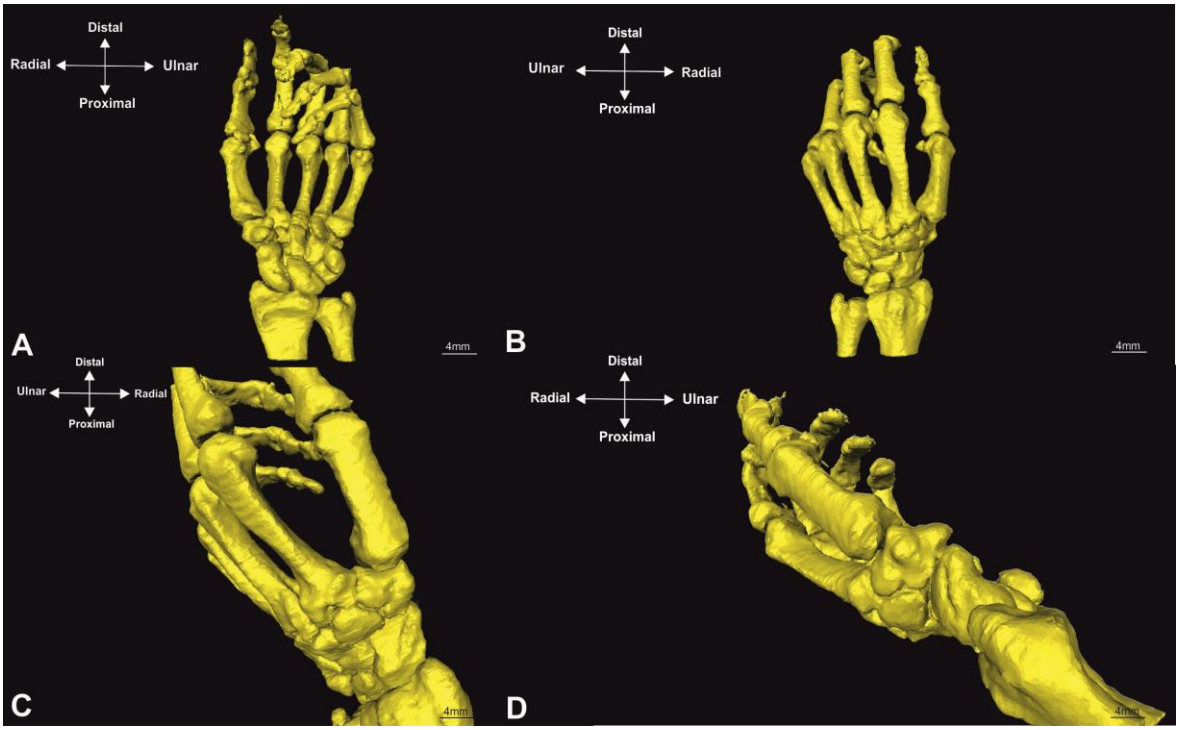

Figure 5.6: Multiple views of a whole hand. Bones rendered in a 3D virtual space by Amira 3D software.
A. Palmar view B. Dorsal view C. Radial view D. Radio-distal view.

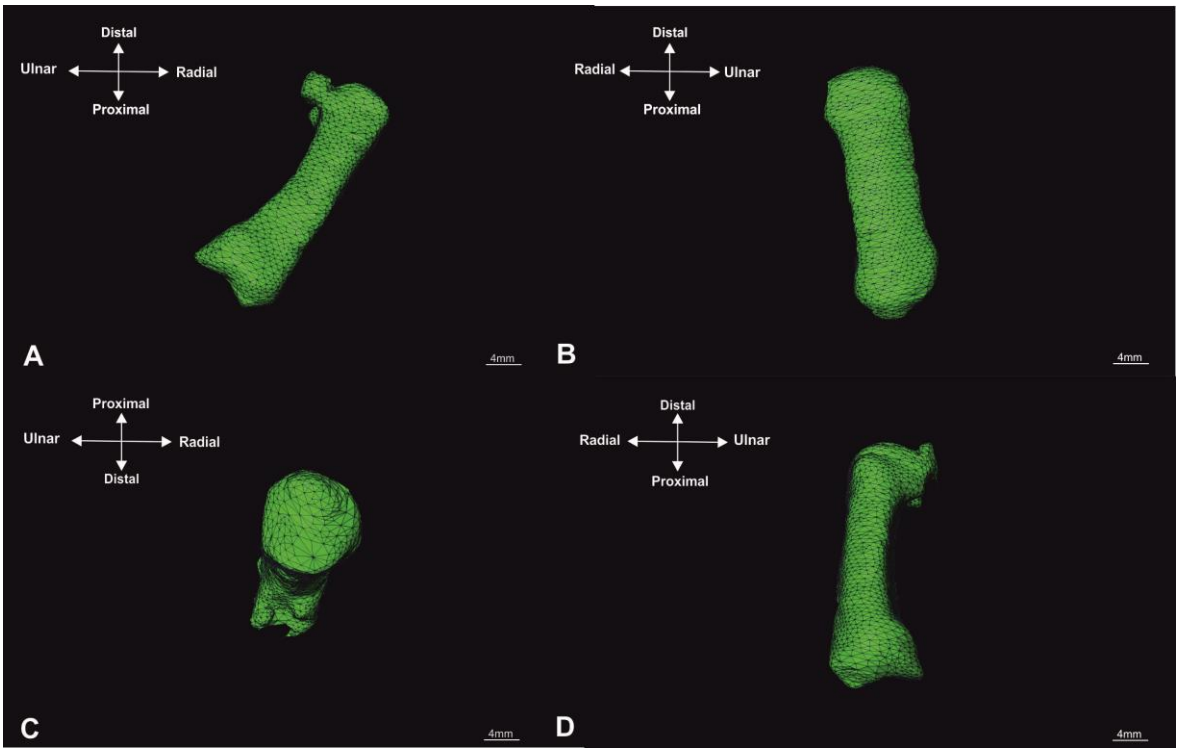

Figure 5.7: Multiple views of the 1st MC bone rendered in a 3D virtual space by Amira 3D software. A. Radial view, B. Dorsal view, C. Proximo-distal or facet view, D. Ulnar view.

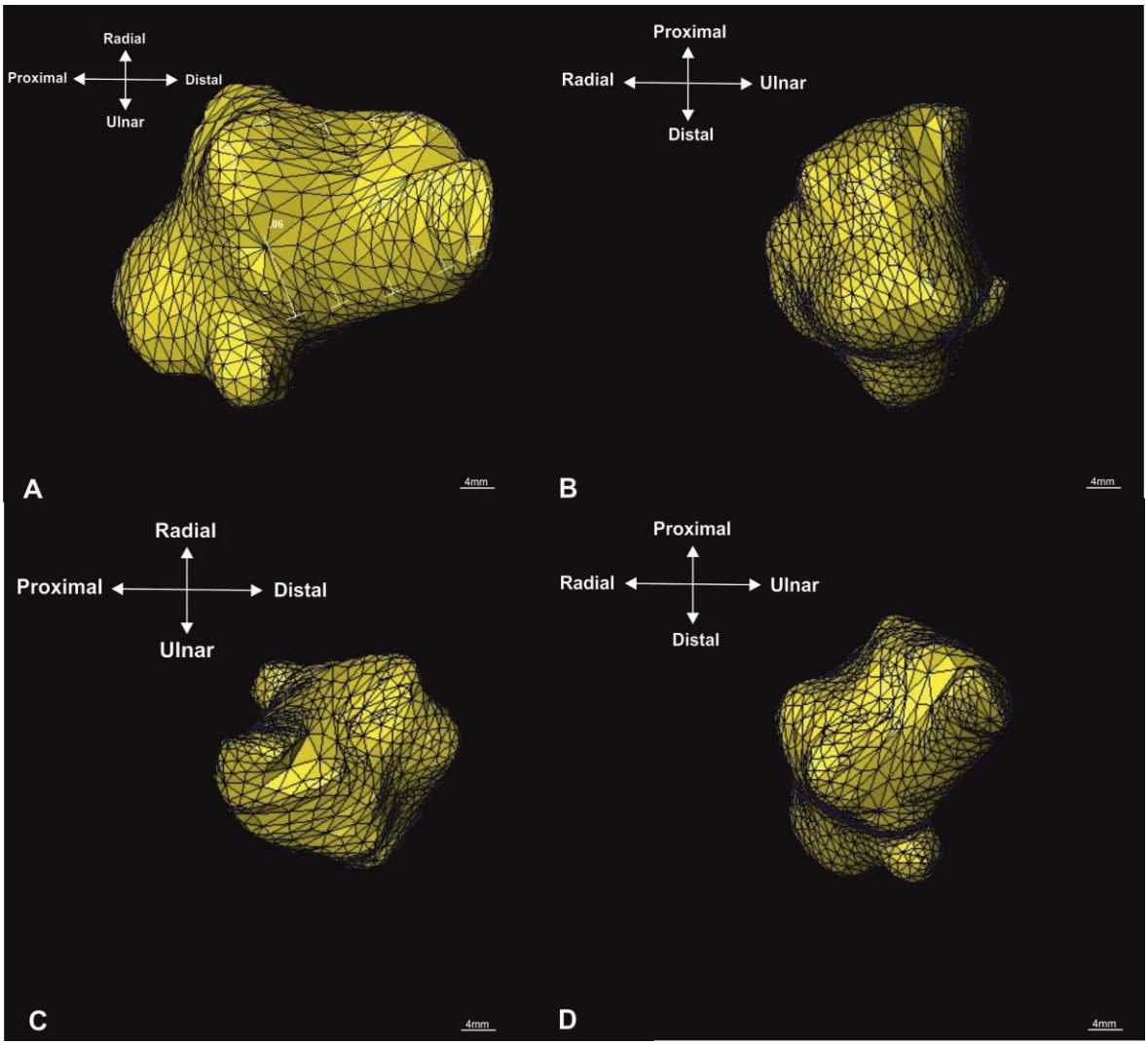

Figure 5.8: Multiple views of the TM bone rendered in a 3D virtual space by Amira 3D software. A. radial view, B. palmo-ulnar view, C. dorso-ulnar view, D. palmo-radial view.

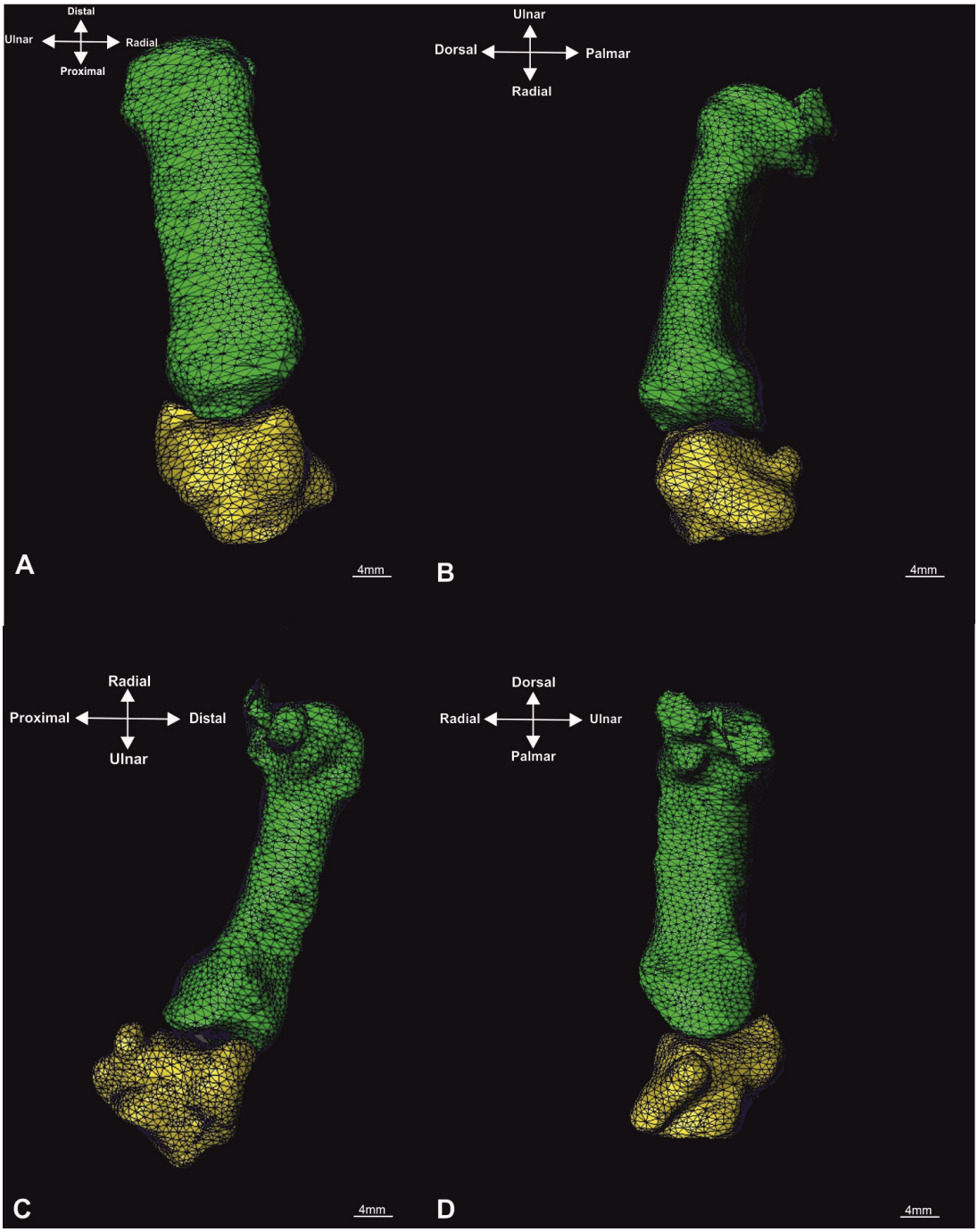

Figure 5.9: Multiple views of the trapeziometacarpal joint (TMC) rendered in a 3D virtual space by Amira 3D software. The figure illustrates the 1st MC bone in green and the TM bone in yellow. A. Dorsal view, B. Radial view, C. Ulnar view, D. Palmar view.

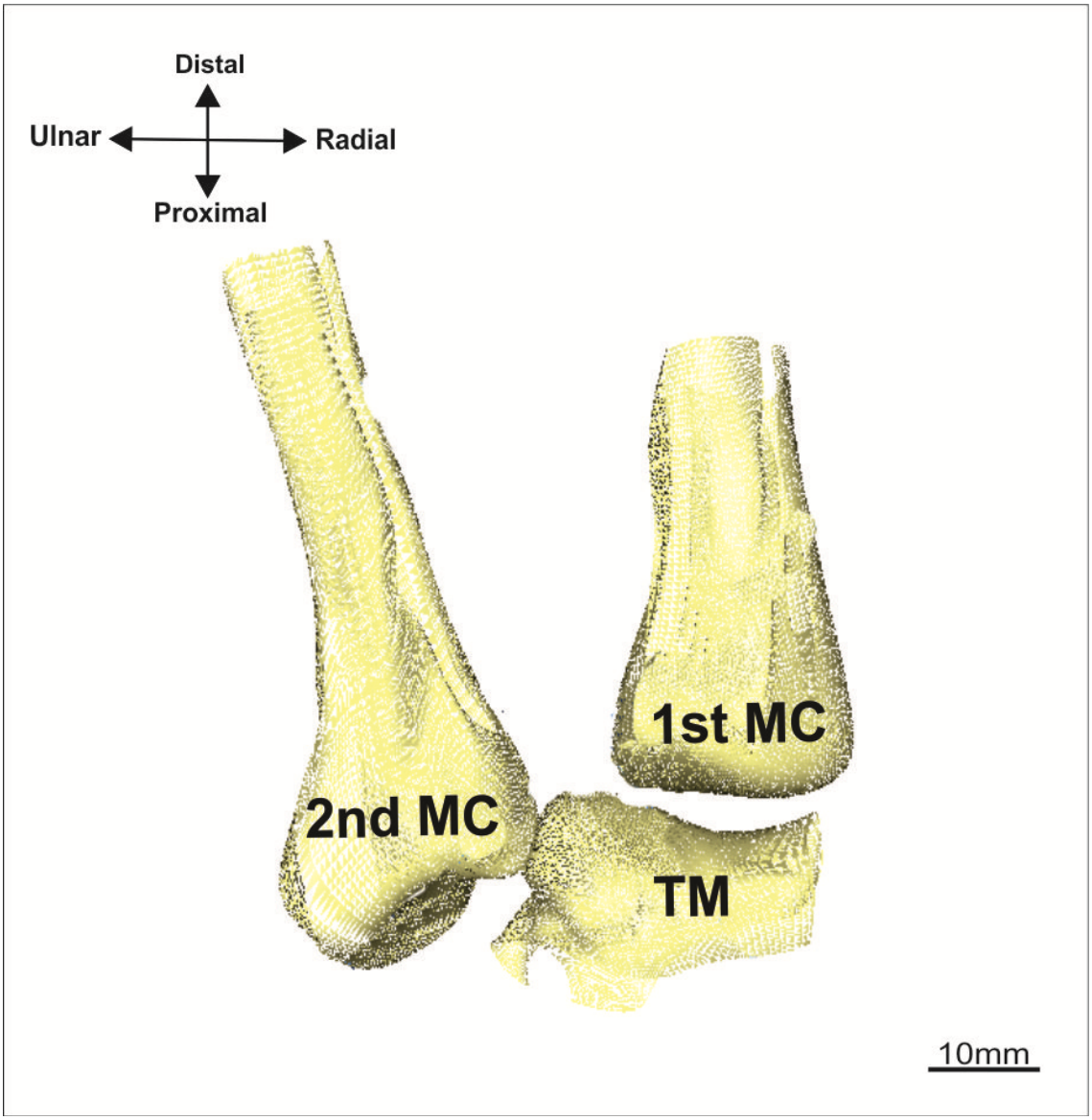

Figure 5.10: The trapeziometacarpal joint (TMC) rendered in a 3D virtual space by Landmark 3D software.TM: trapezium bone, 1st MC: first metacarpal bone, 2nd MC: second metacarpal bone.

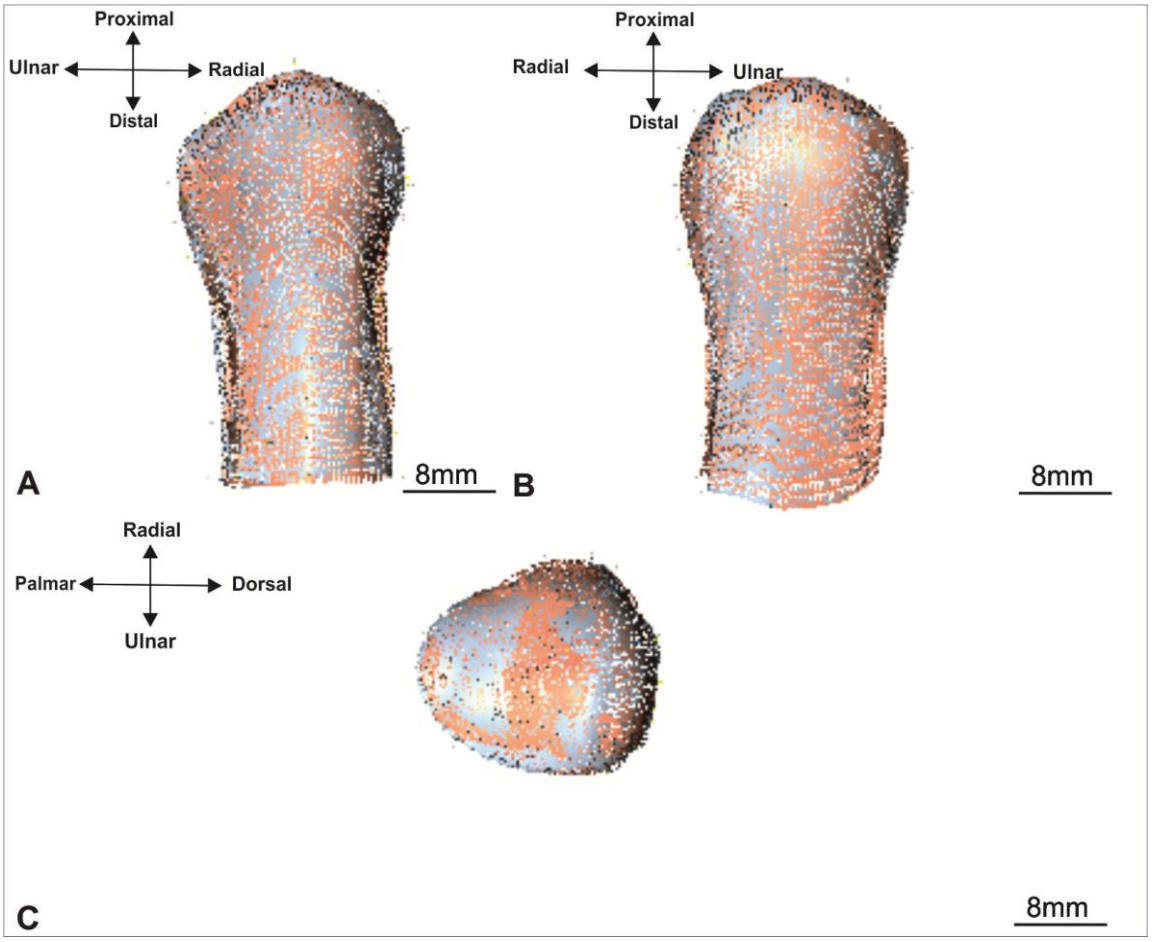

Figure 5.11: Multiple views of the 1st MC bone rendered in a 3D virtual space by Landmark 3D software. A: palmar view, B: dorsal view, C: facet view.

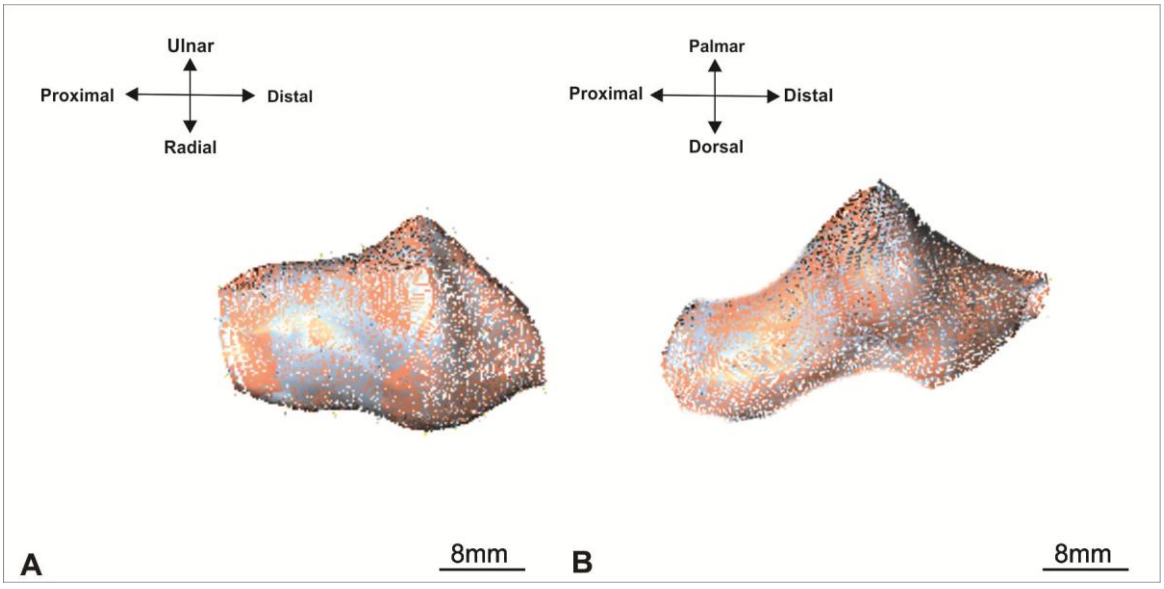

Figure 5.12: Multiple views of the TM bone rendered in a 3D virtual space by Landmark 3D software. A: facet view, B: radial view.

Fifty dry cadaver trapezium and 1st metacarpal bones (25 right and 25 left) of unknown age and sex were used for **Rhinoceros 5.0.** Ten hand cadavers (5 right and 5 left) of unknown age and sex were used for computed tomography with **Amira 3D.** Thirty-two dry cadaver bones of unknown age and sex (8 left TM, 8 right TM, 8 left 1st MC and 8 right 1st MC) were used for **Landmark software.**

The explanation of how each software works can be found previously in this chapter (page 290).

The bones that used for Landmark software were divided into:

1. First stage: Consisted of 16 dry bones of each TM and 1st MC, distributed into 8 groups; group A, group B, group C, group D, group E, group F, group G, and group H (Figures 5.13–5.14). Each group had 2 dry bones. The landmark software would analyse and process the bones to produce a new 3D modelled shape of the bones. This procedure needed to preserve some points on a whole shape of the bone and would neglect some points that were not a necessary to model the shape of the bone. Thus, the trapezium (TM) bone was divided into two views: facet view (view of 1st metacarpal facet of the trapezium bone), and radial view (radially direction of 1st metacarpal facet of the trapezium bone). Those divisions were made based on the articulation area between trapezium and 1st metacarpal bones (Figure 5.12). The 1st metacarpal (1st MC) bone was divided into three views: palmar view, dorsal view and facet view (trapezium facet of 1st MC) (Figure 5.11).

2. Second stage: Consisted of four groups. Group A1 combined groups A and B. Group B1 combined groups C and D. Group C1 combined groups E and F. Group D1 combined groups G and H (Figures 5.13–5.14-5.15-5.16).

3. Third stage: Consisted of two groups. Group A2 combined groups A1 and B1. Group B2 combined groups C1 and D1 (Figures 5.13–5.14-5.15-5.16).

4. Final stage: Combined groups A2 and B2 (Figure 5.17). The landmark software merged the dry bones at a specific single point placed on the surface. The single point coordination method will be explained in detail separately for the TM and 1st MC bones later in this chapter.

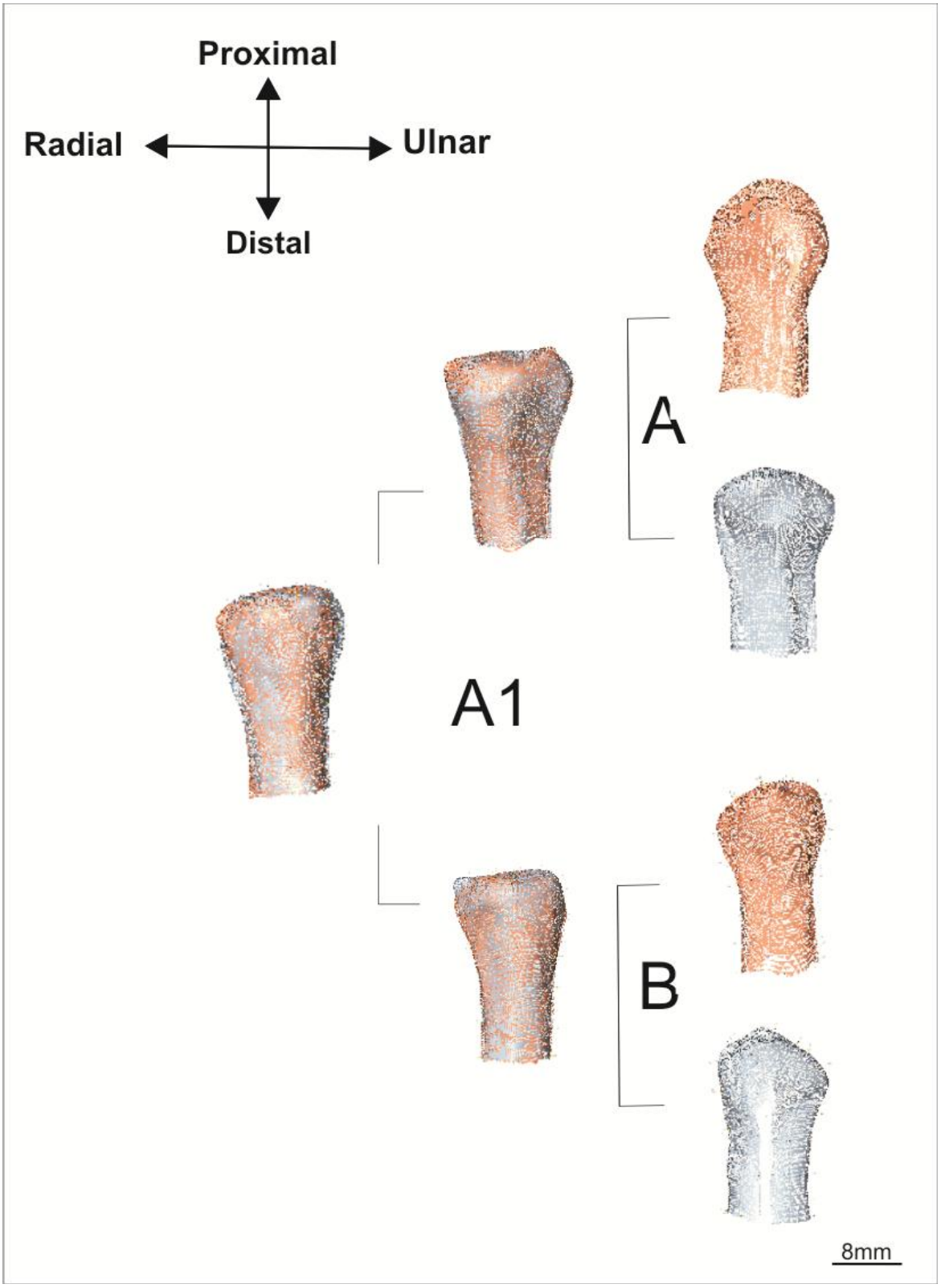

Figure 5.13: First, second and third stages of the division the 1st MC bone using Landmark 3D software. The figure illustrates the division of the 1st MC bone into: groups A, B and their summation which was A1.

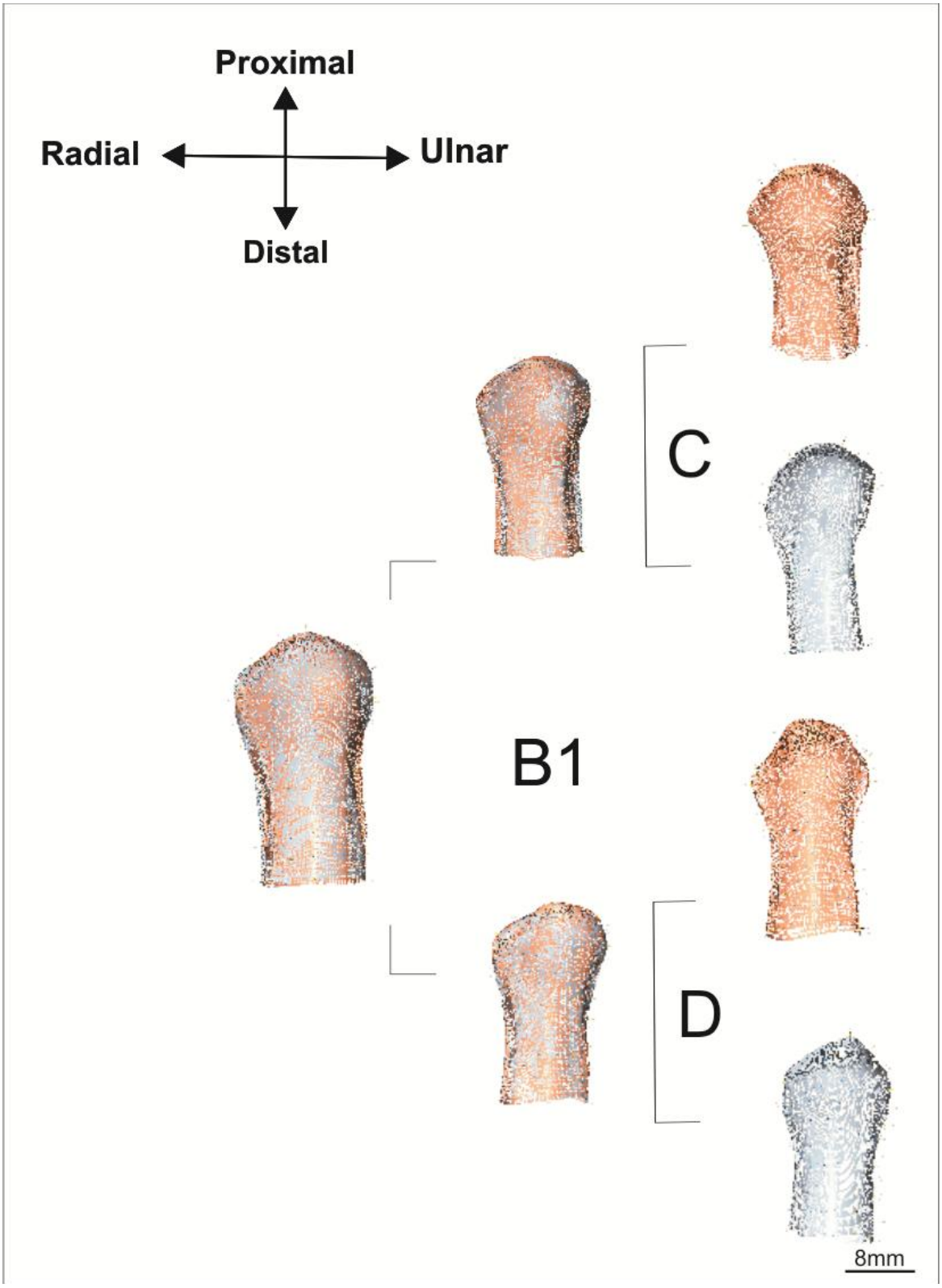

Figure 5.14: First, second and third stages of the division the 1st MC bone using Landmark 3D software. The figure illustrates the division of the 1st MC bone into: groups C, D and their summation which was B1.

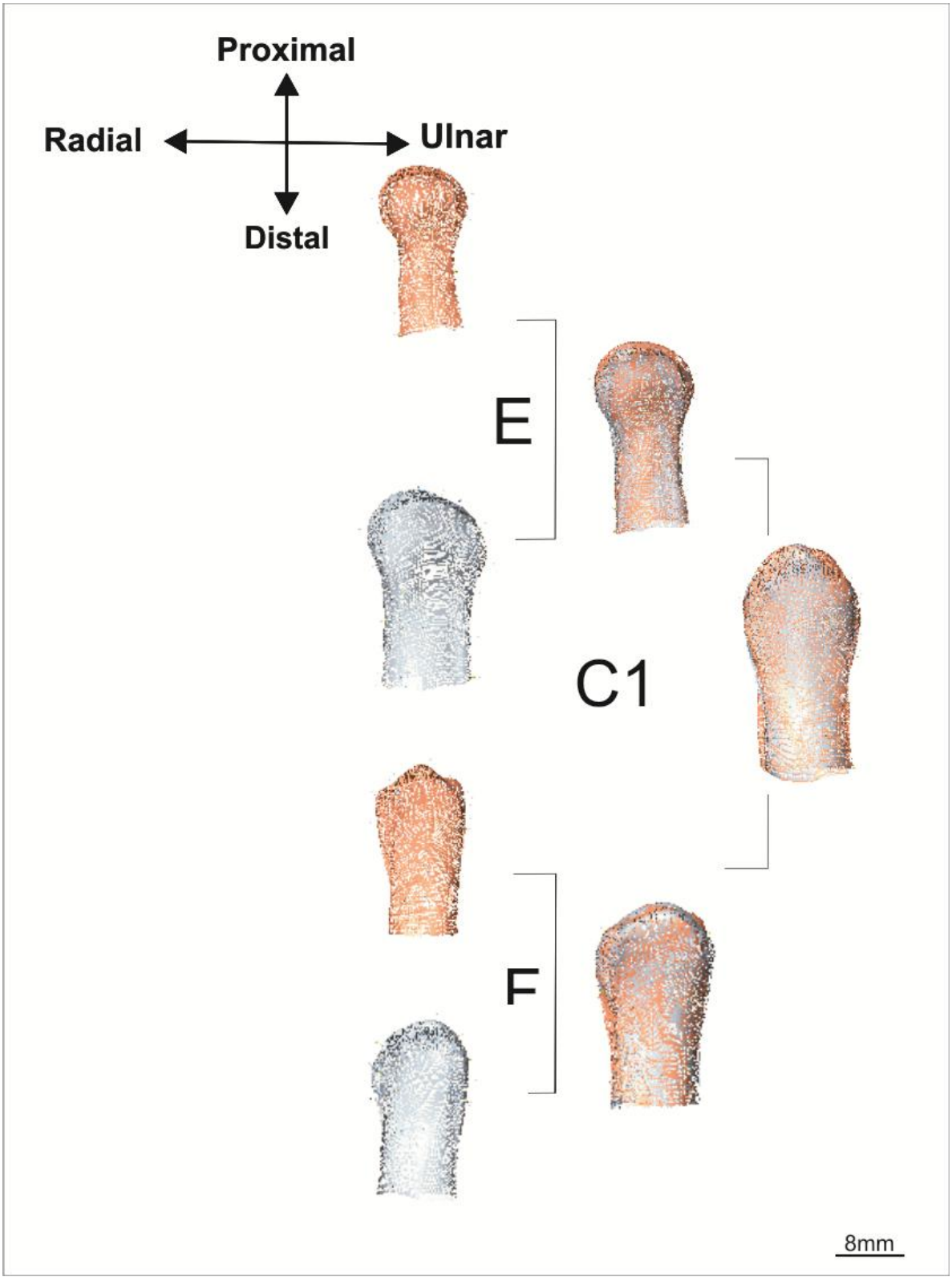

Figure 5.15: First, second and third stages of the division the 1st MC bone by Landmark 3D software. The figure illustrates the division of the 1st MC bone into groups: groups E, F and their summation which was C1

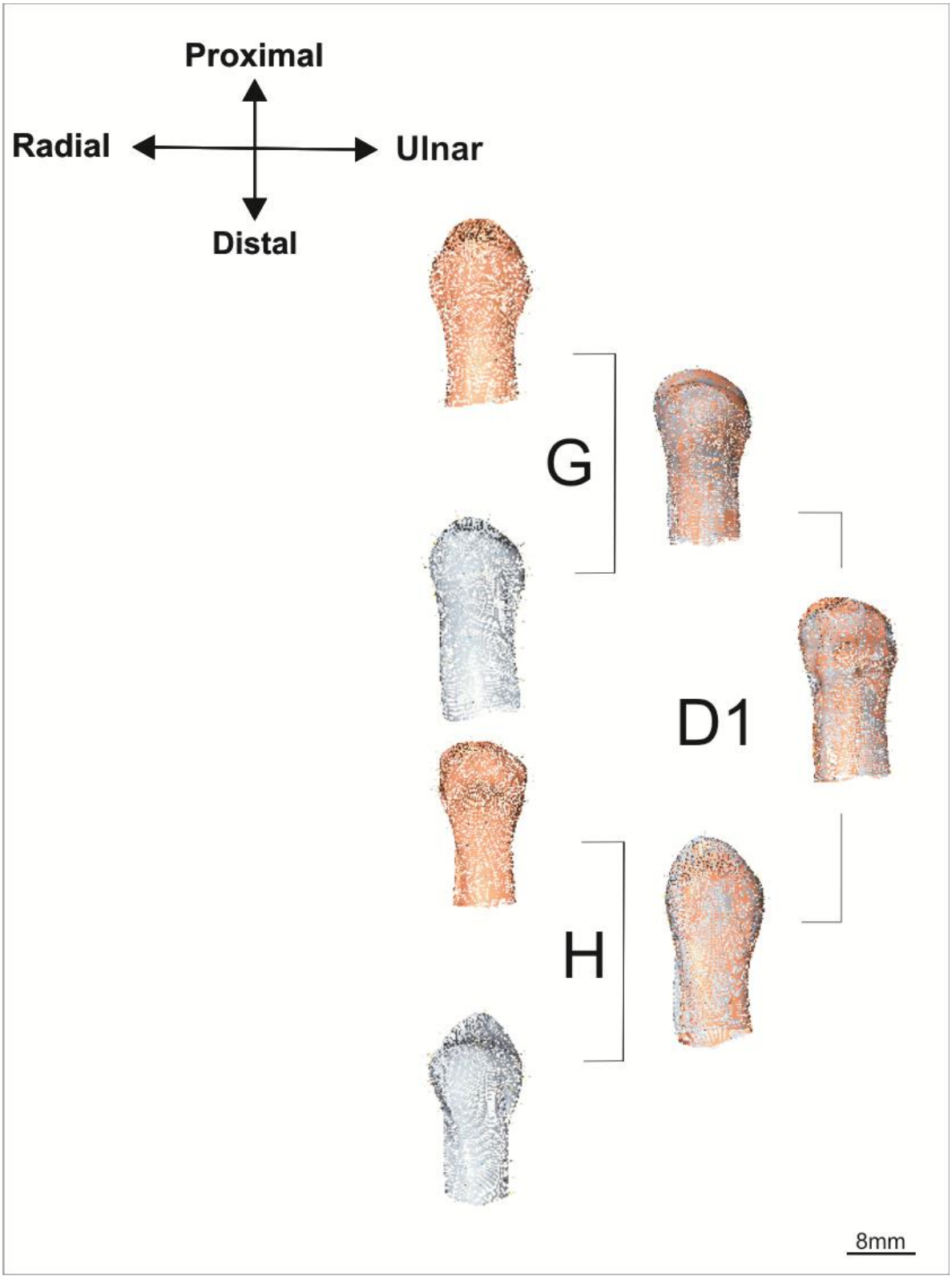

Figure 5.16: First, second and third stages of the division the 1st MC bone by Landmark 3D software. The figure illustrates the division of the 1st MC bone into groups: groups G, H and their summation which was D1

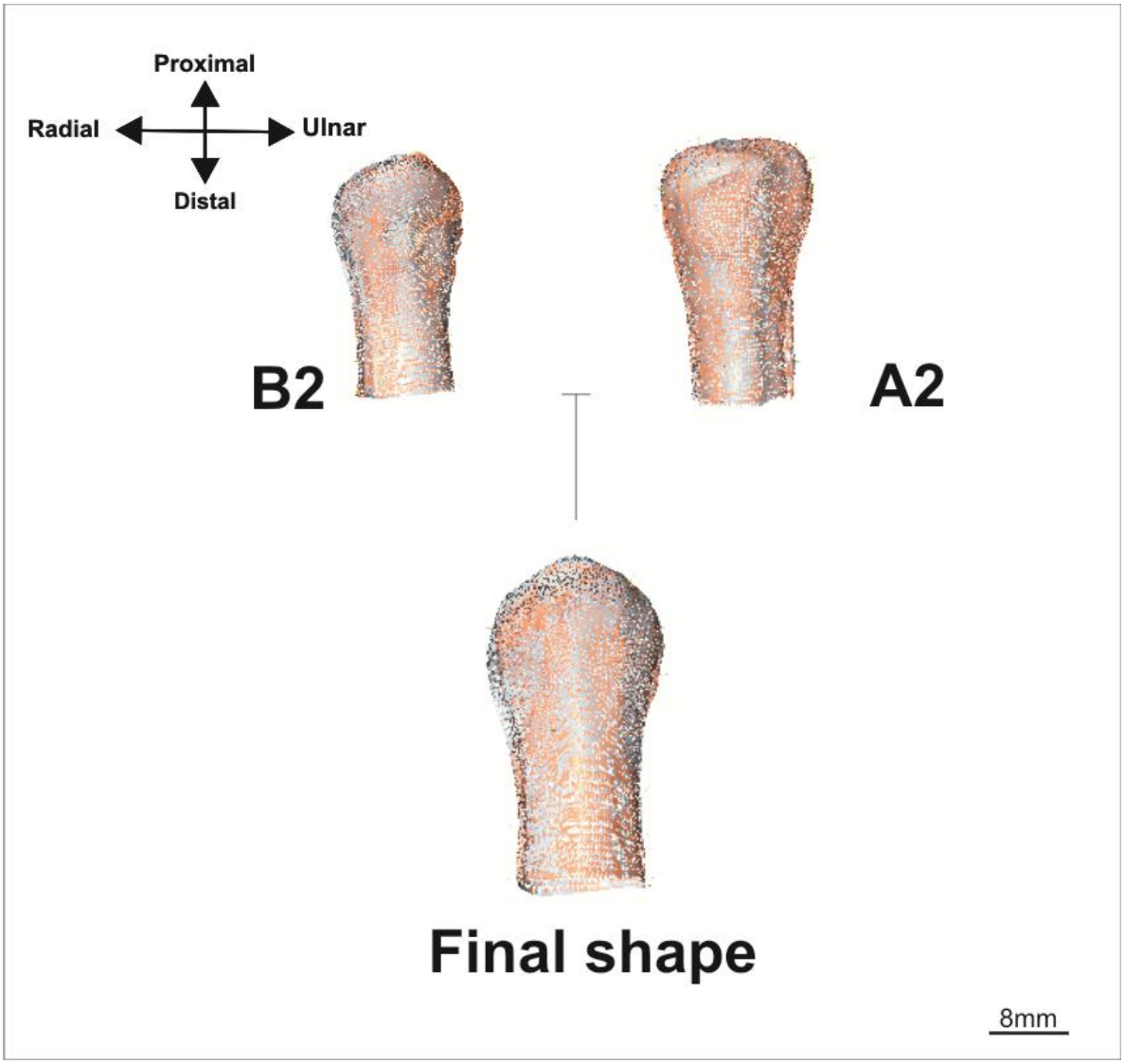

Figure 5.17: Final stage of the division the 1st MC bone by Landmark 3D software. The figure illustrates B2, which was the summation of C1 and D1, and A2, which was the summation of A1 and B1.

5.2.2 Morphological analysis

The TM has three facets:

1) the largest is with the 1st MC bone, where it has a concavo-convex shape, 2) with the trapezoid bone, where it is concave at ulnar surface, and 3) with scaphoid bone, where it is slightly concave at the proximal surface. The TM also has four surfaces: palmar, dorsal, proximal and distal. The shape of the 1st MC described mainly from the palmar, dorsal surfaces and from its facet with the trapezium (Nanno *et al.* 2006a; Snell 1995; Snell 2004).

5.2.2.1 Trapezium bone (TM)

The trapezium consist of four surfaces:

1) The palmar surface which has the palmar tubercle and a groove for the tendon of flexor carpi radialis.

2) The dorsal surface which is rough and has dorso-ulnar tubercle that elongates at the ulnar side; the branches of the radial artery lie in this situation; it also has a dorso-radial tubercle that has a longer projection than dorso-ulnar tubercle.

3) The proximal surface has a facet with scaphoid bone; the facet of the trapezoid bone goes ulnarly to the scaphoid facet (Figures 5.18-5.19).

4) The only large facet of the TM bone was 1st MC facet, and it lies at the radial-side articulation with the 1st MC bone to contain the trapeziometacarpal joint (TMC). There was a small trapezial ridge at the palmar surface most nearly to the ulnar side of the trapezium bone. The radial tubercle sits at the radial side, and it was considered one of the most prominent tubercle of the trapezium bone (Figures 5.20-5.21).

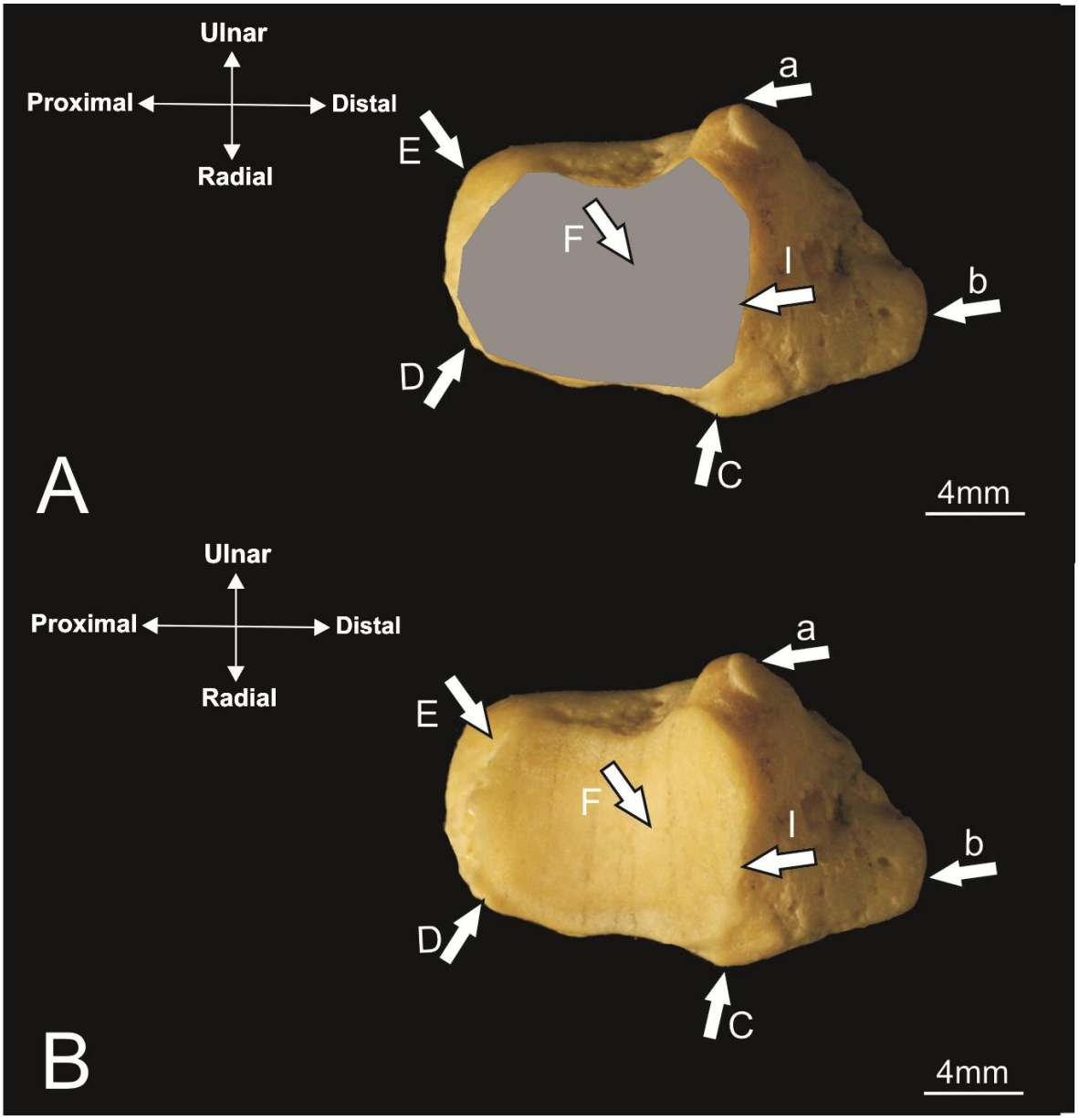

Figure 5.18: Radial view of the right TM bone. a: eminence of the trapezial ridge, b: radial tubercle, C: dorso-ulnar tubercle, D: dorso-radial tubercle, E: palmar tubercle, F: facet of 1st MC of TM bone, I: distal border of 1st MC.

A. Dry TM bone, the articular surface with first metacarpal bone coloured by Grey colour to illustrates a whole facet area.
B. Dry TM bone.

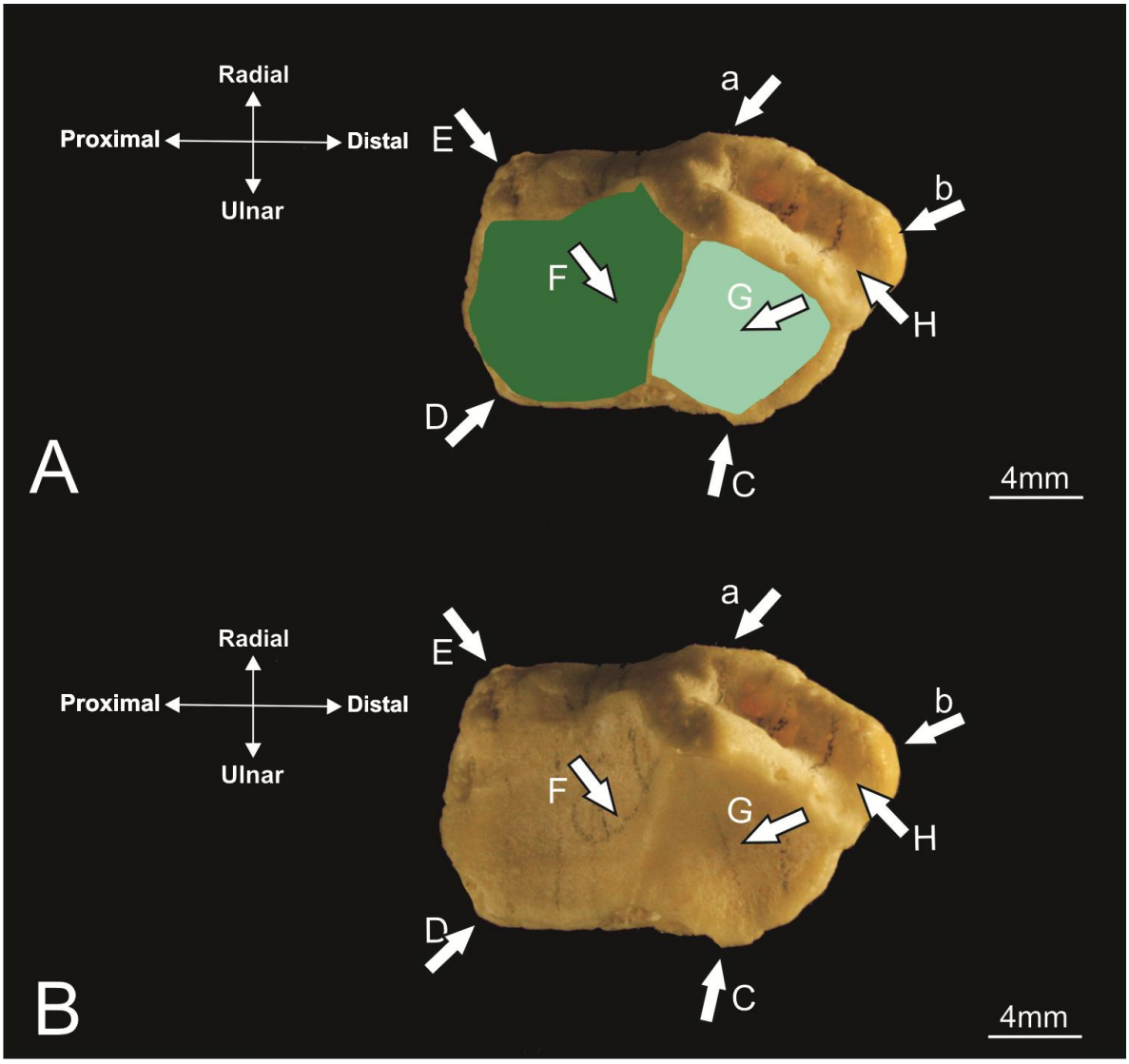

Figure 5.19: Ulnar view of the right TM bone. a: eminence of the trapezial ridge, b: radial tubercle, C: dorso-ulnar tubercle, D: dorso-radial tubercle, E: palmar tubercle, F: facet of trapezoid bone, G: facet of the scaphoid bone, H: groove of the palmar surface for flexor carpi radialis tendon.

A. Dry TM bone, the articular surface with trapezoid bone coloured by dark green colour. And the articular surface with scaphoid bone coloured by light green colour to illustrates a whole facet area.
B. Dry TM bone.

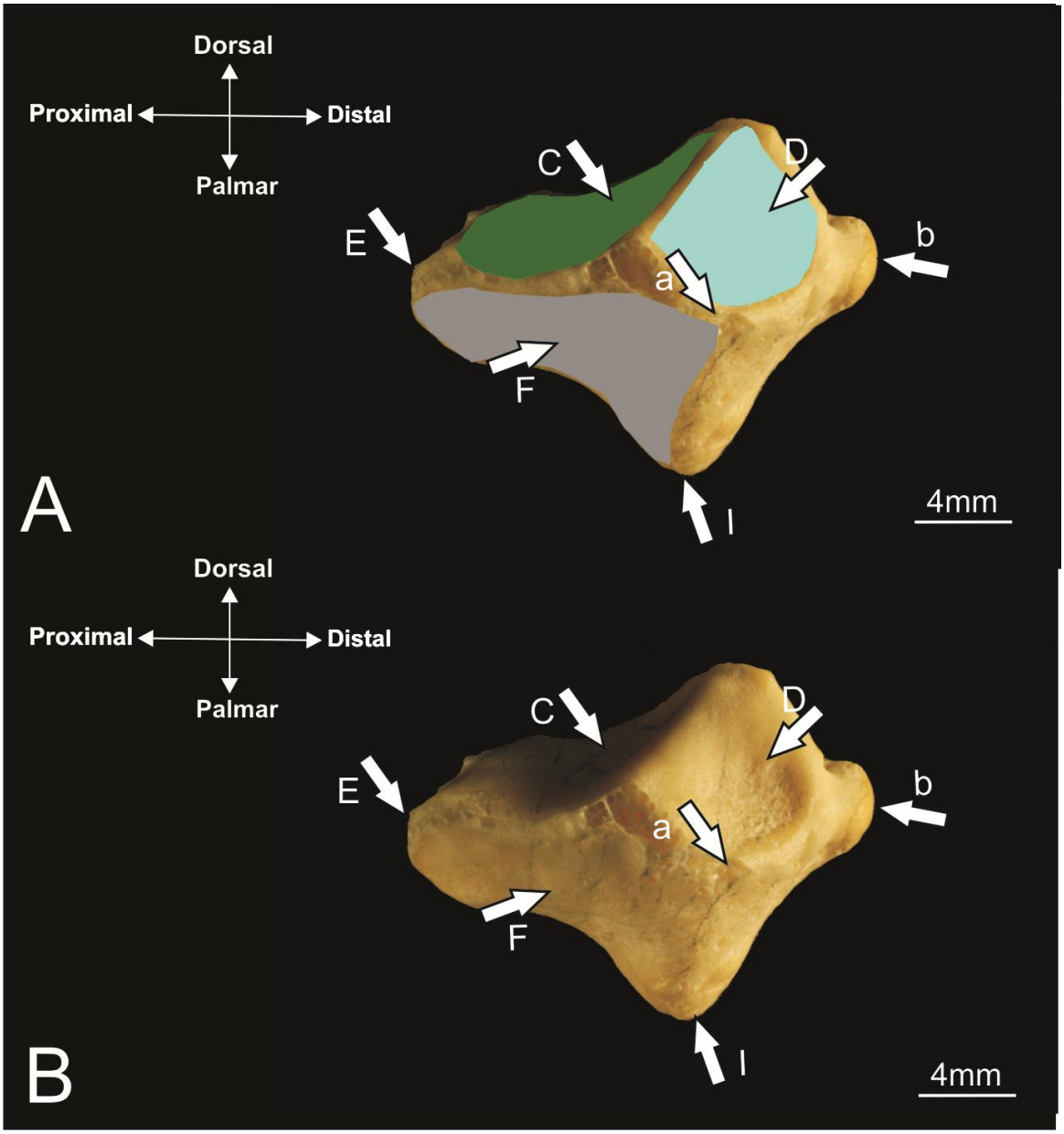

Figure 5.20**:** Dorsal view of the right TM bone. a: eminence of the trapezial ridge, b: radial tubercle, C: facet of trapezoid bone, D: facet of the scaphoid bone, E: palmar tubercle, F: facet of 1st MC of TM bone, I: distal border of the 1st MC facet of the TM bone.

A. Dry TM bone, the articular surface with trapezoid bone coloured by dark green colour. And the articular surface with scaphoid bone coloured by light green colour, the articular surface with first metacarpal bone coloured by Grey colour to illustrates a whole facet area.
B. Dry TM bone.

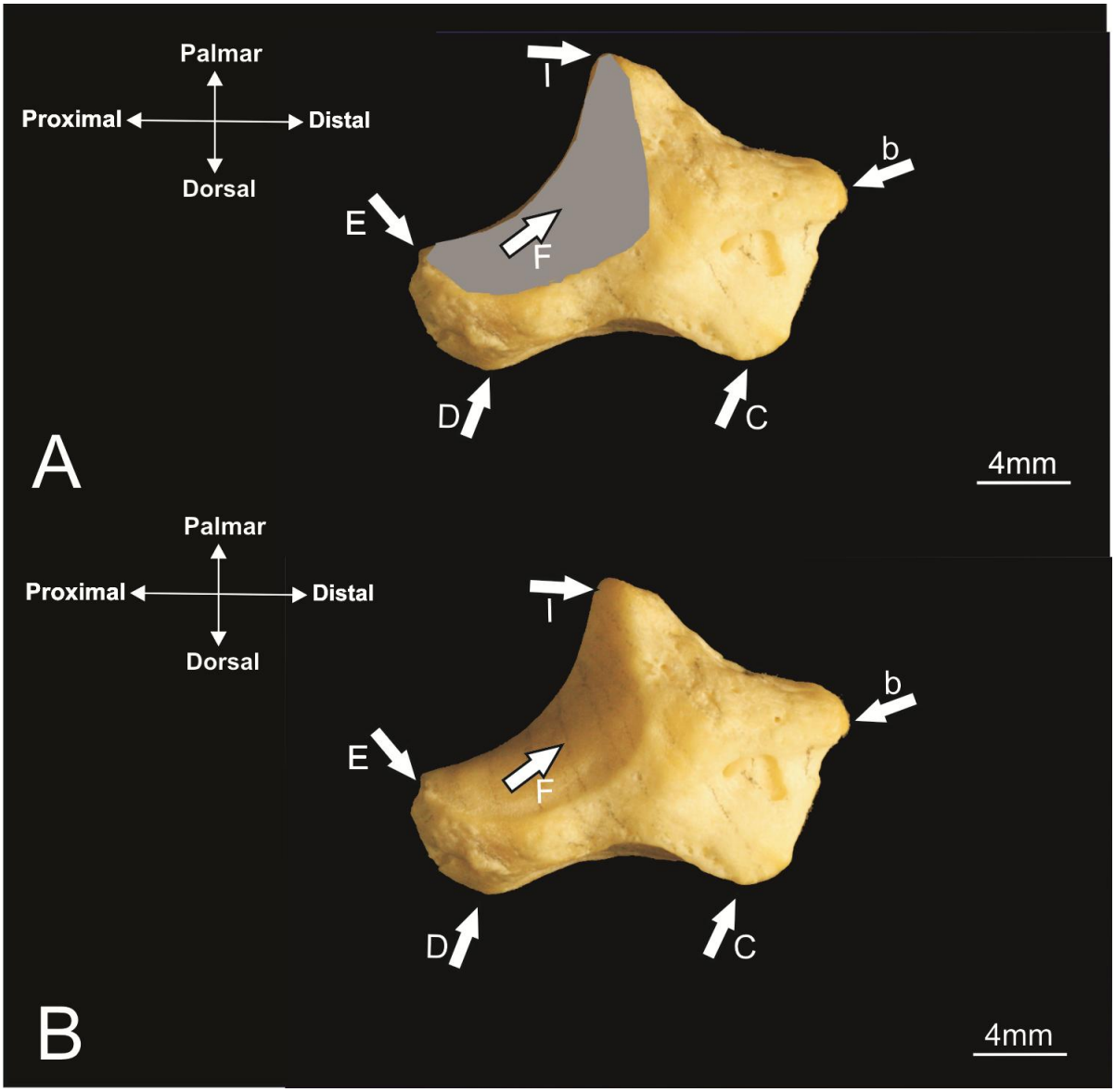

Figure 5.21: Palmar view of the right TM bone. b: radial tubercle, C: dorso-ulnar tubercle, D: dorso-radial tubercle, E: palmar tubercle, F: facet of 1st MC of TM bone, I: distal border of the 1st MC facet of the TM bone.

A. Dry TM bone, the articular surface with first metacarpal bone coloured by Grey colour to illustratesa whole facet area.
B. Dry TM bone.

5.2.2.2 First metacarpal bone (1st MC)

The palmar surface is longitudinally concave and divided by a ridge into a large lateral or anterior part and smaller ulnar or posterior part. It also has the anterior eminence of the 1st MC facet and the palmo-ulnar tubercle on the ulnar side of the palmar surface. The ridge is called the proximal ridge at the proximal side of the palmar surface of the 1st MC. The proximal ridge in this situation has the highest part and the shortest part appears distally of the base near the middle of the shaft of the 1st MC. At that point it is called the distal ridge (Figures 5.22-5.23-5.24).

Three features appear on the dorsal surface of the 1st MC: 1) the posterior eminence of the 1st MC, 2) the dorso-ulnar tubercle at the ulnar side of the dorsal surface of the 1st MC, and 3) the dorso-radial tubercle at the radial side of dorsal surface of the 1st MC (Figures 5.23-5.24-5.25).

The facet of the 1st MC has two borders: the radial border on the radial side and the ulnar border on the ulnar side. It also has two eminences: the anterior eminence at the edge of the palmar side of the facet, and the posterior eminence at the edge of the dorsal side of the facet. The dorso-ulnar tubercle appears at the dorsal side of the facet distally from posterior eminences (Figure 5.26).

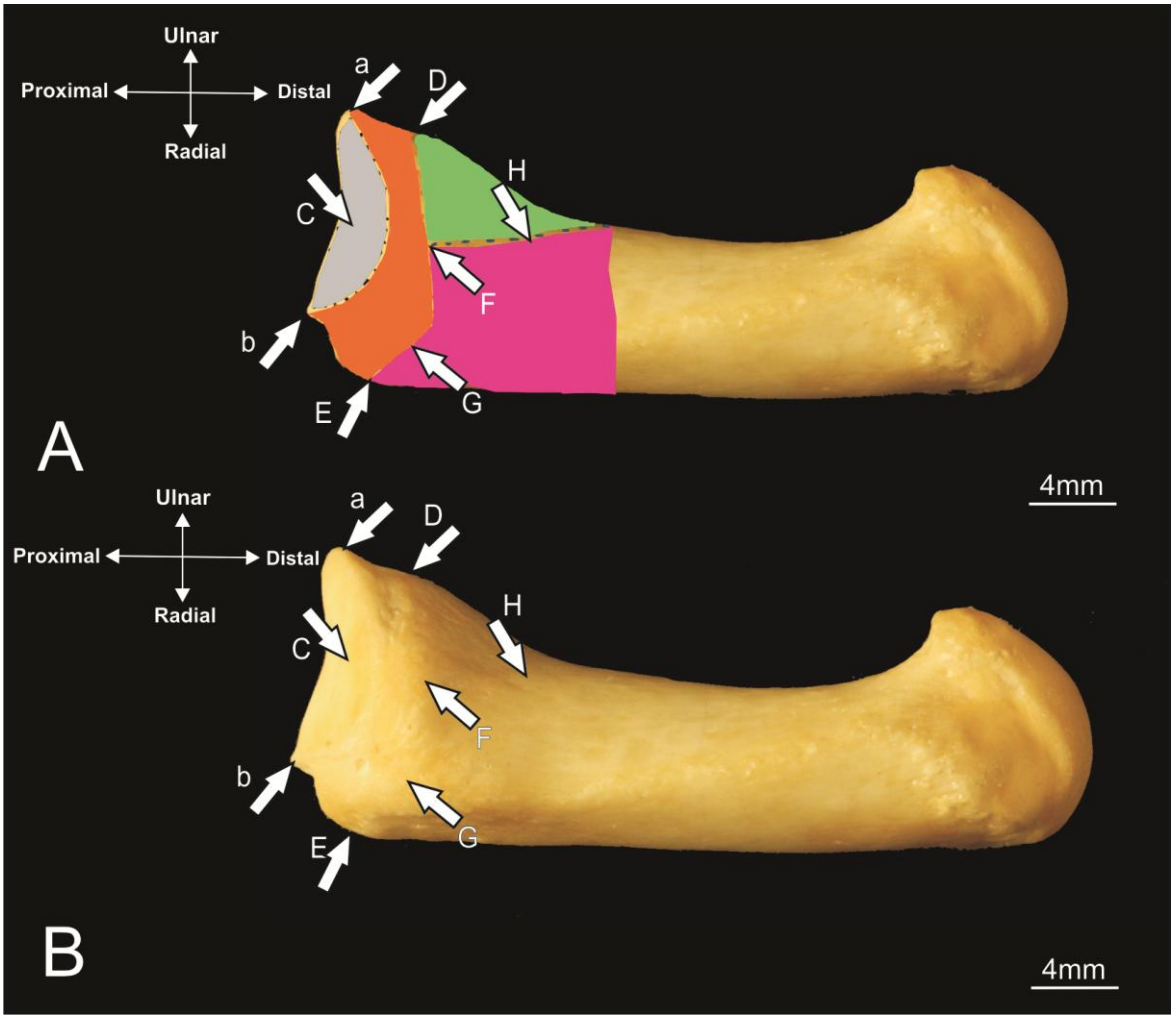

Figure 5.22: Radial view of the right 1st MC bone. a: anterior eminence, b: posterior eminence, C: facet of the TM bone of the 1st MC bone, D: palmo-ulnar tubercle, E: palmo-radial tubercle, F: proximal ridge of palmar surface, G: dorso-ulnar tubercle, H: distal ridge of palmar surface.

A. Dry 1st MC bone, the articular surface coloured by grey colour represents the articular area with TM facet of the 1st MC bone. Orange colour represents the area between the facet of the TM of the 1st MC bone and palmar surface. Green colour represents the area of the small part of ulnar area of the palmar surface of the 1st MC bone. Pink colour represents the area of a large part of the radial area of the palmar surface of the 1st MC bone.
B. Dry 1st MC bone.

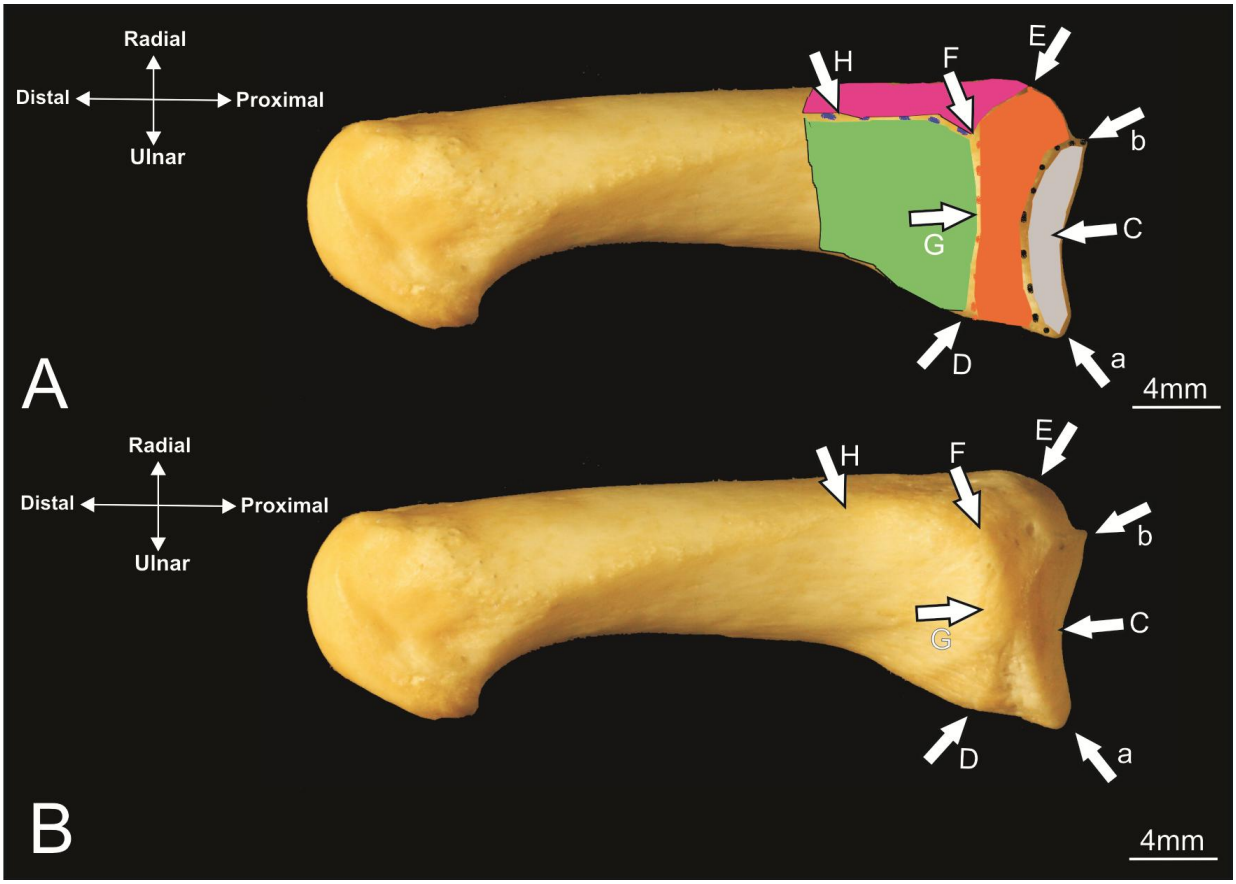

Figure 5.23: Ulnar view of the right 1st MC bone. a: anterior eminence, b: posterior eminence, C: facet of the TM bone of the 1st MC bone, D: palmo-ulnar tubercle, F: proximal ridge of palmar surface, G: dorso-ulnar tubercle, H: distal ridge of palmar surface.

A. Dry 1st MC bone, the articular surface coloured by grey colour represents the articular area with TM facet of the 1st MC bone. Orange colour represents the area between the facet of the TM of the 1st MC bone and palmar surface. Green colour represents the area of the small part of ulnar area of the palmar surface of the 1st MC bone. Pink colour represents the area of a large part of the radial area of the palmar surface of the 1st MC bone.
B. Dry 1st MC bone.

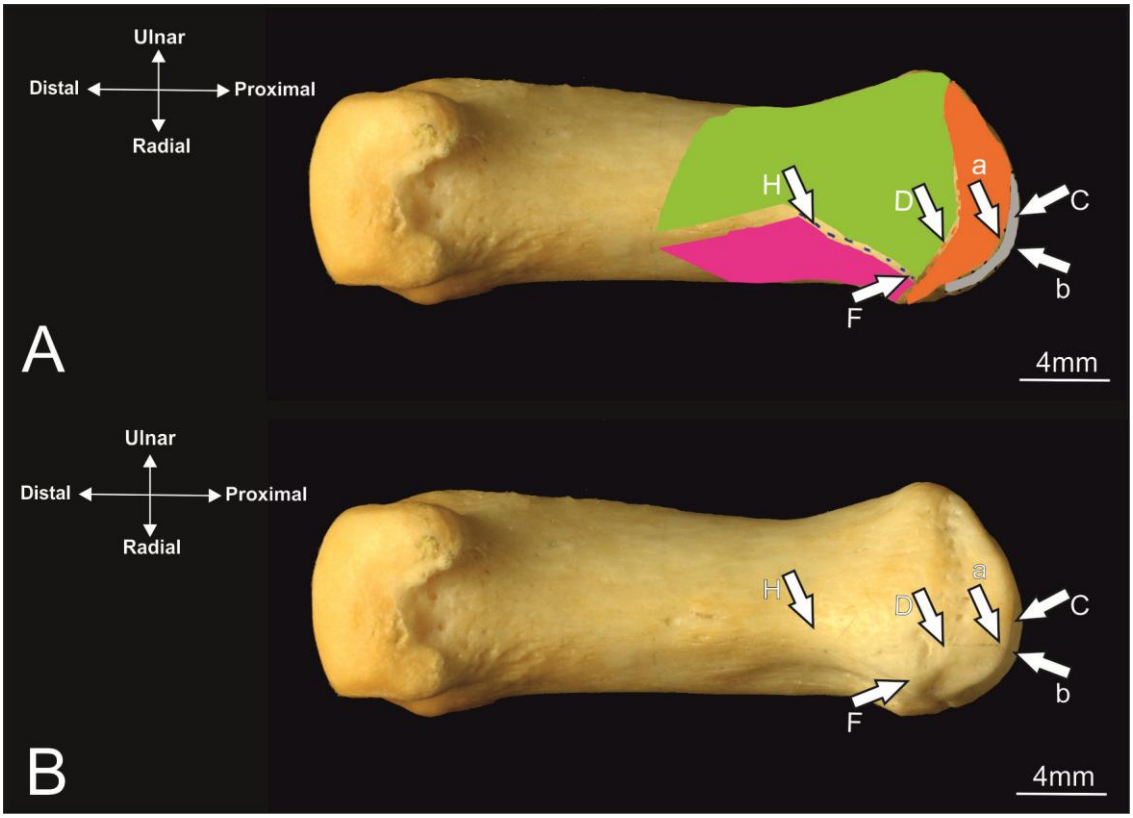

Figure 5.24: Palmar view of the right 1st MC bone. a: anterior eminence, b: Posterior eminence, C: Facet of the TM bone of the 1st MC bone, D: Palmo-ulnar tubercle, F: Proximal ridge of palmar surface, H: Distal ridge of palmar surface.

A. Dry 1st MC bone, the articular surface coloured by grey colour represents the articular area with TM facet of the 1st MC bone. Orange colour represents the area between the facet of the TM of the 1st MC bone and palmar surface. Green colour represents the area of the small part of ulnar area of the palmar surface of the 1st MC bone. Pink colour represents the area of a large part of the radial area of the palmar surface of the 1st MC bone.
B. Dry 1st MC bone.

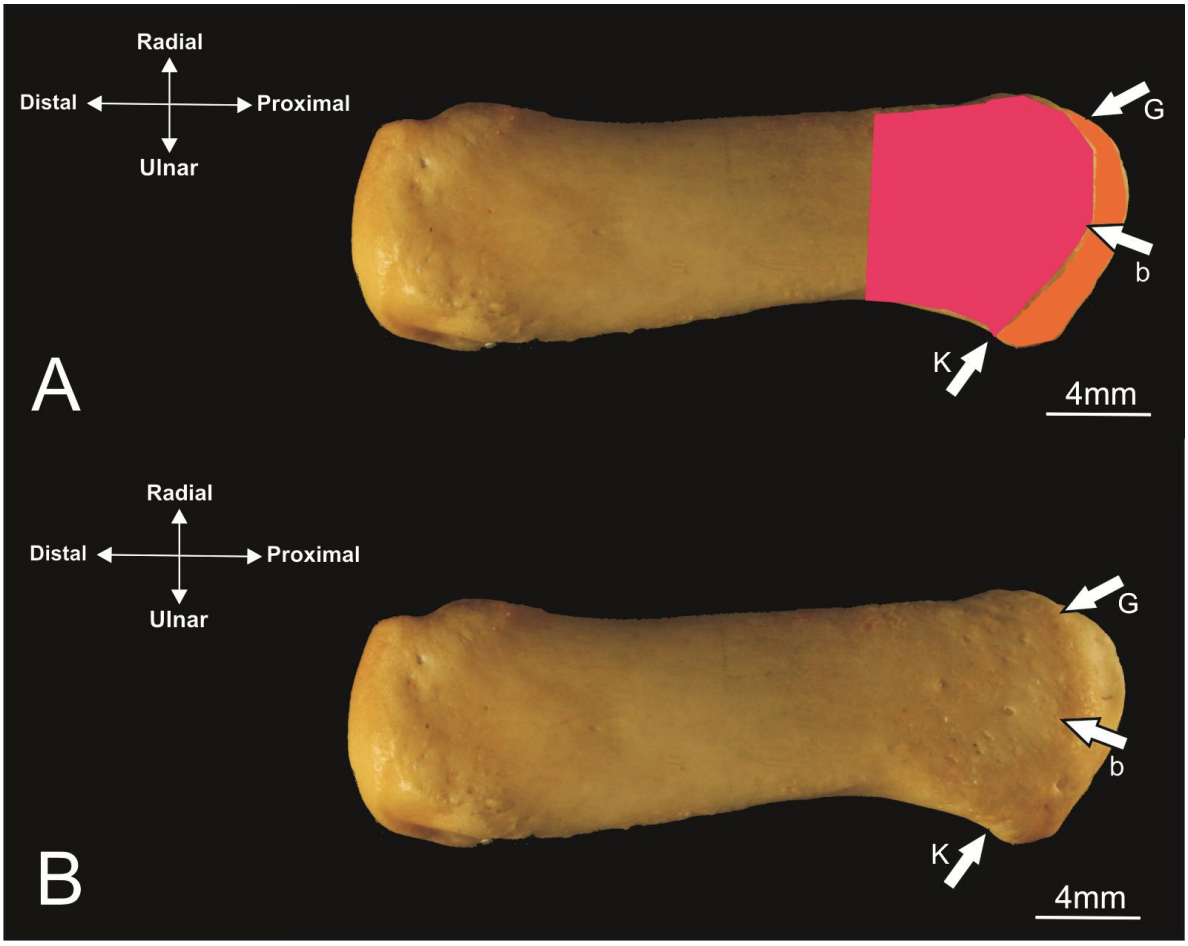

Figure 5.25: Dorsal view of the right 1st MC bone. b: posterior eminence, G: dorso-ulnar tubercle, K: dorso-radial tubercle.

A. Dry 1st MC bone. pink colour represents the area of the base of the 1st MC at the dorsal surface of the 1st MC bone. Orange colour represents the area between the facet of the TM of the 1st MC bone and dorsal surface.
B. Dry 1st MC bone.

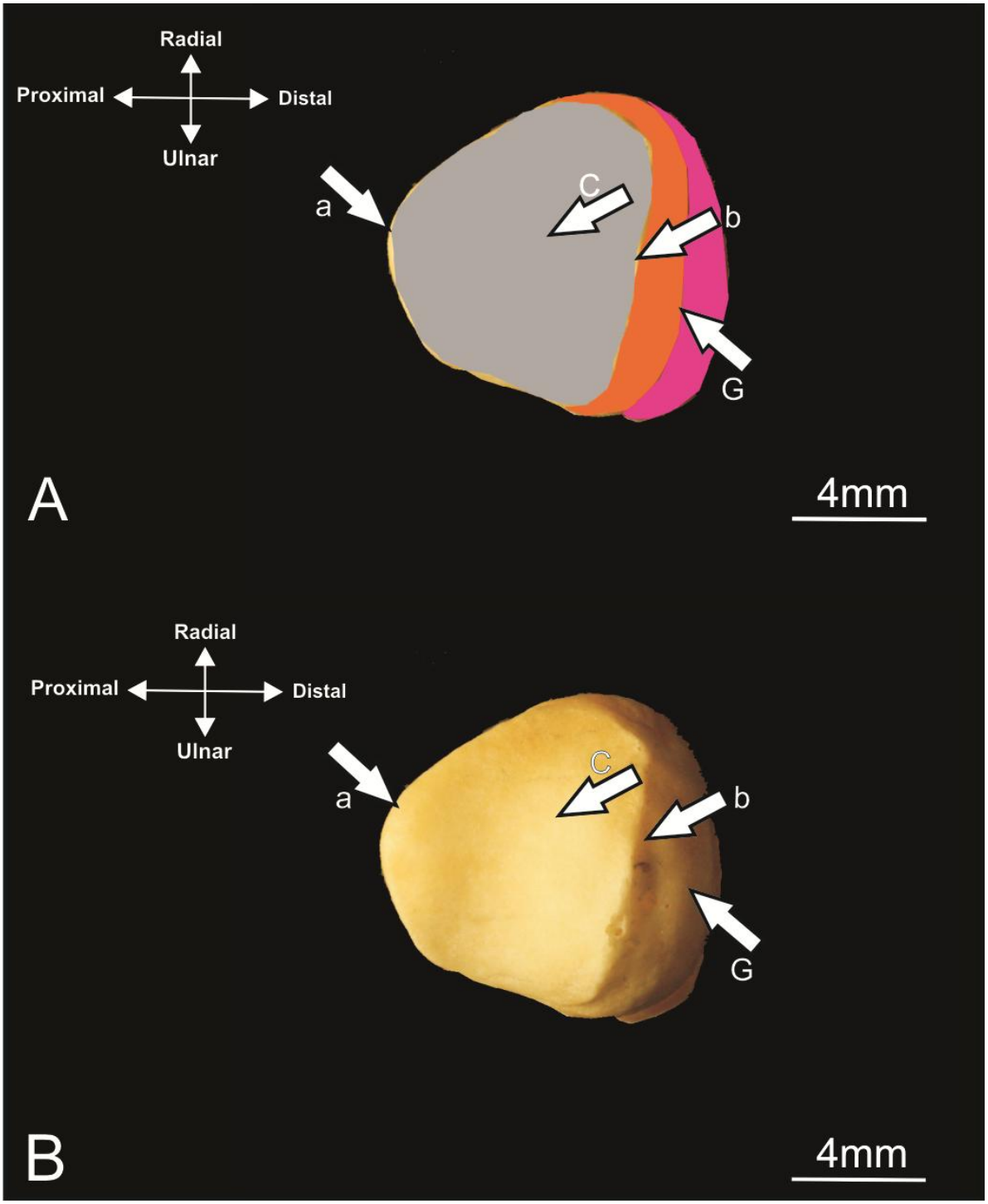

Figure 5.26: Facet view of the right 1st MC bone. a: anterior eminence, b: posterior eminence, C: facet of the TM bone of the 1st MC bone, G: dorso-ulnar tubercle.

A. Dry 1st MC bone. Grey colour represents the articular area with the TM bone. Orange colour represents the area between the facet of the TM of the 1st MC bone and dorsal surface. Pink colour represents the area of the base of the 1st MC at dorsal surface of the 1st MC bone.
B. Dry 1st MC facet.

5.2.3 Single point coordination

Single point coordination distributes points over the whole surface of the model based on the curvatures, prominences, and declines of the surface. The process of distributing the points by special software tools, which is called single point coordination, merges both models together using these points to make a new model. This model has a median between the two models. Also, the importance of these points comes from the critical position of the each point along the surface of model. The mechanics of how these points work are mentioned earlier in this chapter (page 290).

5.2.3.1 Trapezium bone (TM)

Five coordination points on the TM bone, from the radial view or in the radial direction of 1st MC facet of the TM bone, are depicted as follows (Figure 5.27):

1. Point 1. Trapezial-radial point (TR1): This point was set at the distal border of the 1st MC facet.
2. Point 2. Trapezial-radial point (TR2): This point was set at the radial tubercle of the 1st MC bone.
3. Point 3. Trapezial-radial point (TR3): This point was set at the dorso-ulnar tubercle of the 1st MC bone.
4. Point 4. Trapezial-radial point (TR4): This point was set at the dorso-radial tubercle of the 1st MC bone.
5. Point 5. Trapezial-radial point (TR5): This point was set at the palmar tubercle of the 1st MC bone.

Four coordination points on the TM bone from the facet view were depicted as follows (Figure 5.28):

1. Point 1. Trapezial-distal point (TD1): This point was set disto-radially at the radial tubercle.

2. Point 2. Trapezial- distal point (TD2): This point was set disto-radially at the eminence of the trapezial ridge.

3. Point 3. Trapezial-distal point (TD3): This point was set disto-radially from the border of the facet at the dorso-radial tubercle.

4. Point 4. Trapezial-distal point (TD4): This point was set disto-radially from the border of the facet at the palmar tubercle.

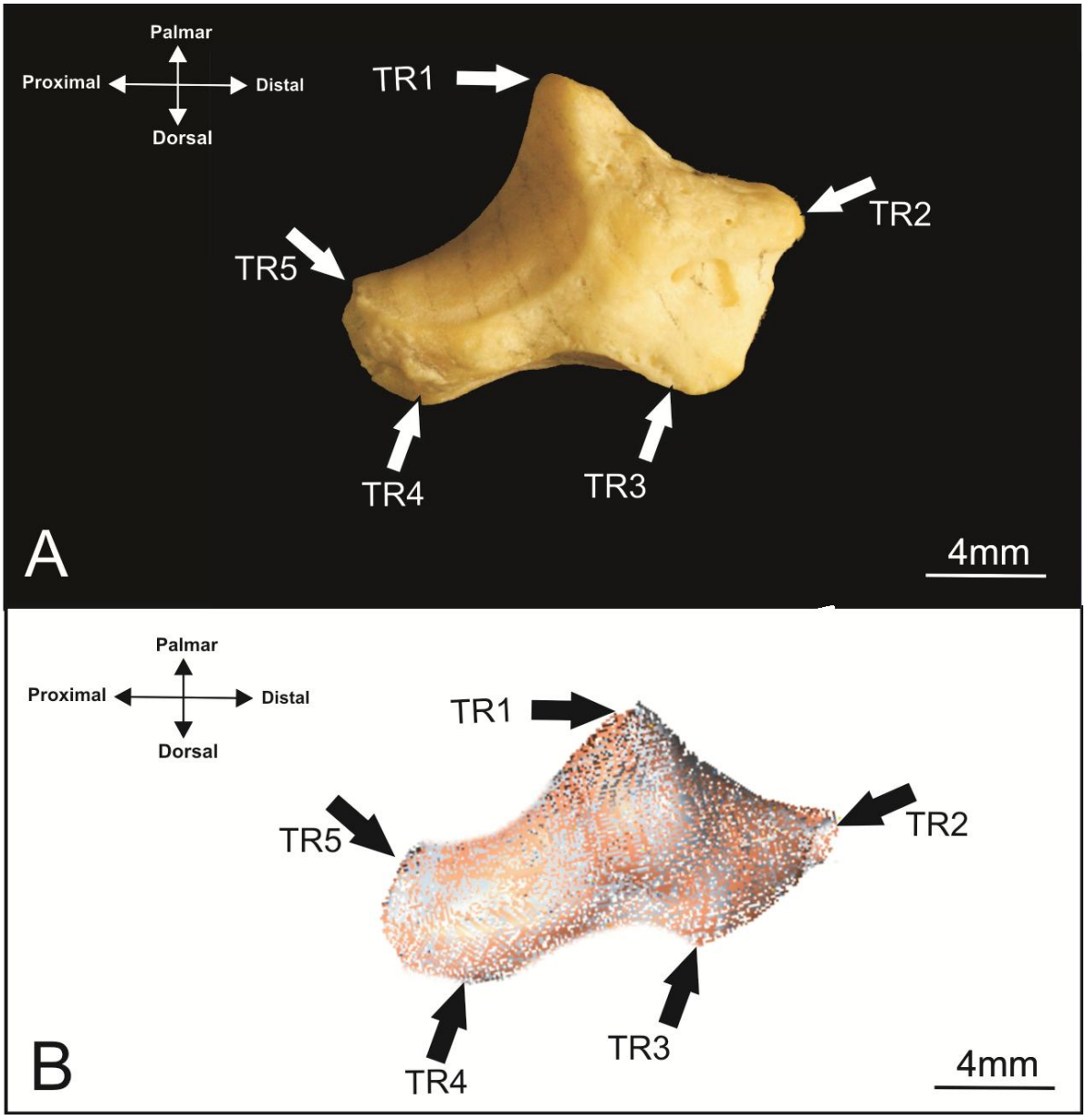

Figure 5.27: Radial view of right 1st MC facet of the TM bone.

A. Dry TM bone illustrates the coordination points. TR1: set at the distal border of the 1st MC facet, TR2: set at the radial tubercle of the 1st MC bone, TR3: set at the dorso-ulnar tubercle of the 1st MC bone, TR4: set at the dorso-radial tubercle of the 1st MC bone, TR5: set at the palmar tubercle of the 1st MC bone.
B. TM bone rendered in a 3D virtual space by Landmark 3D software.

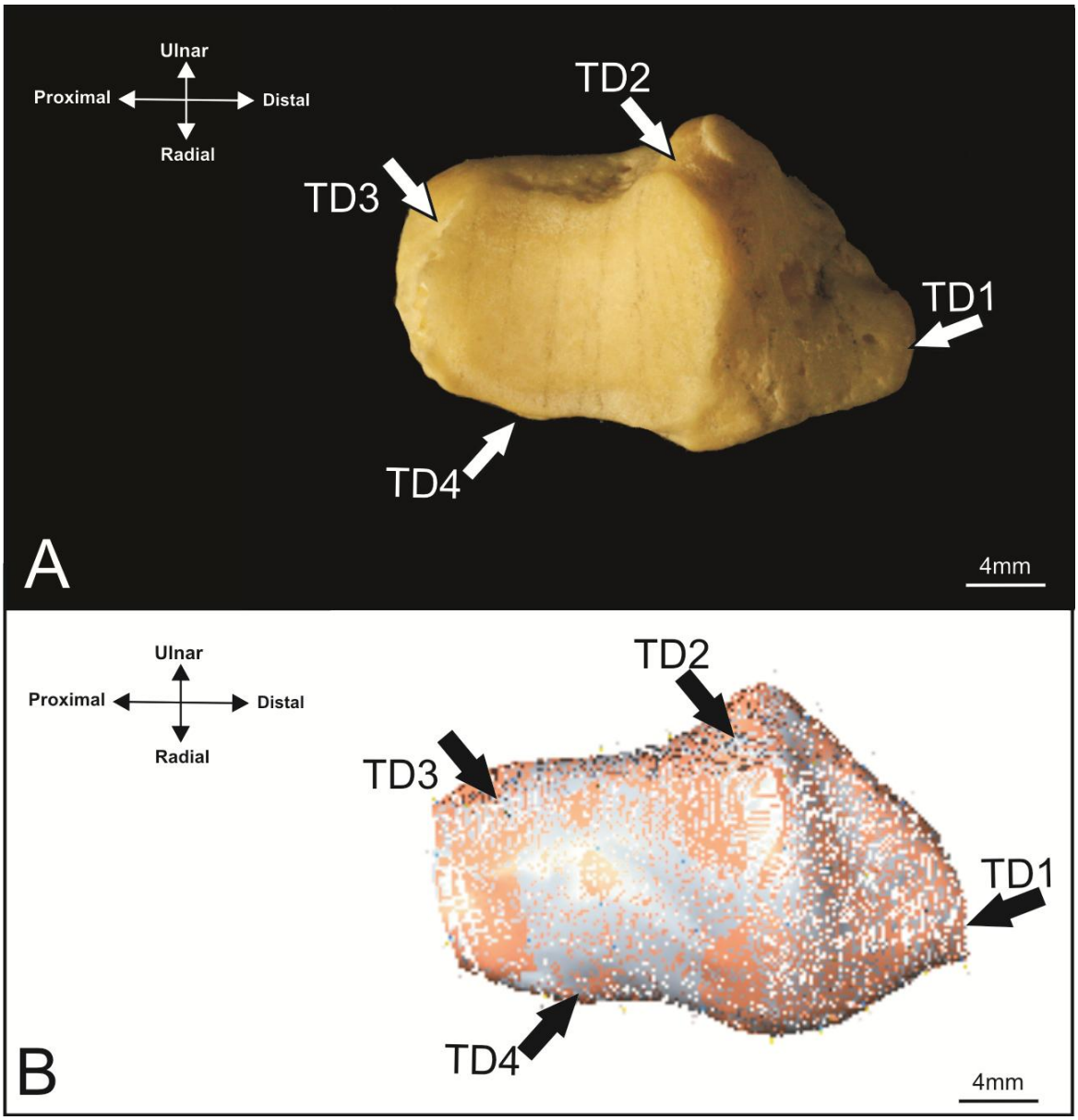

Figure 5.28: Facet view right of the TM bone.

A. Dry TM bone illustrates the coordination points of the TM bone. TD1: Set at the radial tubercle disto-radially, TD2: Set at the eminence of the trapezial ridge disto-radially, TD3: Set at the dorso-ulnar tubercle of the 1st MC bone, TD4: Set at the palmar tubercle disto-radially from the border of the facet.
B. TM bone rendered in a 3D virtual space by Landmark 3D software.

5.2.3.2 First metacarpal (1st MC) bone

Five coordination points on the palmar view of the 1st MC bone are depicted on the TM bone as follows (Figure 5.29):

1. Point 1. Metacarpal-palmar point (MP1): This point was set at the middle of the palmar surface near the radial border of the 1st MC shaft.
2. Point 2. Metacarpal-palmar point (MP2): This point was set at the palmar surface near the palmo-ulnar tubercle of the 1st MC bone.
3. Point 3. Metacarpal-palmar point (MP3): This point was set palmarly at the middle of the anterior eminence.
4. Point 4. Metacarpal-palmar point (MP4): This point was set at the palmar surface near the palmo-radial tubercle of the 1st MC bone.
5. Point 5. Metacarpal-palmar point (MP5): This point was set at the middle of the palmar surface near the ulnar border of the 1st MC shaft.

Five coordination points on the dorsal view of the 1st MC bone were depicted on the 1st MC bone as follows (Figure 5.30):

1. Point 1. Metacarpal-dorsal point (MD1): This point was set at the middle of the dorsal surface near the radial border of the 1st MC shaft.
2. Point 2. Metacarpal-dorsal point (MD2): This point was set at the dorsal surface proximally to the dorso-ulnar tubercle.
3. Point 3. Metacarpal-dorsal point (MD3): This point was set dorsally at the middle of the posterior eminence.
4. Point 4. Metacarpal-dorsal point (MD4): This point was set at the dorsal surface of the dorso-radial tubercle.
5. Point 5. Metacarpal-dorsal point (MD5): This point was set at the middle of dorsal surface near the ulnar border of the 1st MC shaft.

The facet of the 1st MC was also depicted by four coordination points as follows (Figure 5.31):

1. Point 1. Metacarpal-proximal point (MPR1): This point was set at the posterior eminence of the 1st MC.

2. Point 2. Metacarpal-proximal point (MPR2): This point was set at the middle of the radial border of the 1st MC facet.

3. Point 3. Metacarpal-proximal point (MPR3): This point was set at the anterior eminence of the 1st MC.

4. Point 4. Metacarpal-proximal point (MPR4): This point was set at the middle of the ulnar border of the 1st MC facet.

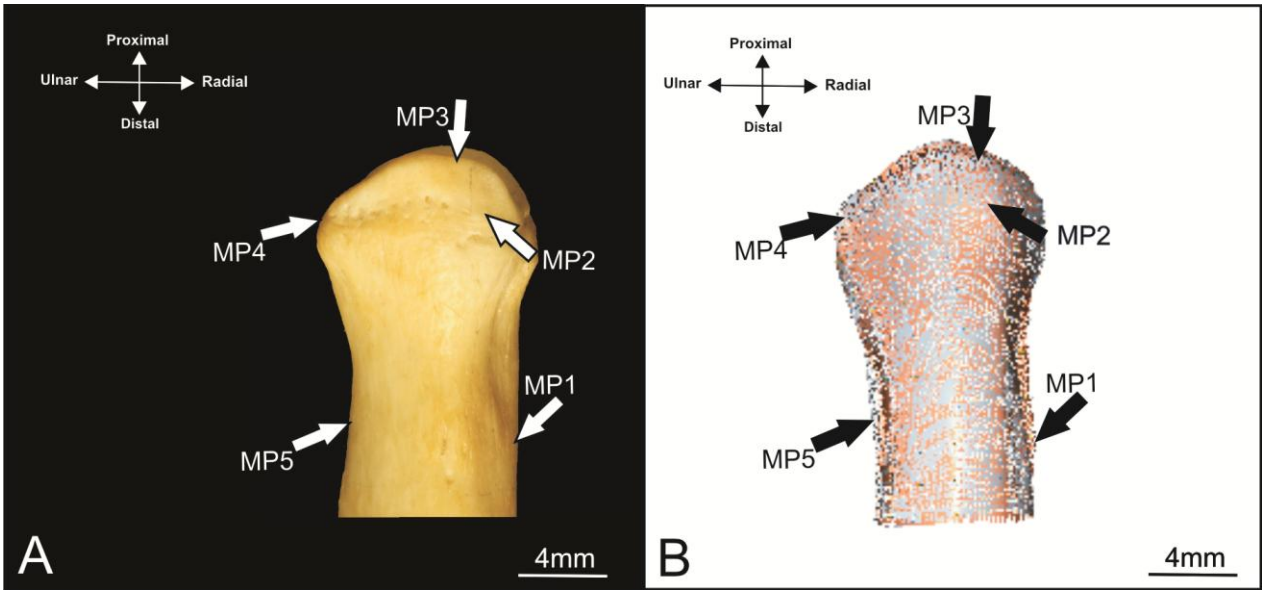

Figure 5.29: Palmar view of the right 1st MC bone.

A. Dry 1st MC bone illustrates the coordination points of the 1st MC bone. MP1: Set at the middle of the palmar surface near the radial border of the 1st MC shaft, MP2: Set at the palmar surface near the palmo-ulnar tubercle of the 1st MC bone, MP3: Set palmarly at the middle of the anterior eminence, MP4: Set at the palmar surface near the palmo-radial tubercle of the 1st MC bone, MP5: Set at the middle of the palmar surface near the ulnar border of the 1st MC shaft.
B. 1st MC bone rendered in a 3D virtual space by Landmark 3D software.

.

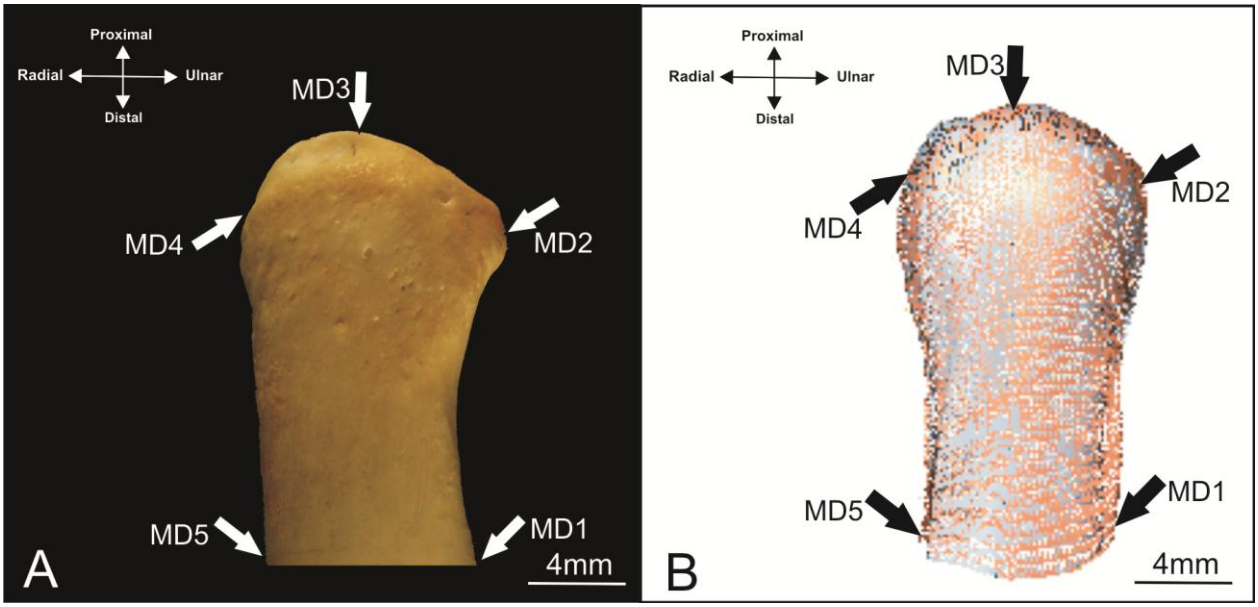

Figure 5.30: Dorsal view of the right 1st MC bone.

A. Dry 1st MC bone illustrates the coordination points of the 1st MC bone. MD1: Set at the middle of the dorsal surface near the radial border of the 1st MC shaft, MD2: Set at the dorsal surface proximally to the dorso-ulnar tubercle, MD3: Set dorsally at the middle of the posterior eminence, MD4: Set at the dorsal surface at the dorso-radial tubercle, MD5: Set at the middle of dorsal surface near the ulnar border of the 1st MC shaft.
B. 1st MC bone rendered in a 3D virtual space by Landmark 3D software.

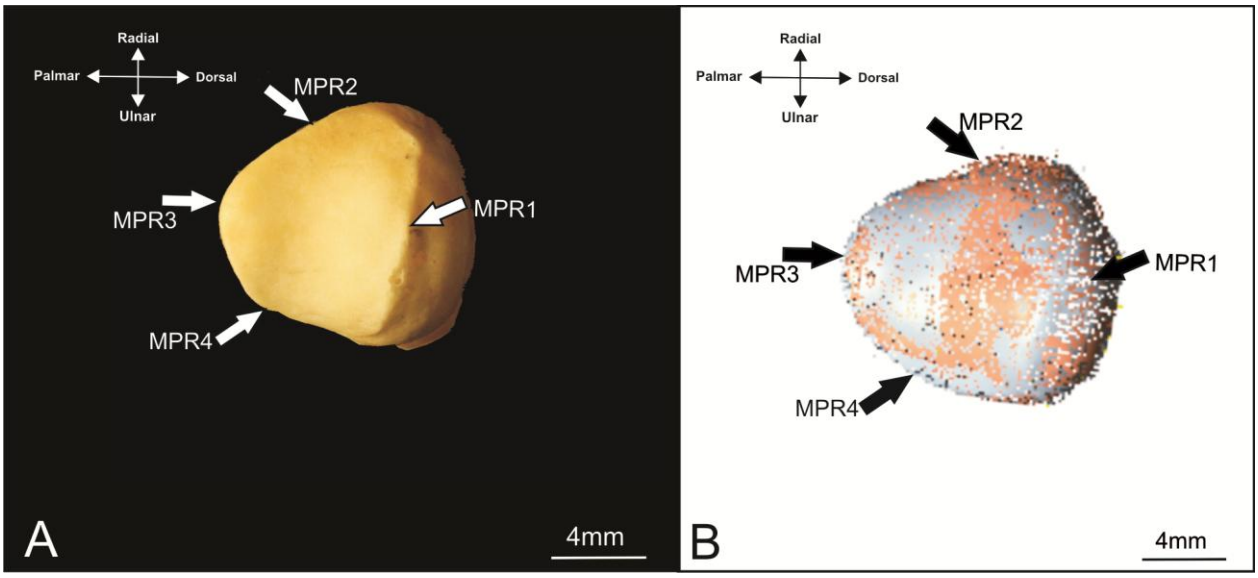

Figure 5.31: Facet view of the right 1st MC bone.

A. Dry 1st MC bone illustrates the coordination points of the 1st MC bone. MPR1: set at the posterior eminence of the 1st MC, MPR2: set at the middle of the radial border of the 1st MC facet, MPR3: set at the anterior eminence of the 1st MC, MPR4: set at the middle of the ulnar border of the 1st MC facet.
B. 1st MC bone rendered in a 3D virtual space by Landmark 3D software.

The choice of these coordination points was based on the anatomical importance of the points' location on the TM and 1st MC bones, and because the Landmark 3D software deals with each point individually to render the virtual 3D shape. The statistical calculations of the Landmark 3D software deal with each point alone to preserve the shape of the TM and 1st MC bones throughout the sample population. The software may neglect a point when there was a more important point found on the shape during the Landmark 3D software calculations (Figures 5.32-5.33).

In addition, each coordination point was chosen carefully, as previously mentioned, based on 1) the importance of the position of the point as that position relates to the bone shape, 2) the distribution of all points to cover the whole shape of the bone and 3) the view of the bone as it relates to the other bones that are contained in the joint. For instance, the facet view of the both TM and 1st MC bones were very important because this face of the bone has two facets that are contained in the TMC joint. Further, the radial direction of the TM bone was chosen because this view is related to other morphological parts of the 1st MC bone, such as the anterior and posterior eminences of the 1st MC. Those eminences are considered as the projection of the base of the 1st MC bone, with little projections toward the ulnar and radial borders.

Moreover, the palmar and dorsal surfaces of the 1st MC are related to facet area of the TM bone, and to some structures such as the radial artery, its branches and the TMC ligament attachments .

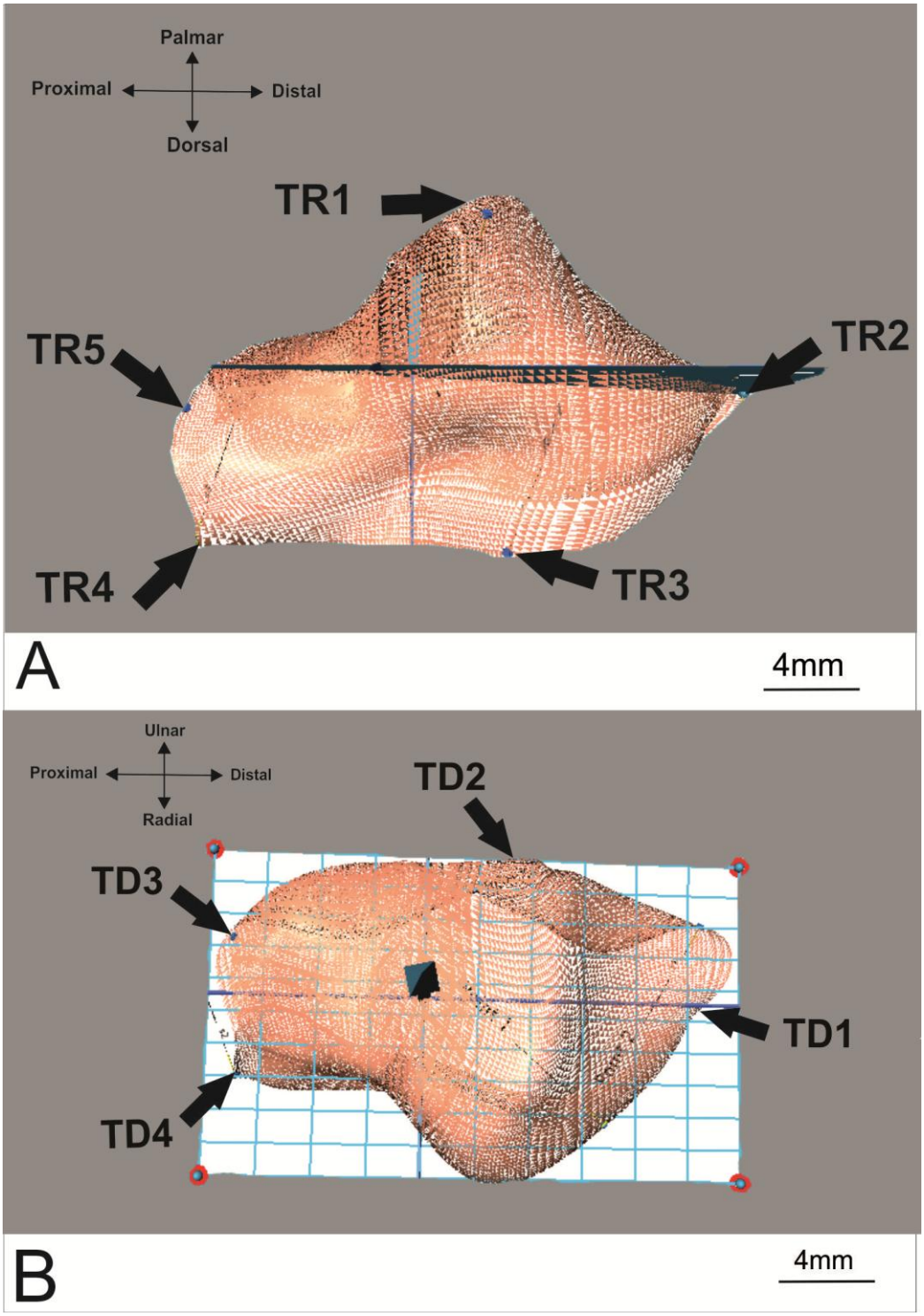

Figure 5.32: Radial and facet views of the right TM bone by Landmark 3D software.

A. Radial view of the right TM bone illustrates the single coordination points of the TM bone. TR1: set at the distal border of the 1st MC facet, TR2: set at the radial tubercle of the 1st MC bone, TR3: set at the dorso-ulnar tubercle of the 1st MC bone, TR4: set at the dorso-radial tubercle of the 1st MC bone, TR5: set at the palmar tubercle of the 1st MC bone.
B. Facet view of the right TM bone illustrates TD1: set disto-radially at the radial tubercle, TD2: set disto-radially at the eminence of the trapezial ridge, TD3: set at the dorso-ulnar tubercle of the 1st MC bone, TD4: set at the palmar tubercle disto-radially from the border of the facet.

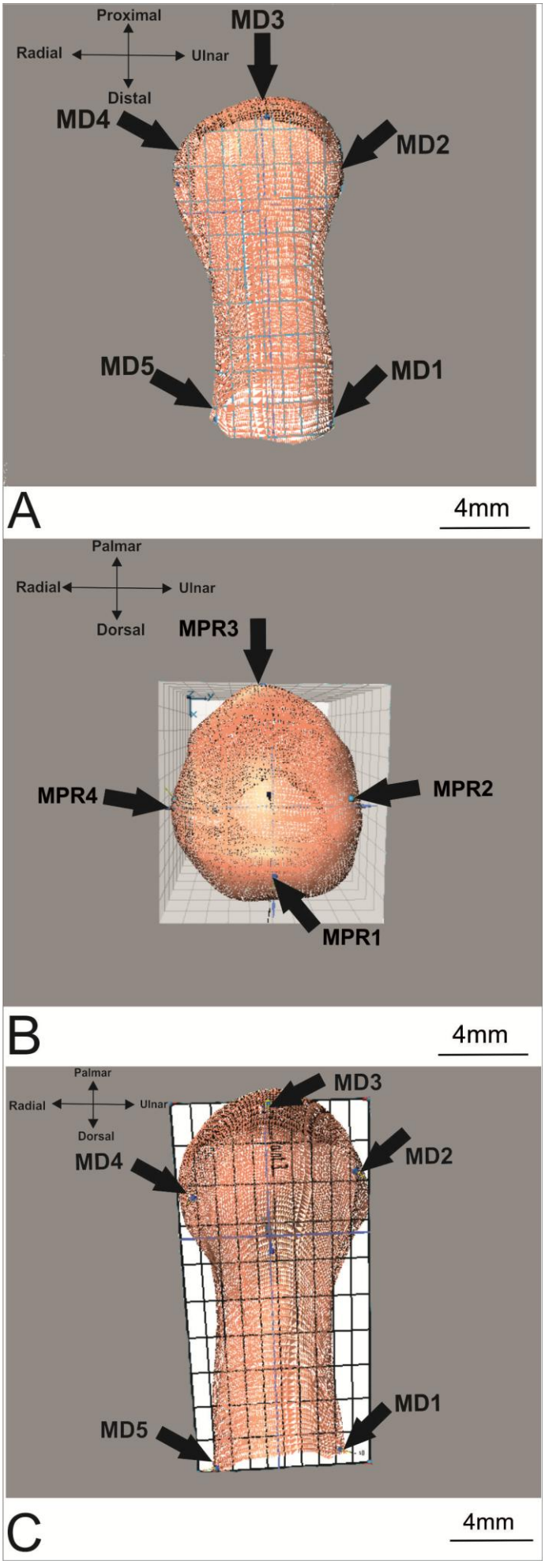

Figure 5.33: Pamar,facet and dorsal views of the right 1st MC bone by Landmark 3D software.

A. Dorsal view of right 1st MC bone illustrates the single coordination points of the 1st MC bone. MD1: set at the middle of the dorsal surface near the radial border of the 1st MC shaft, MD2: set at the dorsal surface proximally to the dorso-ulnar tubercle, MD3: set dorsally at the middle of the posterior eminence, MD4: set at the dorsal surface at the dorso-radial tubercle, MD5: set at the middle of dorsal surface near the ulnar border of the 1st MC shaft.
B. Facet view of right 1st MC bone illustrates the single coordination points of the 1st MC bone. MPR1: set at the posterior eminence of the 1st MC, MPR2: set at the middle of the radial border of the 1st MC facet, MPR3: set at the anterior eminence of the 1st MC, MPR4: set at the middle of the ulnar border of the 1st MC facet.
C. Palmar view of the right 1st MC bone illustrates the single coordination points of the 1st MC bone. MP1: set at the middle of the palmar surface near the radial border of the 1st MC shaft, MP2: set at the palmar surface near the palmo-ulnar tubercle of the 1st MC bone, MP3: set at the middle of the anterior eminence palmarly, MP4: set at the palmar surface near the palmo-radial tubercle of the 1st MC bone, MP5: set at the middle of the palmar surface near the ulnar border of the 1st MC shaft.

5.2.4 Data analysis of single coordination points

Regression analysis testing was used to calculate the changes that occurred on the coordination points. This ensured that each coordination point either preserved its position on the shape or changed through the first stage to another position (Rudemo 2000).

R-squared was calculated as follows:

R-squared = Explained variation / Total variation

R-squared was always between 0 and 100%.

A value of 0% indicates that the model explains none of the variability of the response data around its mean. A value of100% indicates that the model explains all the variability of the response data around its mean. If the variances between the means of two populations were significantly different, the F-factor was also determined (Rudemo 2000).

5.2.5 Measurement procedures

The measurement of the TM and 1st MC bones was made by dividing each bone's articulation surface into length and width.

The length of the TM facet is from the border of dorso-ulnar tubercle in the facet direction, from the palmar tubercle toward distal border of the 1st MC and from the facet border of the dorso-ulnar tubercle. The width of the TM facet is from the facet borders of both palmar and dorsal surfaces of the TM bone (Figure 5.34).

The length of the 1st MC facet is from the anterior eminence parallel to the ulnar and radial borders of the 1st MC facet toward the posterior eminence of the 1st MC bone. The width of the 1st MC facet is from the radial border of the 1st MC facet parallel to the anterior and posterior eminences of the 1st MC facet toward ulnar border of the 1st MC facet (Figure 5.35).

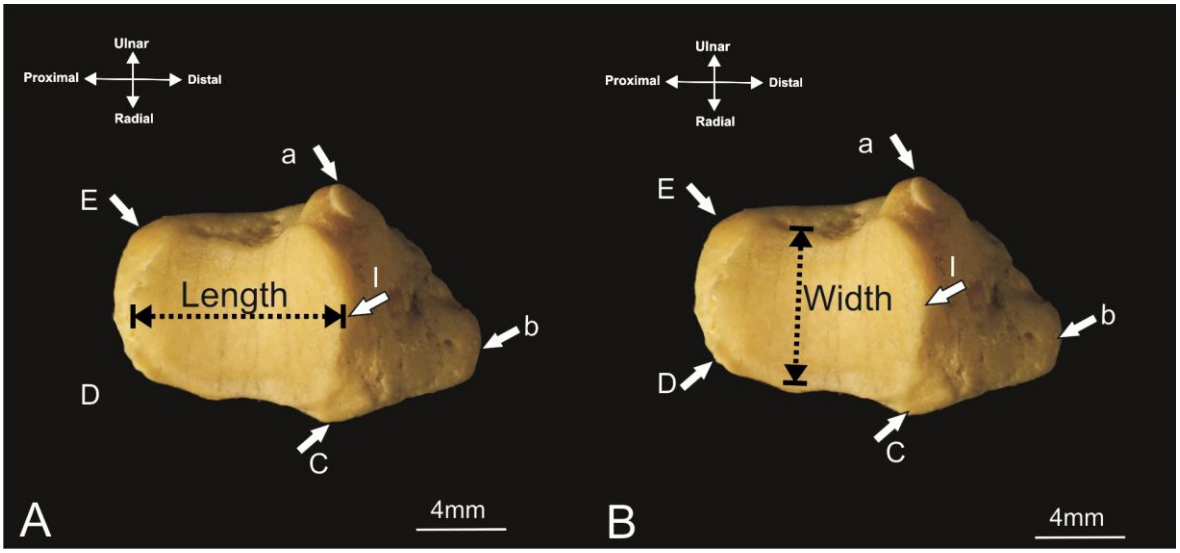

Figure 5.34: Length and width measurement of the right TM facet.

A. Length measurement of TM articular surface
B. Width measurement of TM articular surface.
a: eminence of the trapezial ridge, b: radial tubercle, C: dorso-ulnar tubercle, D: dorso-radial tubercle, E: palmar tubercle, I: distal border of 1st MC facet.

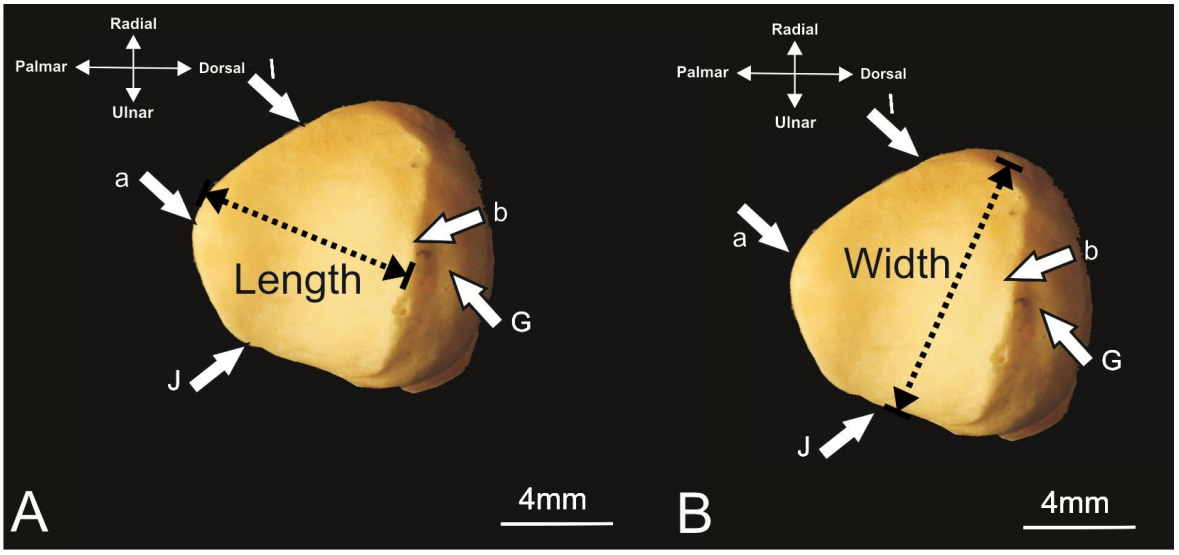

Figure 5.35: Length and width measurement of the right 1st MC facet.

A. Length measurement of 1st MC articular surface
B. Width measurement of 1st MC articular surface.
a: anterior eminence, b: posterior eminence, G: dorso-ulnar tubercle, I: radial border of TM facet of 1st MC bone, J: ulnar border of TM facet of the 1st MC bone

The articulation surface was covered in length and width by five parallel lines. The lines represented the difference between the widest and narrowest areas of the facets of the TM and 1st MC. Based on the anatomical description, the lines were named as follows.

Length lines of the trapezium (TM) bone (Figure 5.36):

1. First eminence trapezial ridge line (ETL1): This line began at the palmar tubercle near the facet toward distal border of the TM facet.

2. Second eminence trapezial ridge line (ETL2): This line was parallel to the ETL1 line near the central length line (CLL).

3. Central length line (CLL): This line was set longitudinally at the centre of the TM facet between both lines (ETL) and dorso-radial tubercle line (DRTL).

4. Second dorso-radial tubercle line (DRTL2): This line began at the dorso-radial tubercle at the facet border and proceeded distally from dorso-ulnar tubercle toward distal border of the TM facet.

5. First dorso-radial tubercle line (DRTL1): This line was parallel to the DRTL and proceeded distally from the edge of the TM facet.

According to the previous division, the areas were presented as follows (Figure 5.37):

1. The area of the facet eminence lines covered lines ETL1 and ETL2.

2. The area of the facet central line covered only the CLL.

3. The area of the facet dorso-radial lines covered lines DRTL1 and DRTL2.

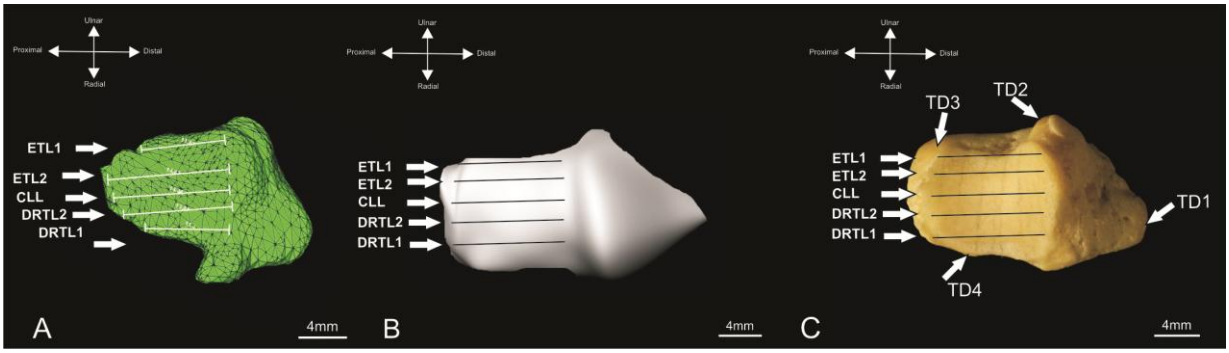

Figure 5.36: Length lines and single-point coordination of the right TM facet.

A. Length lines and single-point coordinations rendered by Amira 3D, depicted the five length lines.
B. Length lines and single-point coordinations rendered by Rhinoceros 0.5, depicted the five length lines.
C. Dry TM bone. TD1: set at the radial tubercle disto-radially, TD2: set disto-radially at the eminence of the trapezial ridge, TD3: set at the dorso-ulnar tubercle of the 1st MC bone, TD4: set at the palmar tubercle disto-radially from the border of the facet.

The five length lines were defined as follows:

1. (ETL1) began at the palmar tubercle near the facet and proceeded toward distal border of the TM facet.

2. (ETL2) was parallel to ETL1 near the central length line (CLL).

3. (CLL) was set longitudinally at the central position of the TM facet between both lines (ETL) and dorso-radial tubercle line (DRTL).

4. (DRTL2) began at the dorso-radial tubercle at the facet border and proceeded distally from dorso-ulnar tubercle toward the distal border of the TM facet.

5. (DRTL1) was parallel to the DRTL and proceeded distally to the edge of the TM facet.

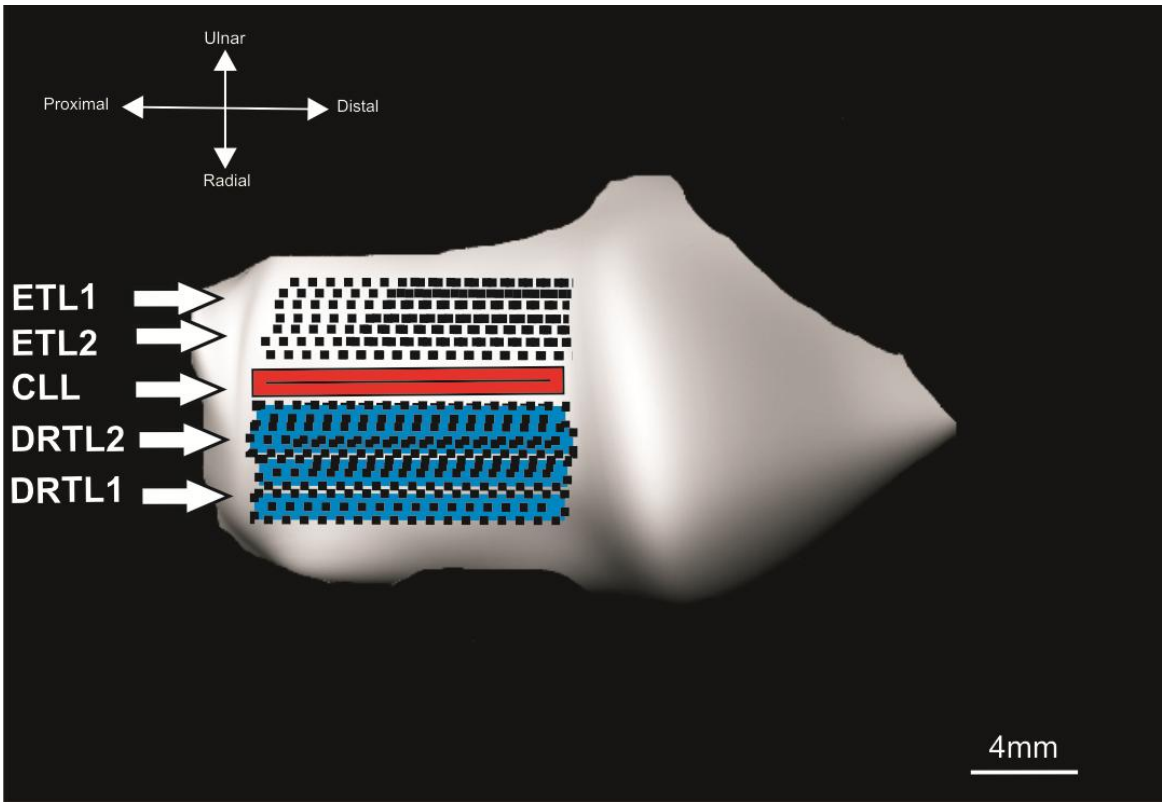

Figure 5.37: Areas divided by the length lines of the right TM facet. The black area was the facet eminence lines. The red area was the central length line. The blue area was the dorso-radial tubercle lines.

The width lines of the trapezium (TM) bone were defined as follows (Figure 5.38).

1. First palmar tubercle line (PTL1): proceeded from the palmar tubercle at the facet border distally toward the dorso-radial tubercle.

2. Second palmar tubercle line (PTL2): parallel to PTL1 near the central width line (CWL).

3. Central width line (CWL): transversely set at the centre of the TM facet.

4. Second distal border line (DBL2): proceeded from the distal border of the TM facet distally to the eminence of the trapezial ridge toward the facet edge near the proximal end of the dorso-ulnar tubercle.

5. First distal border line (DBL1): distal and parallel to the DBL1.

According to the previous divisions, the areas were presented as follows (Figure 5.39).

1. The area of the palmar facet tubercle covered lines PTL1 and PTL2.

2. The area of the central facet covered only the CWL line.

3. The area of the distal facet border covered DBL1 and DBL2.

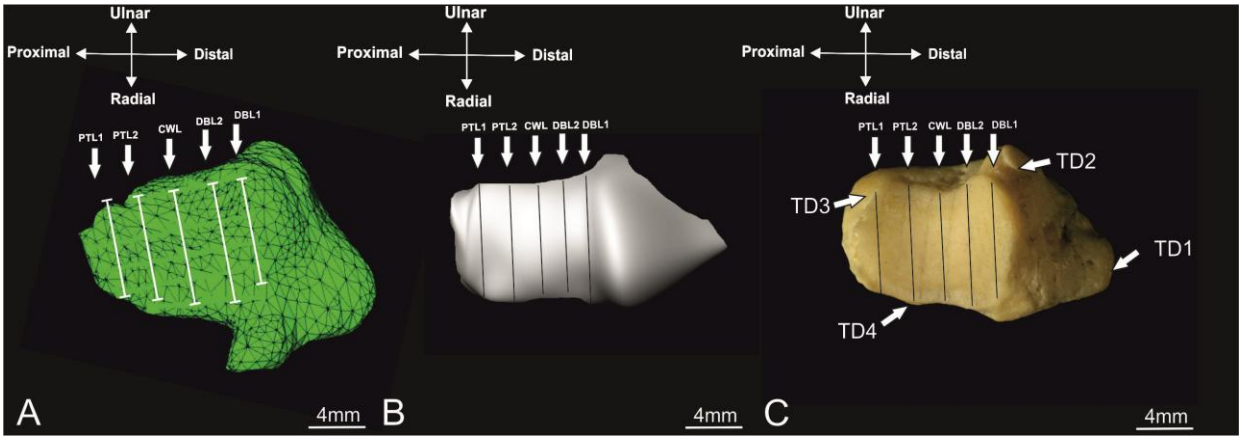

Figure 5.38: Width lines and single-point coordination of the right TM facet.

A. Width lines and single-point coordinations rendered by Amira 3D, depicted the five length lines.
B. Width lines and single-point coordinations rendered by Rhinoceros 0.5, depicted the five length lines.
C. Dry TM bone. TD1: set disto-radially at the radial tubercle, TD2: set disto-radially at the eminence of the trapezial ridge, TD3: set at the dorso-ulnar tubercle of the 1st MC bone, TD4: set at the palmar tubercle disto-radially from the border of the facet.

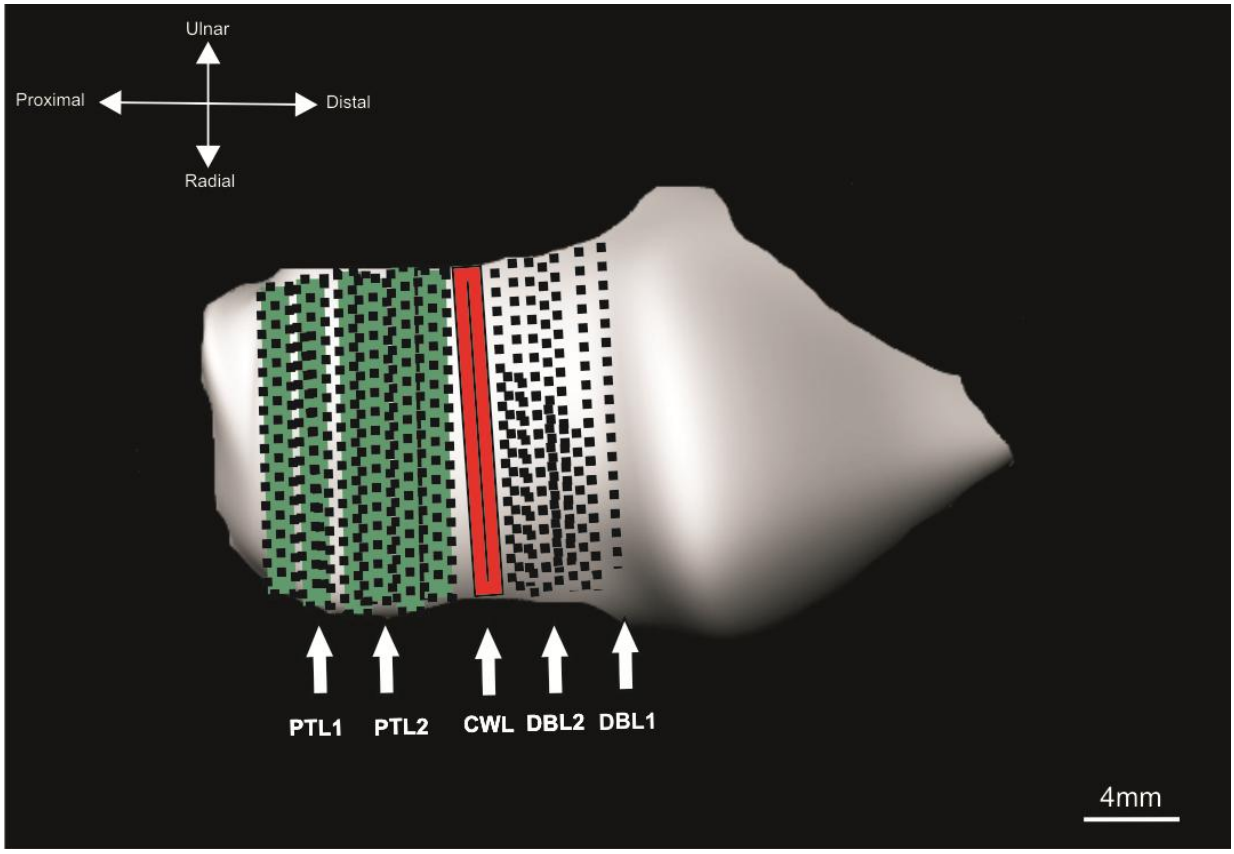

Figure 5.39: The division of areas and the width lines of the right TM facet. Black indicates distal border lines. Red indicates the central width line. Green indicates the palmar tubercle lines.

The length lines of 1st MC bone were defined as follows (Figure 5.40).

1. First radial border line (RBL1): began at the posterior eminence and proceeded radially toward the anterior eminence.
2. Second radial border line (RBL2): ulnar and parallel to RBL1.
3. Central length line (CLL): longitudinal and set at the centre of the 1st MC facet.
4. Second ulnar border line (UBL2): began at the posterior eminence and proceeded ulnarly toward the anterior eminence.
5. First ulnar border line (UB1): ulnar and parallel to UBL2.

According to the previous division, the areas presented were as follows (Figure 5.41).

1. The area of the facet radial border lines covered lines RBL1 and RBL2.

2. The area of the facet central length line covered only CLL.

3. The area of the facet ulnar border lines covered UBL1 and UBL2.

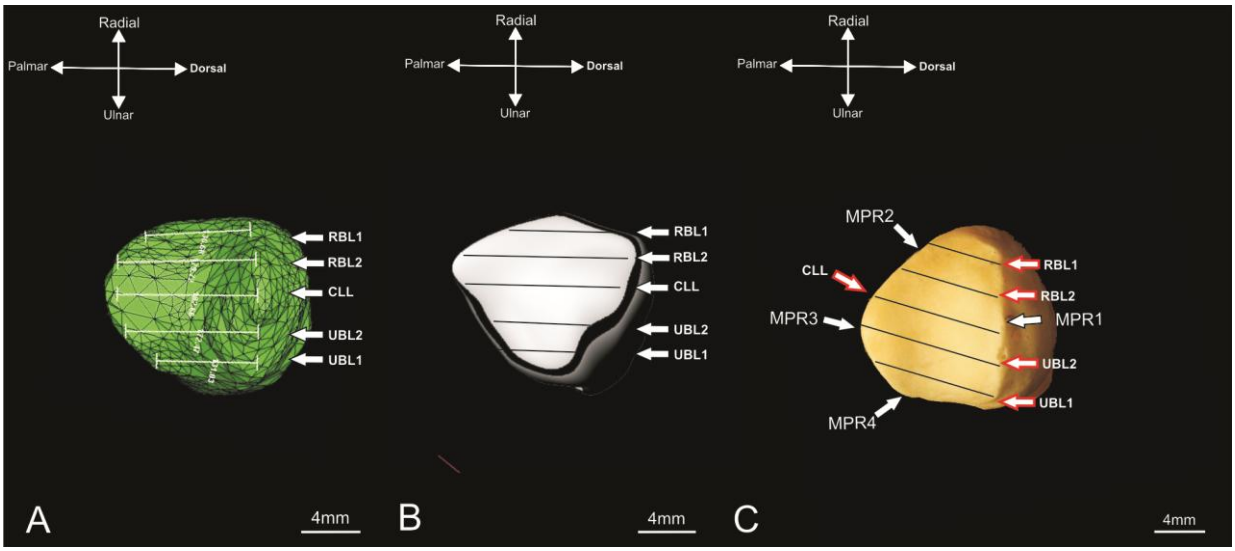

Figure 5.40: Length lines and single-point coordination of the right 1st MC facet.

A. Length lines and single-point coordinations rendered by Amira 3D, depicted the five length lines.
B. Length lines and single-point coordinations rendered by Rhinoceros 0.5, depicted the five length lines.
C. Dry TM bone. MPR1: set at the posterior eminence of the 1st MC, MPR2: set at the middle of the radial border of the 1st MC facet, MPR3: set at the anterior eminence of the 1st MC. MPR4: set at the middle of the ulnar border of the 1st MC facet.

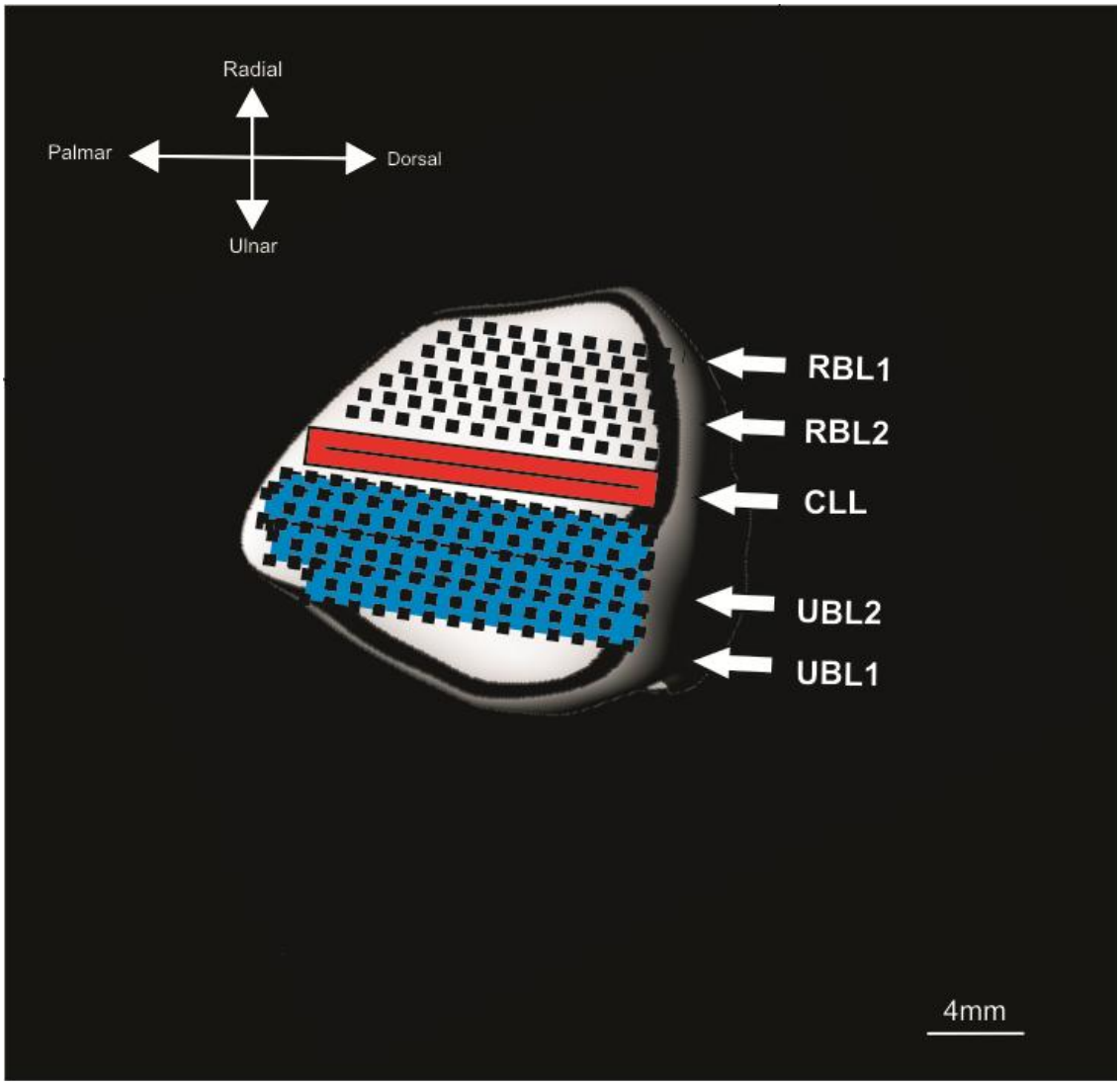

Figure 5.41: Areas defined by the length lines of the right 1st MC facet. Black area was radial border lines. Red area was the central length line. Blue area was the ulnar border lines.

The width lines of 1st MC bone were defined as follows (Figure 5.42).

1. First anterior eminence line (AEL1): began at the radial border and proceeded ulnarly toward ulnar border.

2. Second anterior eminence line (AEL2): ulnar and parallel to AEL1.

3. Central width line (CWL): set transversely at the centre of the 1st MC facet.

4. Second posterior eminence line (PEL2): began at ulnar border and proceeded radially toward radial border.

5. First posterior eminence line (PEL1): radial and parallel to PEL2.

According to the previous division, the areas were presented as follows (Figure 5.43).

1. The area of the facet anterior eminence lines covered AEL1 and AEL2.

2. The area of the facet central width line covered only CWL.

3. The area of the facet posterior eminence lines covered PEL1 and PEL2.

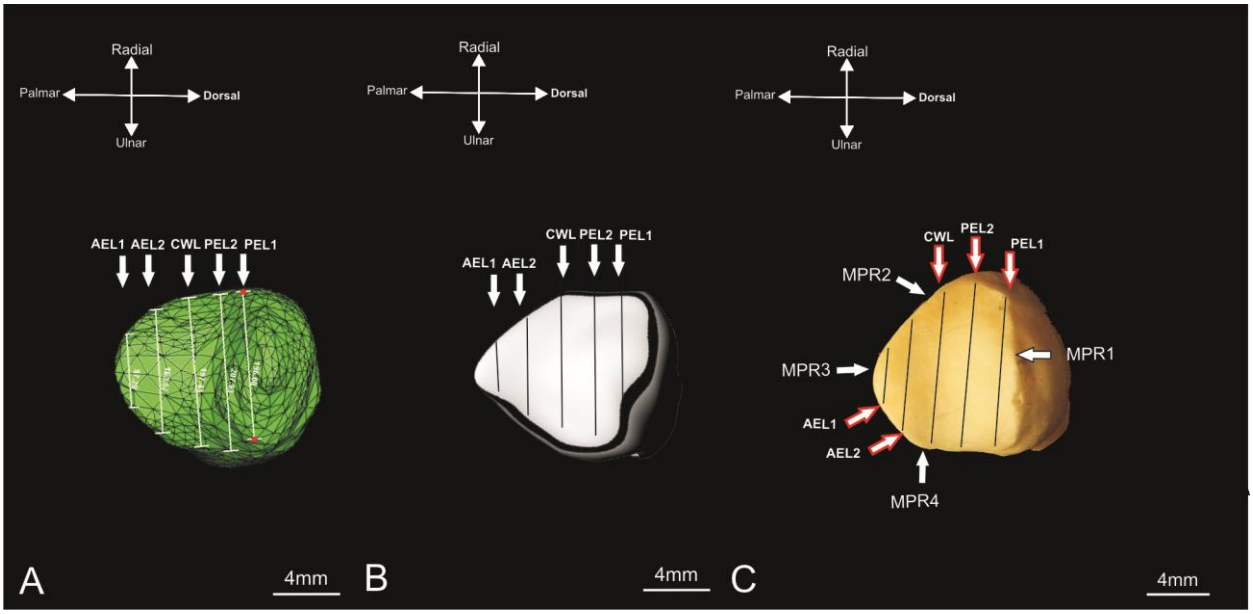

Figure 5.42: Width lines and single-point coordination of the right 1st MC facet.

A. Width lines and single-point coordinations rendered by Amira 3D, depicted the five length lines.
B. Width lines and single-point coordinations rendered by Rhinoceros 0.5, depicted the five length lines.
C. Dry TM bone. MPR1: set at the posterior eminence of the 1st MC, MPR2: set at the middle of the radial border of the 1st MC facet, MPR3: set at the anterior eminence of the 1st MC, MPR4: set at the middle of the ulnar border of the 1st MC facet.

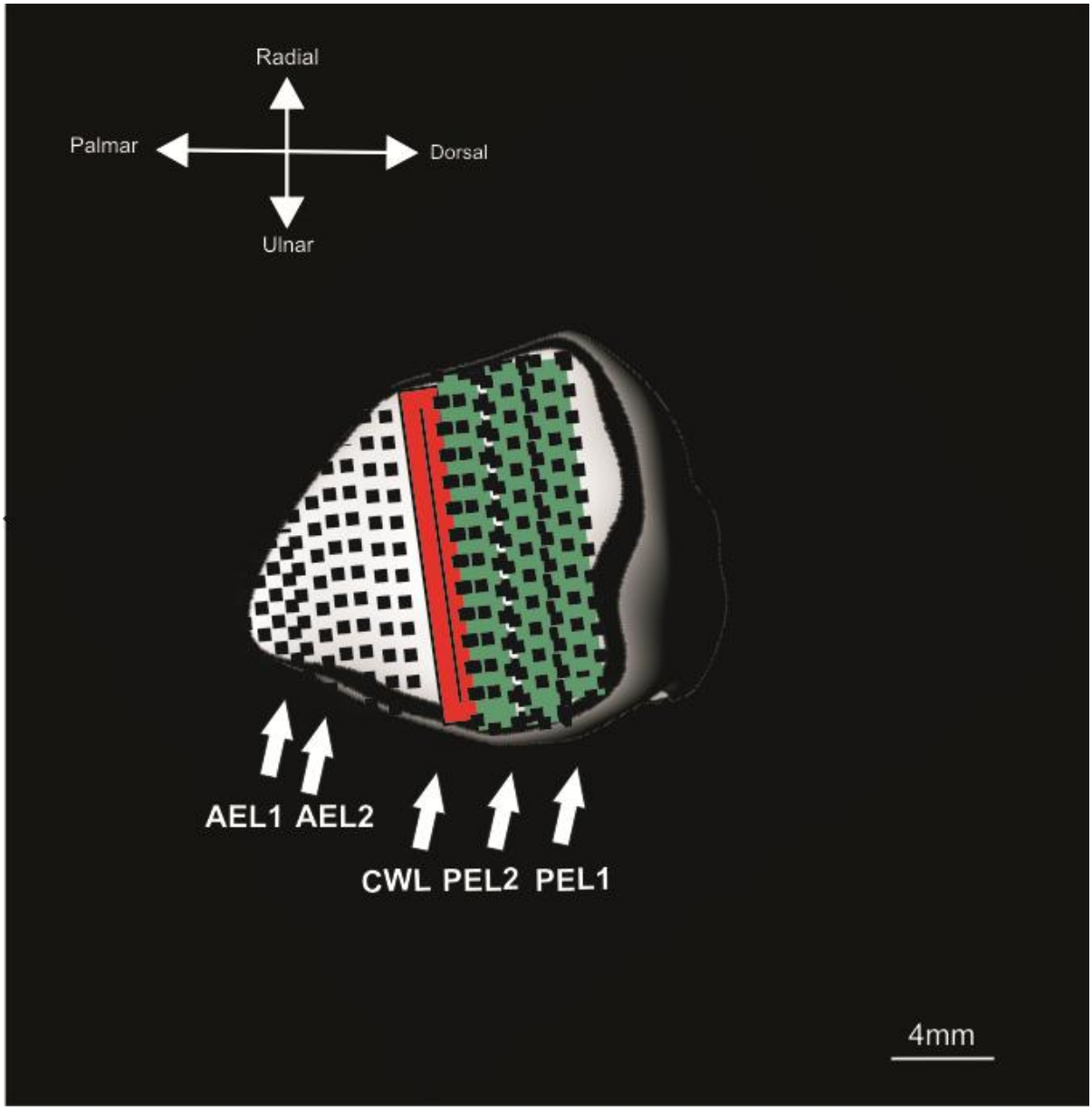

Figure 5.43: Areas defined by the width lines of the right 1st MC facet. Black area was anterior eminence lines. Red area was the central width line. Green area was the posterior eminence lines.

The greatest and least length and width of both articulating surfaces were assessed in Rhinoceros 5.0 and Amira 3D software. The area of the articulation surface of both bones was calculated (Figure 5.44). A comparison between the results of each software was made. The right and left sides of both bones were assessed (Figures 5.45-5.46).

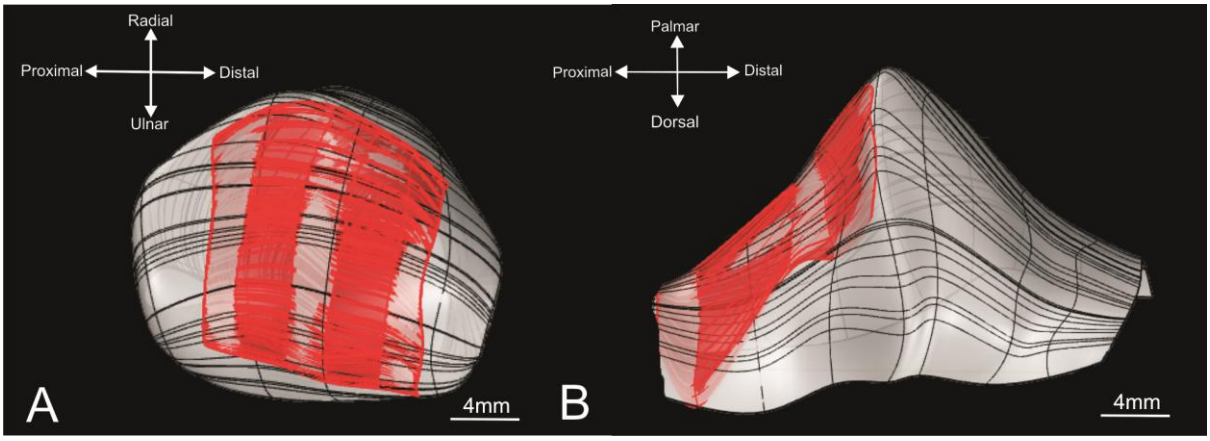

Figure 5.44: Right 1st MC and right TM articulation surface area rendered in virtual 3D by Rhinoceros 5.0 software.

A. 1st MC bone, the red colour presents the articular surface of the 1st MC bone.
B. TM bone, the red colour presents the articular surface of the TM bone.

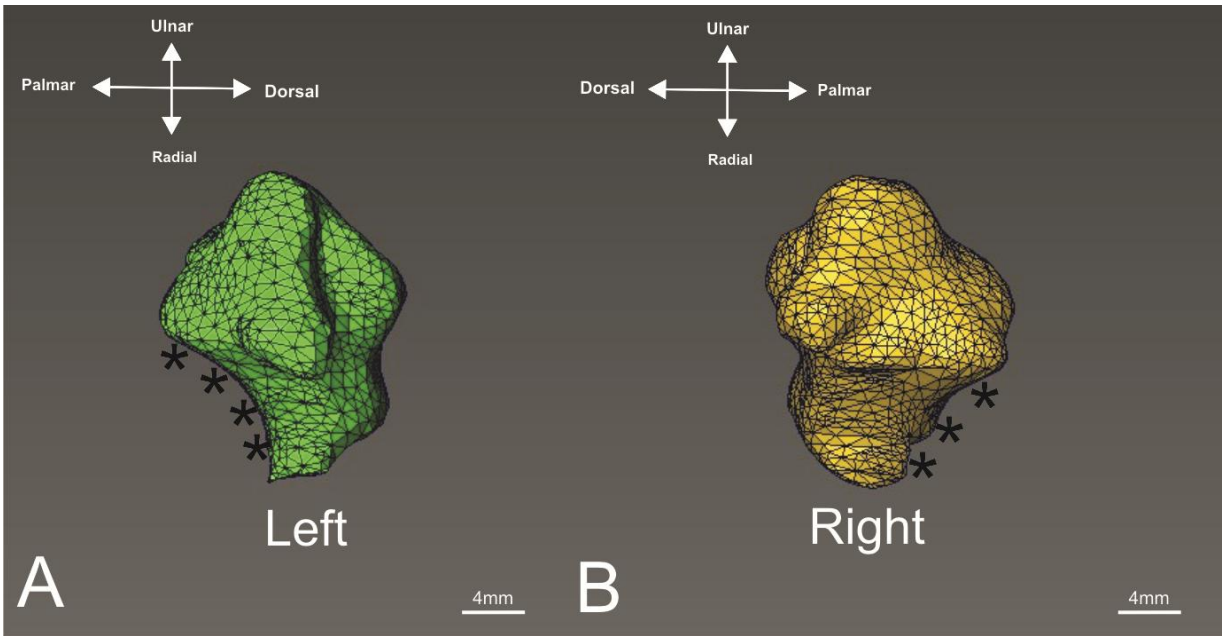

Figure 5.45: Both left and right TM bone.
A. Left TM bone rendered by Amira 3D software.
B. Right TM bone rendered by Amira 3D software.
(*****) indicates to the articulation with 1st MC bone.

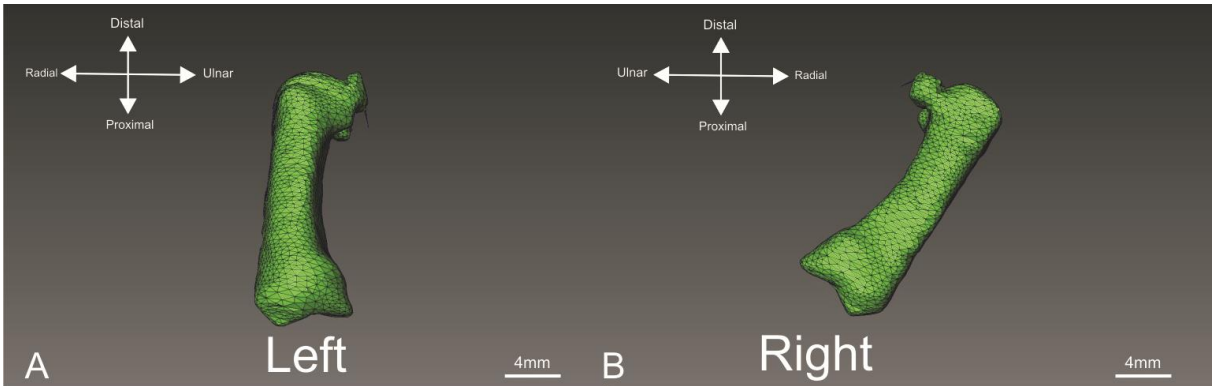

Figure 5.46: Both left and right 1st MC bone.
A. Left 1st MC bone rendered by Amira 3D software.
B. Right 1st MC bone rendered by Amira 3D software.

5.3 Results

5.3.1 Single point coordination of TM bone

5.3.1.1 Facet view of the TM bone

5.3.1.1.1 First trapezial- distal point (TD1)

The R^2 value of the regression point was 0.002 and the significance F was 0.77. The regression point showed that the TD1 point was influenced by the square of single coordination points. TD1 has no relationship with the same point on the other dry TM bones, which means that this coordination point changed from the first stage to the final by 0.2%, without preserving its anatomical place through the sample population (Figure 5.47).

The significance factor F indicated that the regression analysis was not significant (F>0.05). The TD1 point significantly changed from the first stage to the final.

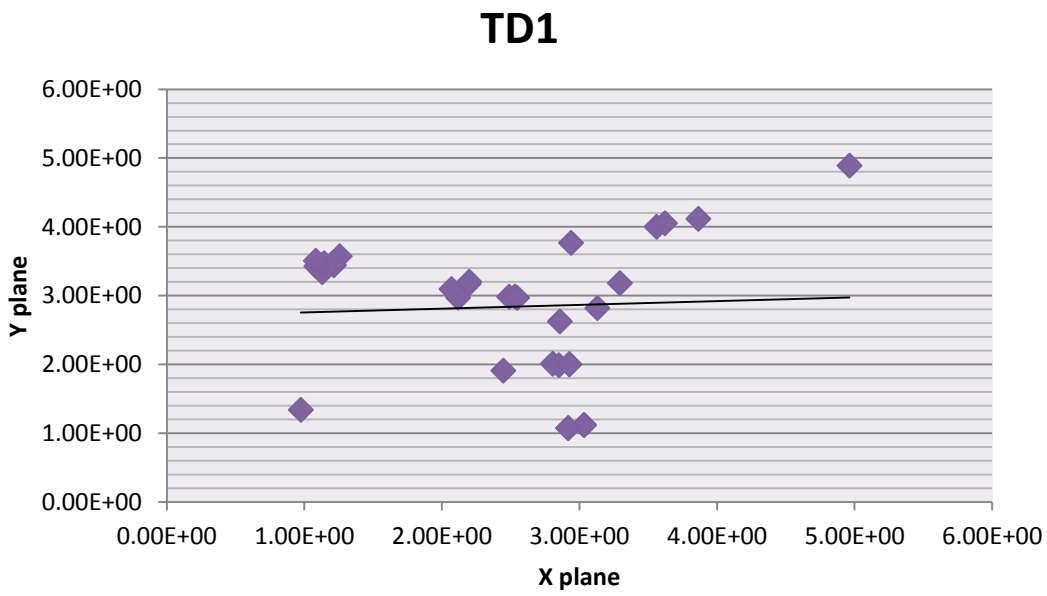

Figure 5.47: Linear regression model of the TD1 single coordination point for the TM facet view.TD1 has no relationship with the same point on the other dry TM bones, the significance factor F indicated that the regression analysis was not significant (F>0.05). N=32.

5.3.1.1.2 Second trapezial- distal point (TD2)

The R^2 value of the regression point was 0.02 and the significance F was 0.42. The regression point showed that the TD2 point was influenced by the square of single coordination points. TD2 has no relationship with the same point on the other dry TM bones, which means that this coordination point changed from the first stage to the final by 20%, without preserving its anatomical place through the sample population (Figure 5.48).

The significance factor F indicated that the regression analysis was not significant (F>0.05). TD2 significantly changed from the first stage to the final.

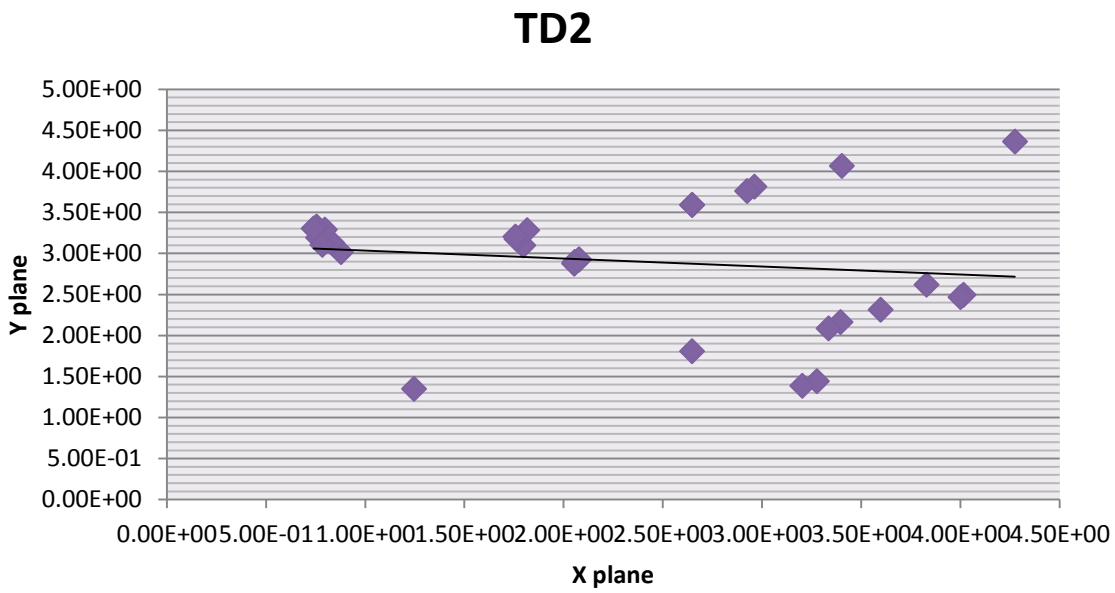

Figure 5.48: Linear regression model of the TD2 single coordination point from the TM facet view. TD2 has no relationship with the same point on the other dry TM bones, the significance factor F indicated that the regression analysis was not significant (F>0.05). N=32.

5.3.1.1.3 Third trapezial- distal point (TD3)

The R^2 value of the regression point was 0.69 and the significance F was 3.92. The regression point showed that the TD3 point was influenced by the square of the single coordination points. TD3 has no relationship with the same point on the other dry TM bones, which means that this coordination point was changed from the first stage to the final by 69%, without preserving its anatomical place through the sample population (Figure 5.49).

The significance factor F indicated that regression analysis was not significant (F>0.05). TD3 significantly changed from the first stage to the final.

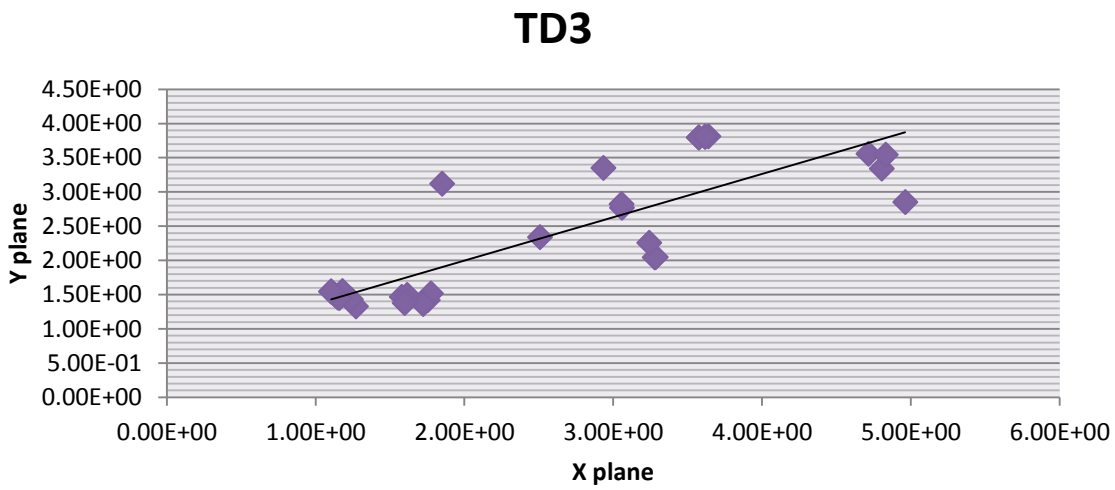

Figure 5.49: Linear regression model of the TD3 single coordination point from the TM facet view. TD3 has no relationship with the same point on the other dry TM bones, the significance factor F indicated that regression analysis was not significant (F>0.05). N=32.

5.3.1.1.4 Fourth trapezial- distal point (TD4)

The R^2 value of the regression point was 0.43 and the significance F was 4.45. The regression point showed that the TD4 point was influenced by the square of the single coordination points. TD4 had no relationship with the same point on the other dry TM bones, which means that this coordination point was changed from the first stage to the final by 43%, without preserving its anatomical place through the sample population (Figure 5.50).

The significance factor F indicated that the regression analysis was not significant (F>0.05). TD4 significantly changed from the first stage to the final.

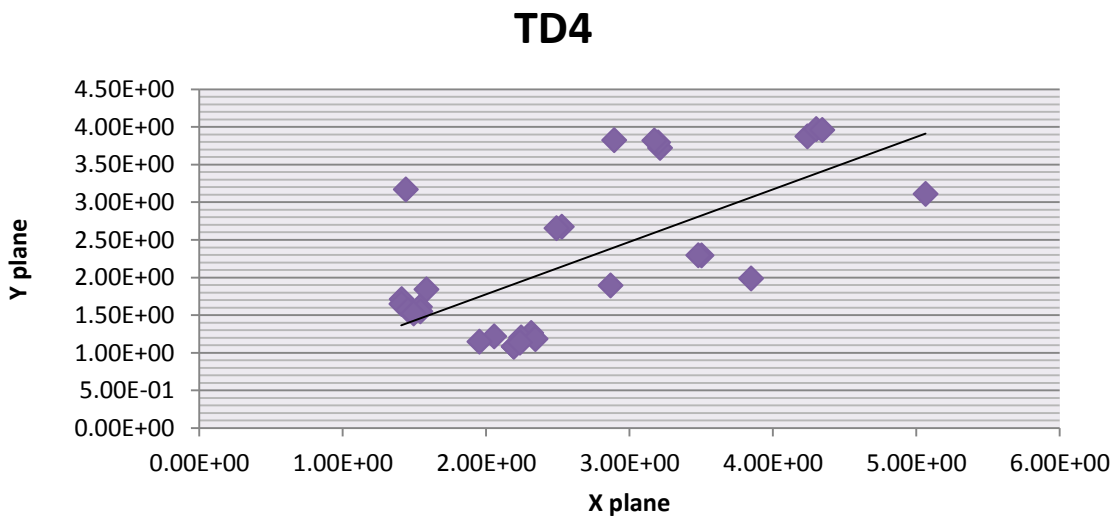

Figure 5.50: Linear regression model of the TD4 single coordination point from the TM facet view. TD4 had no relationship with the same point on the other dry TM bones, the significance factor F indicated that the regression analysis was not significant (F>0.05). N=32.

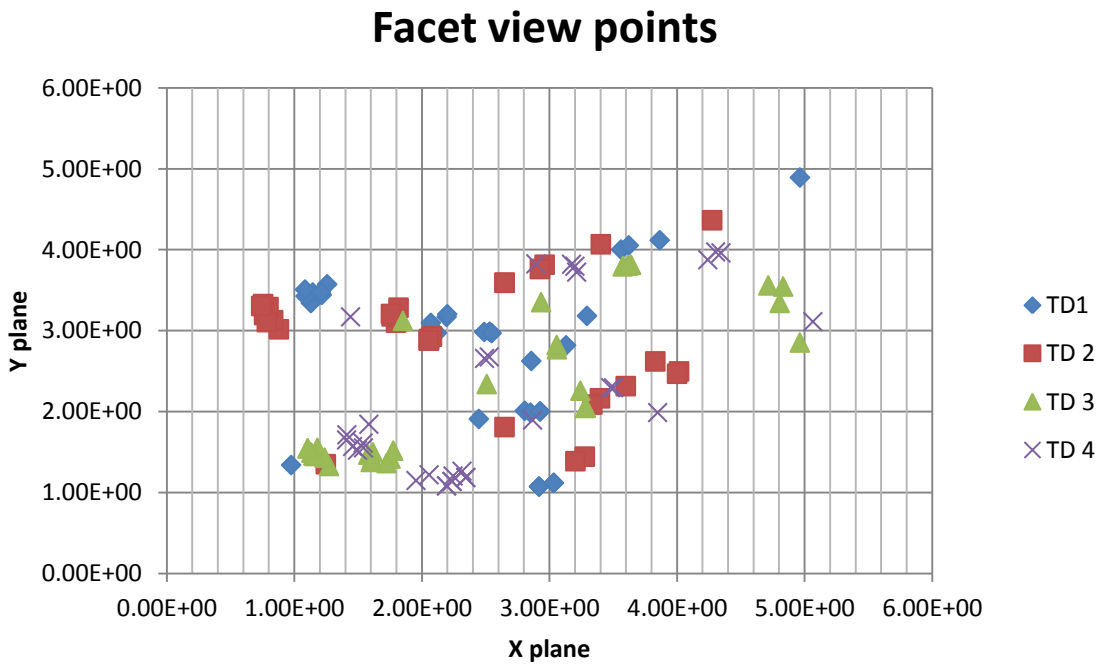

Figure 5.51: Linear regression model of all single coordination points from the facet view of TM bone. N= 32.

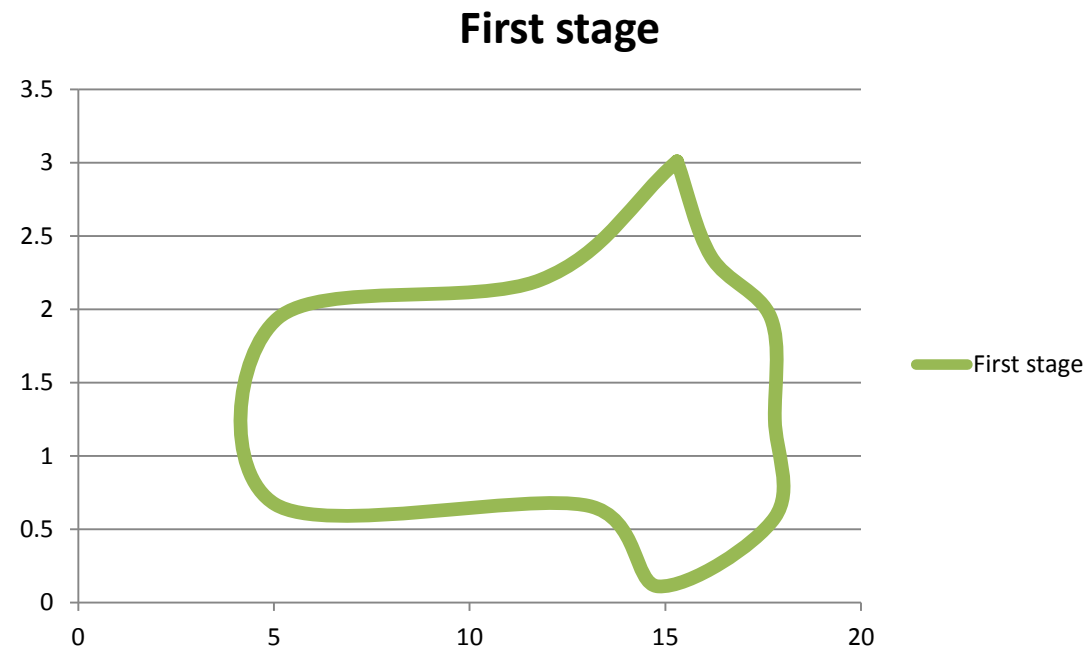

Figure 5.52: First stage of the default geometrical shape of the facet view of the TM bone.

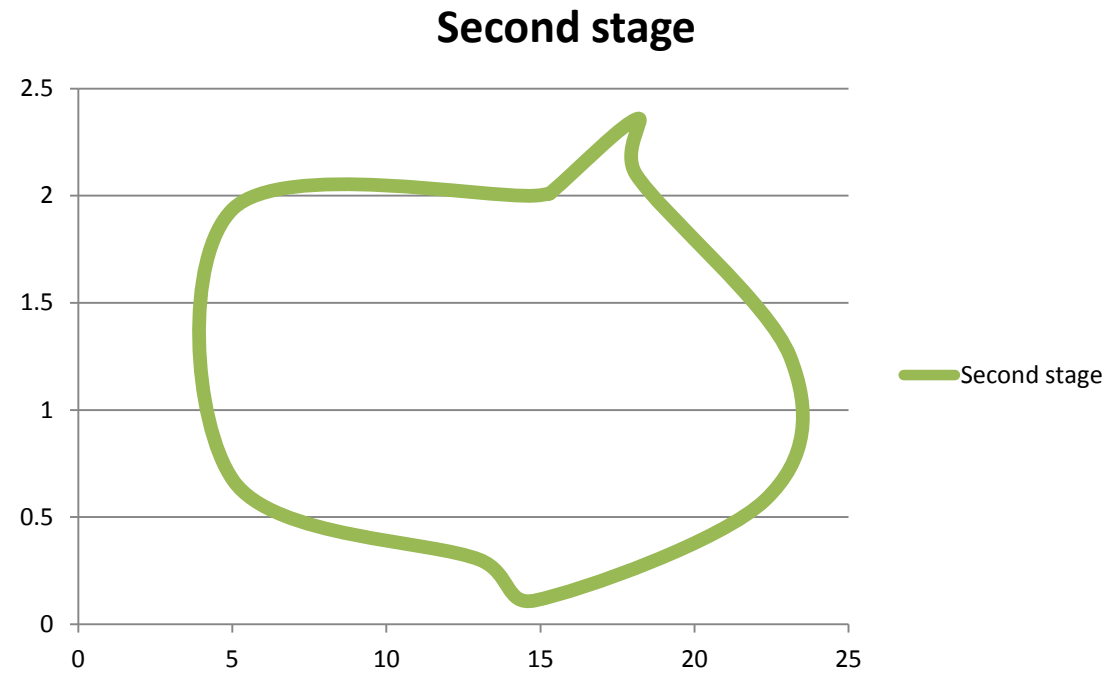

Figure 5.53: Second stage of the default geometrical shape of the facet view of the TM bone.

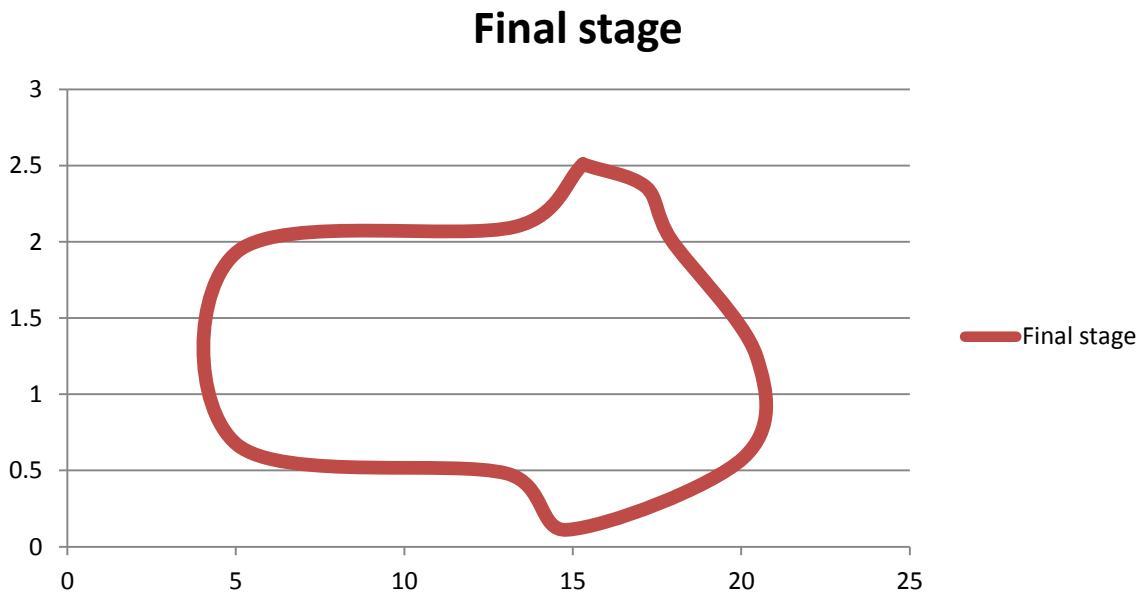

Figure 5.54: Final stage of the default geometrical shape of the facet view of the TM bone.

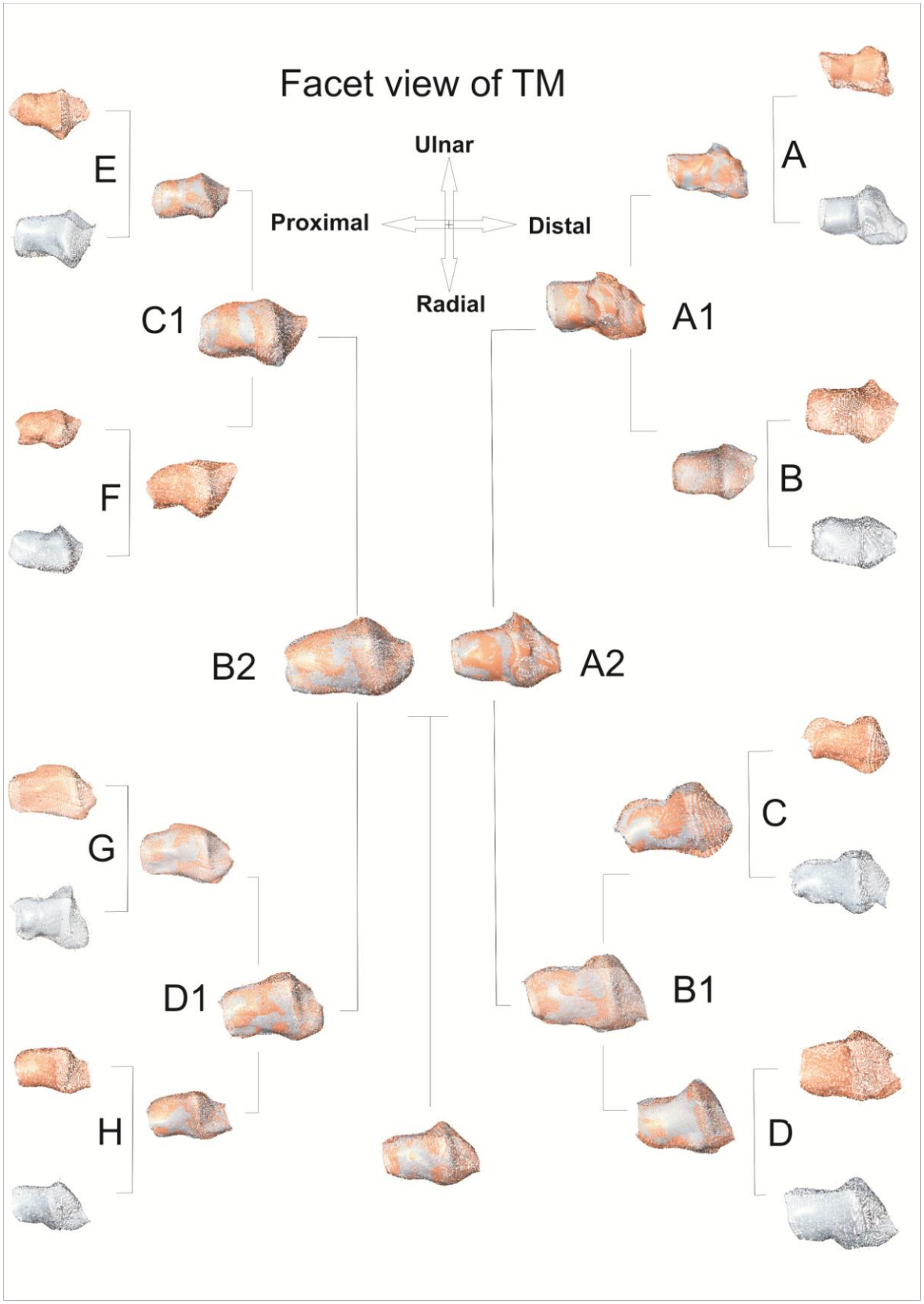

Figure 5.55: Stages of the facet view of the TM bone. Illustrates the first stage with its summation shapes (A1, B1, C1, and D1), the second stage with its summation shapes (A2, and B2) and the final stage with its summation final shape.

5.3.1.2 Radial view of the TM bone

5.3.1.2.1 First trapezial-radial point (TR1)

The R^2 value of the regression point was 0.22 and the significance F was 0.99. The regression point showed that the TR1 point was influenced by the square of single coordination points. TR1 had no relationship with the same point on the other dry TM bones, which means that this coordination point changed from the first stage to the final by 22%, without preserving its anatomical place through the sample population (Figure 5.56).

The significance factor F indicated that regression analysis was not significant (F>0.05). TR1 significantly changed from the first stage to the final.

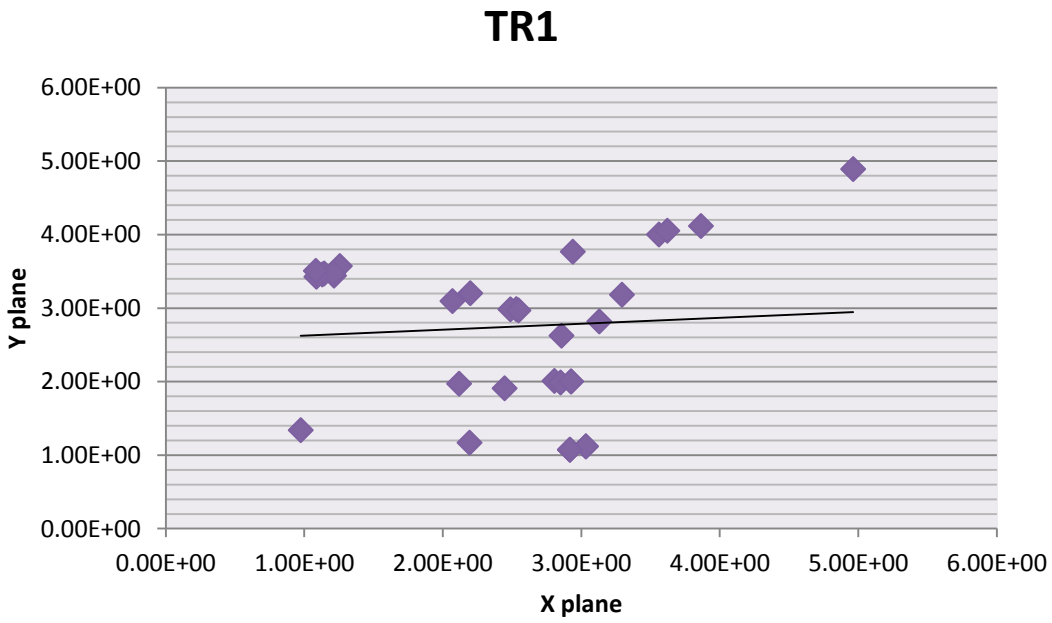

Figure 5.56: Linear regression model of the TR1 coordination point from the TM radial view. TR1 had no relationship with the same point on the other dry TM bones, the significance factor F indicated that regression analysis was not significant (F>0.05). N=32.

5.3.1.2.2 Second trapezial-radial point (TR2)

The R^2 value of the regression point was 0.04 and the significance F was 0.24. The regression point showed that the TR2 point was influenced by the square of single coordination points. TR2 had no relationship with the same point

on the other dry TM bones, which means that this coordination point was changed from the first stage to the final by 4%, without preserving its anatomical place through the sample population (Figure 5.57).

The significance factor F indicated that regression analysis was not significant (F>0.05). TR2 significantly changed from the first stage to the final.

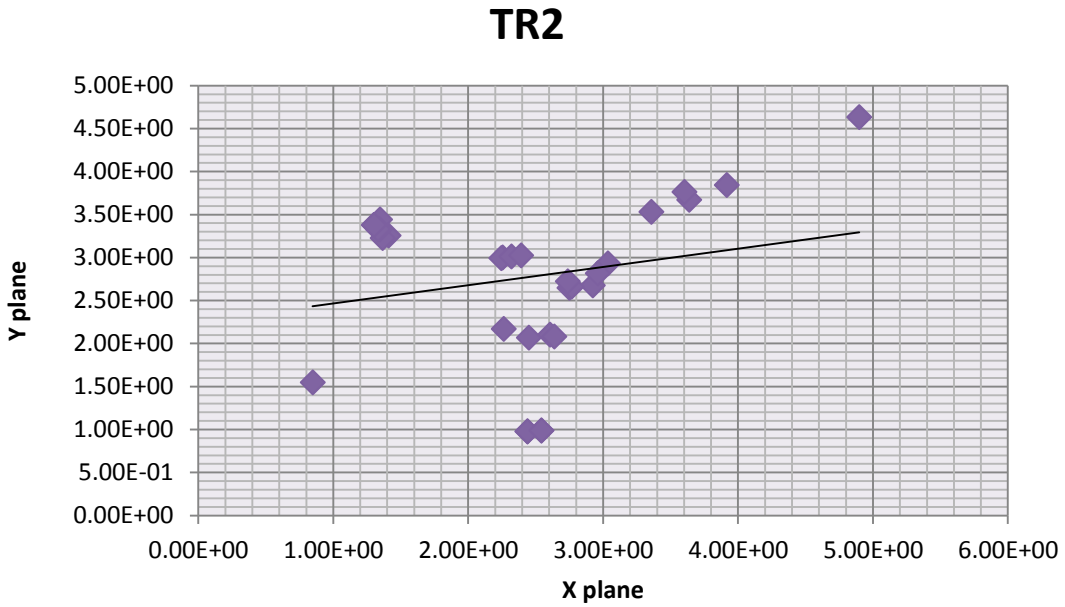

Figure 5.57: Linear regression model of the TR2 coordination point from the TM radial view. TR2 had no relationship with the same point on the other dry TM bones, the significance factor F indicated that regression analysis was not significant (F>0.05). N=32.

5.3.1.2.3 Third trapezial-radial point (TR3)

The R^2 value of the regression point was 0.33 and the significance F was 0.005. The regression point showed that the TR3 point was not influenced by the square of single coordination points. TR3 had a strong relationship with the same point on the other dry TM bones, which means that this coordination point was not changed from the first stage to the final by 33%, and preserved its anatomical place through the sample population (Figure 5.58).

The significance factor F indicated that regression analysis was significant (F<0.05). TR3 did not significantly change from the first stage to the final.

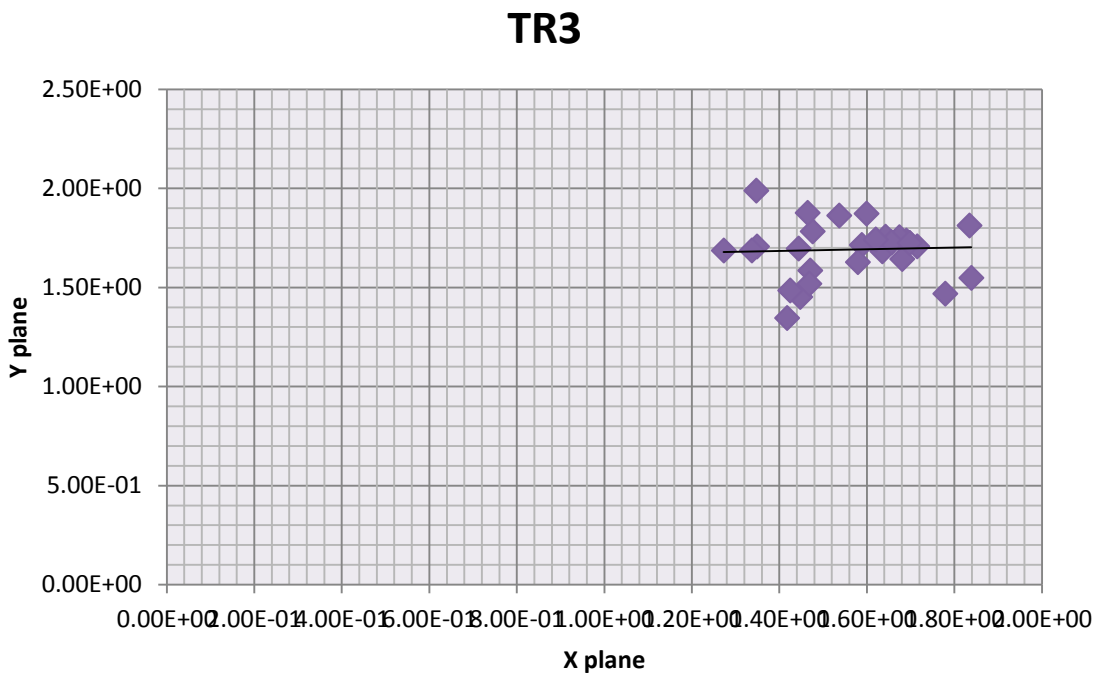

Figure 5.58: Linear regression model of the TR3 coordination point from the TM radial view. TR3 had a strong relationship with the same point on the other dry TM bones, the significance factor F indicated that regression analysis was significant (F<0.05). N=32.

5.3.1.2.4 Fourth trapezial-radial point (TR4)

The R^2 value of the regression point was 0.24, and the significance F was 0.0024. The regression point showed that the TR4 point was not influenced by the square of single coordination points. TR4 had a relationship with the same point on the other dry TM bones, which means that this coordination point did not change from the first stage to the final by 24%, and preserved its anatomical place through the sample population (Figure 5.59).

The significance factor F indicated that regression analysis was significant (F<0.05). TR4 did not significantly change from the first stage to the final.

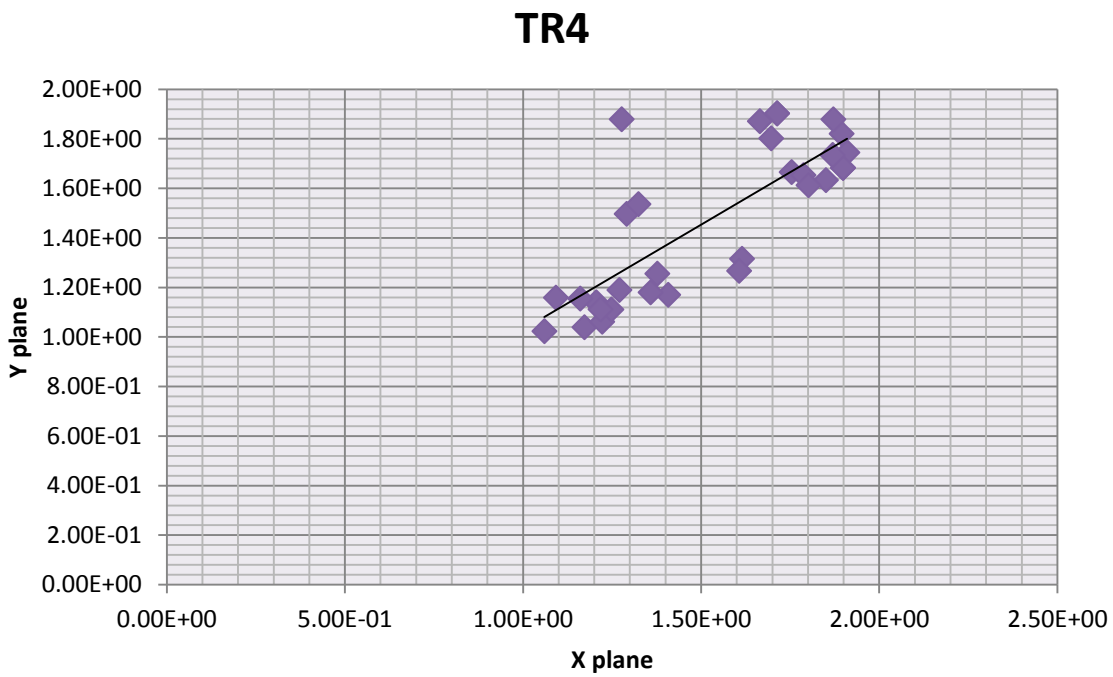

Figure 5.59: Linear regression model of the TR4 coordination point from the TM radial view. TR4 had a relationship with the same point on the other dry TM bones, the significance factor F indicated that regression analysis was significant (F<0.05). N=32.

5.3.1.2.5 Fifth trapezial-radial point (TR5)

The R^2 value of the regression point was 0.31, and the significance F was 0.0085. The regression point showed that the TR5 point was not influenced by the square of single coordination points. TR5 had a strong relationship with the same point on the other dry TM bones, which means that this coordination point did not change from the first stage to the final by 31%, and preserved its anatomical place through the sample population (Figure 5.60).

The significance factor F indicated that regression analysis was significant (F<0.05). TR5 did not significantly change from the first stage to the final.

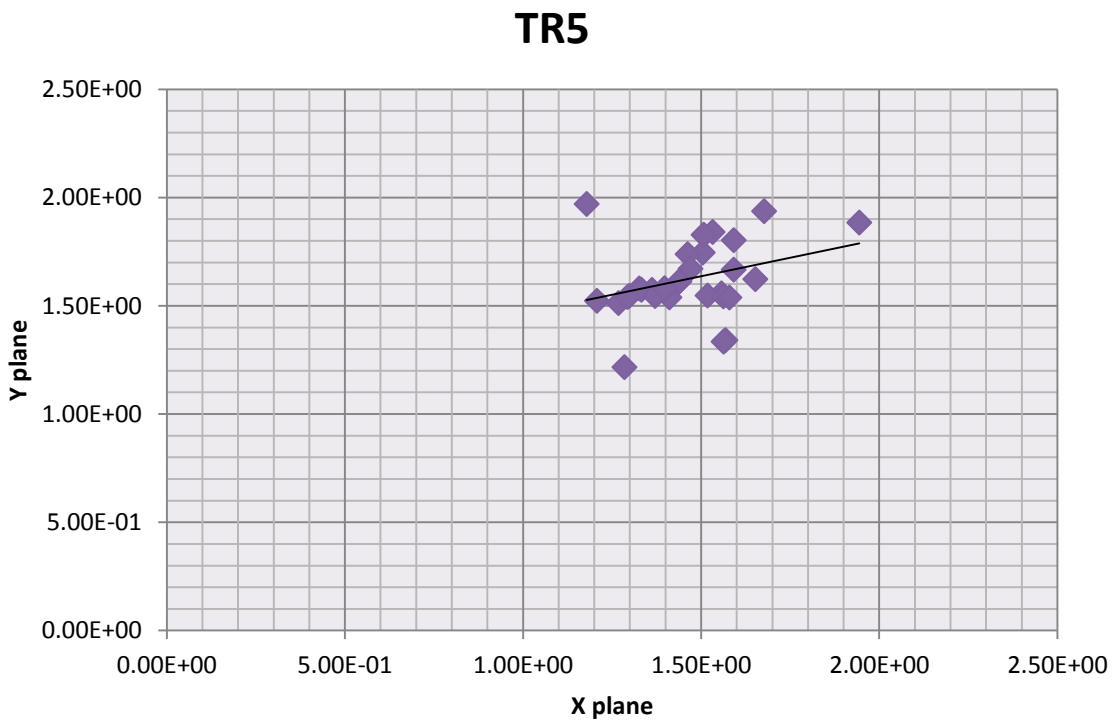

Figure 5.60: Linear regression model of the TR5 coordination point from the TM radial view. TR5 had a strong relationship with the same point on the other dry TM bones, the significance factor F indicated that regression analysis was significant (F<0.05). N=32.

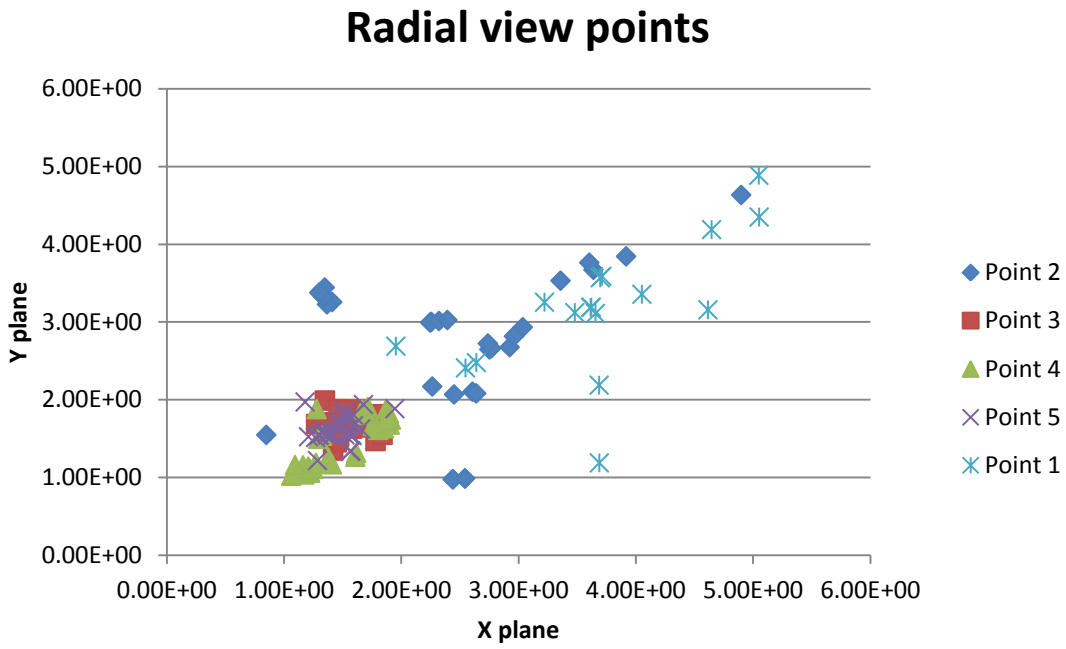

Figure 5.61: Linear regression model of all coordination points from the radial view of TM bone. N=32.

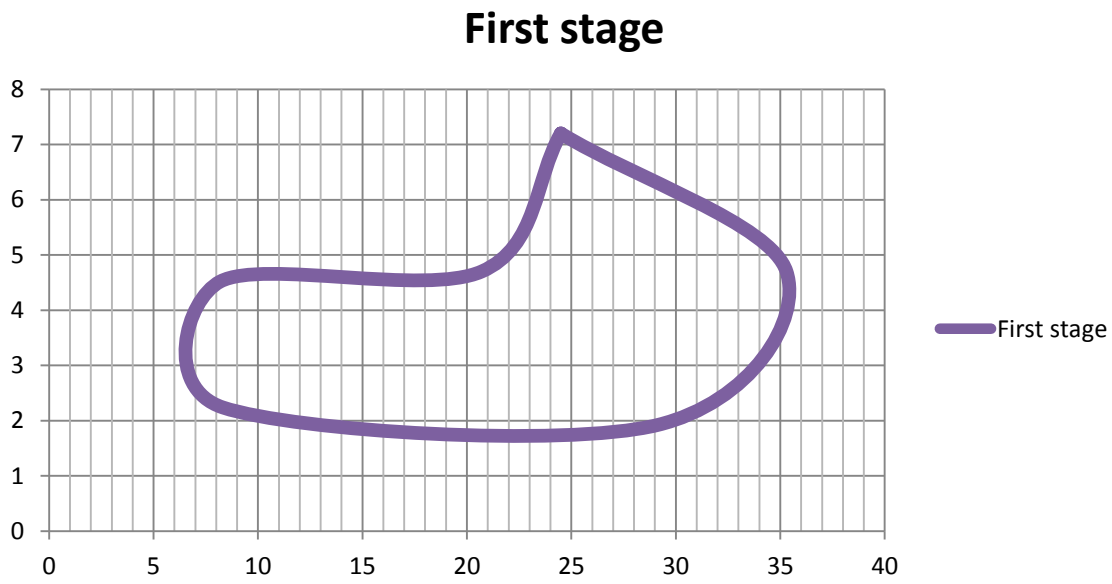

Figure 5.62: First stage of the default geometrical shape of the radial view of the TM bone.

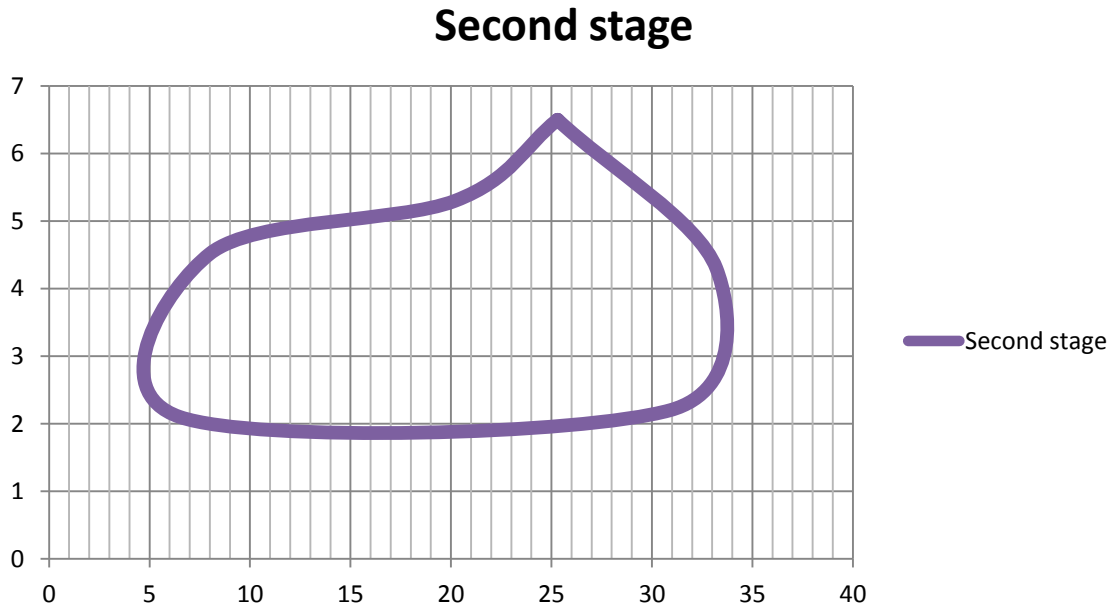

Figure 5.63: Second stage of the default geometrical shape of the radial view of the TM bone.

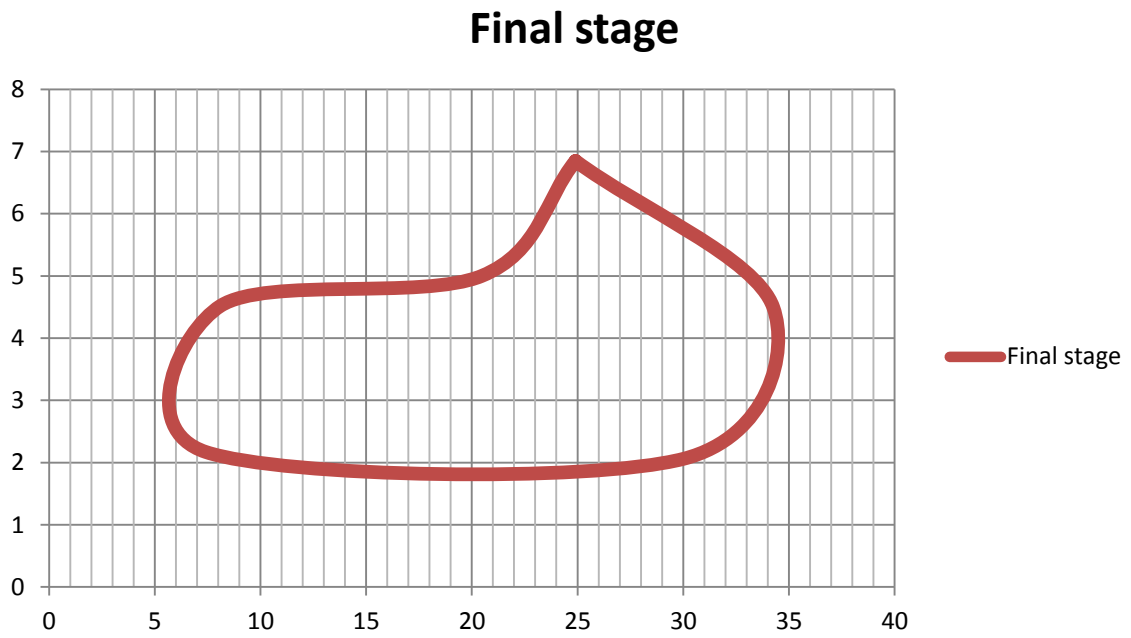

Figure 5.64: Final stage of the default geometrical shape of the radial view of the TM bone.

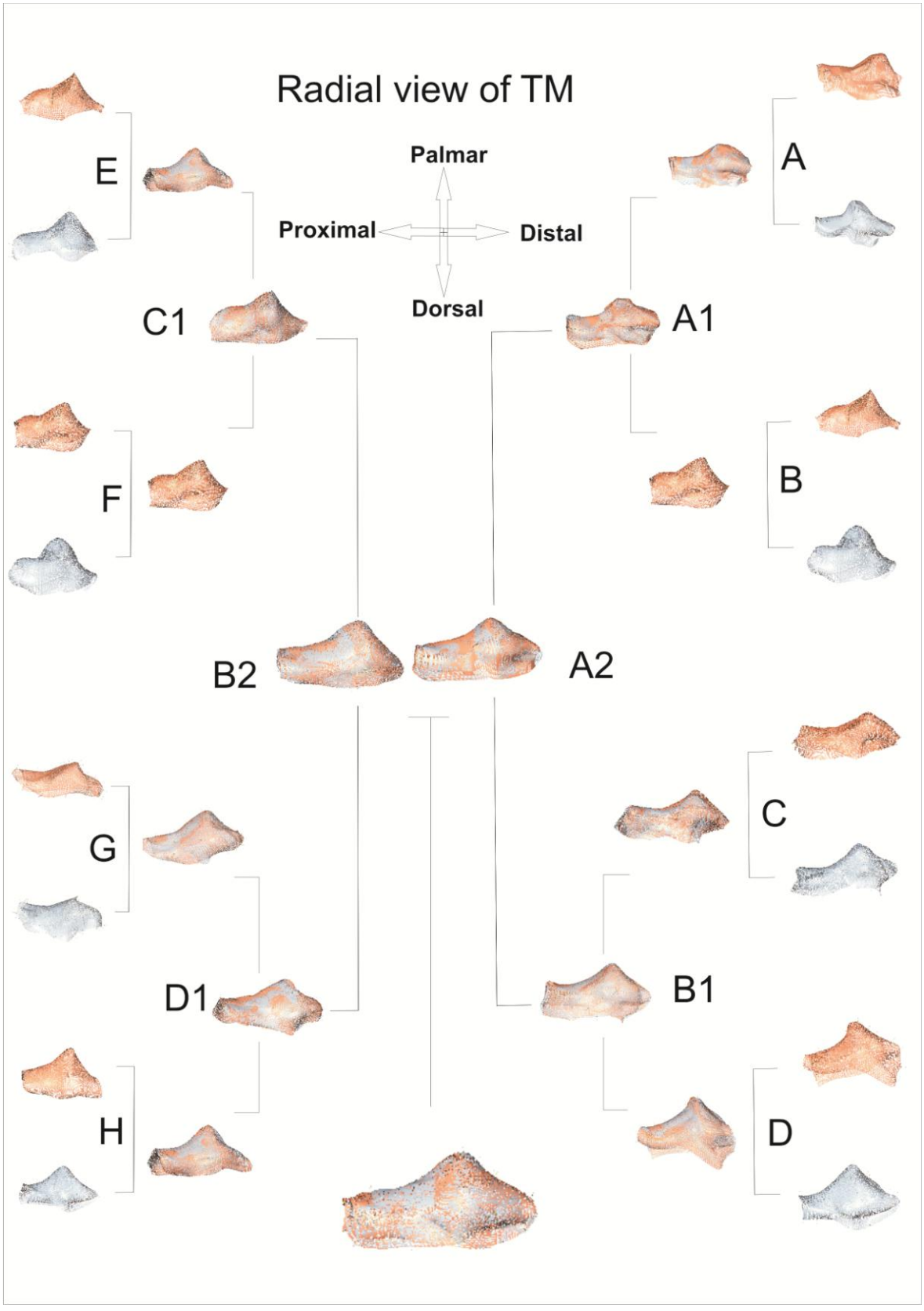

Figure 5.65: Stages of the radial view of the TM bone. Illustrates the first stage with its summation shapes (A1, B1, C1 and D1), the second stage with its summation shapes (A2 and B2), and the final stage with its summation final shape.

5.3.1.3 Palmar view of the 1st MC bone

5.3.1.3.1 First metacarpal-palmar point (MP1)

The R^2 value of the regression point was 0.30, and the significance F was 0.0012. The regression point showed that the MP1 point was not influenced by the square of single coordination points. MP1 had a strong relationship with the same point on the other dry 1st MC bones, which means that this coordination point did not change from the first stage to the final by 30%, and preserved its anatomical place through the sample population (Figure 5.66).

The significance factor F indicated that regression analysis was significant (F<0.05). The MP1 point did not significantly change from the first stage to the final.

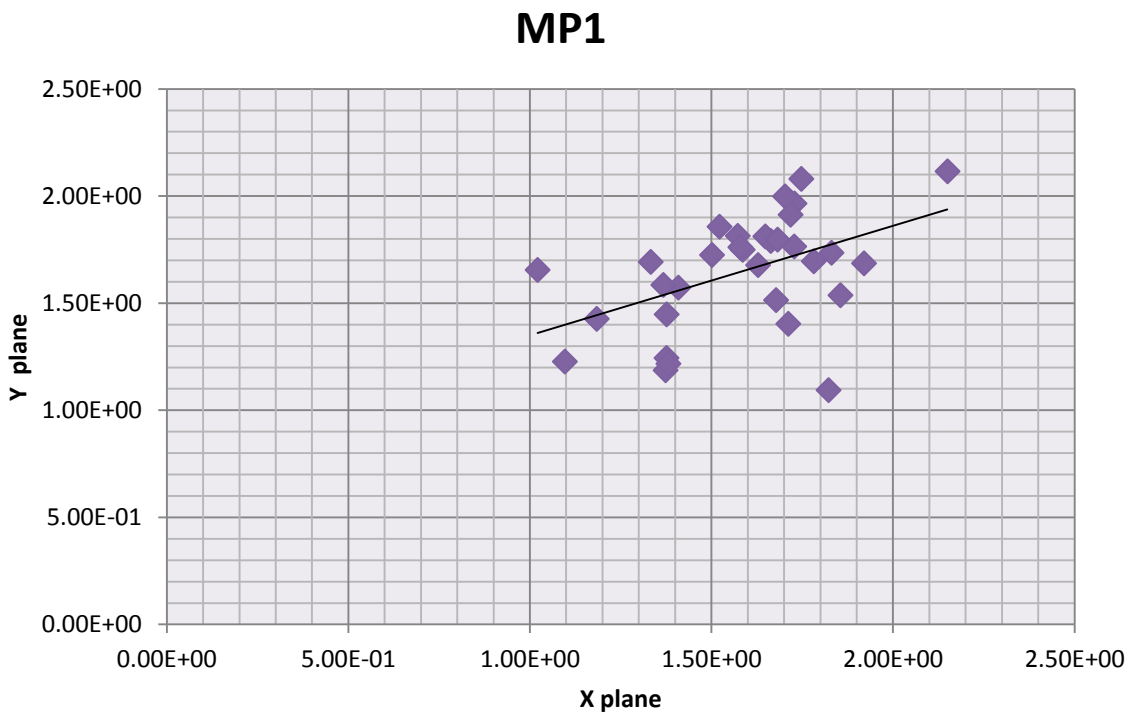

Figure 5.66: Linear regression model of the MP1 coordination point from the palmar view of the 1st MC. MP1 had a relationship with the same point on the other dry 1st MC bones, the significance factor F indicated that regression analysis was significant (F<0.05). N=32.

5.3.1.3.2 Second metacarpal-palmar point (MP2)

The R^2 value of the regression point was 0.15 and the significance F was 0.02. The regression point showed that the MP2 point was not influenced by the square of single coordination points. MP2 had a relationship with the same point on the other dry 1st MC bones, which means that this coordination point did not change from the first stage to the final by 15%, and preserved its anatomical place through the sample population (Figure 5.67).

The significance factor F indicated that regression analysis was significant (F<0.05). The MP2 point did not significantly change from the first stage to the final.

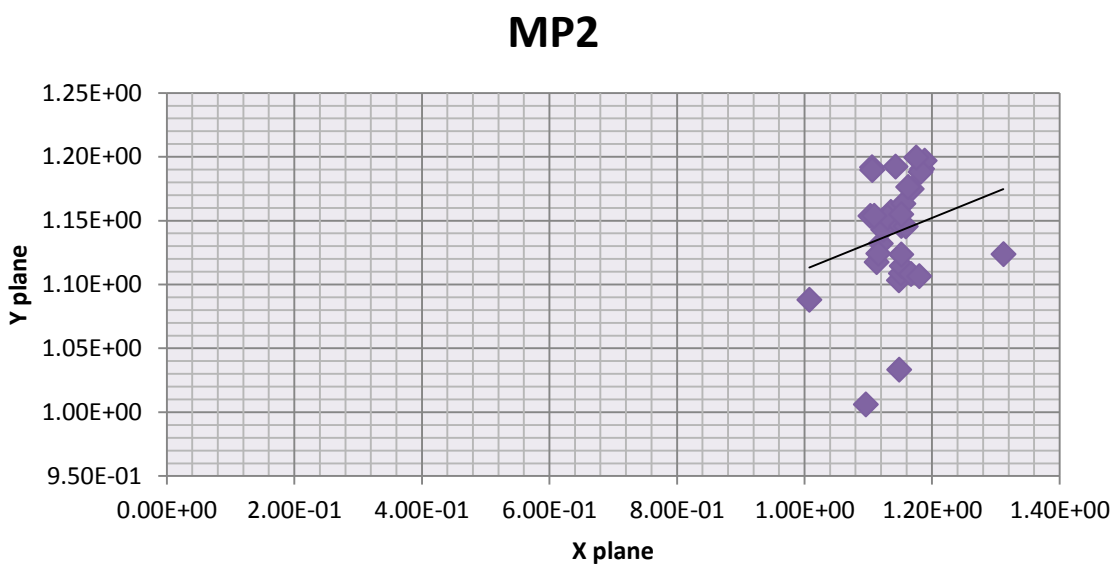

Figure 5.67: Linear regression model of the MP2 coordination point from the 1st MC palmar view. MP2 had a relationship with the same point on the other dry 1st MC bones, the significance factor F indicated that regression analysis was significant (F<0.05). N=32.

5.3.1.3.3 Third metacarpal-palmar point (MP3)

The R^2 value of the regression point was 0.003 and the significance F was 0.91. The regression point showed that the MP3 point was influenced by the square of single coordination points. MP3 had no relationship with the same point on the other dry 1st MC bones, which means that this coordination point significantly changed from the first stage to the final by 3%, without preserving its anatomical place through the sample population (Figure 5.68).

The significance factor F indicated that regression analysis was not significant (F>0.05). The MP3 point significantly changed from the first stage to the final.

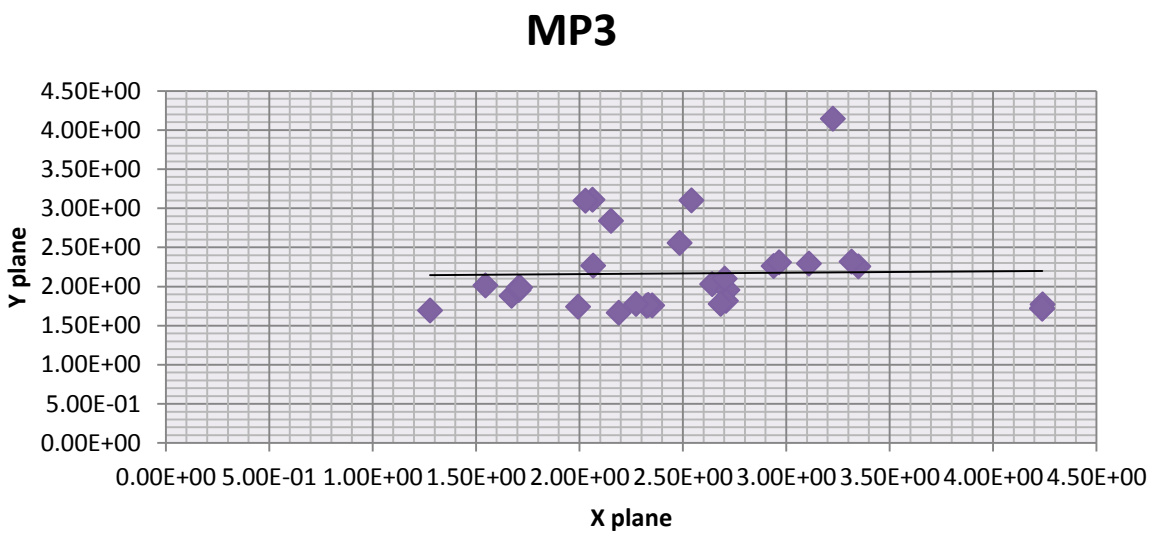

Figure 5.68: Linear regression model of the MP3 coordination point from the 1st MC palmar view. MP3 had no relationship with the same point on the other dry 1st MC bones, the significance factor F indicated that regression analysis was not significant (F>0.05). N=32.

5.3.1.3.4 Fourth metacarpal-palmar point (MP4)

The R^2 value of the regression point was 0.006 and the significance F was 0.6. The regression point showed that the MP4 point was influenced by the square of the single coordination points. MP4 had no relationship with the same point on the other dry 1st MC bones, which means that this coordination point changed from the first stage to the final by 6%, without preserving its anatomical place through the sample population (Figure 5.69).

The significance factor F indicated that regression analysis was not significant (F>0.05). MP4 significantly changed from the first stage to the final.

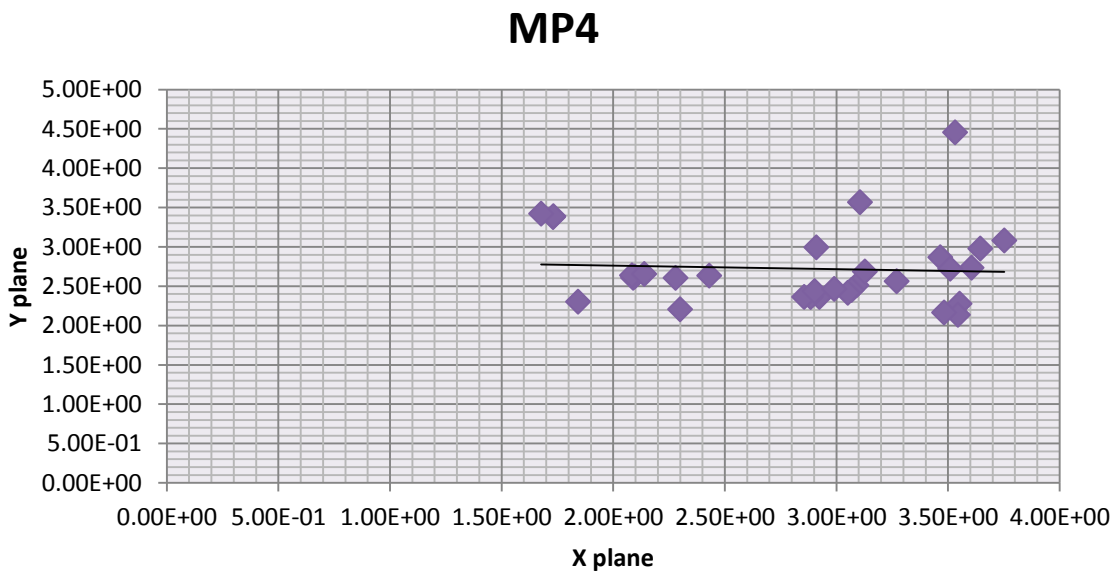

Figure 5.69: Linear regression model of the MP4 coordination point from the 1st MC palmar view. MP4 had no relationship with the same point on the other dry 1st MC bones, the significance factor F indicated that regression analysis was not significant (F>0.05). N=32.

5.3.1.3.5 Fifth metacarpal-palmar point (MP5)

The R^2 value of the regression point was 0.10 and the significance F was 0.007. The regression point showed that the MP5 point was not influenced by the square of single coordination points. MP5 had a relationship with the same point on the other dry 1st MC bones, which means that this coordination point did not change from the first stage to the final by 1%, and preserved its anatomical place through the sample population (Figure 5.70).

The significance factor F indicated that regression analysis was significant (F<0.05). The MP5 point did not significantly change from the first stage to the final.

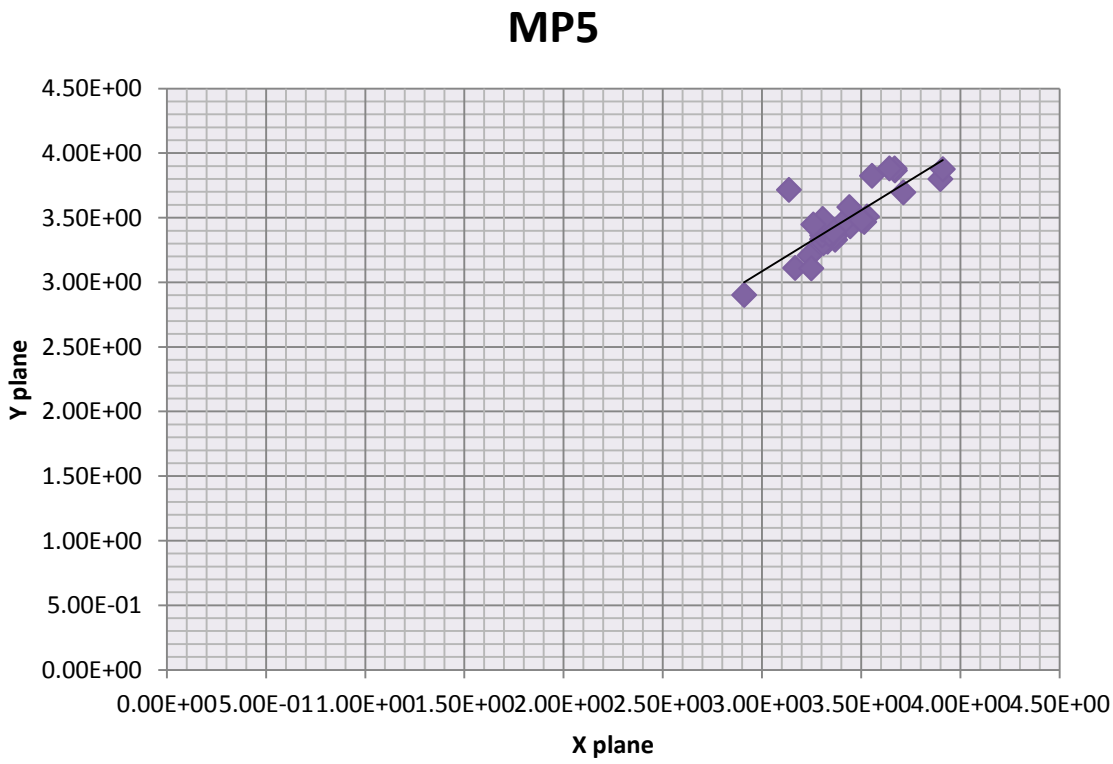

Figure 5.70: Linear regression model of the MP5 coordination point from the 1st MC palmar view. MP5 had a relationship with the same point on the other dry 1st MC bones, the significance factor F indicated that regression analysis was significant (F<0.05). N=32.

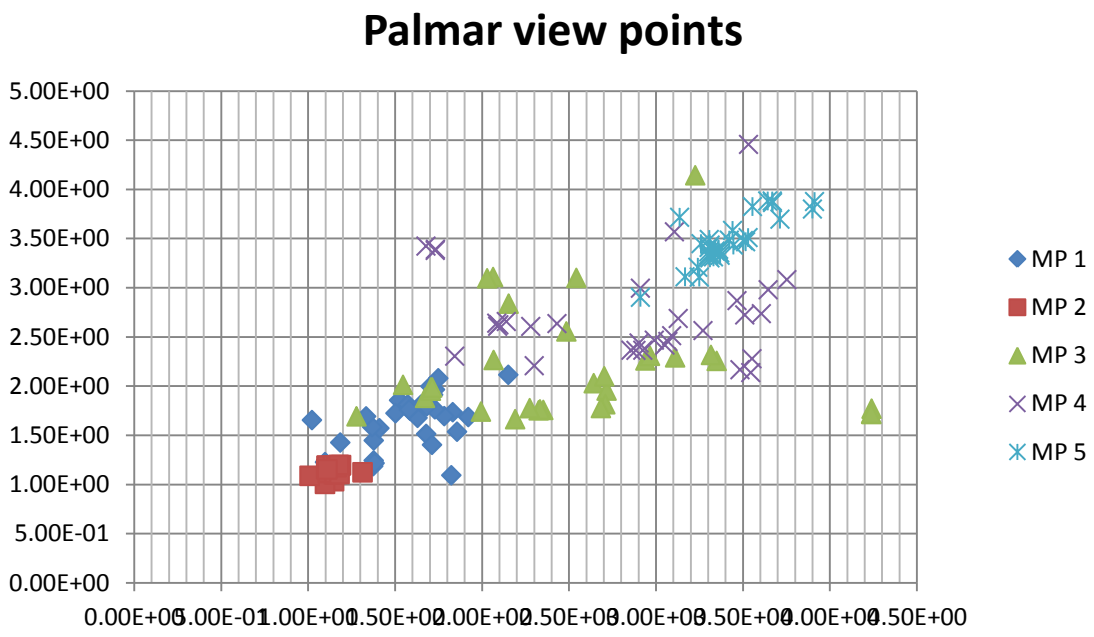

Figure 5.71: Linear regression model of all single coordination points from the palmar view of 1st MC bone. N=32.

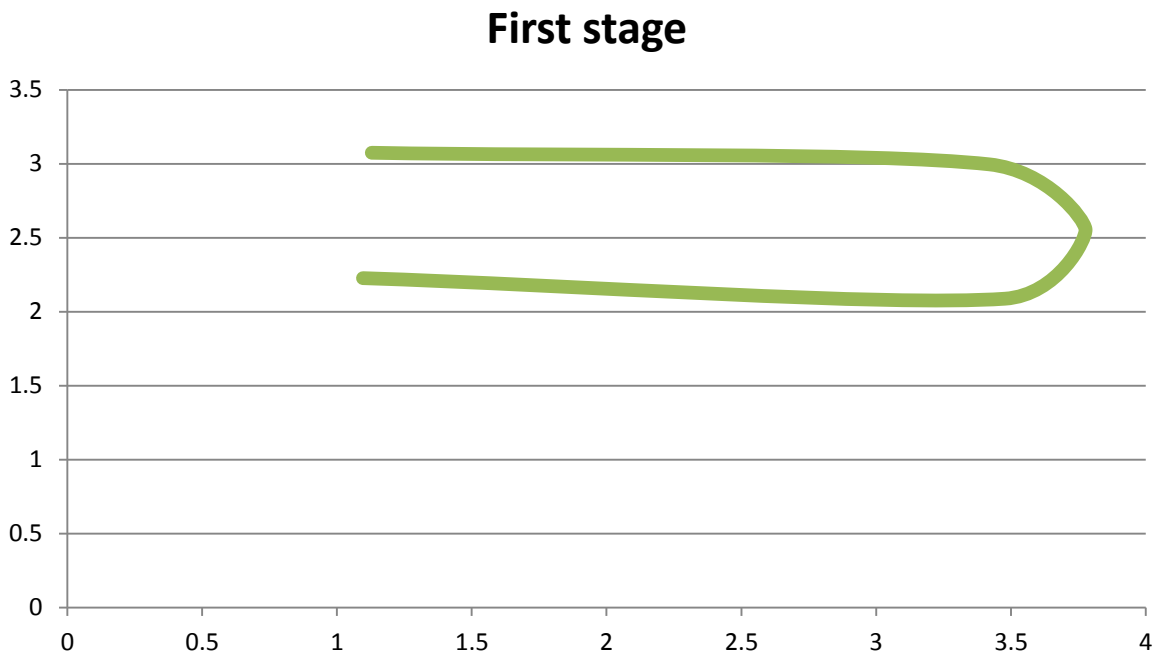

Figure 5.72: First stage of the default geometrical shape of the palmar view of the 1st MC bone.

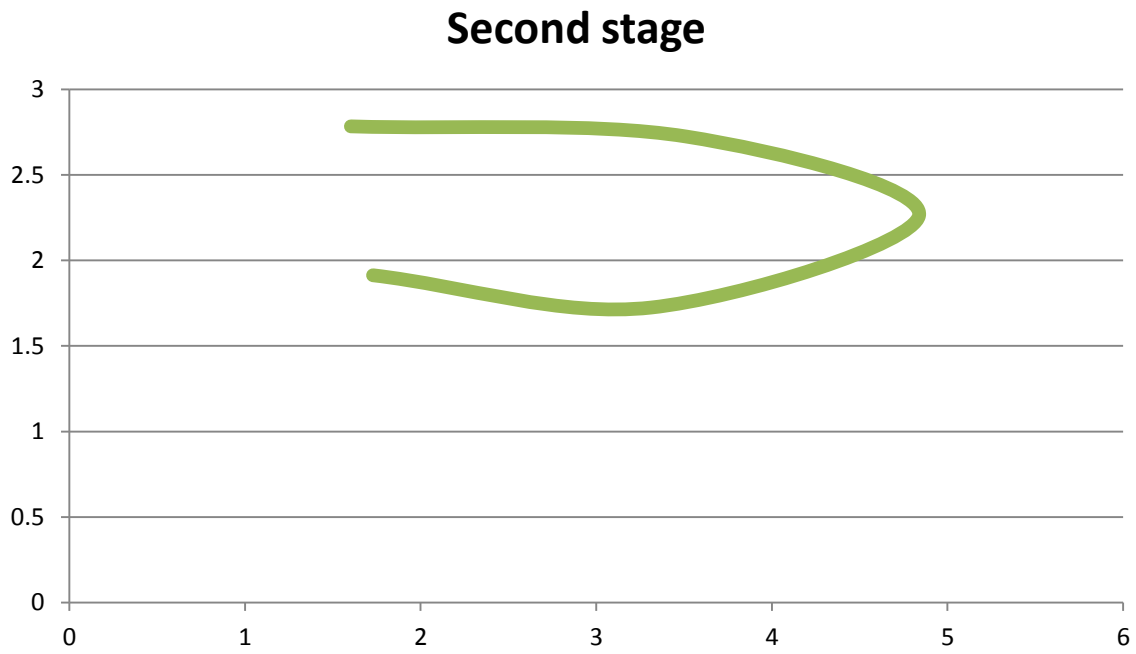

Figure 5.73: Second stage of the default geometrical shape of the palmar view of the 1st MC bone.

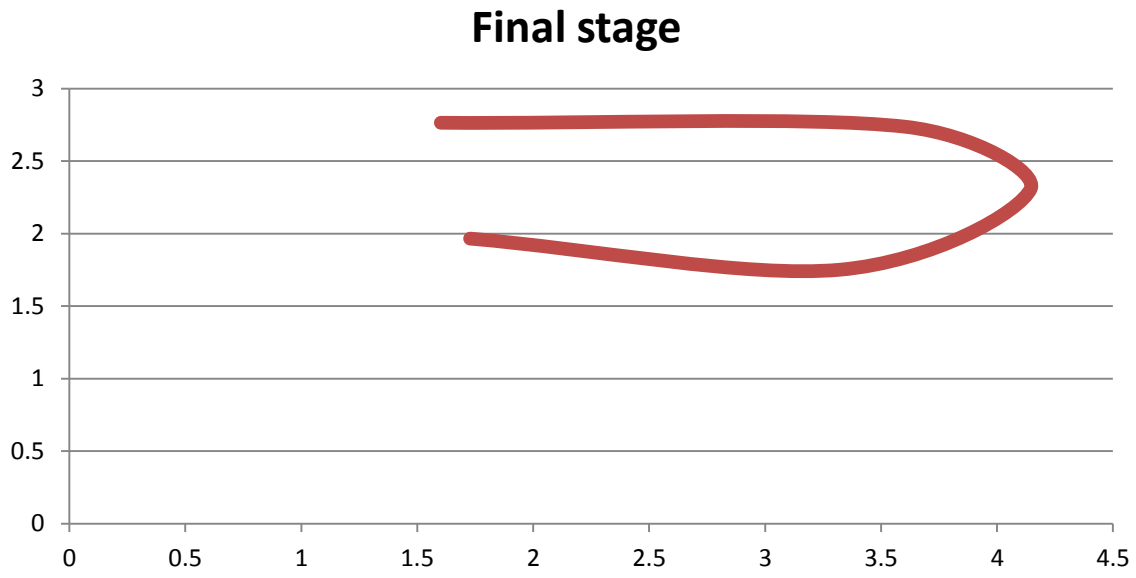

Figure 5.74: Final stage of the default geometrical shape of the palmar view of the 1st MC bone.

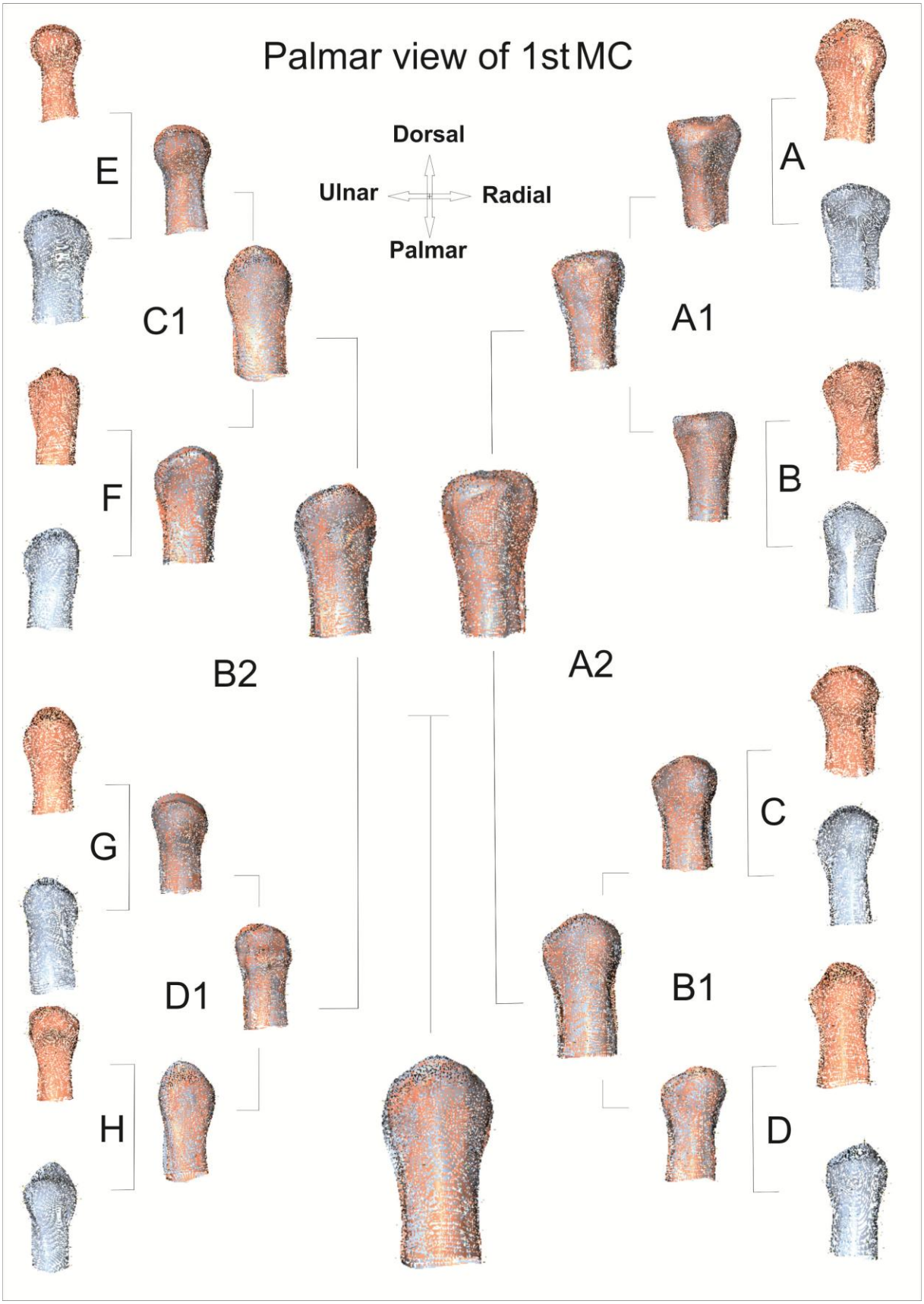

Figure 5.75: Stages of the palmar view of the 1st MC bone. Illustrates the first stage with its summation shapes (A1, B1, C1 and D1), the second stage with its summation shapes (A2 and B2) and the final stage with its summation final shape.

5.3.1.4 Dorsal view of the 1st MC bone

5.3.1.4.1 First metacarpal-dorsal point (MD1)

The R^2 value of the regression point was 0.17 and the significance F was 0.0018. The regression point showed that the MD1 point was not influenced by the square of single coordination points. MD1 had a strong relationship with the same point on the other dry 1st MC bones, which means that this coordination point did not change from the first stage to the final by 17%, and preserved its anatomical place through the sample population (Figure 5.76).

The significance factor F indicated that regression analysis was significant (F<0.05). The MD1 point did not significantly change from the first stage to the final stage.

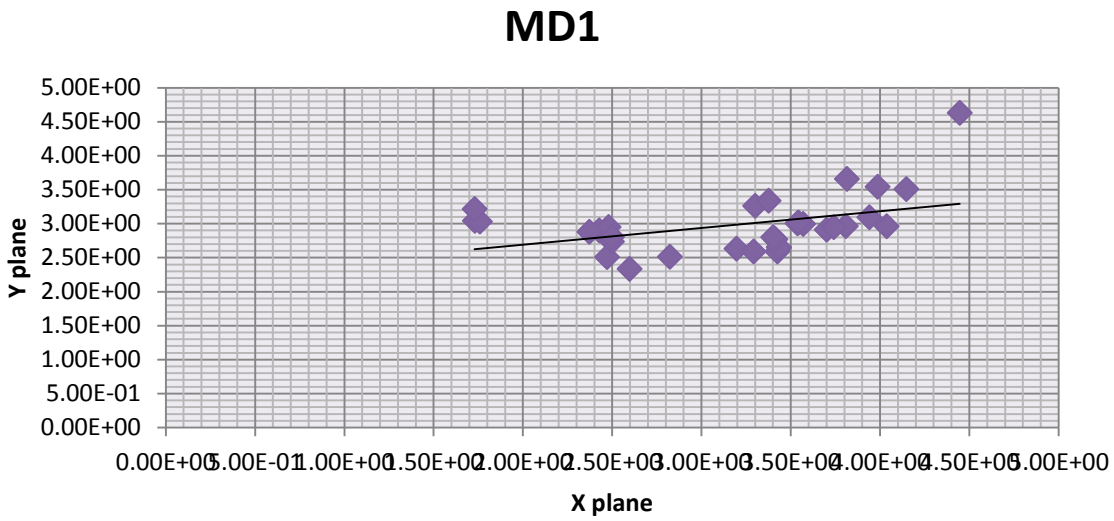

Figure 5.76: Linear regression model of the MD1 coordination point from the 1st MC dorsal view. MD1 had a strong relationship with the same point on the other dry 1st MC bones the significance factor F indicated that regression analysis was significant (F<0.05). N=32.

5.3.1.4.2 Second metacarpal-dorsal point (MD2)

The R^2 value of the regression point was 0.018 and the significance F was 0.45. The regression point showed that the MD2 point was influenced by the square of single coordination points. MD2 had no relationship with the same point

on the other dry 1st MC bones, which means that this coordination point changed from the first stage to the final by 1.8%, without preserving its anatomically place through the sample population (Figure 5.77).

The significance factor F indicated that regression analysis was not significant (F>0.05). The MD2 point changed significantly from the first stage.

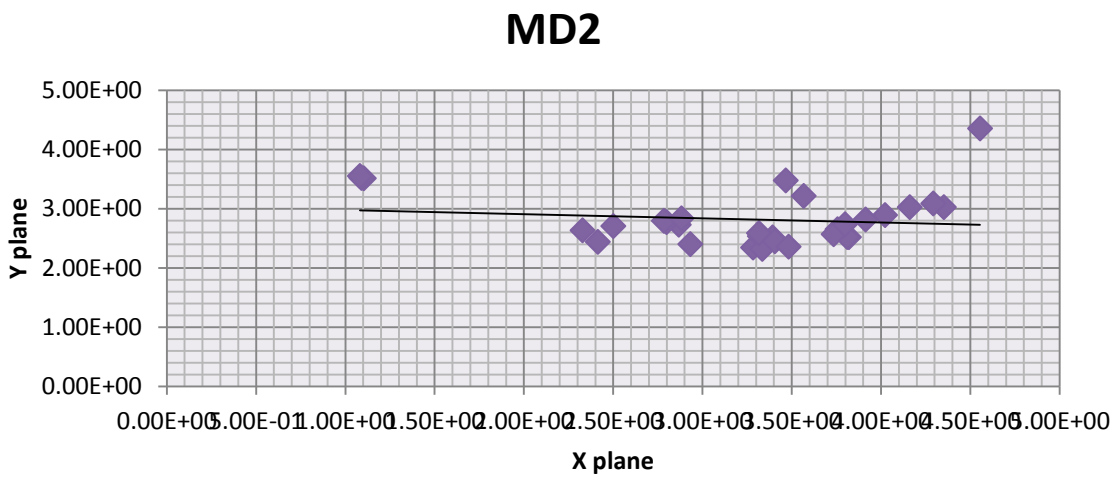

Figure 5.77: Linear regression model of the MD2 coordination point from the 1st MC dorsal view. MD2 had no relationship with the same point on the other dry 1st MC bones, the significance factor F indicated that regression analysis was not significant (F>0.05). N=32.

5.3.1.4.3 Third metacarpal-dorsal point (MD3)

The R^2 value of the regression point was 0.0057 and the significance F was 0.68. The regression point showed that the MD3 point was influenced by the square of single coordination points. MD3 had no relationship with the same point on the other dry 1st MC bones, which means that this coordination point changed from the first stage to the final by 0.57%, without preserving its anatomical place through the sample population (Figure 5.78).

The significance factor F indicated that regression analysis was not significant (F>0.05). The MD3 point changed significantly from the first stage.

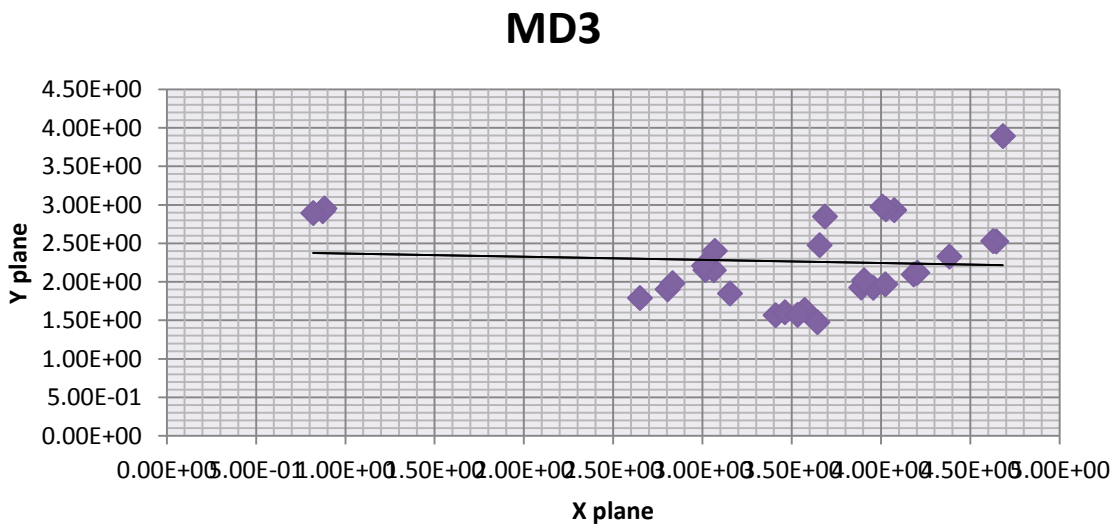

Figure 5.78: Linear regression model of the MD3 coordination point from the 1st MC dorsal view. MD3 had no relationship with the same point on the other dry 1st MC bones, the significance factor F indicated that regression analysis was not significant (F>0.05). N=32

5.3.1.4.4 Fourth metacarpal-dorsal point (MD4)

The R^2 value of the regression point was 0.0075 and the significance F was 0.13. The regression point showed that the MD4 point was influenced by the square of single coordination points. MD4 had no relationship with the same point on the other dry 1st MC bones, which means that this coordination point changed from the first stage to the final by 0.75%, without preserving its anatomical place through the sample population (Figure 5.79).

The significance factor F indicated that regression analysis was not significant (F>0.05). The MD4 point significantly changed from the first stage.

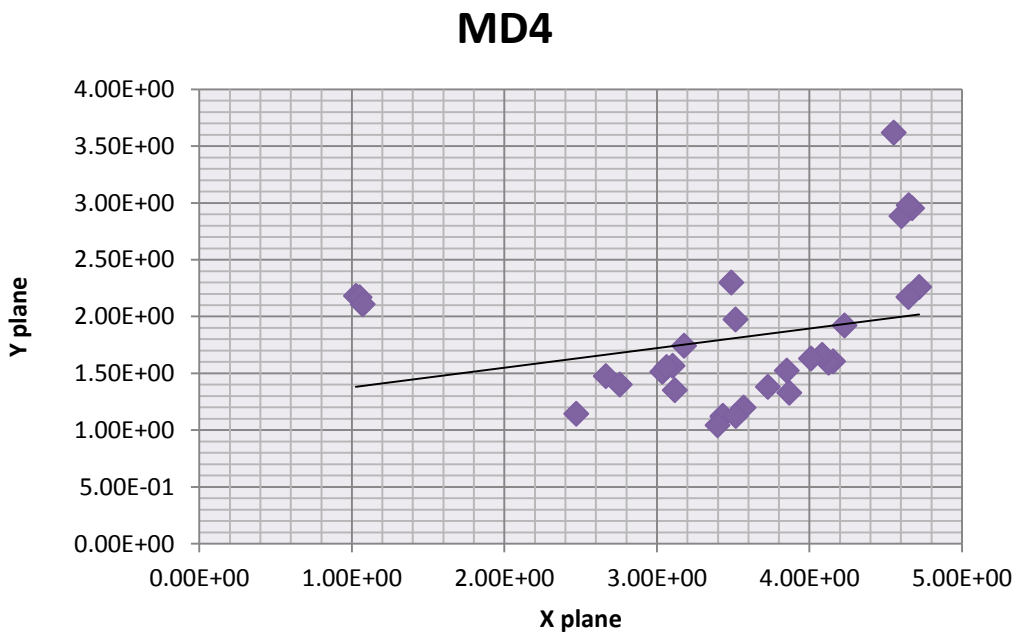

Figure 5.79: Linear regression model of the MD4 coordination point from the 1st MC dorsal view. MD4 had no relationship with the same point on the other dry 1st MC bones, the significance factor F indicated that regression analysis was not significant (F>0.05). N=32.

5.3.1.4.5 Fifth metacarpal-dorsal point (MD5)

The R^2 value of the regression point was 0.29 and the significance F was 0.0014. The regression point showed that the MD5 point was not influenced by the square of single coordination points. MD5 had a strong relationship with the same point on the other dry 1st MC bones, which means that this coordination point did not change from the first stage to the final by 29%, and preserved its anatomical place through the sample population (Figure 5.80).

The significance factor F indicated that regression analysis was significant (F<0.05). The MD5 point did not significantly change from the first stage to the final stage.

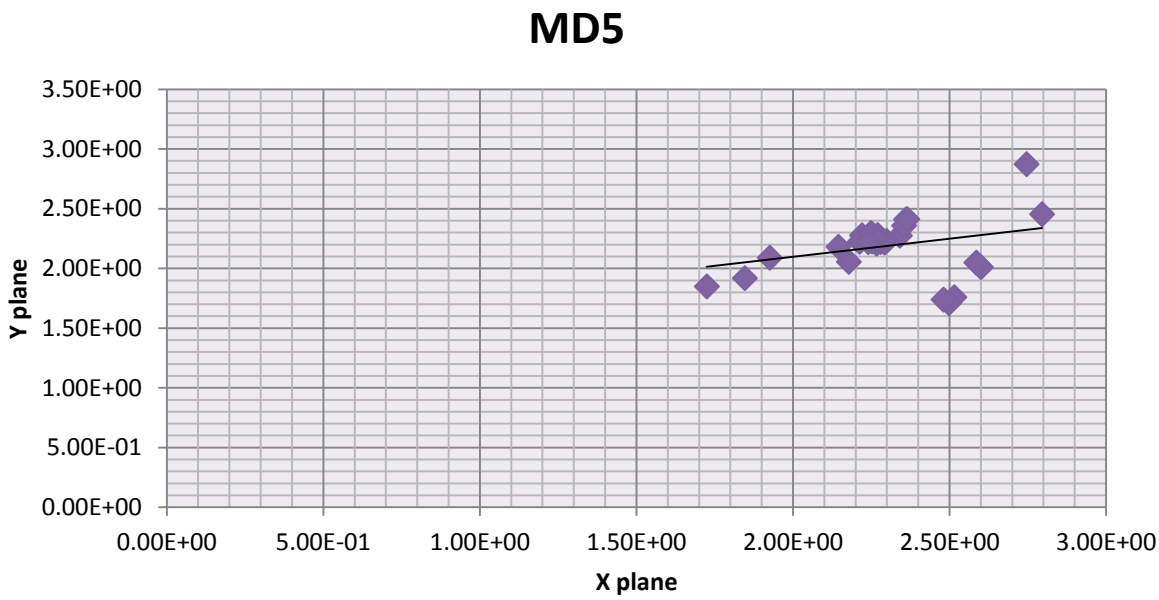

Figure 5.80: Linear regression model of the MD5 coordination point from the 1st MC dorsal view. MD5 had a strong relationship with the same point on the other dry 1st MC bones, the significance factor F indicated that regression analysis was significant (F<0.05). N=32.

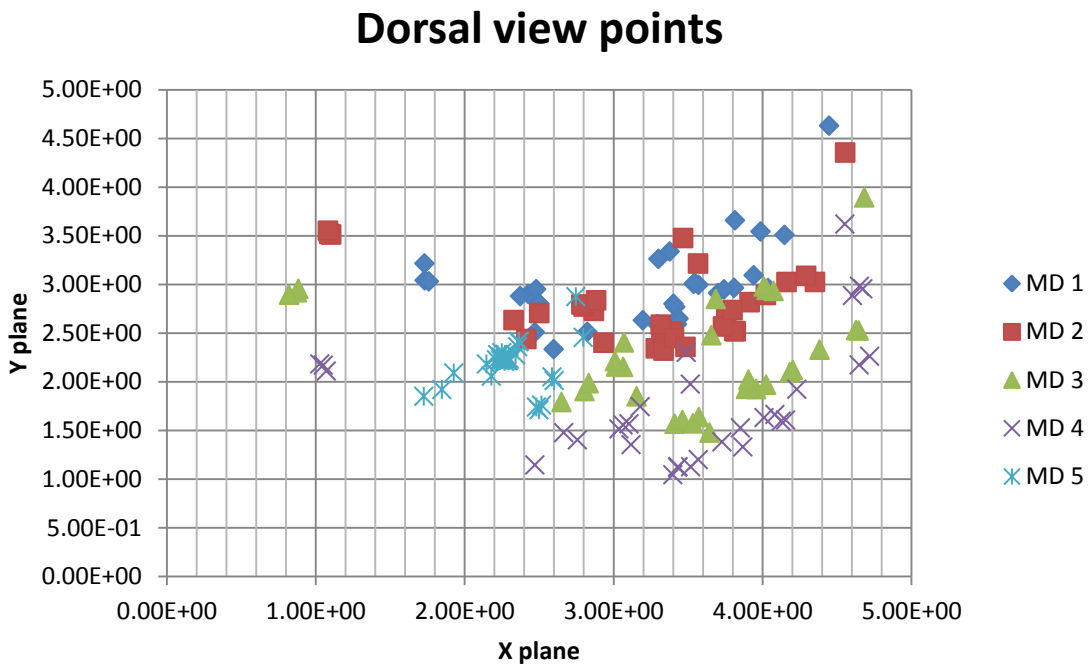

Figure 5.81: Linear regression model of all single coordination points from the dorsal view of 1st MC bone. N=32.

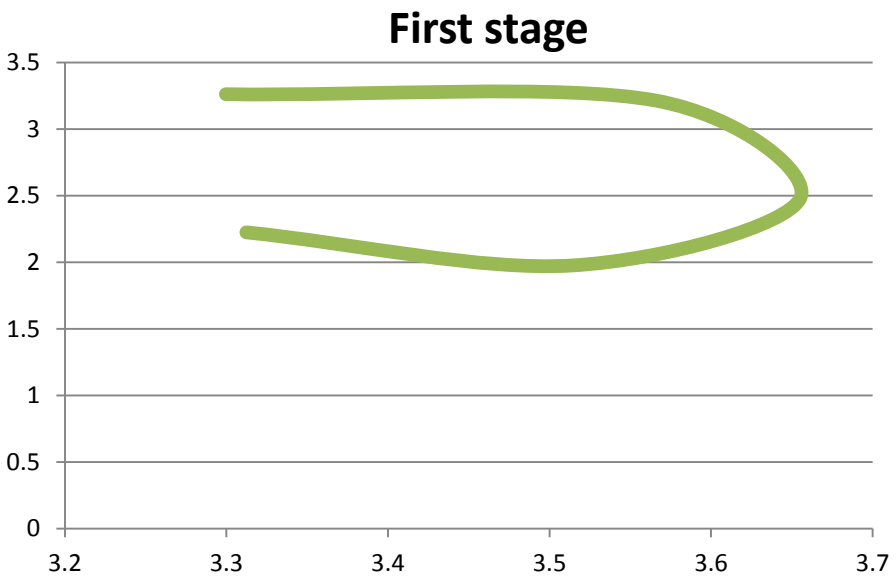

Figure 5.82: First stage of the default geometrical shape of the dorsal view of the 1st MC bone.

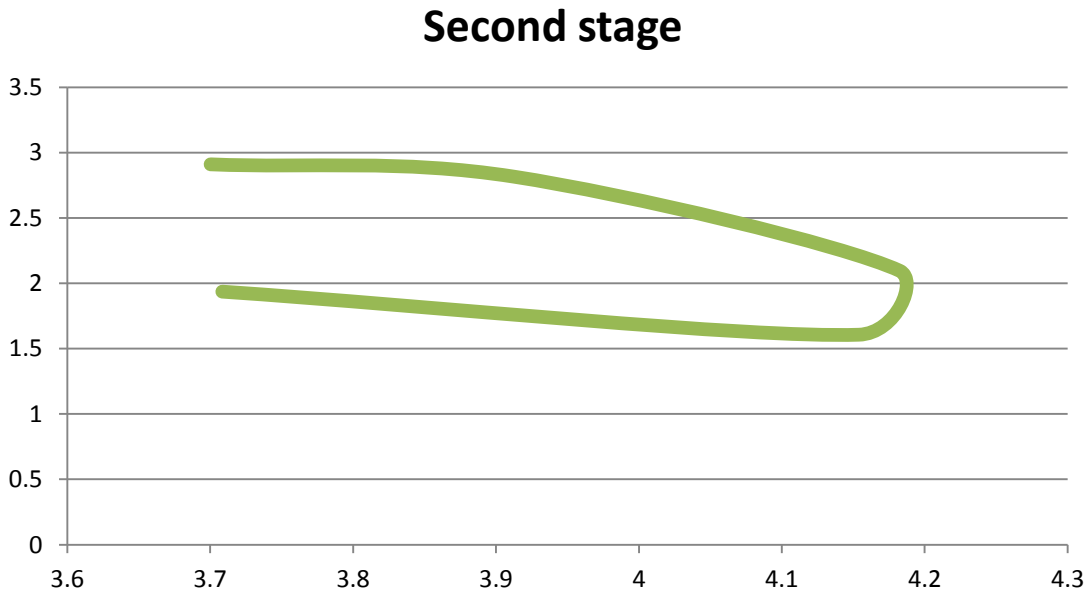

Figure 5.83: Second stage of the default geometrical shape of the dorsal view of the 1st MC bone.

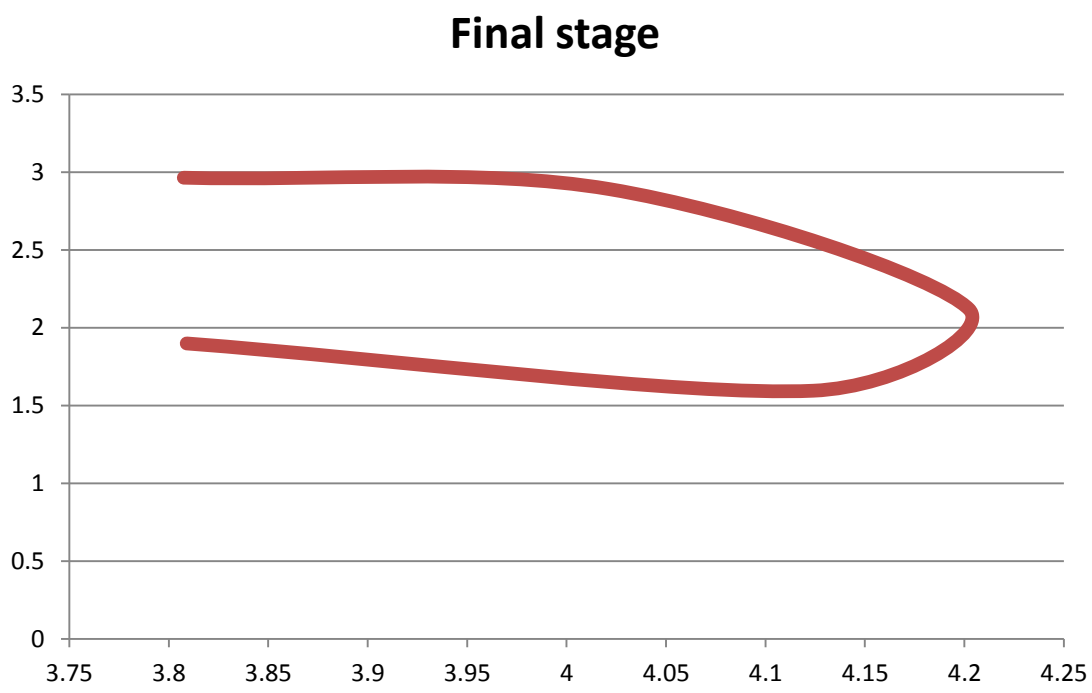

Figure 5.84: Final stage of the default geometrical shape of the dorsal view of the 1st MC bone.

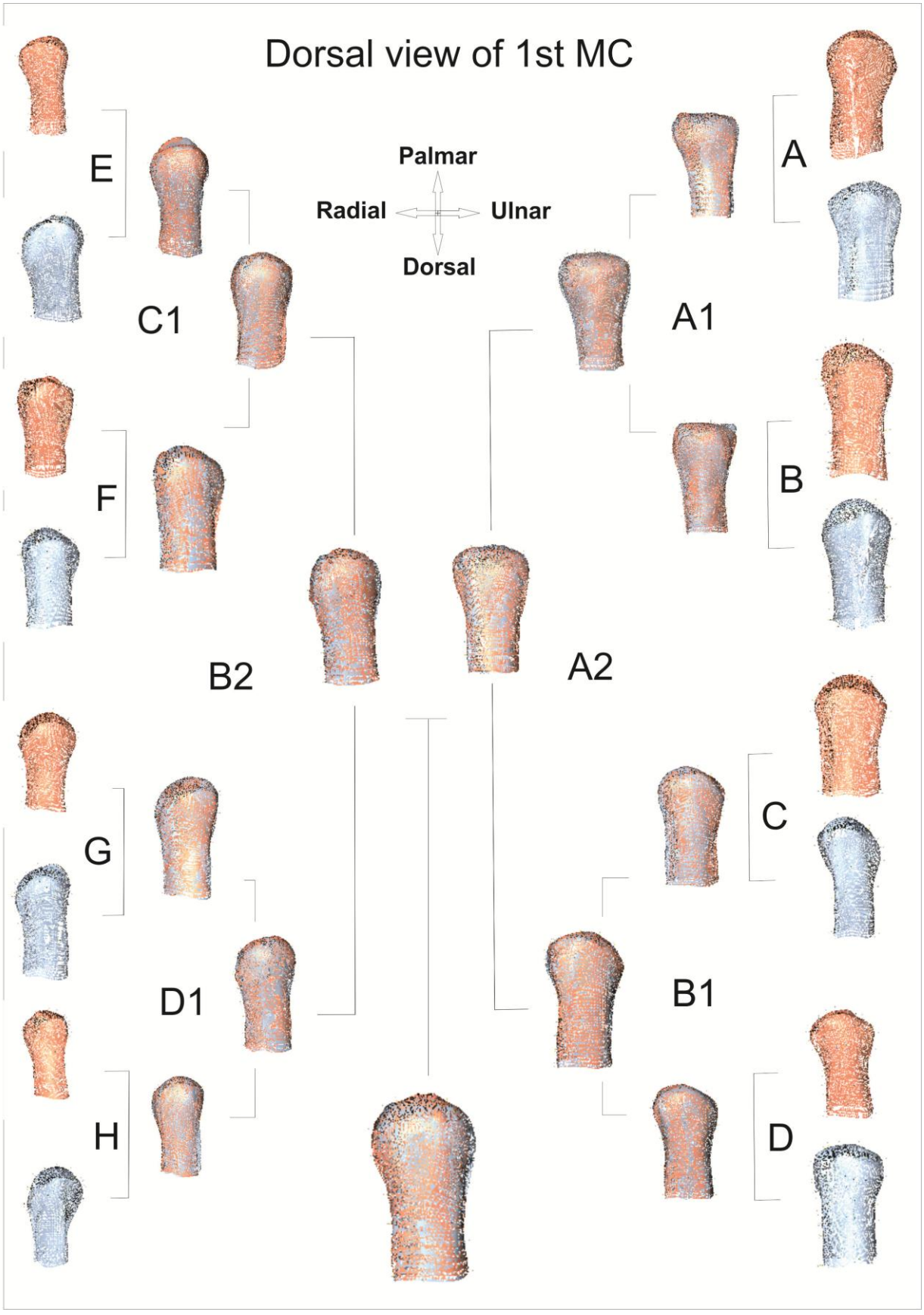

Figure 5.85: Stages of the dorsal view of the 1st MC bone. Illustrates the first stage with its summation shape (A1, B1, C1 and D1), the second stage with its summation shape (A2 and B2) and the final stage with its summation final shape.

5.3.1.5 Facet view of the 1st MC bone

5.3.1.5.1 First metacarpal- proximal point (MPR1)

The R^2 value of the regression point was 0.02 and the significance F was 0.14 The regression point showed that the MPR1 point was influenced by the square of single coordination points. MPR1 had no relationship with the same point on the other dry 1st MC bones, which means that this coordination point changed from the first stage to the final by 2%, without preserving its anatomical place through the sample population (Figure 5.86).

The significance factor F indicated that regression analysis was not significant (F>0.05). The MPR1 point significantly changed from the first stage.

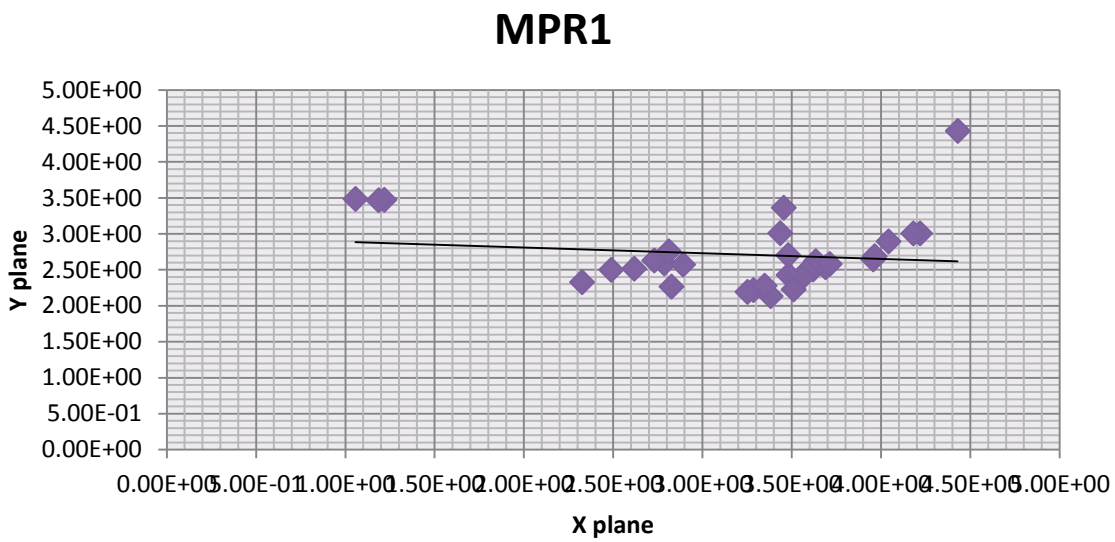

Figure 5.86: Linear regression model of the MPR1 coordination point from the 1st MC facet view. MPR1 had no relationship with the same point on the other dry 1st MC bones, the significance factor F indicated that regression analysis was not significant (F>0.05). N=32.

5.3.1.5.2 Second metacarpal- proximal point (MPR2)

The R^2 value of the regression point was 0.01 and the significance F was 0.5. The regression point showed that the MPR2 point was influenced by the square of single coordination points. MPR2 had no relationship with the same

point on the other dry 1st MC bones, which means that this coordination point changed from the first stage to the final by 1%, without preserving its anatomical place through the sample population (Figure 5.87).

The significance factor F indicated that regression analysis was not significant (F>0.05). The MPR2 point significantly changed from the first stage.

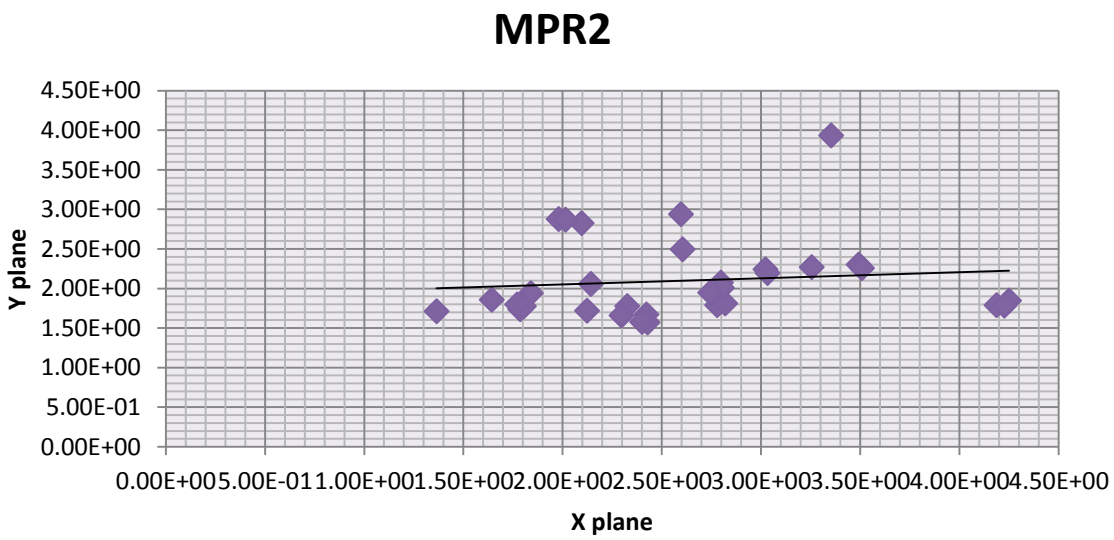

Figure 5.87: Linear regression model of the MPR2 coordination point from the 1st MC facet view. MPR2 had no relationship with the same point on the other dry 1st MC bones, the significance factor F indicated that regression analysis was not significant (F>0.05). N=32.

5.3.1.5.3 Third metacarpal- proximal point (MPR3)

The R^2 value of the regression point was 0.017 and the significance F was 0.48. The regression point showed that the MPR3 point was influenced by the square of single coordination points. MPR3 had no relationship with the same point on the other dry 1st MC bones, which means that this coordination point changed from the first stage to the final by 1.7%, without preserving its anatomical place through the sample population (Figure 5.88).

The significance factor F indicated that regression analysis was not significant (F>0.05). The MPR3 point significantly changed from the first stage.

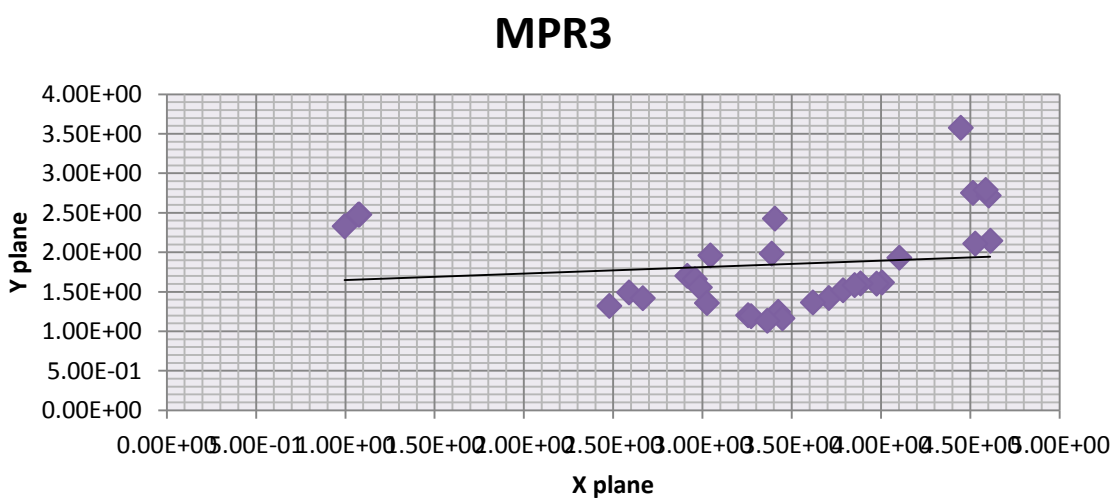

Figure 5.88: Linear regression model of the MPR3 coordination point from the 1st MC facet view. MPR3 had no relationship with the same point on the other dry 1st MC bones, the significance factor F indicated that regression analysis was not significant (F>0.05). N=32.

5.3.1.5.4 Fourth metacarpal- proximal point (MPR4)

The R^2 value of the regression point was 0.10 and the significance F was 0.0058. The regression point showed that the MPR4 point was not influenced by the square of single coordination points. MD5 had a relationship with the same point on the other dry 1st MC bones, which means that this coordination point did not change from the first stage to the final by 10%, and preserved its anatomical place through the sample population (Figure 5.89).

The significance factor F indicated that regression analysis was significant (F<0.05). The MD5 point did not significantly change from the first stage to the final stage.

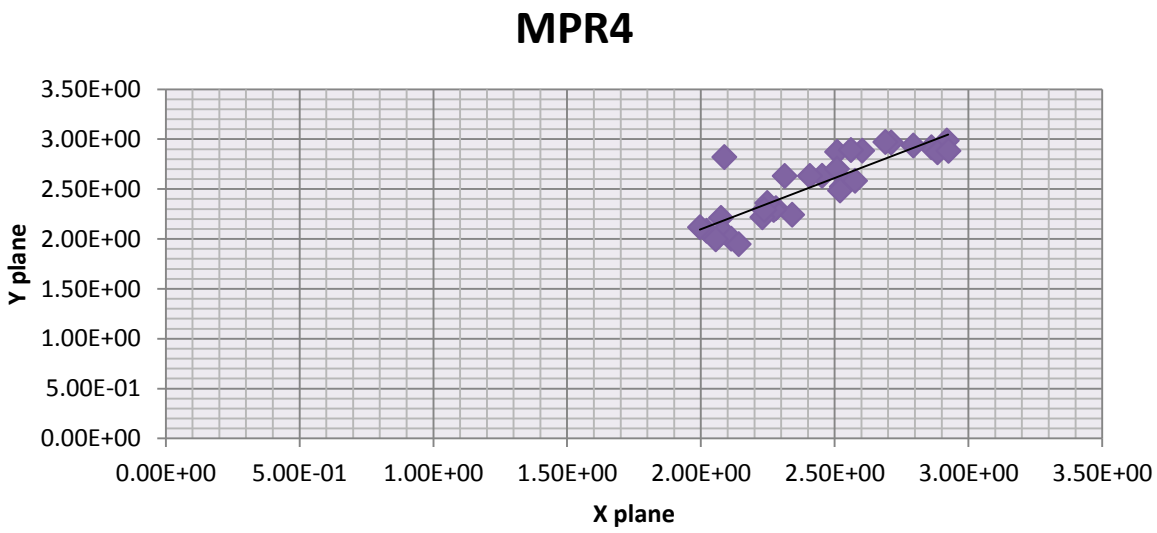

Figure 5.89: Linear regression model of the MPR4 coordination point from the 1st MC facet view. MD5 had a relationship with the same point on the other dry 1st MC bones, the significance factor F indicated that regression analysis was significant (F<0.05). N=32.

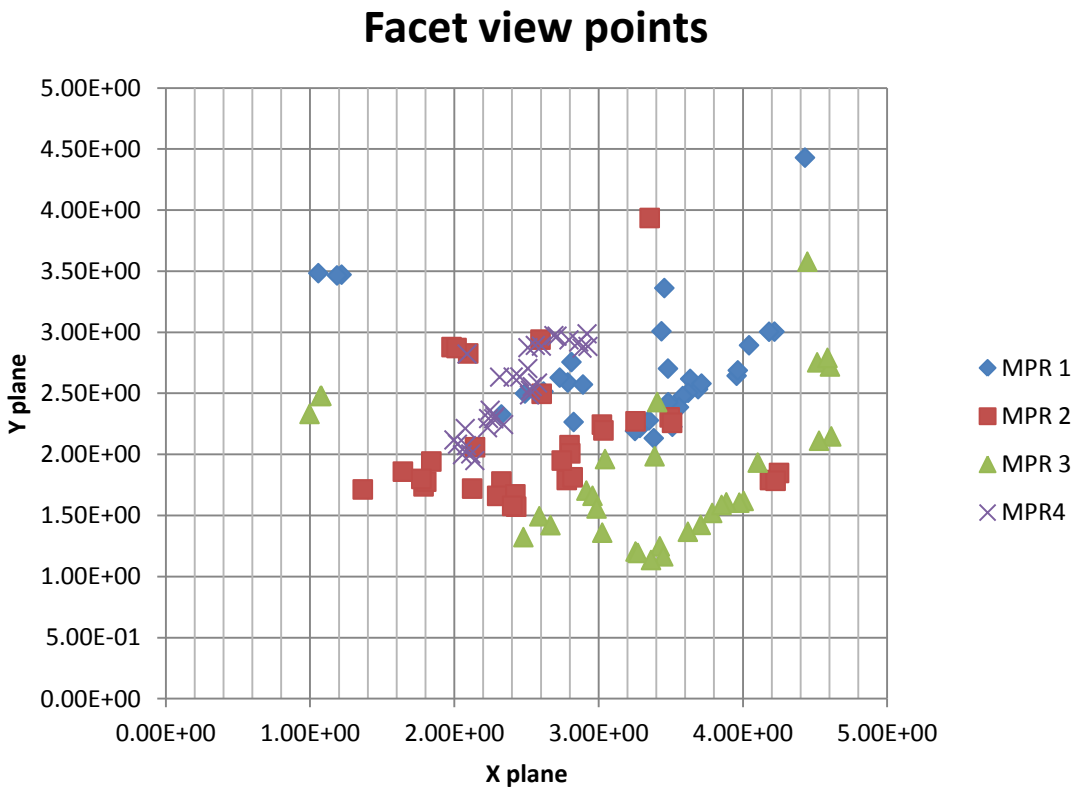

Figure 5.90: Linear regression model of all single coordination points from the facet view of 1st MC bone. N=32.

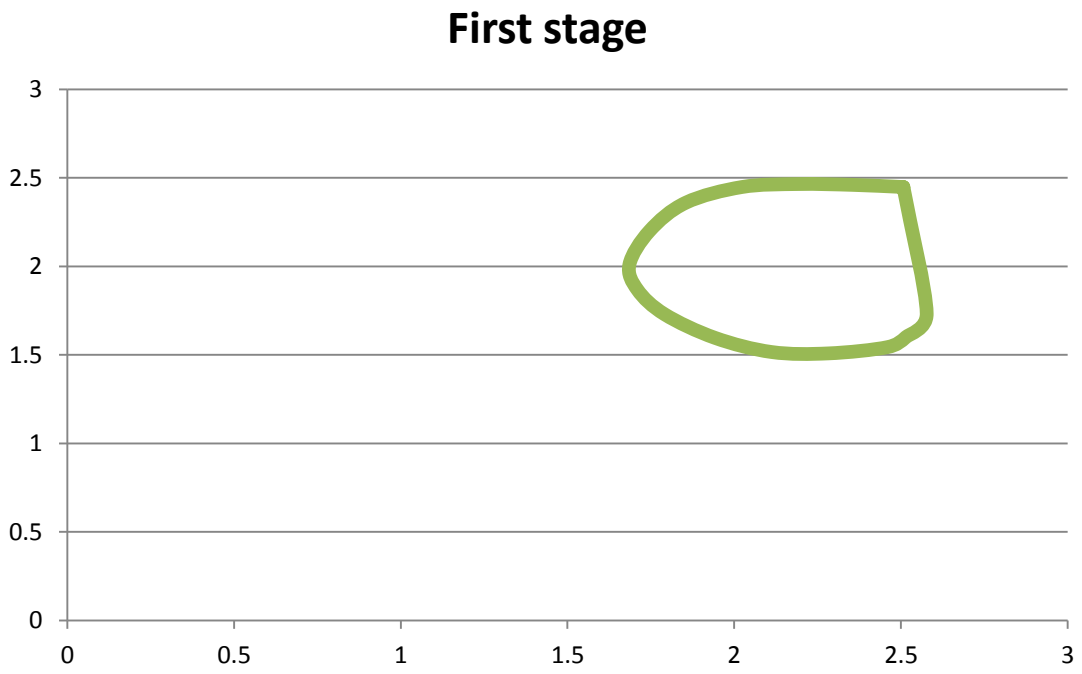

Figure 5.91: First stage of the default geometrical shape of the facet view of the 1st MC bone.

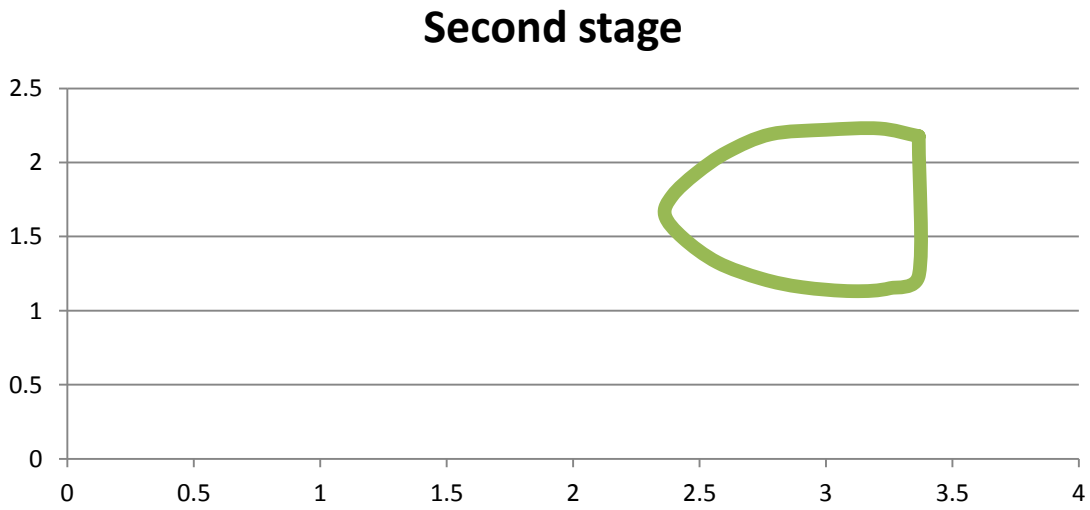

Figure 5.92: Second stage of the default geometrical shape of the facet view of the 1st MC bone.

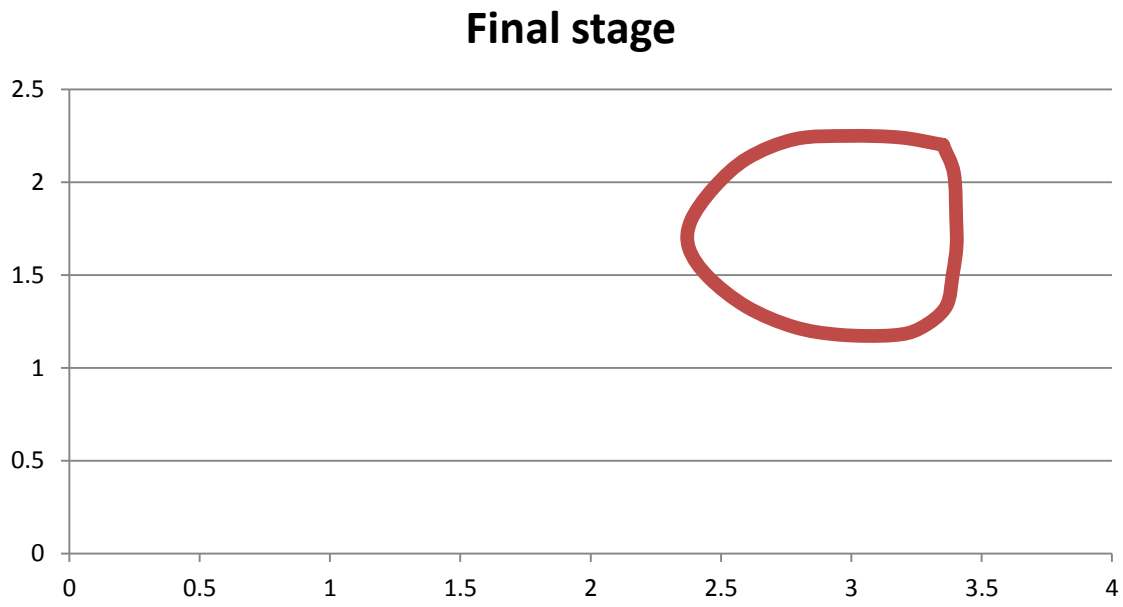

Figure 5.93: Final stage of the default geometrical shape of the facet view of the 1st MC bone.

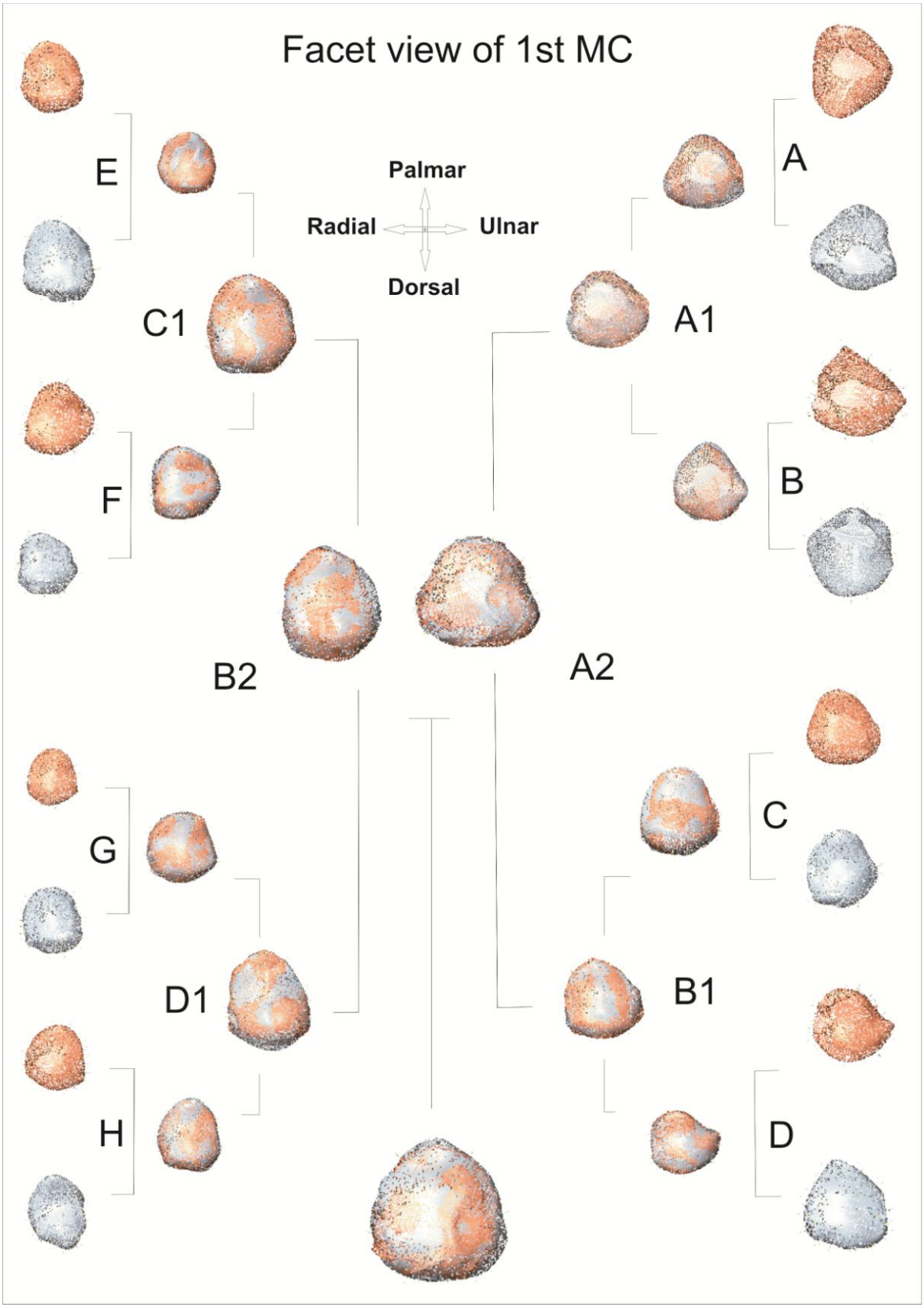

Figure 5.94: Stages of the facet view of the 1st MC bone. Illustrates the first stage with its summation shapes (A1, B1, C1 and D1), the second stage with its summation shapes (A2 and B2) and the final stage with its summation final shape.

5.3.2 Measurement of the articulation surface

5.3.2.1 Length of TM articulation surface

The longest length line from the Amira 3D software was CCL. The right articulation surface was 14.47 mm and the left was 14.22 mm. The shortest length line from the Amira 3D software was DRTL1. The right articulation surface was 9.31 mm and the left was 8.79 mm (Figure 5.95).

The longest length line of the Rhinoceros software was ETL2. The right articulation surface was 14.33 mm and the left was 15.1 mm. The shortest length line of the Rhinoceros software was ETL1. The right articulation surface was 9.91 mm and the left was 9.43 mm (Figure 5.96).There were not significant differences (P> 0.05, 0.001) between the right and left articulation surfaces from the two programs (Figures 5.97-5.98).

The facet central length and the facet first eminence tubercle lines were the longest length lines on the TM articulation surface and the length of the facet eminence tubercle ridge and the dorso-radial tubercle lines were the shortest length lines on the TM articulation surface.

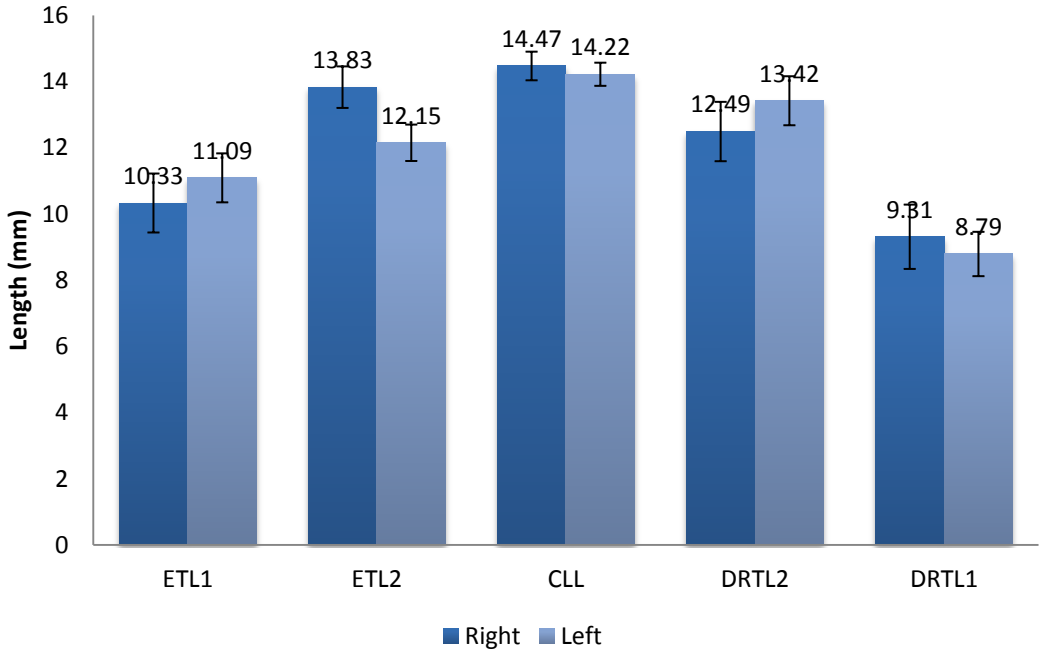

Figure 5.95: Length measurements of the articulation surface of the TM by Amira 3D software. The shortest length line was DRTL1. N=10.

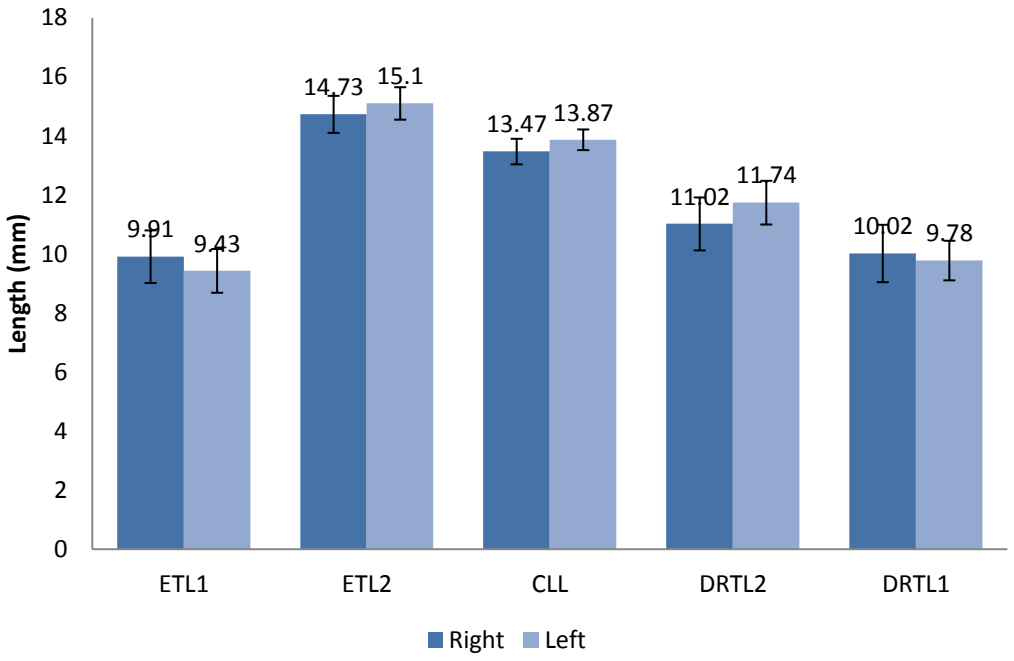

Figure 5.96: Length measurements of the articulation surface of the TM by Rhinoceros software. The longest length line was ETL2. N=50.

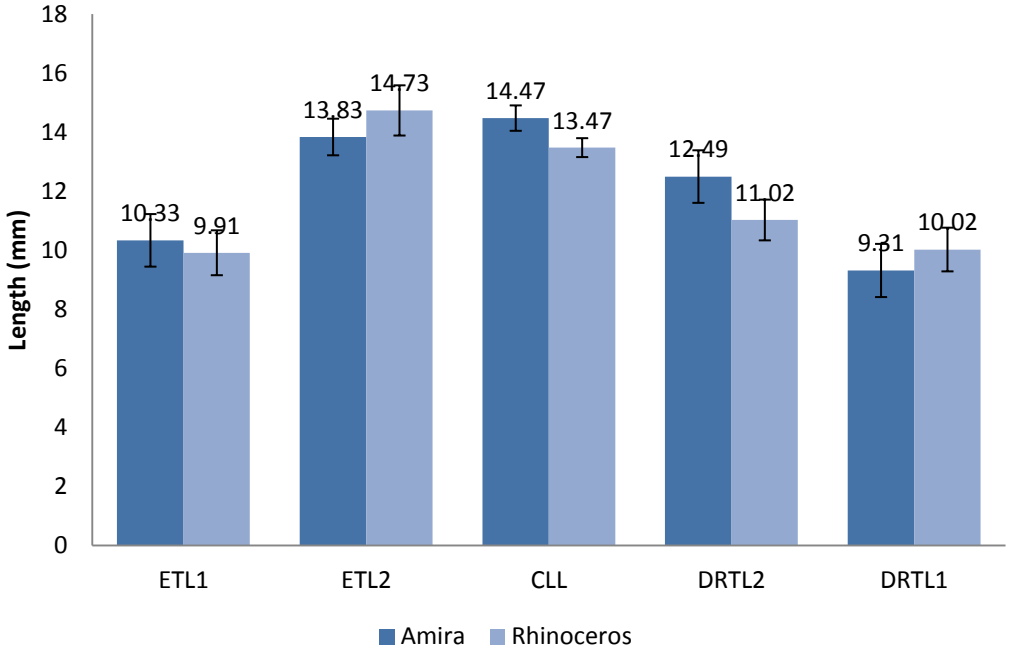

Figure 5.97: Comparison of the right articulation surface length lines between Amira 3D and Rhinoceros software. There were not significant differences (P> 0.05) between the right articulation surfaces from the two programs.N=60.

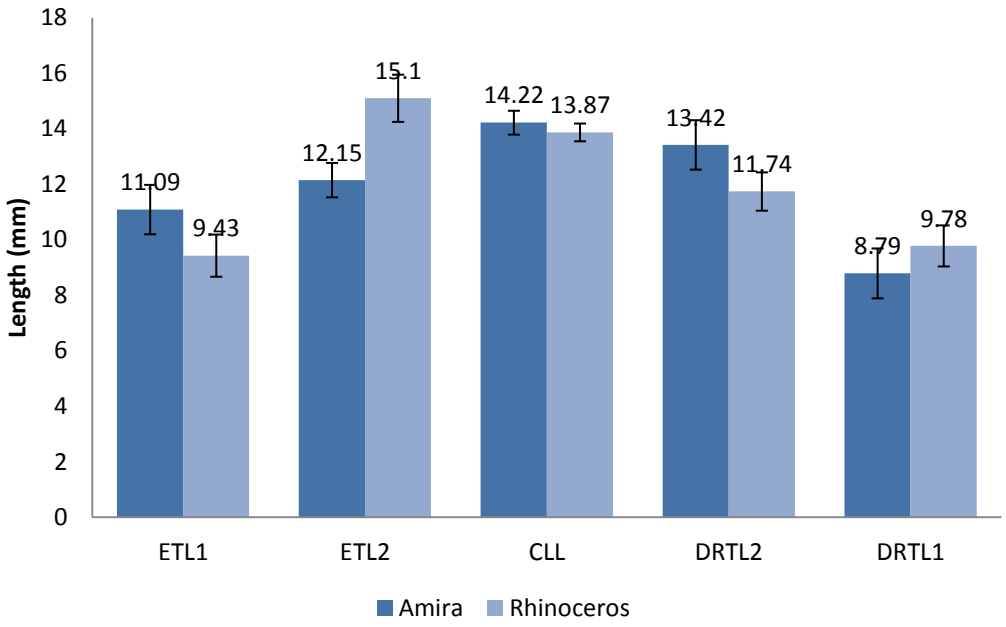

Figure 5.98: Comparison of the left articulation surface length lines between Amira 3D and Rhinoceros software. There were not significant differences (P> 0.05) between the left articulation surfaces from the two programs. N=60.

5.3.2.2 Width of the TM articulation surface

The longest width line from the Amira 3D software was PTL2. The right articulation surface was14.03 mm. The longest width line of the left was DBL2 and the left articulation surface width was14.9 mm. The shortest width line from the Amira 3D software was PTL1. The right articulation surface was 9.82 mm and the left was 10.05 mm (Figure 5.99).

The longest width line from the Rhinoceros software was CWL. The right articulation surface was 14.43 mm and the left was 14.2 mm. The shortest width line from the Rhinoceros software was PTL1. The right articulation surface was 9.36mm and the left was 9.47 mm (Figure 5.100).There were no significant differences (P> 0.05, 0.024) between the right and left articulation surfaces from each program (Figures 5.101-5.102).

The facet second palmar tubercle, the facet distal border, and the facet central width lines represented the widest area of the TM articulation surface and the area of the facet first palmar tubercle line represented the narrowest area of the TM articulation surface.

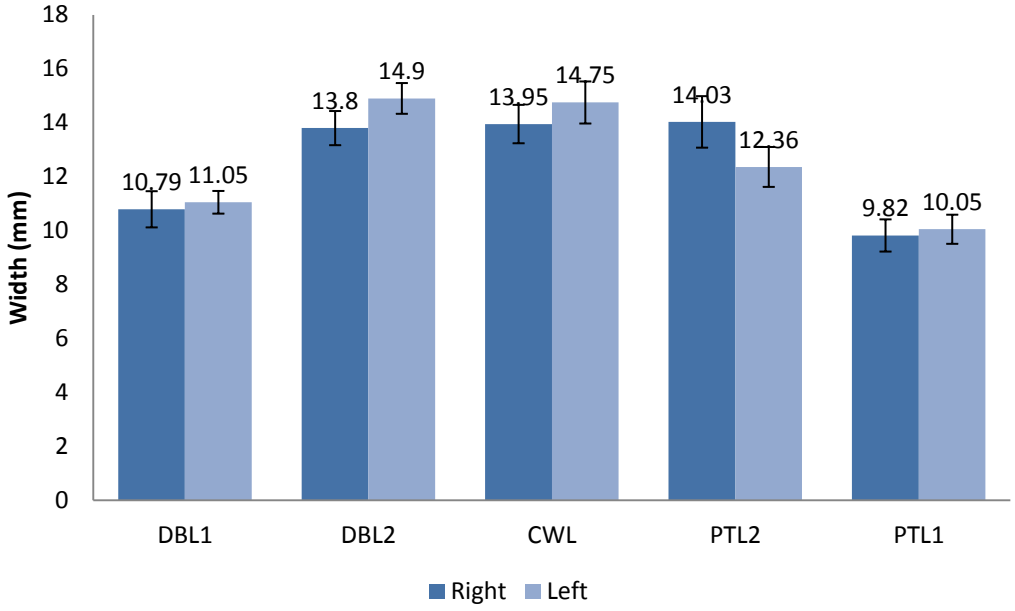

Figure 5.99: Width measurements of the articulation surface of the TM by Amira 3D software. The shortest width line was PTL1. N=10.

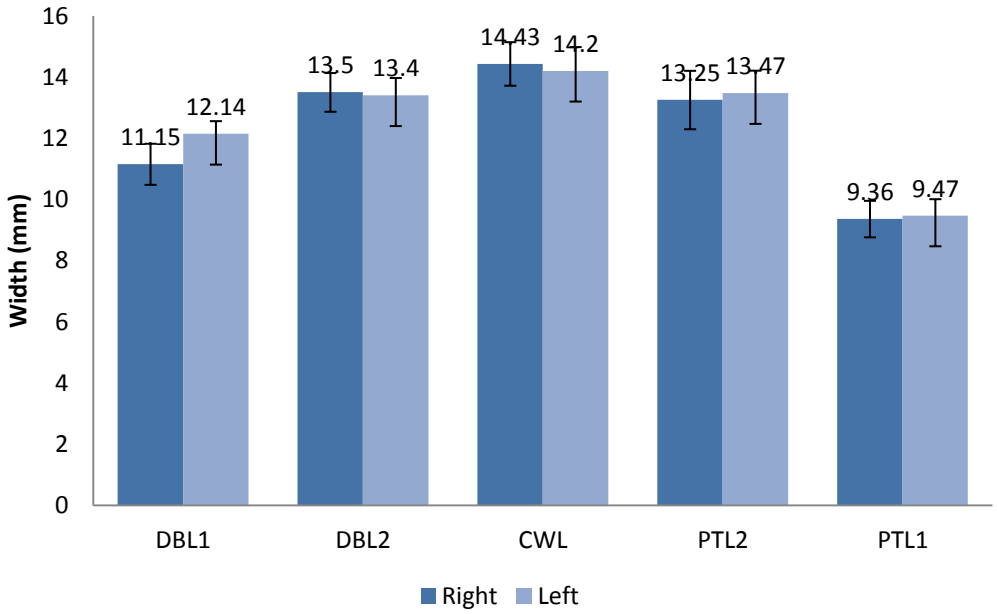

Figure 5.100: Width measurements of the articulation surface of the TM by Rhinoceros software. The shortest width line was PTL1. N=50.

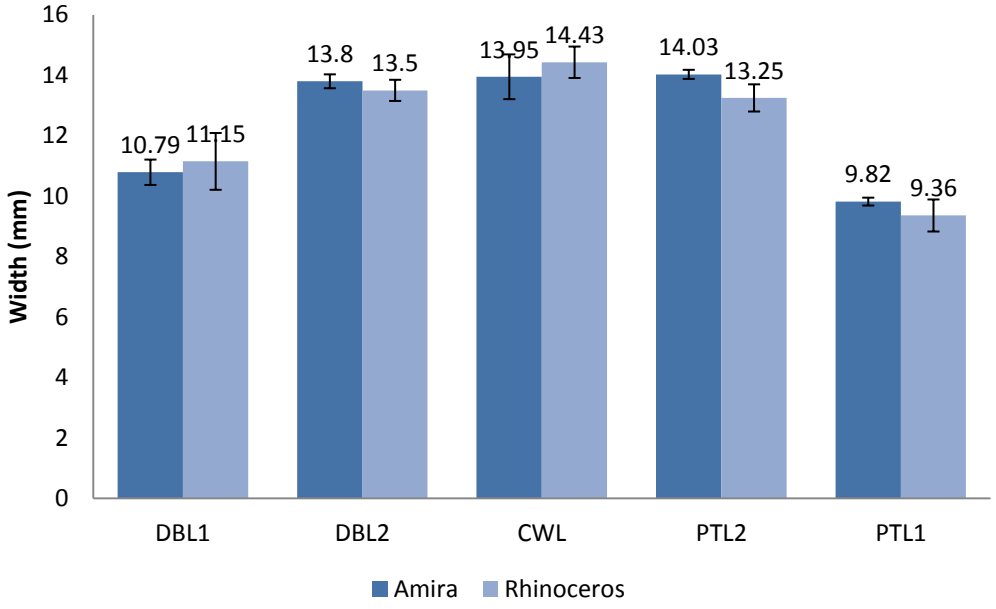

Figure 5.101: Comparison of the right articulation surface width lines between Amira 3D and Rhinoceros software. There were no significant differences (P> 0.05) between the right articulation surfaces from each program. N=60.

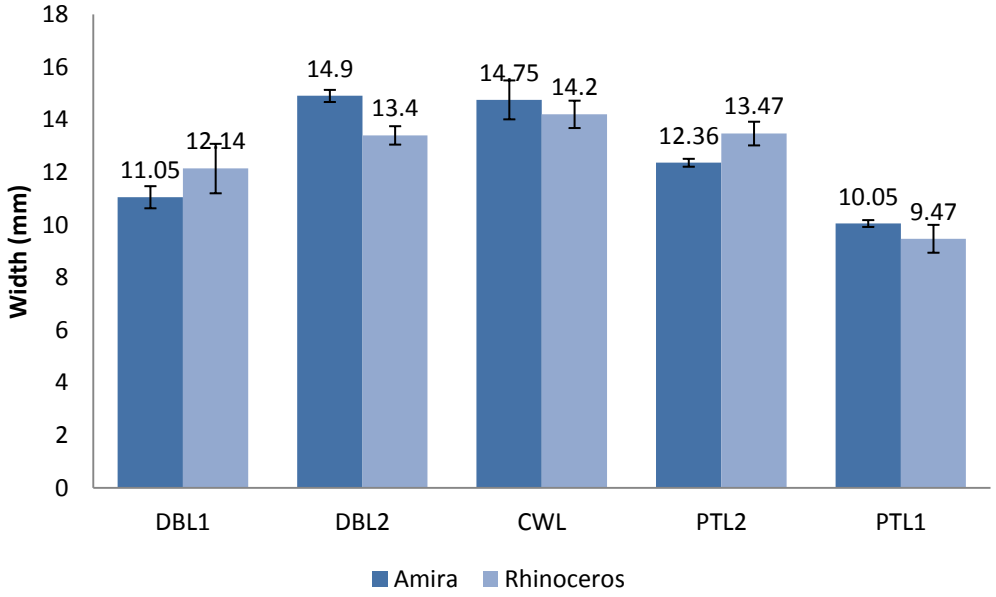

Figure 5.102: Comparison of the left articulation surface width lines between Amira 3D and Rhinoceros software. There were no significant differences (P> 0.05) between the left articulation surfaces from each program.N= 60.

5.3.2.3 Length of the 1st MC articulation surface

The longest line from the Amira 3D software was CCL. The right articulation surface was 11.33 mm and the left was 11.1 mm. The shortest line from the Amira 3D software was RBL1. The right articulation surface was 4.79 mm and the left was 5.35 mm (Figure 5.103).

The longest line from the Rhinoceros software was CCL. The right articulation surface was 11.25 mm and the left was 12.01 mm. The shortest line from the Rhinoceros software was RBL1. The right articulation surface was 6.2 mm and the left was 4.9 mm (Figure 5.104).There were no significant differences (P> 0.05, 0.019) between the right and left articulation surfaces form each program (Figures 5.105-5.106).

The facet central length line was the longest line on the 1st MC articulation surface, while the length of the facet radial border line was the shortest line on the 1st MC articulation surface.

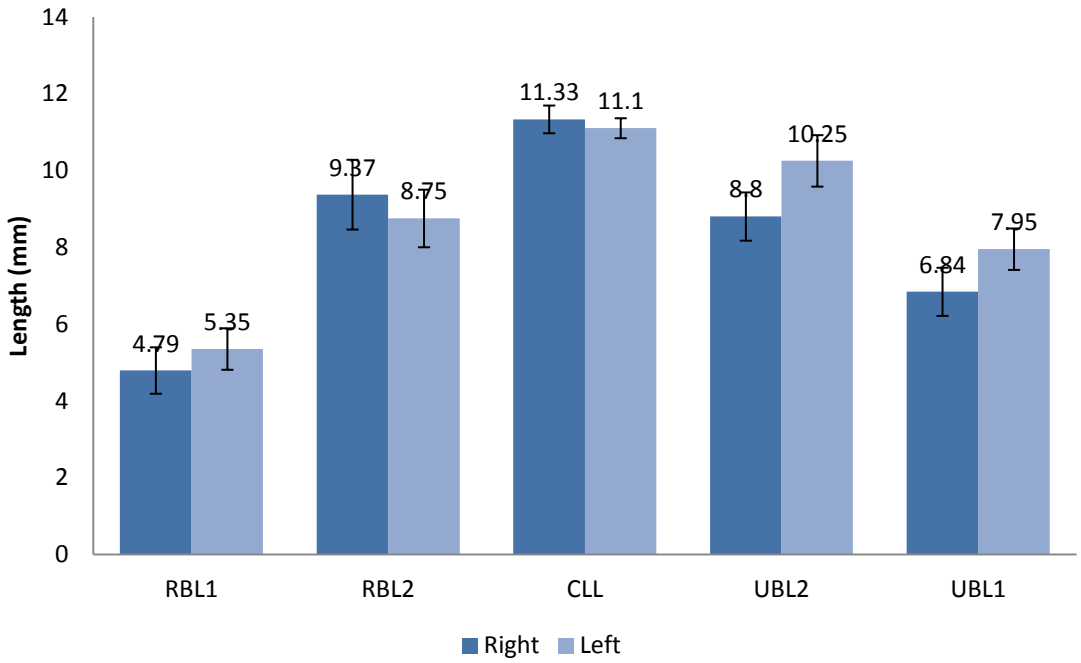

Figure 5.103: Length measurements of the articulation surface of the 1st MC by Amira 3D software. The shortest line was RBL1. N=10.

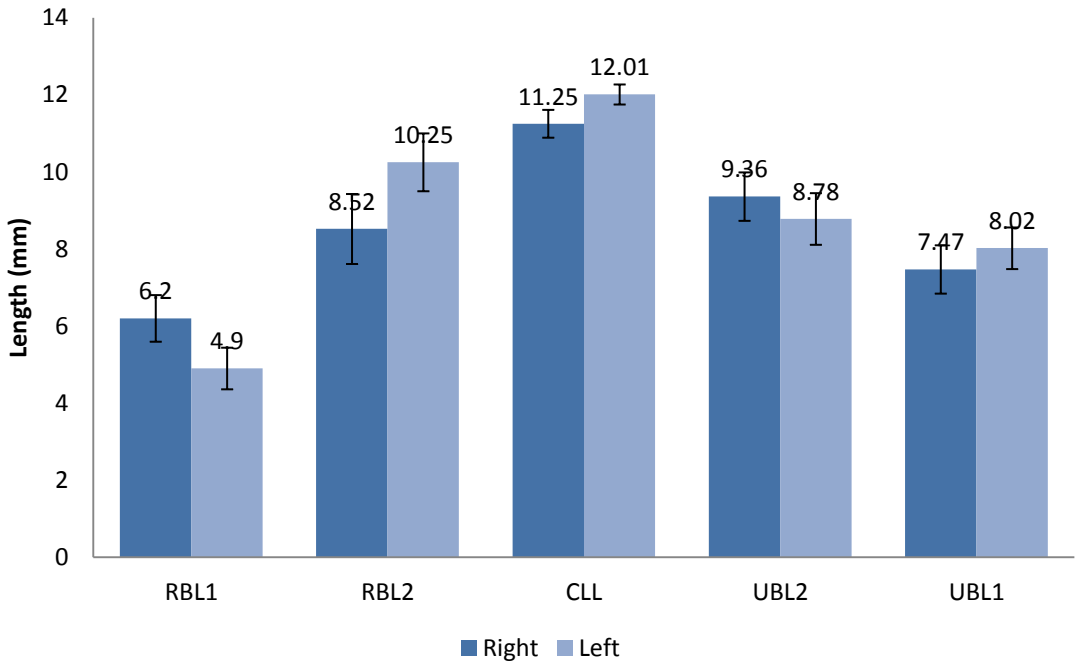

Figure 5.104: Length measurements of the articulation surface of the 1st MC by Rhinoceros software. The shortest line from the Rhinoceros software was RBL1. N=50.

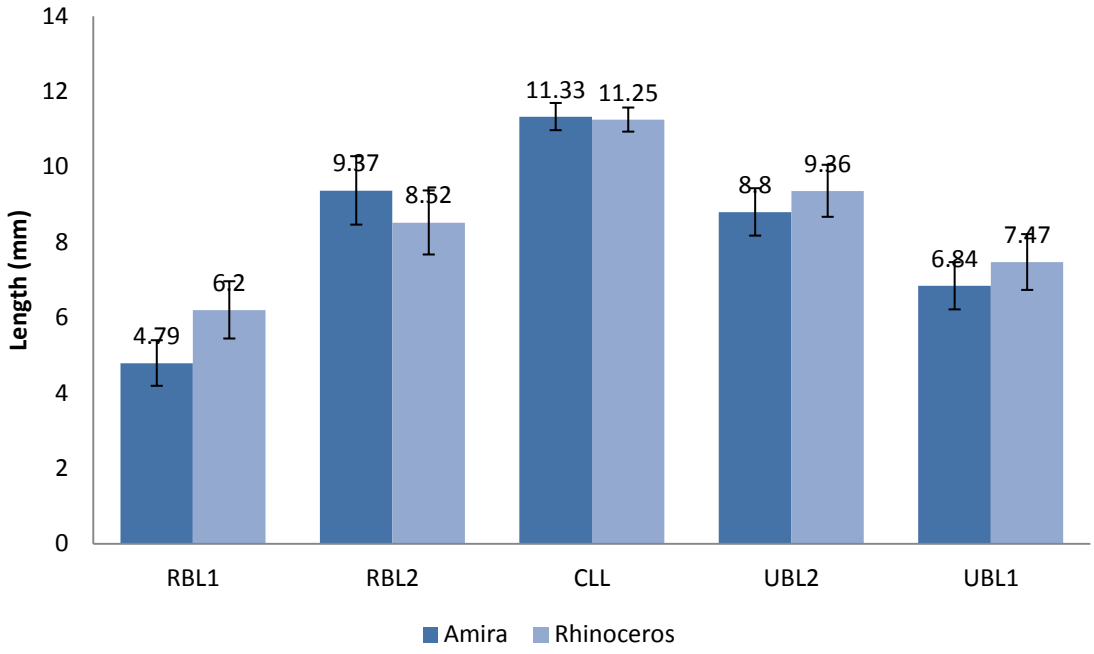

Figure 5.105: Comparison of the right articulation surface length lines between Amira 3D and Rhinoceros software. There were no significant differences (P> 0.05) between the right articulation surfaces form each program. N=60.

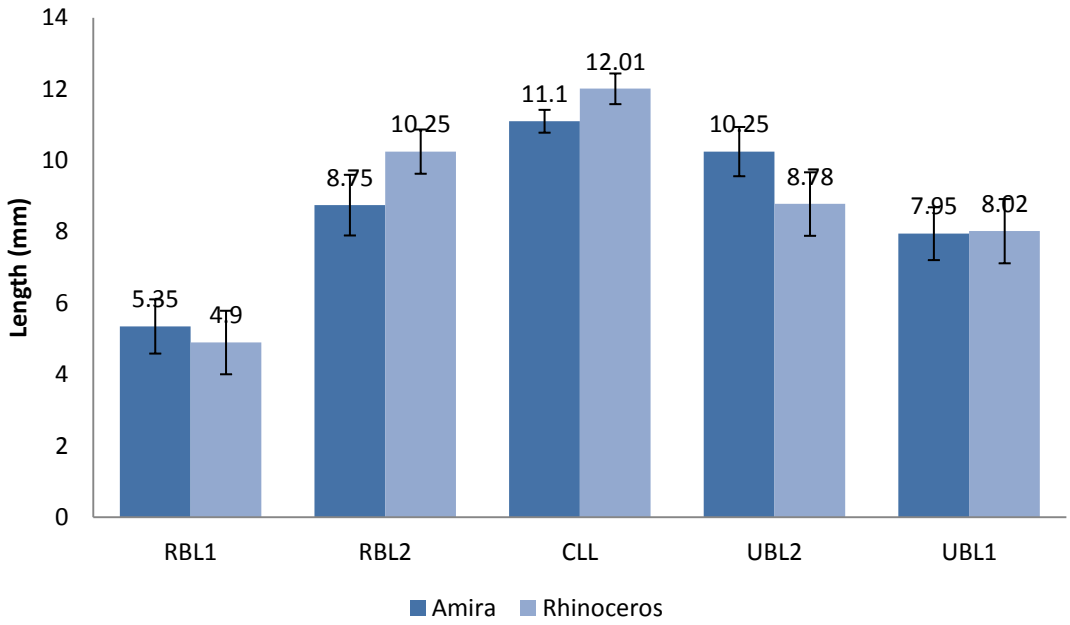

Figure 5.106: Comparison of the left articulation surface length lines between Amira 3D and Rhinoceros software. There were no significant differences (P> 0.05) between the left articulation surfaces form each program. N=60.

5.3.2.4 Width of the 1st MC articulation surface

The longest width line from the Amira 3D software was PEL2. The right articulation surface was 16.39 mm and the left was 17.36 mm. The shortest width line from the Amira 3D software was AEL1. The right articulation surface was 3.85 mm and the left was 4.23 mm (Figure 5.107).

The longest width line from the Rhinoceros software was PEL2. The right articulation surface was 17.96 mm and the left was 16.54 mm. The shortest width line from the Rhinoceros software was AEL1. The right articulation surface was 4.01 mm and the left was 3 mm (Figure 5.108).There were no significant differences (P> 0.05, 0.047) between the right and left articulation surfaces from each program (Figures 5.109-5.110).

The facet of the second posterior eminence line was the widest area of the 1st MC articulation surface, while the length of the facet's first anterior eminence line was narrowest section of the 1st MC articulation surface.

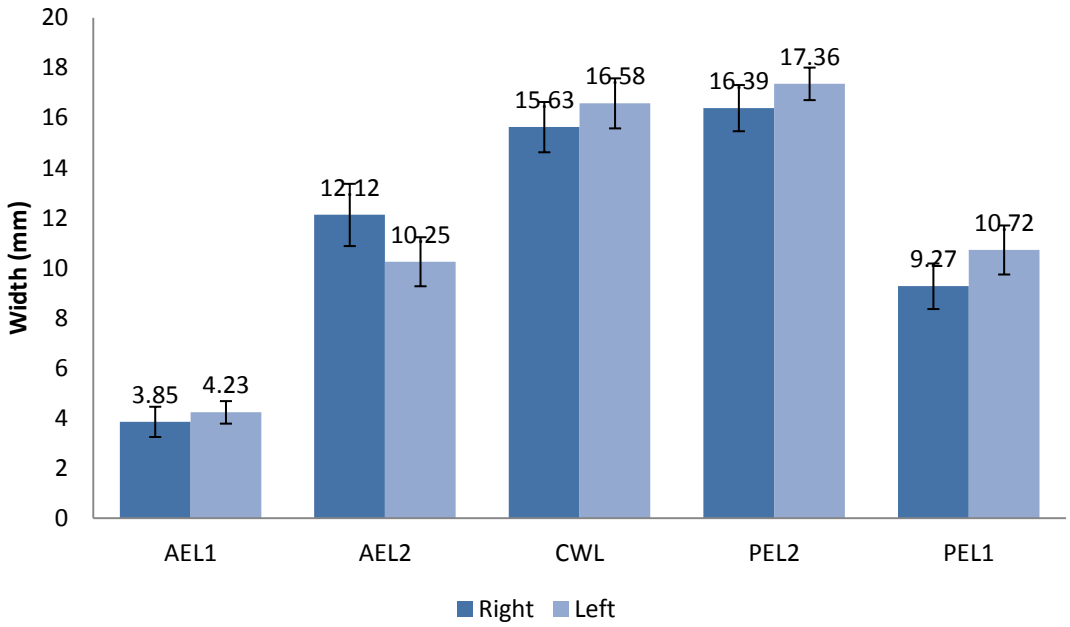

Figure 5.107: Width measurements of the articulation surface of the 1st MC by Amira 3D software. The shortest width line was AEL1. N=10.

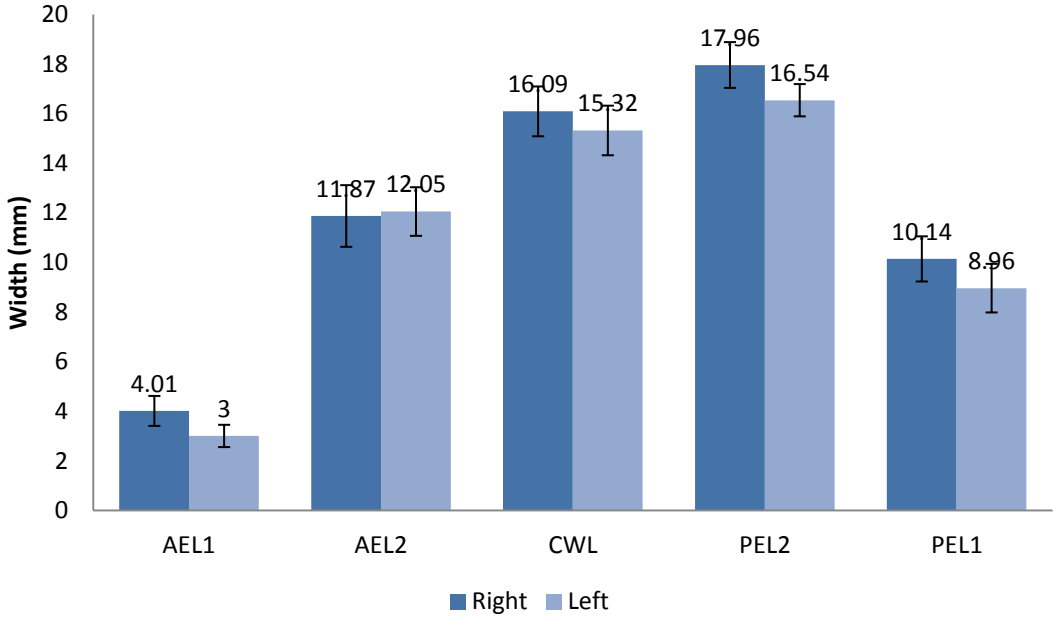

Figure 5.108: Width measurements of the articulation surface of the 1st MC by Rhinoceros software. The shortest width line was AEL1. N=50.

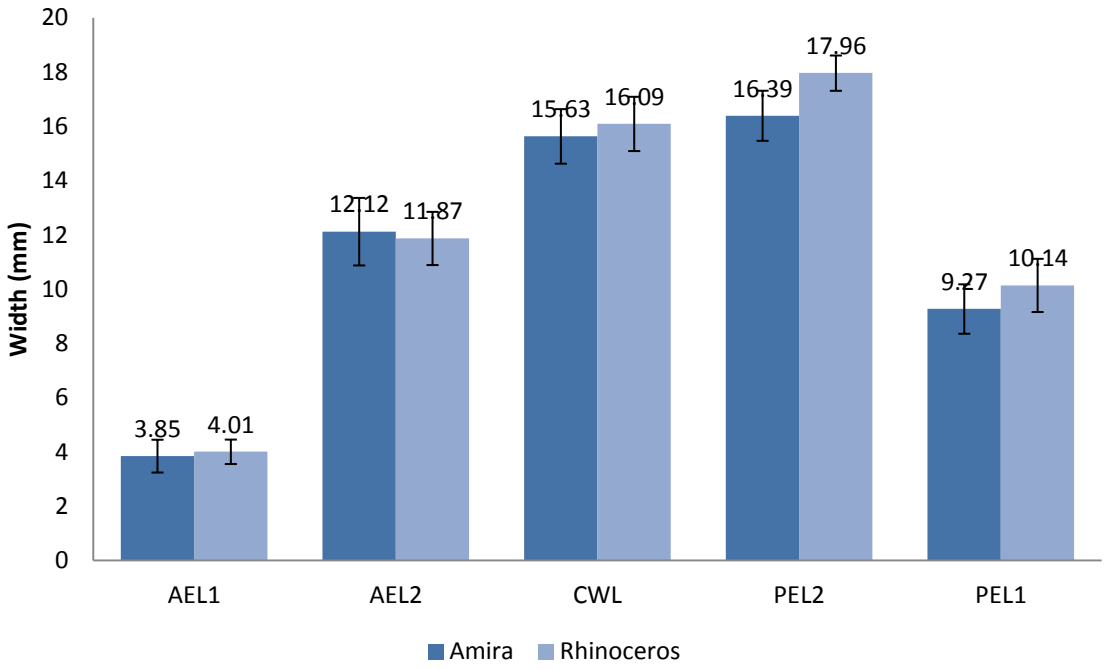

Figure 5.109: Comparison of the right articulation surface width lines between Amira 3D and Rhinoceros software. There were no significant differences (P> 0.05) between the right articulation surfaces from each program. N=60.

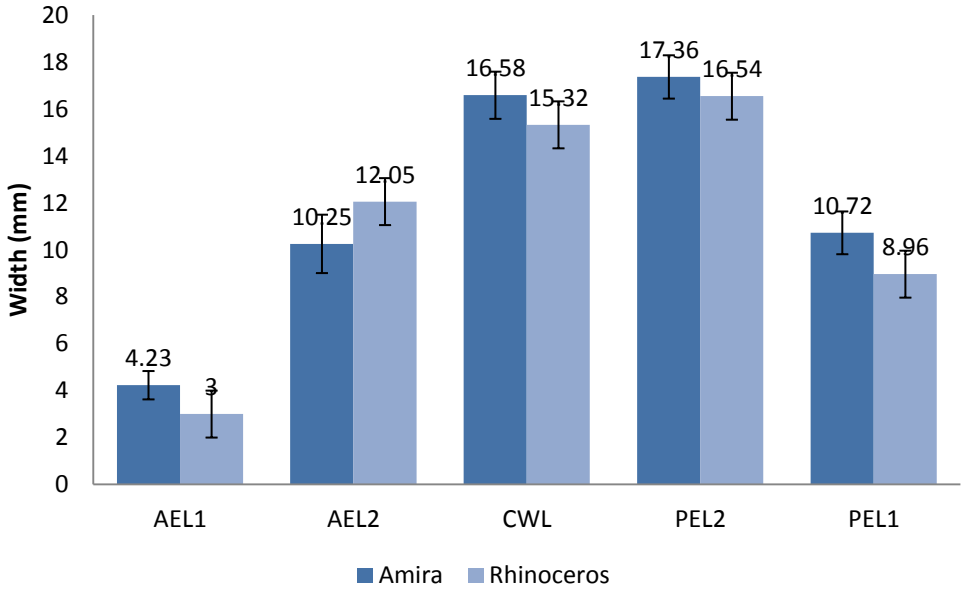

Figure 5.110: Comparison of the left articulation surface width lines between Amira 3D and Rhinoceros software. There were no significant differences (P> 0.05) between the left articulation surfaces from each program. N=60.

5.3.2.5 Area of the TM articulation surface

The area of right TM articulation surface by Amira 3D software was 91.84 mm² and that of the left was 90.52 mm² (Figure 5.111). The area of right TM

articulation surface by Rhinoceros was 93.06 mm² and that of the left was 95.12 mm² (Figure 5.112). There were no significant differences (P> 0.05) between the right and left articulation surfaces from each of the programs (Figure 5.113).

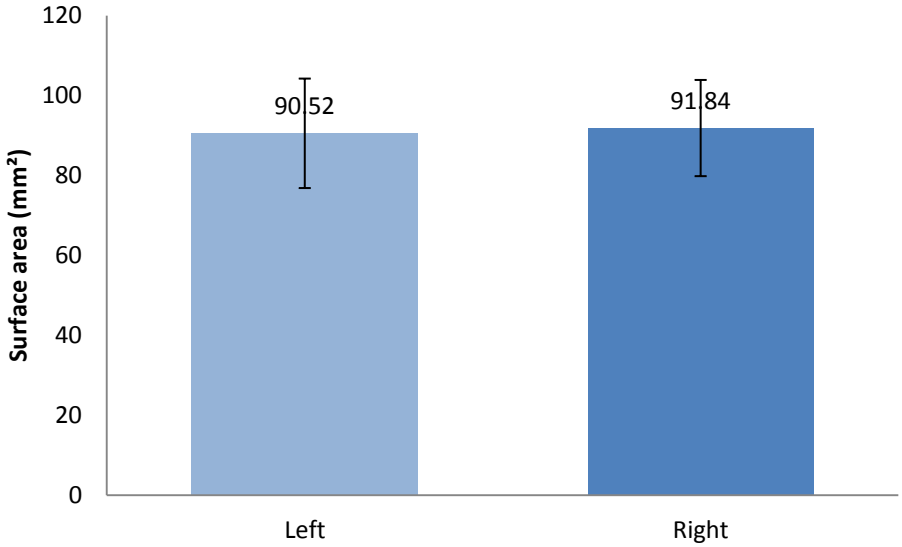

Figure 5.111: Area measurements of the articulation surfaces of the TM facet by Amira 3D software. N=10.

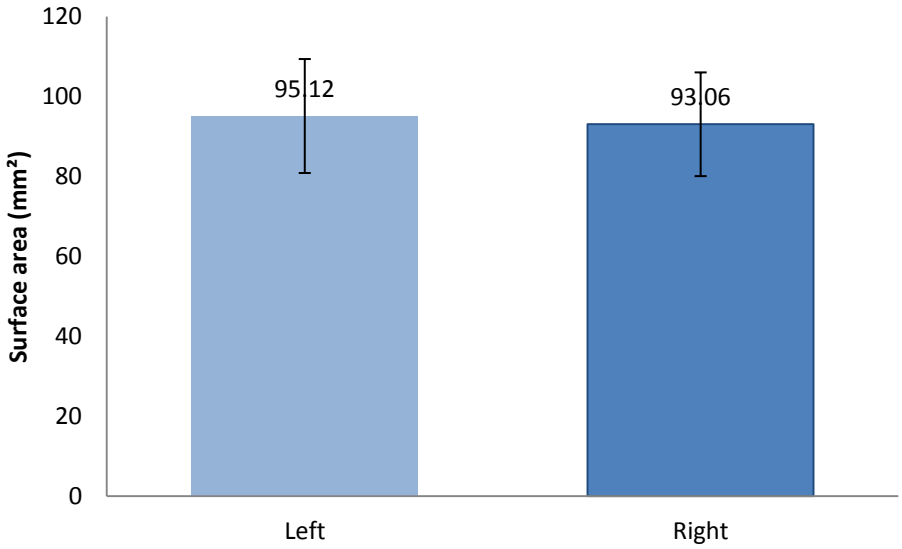

Figure 5.112: Area measurements of the articulation surfaces of the TM facet by Rhinoceros software. N=50.

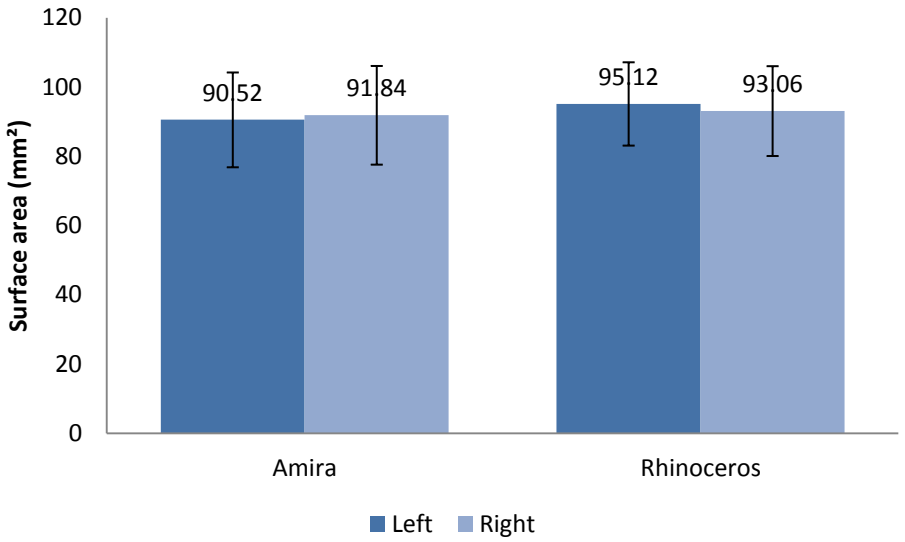

Figure 5.113: Comparison of the left and right TM articulation surfaces by Amira 3D and Rhinoceros software. There were no significant differences (P> 0.05) between the right and left articulation surfaces from each of the programs. N= 60.

5.3.2.6 Area of the 1st MC articulation surface

The area of right 1st MC articulation surface by Amira 3D software was 106.95 mm² and that of the left was 100.35 mm² (Figure 5.114). The area of right 1st MC articulation surface by Rhinoceros was 101.01 mm² and that of the left was 99.24 mm² (Figure 5.115). There were no significant differences (P> 0.05, 0.033) between the right and left articulation surfaces from each program (Figure 5.116).

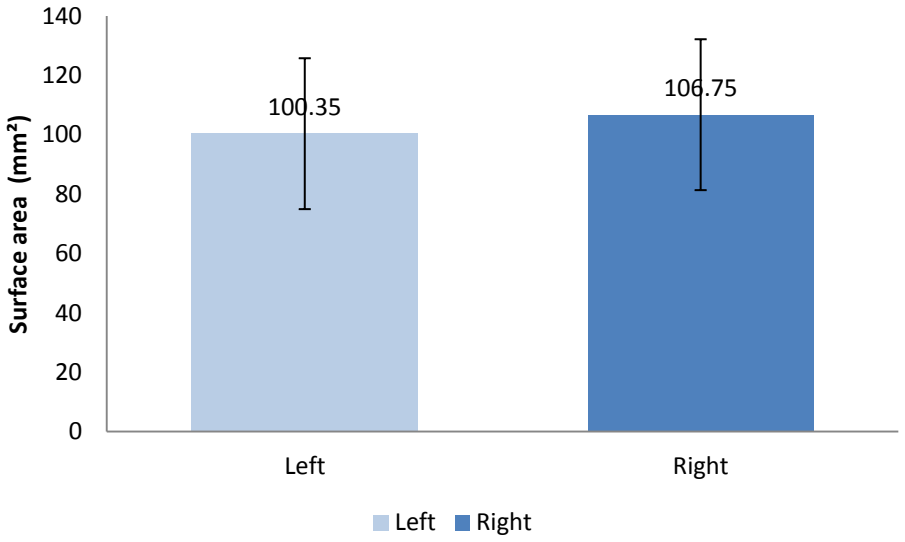

Figure 5.114: Area measurements of the articulation surfaces of the 1st MC facet by Amira 3D software. N=10.

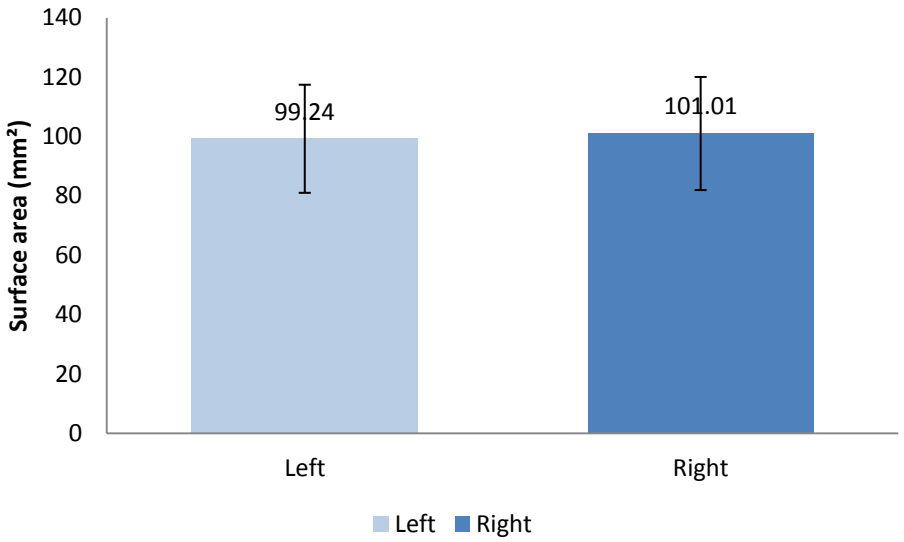

Figure 5.115: Area measurements of the articulation surfaces of the 1st MC facet by Rhinoceros software. N=50.

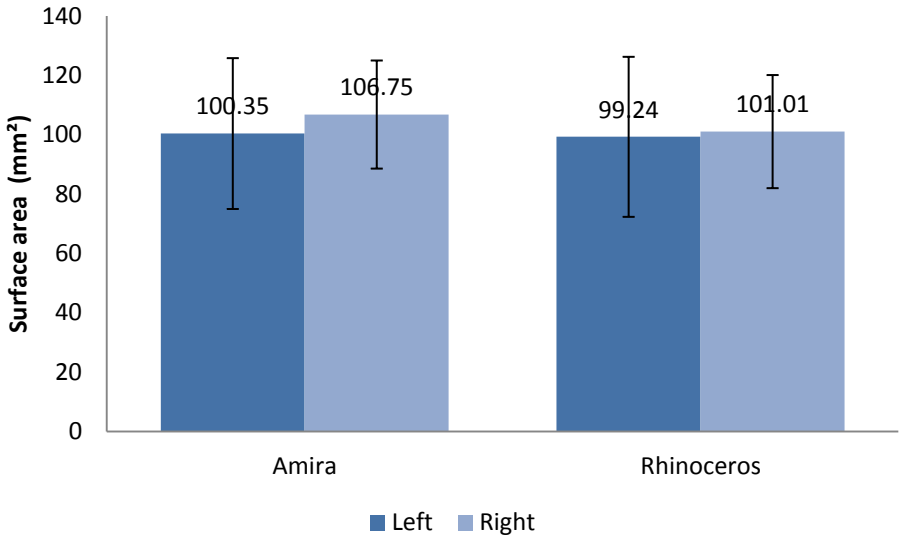

Figure 5.116: Comparison of the left and right 1st MC articulation surfaces by Amira 3D and Rhinoceros software. There were no significant differences (P> 0.05) between the right and left articulation surfaces from each program. N=60.

5.4 Discussion

The morphological descriptions of the TM and 1st MC bones have been investigated by several authors (Ateshian *et al.* 1992; Buffi *et al.* 2013; Ceri *et al.* 2004; El Ibrahimi *et al.* 2009; Humes *et al.* 2004; Simoens 2006), but some features did not fit the descriptions clearly. The current study has defined new and consistent osteological landmarks, and has provided a nomenclature for the body of the TM and the base of the 1st MC.

For instance, the distal border at the 1st MC facet of the TM bone was considered (Figure 5.18). The dorso-ulnar and dorso-radial tubercles were described regarding the anatomical position of the bone in a 3D field. Therefore, they may not have the same descriptions as in previous studies and textbooks (Ateshian *et al.* 1992; Frazer 1965; Gray 2005; Humes *et al.* 2004; Snell 2004). The current study described features modelled in 3D by several software programs, which provided a greater chance for better accuracy throughout the X, Y and Z axes.

Three types of 3D software were used: Rhinoceros, Landmark, and Amira. The reason these software were chosen:

- To make a comparison between the software to ensure the best and most accurate 3D model. The results show that all of them have the ability to create an accurate geometrical 3D model.

- To analyse the process of importing the data inside the software, such as Amira, which depends on the (DICOM) file of a CT scan, while the Rhinoceros depends on the input of the microscribe device. In addition, the Landmark software depends on the 3D model of Rhinoceros. Different ways of importing data plays a very important role.

- To make comparisons between the results of the software, especially the measurements. These results give a good idea of which software has the most accurate results. However, tests have shown no significant differences between the software, which means the results of this study recommend using any software for measuring the 3D model.

- To find the proper features of the TM and first MC bones. To deal with this issue Landmark was used, which has the ability to merge two 3D model models and export one 3D model which has the most important features from the both models, by using a single coordination points. However, the goal of using this software was achieved by creating a model that was a median between the two original models. Through analysis, each median model showed important features on the surfaces of TM and first MC bones. While there were other sets that had no important data, this analysis provided important data about the morphology of the TMC bones.

The base of the 1st MC bone was observed, particularly the area that articulates with the TM bone and the area related to the attachments of the TMC ligaments. Therefore, the most interesting surfaces were found around the facet that articulates with the TM bone, and the palmar and dorsal areas of the shaft of the 1st MC bone. New features were recorded, such as the dorso-radial tubercle, and ulnar and radial borders of the 1st MC facet (Figures 5.22-5.23).

The eminence of the 1st MC facet was divided into anterior and posterior eminences (Figure 5.23). The ridge that divides the palmar surface of the 1st MC into radial and ulnar surfaces was also described in detail in the current study (Figure 5.24). Based on the 3D field, the current study observed that the proximal set of the ridge was more prominent than the distal set of the palmar surface of the 1st MC (Nanno *et al.* 2006a). The importance of this feature relates to the fact that most TMC ligaments insert at or around this feature.

The facet view of the TM and 1st MC bones was chosen due to their congruity and because the TMC joint is built around these areas. The radial view of the TM bone was chosen because of its relation to the features at this set from the palmar view of the 1st MC bone. The dorsal view of the 1st MC bone may not be as important as the palmar view, but it was added to this study for the sake of completing the entire shape of the base of the 1st MC. It also is flattened, so there were no particular features on the dorsal surface related to the structures of the TMC joint, except for some structures such as the radial artery, tendons of extensor pollicis longus, extensor pollicis brevis and abductor pollicis longus (Snell 2004).

Accordingly, the TM and 1st MC bones were explained in detail as were nomenclature features that are strongly related to the insertion, origination and/or passage ligaments, tendons, muscles and arteries. The methods used in the current study will help the understanding of bone description. Most of the techniques used were related to bone description techniques such as the use of coordination points and lines for length and width measurements.

The coordination points utilized a description of a specific point on the surface of the bone (Bookstein 1997). This is the process used by the 3D Landmark software, which treated each shape as a whole without any segmentation (James Rohlf and Marcus 1993; Parsons *et al.* 2003; Williams and Richtsmeier 2003). In the current study, the shape of the TM bone was segmented into two views: facet and radial. The 1st MC was segmented into three views: facet, palmar and dorsal. The software rendered these views into 3D virtual shapes.

Coordination points were distributed across each view based on the importance of each point as it related to the morphological features of the entire shape. Thus, five coordination points were distributed across the radial view, and four across the facet view (Figures 5.32-5.33).

In addition, the 1st MC had five coordination points across both palmar and dorsal views, while the remaining facet view had four points. The study hypothesises that the location of the points comes from the following:

1. The prominent sharpness presented by the tubercle on the bone surface is associated with TD1, TD3, TD4, TR2, TR3, TR4,TR5, MD2, MD4, MP2 and MP4 (Figures 5.32-5.33).

2 The tapered prominence and edge of facet border presented by the on the bone surface is associated with TD2, TR1, MD1, MD3, MD5, MP1, MP3, MF5, MPR1, MPR2, MPR3 and MPR4 (Figures 5.32-5.33). The coordination points occasionally shifted distally or proximally, related to the facet of articulation, which appeared in the facet view. This was due to these points moving closer to the facet articulation surface of the TM bone.

The stages were divided into first, second and final, and were based on the new 3D virtual shapes. Each new shape was modelled from two bones at each

stage, and each stage resulted a new default new shape that resembled that of the previous stage. The 3D Landmark software calculated the position of each point at every stage (James Rohlf and Marcus 1993), not with the shape of the bone in its entirety. The software calculated the location of each point in each view statistically.

Linear regression tests were performed to determine whether and by how much each point changed its location from one stage to the other (Rudemo 2000). A changed location of a point reflected a changed shape of the bone at that point.

Linear regression was also helpful in clarifying the direction of lines. Some points presented positive lines, which indicated that the point protruded and thus that the tubercle had increased sharpness or prominence compared to the previous stage. If a line presented a negative value, that meant that the point was slumped or that the eminence experienced an increase in taper.

The coordination points from the facet view of the TM bone were not related to each other during transfer from the first stage to the final (Figure 5.81). The palmar tubercle, presented by TD3, had the greatest change among the facet view coordination points, a change of 69%. The radial tubercle, presented by TD1, had the least amount of change, only 0.2%. However, whole points did change, which means that the surface of the TM bone, especially at the facet, had not the necessary number of coordination points or that the position of the coordination points could have been better.

The shape of the facet of the TM bone is prominent and convex at the palmar tubercle (TD3) and at the dorso-radial tubercle. It is also tapered and concave at the radial tubercle (TD1) and the eminence of trapezial ridge.

The radial view of the TM bone changed only at two coordination points (Figure 5.61): the distal border of 1st MC facet (TR1) and the radial tubercle (TR2). TR1 had the greatest changed, of 22%, while TR2 was the least changed, by only 4%. The dorso-ulnar tubercle (TR3), the dorso-radial tubercle (TR4) and the palmar tubercle (TR5) from the TM radial view also were not changed from the first stage to those following.

The dorso-ulnar tubercle showed the greatest change, of 33%, while the dorso-radial tubercle was the least changed, by 24%. Therefore, both the distal

border of the 1st MC facet and radial tubercle were changed to become more prominent.

From the radial view, the coordination points preserved the TM bone shape, especially at three points (TR3, TR4 and TR5). Two points, however, did not preserve the TM bone shape (TR1 and TR2). The results also showed that the radial tubercle area had the greatest change in area through the transfer of the TM bone from the first stage to the final shape.

The facet view of the 1st MC bone changed at three coordination points (Figure 5.90): the posterior eminence (MPR1), the middle of the radial border (MPR2) and the anterior eminence (MPR3). The posterior eminence had the greatest change, of 2% and the middle of the radial border has the least amount of change, only 1%. The shape of the 1st MC facet view has prominences or convexities at the middle of the radial border and the anterior eminence. The shape of the 1st MC facet view, by contrast, has a taper or concavity at the posterior eminence.

The palmar view of the 1st MC changed at two points (Figure 5.71): the middle of anterior eminence (MP3) and the palmo-radial tubercle (MP4). The palmo-radial tubercle had the greatest amount of change, 6%, while the middle of the anterior eminence had the least amount of change, 3%.The location of the remaining three points: the middle of the palmar surface near the radial border of 1st MC shaft (MP1), the palmo-ulnar tubercle (MP2) and the middle of the palmar surface near the ulnar border of 1st MC shaft (MP5) did not change through the stages, which means that they preserved their shape through a large sample population. The MP1 point had the greatest amount of preservation, at 30%, while MP5 had the least amount of preservation, at 1%. The shape of change was a taper or concavity.

The dorsal surface of the 1st MC had only one unchanged coordination point (Figure 5.81). It was at the middle of the dorsal surface near the radial border of the 1st MC shaft (MD1). The four remaining points did change through the stages. They were the dorso-ulnar tubercle (MD2), the middle of the posterior eminence (MD3), the dorso-radial tubercle (MD4) and the middle of the dorsal surface near the ulnar border of the 1st MC shaft (MD5).

MD1 preserved the 1st MC shape as defined by the coordination points of the dorsal view by 17%. MD2 had the greatest amount of change, at 1.8%, while MD3 had the least amount of change, at 0.57%. Most of change occurred at MD3 and MD2, which showed a taper and a concavity, respectively.

Normally, the contact area of the TM and 1st MC bones was measured by calculating the length and width of centre line, which is the line which that crosses the articulation surface area in the middle (Momose *et al.* 1999). The curvature of the articulation surface was recorded, and the greatest and least curvatures were noted (Marzke *et al.* 2012).

In addition, other studies have described the articular surface of the TMC joint in early degenerative changes, although without the use of measurement procedures (Lane and Henley 2001; North and Rutledge 1983). The current study hypothesised that the articulation surface of TM and 1st MC could be divided by five lines in length and five lines in width. The articulation surface could therefore be covered entirely and segmented into areas based on the anatomical description of each line, as mentioned previously. Three areas were determined to have changing articulation surfaces.

The second eminence trapezial line (ETL2) was the longest as modelled by Rhinoceros (14.73 mm right, 14.1mm left). The shortest line was the first eminence trapezial line (ETL1) (9.91mm right, 9.43mm left). The longest line as modelled by Amira 3D software was the central length line (CLL) (14.47mm right, 14.22mm left) and the shortest line was first dorso-radial tubercle line (DRTL1) (9.31mm right, 8.79mm left).

Based on these results, the longitudinal area at the centre of the TM facet between both ETLs, the dorso-radial tubercle line DRTL and the area parallel to the ETL1 line near the central length line CLL were considered to be the longest areas of the TM articular surface. The area parallel and distal to the DRTL at the edge of the TM facet and the area from the palmar tubercle near the facet toward the distal border of the TM facet were the shortest areas of TM articular surface (Figures 5.95-5.96-5.97-5.98).

The second distal border line (DBL2) was the widest as modelled by Amira (14.9 mm right). The second palmar tubercle line (PTL2) was 14.03mm right. The widest lines as modelled by both Rhinoceros and Amira 3D software were the first

palmar tubercle line (PTL1) (9.36 mm right, 9.47 mm left and 9.82 mm right, 10.05 mm left, respectively). The widest line as modelled by Amira 3D software was the central width line (CWL) (14.43mm right, 14.2mm left).

The area from the palmar tubercle at the facet border distal toward the dorso-radial tubercle was the narrowest area of TM articulation surface. The area parallel to PTL1 near the central width line (CWL), the area set transversely at the centre of the TM facet and the area from distal border of the TM facet distal to eminence trapezial ridge toward the facet edge near and proximal to the dorso-ulnar tubercle were the widest areas of the TM articulation surface (Figures 5.99-5.100-5.101-5.102).

The central length line (CLL) as modelled by both Amira 3D and Rhinoceros software was the longest line on the 1st MC articulation surface (11.33 mm right, 11.1 mm left and 11.25 mm right, 12.01 mm left, respectively). The first radial border line (RBL1) as modelled by both Amira 3D and Rhinoceros, was the shortest line on the 1st MC articulation surface (4.79 mm right, 5.35 mm left and 6.2 mm right, 4.9 mm left, respectively. The area set longitudinally at the centre of the 1st MC facet was the longest area, while the area that began at the posterior eminence and proceeded radially toward the anterior eminence was the shortest area of the 1st MC articulation surface (Figures 5.103-5.104-5.105-5.106).

The second posterior eminence line (PEL2) as modelled by both Amira 3D and Rhinoceros, represented the widest area of the 1st MC articulation surface (16.39mm right, 17.36 mm left and 17.96 mm right, 16.54 mm left, respectively. The first anterior eminence line (AEL1) as modelled by both Amira 3D and Rhinoceros, represented the narrowest area of the 1st MC articulation surface (3.85 mm right, 4.23 mm left and 4.01 mm right, 3 mm left, respectively. The area that began radially from the ulnar border toward the radial border was widest area of the 1st MC articulation surface, while the area that began ulnarly from radial border toward ulnar border was the narrowest (Figures 5.107-5.108-5.109-5.110).

The shortest observed areas (ETL1, DRTL1) were near the edge of the TM articulation surface and the narrowest (PTL1) area was also restricted to the edge of the TM articulation surface. The shortest area observed on 1st MC (RBL1) was at the edge of 1st MC articulation surface. The narrowest (AEL1) was also near the edge of articulation surface. The edge areas of both TM and 1st MC

articulation surfaces are critical areas, subject to more degenerative change than other areas.

The middle areas of both TM and 1st MC articulation surfaces are subject to the least amount of degenerative change. This is due to the properties of their longest and widest areas, which have good joint space between TM and 1st MC fossa, which prevents degenerative change.

In the current study, there were no significant differences between the right and left dry bones and there were no significant differences between Amira 3D and Rhinoceros.

Four limitations to this study can be identified: 1) the number of samples or population size could be larger, 2) the assessment of the entire TM and 1st MC bone shapes could have been carried out rather than that of the articulation surfaces only, 3) the distribution of coordination points were concentrated in only two views of TM and three views of 1st MC, 4) the age, sex and past medical histories of the sample were not assessed.

Chapter Six

6.1 General Discussion

The controversy over the stabilization of the TMC ligaments was noted throughout the literature review; the PIML was found to be the main stabilizer (Pagalidis *et al.* 1981), while the RTML and PUTML were described as secondary stabilizers (Imaeda *et al.* 1993). Also, this ligament is considered to be one of the dorsal ligament complexes that maintains the TMC joint in dorsal subluxation associated with PTML, PIML,DUTML, and PUTML (Strauch *et al.* 1994). The PTML was mentioned as the primary stabilizer (D'Agostino *et al.* 2014; Eaton and Littler 1969; Pieron 1973; Rongieres 2004; Strauch *et al.* 1994), and the superficial layer played a role in preventing the palmar subluxation (Colman *et al.* 2007). Also, the DUTML was observed to be a stabilizer of the TMC joint (Lin *et al.* 2013).

In this thesis, chapter two investigated the TMC ligaments during the neutral and full abduction positions in 2D—the experiments used the 2D technique. Moreover, the measurements aided in the determining which TMC ligaments served as primary and secondary stabilizers. The results revealed that the PIML and DIML were the main stabilizers through the experiments and that the DUTML and PUTML served as associated ligaments to prevent TMC joint dislocation. The RTML prevented radial subluxation, while the superficial and deep layers of the PTML acted as a pivot for the movement of the TMC joint and assisted in preventing a palmar subluxation. The experiments results supported the concept of the combined work of the TMC ligaments; that is, each of the TMC ligaments have individually specialized functions, as mentioned previously, but the function of protecting the TMC joint from injury such as dislocation or subluxation is still performed by the combined work of TMC ligaments. The strengthening of the TMC joint can prevent injury from a sudden external force by working all the TMC ligaments as a group to maintain the joint at the natural position (anatomical position).

In addition, descriptions of the TMC ligaments' attachment were studied (Luria *et al.* 2010; Pichler *et al.* 2010; Pieron 1973; Pizon and Wang 2010; Shuler *et al.* 2008). In this thesis (Chapter Two), it has been shown that the RTML originates proximally from the distal edge of the transverse carpal ligament (TCL) and the

trapezial ridge and attaches distally on the radio-palmar side of the first metacarpal bone. The sPTML has a large attachment proximal to the palmar edge of the trapezium bone, and this ligament attaches distally to the palmar edge of the first metacarpal base. The dPTML originates proximally on the ulno-palmar edge of the trapezium bone, and this ligament attaches distally on the ulno-palmar edge of the base of the first metacarpal. The PUTML attaches distally to the palmo-ulnar edge of the first metacarpal base and proximally to the dorso-ulnar trapeziometacarpal ligament (DUTML). The DUTML originates proximally to the dorso-radial tubercle of the trapezium bone and is attached to the dorso-ulnar edge of the first metacarpal bone. The PIML originates ulnarly to the radio-palmar base of the second metacarpal and inserts on the radial side of the radio-palmar base of the first metacarpal. The DIML originates ulnarly to the dorso-radial tubercle of the second metacarpal bone and inserts radially to the dorso-ulnar side of the first metacarpal bone.

In addition, the re-naming of the TMC ligaments based on four fundamental processes. Firstly, it was based on the anatomical positions of the TMC ligaments throughout the planned two-dimensional reconstruction in a three-dimensional virtual environment. It was based secondly on the orientations of the attachment between the first metacarpal, second metacarpal, and the trapezium bones. Thirdly, TMC ligaments were divided into two groups. The first group consists of the five ligaments attached between the first metacarpal and trapezium bones: the sAOL, deep anterior oblique ligament (dAOL), POL, UCL, and DRL. The second group consists of the two ligaments attached between the first metacarpal and second metacarpal: the palmar intermetacarpal ligament (PIML) and DIML. Fourthly, terminology was added, such as palmar and trapeziometacarpal, for some of the ligaments in order to be more precise and accurate. Some terminology was also changed, such as the ulnar collateral ligament (UCL) to the radial trapeziometacarpal ligament (RTML). However, other terminology remained unchanged, such as the dorsal intermetacarpal ligament (DIML) and palmar intermetacarpal ligament (PIML).

3D and 2D studies have deepened the understanding of large ligaments such as those of the knee, hip, and foot (Agur *et al.* 2003; Henning *et al.* 1985; Hirokawa and Tsuruno 2000; Momersteeg *et al.* 1995; Pioletti *et al.* 1995; Stark *et al.* 2012), whereas small ligaments such as the carpal ligament are still not well

understood. One of the aims of this thesis was to use 2D and 3D experiments to increase the understanding particularly of small ligaments such as TMC ligaments.

The investigation took place during a static neutral abduction and static full abduction in 3D (Chapter Three), and the experiments utilized a new design called a ligament stretcher. This device was used to stretch the TMC ligaments when the ligament was outside the joint for static full abduction investigations. These experiments also measured the thickness of the proximal cross-sectional area, middle cross-sectional area, and distal cross-sectional area of the TMC ligaments, while the previous experiments (Chapter Two) measured only the length and width and surface area of the TMC ligaments.

Based on the 3D visualization, the orientation of the TMC ligaments were clear and thus the descriptions of the ligaments' tensions and the edge analysis could be identified clearly. The results of the 3D experiments (Chapter Three) supported the 2D experiments (Chapter Two) in that the DIML and PIML were the main stabilizers. Also, the RTML, sPTML, and dPTML were distinguished by relaxing during the full abduction position and stretching in the neutral position, and the RTML was mostly a curved ligament, especially in the neutral position. The shape of the sPTML curved near the proximal surface zone in the neutral position, and the curvature that changed in the full abduction position was concentrated at the middle surface zone near the ulnar attachment zone. Due to the position of the dPTML, it must curve with the sPTML. But the dPTML curved in the full abduction position at the centre, between the middle and proximal surface zones. However, this ligament worked mostly with the sPTML as one ligament.

The PUTML and DUTML are anatomically placed beside each other, but the DUTML has a half arch at the middle and distal surface zones. Both ligaments have the same characteristics of curving during the full abduction position and curve from the middle and distal surface zones. Extreme tension and curvature were shown for the PIML and DIML during the neutral and full abduction positions, respectively. Therefore, the roles of these ligaments were very important in the stabilization of the TMC joint during the motion from the neutral toward full abduction position. According to the anatomical position of the PIML, the curvatures acted at the proximal and middle surface zones, because the PIML was placed between the first and second metacarpal bones palmarly, and the

attachment of the PIML was located near the transverse carpal ligament (TCL). Therefore, the PIML ligament curved proximo-ulnarly. The DIML curved disto-ulnarly with tension upon the ligament during the full abduction position. Also, the tension of both ligaments increased somewhat in the full abduction position, and there was no relaxation potentially affecting the status of these ligaments, except the PIML relaxed a little at the middle surface zone. However, both ligaments play a role as a primary stabilizer of the TMC joint.

Moreover, the volume measurement that was investigated (Chapter Three) by using a B-spline shape to harden the ligaments (tube), and the diameter was 0.158 mm. The anistropic scale must be near zero to be solid in shape, and at the same time it can measure the volume precisely. The process of measuring the volume included summing the volume of all B-splines (tubes) of each ligament individually.

The entheses of the TMC ligaments have been observed and analysed (Benjamin *et al.* 2002; Benjamin *et al.* 2006; Chung 2007; Claudepierre and Voisin 2005; Francois *et al.* 2001; Freemont 2002; Moriggl *et al.* 2003), and the entheses have been classified into fibrous and fibrocartilagenous according to the tissue present at the skeleton attachment site (Patel and Buckland-Wright 1999; Slobodin *et al.* 2007). Moreover, the main structure used to illustrate the type of the entheses was the tidemark line, which was the basophilic line separating the calcified and uncalcified fibrocartilagenous entheses.

In this thesis, the TMC ligaments attachments were found to be of the fibrocartilagenous type, and this was observed at each of the TMC ligament attachments, proximal and distal. The fibrous type often seems in healthy tissues, while the fibrocartilagenous type appears in the tissues degenerative process. However, the ages of the cadavers that were used for the experiments could have affected the results.

The staining of the histological slides used to explore the structures of the tissues and to distinguish the tiny structures between each have been investigated (Asonova and Migalkin 1996; Carleton *et al.* 1980; Miller 1971), and the type of stain has importance in visualizing and identifying the structures of the slides. In

addition, in this thesis (Chapter Four), the experiments used different types of staining, such as MMT and ME.

The development of the procedures for staining, especially the combination of two stains (MMT and ME), was a unique idea in that the process alternated the two stains, one beginning with MME and another beginning with ME. Therefore, the fascicles of the ligaments were difficult to distinguish. The contrast of the blue colour that appeared in the combination beginning with MMT made it difficult to identify the fascicles, but the combination that began with ME was better than that beginning with MME—the colours were near to those of the MMT results, but the MMT alone was clearest.

The ME stain was utilized to detect the elastin fibres of the connective tissues, such as ligaments and tendons (Miller 1971). In this thesis (Chapter Four), this stain was used to differentiate between all the TMC ligaments, and the re-timing of the ME protocol experiments clarified which protocol should be followed to get the clearest view of the tissues slides. The process depended on the two solutions—Van Gieson's and Miller's Elastin—one of which was increased for five seconds and the other was decreased for five seconds, and the results showed that the experiment with 2.5 hours of Miller's Elastin and 15 seconds of Van Gieson's solution was the best of all experiments in that the elastin fibres were clearest, and the other structures could be distinguished most clearly.

The purpose of the elastin fibres is to provide laxity to the ligament so that the ligament can stretch and shorten without tearing and so that the joint has flexibility in all directions except in the direction that is restricted by the ligament at the maximum stretch of the ligament itself.

The HREM technique used the Amira 3D software (Geyer *et al.* 2009; Mohun and Weninger 2012; Rosenthal *et al.* 2004; Weninger *et al.* 2006). In this thesis (Chapter Four) the HREM technique was used to explore the overlap between the DUTML and flexor retinaculum and the 3D visualization of the DUTML in a virtual environment was remarkable for following the collagen fibres of the ligament, as well as the bones of the TMC joint. The results of this experiment showed no connection between the collagen fibres of both the DUTML and flexor retinaculum.

The first metacarpal and trapezium bones have been analysed (Ateshian *et al.* 1992; Buffi *et al.* 2013; Daud *et al.* 2014; Humes *et al.* 2004; Schild *et al.* 1981; Slocum 1943); however, the present study (Chapter Five) analysed each prominence, decline, ridge, and groove to increase the anatomical knowledge of the osteological features of the TMC joint.

The 3D software of Amira, Landmark, and Rhinoceros were used to analyse the shape of the TMC joint bones and also to measure the articular surface of both the first MC and TM bones. In addition, this study (Chapter Five) employed the unique idea of single coordination points (Bookstein 1997) to observe the edges of both 1st MC and TM bones, and these points were chosen based on the position of origin and attachment of the TMC ligament, which gave a much clearer understanding of how the TMC joint bones changed throughout different, large-sample populations.

The results of the experiments showed that the shape of the facet of the TM bone is prominent and convex at the palmar tubercle (TD3) and at the dorso-radial tubercle and that it is also tapered and concave at the radial tubercle (TD1) and at the eminence of trapezial ridge. The radial view of the TM bone changed only at two coordination points: the distal border of the 1st MC facet (TR1) and the radial tubercle (TR2). TR1 showed the greatest change, of 22%, while TR2 was the least changed, by only 4%. Moreover, the dorso-ulnar tubercle (TR3), the dorso-radial tubercle (TR4), and the palmar tubercle (TR5) from the TM radial view showed no change from the first stage to those following.

In addition, the dorso-ulnar tubercle showed the greatest change, of 33%, while the dorso-radial tubercle was the least changed, by 24%. Therefore, both the distal border of the 1st MC facet and radial tubercle were changed to become more prominent. From the radial view, the coordination points preserved the TM bone shape, especially at three points (TR3, TR4 and TR5). Two points, however, did not preserve the TM bone shape (TR1 and TR2). The results also showed that the radial tubercle area had the greatest change in area through the transfer of the TM bone from the first stage to the final shape. Also, the facet view of the 1st MC bone changed at three coordination points: the posterior eminence (MPR1), the middle of the radial border (MPR2), and the anterior eminence (MPR3). The posterior eminence had the greatest change, of 2%, and the middle of the radial

border had the least amount of change, by only 1%. The shape of the 1st MC facet view has prominences or convexities at the middle of the radial border and the anterior eminence. The shape of the 1st MC facet view, by contrast, has a taper or concavity at the posterior eminence.

Moreover, the palmar view of the 1st MC changed at two points: the middle of anterior eminence (MP3) and the palmo-radial tubercle (MP4). The palmo-radial tubercle had the greatest amount of change, of 6%, while the middle of the anterior eminence had the least amount of change, of 3%.The location of the remaining three points—the middle of the palmar surface near the radial border of 1st MC shaft (MP1), the palmo-ulnar tubercle (MP2), and the middle of the palmar surface near the ulnar border of 1st MC shaft (MP5)—did not change throughout the stages, which means that they preserved their shape over a large sample population. The MP1 point had the greatest amount of preservation, at 30%, while MP5 had the least amount of preservation, at 1%. The shape of the change was that of a taper or concavity.

The dorsal surface of the 1st MC had only one unchanged coordination point; it was at the middle of the dorsal surface near the radial border of the 1st MC shaft (MD1). The four remaining points did change throughout the stages; these included the dorso-ulnar tubercle (MD2), the middle of the posterior eminence (MD3), the dorso-radial tubercle (MD4), and the middle of the dorsal surface near the ulnar border of the 1st MC shaft (MD5).

6.2 Clinical implications

The TMC articulation is a saddle-type joint, and the stability of the TMC joint relies on the muscle, tendons, and ligaments crossing the joint. Decrease of laxity of the TMC ligaments, which results from the development of OA in the TMC joint (Batra and Kanvinde 2007), and the strength of the TMC ligaments decreasing with age suggest that the decrease in strength is related to the patho-genesis of the TMC joint (Najima et al. 1997). Aging alone does not significantly affect the kinematics of the TMC joint as other factors are involved in the progression of OA along with aging.

In addition, the recurrent subluxation of the TMC joint increases the prevalence of the development the OA from friction between the articular cartilage of both 1st MC and TM bones (El Ibrahimi et al. 2009; Pellegrini 2001). Traumatic dislocation has been treated by Slocum (Slocum 1943) with an intra-articular palmaris longus graft. Later, Eggers (Eggers 1945) used a portion of the extensor carpi radialis longus as a tendon transfer through a drill hole, and the extensor pollicis brevis tendon was re-routed through drill holes by Kestler (Kestler 1946); however, Kestler subsequently advised the use of the abductor pollicis longus. Nevertheless, the techniques of intervention on the TMC joint have developed over the years.

The classifications of the TMC joint subluxations include plamar, dorsal, palmo-radial, and lateral metacarpal subluxations (Colman et al. 2007; D'Agostino et al. 2014; Lin et al. 2011). Excessive movement in the flexion direction leads to dorsal subluxation, while excessive movement toward abduction leads to lateral subluxation. palmar subluxation occurs during excessive movement toward extension.

However, the results of the current experiments on the kinematics of the TMC joint (Chapters Two and Three) show that the preservation or reconstruction of all TMC ligaments is not always possible during surgery. A choice must then be made to reconstruct certain ligaments. The PIML and DIML based on the current results serve as main stabilizers of the TMC joint, thus our findings suggest a need to reconsider the importance of PIML, DIML, and RTML and that they should be taken into account when planning surgeries with ligament reconstruction of the TMC joint. The RTML also has a role in preventing the lateral or radial subluxtion that is based on the anatomical description of this ligament.

The fracture cases that often occur with dislocations, such as Bennett’s fracture, are a common reasons in the development of OA (El Ibrahimi et al. 2009). The contact areas of the 1st MC and TM bones have factors that increase the possibility of OA (Miura *et al.* 2004a), and the distance between 1st MC and TM articular surfaces also reflect the degree of OA affecting the TMC joint (Eaton and Littler 1969). However, the prophylactic treatment considered as early treatment has many stages: decrease pain; increase the muscles, tendons, and ligaments crossing the TMC joint, and increase TMC joint mobility—which can be

accomplished with medications and rehabilitation. Reconstruction surgery can be considered if the prophylactic treatment is not successful.

The entheses for clinical purposes have shown that the spondyloarthropathies provide the most striking examples of entheseal involvement in inflammatory joint disease (Claudepierre and Voisin 2005). Also, tennis elbow, golfer's elbow, and jumper's knee provide stress concentration such as an issue in entheses (Chung 2007), and the mechanical load and excessive exercise at sites of stress concentration at the region where tendons and ligaments attach to bone lead to development of enthesopathies (Benjamin et al. 2006). However, the aging is associated with an increased prevalence of asymptomatic radiological enthesopathy.

Fibrous entheses is not considered to be a pathological state due to the normalities of the fibrous matrix at the site of attachment with the bone. In contrast, fibrocartilagenous has a changed fibrous matrix, from fibrous to cartilaginous at the attachment sites. Thus, the tidemark line has been shown, and the calcified and uncalcified areas have also been shown, and these structures are considered to be a pathological state or case. The reasons for enthesopathy include aging and the athletes frequently seek medical advice. Chapter Four discussed the fibrocartilagenous type of entheses and the calcified and uncalcified interruption by the tidemark line was shown on most slides of the proximal and distal attachment zone of the TMC ligament. The age of the cadavers may have played a major role in revealing the fibrocartilagenous type.

The osteological findings have led to a new naming of the 1st MC and TM features (Chapter Five) such as the distal border of 1st MC facet, the distal and proximal ridge of the palmar surface of 1st MC, and the eminences of the trapezial ridge of the TM. Thus, our findings provide a new osteological definition of the1st MC and TM bones, which increases the understanding the radiological anatomy and therefore of its complex fracture patterns and increases the anatomical knowledge of the fractures classifications of the 1st MC and TM bones.

6.3 Conclusion

In this thesis, many of novel concepts were used to observe the most accurate and precise movement of the TMC joint and its ligaments. As mentioned in the first chapter, there were many of difficulties determining which ligament of TMC ligaments worked to stabilize the TMC joint (Kuo *et al.* 2004; Miura *et al.* 2004b; Zhang *et al.* 2005). Also, the number of ligaments around TMC joint was unclear (Bettinger *et al.* 1999; Eaton and Littler 1969; Imaeda *et al.* 1994; Kapandji and Kapandji 1993; Kaplan 1965), as well as the naming of the TMC ligaments (Imaeda *et al.* 1993; Kuo *et al.* 2002). Thus, the experiments must have new materials, ideas, and devices to solve these problems.

The 3D model in the last century has achieved the best results for medical and biomechanical science (Kuo *et al.* 2009a; Kuo 2003; Miura *et al.* 2004b; Nanno *et al.* 2006a; Oberlin *et al.* 1992; Su *et al.* 2014). Developers struggled to produce much of the software used to render the shape of the 3D model, and created the best options to produce 3D models in a 3D virtual environment. In addition, they used their abilities to make the software accurate and easy to use by researchers, especially for measuring 3D models.

In this thesis three types of software were used to render the shape of the TMC ligaments and bones into 3D model, then use this model to measure results to prove a specific hypothesis. Rhinoceros software was the main software for rendering the TMC ligaments and bones in all experiments, but mostly used for chapters two, three, and five. It is good software and has high rate of accuracy. By using this software the results of the measurements illustrate the properties of the main stabilizer of the TMC joint, particularly in the neutral and full abduction positions. Also, it allows precise manipulation in the 3D virtual environment, which aids in describing the anatomical position of each TMC ligament and naming the ligaments based on their new orientations.

The second software used was Landmark 3D software. This software has the ability to deal with two 3D models and merge them together into one 3D model. This merged model has the most important points that are shared between the two models. This software was mainly used in chapter five, and it succeeded in

combining the bones of the TMC joint, and analysing the features of the surfaces of these bones (TM and first MC).

The third software used was Amira 3D, which is the newest of the 3D modelling software. It deals with CT scan files (DICOM) and renders it into a 3D model. Moreover, it was used to compare results between itself and Rhinoceros. The results have shown that there were no significant changes between of both of them. However, each software has a specific uses in this thesis to provide stabilization and to identify the ligaments around the TMC joint, as well as to re-name them.

Rendering the small ligaments into a 3D model was previously very difficult, but now, by using this software, it is easier. Moreover, the comparison between the 2D reconstruction and 3D model of the TMC ligaments successfully proved the stabilization of the TMC ligaments, which occurred in the chapter three. The hypothesis of comparing two different shapes is also a unique feature of this thesis.

The combination of two stains was used in most of the previous experiments (Asonova and Migalkin 1996; Goldner 1938; Miller 1971; O'Connor and Valle 1982; Veuthey *et al.* 2014), but a new procedure combining the MMT with ME stains was used this time. The hypothesis was tested to identify both the collagen fibres and elastin fibres on one figure. This was shown in chapter four. Also, the re-timing of the reactions of the Miller elastin and Van Gieson solutions with TMC ligaments slides were unique procedures. Therefore, clear visibility of the elastin fibres under the microscope has been achieved with 2.5 hours of Miller elastin solution and 15 seconds of Van Gieson solution.

In the anatomical descriptions of the RTML ligaments, the relationship between the RTML ligament and TCL ligament was observed. Thus, the experiment using Amira software and a special technique, called HREM, to distinguish the relationship between RTML and TCL ligaments, was unique. However, the results have shown no relationship between them.

I addition, the TMC joint, particularly the TM and first MC bones, which contain the TMC joint, were observed, measured, and analysed in chapter five. The

hypothesis was that the area of the TM nor the first MC has changed morphologically. The results have shown morphological change in some sets of both TM and first MC bones, while some sets have preserved the shape.

Normally, Landmark is used paleontology to discover the age and change of the fossils through the years. The hypothesis to use this software for human bones was unique and achieved successful analysis of the prominences and declines of the TM and first MC bones.

Finally, the utilization of multiple 3D software suites to achieve the target goals of this thesis proves the arguments were of the previous studies. The stabilization of the TMC joint, numbering of the TMC ligaments around the TMC joint, naming of the TMC ligaments, identifying the most important set of the TMC bones (TM and first MC), measuring the articular surface and ligaments, identification of the TMC ligaments, and determining the tissue level of the TMC ligaments were all achieved in this thesis.

6.4 Future studies

The nature of this project has been to explore TMC joint stability, morphology, and osteology. The results shown in my thesis suggest important future experiments in various directions.

In the current study, I have used 2D and 3D models of TMC joint ligaments and bones. In order to discriminate the anatomical features of both ligaments and bones, a new form of software, for instance 3D photo modeller, will give a more accurate 3D model. Also, advances devices or accessories such as Rhinoceros' scanner will give a more precise 3D model for more accurately measured results.

In the current study, I have investigated only the TMC ligament and bones; the nerves, blood supplies, and muscles of this joint were not studied throughout these experiments. The blood supplies, nerves, and muscles are very important for increasing the anatomical knowledge of the TMC joint and to determine the nature of the TMC joint (healthy or diseased).

In the current study, I have observed every structure of the TMC joint separately. A study on the relationship between these structures (ligaments, bone, arteries, veins, muscles, and nerves) will also help in the development of future therapeutic procedures (surgery).

In the current study, I have concentrated on both the neutral and full abduction positions (static and dynamic study); a variety movement such as those on flexion, extension, and opposition motion will increase the information on TMC joint displacement.

In the current study, I have used the histological findings for identifying the structures of the TMC ligament, but there were no measurement procedures for these structures. The measurement of the structures particularly at a magnification of 2.5 or 10 would be more accurate.

Appendix 1 Tissue preparing

Accelerate Decalcification

Ingredients:
1% EDTA
9.5% nitric acid ($HNO_{3)}$
Distilled H_2O

Double Embedding

This double-embedding procedure was adopted to combat the difficulties faced with the traditional single-embedding procedure. The double-embedding procedure was as following:
1- 50% alcohol all day
2- 70% alcohol overnight
3- 95% alcohol all day
4- Absolute alcohol 1.5 hours
5- Absolute alcohol (new change) overnight
6- 50% alcohol: 50% diethyl-ether half day
7- 1% cellulose nitrate in 50% alcohol: 50% diethyl-ether half day
8- 1% cellulose nitrate in 50% alcohol: 50% diethyl-ether over night
9- 1% cellulose nitrate in 50% alcohol: 50% diethyl-ether half day
10- Amyl acetate or chloroform 30 minutes
11- Dry on paper
12- Immerse in liquid paraffin wax (1^{st} wax) 60 minutes **in oven**
13- 2^{nd} wax (new wax) 60 minutes **in oven**
14- 3^{rd} wax (new wax) in vacuum @ 800 30 minutes **in vacuum oven**
15- Don **NOT** change wax or open oven; Increase vacuum to 500 30 minutes **in vacuum oven**
16- **Gently** release vacuum, then open oven
17- 4^{th} wax (new wax) in vacuum @ 500 1-2 hours **in vacuum oven**
18- Mount tissue in block

Slide Coating and Weighting OPTINAL

To facilitate section adhesion to the slides each slide was coated with a gelatin mixture.

Solution

2.5 g gelatin
0.25 g chromium III potassium sulphate ($CrK(SO_4)_2\,12H_2O$)
500 mL distilled water
Gelatin dissolved into 250 mL distilled water on medium heat with stirrer
Chromium dissolved in 250 mL of distilled water
Gelatin solution added to chromium solution through filter paper

Procedure

Slides were cleaned with soapy water
Rinsed in warm water
Placed in warm gelatin solution and carefully removed to avoid creating bubbles on the slides surface
Placed in oven (50° C) overnight, Sealed in airtight container until used

Appendix 2 Modified Masson's Trichrome Staining (MMT)

Technique after Fogg 2004

Stain

1- Cytoplasmic Red **

A = 1% ponceau de xylidine in 1% acetic acid
B = 1% acid fuchsin in 1% acetic acid
Mix together in a ration of 2A:1B
To make 300 mL
A = 2 g ponceau de xylidine + 2 mL acetic acid in 200 mL H_2O
B = 1 g acid fuchsin + 1 mL acetic acid in 100 mL H_2O
The final pH ≈ 3.05

2- Light Green

2 g Light green SF + 2 mL acetic acid + 100 mL H_2O
Final pH ≈ 2.85

Procedure

1- Dewax slides in Histoclear	10-15 minutes
Hydration	
2- 1st Absolute alcohol	2 minutes
3- 2nd Absolute alcohol	2 minutes
4- 90% Alcohol	4 minutes
5- 70% Alcohol	4 minutes
6- Wash in water	4 minutes
Stain	
7- Place slides in Mayer's haematoxylin	8 minutes
8- Blue in water	
9- Place slides in Cytoplasmic red	1 minute
10- Wash in 2 dips of 1% Acetic acid	
11- Displace in 4% phosphomolybdic acid	2 minutes
12- Wash in 1% Acetic acid	
13- Place slides in 1% Light green	35-70 seconds
14- Wash in 1% Acetic acid	
Dehydrate	
16- 70% Alcohol	1 minute
17- 90% Alcohol	1 minute
18- 1st Absolute alcohol	2 minutes
19- 2nd Absolute alcohol	3 minutes
20- Clear in Histoclear	10-15 minutes
21- 2nd Histoclear	5 minutes
22- Mount slides in Histomount / DPX	

Results

Nuclei – Blue / Black
Cytoplasm, muscle and acidophil granules – Red
Collagen, cartilage, mucin and basophil granules – Green

(Fogg 2004)

Appendix 3 Milller's Elastin staining (ME)

Ingredient

Victoria blue 4R 1g
New fuchsin 1g
Crystal violet 1g.
200 mL hot water
Resorcein 4g
Dextrin 1g
Fresh 30% aq ferric chloride 50 mL
200 mL of 95% Alcohol
2 mL conc hydrochloric acid
0.5% Potassium permanganate
1% Oxalic acid
Nitric acid
Water
$4\ ROH + 4\ CO + O_2 \rightarrow 2\ (CO_2R)_2 + 2\ H_2O$
Van Gieson

Stain

1- Miller's Elastin stain

Victoria blue 4R 1g
New fuchsin 1g
Crystal violet 1g.
200 mL hot water
Resorcein 4g
Dextrin 1g
Fresh 30% aq ferric chloride 50 mL
200 mL of 95% Alcohol
2 mL conc hydrochloric acid

2- Oxalic acid

Nitric acid 50 mL
Water 750 mL

3- Van Gieson

Picric acid
Acid fuchsin
Celestin Blue
5% ammonium ferric sulphate 100ml
Celestin Blue 5 g
Curtis Stain
Saturated aqueous picric acid 90 mL
1% ponceau S 10 mL
Glacial acetic acid 10 mL

1% Ponceau S
Ponceau S 1 gm
Distilled water 100 mL

Procedure

1- Dewax slides in Histoclear	10-15 minutes
Hydration	
2- 1st Absolute alcohol	30 seconds
3- 2nd Absolute alcohol	30 seconds

4- 90% Alcohol	30 seconds
5- 70% Alcohol	1 minute
6- Wash in water	2 minutes

Stain

7- Place slides in 0.5% Potassium permangonate	5 minutes
8- Wash in water	
9- Place slides in 1% Oxalic acid	until clear
10- Wash in water	
11- Place slides in Miller's Elastin stain	2 Hours
12- Rinse in 90% Alcohol to remove excess stain	
13- Wash in water	
14- Counterstain with Van Gieson	30 seconds
15- Wash briefly in water	30 seconds

Dehydrate

16- 70% Alcohol	30 seconds
17- 90% Alcohol	30 seconds
18- 1st Absolute alcohol	1 minute
19- 2nd Absolute alcohol	2 minutes
20- Clear in Histoclear	10-15 minutes
21- 2nd Histoclear	5 minutes
22- Mount slides in Histomount / DPX	

Results

Elastin fibres – Black
Collagen – Deep red
Cytoplasm, muscle, fibrin, RBCs- Yellow

Appendix 4 Combination staining start with Modified Masson's Trichrom (MMT)

Procedure

1- Dewax slides in Histoclear	10-15 minutes
Hydration	
2- 1st Absolute alcohol	2 minutes
3- 2nd Absolute alcohol	2 minutes
4- 90% Alcohol	4 minutes
5- 70% Alcohol	4 minutes
6- Wash in water	4 minutes

Stain

7- Place slides in Mayer's haematoxylin	8 minutes
8- Blue in water	
9- Place slides in Cytoplasmic red	1 minute
10- Wash in 2 dips of 1% Acetic acid	
11- Displace in 4% phosphomolybdic acid	2 minutes
12- Wash in 1% Acetic acid	
13- Place slides in 1% Light green	35-70 seconds
14- Wash in 1% Acetic acid	
15- Place slides in 0.5% Potassium permangonate	5 minutes
16- Wash in water	
17- Place slides in 1% Oxalic acid	until clear
18- Wash in water	
19- Place slides in Miller's Elastin stain	2 Hours
20- Rinse in 90% Alcohol to remove excess stain	
21- Wash in water	
22- Counterstain with Van Gieson	30 seconds
23- Wash briefly in water	30 seconds

Dehydrate

24- 70% Alcohol	30 seconds
25- 90% Alcohol	30 seconds
26- 1st Absolute alcohol	1 minute
27- 2nd Absolute alcohol	2 minutes
28- Clear in Histoclear	10-15 minutes
29- 2nd Histoclear	5 minutes
30- Mount slides in Histomount / DPX	

Results

Nuclei – Black
Cytoplasm, muscle and acidophil granules – Blue
Collagen, cartilage, mucin and basophil granules – Deep blue

Appendix 5 Combination staining start with Miller's Elastin (ME)

Procedure

1- Dewax slides in Histoclear	10-15 minutes
Hydration	
2- 1st Absolute alcohol	30 seconds
3- 2nd Absolute alcohol	30 seconds
4- 90% Alcohol	30 seconds
5- 70% Alcohol	1 minute
6- Wash in water	2 minutes

Stain

7- Place slides in 0.5% Potassium permangonate	5 minutes
8- Wash in water	
9- Place slides in 1% Oxalic acid	until clear
10- Wash in water	
11- Place slides in Miller's Elastin stain	2 Hours
12- Rinse in 90% Alcohol to remove excess stain	
13- Place slides in Mayer's haematoxylin	8 minutes
14- Blue in water	
15- Place slides in Cytoplasmic red	1 minute
16- Wash in 2 dips of 1% Acetic acid	
17- Displace in 4% phosphomolybdic acid	2 minutes
18- Wash in 1% Acetic acid	
19- Place slides in 1% Light green	35-70 seconds
20- Wash in 1% Acetic acid	

Dehydrate

21- 70% Alcohol	1 minute
22- 90% Alcohol	1 minute
23- 1st Absolute alcohol	2 minutes
24- 2nd Absolute alcohol	3 minutes
25- Clear in Histoclear	10-15 minutes
26- 2nd Histoclear	5 minutes
27- Mount slides in Histomount / DPX	

Results

Nuclei – Blue / Black
Cytoplasm, muscle and acidophil granules – Deep red
Collagen, cartilage, mucin and basophil granules – Deep green

Not: the Van Gieson stain not utilize in this protocol

Appendix 6 Re-timing protocol of Miller's Elastin (ME) stain

Procedure

1- Dewax slides in Histoclear	10-15 minutes
Hydration	
2- 1st Absolute alcohol	30 seconds
3- 2nd Absolute alcohol	30 seconds
4- 90% Alcohol	30 seconds
5- 70% Alcohol	1 minute
6- Wash in water	2 minutes

Stain

7- Place slides in 0.5% Potassium permangonate	5 minutes
8- Wash in water	
9- Place slides in 1% Oxalic acid	until clear
10- Wash in water	
11- **Place slides in Miller's Elastin stain**	
1st experiment	**2 hours**
2nd experiment	**2 hours**
3rd experiment	**2.5 hours**
4th experiment	**2.5 hours**
5th experiment	**3 hours**
12- Rinse in 90% Alcohol to remove excess stain	
13- Wash in water	
14- **Counterstain with Van Gieson**	
1st experiment	**30 seconds**
2nd experiment	**15 seconds**
3rd experiment	**15 seconds**
4th experiment	**10 seconds**
5th experiment	**10 seconds**
15- Wash briefly in water	30 seconds

Dehydrate

16- 70% Alcohol	30 seconds
17- 90% Alcohol	30 seconds
18- 1st Absolute alcohol	1 minute
19- 2nd Absolute alcohol	2 minutes
20- Clear in Histoclear	10-15 minutes
21- 2nd Histoclear	5 minutes
22- Mount slides in Histomount / DPX	

Results

1st experiment

Elastin fibres – Black
Collagen – Deep red
Cytoplasm, muscle, fibrin, RBCs- Yellow

2nd experiment

Elastin fibres – Mild Black near to pink
Collagen – Light red
Cytoplasm, muscle, fibrin, RBCs- Yellow near to orange

3rd experiment

Elastin fibres – Mild Black near to pink

Collagen – Deep red
Cytoplasm, muscle, fibrin, RBCs- Yellow near to orange

4th experiment
Elastin fibres – Mild Black near to pink
Collagen – Mild deep red
Cytoplasm, muscle, fibrin, RBCs- Yellow near to orange

5th experiment
Elastin fibres – Mild Black near to pink
Collagen – deep red
Cytoplasm, muscle, fibrin, RBCs- Yellow near to oran

References

Agur, AM, Ng-Thow-Hing, V, Ball, KA, Fiume, E and McKee, NH (2003). Documentation and three-dimensional modelling of human soleus muscle architecture. *Journal of Clinical Anatomy* **16(4)**: 285-293.

Asonova, SN and Migalkin, NS (1996). [Use of Masson's trichrome method for staining decalcified bone tissue]. *Journal of Arkh Patol* **58(1)**: 66-67.

Ateshian, GA, Rosenwasser, MP and Mow, VC (1992). Curvature characteristics and congruence of the thumb carpometacarpal joint: Differences between female and male joints. *Journal of Biomechanics* **25(6)**: 591-607.

Batra, S and Kanvinde, R (2007). Osteoarthritis of the thumb trapeziometacarpal joint. *Journal of Current Orthopaedics* **21(2)**: 135-144.

Benjamin, M, Kumai, T, Milz, S, Boszczyk, BM, Boszczyk, AA and Ralphs, JR (2002). The skeletal attachment of tendons tendon entheses. *Comparative Biochemistry and Physiology Part A: Molecular & Integrative Physiology* **133(4)**: 931-945.

Benjamin, M, Toumi, H, Ralphs, JR, Bydder, G, Best, TM and Milz, S (2006). Where tendons and ligaments meet bone: attachment sites ('entheses') in relation to exercise and/or mechanical load. *Journal of Anatomy* **208(4)**: 471-490.

Bettinger, PC, Linscheid, RL, Berger, RA, Cooney Iii, WP and An, K-N (1999). An Anatomic Study of the Stabilizing Ligaments of the Trapezium and Trapeziometacarpal Joint. *The Journal of Hand Surgery* **24(4)**: 786-798.

Bettinger, PC, Smutz, WP, Linscheid, RL, Cooney, WP, 3rd and An, KN (2000). Material properties of the trapezial and trapeziometacarpal ligaments. *Journal of Hand Surgery American Volume* **25(6)**: 1085-1095.

Bojsen-Moller, F (1976a). Osteoligamentous guidance of the movements of the human thumb. *American Journal of Anatomy* **147(1)**: 71-80.

Bojsen-Moller, F (1976b). Osteoligamentous guidance of the movements of the human thumb. *American Juornal of Anatomy* **147(1)**: 71-80.

Bookstein, FL (1997). Landmark methods for forms without landmarks: morphometrics of group differences in outline shape. *Medical Image Analysis* **1(3)**: 225-243.

Buffi, JH, Crisco, JJ and Murray, WM (2013). A method for defining carpometacarpal joint kinematics from three-dimensional rotations of the metacarpal bones captured in vivo using computed tomography. **46:** 2104-2108.

Burkhart, KJ, Nowak, TE, Blum, J, Kuhn, S, Welker, M, Sternstein, W, Mueller, LP and Rommens, PM (2010). Influence of formalin fixation on the biomechanical properties of human diaphyseal bone. *Journal of Biomedical Engineering* **55(6)**: 361-365.

Cardoso, FN, Kim, H-J, Albertotti, F, Botte, MJ, Resnick, D and Chung, CB (2009). Imaging the Ligaments of the Trapeziometacarpal Joint: MRI Compared with MR Arthrography in Cadaveric Specimens. *American Journal of Roentgenology* **192(1)**: W13-W19.

Carleton, HM, Drury, RAB and Wallington, EA (1980). *Carleton's Histological technique*. Oxford ; New York, Oxford University Press.

Ceri, N, Korman, E, Gunal, I and Tetik, S (2004). The morphological and morphometric features of the scaphoid. *The Journal of Hand Surgery: British & European Volume* **29(4)**: 393-398.

Cerveri, P, De Momi, E, Marchente, M, Lopomo, N, Baud-Bovy, G, Barros, RM and Ferrigno, G (2008). In vivo validation of a realistic kinematic model for

the trapezio-metacarpal joint using an optoelectronic system. *Annals of Biomedical Engineering* **36(7)**: 1268-1280.

Cheze, L, Dumas, R, Comtet, JJ, Rumelhart, C and Fayet, M (2009). A joint coordinate system proposal for the study of the trapeziometacarpal joint kinematics. *Journal of Computer Methods Biomechanical and Biomedical Engineering* **12(3)**: 277-282.

Chiavaras, MM, Harish, S, Oomen, G, Popowich, T, Wainman, B and Bain, JR (2010). Sonography of the anterior oblique ligament of the trapeziometacarpal joint: a study of cadavers and asymptomatic volunteers. *American Journal of Roentgenology* **195(6)**: W428-434.

Chidgey, LK, Dell, PC, Bittar, ES and Spanier, SS (1991). Histologic anatomy of the triangular fibrocartilage. *The Journal of Hand Surgery* **16(6)**: 1084-1100.

Chung, Ka (2007). 120 Entheses (tendon and ligament attachment sites): basic considerations for considering enthesopathies in sport. *Journal of Science and Medicine in Sport* **10, Supplement 1(0)**: 49.

Claudepierre, P and Voisin, M-C (2005). The entheses: histology, pathology, and pathophysiology. *Joint Bone Spine* **72(1)**: 32-37.

Cobb, TK, Dalley, BK, Posteraro, RH and Lewis, RC (1993). Anatomy of the flexor retinaculum. *The Journal of Hand Surgery* **18(1)**: 91-99.

Cole, KJ and Abbs, JH (1986). Coordination of three-joint digit movements for rapid finger-thumb grasp. *Journal of Neurophysiology* **55(6)**: 1407-1423.

Colman, M, Mass, DP and Draganich, LF (2007). Effects of the deep anterior oblique and dorsoradial ligaments on trapeziometacarpal joint stability. *Journal of Hand Surgery American Volume* **32(3)**: 310-317.

Connell, DA, Pike, J, Koulouris, G, van Wettering, N and Hoy, G (2004). MR imaging of thumb carpometacarpal joint ligament injuries. *Journal of Hand Surgery British Volume* **29(1)**: 46-54.

Cooney, WP, 3rd and Chao, EY (1977). Biomechanical analysis of static forces in the thumb during hand function. *Journal of Bone Joint Surgery American Volume* **59(1)**: 27-36.

Cooney, WP, 3rd, Lucca, MJ, Chao, EY and Linscheid, RL (1981). The kinesiology of the thumb trapeziometacarpal joint. *Journal of Bone Joint Surgery American Volume* **63(9)**: 1371-1381.

Crisco, JJ, Coburn, JC, Moore, DC and Upal, MA (2005). Carpal bone size and scaling in men versus in women. *The Journal of Hand Surgery* **30(1)**: 35-42.

Currey, JD, Brear, K, Zioupos, P and Reilly, GC (1995). Effect of formaldehyde fixation on some mechanical properties of bovine bone. *Journal of Biomaterials* **16(16)**: 1267-1271.

D'Agostino, P, Kerkhof, FD, Shahabpour, M, Moermans, JP, Stockmans, F and Vereecke, EE (2014). Comparison of the Anatomical Dimensions andÂ Mechanical Properties of the Dorsoradial andÂ Anterior Oblique Ligaments of the Trapeziometacarpal Joint. *The Journal of Hand Surgery* **39(6)**: 1098-1107.

Daud, R, Abdul Kadir, MR, Izman, S, Md Saad, AP, Lee, MH and Che Ahmad, A (2014). Three-Dimensional Morphometric Study of the Trapezium Shape of the Trochlea Tali. *The Journal of Foot and Ankle Surgery* **52(4)**: 426-431.

Doerschuk, SH, Hicks, DG, Chinchilli, VM and Pellegrini, VD, Jr. (1999). Histopathology of the palmar beak ligament in trapeziometacarpal osteoarthritis. *Journal of Hand Surgery American Volume* **24(3)**: 496-504.

Doschak, MR, LaMothe, JM, Cooper, DML, Hallgrimsson, B, Hanley, DA, Bray, RC and Zernicke, RF (2005). Bisphosphonates reduce bone mineral loss at ligament entheses after joint injury. *Osteoarthritis and Cartilage* **13(9)**: 790-797.

Drake, MGH (2005). Gray's anatomy Elsevier/Churchill Livingstone.
Drake, RLMGH (2010). *Gray's anatomy* Philadelphia, PA, Churchill Livingstone/Elsevier.
Dumas, R, Cheze, L, Fayet, M, Rumelhart, C and Comtet, JJ (2008). Comment définir sans ambiguïté les mouvements d'une articulation : proposition de standardisation pour l'articulation trapézométacarpienne. *Chirurgie de la Main* **27(5)**: 195-201.
Eaton, RG and Littler, JW (1969). A study of the basal joint of the thumb. Treatment of its disabilities by fusion. *Journal of Bone Joint Surgery American Volume* **51(4)**: 661-668.
Ebskov, B and Boe, C (1966). The hexatron. A new thumbgonimeter. *Journal of Acta Orthop Scandinavica* **37(1)**: 58-66.
Edmunds, JO (2011). Current concepts of the anatomy of the thumb trapeziometacarpal joint. *Journal of Hand Surgery American Volume* **36(1)**: 170-182.
Eggers, GWN (1945). *chronic dislocation of the base of the metacarpal of the thumb*.
El Ibrahimi, A, Amar, F, Chbani, B, Daoudi, A, Elmrini, A and Boutayeb, F (2009). Dislocation of the carpometacarpal joint of the thumb associated with trapezium and Bennett's fractures. *Journal of Hand New York* **4(2)**: 191-193.
Fogg, QA (2004). Scaphoid variation and an anatomical basis for variable carpal mechanics. *Department of Anatomical Sciences*. Adelaide, University of Adelaide. **Doctor of Philosophy:** 284.
Francois, RJ, Braun, J and Khan, MA (2001). Entheses and enthesitis: a histopathologic review and relevance to spondyloarthritides. *Curr Opin Rheumatol* **13(4)**: 255-264.
Frazer, JES. (1920). The anatomy of the human skeleton. Ed. 2., from http://ebooks.library.ualberta.ca/local/anatomyofhumansk00frazuoft
Materials specified: Free Access http://ebooks.library.ualberta.ca/local/anatomyofhumansk00frazuoft.
Frazer, JESBAS (1965). *Frazer's anatomy of the human skeleton*. London, Churchill.
Frazer, JESBAS and ed (1965). *Anatomy of the human skeleton*. Boston, Little, Brown.
Freemont, AJ (2002). Enthesopathies. *Current Diagnostic Pathology* **8(1)**: 1-10.
Garcia-Elias, M and Orsolini, C (2011). Relationship between thumb laxity and trapezium kinematics. *Chirurgie de la Main* **30(3)**: 224-227.
Geyer, SH, Mohun, TJ and Weninger, WJ (2009). Visualizing vertebrate embryos with episcopic 3D imaging techniques. *ScientificWorldJournal* **9**: 1423-1437.
Ghavami, A and Oishi, SN (2006). Thumb trapeziometacarpal arthritis: treatment with ligament reconstruction tendon interposition arthroplasty. *Journal of Plastic and Reconstructive Surgery* **117(6)**: 116e-128e.
Goitz, RJ, Fowler, JR and Li, ZM (2014). The transverse carpal ligament: anatomy and clinical implications. *Journal of Wrist Surgery* **3(4)**: 233-234.
Goldner, J (1938). A modification of the masson trichrome technique for routine laboratory purposes. *The American Journal of Pathology* **14(2)**: 237-243.
Goubier, JN, Devun, L, Mitton, D and Lavaste, F (2011). In vivo kinematics of the first carpometacarpal joint after trapezectomy. *Chirurgie de la Main* **30(2)**: 97-101.
Goubier, JN, Devun, L, Mitton, D, Lavaste, F and Papadogeorgou, E (2009). Normal range-of-motion of trapeziometacarpal joint. *Chirurgie de la Main* **28(5)**: 297-300.

Gray, H (2005). *Gray's anatomy : the anatomical basis of clinical practice*. Edinburgh, New York.

Hagert, E, Lee, J and Ladd, AL (2012). Innervation Patterns of Thumb Trapeziometacarpal Joint Ligaments. *The Journal of Hand Surgery* **37(4)**: 706-714.e701.

Haines, RW (1944). The mechanism of rotation at the first carpo-metacarpal joint. *Journal of Anatomy* **78(Pt 1-2)**: 44-46.

Harvey, FJ and Bye, WD (1976). Bennett's fracture. *Journal of Hand Surgery European Volume* **8(1)**: 48-53.

Henning, CE, Lynch, MA and Glick, KR, Jr. (1985). An in vivo strain gage study of elongation of the anterior cruciate ligament. *American Journal of Sports Medicine* **13(1)**: 22-26.

Hirokawa, S and Tsuruno, R (1997). Hyper-elastic model analysis of anterior cruciate ligament. *Medical Engineering & Physics* **19(7)**: 637-651.

Hirokawa, S and Tsuruno, R (2000). Three-dimensional deformation and stress distribution in an analytical/computational model of the anterior cruciate ligament. *Journal of Biomechanics* **33(9)**: 1069-1077.

Humes, D, Jahnich, H, Rehm, A and Compson, JP (2004). The osteology of the trapezium. *Journal of Hand Surgery British Volume* **29(1)**: 42-45.

Humphrey, JD, Strumpf, RK and Yin, FC (1989). A theoretically-based experimental approach for identifying vascular constitutive relations. *Biorheology* **26(4)**: 687-702.

Imaeda, T, An, K-N, Cooney Iii, WP and Linscheid, R (1993). Anatomy of trapeziometacarpal ligaments. *The Journal of Hand Surgery* **18(2)**: 226-231.

Imaeda, T, Niebur, G, An, K-N and Cooney, WP (1994). Kinematics of the trapeziometacarpal joint after sectioning of ligaments. *Journal of Orthopaedic Research* **12(2)**: 205-210.

Imaeda, T, Niebur, G, Cooney, W, Linscheid, R and An, K-N (1997). Ligament length during circumduction of the trapeziometacarpal joint. *Journal of Orthopaedic Science* **2(5)**: 319-327.

Isa, MG and Hoo, PC (1980). A technique for the simultaneous staining of osteocytes and osteons in frozen sections of decalcified bone. *Stain Technol* **55(1)**: 47-48.

James Rohlf, F and Marcus, LF (1993). A revolution morphometrics. *Trends Ecol Evol* **8(4)**: 129-132.

Jantea, C, Kurz, R, Clahsen, H, Arnold, G and Rüther, W (1994). Experimental study on the stability of the CMC-joint of the thumb. *The Journal of Hand Surgery: British & European Volume* **19, Supplement 1(0)**: 23-24.

Jonsson, H, Valtysdottir, ST, Kjartansson, O and Brekkan, A (1996). Hypermobility associated with osteoarthritis of the thumb base: a clinical and radiological subset of hand osteoarthritis. *Ann Rheum Dis* **55(8)**: 540-543.

Kapandji, AI (1989). [Prehension of the human hand]. *Ann Chir Main* **8(3)**: 234-241.

Kapandji, AI and Heim, UF (2002). [Reorientation osteotomy of the trapezial saddle]. *Chir Main* **21(2)**: 124-133.

Kapandji, TG and Kapandji, AI (1993). [New radiologic data on the trapezo-metacarpal joint. The results of 330 cases]. *Ann Chir Main Memb Super* **12(4)**: 263-274.

Kaplan, EB (1965). *Functional and surgical anatomy of the hand*. Philadelphia, Lippincott.

Kauer, JM (1987). Functional anatomy of the carpometacarpal joint of the thumb. *Journal of Cinical Orthopaedics and Related Research***(220)**: 7-13.

Kestler, OC (1946). *Recurrent Dislocation of the First Carpometacarpal Joint Repaired by Funcational Tenodesis*.

Koff, MF, Ugwonali, OF, Strauch, RJ, Rosenwasser, MP, Ateshian, GA and Mow, VC (2003). Sequential wear patterns of the articular cartilage of the thumb carpometacarpal joint in osteoarthritis. *Journal of Hand Surgery American Volume* **28(4)**: 597-604.

Kraus, VB, Li, YJ, Martin, ER, Jordan, JM, Renner, JB, Doherty, M, Wilson, AG, Moskowitz, R, Hochberg, M, Loeser, R, Hooper, M and Sundseth, S (2004). Articular hypermobility is a protective factor for hand osteoarthritis. *Arthritis Rheum* **50(7)**: 2178-2183.

Kuczynski, K (1974). Carpometacarpal joint of the human thumb. *Journal of Anatomy* **118(Pt 1)**: 119-126.

Kume, A, Dryden, IL and Le, H (2007). Shape-space smoothing splines for planar landmark data. *Journal of Biometrika* **94(3)**: 513-528.

Kuo, L-C, Chiu, H-Y, Chang, C-W, Hsu, H-Y and Sun, Y-N (2009a). Functional workspace for precision manipulation between thumb and fingers in normal hands. *Journal of Electromyography and Kinesiology* **19(5)**: 829-839.

Kuo, L-C, Cooney, WP, Kaufman, KR, Chen, Q-S, Su, F-C and An, K-N (2004). A quantitative method to measure maximal workspace of the trapeziometacarpal joint—normal model development. *Journal of Orthopaedic Research* **22(3)**: 600-606.

Kuo, L-C, Su, F-C, Chiu, H-Y and Yu, C-Y (2002). Feasibility of using a video-based motion analysis system for measuring thumb kinematics. *Journal of Biomechanics* **35(11)**: 1499-1506.

Kuo, L (2003). Feasibility of using surface markers for assessing motion of the thumb trapeziometacarpal joint. *Clinical Biomechanics* **18(6)**: 558-563.

Kuo, LC, Cooney, WP, 3rd, An, KN, Lai, KY, Wang, SM and Su, FC (2009b). Effects of age and gender on the movement workspace of the trapeziometacarpal joint. *Proc Inst Mech Eng H* **223(2)**: 133-142.

Ladd, AL, Lee, J and Hagert, E (2012). Macroscopic and microscopic analysis of the thumb carpometacarpal ligaments: a cadaveric study of ligament anatomy and histology. *Journal of Bone Joint Surgery American Volume* **94(16)**: 1468-1477.

Ladd, AL, Weiss, AP, Crisco, JJ, Hagert, E, Wolf, JM, Glickel, SZ and Yao, J (2013). The thumb carpometacarpal joint: anatomy, hormones, and biomechanics. *Instructional Course Lectures* **62**: 165-179.

Lane, LB and Henley, DH (2001). Ligament reconstruction of the painful, unstable, nonarthritic thumb carpometacarpal joint. *Journal of Hand Surgery American Volume* **26(4)**: 686-691.

Li, Q, Gong, XQ, Ma, FC, Zhao, YL and Zhu, XH (2005). [Application of histochemical staining in diagnosis of osteosarcomas]. *Zhonghua Zhong Liu Za Zhi* **27(8)**: 489-491.

Lin, H-T, Kuo, L-C, Liu, H-Y, Wu, W-L and Su, F-C (2010). The three-dimensional analysis of three thumb joints coordination in activities of daily living. *Clinical Biomechanics* **26(4)**: 371-376.

Lin, H-T, Kuo, L-C, Liu, H-Y, Wu, W-L and Su, F-C (2011). The three-dimensional analysis of three thumb joints coordination in activities of daily living. *Clinical Biomechanics* **26(4)**: 371-376.

Lin, J, Karl, J and Strauch, R (2013). Trapeziometacarpal Joint Stability: The Evolving Importance of the Dorsal Ligaments. *Clinical Orthopaedics and Related ResearchÂ®*: 1-8.

Linde, F and Sorensen, HC (1993). The effect of different storage methods on the mechanical properties of trabecular bone. *Journal of Biomechanical* **26(10)**: 1249-1252.

Loy, A, Busilacchi, S, Costa, C, Ferlin, L and Cataudella, S (2000). Comparing geometric morphometrics and outline fitting methods to monitor fish shape variability of Diplodus puntazzo (Teleostea: Sparidae). *Aquacultural Engineering* **21(4)**: 271-283.

Lubahn, J, Ivance, D, Konieczko, E and Cooney, T (2006). Immunohistochemical detection of relaxin binding to the volar oblique ligament. *Journal of Hand Surgery American Volume* **31(1)**: 80-84.

Luria, S, Hoch, S, Liebergall, M, Mosheiff, R and Peleg, E (2010). Optimal Fixation of Acute Scaphoid Fractures: Finite Element Analysis. *The Journal of Hand Surgery* **35(8)**: 1246-1250.

MacBride, RG (1998). Potential use of embalmed cadavers to study mast cell presence. *Journal of Anatomical Record* **250(1)**: 117-120.

Maes-Clavier, C, BellemÃ¨re, P, Gabrion, A, David, E, Rotari, V and Havet, E (2014). Anatomical study of the ligamentous attachments and articular surfaces of the trapeziometacarpal joint. Consequences on surgical management of its osteoarthrosis. *Chirurgie de la Main* **33(2)**: 118-123.

Manley, M, Boardman, M and Goitz, RJ (2013). The carpal insertions of the transverse carpal ligament. *Journal of Hand Surgery American Volume* **38(4)**: 729-732.

Marzke, MW, Tocheri, MW, Marzke, RF and Femiani, JD (2012). Three-Dimensional Quantitative Comparative Analysis of Trapezial-Metacarpal Joint Surface Curvatures in Human Populations. *The Journal of Hand Surgery* **37(1)**: 72-76.

McElhaney, J, Fogle, J, Byars, E and Weaver, G (1964). Effect of Embalming on the Mechanical Properties of Beef Bone. *Journal of Applied Physiology* **19**: 1234-1236.

Miller, PJ (1971). An elastin stain. *Med Lab Technol* **28(2)**: 148-149.

Miura, T, Ohe, T and Masuko, T (2004a). Comparative in vivo kinematic analysis of normal and osteoarthritic trapeziometacarpal joints. *Journal of Hand Surgery American Volume* **29(2)**: 252-257.

Miura, T, Ohe, T and Masuko, T (2004b). Comparative in vivo kinematic analysis of normal and osteoarthritic trapeziometacarpal joints. *The Journal of Hand Surgery* **29(2)**: 252-257.

Mohun, TJ and Weninger, WJ (2012). Embedding embryos for high-resolution episcopic microscopy (HREM). *Cold Spring Harb Protoc* **2012(6)**: 678-680.

Momersteeg, TJ, Blankevoort, L, Huiskes, R, Kooloos, JG, Kauer, JM and Hendriks, JC (1995). The effect of variable relative insertion orientation of human knee bone-ligament-bone complexes on the tensile stiffness. *Journal of Biomechanical* **28(6)**: 745-752.

Momose, T, Nakatsuchi, Y and Saitoh, S (1999). Contact Area of the Trapeziometacarpal Joint. *The Journal of Hand Surgery* **24(3)**: 491-495.

Moriggl, B, Kumai, T, Milz, S and Benjamin, M (2003). The structure and histopathology of the "enthesis organ" at the navicular insertion of the tendon of tibialis posterior. *Journal of Rheumatology* **30(3)**: 508-517.

Munoz, JI, Linares-Iglesias, M, Suarez-Penaranda, JM, Mayo, M, Miguens, X, Rodriguez-Calvo, MS and Concheiro, L (2001). Stature estimation from radiographically determined long bone length in a Spanish population sample. *Journal of Forensic Science* **46(2)**: 363-366.

Musgrave, JH and Harneja, NK (1978). The estimation of adult stature from metacarpal bone length. *American Journal of Physical Anthropology* **48(1)**: 113-119.

Najima, H, Oberlin, C, Alnot, JY and Cadot, B (1997). Anatomical and biomechanical studies of the pathogenesis of trapeziometacarpal degenerative arthritis. *Journal of Hand Surgery British Volume* **22(2)**: 183-188.

Nallakaruppan, V, Tung, EY, Sebastin, SJ, Karjalainen, T and Peng, YP (2012). The effect of blocking radial abduction on palmar abduction strength of the thumb. *Journal Hand Surgery European Volume* **37(3)**: 269-274.

Nanno, M, Buford Jr, WL, Patterson, RM, Andersen, CR and Viegas, SF (2006a). Three-Dimensional Analysis of the Ligamentous Attachments of the First Carpometacarpal Joint. *The Journal of Hand Surgery* **31(7)**: 1160-1170.

Nanno, M, Patterson, RM and Viegas, SF (2006b). Three-Dimensional Imaging of the Carpal Ligaments. *Hand Clinics* **22(4)**: 399-412.

Napier, JR (1955). The form and function of the carpo-metacarpal joint of the thumb. *Journal of Anatomy* **89(Pt 3)**: 362-369.

Ng-Thow-Hing, V (2001). Anatomically-based models for physical and geometric reconstruction of humans and other animals, University of Toronto**:** 189.

Nigro, RO (2001). Anatomy of the flexor retinaculum of the wrist and the flexor carpi radialis tunnel. *Hand Clin* **17(1)**: 61-64, vi.

North, ER and Rutledge, WM (1983). The trapezium-thumb metacarpal joint: The relationship of joint shape and degenerative joint disease. *The Hand* **15(2)**: 201-206.

O'Connor, WN and Valle, S (1982). A combination Verhoeff's elastic and Masson's trichrome stain for routine histology. *Stain Technol* **57(4)**: 207-210.

Oberlin, C, Salon, A, Pigeau, I, Sarcy, JJ, Guidici, P and Treil, N (1992). Three-dimensional reconstruction of the carpus and its vasculature: An anatomic study. *The Journal of Hand Surgery* **17(4)**: 767-772.

Oehmke, MJ, Podranski, T, Klaus, R, Knolle, E, Weindel, S, Rein, S and Oehmke, HJ (2009). The Blood Supply of the Scaphoid Bone. *Journal of Hand Surgery (European Volume)* **34(3)**: 351-357.

Ohtera, K, Yamada, Y, Aoki, M, Sasaki, T and Yamakoshi, K (2000). Effects of periosteum wrapped around tendon in a bone tunnel: A biomechanical and histological study in rabbits. *Crit Rev Biomed Eng* **28(1-2)**: 115-118.

Olah, AJ, Simon, A, Gaudy, M, Herrmann, W and Schenk, RK (1977). Differential staining of calcified tissues in plastic embedded microtome sections by a modification of Movat's pentachrome stain. *Stain Technol* **52(6)**: 331-337.

Pacek, CA, Chakan, M, Goitz, RJ, Kaufmann, RA and Li, ZM (2010). Morphological analysis of the transverse carpal ligament. *Journal of Hand New York* **5(2)**: 135-140.

Pagalidis, T, Kuczynski, K and Lamb, DW (1981). Ligamentous stability of the base of the thumb. *The Hand* **13(1)**: 29-35.

Park, K, Kim, K and Choi, YS (2011). Comparison of mechanical rigidity between plate augmentation leaving the nail in situ and interlocking nail using cadaveric fracture model of the femur. *Journal of International Orthopaedics* **35(4)**: 581-585.

Parsons, K, Robinson, B and Hrbek, T (2003). Getting into Shape: An Empirical Comparison of Traditional Truss-Based Morphometric Methods with a Newer Geometric Method Applied to New World Cichlids. *Environmental Biology of Fishes* **67(4)**: 417-431.

Patel, N and Buckland-Wright, C (1999). Advancement in the zone of calcified cartilage in osteoarthritic hands of patients detected by high definition macroradiography. *Osteoarthritis and Cartilage* **7(6)**: 520-525.

Pearlman, JL, Roach, SS and Valero-Cuevas, FJ (2004). The fundamental thumb-tip force vectors produced by the muscles of the thumb. *Journal of Orthopaedic Research* **22(2)**: 306-312.

Pellegrini Jr, VD, Olcott, CW and Hollenberg, G (1993). Contact patterns in the trapeziometacarpal joint: The role of the palmar beak ligament. *The Journal of Hand Surgery* **18(2)**: 238-244.

Pellegrini, VD, Jr. (1991). Osteoarthritis of the trapeziometacarpal joint: the pathophysiology of articular cartilage degeneration. I. Anatomy and pathology of the aging joint. *Journal of Hand Surgery American Volume* **16(6)**: 967-974.

Pellegrini, VD, Jr. (2001). Pathomechanics of the thumb trapeziometacarpal joint. *Journal of Hand Clinical* **17(2)**: 175-184, vii-viii.

Pichler, W, Windisch, G, Schaffler, G, Heidari, N, Dorr, K and Grechenig, W (2010). Computer-assisted 3-dimensional anthropometry of the scaphoid. *Orthopedics* **33(2)**: 85-88.

Pieron, AP (1973). The mechanism of the first carpometacarpal (CMC) joint. An anatomical and mechanical analysis. *Acta Orthop Scand Suppl* **148**: 1-104.

Pioletti, DP, Heegaard, JH, Rakotomanana, RL, Leyvraz, PF and Blankevoort, L (1995). Experimental and mathematical methods for representing relative surface elongation of the ACL. *Journal of Biomechanical* **28(9)**: 1123-1126.

Pizon, AF and Wang, HE (2010). Carpometacarpal Dislocation of the Thumb. *The Journal of Emergency Medicine* **38(3)**: 376-377.

Presazzi, A, Bortolotto, C, Zacchino, M, Madonia, L and Draghi, F (2011). Carpal tunnel: Normal anatomy, anatomical variants and ultrasound technique. *Journal of Ultrasound* **14(1)**: 40-46.

Punsola-Izard, V, Salas-GÃ³mez, D, Sirvent-Rivalda, E and Esquirol-CaussÃ , J (2012). Functional patterns of thumb key pinch and their influence on thumb strength and stability. *Hand Therapy* **17(4)**: 78-86.

Rongieres, M (2004). Anatomie et physiologie de l'articulation trapézométacarpienne humaine. *Chirurgie de la Main* **23(6)**: 263-269.

Rosenthal, J, Mangal, V, Walker, D, Bennett, M, Mohun, TJ and Lo, CW (2004). Rapid high resolution three dimensional reconstruction of embryos with episcopic fluorescence image capture. *Birth Defects Res C Embryo Today* **72(3)**: 213-223.

Rudemo, M (2000). Statistical Shape Analysis. I. L. Dryden and K. V. . *Journal of Statistics in Medicine* **19(19)**: 2716-2717.

Schild, H, Walde, HJ, Rudigier, J and Schwarzkopf, W (1981). The trapezium bone--anatomy, radiography and traumatology. *Handchirurgie* **13(3-4)**: 238-241.

Shuler, MS, Luria, S and Trumble, TE (2008). Basal joint arthritis of the thumb. *Journal of American Academey Orthopaedic Surgeons* **16(7)**: 418-423.

Simoens, P (2006). Anatomie comparée de la main. *Chirurgie de la Main* **25(3-4)**: 111-118.

Slobodin, G, Rozenbaum, M, Boulman, N and Rosner, I (2007). Varied Presentations of Enthesopathy. *Seminars in Arthritis and Rheumatism* **37(2)**: 119-126.

Slocum, DB (1943). Stabilization of the articulation of the greater multangular and the first metacarpal. *Journal of Bone and Joint Surgery* **25**: 626-630.

Smith, EM, Juvinall, RC, Bender, LF and Pearson, JR (1964). Role of the Finger Flexor in Rheumatoid Deformlties of the Metacarpophalangeal Joints. *Journal of Arthritis Rheumotology* **7**: 467-480.

Snell, RS (1995). *Clinical anatomy* Boston, Little, Brown.

Snell, RSSRS (2004). Clinical anatomy, Lippincott Williams & Wilkins.

Song, Y, Debski, RE, Musahl, V, Thomas, M and Woo, SLY (2004). A three-dimensional finite element model of the human anterior cruciate ligament: a computational analysis with experimental validation. *Journal of Biomechanics* **37(3)**: 383-390.

Stark, H, Frober, R and Schilling, N (2012). Intramuscular architecture of the autochthonous back muscles in humans. *Journal of Anatomy*.

Sterling, TR, Pope, DS, Bishai, WR, Harrington, S, Gershon, RR and Chaisson, RE (2000). Transmission of Mycobacterium tuberculosis from a cadaver to an embalmer. *New England Journal of Medicine* **342(4)**: 246-248.

Steven, W (2009). CHAPTER 55 - The Carpometacarpal Joint. *Pain Review*. Philadelphia, W.B. Saunders**:** 105.

Strauch, RJ, Behrman, MJ and Rosenwasser, MP (1994). Acute dislocation of the carpometacarpal joint of the thumb: An anatomic and cadaver study. *The Journal of Hand Surgery* **19(1)**: 93-98.

Su, F-C, Kuo, L-C, Chiu, H-Y and Chen-Sea, M-J (2003). Video-computer quantitative evaluation of thumb function using workspace of the thumb. *Journal of Biomechanics* **36(7)**: 937-942.

Su, F-C, Lin, C-J, Wang, C-K, Chen, G-P, Sun, Y-N, Chuang, AK and Kuo, L-C (2014). In vivo analysis of trapeziometacarpal joint arthrokinematics during multi-directional thumb motions. **29:** 1009-1015.

Tan, J, Xu, J, Xie, RG, Deng, AD and Tang, JB (2011). In Vivo Length and Changes of Ligaments Stabilizing the Thumb Carpometacarpal Joint. *The Journal of Hand Surgery* **36(3)**: 420-427.

Thiel, W (2002). [Supplement to the conservation of an entire cadaver according to W. Thiel]. *Journal of Annals of Anatomy***184(3)**: 267-269.

Tocheri, MW, Razdan, A, Williams, RC and Marzke, MW (2005). A 3D quantitative comparison of trapezium and trapezoid relative articular and nonarticular surface areas in modern humans and great apes. *Journal of Human Evolution* **49(5)**: 570-586.

Van Brenk, B, Richards, RR, Mackay, MB and Boynton, EL (1998). A biomechanical assessment of ligaments preventing dorsoradial subluxation of the trapeziometacarpal joint. *Journal of Hand Surgery American Volume* **23(4)**: 607-611.

van Haaren, EH, van der Zwaard, BC, van der Veen, AJ, Heyligers, IC, Wuisman, PI and Smit, TH (2008). Effect of long-term preservation on the mechanical properties of cortical bone in goats. *Jounal of Acta Orthopaedica* **79(5)**: 708-716.

Veuthey, T, Herrera, G and Dodero, VI (2014). Dyes and stains: from molecular structure to histological application. *Front Biosci (Landmark Ed)* **19**: 91-112.

Watt, N and Hooper, G (1987). Dislocation of the trapezio-metacarpal joint. *The Journal of Hand Surgery: British & European Volume* **12(2)**: 242-245.

Weninger, WJ, Geyer, SH, Mohun, TJ, Rasskin-Gutman, D, Matsui, T, Ribeiro, I, Costa Lda, F, Izpisua-Belmonte, JC and Muller, GB (2006). High-resolution episcopic microscopy: a rapid technique for high detailed 3D analysis of gene activity in the context of tissue architecture and morphology. *Journal of Anatomy and Embryology* **211(3)**: 213-221.

Wilke, HJ, Krischak, S and Claes, LE (1996). Formalin fixation strongly influences biomechanical properties of the spine. *Journal of Biomechanical* **29(12)**: 1629-1631.

Williams, FL and Richtsmeier, JT (2003). Comparison of mandibular landmarks from computed tomography and 3D digitizer data. *Journal of Clinical Anatomy* **16(6)**: 494-500.

Zancolli, EA, Ziadenberg, C and Zancolli, E, Jr. (1987). Biomechanics of the trapeziometacarpal joint. *Journal of Clinical Orthopaedic Related Research***(220)**: 14-26.

Zhang, X, Braido, P, Lee, SW, Hefner, R and Redden, M (2005). A normative database of thumb circumduction in vivo: center of rotation and range of motion. *Journal of the Human Factors and Ergonomics Society* **47(3)**: 550-561.

.....